



저작자표시-비영리-변경금지 2.0 대한민국

이용자는 아래의 조건을 따르는 경우에 한하여 자유롭게

- 이 저작물을 복제, 배포, 전송, 전시, 공연 및 방송할 수 있습니다.

다음과 같은 조건을 따라야 합니다:



저작자표시. 귀하는 원저작자를 표시하여야 합니다.



비영리. 귀하는 이 저작물을 영리 목적으로 이용할 수 없습니다.



변경금지. 귀하는 이 저작물을 개작, 변형 또는 가공할 수 없습니다.

- 귀하는, 이 저작물의 재이용이나 배포의 경우, 이 저작물에 적용된 이용허락조건을 명확하게 나타내어야 합니다.
- 저작권자로부터 별도의 허가를 받으면 이러한 조건들은 적용되지 않습니다.

저작권법에 따른 이용자의 권리는 위의 내용에 의하여 영향을 받지 않습니다.

이것은 [이용허락규약\(Legal Code\)](#)을 이해하기 쉽게 요약한 것입니다.

[Disclaimer](#)

약학박사학위논문

Design and development of multi-targeted
anticancer agents for anti-angiogenic therapy
or tumor tissue-selective delivery

혈관신생억제 및 종양선택적 전달을 위한
다중표적형 항암제의 설계와 개발

2015년 2월

서울대학교 대학원

약학과 약제과학전공

정 성 우

ABSTRACT

Despite the rapid advances of cancer research, cancer is still one of the leading causes of mortality worldwide. During the past decades, research of anticancer agents mostly focused on selective targeting of tumor-specific antigens in the context of molecular targeted therapy as well as targeted drug delivery to improve the therapeutic index of the traditional chemotherapy. However, due to the intrinsic genetic diversity and complexity of tumors, the targeted therapeutics showed only limited improvements. Therefore, a breakthrough of the fundamental concept in cancer treatment has been deemed necessary. In this dissertation, novel therapeutic alternatives are proposed and evaluated that could contribute to the further advance in the cancer therapeutics.

Part one concerns development of a heparin-based anti-angiogenic agent LHT7 – a sodium taurocholate conjugated LMWH – that inhibits multiple stages of angiogenesis, and investigation of its mode of action. This study showed that the conjugation of sodium taurocholates abolished the intrinsic capability of LMWH to interact with ATIII while enhancing the binding property on VEGF, resulting in decreased anticoagulant activity and enhanced anti-angiogenic activity. The differential effects of sodium taurocholate conjugation to LMWH on its interaction between ATIII and VEGF were attributable to the unique structure of sodium taurocholate: the bulky and rigid sterane core of taurocholate sterically concealed the ATIII-binding pentasaccharide unit of LMWH, while the terminal sulfate group generated additional interactions with VEGF leading to a stronger binding.

The major advantage of exploiting heparin as a lead compound for the development of novel anti-angiogenic agents comes from the intrinsic capability of interacting and regulating wide array of pro-angiogenic factors. LHT7 was speculated to block FGF2 and PDGF-B in addition to VEGF. Since these three pro-angiogenic factors play key roles in multiple stages of angiogenesis, simultaneous blockade of these factors resulted in potent suppression of tumor angiogenesis as well as tumor growth. The results of this

study suggested that LHT7 would potentially overcome the resistance issue shown in the conventional anti-angiogenic agents.

Part two discusses development of doxorubicin prodrugs that target induced-apoptosis for effective delivery of chemotherapeutics to the tumor regardless of its genomic property. The first doxorubicin prodrug involves two distinct features for an effective tumor targeting: EPR effect-mediated tumor accumulation with extended plasma half-life, and radiation-induced apoptosis targeting. This prodrug – EMC-DEVD-S-DOX – comprises a maleimide group, which binds to the circulating albumin after intravenous administration, and a DEVD motif, which is cleaved by caspase-3 upregulated in the tumor cells that are exposed to radiation. The EMC-DEVD-S-DOX showed a prolonged plasma half-life with selective accumulation within tumor tissue, and released free doxorubicin only when combined with radiotherapy.

The second doxorubicin prodrug – RGDEVD-DOX – comprises an integrin $\alpha\beta3$ recognizing RGD sequence and a DEVD sequence. The RGD moiety selectively delivers the prodrug to the tumor during the initial phase of administration and induces apoptosis in certain subclone of tumor cells as well as tumor endothelial cells that overexpress integrin $\alpha\beta3$. The caspase-3 from the apoptotic cells further activates other molecules of the prodrug, forcing those to release hydrophobic active compound with facilitated cell penetration regardless of integrin $\alpha\beta3$ expression. Therefore, it could affect broader range of tumor cells within the tumor tissue, thereby providing more effective therapeutic outcomes. Since the upregulation of the caspase-3, which is the key event of the proposed drug delivery strategy, is common during the apoptosis, the genomic diversity of tumor cells hardly influences the efficacy of the currently developed prodrugs.

Keywords: Heparin; anticancer agent; angiogenesis inhibitor, multi-targeting; VEGF; FGF; PDGF; doxorubicin; prodrug; caspase-3; DEVD; albumin; RGD; integrin $\alpha\beta3$.

Student number: 2010-31129

Table of Contents

ABSTRACT	i
Table of Contents	iii
List of Tables	ix
List of Figures	ix
Abbreviations	xvi
Introduction	1
References	3
Part I. Study of mode of action and multiple pathway inhibitory capability in tumor angiogenesis of heparin-based agent LHT7	5
1. General Introduction	7
1.1. Tumor angiogenesis	7
1.1.1. Physiology of tumor angiogenesis	7
1.1.2. Angiogenesis inhibition	10
1.1.3. Resistance to angiogenesis inhibitors	13
1.2. Heparin	17
1.2.1. Structural Characteristics of Heparin	18
1.2.2. Anticoagulant Activity of Heparin	19
1.2.2. Heparin in Cancer	20
1.3. Rationale of the research	22
References	23
2. Potentiation of anti-angiogenic activity of heparin by blocking the ATIII- interacting pentasaccharide unit and increasing net anionic charge	35
2.1. Introduction	36
2.2. Materials and Methods	38
2.2.1. Cell lines	38
2.2.2. Synthesis	38
2.2.3. Characterization of the synthesized LMWH-derivatives	41
2.2.4. Surface plasmon resonance (SPR) analysis	43
2.2.5. Molecular dynamics	43
2.2.6. Computer simulated molecular docking	44

2.2.7. X-ray μ CT angiography	45
2.2.8. Tumor growth suppression	46
2.2.9. Histological analysis	46
2.2.10. Ex vivo imaging of whole-body distribution.....	46
2.2.11. Immunofluorescence	47
2.2.12. Platelet uptake study of fluorescent-labeled LHT7.....	47
2.2.13. Statistical analysis	48
2.3. Results.....	48
2.3.1. Effects of the conjugated sodium taurocholate between the interaction of LMWH and ATIII determined by computerized docking simulation.....	48
2.3.2. Anticoagulant activities of LHT7 and its structural analogs	49
2.3.3. Effects of the conjugated sodium taurocholate between the interaction of LMWH and VEGF determined by computerized molecular dynamics	50
2.3.4. VEGF binding affinities of LHT7 and its structural analogs.....	51
2.3.5. Effect of LHT7 on tumor angiogenesis in vivo	52
2.3.6. Anticancer effects of LHT7 on distinct types of carcinoma xenografts.....	53
2.3.7. Intratumor localization of LHT7.....	54
2.3.8. LHT7 uptake by platelets	54
2.4. Discussion	70
2.5. Conclusion.....	76
References.....	76
3. Multiple-stage angiogenesis inhibition of LHT7 by blocking VEGF, FGF2, and PDGF-B	81
3.1. Introduction	82
3.2. Materials and Methods.....	84
3.2.1. Cell lines.....	84
3.2.2. Transwell chemotactic migration assay	84
3.2.3. MTT cytotoxicity assay.....	85
3.2.4. HUVEC spheroid sprouting assay	85
3.5.5. Endothelial tube formation assay.....	86

3.2.6. Matrigel plug angiogenesis assay	87
3.2.7. Receptor tyrosine kinase phosphorylation studies	87
3.2.8. In vitro pericyte migration to endothelial tube	88
3.2.9. In vitro pericyte-endothelium adhesion assay	88
3.2.10. Surface plasmon resonance (SPR) analysis.....	89
3.2.11. Dynamic contrast enhanced magnetic resonance imaging.....	89
3.2.12. Statistical analysis.....	90
3.3. Results	90
3.3.1. HUVEC migration inhibitory effect and cytotoxicity evaluation of LHT7	90
3.3.2. Inhibitory effect of LHT7 in endothelial sproutings	91
3.3.3. Inhibitory effect of LHT7 in endothelial tubular differentiation ...	92
3.3.4. Inhibitory effect of LHT7 in the angiogenesis induced by VEGF and FGF2 in matrigel plugs	92
3.3.5. VEGF-VEGFR2 and FGF2-FGFR1 signaling pathway blockade by LHT7	93
3.3.6. Inhibitory effect of LHT7 on pericyte recruitment to endothelium linings	94
3.3.7. Determination of cytotoxicity on pericytes and possible effects in the endothelial cell and pericyte adhesion of LHT7.....	95
3.3.8. Inhibitory effect of LHT7 on PDGF-B-induced angiogenesis in matrigel plugs	95
3.3.9. PDGFB-PDGFR β signaling pathway blockade by LHT7	96
3.3.10. Characterization of tumor vasculatures in LHT7-treated tumor-bearing animals using DCE-MRI.....	97
3.4. Discussion.....	112
3.5. Conclusion	115
References	115
Part II. Novel strategy for site-specific delivery system and development of doxorubicin prodrugs	119
4. General Introduction	121
4.1. Tumor heterogeneity	121
4.1.1. Intertumor heterogeneity.....	121
4.1.2. Intratumor heterogeneity.....	122

4.2. Apoptosis targeted prodrug system.....	124
4.2.1. Caspase in apoptosis	125
4.2.2. Substrate recognition by caspases.....	127
4.3. Tumor targeting strategies.....	131
4.3.1. Passive tumor targeting	131
4.3.1.1. Albumin as a carrier for tumor targeting	134
4.3.1.2. Exploiting endogenous albumin for albumin-bound agents	137
4.3.2. Active tumor targeting strategy	140
4.3.2.1. Integrins.....	144
4.3.2.2. RGD peptide sequence for targeting integrin $\alpha\beta 3$	146
4.4. Rationale of the research.....	148
References.....	149
5. Albumin-binding radiation-induced apoptosis targeted doxorubicin prodrug .	165
5.1. Introduction	166
5.2. Materials and methods	169
5.2.1. Cell lines.....	169
5.2.2. Synthesis.....	169
5.2.3. EMC-DEVD-S-DOX binding study with HSA	171
5.2.4. HSA-DEVD-S-DOX analysis by SDS-PAGE	171
5.2.5. Determination of thiol concentration of HSA using Ellman's test	
.....	172
5.2.6. Preparation and characterization of HSA-DEVD-S-DOX	172
5.2.7. EMC-DEVD-S-DOX incubation study in plasma	173
5.2.8. Western blot.....	173
5.2.9. MTT cytotoxicity assay.....	174
5.2.10. Cellular uptake imaging	174
5.2.11. HPLC determination of caspase-mediated activation	175
5.2.12. Pharmacokinetic study	175
5.2.13. Ex vivo biodistribution imaging	176
5.2.14. Tumor growth suppression	176
5.3. Results.....	177
5.3.1. Synthesis of EMC-DEVD-S-DOX	177

5.3.2. Albumin-binding of EMC-DEVD-S-DOX	177
5.3.3. Caspase-3-mediated cleavage of HSA-DEVD-S-DOX	179
5.3.4. In vitro efficacy of HSA-DEVD-S-DOX.....	180
5.3.5. Caspase-3 upregulation induced by activated HSA-DEVD-S-DOX	180
5.3.6. Pharmacokinetic study	181
5.3.7. Tumor accumulation of EMC-DEVD-Cy5.5	181
5.3.8. Tumor growth suppression of EMC-DEVD-S-DOX.....	182
5.4. Discussion	198
5.5. Conclusion	200
References	201
6. Integrin $\alpha\beta 3$ targeted caspase-3-dependently activated doxorubicin prodrug	203
6.1. Introduction.....	204
6.2. Materials and Methods	206
6.2.1. Cell lines	206
6.2.2. Synthesis	206
6.2.2. Integrin $\alpha\beta 3$ dependent cellular uptake imaging	208
6.2.3. siRNA transfection.	209
6.2.4. Flow cytometry.....	210
6.2.5. HPLC determination of caspase-mediated activation.....	210
6.2.6. MTT cytotoxicity assay	211
6.2.7. Western blots.....	211
6.2.8. Caspase-3 cellular activity assay	212
6.2.9. Cellular caspase-3 stain.....	213
6.2.10. Animal study	213
6.2.11. Statistical analysis.....	214
6.3. Results	214
6.3.1. Synthesis of RGDEVD-DOX.....	214
6.3.2. Integrin $\alpha\beta 3$ dependent cellular uptake of RGDEVD peptide... 214	
6.3.2. Caspase-3-mediated cleavage of RGDEVD-DOX	216
6.3.3. In vitro efficacy of RGDEVD-DOX.....	216
6.3.4. Caspase-3 upregulation induced by RGDEVD-DOX.....	217

6.3.5. Tumor growth suppression of RGDEVD-DOX	219
6.4. Discussion	238
6.5. Conclusion.....	240
References.....	240
Concluding remarks	243

List of Tables

Table 2.1. Characteristics of LHT7 and its analogs	57
Table 3.1. Dissociation constants of LHT7 on VEGF, FGF2 or PDGF-B	99
Table 4.1. Optimal substrate sequences for caspases	129
Table 5.1. Pharmacokinetic parameters in SD rats (1 mg/kg dox molar eq.) .	183

List of Schemes

Scheme 5.1. Chemical synthesis of EMC-DEVD-S-DOX	185
Scheme 6.1. Chemical synthesis of RGDEVD-DOX	223

List of Figures

Figure 2.1. (A) Computerized molecular docking of LMWH (left) and LHT7 (right) on the ATIII heparin binding site (arrow). The pairs were allowed to reach the minimum intermolecular energy level and the final appearances were examined. (B) Representative chemical structures of LMWH **1**, cholic acid conjugated LMWH **2**, taurine conjugated LMWH **3**, and LHT7 **4**. (C) The model structure of LHT7 and VEGF-HBD complex when the intermolecular energy level has reached the minimum during molecular dynamics. 59

Figure 2.2. (A) Representative images of saline (control), LMWH, and LHT7 treated SCC7 tumors obtained by X-ray μ CT. Scale bar, 5 mm. (B) Tumor vessel volumes (left) and vessel fractions (right) calculated through reconstruction of vasculatures followed by computed calculation of the volumes. * $P < 0.05$, ** $P < 0.005$, and *** $P < 0.001$ versus control. Data are expressed as mean \pm s.e.m. 61

Figure 2.3. Tumor growth suppression on A549 (A) and HT-29 (B) xenografts. The three groups received either saline as control (\circ) or LHT7 in two different doses: 1 mg/kg (\bullet) and 5 mg/kg (\square) administered intravenously every other day.

n = 9. Data presented as mean \pm s.e.m. (C) Histological analysis of A549 (left) and HT-29 (right) tumor sections. Immunostaining of the upper and lower panels indicates CD34 and α SMA, respectively. Scale bar, 50 μ m. 63

Figure 2.4. (A) Tumor growth suppression of AMC-HN9 xenografts. Mice received either saline as control (\circ) or LHT7 in different doses: 1 mg/kg (\bullet) and 5 mg/kg (\square) administered every other day. n = 9. (B) Histological analysis of AMC-HN9 tumor sections. Immunostaining of the left and right panels indicates CD34 and α SMA, respectively. Scale bar, 50 μ m. (C) CD34 (left) and HE (right) staining of the tumor specimens. Arrows depict a subset of red blood cells. Scale bar, 50 μ m. 65

Figure 2.5. (A) *Ex vivo* biodistribution observations of the fluorescent-labeled LHT7 after intravenous administration in mice. (B) Immunostaining of tumor specimens at post-administration of LHT7. Red and green color represents CD31 and LHT7, respectively. Scale bar, 50 μ m. 67

Figure 2.6. (A) FACS analysis of platelets that have taken up LHT7 after incubation with a series of concentrations of fluorescent-labeled LHT7. Numbers represent the gated percentage in the assigned range. (B) Quantitative analysis of released (\circ) and bound (\bullet) LHT7 on the pellet of the platelets after activation of platelets incubated with fluorescent-labeled LHT7. Data are expressed as means \pm s.d. (C) Immunocytochemical staining of platelets incubated with fluorescent-labeled LHT7. Green and red represents LHT7 and P-selectin in α -granules of platelets, respectively. Scale bar, 2 μ m. 69

Figure 3.1. (A) Transwell chemotactic cell migration of HUVECs induced by VEGF or FGF2. Degree of migration in control (white) and LHT7-treated group (black) was assessed. (B) Cytotoxicity evaluation of LHT7 on HUVECs by using MTT cell proliferation assay at a concentration range of 0.01 to 1 mg/ml. (C) Representative images of VEGF and/or FGF2-induced angiogenic sprouting of HUVEC spheroid of control and LHT7-treated groups. Scale bar, 50 μ m. 101

Figure 3.2. (A) HUVEC tube formation induced by VEGF and/or FGF2. HUVECs were stained in green fluorescence. Scale bar, 500 μ m. (B) Quantitative analysis of HUVEC tubes by ImageJ angiogenesis analyzer. Number of nodes (left panel) and branches (right panel) of control (empty column) and LHT7 treated group (filled column) were calculated. * $P < 0.05$ versus control. Data are presented as mean \pm s.d. 103

Figure 3.3. (A) *In vivo* matrigel plug angiogenesis assay using VEGF or FGF2 as an angiogenic stimulator. The inhibition of phosphotyrosine level of VEGFR2 stimulated by VEGF (B) and FGFR1 stimulated by FGF2 (C) on HUVECs (left) and HDMECs (right) by LHT7 are shown by immunoblots. . 105

Figure. 3.4. Representative images of HUVECs (red) and pericytes (green) coculture system *in vitro*. (A) Pericytes were seeded after endothelial tubes were formed. Recruitment of pericytes to HUVEC tubes in control, anti-VEGF mAb, and LHT7-treated groups were observed after 2 h and 18 h of pericyte addition. Scale bars, 500 μ m. (B) Quantitative analysis of remaining endothelial tubes after 18 h of pericyte addition by ImageJ angiogenesis analyzer. Number of nodes (left panel) and branches (right panel) were calculated and shown as means \pm s.d. with individual plot. * $P < 0.05$ versus control. (C) Cytotoxic effect of LHT7 evaluated by MTT assay at a concentration range of 0.01 to 1 mg/ml. (D) Pericytes adhesion on confluent HUVEC monolayer. Single image was obtained in the center of the each well (n = 3) at 40x magnification and number of the adhered pericytes were counted and averaged. Data are expressed as means \pm s.d. 107

Figure 3.5. (A) *In vivo* matrigel plug angiogenesis assay using PDGF-B and PDGF-B/FGF2 mixture as angiogenic stimulators. (B) Western blots of phosphotyrosine level of PDGFR β on pericytes stimulated by PDGF-B in the presence or absence of LHT7 or neutralizing antibody. 109

Figure 3.6. MDA-MB-231 tumor-bearing mice were treated with LHT7 at a dose of 5 mg/kg intravenously daily for three weeks (●) and compared with

control (○). Tumor growth (A) and body weight (B) change were measured. DCE-MRI parameters were measured during the treatment at day 0, 7, 14 and 21. The values of K_{trans} (C), K_{ep} (D), initial slope (E), and K_{el} (F) were calculated. $n = 3$. Data are expressed as mean \pm s.d. * $P < 0.05$ versus control.

..... 111

Figure 5.1. (A) Schematic diagram of EMC-DEVD-S-DOX therapeutic strategy. (B) Chemical structure of EMC-DEVD-S-DOX. 187

Figure 5.2. (A) Analytical HPLC chromatogram of the final product detected under fluorescence detector (470/580 nm). (B) Mass spectrum of the final product determined by LC/ESI-MS..... 189

Figure 5.3. (A) HPLC chromatograms of EMC-DEVD-S-DOX and that incubated with commercially available HSA (3, 60 min), EMC-DEVD-S-DOX incubated with HSA blocked with excess GMB (60 min), and only HSA. (B) SDS-PAGE of EMC-DEVD-S-DOX or DEVD-S-DOX incubated with HSA or HSA blocked with excess GMB. (C) MALDI-TOF MS results of commercially available HSA (grey), and that incubated with EMC-DEVD-S-DOX in PBS (pH 7.4; black). (D) HPLC chromatograms of EMC-DEVD-S-DOX and that incubated in human plasma (3, 60 min), EMC-DEVD-S-DOX incubated with the plasma blocked with excess GMB (60 min), and only plasma..... 191

Figure 5.4. (A) HPLC chromatograms of HSA-DEVD-S-DOX and that incubated in the presence or absence of caspase-3, HSA-DEVD-S-DOX incubated with the caspase-3 pretreated with caspase inhibitor, and doxorubicin. (B) Concentration-dependent cytotoxicity of doxorubicin (○), HSA-DEVD-S-DOX (■), and HSA-DEVD-S-DOX incubated with recombinant human caspase-3 (□) on SCC7 (left) and MDA-MB-231 (right) cells determined by MTT assay. (C) Cellular uptake and intracellular distribution of doxorubicin (left), HSA-DEVD-S-DOX (center), and HSA-DEVD-S-DOX incubated with caspase-3 (right) in SCC7 (upper) and MDA-MB-231 (lower) cells observed under confocal microscopy. The substances were detected through intrinsic

fluorescence of doxorubicin and represented as red color. Scale bar, 50 μm . (D) Western blots of SCC7 (upper) or MDA-MB-231 (lower) cells treated with HSA-DEVD-S-DOX or HSA-DEVD-S-DOX incubated with recombinant human caspase-3 (Cleaved HSA-DEVD-S-DOX) at a concentration of 1, 5, and 10 μM . The immunoblots were carried out using procaspase-3 (upper), cleaved caspase-3 (center), and β -actin (lower) antibodies. 193

Figure 5.5. (A) Logarithmic plasma concentration for time profiles of EMC-DEVD-S-DOX (\circ) and DEVD-S-DOX (\bullet) administered to SD rats ($n = 3$) via intravenous route at a dose of 1 mg/kg molar equivalent to doxorubicin. The plasma concentration was calculated based on the mass concentration of doxorubicin content. Lower graph depicts enlarged plasma concentration profile showing until 2 h. (B) Ex vivo imaging of whole body distribution of EMC-DEVD-Cy5.5 in U87 MG tumor-bearing mice. 195

Figure 5.6. Animal study result of SCC7-tumor bearing C3H/HeN mice that received normal saline (\circ), radiation (\bullet), DEVD-S-DOX accompanied by radiation (Δ), EMC-DEVD-S-DOX (\square), or EMC-DEVD-S-DOX accompanied by radiation (\blacksquare). EMC-DEVD-S-DOX or DEVD-S-DOX was intravenously administered daily for 7 days at 1 mg/kg molar equivalent to doxorubicin from day 0 ($n = 5$). Radiation was given at a dose of 4 Gy single time at day 0. Tumor growth profile (A) and body weight profile (B) are shown. Data are presented as mean \pm s.e.m. 197

Figure 6.1. (A) Schematic diagram of the suggested prodrug strategy. (B) The major difference of the conventional targeted delivery system and the currently proposed targeted delivery system. (C) Chemical structure and compartment of the RGDEVD-DOX prodrug and its active compound. 225

Figure 5.2. (A) Analytical HPLC chromatogram of the final product detected under UV detector (214 nm) and ESI-MS. (B) Mass spectrum of the final product determined by LC/ESI-MS. 227

Figure 6.3. (A) Confocal microscopy images of HUVECs (left), HDMEC (center), and U87 MG cells (right) exposed to RDEVD (upper panel) or RGDEVD peptide (lower panel) labeled with Cy5.5. Green fluorescence represents the peptides. Cell nuclei are stained with DAPI (blue). Scale bar, 50 μ m. (B) Western blots of integrin α v after ITGAV siRNA transfection of HDMECs and U87 MG cells. (C) Confocal microscopy images of Cy5.5-labeled RGDEVD peptide given to HDMECs (left) and U87 MG cells (right) that were mock-transfected (upper) or ITGAV siRNA transfected (lower). Green fluorescence represents the peptides. Cell nuclei are stained with DAPI (blue). Scale bar, 50 μ m. (D) Histograms of flow cytometry analysis. Mock-transfected (blue) and ITGAV siRNA transfected (pink) U87 MG cells were analyzed after RGDEVD peptide treatment and integrin α v β 3 immunostaining. The cells were detected against Alexa488-labeled integrin α v β 3 antibody (left) and Cy5.5-labeled RGDEVD peptide (right). Non-stained non-treated U87 MG cells were also analyzed (grey). (E) Confocal microscopy images of U87 MG cells exposed to RDEVD-DOX (left) or RGDEVD-DOX (right). The red fluorescence represents the doxorubicin moiety. The cells are also stained with DAPI (blue). All the acquired channels (red, blue, and DIC) were merged and shown in the lower panel. Scale bar, 50 μ m. 229

Figure 6.4. (A) HPLC chromatograms of RGDEVD-DOX incubated in the presence of recombinant human caspase-3 for 0, 15, 30, and 60 min. Chromatograms of RGDEVD-DOX incubated for 120 min with the caspase-3 pretreated with caspase inhibitor, and RGDEVD-DOX incubated for 120 min without addition of caspase-3 were also shown. (B) Mean intensity of doxorubicin fluorescence in the cell nuclei quantified depending on the drug exposure time. Doxorubicin (\circ), RGDEVD-DOX (\square), or cleaved RGDEVD-DOX (\blacksquare) was treated on U87 MG (left) and HT-29 (right) cells. Data are presented as mean \pm s.e.m. (C) Representative images of doxorubicin (left), RGDEVD-DOX (center), and cleaved RGDEVD-DOX (right) treated on U87 MG (upper) and HT-29 (lower) cells for 1 h. Scale bar, 50 μ m. 231

Figure 6.5. (A) Concentration-dependent cytotoxicity of doxorubicin (○), RGDEVD-DOX (□), and RGDEVD-DOX incubated with recombinant human caspase-3 (cleaved RGDEVD-DOX; ■) on U87 MG (left) and HT-29 (right) cells when exposed 2 h determined by MTT assay. (B) Exposure time-dependent IC50 values of the drugs on U87 MG cells. Data are presented as mean ± s.e.m.233

Figure 6.6. (A) Western blots of U87 MG cells treated with RGDEVD -DOX or RGDEVD-DOX incubated with recombinant human caspase-3 (cleaved RGDEVD-DOX) at a concentration of 0.1, 1, and 10 μM. The immunoblots were carried out using procaspase-3 (upper), cleaved caspase-3 (center), and beta-actin (lower) antibodies. (B) Cellular caspase activities of U87 MG cells treated with cleaved RGDEVD-DOX (white) or RGDEVD-DOX (grey) at a concentration of 0, 0.1, 1, and 10 μM. Data are presented as mean ± s.e.m. (C) Cellular caspase-3 staining of U87 MG cells after 48 h exposure to cleaved RGDEVD-DOX (center) and RGDEVD-DOX (right). Control cells that have not been treated with any drugs were also shown (left). Green fluorescence represents the active caspase-3. Nuclei of control cells were stained with DAPI (blue). Nuclei of drug treated cells were accumulated with the drug (red) and were not stained with DAPI. Scale bar, 10 μm.235

Figure 6.7. Animal study result of U87 MG-tumor bearing BALC/cSlc-nu mice that received normal saline (○), doxorubicin (7 × 3 mg/kg, ●), RDEVD-DOX (7 × 3 mg/kg, Δ), and RGDEVD-DOX in three different doses (7 × 1 mg/kg, ▲; 7 × 3 mg/kg, □; 7 × 5 mg/kg, ■). The animals received the agents intravenously daily for 7 days. The doses are expressed at molar equivalent of doxorubicin. Tumor growth profiles (A), isolated tumor weights (C), and body weight profiles (B) are shown. Data are presented as mean ± s.e.m.237

Abbreviations

A

Ab	Antibody
ADC	Antibody-drug conjugate
AIF	Apoptosis-inducing factor
AMC	7-amino-4-methylcoumarin (not for AMC-HN9)
AML	Acute myeloid leukemia
Ang	Angiopoietin
ANOVA	Analysis of variance
APAF1	Apoptotic-proteases-activating factor-1
APF	Amino acid positional fitness
APO-1	Apoptosis antigen 1
AT	Antithrombin
ATP	Adenosine triphosphate
AUC	Area under the concentration-time curve

B

BBB	Blood-brain barrier
BCA	Bicinchoninic acid
Bcl	B-cell lymphoma
BID	BH3 interacting-domain death agonist
BMDC	Bone marrow-derived cell
BSA	Bovine serum albumin

C

CAF	Carcinoma-activated fibroblast
CAM	Cell adhesion molecule
CD	Cluster of differentiation protein
CHAPS	3-[(3-Cholamidopropyl)dimethylammonio]-1-propanesulfonate
CL	Clearance
C_{max}	Maximum concentration
COX-2	Cyclooxygenase-2
CT	Computed tomography
CXCL	C-X-C chemokine ligand
CXCR	C-X-C chemokine receptor
Cy	Cyanine

D

D4-GDI	D4 GDP dissociation inhibitor
Da	Dalton
DAB	Diaminobenzidine
DAPI	4',6-Diamidino-2-phenylindole

DCE-MRI	Dynamic contrast enhanced magnetic resonance imaging
DIABLO	Direct inhibitor of apoptosis (IAP)-binding protein with low pi
DIEA	<i>N,N</i> -diisopropylethylamine
DISC	Death-inducing signaling complex
DLL	Delta-like ligand
DMEM	Dulbecco's modified eagle medium
DMF	Dimethyl formamide
DNA	Deoxyribonucleic acid
DNA-PKcs	DNA-dependent protein kinase catalytic subunit
DOX	Doxorubicin
DTT	Dithiothreitol
DVT	Deep vein thrombosis
DW	Distilled water
E	
EBM	Endothelial basal medium
ECGM	Endothelial cell growth medium
ECM	Extracellular matrix
EDC	<i>N</i> -(3-dimethylaminopropyl)- <i>N'</i> -ethylcarbodiimide
EDTA	Ethylenediaminetetraacetic acid
EEDQ	<i>N</i> -Ethoxycarbonyl-2-ethoxy-1,2-dihydroquinoline
EGF	Epidermal growth factor
EGFR	Epidermal growth factor receptor
EMC	ϵ -maleimidocaproylamide
EMCS	ϵ -maleimidocaproyl succinimide
EMT	Epithelial-mesenchymal transition
EndoG	Endonuclease G
EPC	Endothelial progenitor cells
EPR	Enhanced permeation and retention
ErbB	Erythroblastosis oncogene B
ESI-MS	Electrospray ionization mass spectrometry
EtSTC	Ethylamine sodium taurocholate
F	
FACS	Fluorescence-activated cell sorting
FADD	Fas-associated protein with death domain
FAM	Carboxyfluorescein
FasL	Fas ligand
FBS	Fetal bovine serum
FcRn	Neonatal Fc receptor
FDA	Food and drug administration
FGF	Fibroblast growth factor
FGFR	Fibroblast growth factor receptor

FITC	Fluorescein isothiocyanate
FLICA	Fluorescent-Labeled Inhibitors of Caspases
FMK	Fluoromethyl ketone
FR	Folate receptor
FXa	Factor Xa
G	
GBM	Glioblastoma multiforme
GCSF	Granulocyte colony-stimulating factor
Gd-DOTA	Gadolinium- tetraazacyclododecanetetraacetic acid
Glc	Glucosamine
GMB	γ -maleimidobutyric acid
gp60	60 kDa glycoprotein
GPNMB	Transmembrane glycoprotein NMB
H	
HB-EGF	Heparin-binding epidermal growth factor
HBSS	Hank's balanced salt solution
HDMEC	Human dermal microvascular endothelial cell
HE	Hematoxylin and eosin
HEPES	4-(2-hydroxyethyl)-1-piperazineethanesulfonic acid
HER	Human epidermal growth factor receptor
HGF	Hepatocyte growth factor
HIF	Hypoxia-inducible factor
HPLC	High performance liquid chromatography
HRMS	High resolution mass spectrometry
HRP	Horseradish peroxidase
HSA	Human serum albumin
HSGAG	Heparan sulfate glycosaminoglycan
HTRA2	High-temperature-requirement protein A2
HUVEC	Human umbilical vein endothelial cell
I	
IDH	Isocitrate dehydrogenase
IdoA	Iduronic acid
IgG	Immunoglobulin G
IL	Interleukin
IPTT	Induced-phenotype targeted therapy
ITGAV	Integrin α v
L	
LIF	Leukemia inhibitory factor
LMWH	Low-molecular-weight heparin
LRP1	Lipoprotein receptor-related protein 1
M	

mAb	Monoclonal antibody
MAC-1	Macrophage-1 antigen
MALDI-TOF MS	Matrix-assisted laser desorption/ionization time-of-flight mass spectrometry
MAPK	Mitogen-activated protein kinase
MDR	Multidrug resistance
MMAE	Monomethyl auristatin E
MMP	Matrix metalloproteinase
MRI	Magnetic resonance imaging
mRNA	Messenger ribonucleic acid
MT1-MMP	Membrane type 1 matrix metalloproteinase
mTOR	Mechanistic target of rapamycin
MTT	3-(4,5-Dimethylthiazol-2-yl)-2,5-diphenyltetrazolium bromide
N	
NG2	Neural/glial antigen 2
NHS	<i>N</i> -hydroxysuccinimide
NMR	Nuclear magnetic resonance
NPC	Nitrophenyl chloroformate
NPM	Nucleophosmin
NRP	Neuropilin
NSCLC	Non-small-cell lung cancer
O	
OAlI	Allyl ester
ODS	Octadecylsilane
OMI	Oocyte maturation inhibitor
OPLS	Optimized Potentials for Liquid Simulations
P	
PABC	<i>para</i> -aminobenzylcarbamate
PARP	Poly(ADP-ribose) polymerase
PBS	Phosphate buffered saline
PDB	Protein data bank
PDGF	Platelet-derived growth factor
PDGFR	Platelet-derived growth factor receptor
PE	Pulmonary embolism
PECAM	Platelet endothelial cell adhesion molecule
PEG	Polyethylene glycol
PFA	Paraformaldehyde
PGI	Prostaglandin I
PI3K	Phosphoinositide 3-kinase
PKC	Protein kinase C
PIGF	Placental growth factor

<i>p</i> NA	<i>para</i> -Nitroaniline
PRKCD	Protein kinase C δ
PS-SCL	Positional scanning synthetic combinatorial library
R	
RESPA	Reversible reference system propagator algorithm
RIATC	Radiation-induced apoptosis targeted chemotherapy
RIPA	Radioimmunoprecipitation assay
RNA	Ribonucleic acid
RNAi	RNA interference
RNS	Reactive nitrogen species
ROS	Reactive oxygen species
RTKI	Receptor tyrosine kinase inhibitors
RU	Response unit
S	
SCF	Stem cell factor
SDF	Stromal cell-derived factor
SDS-PAGE	Sodium dodecyl sulfate polyacrylamide gel electrophoresis
siRNA	Small interference RNA
SMA	Smooth muscle actin
SMAC	Second mitochondria-derived activator of caspase
SNRNP70	Small nuclear ribonucleoprotein 70kda (U1)
SPARC	Secreted protein acidic and rich in cysteine
SPR	Surface plasmon resonance
SREBP	Sterol regulatory element-binding proteins
STC	Sodium taurocholate
T	
$t_{1/2}$	Half-life
TEA	Triethylamine
TFA	Trifluoroacetic acid
TfR	Transferrin receptor
TIE	Tyrosine kinase with immunoglobulin-like and EGF-like domains
TIP3P	Transferable intermolecular potential 3P
TNF	Tumor necrosis factor
U	
UFH	Unfractionated heparin
uPA	Urokinase-type-plasminogen activator
UV	Ultraviolet
V	
VEGF	Vascular endothelial growth factor
VEGFR	Vascular endothelial growth factor receptor
VHBD	VEGF-heparin binding domain

VHL
VTE

von Hippel Lindau
Venous thromboembolism

Introduction

Since Paul Ehrlich proposed a concept of “magic bullet” more than a century ago, there was an enormous advance in the cancer therapeutics towards development of more selective anticancer agents¹. The early generation of anticancer agents was developed based on the practical knowledge that cancer cells proliferate at a higher rate than normal cells. These agents including alkylating agents, topoisomerase inhibitors, antimetabolites, and vinca alkaloids arrest cell division by inhibiting various pathways required for the DNA replication or cell mitosis, ultimately leading to cell death². Therefore, cells with higher proliferation rate are more prone to these cytotoxic agents, which is the fundamental basis for their tumor cell selectivity over normal cells in the therapeutic aspect¹.

Although cancer cells are more susceptible to the cytotoxic agents, normal cells are also affected since they too proliferate albeit in slower rate³. Moreover, the cytotoxic agents distribute to the cells in non-selective manner since their target molecules such as DNA or topoisomerases exist in similar quantity in both tumor and normal cells². Therefore, despite the potent anticancer effect, they also showed severe toxicities on the normal tissues and organs that were some times even lethal.

The increased understandings of the molecular biology involved in tumor progression have led to the idea of the molecular targeted therapy in aim to develop more selective anticancer agents with reduced risk of adverse effects⁴. Many new molecular targets were revealed that are specifically expressed or biologically significant only in tumor cells, those including several kinds of growth factors, signaling molecules, cell-cycle proteins, modulators of apoptosis, and pro-angiogenic factors⁵. The advances in biotechnology and combinatorial chemistry allowed the development of molecular targeted agents such as monoclonal antibodies and small molecule tyrosine kinase inhibitors (smTKIs) that could selectively block the downstream signaling pathways of their target molecules or deliver cytotoxic agents to the tumor cells expressing

the target molecules on their cell surface^{6,7}. Especially, antibody-drug conjugates (ADCs), which could deliver the cytotoxic agents selectively to the tumor cells, gained increasing interests after the recent clinical approval of two new agents, brentuximab vedotin and ado-trastuzumab emtansine⁷. As a result of the highly selective property of the molecular targeted agents to the target molecules, they showed favorable toxicity profile at the therapeutically effective doses.

However, the clinical outcomes of the molecular targeted agents were disappointing than have been expected, showing only limited improvements in the overall survival of the patients³. The inherent genomic instability and complexity of the tumor cells largely contribute to their resistance against the anticancer therapies⁸. Due to the high frequency of mutations, tumor cells easily adapt to the therapy and acquire an evasive pathway for their survival. Moreover, molecular and genomic heterogeneities of the tumor lead to only partial response to the targeted therapies, resulting in regrowth from the unaffected population of the tumor subclones. There are still a lot of endeavors to discover new molecular targets in a belief that there exists a critical cellular signaling pathway that is irreplaceable and specifically occurs only in tumor in order to overcome the many known issues shown in the modern molecular targeted therapies. However, when considering the genomic instability and the heterogeneity of the tumors, that effort seems to be not that much promising.

The major hurdles in using molecular targeted agents, such as limited therapeutic effect and easily acquired resistance, are ironically due to the highly selective property of those agents. As much as the narrowed target reduced the adverse effects in the normal tissues, it also limited the actions in the tumors, which has dynamic and complex nature. The well refined targeting capability towards the limited number of molecular targets of the targeted agents allow tumor cells to easily evade the therapy by acquiring alternative pathways. Also, regarding that many distinct subclones of tumor cells exist in a tumor mass, the highly selective property of the targeted therapy limit the number of therapeutically affected tumor cell subclones, thus leaving many tumor cells

unaffected. But according to the past experience, the selectivity of the anticancer agent between the normal tissue and the tumor tissue cannot be renounced to avoid any toxic adverse effects during therapy. Therefore, an ideal anticancer agent should selectively act to the tumor, but act in a non-selective manner among the distinct subclones of tumor cells or molecular targets that are associated with the given pathological condition. In other words, selective and non-selective natures should coexist, but in differential aspects, in the anticancer agents for effective and enduring cancer treatment.

This dissertation discusses about two different strategies that concern the coexistence of selectivity and non-selectivity in a single therapeutic agent. Part one demonstrates development of heparin-based anti-angiogenic agent LHT7 that inhibits multiple stages of pathological angiogenesis by blocking VEGF, FGF2, and PDGF-B at the same time, and stresses its mode of action. This shows the benefit of blocking broad range of pro-angiogenic factors associated in tumor angiogenesis than simply blocking single pro-angiogenic factor. Part two discusses about the development of doxorubicin prodrugs that employ two distinct targeted delivery strategies for an effective delivery of chemotherapeutics to the tumor. Basically, these prodrugs involve traditional targeted delivery system and induced-phenotype targeted prodrug system, allowing the doxorubicin to be selectively delivered to the tumor tissue regardless of the genomic profiles of the tumor cells, followed by non-selective distribution of the active compound to the tumor cells.

References

- 1 Strebhardt, K. & Ullrich, A. Paul Ehrlich's magic bullet concept: 100 years of progress. *Nat Rev Cancer* **8**, 473-480 (2008).
- 2 Gerber, D. E. Targeted therapies: a new generation of cancer treatments. *Am Fam Physician* **77**, 311-319 (2008).
- 3 Holohan, C., Van Schaeybroeck, S., Longley, D. B. & Johnston, P. G. Cancer drug resistance: an evolving paradigm. *Nat Rev Cancer* **13**, 714-726 (2013).
- 4 Schrama, D., Reisfeld, R. A. & Becker, J. C. Antibody targeted drugs as cancer therapeutics. *Nat Rev Drug Discov* **5**, 147-159 (2006).

- 5 Hanahan, D. & Weinberg, R. A. The hallmarks of cancer. *Cell* **100**, 57-70 (2000).
- 6 Imai, K. & Takaoka, A. Comparing antibody and small-molecule therapies for cancer. *Nat Rev Cancer* **6**, 714-727 (2006).
- 7 Hughes, B. Antibody-drug conjugates for cancer: poised to deliver? *Nat Rev Drug Discov* **9**, 665-667 (2010).
- 8 Burrell, R. A., McGranahan, N., Bartek, J. & Swanton, C. The causes and consequences of genetic heterogeneity in cancer evolution. *Nature* **501**, 338-345 (2013).

Part I

**Study of mode of action and multiple pathway
inhibitory capability in tumor angiogenesis of
heparin-based agent LHT7**

Chapter 1

General Introduction

1.1. Tumor angiogenesis

Tumor angiogenesis refers to a new blood vessel formation within tumor, which plays a critical role in mass growth and metastasis of tumor¹. Since the diffusion limit of the oxygen and nutrients from the blood vessel is ranged within 100-200 μm , tumors demand their own blood vessels for the survival and to grow beyond certain size¹. The observations of angiogenesis in the tumor were reported decades ago, which led to an establishment of hypothesis that the tumors may express some driving forces that could recruit blood vessels around themselves². Following studies suggested that tumor cells secrete diffusible substances that could stimulate angiogenesis rather than require direct contact to the nearby endothelium^{3,4}, which eventually guided to the discovery and isolation of several pro-angiogenic factors⁵. In the basis of extensive study about the critical role of angiogenesis in tumor progression combined with the identification of pro-angiogenic factors, Judah Folkman proposed a novel strategy for treatment of cancer through inhibition of angiogenesis by blocking the pro-angiogenic factors in 1971⁶.

1.1.1. Physiology of tumor angiogenesis

Large quantity of studies in angiogenesis have revealed a number of angiogenic factors that are secreted by tumor cells as well as stromal cells, endothelial cells, and blood cells, which indicated complex interplay of tumor and host stroma during the angiogenic process⁷. The past studies not only identified pro-angiogenic factors, but also discovered numbers of endogenous anti-angiogenic factors. In normal condition, the balance of pro-angiogenic and anti-angiogenic

factors tightly regulates physiological angiogenesis. However, in certain pathological condition, such as in malignancy or inflammation, the balance between the pro-angiogenic and anti-angiogenic factors is collapsed by the excessive production of pro-angiogenic factors. This phenomenon is termed as ‘angiogenic switch’, and leads to stimulation of angiogenesis¹. The normal blood vessels are developed in the well-balanced pro-angiogenic and anti-angiogenic signaling, which generates well-organized endothelial cell linings tightly surrounded by vascular smooth muscle cells and basement membranes in order to ensure their optimal function. In contrast, due to the highly leaned balance toward the pro-angiogenic signaling during tumor progression, tumor vasculatures have irregular and disorganized structure with tortuous and dilated vessels. In addition, the endothelial cell that constitutes the vessel wall does not form homogenous layer, and the vessels lack functional mural cells, which plays role in stabilization of the vasculatures⁸.

Multiple steps are involved in the angiogenesis⁹. The sprouting from pre-existing vessels to the avascular region of the tissue requires the opening of the vessels and degradation of the surrounding extracellular matrix (ECM), which allows infiltration of the endothelial cells. Hypoxic conditions in the microenvironment induce endothelial cells to express hypoxia-inducible factor-1 α (HIF-1 α), leading to expression of vascular endothelial growth factor A (VEGF-A) and vascular endothelial growth factor receptor 2 (VEGFR2)¹⁰. VEGF-A is the most predominant pro-angiogenic factor that guides endothelial cells into the avascular regions, mainly through the interaction with the VEGFR2 expressed on the surface of endothelial cells¹¹. The concentration gradient of VEGF-A induces formation of ‘tip cells’, which could proteolytically degrade the basement membrane and guide the direction of sprouting, and stimulates the proliferation of trailing stalk cells for the successful endothelial sprout formations¹². During the sprouting, the tip cells secrete membrane type 1-matrix metalloproteinase (MT1-MMP), which degrades and opens the surrounding ECM. The MT1-MMP is downregulated in the late stage of angiogenesis when the stalks cells contact with the recruited

mural cells¹³. The tip cells also express delta-like ligand 4 (DLL4), which binds to Notch 1 and Notch 4 expressed on the adjacent stalk cells when exposed to VEGF-A. The DLL4-Notch signaling restricts the angiogenic potential of the nearby stalk cells by downregulating the VEGFR2 expression; hence prevent the participation of the nearby cells in developing sprout and promote orderly development of the new vessels¹⁴.

The maturation and stabilization of the nascent vessels involve mural cells. When the primitive vascular network is established, the endothelial cells secrete platelet-derived growth factor B (PDGF-B): this promotes migration, recruitment, and proliferation of mural cells such as pericytes and vascular smooth muscle cells¹⁵. The secreted PDGF-B binds to the heparan sulfate proteoglycans that present in the ECM surrounding the endothelium through the carboxyl-terminal retention motif, generating a concentration gradient that acts as a guidance cue for the migration of the mural cells¹⁵. Recent studies suggested that sonic hedgehog (Shh) is involved in the PDGF-B-mediated migration of mural cells by inducing ERK1/2 and Akt phosphorylation¹⁶. In addition, SDF-1 α is also reported to regulate PDGF-B-mediated-differentiation of bone-marrow derived pericytes¹⁷. These mural cells are essential for nascent vessels to be matured into functional blood vessels¹⁸. The recruited mural cells express angiopoietin 1 (Ang1) on their surface that interacts with the tyrosine kinase with immunoglobulin-like and EGF-like domains 2 (TIE2) on the endothelial cells, which the downstream signalings contribute to the stabilization of the blood vessels¹⁹. The Ang1/TIE2 signal also stimulates the expression of heparin-binding EGF-like growth factor (HB-EGF) by endothelial cells, which facilitates the migration of mural cells via the epidermal growth factor receptors (EGFRs)²⁰. Recent studies suggested that PDGF-C and PDGF-D could also facilitate the coverage of the nascent vessels by mural cells^{21,22}. FGF2 was also demonstrated to stimulate the migration and proliferation of pericytes, and increased the pericyte coverage²³. When the fully functional blood vessels are developed in the tumor, VEGF level decreases as the local concentration of oxygen increases, thereby terminating the angiogenesis²⁴.

Generally, hypoxic microenvironment stimulates the activation of angiogenesis through expression of hypoxia-inducible factors (HIFs)²⁵. In tumor, however, other pathways can aberrantly upregulate the expression of HIF-1 α under normoxic conditions, which is known as hypoxic mimicry²⁶. Mutations in the tumor suppressor gene von Hippel Lindau (*VHL*) enhance the activity of HIF-1 α by preventing its polyubiquitylation and proteasomal degradation²⁷. Moreover, mutations in several oncogenes that results in the activation of mitogen-activated protein kinase (MAPK), phosphoinositide 3-kinase (PI3K) or protein kinase C (PKC) pathways can also increase the activation or the synthesis of HIF-1 α ²⁸. Other factors including reactive oxygen species (ROS) and reactive nitrogen species (RNS), loss of a tumor suppressor gene function, or the expression of viral oncogenes can also induce the upregulation of HIF-1 α ²⁶. As a result of these environmental cues, VEGF-A expression is upregulated in tumors²⁹. VEGF-A secreted from tumors functions not only as a paracrine mediator for stimulating angiogenesis via endothelial cells, but also as an autocrine signal directly to the tumor cells: it promotes the survival, proliferation, and invasiveness of tumor cells independent of angiogenesis³⁰⁻³². It is recognized that in addition to VEGFRs, neuropilins (NRPs) play central role as crucial effectors in the autocrine VEGF signaling in tumors. Recent finding also suggested that VEGF-A contributes to the epithelial-mesenchymal transition (EMT) and the cancer stemness of the tumor cells, which could initiate tumor propagation and metastatic spread from the primary tumor^{33,34}.

1.1.2. Angiogenesis inhibition

Over the past decades, intensive efforts have been undertaken to develop angiogenesis inhibitors for use in the clinical oncology. Among many pro-angiogenic factors identified so far, VEGF has been considered as the most attractive target molecule for its critical role in angiogenesis³⁵. The pioneer of the clinical proof-of-concept as an angiogenesis inhibitor as well as the first VEGF inhibitor to be approved for the clinical use is the humanized monoclonal VEGF antibody, bevacizumab (Avastin[®], Genentech/Roche). Since the FDA

approval in 2004 for treatment of metastatic colorectal cancer, bevacizumab was further approved for the clinical use in treating patients with recurrent or metastatic non-squamous non-small-cell lung cancer (NSCLC), metastatic human epidermal growth factor receptor 2 (HER2, also known as ErbB2)-negative breast cancer (the approval has been withdrawn in 2011), glioblastoma, metastatic renal cell carcinoma, and most recently approved for recurrent or late-stage (metastatic) cervical cancer (FDA approval in August 2014) with combination of chemotherapy³⁶. Additional compounds targeting VEGF signaling axis including VEGF aptamer (Pegaptanib, Macugen[®], Eyetech/Pfizer), VEGF trap (VEGFR fusion protein; Aflibercept, Eylea[®], Regeneron/Bayer), humanized monoclonal VEGFR2 antibody (Ramucirumab, Cyramza[®], ImClone/Eli Lilly), and receptor tyrosine kinase inhibitors (RTKIs) that target VEGFR, such as sorafenib (Nexavar[®], Bayer) and sunitinib (Sutent[®], Pfizer), were developed and clinically approved to treat various types of cancers as well as other pathological conditions related to angiogenesis³⁷.

The VEGF inhibitors arrest proliferation of the endothelial cells and suppress mobilization of the endothelial progenitor cells (EPCs) from the bone marrow, thus prevent growth of the blood vessels in tumor. They could also regress the immature blood vessels, which are predominant in tumor vasculatures, since the immature vessels are susceptible to depletion of VEGF signaling required for their maintenance. Moreover, although yet controversial, VEGF inhibitors are suggested to improve delivery of chemotherapeutic agents to the tumor by normalizing the disorganized and abnormal architecture of tumor vasculatures, which improves chaotic blood flow, reduces vascular permeability and interstitial fluid pressure³⁸.

Angiogenesis inhibitors that target cells other than the endothelial cells are also investigated. Although not as tightly covered as the normal vessels, tumor vessels are also covered by mural cells³⁸. These mural cells are differentiated from the bone marrow-derived mural progenitor cells, which are recruited in the response to PDGF-B that is secreted by endothelial cells³⁹. The mural cells covering the endothelium promote the endothelial cell survival by producing

VEGF that acts in a juxtacrine manner, and by inducing anti-apoptotic protein Bcl-w in the endothelial cells^{40,41}. Therefore, the survival of the endothelium covered with mural cells is independent of the external VEGF. For this reason, depletion of VEGF does not affect the integrity of the blood vessels that are already covered and stabilized by the mural cells³⁶.

The overexpression of PDGF-B by tumor facilitates the stabilization of the blood vessels by mural cells, leading to an accelerated growth of the tumor⁴². Conversely, inhibition of PDGF-B signaling axis by using the PDGF receptor β (PDGFR β) inhibitor results in loss of mural cells on the endothelium and increased apoptosis of the endothelial cells. Such destabilization of the matured vessels transforms the tumor vessels to be more susceptible to the VEGF inhibitors. Indeed, previous study has demonstrated that simultaneous treatment of RTKIs that target VEGFRs and PDGFR β synergistically enhanced the angiogenesis inhibition even in the late-stage solid tumors, which are often resistant to the VEGF inhibitors³⁶. Blockade of stromal cell-derived factor 1 α (SDF-1 α ; also known as CXCL12 α)/C-X-C chemokine receptor type 4 (CXCR4) axis was also recently reported to downregulate PDGF-B, and inhibited the bone marrow-derived pericyte differentiation and tumor vascular expansion⁴³.

Carcinoma-activated fibroblasts (CAFs) are another kind of the stromal cells that are highlighted for their significant role in the progression of tumor. CAFs are reported to accelerate tumor growth, increase malignancy, and affect tumor angiogenesis. CAFs express PDGFR β , and in response to PDGF-B, they are recruited to the tumor and release several pro-angiogenic factors including VEGF and placental growth factor (PlGF)⁴². Stromal fibroblasts are also involved in angiogenesis as they recruit EPCs by releasing SDF-1 α . Inhibition of this chemokine was also effective in the tumor growth suppression⁴⁴.

1.1.3. Resistance to angiogenesis inhibitors

Angiogenesis inhibitors including bevacizumab, sunitinib, and sorafenib have proven their therapeutic benefits in many aggressive tumors. However, the angiogenesis inhibitors, particularly the inhibitors of VEGF pathway, failed to produce enduring clinical responses and showed only transient improvements in most patients^{45,46}. Clinical use of chemotherapeutic agents often suffers in the occurrence of multidrug resistance (MDR), which makes the efficacy of the agent significantly decrease. The MDR is fundamentally caused by the genetically unstable nature of tumor cells. Considering that the angiogenesis inhibitors target majorly endothelial cells, which is genetically stable unlike tumor cells, those were initially regarded to be an ideal therapeutic strategy having no resistant issues³⁷. Therefore, the occurrence of the acquired resistance against angiogenesis inhibitors was unexpected to many researchers and clinicians. Even though the mechanisms of resistance are not fully understood, several mechanisms have been suggested in many studies. Contrary to the traditional means of resistance against chemotherapeutic agents, which involves mutational alteration of the gene encoding a drug target or by alterations in drug uptake and efflux^{47,48}, the resistance against the angiogenesis inhibitors is largely indirect by variously acquiring evasive pathways during the therapeutic blockade of angiogenesis^{49,50}. The observations showed that the specific therapeutic target of the angiogenesis inhibitor still remained inhibited when the tumors acquired resistance, but the alternative pathways were activated to evade the therapy and sustain the tumor growth^{49,51,52}. There are at least four distinct adaptive mechanisms suggested in the evasive resistance to the anti-angiogenic therapies: first, upregulation of alternative pro-angiogenic signaling pathways in the tumor; second, recruitment of bone marrow-derived pro-angiogenic cells that could surmount the depletion of VEGF signaling; third, coverage of tumor vessels by mural cells, which improves the stability of the vessels and attenuate the demand for VEGF signaling for the survival of endothelial cells; and fourth,

facilitated invasion and metastasis of tumor cells to access to the distant normal vasculatures³⁶.

Upregulation of alternative pro-angiogenic factors during blockade of VEGF signaling pathway was demonstrated by several preclinical studies. When genetically engineered mice with pancreatic neuroendocrine cancer (*Rip1-Tag2* mice) were treated with a monoclonal antibody against VEGFR2 (DC101; now ramucirumab or Cyramza[®]), the tumor only showed transient response (10-14 days) followed by regrowth that was accompanied by restoration of the tumor vasculatures⁴⁹. The relapsing tumors had increased levels of the mRNAs of fibroblast growth factor 1 (FGF1), fibroblast growth factor 2 (FGF2), ephrin A1, ephrin A2, and Ang1. The upregulation of these mRNAs was closely associated with the hypoxia induced by the initial regression of vasculature by the DC101 treatment. When the animals were treated with the DC101 followed by the treatment of FGF trap (FGFR-Fc fusion protein), the revascularization and the tumor growth were significantly delayed. This indicated that FGF signaling induced the restoration of angiogenesis that occurred after blockade of the VEGF signaling. Other studies have also demonstrated upregulation of interleukin 8 (IL8) and PDGF-A in the refractory tumors that were initially treated with the anti-angiogenic therapy^{51,53}. The evasive resistance by upregulation of FGF2 was also shown in the clinical observations involving a study of glioblastoma patients being treated with VEGFR inhibitor (Cediranib, Recentin[®], Astra Zeneca)⁵⁴. During the treatment, plasma levels of FGF2 were elevated in the patients during the relapsing phase than in the response phase. Concurrent study showed that the tumor relapse of the glioma patients treated with the cediranib was accompanied by re-initiation of the tumor angiogenesis and loss of the vascular normalization revealed by vascular imaging, which could be highly related to the upregulated FGF2 level in the plasma. Other clinical studies have demonstrated transiently increased plasma levels of VEGF and PlGF in the patients treated with receptor tyrosine kinase inhibitors^{55,56}. The upregulation of the alternative pro-angiogenic factors induced by the host was also observed. The increased levels of the pro-angiogenic factors including

granulocyte colony-stimulating factor (G-CSF), SDF-1 α , stem cell factor (SCF; also known as c-kit ligand), and osteopontin were observed in the non-tumor bearing mice that received sunitinib, implicating a systemic endocrine response to inhibition of VEGF and PDGF signaling in the host tissue⁵⁷. Recent report demonstrated that the upregulation of SDF-1 α could induce the expression of PDGF-B in the VEGF inhibited Ewing's sarcoma. The secreted PDGF-B increased infiltration and differentiation of PDGFR β ⁺ bone marrow-derived cells (BMDCs) into desmin and NG2 expressing matured pericytes, thereby re-initiating the tumor growth¹⁷.

Hypoxia caused by the vessel regression by the anti-angiogenic therapy also stimulates the recruitment of BMDCs that are capable to elicit neovasculatures in the tumor tissues³⁶. The BMDCs consist of vascular progenitors and vascular modulatory cells. Endothelial and pericyte progenitor cells are the vascular progenitor cells, which eventually become the physical compositions of the blood vessels^{39,58}. TAMs (tumor-associated macrophages)⁵⁹, TIE2⁺ (also known as TEK⁺) monocytes⁶⁰, VEGFR1⁺ hemangiocytes⁶¹, and CD11b⁺ (also known as ITGAM⁺) myeloid cells⁶² play role as the vascular modulators by expressing various cytokines, growth factors, and proteases during angiogenesis⁶³. In the experimentally induced ischemic tissue, endothelial progenitor cells and other CXCR4⁺ BMDCs were recruited through increased HIF-1 α , SDF-1 α , and VEGF⁶⁴⁻⁶⁶. Recruitment of various bone marrow-derived CD45⁺ (also known as PTPRC⁺) myeloid cells, mature F4/80⁺ tumor-associated macrophages, as well as the endothelial and the pericyte progenitor cells mediated by HIF-1 α were also observed during neovascularization of glioblastoma multiforme (GBM), which is characterized as a highly hypoxic and necrotic tumor⁶³. Conversely, GBMs deficient in HIF-1 α had few BMDCs recruited, and the vascularization and the mass growth was severely impaired. These results collectively suggested that hypoxia induced by anti-angiogenic therapy recruited BMDCs that facilitated the revascularization of the tumor. Experimental study showed that vascular disrupting agent, which induces acute hypoxia and necrosis within tumor, triggered the accumulation of the endothelial progenitor cells that were

sufficient for the revascularization at the tumor margins⁶⁷. By contrast, untreated tumor showed no significant infiltration of the BMDCs, indicating that the recruitment of the BMDCs contributes to the adaptive response to the anti-angiogenic therapy.

Number of evidences have also suggested that the coverage of endothelial vessels by pericytes protected the vessels from the anti-angiogenic therapy⁶⁸. Several studies have reported that distinctive functional vessels that were tightly covered with pericytes remained after the substantial reduction of the tumor vasculatures by the VEGF inhibition⁶⁹⁻⁷¹. These vessels from the refractory tumors were distinguishable from the typical vessels in the untreated tumors, which are, by contrast, sporadically covered with less closely associated pericytes⁷². These reports collectively indicated that the pericyte coverage of the tumor blood vessels contribute to the resistance to anti-angiogenic therapy. Experimental study showed that the tumor vessels with inadequate pericyte coverage were more vulnerable to the depletion of VEGF signaling⁷³, and this was further elucidated by the fact that pericytes support the endothelial survival in juxtacrine manner by expressing appreciable amount of VEGF and other factors that are critical in survival of endothelial cells^{39,40}. Moreover, the pericytes attenuate the proliferation rate of the endothelial cells as a part of the vessel stabilization process, which reduces the necessity of the VEGF in the endothelial cells⁷⁴.

The increased invasiveness of the tumor cells has been suggested as another mechanism of the evasive resistance to the anti-angiogenic therapy. Preclinical studies in orthotopic GBM mouse model demonstrated an aggressive invasion of the malignant cells and the continuous growth of tumor, albeit more slowly, when angiogenesis was impeded by genetically deleting pro-angiogenic factors such as VEGF, HIF-1 α , and matrix metalloproteinase 9 (MMP-9). Similar result was shown when the angiogenesis was inhibited pharmacologically with the VEGFR tyrosine kinase inhibitor SU5416 (sunitinib). The glioblastoma cells invaded to the normal tissue and co-opt with the normal blood vessels, using those vessels as channels to penetrated deep into the brain. This perivascular

tumor invasion allowed the tumor cells to evade the vascular deficiency in a dispersed fashion⁷⁵. The pro-invasive adaptation of tumor was also observed in clinical studies in a subset of GBM patients who had developed multifocal recurrence of tumors during the course of bevacizumab treatment^{76,77}. The increased incidence of the metastasis during the anti-angiogenic therapy was also reported in several other tumors. The adaptive mechanisms for the increased tumor invasiveness by the anti-angiogenic therapy were suggested as the follows: firstly, tumors may increase the activity of the pre-existing invasion program in compensation to their loss of angiogenic capability; secondly, tumors might switch on an invasion program that is distinct to that occurs spontaneously during progression; thirdly, VEGF might have a potential role in restricting the tumor cell invasion, thus inhibition of VEGF signaling initiating the intrinsic invasiveness of tumor cells. In fact, a recent study revealed that the VEGF directly inhibit the tumor cell invasiveness by facilitating the protein tyrosine phosphatase 1B (PTP1B) to a MET/VEGFR2 heterocomplex, thereby suppressing the MET-dependent tumor cell migration. The VEGF blockade resulted in increased MET activity in GBM cells in a hypoxia-independent manner and induction of epithelial-mesenchymal transition (EMT)⁷⁸.

Although the transitory clinical outcome of the angiogenesis inhibitors might be construed disappointing, they still possess an important status in the modern cancer therapeutics and are becoming components of gold standard regimens. The growing evidence and knowledge about the mechanistic basis for adaptive evasive resistance provides affirmative opportunities for improving the anti-angiogenic therapy.

1.2. Heparin

Heparin is a naturally occurring highly sulfated glycosaminoglycan that is commonly used as an injectable anticoagulant agent for prevention and treatment of venous thromboembolism (VTE)⁷⁹. About a century ago, Jay McLean and William H. Howard at Johns Hopkins University found that an

extract of canine liver prolonged the plasma clotting time, and isolated an anticoagulant, which the substance was termed as 'heparin' (hepar or ήπαρ means liver in Greek)⁸⁰. Although the heparin was initially extract from the canine liver, pharmaceutical grade of heparin is currently obtained from mucosal tissues, such as porcine intestines or bovine lungs⁸¹. Since the discovery in 1916, heparin still remains one of the most important anticoagulant agents in clinical use⁸². Despite that heparin is only approved for anticoagulation in clinical use, large quantities of studies revealed its regulatory effects in diverse pathophysiological processes, thereby attracting researchers for its potential to be used in other pathological conditions⁸³.

1.2.1. Structural Characteristics of Heparin

Heparin is a linear polysaccharide consisting of alternative disaccharide units with molecular weight range of 5-40 kDa and average molecular weight of 15 kDa⁸⁴. The most common disaccharide unit within the heparin is composed of a 2-*O*-sulfated iduronic acid, and 6-*O*- and *N*-sulfated glucosamine (IdoA(2S)-GlcNS(6S)), which accounts for about 85% and 75% of the heparin composition extracted from bovine lung and porcine intestinal mucosa, respectively⁸⁵. Although IdoA(2S)-GlcNS(6S) unit is the major component, a number of structural variation in the disaccharide unit exists, contributing to the microheterogeneity of the heparin. Another important characteristic of the heparin is the strong anionic charge within the molecule. The IdoA(2S)-GlcNS(6S) disaccharide unit contains three sulfate groups, which provides significant amount of anionic charge to the heparin molecule. In fact, the disaccharide units that compose heparin have average 2.7 sulfate groups. Due to the high content of sulfate and carboxyl groups, heparin is recognized to have the highest anionic charge density among any of the known biological macromolecules, which attributes to its diverse biological activity by interacting with wide-array of endogenous proteins⁸⁴.

1.2.2. Anticoagulant Activity of Heparin

The most relevant activity of heparin is anticoagulation. The heparin shows its anticoagulant activity by binding to antithrombin III (ATIII), a serine protease inhibitor. When heparin is bound, the ATIII undergoes conformational change that initiates its enzymatic activity by the increased flexibility of the reactive center loop sequence⁸⁶. The activation of the ATIII leads to the inhibition of thrombin and other proteases that are crucially involved in blood coagulation cascade. The activation of ATIII through heparin binding increased the inactivation rate of the associated proteases up to 1000-fold⁸⁷. The ATIII binds to a specific pentasaccharide within the heparin polysaccharide, which is identified as GlcNAc/NS(6S)-GlcA-GlcNS(3S,6S)-IdoA(2S)-GlcNS(6S)^{88,89}. The inhibition of factor Xa only needs binding of ATIII to the heparin pentasaccharide unit. However, inactivation of thrombin requires additional binding of the thrombin to the heparin polysaccharide at the site near the pentasaccharide unit, which results in the formation of a ternary complex of ATIII, thrombin, and heparin. The activity of heparin against thrombin is dependent to the length of the heparin oligosaccharide, since the formation of the ternary complex requires at least 18 saccharide units^{90,91}. The different mode of actions in the inhibition of coagulation cascade of heparin depending in its chain length has led to the development of low-molecular-weight heparin (LMWH). The LMWH consists of low-molecular weight fragments of heparin with an average molecular weight of approximately 5,000 Da, and it is obtained by fractionation or by controlled enzymatic or chemical depolymerization of heparin by various methods⁸¹. Because of the relatively shorter oligosaccharide chain, LMWH preferably targets factor Xa than thrombin. The LMWH has more predictable anticoagulant response and longer plasma half-life than the unfractionated heparin (UFH), thereby produces improved therapeutic index with fewer side effects⁹²⁻⁹⁴. For this reason, LMWH is preferred over UFH in patients with VTE, such as pulmonary embolism (PE) and deep vein thrombosis (DVT)^{95,96}.

1.2.2. Heparin in Cancer

Although heparin has been clinically used as an anticoagulant agent, other potential functions in physiological or pathological conditions was reported in number of studies^{82,97}. Among many suggested biological roles of heparin, the regulatory effect in tumor progression was mainly focused. Especially, LMWH was preferably studied than UFH. In fact, the retrospective analysis of cancer patients who received LMWH demonstrated significantly improved survival as compared to UFH recipients^{98,99}, and according to the recent international guidelines, LMWH is the recommended regimen for the cancer patients^{100,101}. Many experimental studies showed that the heparin affected tumor progression by regulating various pathways besides coagulation cascade. It was demonstrated that heparin could induce cell apoptosis^{102,103}, inhibit cell proliferation^{104,105}, metastasis¹⁰⁶⁻¹⁰⁹, and angiogenesis¹¹⁰⁻¹¹², and also modulate immune systems⁸³. The diverse physiological roles of heparin are attributable to the polyanionic groups on the glycosaminoglycan chain, which allows the electrostatic interactions with broad range of endogenous proteins other than ATIII, including cytokines, chemokines, growth factors, and pro-angiogenic factors. Among these heparin-binding proteins, many proteins such as VEGF, FGF, PDGF, HB-EGF, heparanase, MMPs, selectins, and integrins are crucially involved in various stages of tumor progression⁸²⁻⁸⁴. The binding properties of heparin are determined by its saccharide sequence composition, sulfation pattern, charge distribution, overall anionic charge density, and the size of the oligosaccharide^{84,113}.

Among many regulatory roles in tumor progression, the effect of heparin in tumor angiogenesis has been an area of a great interest^{113,114}. Many experimental studies showed anti-angiogenic effect of heparin in both *in vitro* and *in vivo*, which eventually led to suppression of tumor growth in the animal models¹¹⁰⁻¹¹². Considering that the angiogenesis significantly contributes not only to the mass growth of tumor, but also to the metastasis, the anti-angiogenic activity of heparin possesses a great importance in the clinical oncology¹¹⁵.

Tumor cells release various pro-angiogenic factors, which many are heparin-binding proteins, during tumor progression to stimulate angiogenesis within tumor tissue for further growth^{116,117}. The secreted pro-angiogenic factors stimulate angiogenic responses via interactions with their receptors expressed on the endothelial cells. Interestingly, effective interaction between pro-angiogenic factors and their corresponding receptors requires preceded binding of the pro-angiogenic factors on the cell surface heparan sulfate glycosaminoglycans (HSGAGs), which are related substances of heparin.

The HSGAGs are expressed on the surface of every eukaryotic cells including tumor cells and their related cells, and are crucially involved in the tumor progression such as cellular transformation, mass growth, metastasis, and angiogenesis⁸³. Similar to heparin, the HSGAGs interact with broad range of extracellular signaling molecules including the pro-angiogenic factors and allow them to regulate the pathological processes. The HSGAGs prevents diffusion, proteolytic degradation, and inactivation of the bound pro-angiogenic factors in the microenvironment, thus storing and stabilizing those proteins before their action^{116,118-120}. In addition, the HSGAGs act as a cofactor and potentiate the interaction between the pro-angiogenic factors and their receptors, and enhance the downstream angiogenic signals¹²¹⁻¹²⁴. Therefore, it has been suggested that heparin modulate the angiogenesis by interfering the interaction between the pro-angiogenic factors and the HSGAGs by competitive binding, thereby disrupting the proper angiogenic signalings^{125,126}.

Heparin has shown differential regulatory effects in angiogenesis depending in their size¹¹⁴. Many reports have demonstrated that LMWH effectively inhibited angiogenesis, whereas UFH was significantly less effective or even stimulated the angiogenesis^{111,127-132}. In particular, the angiogenesis induced by VEGF or FGF2 was inhibited by the heparin oligosaccharides with less than 20 or 12 saccharide units *in vitro*, respectively^{104,111}. In fact, Soker et al. demonstrated that heparin fragments of 16-18 saccharide units inhibited the binding of VEGF-A to VEGFRs, while the fragments larger than 22 saccharide units enhanced the binding¹¹¹. Other studies have also showed the inhibitory

effects of the small fragment of heparin in VEGF and FGF2-mediated angiogenesis *in vivo*^{129,133}. However, recent study has demonstrated that heparin requires at least eight saccharide units for an efficient binding to VEGF¹³⁴, indicating that there exist a minimum threshold of the polysaccharide size for the heparin to express its regulatory roles.

1.3. Rationale of the research

In the modern cancer therapeutics, molecular targeted therapies gained the most interest by the increased understandings of the molecular basis of cancer progression. As a part of the molecular targeted therapy, a number of angiogenesis inhibitors, especially blocking VEGF signaling pathway, have been developed and approved for many types of tumor³⁵. However, regardless of the initial response, these agents failed to produce enduring clinical benefit in the cancer patients. Since the overexpression of alternative pro-angiogenic factors besides VEGF was found to be substantially responsible to the resistance against angiogenesis inhibitors, simultaneous blockade of the multiple angiogenic signaling pathways has been deemed necessary for effective and enduring inhibition of tumor angiogenesis³⁶.

Currently, the major classes constituting the molecular targeted agents including angiogenesis inhibitors are humanized monoclonal antibodies and small molecule tyrosine kinase inhibitors (smTKIs). The monoclonal antibodies are intrinsically specific to a target molecule and are difficult to be developed as multi-targeted agent. By contrast, smTKIs are relatively non-specific and targets several receptor kinases at the same time, therefore, generally regarded as multi-targeted agents¹³⁵. However, considering that single pro-angiogenic factor acts as a ligand for more than one receptor – for example, VEGF-A interacts with VEGFR1 and VEGFR2 – blocking multiple receptor kinases could only partly block the angiogenic signals from each pro-angiogenic factor. Therefore, blocking multiple pro-angiogenic factors instead of the receptors

could be more effective in practical means of inhibiting the multiple angiogenic signaling pathways³⁶.

Many pro-angiogenic factors including VEGF, FGF, PDGF, HB-EGF, heparanase, and MMPs are inherently heparin-binding proteins and their activities could be inhibited by heparin^{82,84}. Therefore, an appropriate modification of heparin that could retain its capability to interact with broad array of pro-angiogenic factors and eliminate its anticoagulant activity at the same time would produce an ideal multi-targeted angiogenesis inhibitor.

References

- 1 Carmeliet, P. & Jain, R. K. Angiogenesis in cancer and other diseases. *Nature* **407**, 249-257 (2000).
- 2 Goldmann, E. The Growth of Malignant Disease in Man and the Lower Animals, with special reference to the Vascular System. *Proc R Soc Med* **1**, 1-13 (1908).
- 3 Greenblatt, M. & Shubi, P. Tumor angiogenesis: transfilter diffusion studies in the hamster by the transparent chamber technique. *J Natl Cancer Inst* **41**, 111-124 (1968).
- 4 Ehrmann, R. L. & Knoth, M. Choriocarcinoma. Transfilter stimulation of vasoproliferation in the hamster cheek pouch. Studied by light and electron microscopy. *J Natl Cancer Inst* **41**, 1329-1341 (1968).
- 5 Folkman, J. & Klagsbrun, M. Angiogenic factors. *Science* **235**, 442-447 (1987).
- 6 Folkman, J., Merler, E., Abernathy, C. & Williams, G. Isolation of a tumor factor responsible for angiogenesis. *J Exp Med* **133**, 275-288 (1971).
- 7 Fukumura, D., Xavier, R., Sugiura, T., Chen, Y., Park, E. C., Lu, N., Selig, M., Nielsen, G., Taksir, T., Jain, R. K. & Seed, B. Tumor induction of VEGF promoter activity in stromal cells. *Cell* **94**, 715-725 (1998).
- 8 Jain, R. K. A new target for tumor therapy. *N Engl J Med* **360**, 2669-2671 (2009).
- 9 Carmeliet, P. Angiogenesis in health and disease. *Nat Med* **9**, 653-660 (2003).
- 10 Tang, N., Wang, L., Esko, J., Giordano, F. J., Huang, Y., Gerber, H. P., Ferrara, N. & Johnson, R. S. Loss of HIF-1alpha in endothelial cells disrupts a hypoxia-driven VEGF autocrine loop necessary for tumorigenesis. *Cancer Cell* **6**, 485-495 (2004).
- 11 Ferrara, N., Gerber, H. P. & LeCouter, J. The biology of VEGF and its receptors. *Nat Med* **9**, 669-676 (2003).
- 12 Gerhardt, H., Golding, M., Fruttiger, M., Ruhrberg, C., Lundkvist, A., Abramsson, A., Jeltsch, M., Mitchell, C., Alitalo, K., Shima, D. & Betsholtz, C. VEGF guides

- angiogenic sprouting utilizing endothelial tip cell filopodia. *J Cell Biol* **161**, 1163-1177 (2003).
- 13 Chung, A. S., Lee, J. & Ferrara, N. Targeting the tumour vasculature: insights from physiological angiogenesis. *Nat Rev Cancer* **10**, 505-514 (2010).
 - 14 Hellstrom, M., Phng, L. K., Hofmann, J. J., Wallgard, E., Coultas, L., Lindblom, P., Alva, J., Nilsson, A. K., Karlsson, L., Gaiano, N., Yoon, K., Rossant, J., Iruela-Arispe, M. L., Kalen, M., Gerhardt, H. & Betsholtz, C. Dll4 signalling through Notch1 regulates formation of tip cells during angiogenesis. *Nature* **445**, 776-780 (2007).
 - 15 Lindblom, P., Gerhardt, H., Liebner, S., Abramsson, A., Enge, M., Hellstrom, M., Backstrom, G., Fredriksson, S., Landegren, U., Nystrom, H. C., Bergstrom, G., Dejana, E., Ostman, A., Lindahl, P. & Betsholtz, C. Endothelial PDGF-B retention is required for proper investment of pericytes in the microvessel wall. *Genes Dev* **17**, 1835-1840 (2003).
 - 16 Yao, Q., Renault, M. A., Chapouly, C., Vandierdonck, S., Belloc, I., Jaspard-Vinassa, B., Daniel-Lamaziere, J. M., Laffargue, M., Merched, A., Desgranges, C. & Gadeau, A. P. Sonic hedgehog mediates a novel pathway of PDGF-BB-dependent vessel maturation. *Blood* **123**, 2429-2437 (2014).
 - 17 Hamdan, R., Zhou, Z. & Kleinerman, E. S. SDF-1alpha induces PDGF-B expression and the differentiation of bone marrow cells into pericytes. *Mol Cancer Res* **9**, 1462-1470 (2011).
 - 18 Hellstrom, M., Gerhardt, H., Kalen, M., Li, X., Eriksson, U., Wolburg, H. & Betsholtz, C. Lack of pericytes leads to endothelial hyperplasia and abnormal vascular morphogenesis. *J Cell Biol* **153**, 543-553 (2001).
 - 19 Hawighorst, T., Skobe, M., Streit, M., Hong, Y. K., Velasco, P., Brown, L. F., Riccardi, L., Lange-Asschenfeldt, B. & Detmar, M. Activation of the tie2 receptor by angiopoietin-1 enhances tumor vessel maturation and impairs squamous cell carcinoma growth. *Am J Pathol* **160**, 1381-1392 (2002).
 - 20 Iivanainen, E., Nelimarkka, L., Elenius, V., Heikkinen, S. M., Junttila, T. T., Sihombing, L., Sundvall, M., Maatta, J. A., Laine, V. J., Yla-Herttuala, S., Higashiyama, S., Alitalo, K. & Elenius, K. Angiopoietin-regulated recruitment of vascular smooth muscle cells by endothelial-derived heparin binding EGF-like growth factor. *FASEB J* **17**, 1609-1621 (2003).
 - 21 di Tomaso, E., London, N., Fuja, D., Logie, J., Tyrrell, J. A., Kamoun, W., Munn, L. L. & Jain, R. K. PDGF-C induces maturation of blood vessels in a model of glioblastoma and attenuates the response to anti-VEGF treatment. *PLoS One* **4**, e5123 (2009).
 - 22 Liu, J., Liao, S., Huang, Y., Samuel, R., Shi, T., Naxerova, K., Huang, P., Kamoun, W., Jain, R. K., Fukumura, D. & Xu, L. PDGF-D improves drug delivery and efficacy

- via vascular normalization, but promotes lymphatic metastasis by activating CXCR4 in breast cancer. *Clin Cancer Res* **17**, 3638-3648 (2011).
- 23 Ricard, N., Tu, L., Le Hirsch, M., Huertas, A., Phan, C., Thuillet, R., Sattler, C., Fadel, E., Seferian, A., Montani, D., Dorfmüller, P., Humbert, M. & Guignabert, C. Increased pericyte coverage mediated by endothelial-derived fibroblast growth factor-2 and interleukin-6 is a source of smooth muscle-like cells in pulmonary hypertension. *Circulation* **129**, 1586-1597 (2014).
 - 24 Darland, D. C. & D'Amore, P. A. Blood vessel maturation: vascular development comes of age. *J Clin Invest* **103**, 157-158 (1999).
 - 25 Dayan, F., Mazure, N. M., Brahimi-Horn, M. C. & Pouyssegur, J. A dialogue between the hypoxia-inducible factor and the tumor microenvironment. *Cancer Microenviron* **1**, 53-68 (2008).
 - 26 Semenza, G. L. Oxygen homeostasis. *Wiley Interdiscip Rev Syst Biol Med* **2**, 336-361 (2010).
 - 27 Pugh, C. W. & Ratcliffe, P. J. Regulation of angiogenesis by hypoxia: role of the HIF system. *Nat Med* **9**, 677-684 (2003).
 - 28 Liao, D. & Johnson, R. S. Hypoxia: a key regulator of angiogenesis in cancer. *Cancer Metastasis Rev* **26**, 281-290 (2007).
 - 29 Kerbel, R. S. Tumor angiogenesis. *N Engl J Med* **358**, 2039-2049 (2008).
 - 30 Mercurio, A. M., Bachelder, R. E., Bates, R. C. & Chung, J. Autocrine signaling in carcinoma: VEGF and the $\alpha 6 \beta 4$ integrin. *Semin Cancer Biol* **14**, 115-122 (2004).
 - 31 Lichtenberger, B. M., Tan, P. K., Niederleithner, H., Ferrara, N., Petzelbauer, P. & Sibilio, M. Autocrine VEGF signaling synergizes with EGFR in tumor cells to promote epithelial cancer development. *Cell* **140**, 268-279 (2010).
 - 32 Cao, Y., E, G., Wang, E., Pal, K., Dutta, S. K., Bar-Sagi, D. & Mukhopadhyay, D. VEGF exerts an angiogenesis-independent function in cancer cells to promote their malignant progression. *Cancer Res* **72**, 3912-3918 (2012).
 - 33 Beck, B., Driessens, G., Goossens, S., Youssef, K. K., Kuchnio, A., Caauwe, A., Sotiropoulou, P. A., Loges, S., Lapouge, G., Candi, A., Mascré, G., Drogat, B., Dekoninck, S., Haigh, J. J., Carmeliet, P. & Blanpain, C. A vascular niche and a VEGF-Nrp1 loop regulate the initiation and stemness of skin tumours. *Nature* **478**, 399-403 (2011).
 - 34 Fantozzi, A., Gruber, D. C., Pisarsky, L., Heck, C., Kunita, A., Yilmaz, M., Meyer-Schaller, N., Cornille, K., Hopfer, U., Bentires-Alj, M. & Christofori, G. VEGF-mediated angiogenesis links EMT-induced cancer stemness to tumor initiation. *Cancer Res* **74**, 1566-1575 (2014).

- 35 Ellis, L. M. & Hicklin, D. J. VEGF-targeted therapy: mechanisms of anti-tumour activity. *Nat Rev Cancer* **8**, 579-591 (2008).
- 36 Bergers, G. & Hanahan, D. Modes of resistance to anti-angiogenic therapy. *Nat Rev Cancer* **8**, 592-603 (2008).
- 37 Carmeliet, P. Angiogenesis in life, disease and medicine. *Nature* **438**, 932-936 (2005).
- 38 Jain, R. K. Normalization of tumor vasculature: an emerging concept in antiangiogenic therapy. *Science* **307**, 58-62 (2005).
- 39 Song, S., Ewald, A. J., Stallcup, W., Werb, Z. & Bergers, G. PDGFRbeta+ perivascular progenitor cells in tumours regulate pericyte differentiation and vascular survival. *Nat Cell Biol* **7**, 870-879 (2005).
- 40 Darland, D. C., Massingham, L. J., Smith, S. R., Piek, E., Saint-Geniez, M. & D'Amore, P. A. Pericyte production of cell-associated VEGF is differentiation-dependent and is associated with endothelial survival. *Dev Biol* **264**, 275-288 (2003).
- 41 Franco, M., Roswall, P., Cortez, E., Hanahan, D. & Pietras, K. Pericytes promote endothelial cell survival through induction of autocrine VEGF-A signaling and Bcl-w expression. *Blood* **118**, 2906-2917 (2011).
- 42 Ostman, A. PDGF receptors-mediators of autocrine tumor growth and regulators of tumor vasculature and stroma. *Cytokine Growth Factor Rev* **15**, 275-286 (2004).
- 43 Hamdan, R., Zhou, Z. & Kleinerman, E. S. Blocking SDF-1alpha/CXCR4 downregulates PDGF-B and inhibits bone marrow-derived pericyte differentiation and tumor vascular expansion in Ewing tumors. *Mol Cancer Ther* **13**, 483-491 (2014).
- 44 Orimo, A., Gupta, P. B., SgROI, D. C., Arenzana-Seisdedos, F., Delaunay, T., Naeem, R., Carey, V. J., Richardson, A. L. & Weinberg, R. A. Stromal fibroblasts present in invasive human breast carcinomas promote tumor growth and angiogenesis through elevated SDF-1/CXCL12 secretion. *Cell* **121**, 335-348 (2005).
- 45 Saltz, L. B., Lenz, H. J., Kindler, H. L., Hochster, H. S., Wadler, S., Hoff, P. M., Kemeny, N. E., Hollywood, E. M., Gonen, M., Quinones, M., Morse, M. & Chen, H. X. Randomized phase II trial of cetuximab, bevacizumab, and irinotecan compared with cetuximab and bevacizumab alone in irinotecan-refractory colorectal cancer: the BOND-2 study. *J Clin Oncol* **25**, 4557-4561 (2007).
- 46 Kindler, H. L., Niedzwiecki, D., Hollis, D., Sutherland, S., Schrag, D., Hurwitz, H., Innocenti, F., Mulcahy, M. F., O'Reilly, E., Wozniak, T. F., Picus, J., Bhargava, P., Mayer, R. J., Schilsky, R. L. & Goldberg, R. M. Gemcitabine plus bevacizumab compared with gemcitabine plus placebo in patients with advanced pancreatic

- cancer: phase III trial of the Cancer and Leukemia Group B (CALGB 80303). *J Clin Oncol* **28**, 3617-3622 (2010).
- 47 Gorre, M. E. & Sawyers, C. L. Molecular mechanisms of resistance to STI571 in chronic myeloid leukemia. *Curr Opin Hematol* **9**, 303-307 (2002).
- 48 O'Connor, R., Clynes, M., Dowling, P., O'Donovan, N. & O'Driscoll, L. Drug resistance in cancer - searching for mechanisms, markers and therapeutic agents. *Expert Opin Drug Metab Toxicol* **3**, 805-817 (2007).
- 49 Casanovas, O., Hicklin, D. J., Bergers, G. & Hanahan, D. Drug resistance by evasion of antiangiogenic targeting of VEGF signaling in late-stage pancreatic islet tumors. *Cancer Cell* **8**, 299-309 (2005).
- 50 Shojaei, F., Wu, X., Malik, A. K., Zhong, C., Baldwin, M. E., Schanz, S., Fuh, G., Gerber, H. P. & Ferrara, N. Tumor refractoriness to anti-VEGF treatment is mediated by CD11b+Gr1+ myeloid cells. *Nat Biotechnol* **25**, 911-920 (2007).
- 51 Fernando, N. T., Koch, M., Rothrock, C., Gollogly, L. K., D'Amore, P. A., Ryeom, S. & Yoon, S. S. Tumor escape from endogenous, extracellular matrix-associated angiogenesis inhibitors by up-regulation of multiple proangiogenic factors. *Clin Cancer Res* **14**, 1529-1539 (2008).
- 52 Kadenhe-Chiweshe, A., Papa, J., McCrudden, K. W., Frischer, J., Bae, J. O., Huang, J., Fisher, J., Lefkowitz, J. H., Feirt, N., Rudge, J., Holash, J., Yancopoulos, G. D., Kandel, J. J. & Yamashiro, D. J. Sustained VEGF blockade results in microenvironmental sequestration of VEGF by tumors and persistent VEGF receptor-2 activation. *Mol Cancer Res* **6**, 1-9 (2008).
- 53 Mizukami, Y., Jo, W. S., Duerr, E. M., Gala, M., Li, J., Zhang, X., Zimmer, M. A., Iliopoulos, O., Zukerberg, L. R., Kohgo, Y., Lynch, M. P., Rueda, B. R. & Chung, D. C. Induction of interleukin-8 preserves the angiogenic response in HIF-1alpha-deficient colon cancer cells. *Nat Med* **11**, 992-997 (2005).
- 54 Batchelor, T. T., Sorensen, A. G., di Tomaso, E., Zhang, W. T., Duda, D. G., Cohen, K. S., Kozak, K. R., Cahill, D. P., Chen, P. J., Zhu, M., Ancukiewicz, M., Mrugala, M. M., Plotkin, S., Drappatz, J., Louis, D. N., Ivy, P., Scadden, D. T., Benner, T., Loeffler, J. S., Wen, P. Y. & Jain, R. K. AZD2171, a pan-VEGF receptor tyrosine kinase inhibitor, normalizes tumor vasculature and alleviates edema in glioblastoma patients. *Cancer Cell* **11**, 83-95 (2007).
- 55 Bocci, G., Man, S., Green, S. K., Francia, G., Ebos, J. M., du Manoir, J. M., Weinerman, A., Emmenegger, U., Ma, L., Thorpe, P., Davidoff, A., Huber, J., Hicklin, D. J. & Kerbel, R. S. Increased plasma vascular endothelial growth factor (VEGF) as a surrogate marker for optimal therapeutic dosing of VEGF receptor-2 monoclonal antibodies. *Cancer Res* **64**, 6616-6625 (2004).

- 56 Motzer, R. J., Michaelson, M. D., Redman, B. G., Hudes, G. R., Wilding, G., Figlin, R. A., Ginsberg, M. S., Kim, S. T., Baum, C. M., DePrimo, S. E., Li, J. Z., Bello, C. L., Theuer, C. P., George, D. J. & Rini, B. I. Activity of SU11248, a multitargeted inhibitor of vascular endothelial growth factor receptor and platelet-derived growth factor receptor, in patients with metastatic renal cell carcinoma. *J Clin Oncol* **24**, 16-24 (2006).
- 57 Ebos, J. M., Lee, C. R., Christensen, J. G., Mutsaers, A. J. & Kerbel, R. S. Multiple circulating proangiogenic factors induced by sunitinib malate are tumor-independent and correlate with antitumor efficacy. *Proc Natl Acad Sci U S A* **104**, 17069-17074 (2007).
- 58 Asahara, T., Murohara, T., Sullivan, A., Silver, M., van der Zee, R., Li, T., Witzenbichler, B., Schatteman, G. & Isner, J. M. Isolation of putative progenitor endothelial cells for angiogenesis. *Science* **275**, 964-967 (1997).
- 59 Pollard, J. W. Tumour-educated macrophages promote tumour progression and metastasis. *Nat Rev Cancer* **4**, 71-78 (2004).
- 60 De Palma, M., Venneri, M. A., Galli, R., Sergi Sergi, L., Politi, L. S., Sampaolesi, M. & Naldini, L. Tie2 identifies a hematopoietic lineage of proangiogenic monocytes required for tumor vessel formation and a mesenchymal population of pericyte progenitors. *Cancer Cell* **8**, 211-226 (2005).
- 61 Kaplan, R. N., Riba, R. D., Zacharoulis, S., Bramley, A. H., Vincent, L., Costa, C., MacDonald, D. D., Jin, D. K., Shido, K., Kerns, S. A., Zhu, Z., Hicklin, D., Wu, Y., Port, J. L., Altorki, N., Port, E. R., Ruggero, D., Shmelkov, S. V., Jensen, K. K., Rafii, S. & Lyden, D. VEGFR1-positive haematopoietic bone marrow progenitors initiate the pre-metastatic niche. *Nature* **438**, 820-827 (2005).
- 62 Yang, L., DeBusk, L. M., Fukuda, K., Fingleton, B., Green-Jarvis, B., Shyr, Y., Matrisian, L. M., Carbone, D. P. & Lin, P. C. Expansion of myeloid immune suppressor Gr⁺CD11b⁺ cells in tumor-bearing host directly promotes tumor angiogenesis. *Cancer Cell* **6**, 409-421 (2004).
- 63 Du, R., Lu, K. V., Petritsch, C., Liu, P., Ganss, R., Passegue, E., Song, H., Vandenberg, S., Johnson, R. S., Werb, Z. & Bergers, G. HIF1 α induces the recruitment of bone marrow-derived vascular modulatory cells to regulate tumor angiogenesis and invasion. *Cancer Cell* **13**, 206-220 (2008).
- 64 Ceradini, D. J., Kulkarni, A. R., Callaghan, M. J., Tepper, O. M., Bastidas, N., Kleinman, M. E., Capla, J. M., Galiano, R. D., Levine, J. P. & Gurtner, G. C. Progenitor cell trafficking is regulated by hypoxic gradients through HIF-1 induction of SDF-1. *Nat Med* **10**, 858-864 (2004).
- 65 De Falco, E., Porcelli, D., Torella, A. R., Straino, S., Iachininoto, M. G., Orlandi, A., Truffa, S., Biglioli, P., Napolitano, M., Capogrossi, M. C. & Pesce, M. SDF-1

- involvement in endothelial phenotype and ischemia-induced recruitment of bone marrow progenitor cells. *Blood* **104**, 3472-3482 (2004).
- 66 Petit, I., Jin, D. & Rafii, S. The SDF-1-CXCR4 signaling pathway: a molecular hub modulating neo-angiogenesis. *Trends Immunol* **28**, 299-307 (2007).
- 67 Shaked, Y., Ciarrocchi, A., Franco, M., Lee, C. R., Man, S., Cheung, A. M., Hicklin, D. J., Chaplin, D., Foster, F. S., Benezra, R. & Kerbel, R. S. Therapy-induced acute recruitment of circulating endothelial progenitor cells to tumors. *Science* **313**, 1785-1787 (2006).
- 68 Bergers, G. & Song, S. The role of pericytes in blood-vessel formation and maintenance. *Neuro Oncol* **7**, 452-464 (2005).
- 69 Tong, R. T., Boucher, Y., Kozin, S. V., Winkler, F., Hicklin, D. J. & Jain, R. K. Vascular normalization by vascular endothelial growth factor receptor 2 blockade induces a pressure gradient across the vasculature and improves drug penetration in tumors. *Cancer Res* **64**, 3731-3736 (2004).
- 70 Winkler, F., Kozin, S. V., Tong, R. T., Chae, S. S., Booth, M. F., Garkavtsev, I., Xu, L., Hicklin, D. J., Fukumura, D., di Tomaso, E., Munn, L. L. & Jain, R. K. Kinetics of vascular normalization by VEGFR2 blockade governs brain tumor response to radiation: role of oxygenation, angiopoietin-1, and matrix metalloproteinases. *Cancer Cell* **6**, 553-563 (2004).
- 71 Mancuso, M. R., Davis, R., Norberg, S. M., O'Brien, S., Sennino, B., Nakahara, T., Yao, V. J., Inai, T., Brooks, P., Freimark, B., Shalinsky, D. R., Hu-Lowe, D. D. & McDonald, D. M. Rapid vascular regrowth in tumors after reversal of VEGF inhibition. *J Clin Invest* **116**, 2610-2621 (2006).
- 72 Baluk, P., Hashizume, H. & McDonald, D. M. Cellular abnormalities of blood vessels as targets in cancer. *Curr Opin Genet Dev* **15**, 102-111 (2005).
- 73 Bergers, G., Song, S., Meyer-Morse, N., Bergsland, E. & Hanahan, D. Benefits of targeting both pericytes and endothelial cells in the tumor vasculature with kinase inhibitors. *J Clin Invest* **111**, 1287-1295 (2003).
- 74 Orlidge, A. & D'Amore, P. A. Inhibition of capillary endothelial cell growth by pericytes and smooth muscle cells. *J Cell Biol* **105**, 1455-1462 (1987).
- 75 Rubenstein, J. L., Kim, J., Ozawa, T., Zhang, M., Westphal, M., Deen, D. F. & Shuman, M. A. Anti-VEGF antibody treatment of glioblastoma prolongs survival but results in increased vascular cooption. *Neoplasia* **2**, 306-314 (2000).
- 76 Norden, A. D., Young, G. S., Setayesh, K., Muzikansky, A., Klufas, R., Ross, G. L., Ciampa, A. S., Ebbeling, L. G., Levy, B., Drappatz, J., Kesari, S. & Wen, P. Y. Bevacizumab for recurrent malignant gliomas: efficacy, toxicity, and patterns of recurrence. *Neurology* **70**, 779-787 (2008).

- 77 Narayana, A., Kelly, P., Golfinos, J., Parker, E., Johnson, G., Knopp, E., Zagzag, D., Fischer, I., Raza, S., Medabalmi, P., Eagan, P. & Gruber, M. L. Antiangiogenic therapy using bevacizumab in recurrent high-grade glioma: impact on local control and patient survival. *J Neurosurg* **110**, 173-180 (2009).
- 78 Lu, K. V., Chang, J. P., Parachoniak, C. A., Pandika, M. M., Aghi, M. K., Meyronet, D., Isachenko, N., Fouse, S. D., Phillips, J. J., Cheresch, D. A., Park, M. & Bergers, G. VEGF inhibits tumor cell invasion and mesenchymal transition through a MET/VEGFR2 complex. *Cancer Cell* **22**, 21-35 (2012).
- 79 Turchini, J. & Khau Van Kien, L. [Heparin and basophil granulations]. *Montp Med* **41-42**, 967-970 (1952).
- 80 Mc, L. J. The discovery of heparin. *Circulation* **19**, 75-78 (1959).
- 81 Linhardt, R. J. & Gunay, N. S. Production and chemical processing of low molecular weight heparins. *Semin Thromb Hemost* **25 Suppl 3**, 5-16 (1999).
- 82 Lever, R. & Page, C. P. Novel drug development opportunities for heparin. *Nat Rev Drug Discov* **1**, 140-148 (2002).
- 83 Sasisekharan, R., Shriver, Z., Venkataraman, G. & Narayanasami, U. Roles of heparan-sulphate glycosaminoglycans in cancer. *Nat Rev Cancer* **2**, 521-528 (2002).
- 84 Capila, I. & Linhardt, R. J. Heparin-protein interactions. *Angew Chem Int Ed Engl* **41**, 391-412 (2002).
- 85 Gatti, G., Casu, B. & Perlin, A. S. Conformations of the major residues in heparin. H-NMR spectroscopic studies. *Biochem Biophys Res Commun* **85**, 14-20 (1978).
- 86 Chuang, Y. J., Swanson, R., Raja, S. M. & Olson, S. T. Heparin enhances the specificity of antithrombin for thrombin and factor Xa independent of the reactive center loop sequence. Evidence for an exosite determinant of factor Xa specificity in heparin-activated antithrombin. *J Biol Chem* **276**, 14961-14971 (2001).
- 87 Bjork, I. & Lindahl, U. Mechanism of the anticoagulant action of heparin. *Mol Cell Biochem* **48**, 161-182 (1982).
- 88 Lindahl, U., Backstrom, G., Hook, M., Thunberg, L., Fransson, L. A. & Linker, A. Structure of the antithrombin-binding site in heparin. *Proc Natl Acad Sci U S A* **76**, 3198-3202 (1979).
- 89 Jin, L., Abrahams, J. P., Skinner, R., Petitou, M., Pike, R. N. & Carrell, R. W. The anticoagulant activation of antithrombin by heparin. *Proc Natl Acad Sci U S A* **94**, 14683-14688 (1997).
- 90 Petitou, M., Duchaussoy, P., Driguez, P. A., Herault, J. P., Lormeau, J. C. & Herbert, J. M. New synthetic heparin mimetics able to inhibit thrombin and factor Xa. *Bioorg Med Chem Lett* **9**, 1155-1160 (1999).

- 91 Petitou, M., Herault, J. P., Bernat, A., Driguez, P. A., Duchaussoy, P., Lormeau, J. C. & Herbert, J. M. Synthesis of thrombin-inhibiting heparin mimetics without side effects. *Nature* **398**, 417-422 (1999).
- 92 Bara, L., Billaud, E., Kher, A. & Samama, M. Increased anti-Xa bioavailability for a low molecular weight heparin (PK 10169) compared with unfractionated heparin. *Semin Thromb Hemost* **11**, 316-317 (1985).
- 93 Boneu, B., Caranobe, C., Cadroy, Y., Dol, F., Gabaig, A. M., Dupouy, D. & Sie, P. Pharmacokinetic studies of standard unfractionated heparin, and low molecular weight heparins in the rabbit. *Semin Thromb Hemost* **14**, 18-27 (1988).
- 94 Young, E., Prins, M., Levine, M. N. & Hirsh, J. Heparin binding to plasma proteins, an important mechanism for heparin resistance. *Thromb Haemost* **67**, 639-643 (1992).
- 95 Hull, R. D. Treatment of pulmonary embolism: The use of low-molecular-weight heparin in the inpatient and outpatient settings. *Thromb Haemost* **99**, 502-510 (2008).
- 96 Snow, V., Qaseem, A., Barry, P., Hornbake, E. R., Rodnick, J. E., Tobolic, T., Ireland, B., Segal, J. B., Bass, E. B., Weiss, K. B., Green, L., Owens, D. K., American College of, P. & American Academy of Family Physicians Panel on Deep Venous Thrombosis/Pulmonary, E. Management of venous thromboembolism: a clinical practice guideline from the American College of Physicians and the American Academy of Family Physicians. *Ann Intern Med* **146**, 204-210 (2007).
- 97 Mousa, S. A. & Petersen, L. J. Anti-cancer properties of low-molecular-weight heparin: preclinical evidence. *Thromb Haemost* **102**, 258-267 (2009).
- 98 Hull, R. D., Raskob, G. E., Pineo, G. F., Green, D., Trowbridge, A. A., Elliott, C. G., Lerner, R. G., Hall, J., Sparling, T., Brettell, H. R. & et al. Subcutaneous low-molecular-weight heparin compared with continuous intravenous heparin in the treatment of proximal-vein thrombosis. *N Engl J Med* **326**, 975-982 (1992).
- 99 Prandoni, P., Lensing, A. W., Buller, H. R., Carta, M., Cogo, A., Vigo, M., Casara, D., Ruol, A. & ten Cate, J. W. Comparison of subcutaneous low-molecular-weight heparin with intravenous standard heparin in proximal deep-vein thrombosis. *Lancet* **339**, 441-445 (1992).
- 100 Mandala, M., Falanga, A., Piccioli, A., Prandoni, P., Pogliani, E. M., Labianca, R., Barni, S. & working group, A. Venous thromboembolism and cancer: guidelines of the Italian Association of Medical Oncology (AIOM). *Crit Rev Oncol Hematol* **59**, 194-204 (2006).
- 101 Lyman, G. H., Khorana, A. A., Falanga, A., Clarke-Pearson, D., Flowers, C., Jahanzeb, M., Kakkar, A., Kuderer, N. M., Levine, M. N., Liebman, H., Mendelson, D., Raskob, G., Somerfield, M. R., Thodiyil, P., Trent, D., Francis, C. W. &

- American Society of Clinical, O. American Society of Clinical Oncology guideline: recommendations for venous thromboembolism prophylaxis and treatment in patients with cancer. *J Clin Oncol* **25**, 5490-5505 (2007).
- 102 Li, H. L., Ye, K. H., Zhang, H. W., Luo, Y. R., Ren, X. D., Xiong, A. H. & Situ, R. Effect of heparin on apoptosis in human nasopharyngeal carcinoma CNE2 cells. *Cell Res* **11**, 311-315 (2001).
- 103 Berry, D., Lynn, D. M., Sasisekharan, R. & Langer, R. Poly(beta-amino ester)s promote cellular uptake of heparin and cancer cell death. *Chem Biol* **11**, 487-498 (2004).
- 104 Jayson, G. C. & Gallagher, J. T. Heparin oligosaccharides: inhibitors of the biological activity of bFGF on Caco-2 cells. *Br J Cancer* **75**, 9-16 (1997).
- 105 Karti, S. S., Ovali, E., Ozgur, O., Yilmaz, M., Sonmez, M., Ratip, S. & Ozdemir, F. Induction of apoptosis and inhibition of growth of human hepatoma HepG2 cells by heparin. *Hepatogastroenterology* **50**, 1864-1866 (2003).
- 106 Saiki, I., Murata, J., Nakajima, M., Tokura, S. & Azuma, I. Inhibition by sulfated chitin derivatives of invasion through extracellular matrix and enzymatic degradation by metastatic melanoma cells. *Cancer Res* **50**, 3631-3637 (1990).
- 107 Vlodaysky, I., Mohsen, M., Lider, O., Svahn, C. M., Ekre, H. P., Vigoda, M., Ishai-Michaeli, R. & Peretz, T. Inhibition of tumor metastasis by heparanase inhibiting species of heparin. *Invasion Metastasis* **14**, 290-302 (1994).
- 108 Antachopoulos, C. T., Iliopoulos, D. C., Gagos, S., Agapitos, M. V., Karayannacos, P. E., Roboli, S. K. & Skalkas, G. D. In vitro effects of heparin on SW480 tumor cell-matrix interaction. *Anticancer Res* **15**, 1411-1416 (1995).
- 109 Bertozzi, C. R. & Kiessling, L. L. Chemical glycobiology. *Science* **291**, 2357-2364 (2001).
- 110 Folkman, J., Langer, R., Linhardt, R. J., Haudenschild, C. & Taylor, S. Angiogenesis inhibition and tumor regression caused by heparin or a heparin fragment in the presence of cortisone. *Science* **221**, 719-725 (1983).
- 111 Soker, S., Goldstau, D., Svahn, C. M., Vlodaysky, I., Levi, B. Z. & Neufeld, G. Variations in the size and sulfation of heparin modulate the effect of heparin on the binding of VEGF165 to its receptors. *Biochem Biophys Res Commun* **203**, 1339-1347 (1994).
- 112 Takahashi, H., Ebihara, S., Okazaki, T., Asada, M., Sasaki, H. & Yamaya, M. A comparison of the effects of unfractionated heparin, dalteparin and danaparoid on vascular endothelial growth factor-induced tumour angiogenesis and heparanase activity. *Br J Pharmacol* **146**, 333-343 (2005).

- 113 Smorenburg, S. M. & Van Noorden, C. J. The complex effects of heparins on cancer progression and metastasis in experimental studies. *Pharmacol Rev* **53**, 93-105 (2001).
- 114 Norrby, K. Low-molecular-weight heparins and angiogenesis. *APMIS* **114**, 79-102 (2006).
- 115 Ebos, J. M. & Kerbel, R. S. Antiangiogenic therapy: impact on invasion, disease progression, and metastasis. *Nat Rev Clin Oncol* **8**, 210-221 (2011).
- 116 Ruoslahti, E. & Yamaguchi, Y. Proteoglycans as modulators of growth factor activities. *Cell* **64**, 867-869 (1991).
- 117 Folkman, J. Angiogenesis in cancer, vascular, rheumatoid and other disease. *Nat Med* **1**, 27-31 (1995).
- 118 Colin, S., Jeanny, J. C., Mascarelli, F., Vienet, R., Al-Mahmood, S., Courtois, Y. & Labarre, J. In vivo involvement of heparan sulfate proteoglycan in the bioavailability, internalization, and catabolism of exogenous basic fibroblast growth factor. *Mol Pharmacol* **55**, 74-82 (1999).
- 119 Saksela, O., Moscatelli, D., Sommer, A. & Rifkin, D. B. Endothelial cell-derived heparan sulfate binds basic fibroblast growth factor and protects it from proteolytic degradation. *J Cell Biol* **107**, 743-751 (1988).
- 120 Rusnati, M. & Presta, M. Interaction of angiogenic basic fibroblast growth factor with endothelial cell heparan sulfate proteoglycans. Biological implications in neovascularization. *Int J Clin Lab Res* **26**, 15-23 (1996).
- 121 Spivak-Kroizman, T., Lemmon, M. A., Dikic, I., Ladbury, J. E., Pinchasi, D., Huang, J., Jaye, M., Crumley, G., Schlessinger, J. & Lax, I. Heparin-induced oligomerization of FGF molecules is responsible for FGF receptor dimerization, activation, and cell proliferation. *Cell* **79**, 1015-1024 (1994).
- 122 Mason, I. J. The ins and outs of fibroblast growth factors. *Cell* **78**, 547-552 (1994).
- 123 Tessler, S., Rockwell, P., Hicklin, D., Cohen, T., Levi, B. Z., Witte, L., Lemischka, I. R. & Neufeld, G. Heparin modulates the interaction of VEGF165 with soluble and cell associated flk-1 receptors. *J Biol Chem* **269**, 12456-12461 (1994).
- 124 Schlessinger, J., Lax, I. & Lemmon, M. Regulation of growth factor activation by proteoglycans: what is the role of the low affinity receptors? *Cell* **83**, 357-360 (1995).
- 125 Folkman, J., Klagsbrun, M., Sasse, J., Wadzinski, M., Ingber, D. & Vlodavsky, I. A heparin-binding angiogenic protein--basic fibroblast growth factor--is stored within basement membrane. *Am J Pathol* **130**, 393-400 (1988).
- 126 Vlodavsky, I., Ishai-Michaeli, R., Mohsen, M., Bar-Shavit, R., Catane, R., Ekre, H. P. & Svahn, C. M. Modulation of neovascularization and metastasis by species of heparin. *Adv Exp Med Biol* **313**, 317-327 (1992).

- 127 Norrby, K. & Sorbo, J. Heparin enhances angiogenesis by a systemic mode of action. *Int J Exp Pathol* **73**, 147-155 (1992).
- 128 Norrby, K. Heparin and angiogenesis: a low-molecular-weight fraction inhibits and a high-molecular-weight fraction stimulates angiogenesis systemically. *Haemostasis* **23 Suppl 1**, 141-149 (1993).
- 129 Norrby, K. & Ostergaard, P. Basic-fibroblast-growth-factor-mediated de novo angiogenesis is more effectively suppressed by low-molecular-weight than by high-molecular-weight heparin. *Int J Microcirc Clin Exp* **16**, 8-15 (1996).
- 130 Collen, A., Smorenburg, S. M., Peters, E., Lupu, F., Koolwijk, P., Van Noorden, C. & van Hinsbergh, V. W. Unfractionated and low molecular weight heparin affect fibrin structure and angiogenesis in vitro. *Cancer Res* **60**, 6196-6200 (2000).
- 131 Khorana, A. A., Sahni, A., Altland, O. D. & Francis, C. W. Heparin inhibition of endothelial cell proliferation and organization is dependent on molecular weight. *Arterioscler Thromb Vasc Biol* **23**, 2110-2115 (2003).
- 132 Marchetti, M., Vignoli, A., Russo, L., Balducci, D., Pagnoncelli, M., Barbui, T. & Falanga, A. Endothelial capillary tube formation and cell proliferation induced by tumor cells are affected by low molecular weight heparins and unfractionated heparin. *Thromb Res* **121**, 637-645 (2008).
- 133 Norrby, K. & Ostergaard, P. A 5.0-kD heparin fraction systemically suppresses VEGF165-mediated angiogenesis. *Int J Microcirc Clin Exp* **17**, 314-321 (1997).
- 134 Zhao, W., McCallum, S. A., Xiao, Z., Zhang, F. & Linhardt, R. J. Binding affinities of vascular endothelial growth factor (VEGF) for heparin-derived oligosaccharides. *Biosci Rep* **32**, 71-81 (2012).
- 135 Imai, K. & Takaoka, A. Comparing antibody and small-molecule therapies for cancer. *Nat Rev Cancer* **6**, 714-727 (2006).

Chapter 2

Potentialiation of anti-angiogenic activity of heparin by blocking the ATIII-interacting pentasaccharide unit and increasing net anionic charge

Heparin, a potent anticoagulant agent used for the prevention of venous thromboembolism, has been also recognized to inhibit angiogenesis in tumor. However, its clinical application for cancer therapy is limited due to the anticoagulant activity, which may cause the bleeding-associated adverse effects. The current study shows the structural correlation of LHT7, a heparin-based angiogenesis inhibitor, with enhanced anti-angiogenic activity and decreased anticoagulant activity when compared to LMWH. LHT7 is characterized as having average seven molecules of sodium taurocholates conjugated per one molecule of LMWH. The results showed that the sodium taurocholate conjugation distorted the proper binding of LMWH chain to ATIII, while improving the binding to VEGF. The differential effect of sodium taurocholate conjugation was attributable to its unique structure. The bulky and rigid sterane core of the sodium taurocholate hindered the proper interaction between the specific pentasaccharide unit of LMWH and ATIII. By contrast, the terminal sulfate group generated an additional interaction site on VEGF, thereby improving the binding property. The anti-angiogenic activity of LHT7 was further confirmed *in vivo* using three distinct tumor models that differ in their angiogenic potential. The decreased amount of tumor vasculature in tumor tissue after LHT7 administration was also visualized and quantified.

2.1. Introduction

Angiogenesis is a crucial step in tumor progression by which tumor grows and survives beyond the certain size; on the other hand, tumor that has inadequate blood supply turns necrotic or apoptotic¹. When tumor cells become hypoxic, they secrete pro-angiogenic factors to induce angiogenesis. Among the secreted pro-angiogenic factors, VEGF (now known as VEGF-A) is the key regulator in the initial robust angiogenic responses, affecting survival, migration, proliferation, and differentiation of endothelial cells². Therefore, it has been regarded as the most attractive therapeutic target in the inhibition of tumor angiogenesis, leading to development of several angiogenesis inhibitors that block VEGF signaling pathway. However, these angiogenesis inhibitors failed to produce enduring clinical responses by the occurrence of acquired resistance^{3,4}.

Several adaptive mechanisms of the acquired resistance to the angiogenesis inhibitors have been proposed⁵. Among those, the upregulation of alternative pro-angiogenic factors have been suggested as one of the predominant cause of the resistance. Indeed, overexpression of FGF1, FGF2, PDGF-A, PDGF-B, and other pro-angiogenic factors in refractory tumors after the pharmacological blockade of VEGF signaling pathway was observed in many pre-clinical and clinical studies⁶⁻⁸. In addition, the maturation of tumor vasculatures by pericytes were also suggested to be responsible to the resistance, in which the pericyte coverage protecting the blood vessel from the anti-angiogenic therapy⁹. The experimental studies showed that the tumor vessels with inadequate pericyte coverage were more vulnerable to the depletion of VEGF signaling^{10,11}, and this was further elucidated by the fact that the pericytes stabilize the endothelium in juxtacrine manner by expressing appreciable amount of VEGF and other proteins that are critical in the survival of endothelial cells^{12,13}. For this reason, blockade of multiple angiogenic pathways, especially that are involved in the initial angiogenic response as well as the late-stage of angiogenesis, has been suggested for effective and enduring angiogenesis inhibition⁵.

In this context, heparin is a promising lead compound for developing the broad-spectrum angiogenesis inhibitor. Although heparin is clinically approved for use as a potent anticoagulant agent, its other physiological functions mediated by the capability to regulate various endogenous proteins are demonstrated by a number of studies. The heparin-binding proteins include VEGF, FGF, PDGF, HB-EGF, heparanase, MMPs, and selectins, which are crucially involved in many stages of tumor progression¹⁴⁻¹⁶. However, direct clinical application of heparin in the cancer therapy is limited due to its potent anticoagulant activity and relatively insufficient anticancer activity. Therefore, many efforts have been made to develop heparin-based anticancer agents by various approaches including the use of non-anticoagulant fractions of heparin¹⁷, chemical modification of heparin^{18,19} or synthesizing heparin mimetic by oversulfation of oligosaccharides^{20,21}, which demonstrated applicable efficacy in preclinical models, especially focusing on the inhibition of metastasis and angiogenesis.

In our research group, a series of chemically modified heparin has been previously prepared by conjugating different bile acids including deoxycholic acid, lithocholic acid, and taurocholic acid on the carboxylic groups of heparin as heparin-based anticancer therapeutics; they have been demonstrated to have good anticancer effect *in vivo* with very low anticoagulant activity²²⁻²⁵. Among the prepared bile acid-heparin conjugates, LHT7, which was characterized as average seven molecules of sodium taurocholates conjugated on carboxylic groups of low-molecular weight heparin (LMWH), showed the most potent anticancer and anti-angiogenic activity with negligible anticoagulation activity. A preceded study demonstrated that LHT7 had relatively stronger binding affinity against VEGF when compared to the non-modified LMWH²⁶. The chromogenic factor Xa assay showed a gradual decrease in the anticoagulant activity as more sodium taurocholates were conjugated to LMWH, indicating that the conjugated sodium taurocholate could interfere with LMWH from properly interacting with antithrombin III (ATIII).

In order to provide an insight in designing heparin-based anticancer therapeutics, the structural correlation of the LHT7 to the ATIII and VEGF bindings, which are strongly correlated to the respective anticoagulant and anti-angiogenic activity of LMWH, was carried out. In particular, computerized simulated binding studies were performed to determine the binding configuration of LHT7 to ATIII and VEGF. The binding affinities against VEGF and also the anticoagulant activities of LHT7 and its structural analogs were further evaluated. The *in vivo* tumor growth inhibitory effect of LHT7 on various kinds of carcinomas depending on their degree of angiogenesis was evaluated. In addition, the biodistribution of LHT7 in a tumor xenografted animal model was assessed in both macroscopic and microscopic scale.

2.2. Materials and Methods

2.2.1. Cell lines

A549, HT-29, and MDA-MB-231 cells were obtained from the American Type Culture Collection (ATCC; Manassas, VA). AMC-HN9 cells (head and neck carcinoma) were kindly provided from Asan Medical Center, Korea. The cells were grown in high-glucose DMEM (Gibco, Carlsbad, CA) supplemented with 10% FBS (Gibco). The cells were maintained in a humidified 5% CO₂ atmosphere at 37°C.

2.2.2. Synthesis

LHT7 was synthesized by conjugating LMWH with sodium taurocholate as the follows: To conjugate LMWH with sodium taurocholate, 3-OH of the sodium taurocholate was first converted into primary amine group through several synthetic steps in purpose to react it with the carboxylic group of LMWH. Firstly, sodium taurocholate (500 mg, 0.93 mmol; Sigma-Aldrich, St. Louis, MO) was dissolved in anhydrous DMF (4.6 ml; Sigma-Aldrich) and cooled to 4°C. Then triethylamine (778 µl, 5.58 mmol; Sigma-Aldrich) and 4-NPC (937 mg, 4.65 mmol; Sigma-Aldrich) were added to the solution and reacted for an

hour at 4°C, and 6 hours at room temperature. When the reaction was completed, the solution was diluted with 10 ml of DW and extracted with ethyl acetate (10 ml × 3). The remaining aqueous layer was collected and lyophilized to obtain a yellowish powder of carbonate-taurocholate derivative (NPC-STC). The NPC-STC (500 mg, 0.71 mmol) was dissolved in anhydrous DMF (5 ml), 4-methylmorpholine (157 µl, 1.42 mmol; Sigma-Aldrich) was added to the solution, and stirred for an hour at 50°C. Then the solution was dropped slowly to the solution of excess amount of ethylenediamine (5 ml in 10 ml of anhydrous DMF; Sigma-Aldrich) and reacted for 16 hours at room temperature. When the reaction was completed, the solution was transferred to a 10 volume of acetone to precipitate the product. The precipitate was collect by filtration and dried *in vacuo* to obtain EtSTC as a yellowish powder.

The final product, LHT7, was prepared by conjugating LMWH with the synthesized EtSTC. LMWH (100 mg, 22 µmol; Fraxiparin[®], GlaxoSmithKline, Genval, Belgium) was dissolved in 10 ml of 20 mM acetate buffer (pH 4.5) and *N*-(3-dimethylaminopropyl)-*N'*-ethylcarbodiimide HCl (EDC; 56 mg, 294 µmol; Sigma-Aldrich) was added followed by the addition of *N*-hydroxysuccinimide (NHS; 34 mg, 294 µmol; Sigma-Aldrich) on ice bath, and stirred for 30 min. Then, EtSTC (166 mg, 245 µmol) was added, and the solution was reacted further overnight at room temperature. After reaction was completed, unreacted EDC, NHS, and EtSTC were removed by dialysis (molecular weight cutoff 2,000; dialysis membrane obtained from Spectrum Laboratories, Rancho Dominguez, CA) in DW. The solution in the enclosed membrane was collected and lyophilized to obtain white powder of LHT7.

Cholic acid conjugated LMWH was synthesized as follows: Cholic acid (500 mg, 1.22 mmol; Sigma-Aldrich) and *p*-toluenesulfonic acid monohydrate (4.7 mg, 24.7 µmol; Sigma-Aldrich) was dissolved in methanol (10 ml) and refluxed overnight. The solution concentrated to half of its initial volume and cooled to on ice bath for recrystallization. The solid was collected, washed with methanol, and dried *in vacuo* to obtain methylated cholic acid (MeCA) as yellow solid. The obtained MeCA (200 mg, 473 µmol) was dissolved in

dichloromethane (5 ml) and 4-methylmorpholine (65 μ l, 591 μ mol) was added. The solution was heated to 40°C, and then solution of 4-NPC (130 mg, 645 μ mol) in dichloromethane (5 ml) was added slowly and reacted for 3 hours. The solution was cooled to room temperature and extracted with DW (10 ml \times 3). The organic layer was collected, dried by addition of anhydrous MgSO₄ (Sigma-Aldrich), and filtered. The filtrate was evaporated in reduced pressure to remove all the solvents. Then, ethyl acetate (5 ml) was added to the residue and heated to 60°C until the residue was completely dissolved. The concentrated solution was added to 10 volume of n-hexane to form precipitate. The precipitate was collected by filtration and dried in reduced pressure to obtain NPC-MeCA as a yellow solid. Then, the obtained NPC-MeCA (200 mg, 341 μ mol) was dissolved in dichloromethane (5 ml), and 4-methylmorpholine (56 μ l, 509 μ mol) was added slowly and stirred for an hour. The NPC-MeCA solution was slowly added to a solution of ethylenediamine (1 ml) in dichloromethane (2 ml), and reacted for overnight at room temperature. When the reaction was completed, the solution was extracted with DW (10 ml \times 3) and the organic layer was collected, and evaporated to remove the solvent. The residue was redissolved in ethyl acetate (5 ml) and precipitated in 10 volume of n-hexane. The precipitate was collected, washed with n-hexane, and dried *in vacuo* to obtain Et-MeCA. The obtained Et-MeCA (150 mg, 295 μ mol) was dissolved in mixture of methanol (8 ml) and water (2 ml) containing NaOH (120 mg, 3 mmol), and refluxed for 2 hours. The solution was cooled to room temperature and acidified with equal volume of 1N HCl, and then extracted with ethyl acetate (100 ml \times 3). The organic layer was collected and evaporated. The residue was redissolved in methanol (5 ml) and precipitated in 10 volume of DW. The precipitate was collected by filtration and dried *in vacuo* to obtain EtCA.

LMWH (100 mg, 22 μ mol) was dissolved in formamide (5 ml; Sigma-Aldrich) at 70°C, and cooled on ice bath. EDC (103 mg, 588 μ mol) was added to the LMWH solution followed by addition of NHS (68 mg, 588 μ mol), and reacted for 30 min. To the solution of LMWH, EtCA (226 mg, 457 μ mol) in

anhydrous DMF (5 ml) was added, and reacted overnight at room temperature. After reaction was completed, the solution was concentrated under reduced pressure and precipitated in methanol. The precipitate was collected by filtration and washed three times with methanol, and dried. The obtained solid was dissolved in DW and further purified by dialysis (molecular weight cutoff 2,000) in DW. The solution in the enclosed membrane was collected and lyophilized to obtain white powder of cholic acid conjugated LMWH.

Taurine conjugated LMWH was synthesized as follows: LMWH (100 mg, 22 μmol) was dissolved in 10 ml of 20 mM acetate buffer (pH 4.5) and EDC (56 mg, 294 μmol) was added followed by the addition of NHS (34 mg, 294 μmol) on ice bath, and stirred for 30 min. Then, taurine (30 mg, 245 μmol) was added, and the solution was reacted further overnight at room temperature. After reaction was completed, unreacted EDC, NHS, and taurine were removed by dialysis (molecular weight cutoff 2,000) in DW. The solution in the enclosed membrane was collected and lyophilized to obtain white powder of taurine conjugated LMWH.

2.2.3. Characterization of the synthesized LMWH-derivatives

The synthesized products were subjected to $^1\text{H-NMR}$ (Avance III, Bruker, Billerica, MA) and elemental analysis (Flash1112, Thermo Fischer Scientific, Waltham, MA). The coupling ratio of the conjugated bile acids on the LHT7 and cholic acid conjugated LMWH was determined by using the quantitative detection method for bile acids, which will be detailed below²⁷. The anticoagulant activities of the synthesized products were determined using the chromogenic factor Xa assay (Coatest Heparin; Chromogenix, Milan, Italy) according to the manufacturer's instruction. The content of sulfate in the synthesized substances was also quantified according to the previous article²⁸. The detailed procedure is also described below.

The coupling ratio of the conjugated bile acids was determined as follows: The sample solution was prepared in DW at a concentration of 5 mg/ml. The standard solutions of EtSTC (or EtCA) and LMWH were prepared at a

concentration of 2.937, 3.566, 4.093, 4.539, 4.924 mg/ml and 7.0621, 6.4322, 5.9055, 5.4605, 5.0761 mg/ml, respectively, in DW. The final standard solution was prepared by combining the EtSTC (or EtCA) standard solution (100 μ l) and LMWH standard solution (100 μ l) in a same order described above. The final concentration of EtSTC (or EtCA) of each standard solution is 0.0734, 0.0892, 0.1023, 0.1135, and 0.1231 mg/ml. Then, 50 μ l of standard and sample solutions were transferred to microtubes and diluted to 280 μ l with DW, and placed on ice. Pre-chilled sulfuric acid (720 μ l) was transferred and incubated 5 min at 80°C. The solutions were then cooled in ice bath and the absorbance was measured at 420 nm. The concentration of the sample was calculated based on the standard curve. The conjugation ratio was calculated according to the following equation:

$$\text{Conjugation ratio} = \frac{[\text{BA concentration}] \times [\text{LMWH molecular weight}]}{(0.25 - [\text{BA concentration}]) \times [\text{BA molecular weight}]}$$

,where BA represents conjugated bile acid.

The sulfate content of the synthesized LMWH derivatives was determined as follows: When barium ion is in complex with rhodizonate ion, the complex shows color. However, when barium ion binds with inorganic sulfate to form BaSO₄ and dissociate from rhodizonate ion, the color disappears. The content of sulfate in glycosaminoglycans including heparin and heparin derivatives can be determined by measuring the intensity of the color from the barium-rhodizonate complex. Firstly, barium buffer was prepared from 2 M acetic acid (5 ml), 0.01 M BaCl₂ (1 ml) and 0.02 M NaHCO₃ (4 ml), which were adjusted to 150 ml with ethanol. Rhodizonate reagent was prepared by dissolving rhodizonate (5 mg) and L-ascorbic acid (100 mg) in 20 ml of DW, and adjusted to 100 ml with ethanol. The standard solution was prepared from 0.01 M sulfuric acid. The sample solution (1 ml, 10 nmol) and 0.1 M NaOH (20 μ l) were combined and lyophilized. The dried residues were pyrolyzed by heating for 10 sec, and then dissolved in 0.5 ml of DW. The prepared barium buffer (3 ml) and rhodizonate reagent (1.5 ml) were added, and the solution was agitated. The absorbance of the samples was read at 520 nm.

2.2.4. Surface plasmon resonance (SPR) analysis

Biacore T100 (GE Healthcare, Waukesha, WI) was used for the SPR analysis. The sample analytes, LMWH, LHT7, cholic acid conjugated LMWH, and taurine conjugated LMWH, were prepared at concentrations ranging from 50-1000 ng/ml in HBS-EP buffer (GE Healthcare), which the buffer was also used as a running buffer. Recombinant human VEGF₁₆₅ (Peprotech, Rocky Hill, NJ) was immobilized on a sensor chip CM5 (GE Healthcare) by using EDC/NHS amide coupling method, adjusting the level of immobilization to approach 2,000 RU. The flow rate of the overall analysis was 30 μ l/min, and 50 mM of NaOH was used for regeneration of the chip surface after each cycle of analysis. The experiments were done in triplicate at each concentration. Obtained data were globally fitted and calculated for kinetics by BIAevaluation software (GE healthcare).

2.2.5. Molecular dynamics

For molecular dynamics modeling, the coordinates of VEGF-heparin binding domain (VHBD) and heparin were obtained from the RCSB Protein Data Bank (PDB; www.pdb.org). The coordinates of VHBD were obtained from the NMR structure of amino acids 111-165 from VEGF (PDB code 2VGH). The coordinates of heparin were obtained from the crystal structure of a ternary FGF1-FGFR2-heparin complex (PDB code 1E0O). Sodium taurocholate grafts were added at every 6-carboxylic position of the coordinates of heparin in order to build the structure of LHT7. To generate the initial structures for VHBD-LMWH and VHBD-LHT7 complexes, heparin or LHT7 was positioned near Arg124, Lys140, Arg149 and Arg156. In the case of LHT7, some dihedral angles in the structure were adjusted to avoid atom clashes between VHBD and LHT7. The initial structures for VHBD-LMWH and VHBD-LHT7 complexes were oriented in the orthorhombic simulation boxes. The dimensions of the boxes were calculated by using 10 Å buffer distances between any atom and the simulation box boundary. Each system was solvated in a TIP3P water model²⁹.

Sodium and chloride ions were added to maintain physiological salinity (150 μM) and neutral total charge of the systems. All molecular dynamics simulations were performed using the Desmond program. The OPLS-2005 force field was used for simulations and the energy calculation for trajectories. RESPA time step scheduling was used as the simulation integrator with parameters of 2.0 fs, 2.0 fs and 6.0 fs for bonded forces, non-bonded near forces, and non-bonded far forces, respectively. The Nosé-Hoover thermostat and the Martyna-Tobias-Klein barostat were utilized for the NPT ensemble simulations. Long-range electrostatics was treated by the smooth particle-mesh-Ewald method. The SHAKE algorithm was used to constrain heavy atom-hydrogen bonds. Each system was relaxed before the production run. This relaxation process consisted of a series of minimization and short molecular dynamics simulations. After relaxation, each system was simulated for 50 ns at constant temperature (300 K) and pressure (1 bar). Trajectories were saved every 10 ps for analysis. When the intermolecular energy level had reached the minimum, the corresponding structure was commenced with the Truncated Newton Conjugate Gradient minimization algorithm using the derivative convergence criterion of 0.05 kJ/Å/mol.

2.2.6. Computer simulated molecular docking

To investigate the binding of LMWH and LHT7 on ATIII, the ATII-binding pentasaccharide coordinate was used since it is the critical part among entire heparin chain in the interaction with the heparin-binding site of ATIII. The docking of pentasaccharide was simulated using the AutoDock Lamarckian GA version 4.2³⁰. The coordinates of rigid receptor protein ATIII were obtained for the crystal structure of a dimeric form of intact antithrombin III (PDB code 2ANT)³¹. In the structure of ATIII, all hydrogens were added and Gasteiger charges were assigned³². ATIII has the heparin binding residues including Arg13, Arg47, Arg125, and Arg129³³. A grid, with regular cubes of 50 Å per side, was placed on the map to indicate the heparin-binding site (x.y.z = 2.12.105).

2.2.7. X-ray μ CT angiography

X-ray μ CT for the macroscopic analysis of tumor vasculature was carried out as described elsewhere^{34,35}. The animal models were established in a 6-7 weeks old male C3H/HeN mice (Orient Bio, Seongnam, Korea) by dorsal flank subcutaneous inoculation of 1×10^7 SCC7 cells per mouse and allowed to grow. When the tumor volume reached 50-100 mm³, the mice were randomized into three groups and received normal saline, LMWH (5 mg/kg), or LHT7 (5 mg/kg) via intravenous route every other day for 14 days. After the treatment, the mice received a 50 μ l intraperitoneal injection of heparin prior to sacrificing by CO₂ inhalation. The thoracic cavity was opened and an incision was made on the apex of the heart. A polyethylene tube (i.d. 0.58 mm; o.d. 0.96 mm) was cannulated through the left ventricle and secured in the ascending aorta using surgical suture. Nitroprusside (Sigma-Aldrich) in a normal saline solution (0.1 mM, 30 ml) was perfused at a rate of 0.7 ml/min in purpose to replace the blood and vasodilate. Microfil[®] (Flow Tech, Carver, MA), which is a radiopaque polymer solution, was prepared as instructed by the manufacturer. Then 15 ml of the Microfil[®] solution was perfused at a rate of 0.2 ml/min through the cannulated tube. Microfil[®] perfused into the vasculature was allowed to polymerize at room temperature for 2 h and the tumor was dissected, followed by immersion in 4% PFA. Dissected and fixed tumors were scanned and observed using Skyscan 1076 (Bruker, Kontich, Belgium) X-ray micro-computed tomography system at a voxel resolution of $18 \times 18 \times 18 \mu\text{m}$ with the following scanning parameters: 45 kV, 180 μA , 0.5 mm aluminum filter, 590 ms exposure time and 0.5° rotation step. The vessel volume was measured by generating 3D models of the tumor vasculature reconstructed from the acquired cross-section images by Mimics 13.1 software (Materialise, Leuven, Belgium). The vessel volume divided by the tissue volume was presented as the vessel volume fraction.

2.2.8. Tumor growth suppression

The xenograft animal models of A549, HT-29, and AMC-HN9 were established in 6-7 weeks old male BALB/cSlc-nu mice (Orient Bio) by dorsal flank subcutaneous inoculation of 1×10^7 cells per mouse and allowed to grow. When tumors reached the volume of 150 mm³ for A549, 300 mm³ for HT-29 and 50 mm³ for AMC-HN9 xenografts, mice were randomized into three groups (n = 9) and received one of the followings: normal saline as control; 1 or 5 mg/kg of LHT7 every other day. All experimental and surgical procedures were carried out according to the guidelines of the Institute of Laboratory Animal Resources, Seoul National University (IACUC no. SNU-070822-5).

2.2.9. Histological analysis

The xenograft animal models of A549, HT-29, and AMC-HN9 were prepared as described above. At day 16, tumors were isolated, and prepared as FFPE blocks. The specimens were sectioned in 4 µm thicknesses and immunostained with anti-human CD34 antibody (1:50; Dako, Carpinteria, CA) or anti-human αSMA antibody (1:50; Dako). HRP visualization system (Dako) in combination with DAB was used for detection of the primary antibody. The sections were then counterstained with Hematoxylin. Hematoxylin and Eosin (HE) stained sections were additionally prepared for the AMC-HN9 tumor specimens.

2.2.10. Ex vivo imaging of whole-body distribution

Cy7.5 (Amersham Biosciences, Piscataway, NJ) labeled LHT7 were intravenously administered to MDA-MB-231 xenografted 7-week-old female BALB/cSlc-nu mice (Orient Bio) in a dose of 5 mg/kg. Lateral images for tumors were acquired at 15 min, 1, 4, 8, 12, 18, 24, 36, and 48 h after injection using the eXplore Optix imaging system (GE Medical Systems, Milwaukee, WI). Laser power and count time settings on the instrument were adjusted to 8 µW and 0.3 per point, respectively. Excitation and emission spots were raster-scanned in 1 mm steps.

2.2.11. Immunofluorescence

For the microscopic analysis of the tumor vasculatures, mice received Cy7.5-LHT7 intravenously 6 h prior to heart perfusion with 4% PFA, followed by preparation of 10 μm sections from the tumors. Sections were incubated with rat anti-mouse CD31 antibody (1:20; BD Pharmingen, San Diego, CA) and FITC-conjugated secondary antibody (1:200; Jackson ImmunoResearch Laboratories, West Grove, PA), subsequently. The sections were washed with PBS, and the nuclei of cells were stained with DAPI (1:1000; Invitrogen, Carlsbad, CA). The photomicrographs were acquired under confocal laser scanning microscopy (LSM 510, Carl Zeiss, Thornwood, NY).

2.2.12. Platelet uptake study of fluorescent-labeled LHT7

Human blood was obtained from a healthy volunteer and the blood was stabilized with EDTA immediately after withdrawal. Platelets were prepared from the blood as described elsewhere³⁶. The Prepared platelets were washed twice and resuspended carefully in the glucose HEPES-Tryodes buffer (pH 6.5 during washing, pH 7.3 for resuspension) in the presence of prostacyclin (Sigma-Aldrich) at a final concentration of 10 ng/ml. Platelets (4×10^8 PLTs per ml) were incubated with varying concentrations of FITC-labeled LHT7. The flow cytometry analysis and the immunofluorescence microscopic observation were carried out after complete washing of platelets. For the microscopic observation, the platelets were fixed and permeabilized with 4% PFA (Sigma-Aldrich), followed by 0.1% Triton X-100 (Sigma-Aldrich). The α -granules of the platelets were immunostained with Alexa 647 labeled P-selectin mAb (Biolegend, San Diego, CA). The relative amount of the taken up LHT7 was measured by activating the platelets with 5 IU/ml of thrombin (Sigma-Aldrich) at 37°C. Fluorescence intensity was each measured in the supernatant and the platelet pellets.

2.2.13. Statistical analysis

Data were analyzed using unpaired one-way ANOVA followed by the Dunnett's multiple comparisons test. The GraphPad Prism version 5.01 (GraphPad Software, San Diego, CA) was used for the statistical calculations. *P* value less than 0.05 was considered statistically significant.

2.3. Results

2.3.1. Effects of the conjugated sodium taurocholate between the interaction of LMWH and ATIII determined by computerized docking simulation

Previous study have demonstrated that conjugation of sodium taurocholates on LMWH significantly reduced the anticoagulant activity, indicating attenuation of the interaction between LMWH and ATIII²⁶. The anticoagulant activities of the LMWH-taurocholate conjugates were inversely proportional to the number of the conjugated sodium taurocholate on LMWH, showing gradual decrease of the anticoagulant activity following the increased number of the conjugated sodium taurocholate. The anticoagulant activities were determined by the chromogenic factor Xa assay. This assay determines the anticoagulant activity by quantitatively measuring the amount of remaining factor Xa that did not form complex with ATIII in the presence of heparin³⁷. Considering that appropriate binding of heparin to the ATIII triggers the further complex formation with the factor Xa, the decreased anticoagulant activity as a result of sodium taurocholate conjugation implied that the conjugated sodium taurocholate hindered the proper interaction between the ATIII-binding pentasaccharide unit of LMWH and the heparin-binding site of ATIII.

For deeper understanding of such phenomenon, the binding between ATIII and LHT7 were observed through a computerized docking simulation study using AutoDock Lamarckian GA 4.2 software. Since the specific pentasaccharide unit within the heparin plays the predominant role in the interaction with ATIII, the pentasaccharide coordinate was used in the

simulation as a representative molecule of LMWH. Similarly, the same pentasaccharide coordinate that has two molecules of sodium taurocholate conjugated was used for the representative molecule of LHT7.

The simulation results showed that when LHT7 was docked on the designated area around the heparin-binding moiety of ATIII, which comprises Arg13, Arg47, Arg125, and Arg129³³, it did not preferentially bind to the heparin-binding moiety, but rather stabilized on the other location. By contrast, LMWH was properly stabilized on the heparin-binding moiety (**Fig. 2.1A**). The energy transitions that occurred during the binding of LMWH and LHT7 on the ATIII were -1.39 and 7.48 kcal/mol, respectively, indicating relatively more unstable binding of LHT7 to ATIII when compared to that of LMWH: this ultimately led to the decreased anticoagulant activity in LHT7.

2.3.2. Anticoagulant activities of LHT7 and its structural analogs

The results were further supported by the comparison of the anticoagulant activities of the LHT7 and its structural analogs. Since the conjugated sodium taurocholate was considered to be entirely responsible to the altered activities of LHT7, the analogous compounds were prepared by conjugating each of the distinguishing compartment of this molecule – cholic acid and taurine – to LMWH (**1**), thereby producing two distinct LHT7 (**4**) analogs, cholic acid conjugated LMWH (**2**) and taurine conjugated LMWH (**3**), respectively (**Fig. 2.1B**). The rationale of separating the compartment of the sodium taurocholate to cholic acid and taurine is from the idea that the significant characteristics of the sodium taurocholate are the steroidal structure (also called as sterane core) and the strong anionic charge from the sulfate group. The prepared cholic acid conjugated LMWH shares the identical sterane core, and the taurine conjugated LMWH has the same overall charge density with LHT7. Therefore, the comparison of the LHT7 analogs and the LHT7 as well as the LMWH could provide important information in which compartment of the conjugated sodium taurocholate contributed to the altered biological activities.

Similar to LHT7, cholic acid conjugated LMWH showed very low anticoagulant activity; however, taurine conjugated LMWH showed only slight decrease of the activity (**Table 2.1**). As mentioned above, the LHT7 and the cholic acid conjugated LMWH share the same sterane core in their conjugated bile acid moieties. This clearly suggested that the sterane core of the conjugated sodium taurocholate, which has rigid and bulky chemical structure, is mainly responsible to the improper binding of the pentasaccharide unit in the LHT7 to the heparin-binding moiety of ATIII through steric hindrance.

2.3.3. Effects of the conjugated sodium taurocholate between the interaction of LMWH and VEGF determined by computerized molecular dynamics

Preceding study has demonstrated that conjugation of sodium taurocholates on LMWH significantly increased binding affinity against VEGF₁₆₅ (hereafter, VEGF)²⁶. A computerized molecular dynamics simulation was carried out to thoroughly investigate the configuration when LHT7 is bound to VEGF. Intermolecular potential energy, defined as a sum of van der Waals and electrostatic interaction energies, was calculated during the binding simulation between VEGF-heparin binding domain (VHBD) and LMWH or LHT7. The final results showed that VHBD-LHT7 complex had a significantly lower energy state (-2,228 kcal/mol) than that shown in VHBD-LMWH complex (-1,865 kcal/mol) in their respective lowest intermolecular potential energy states. The more stable complex formation of LHT7 than LMWH with the VHBD indicated a stronger binding of LHT7 to the VHBD. The structure that was obtained at the lowest intermolecular energy states of VHBD-LHT7 complex was used as the model structure to describe the origin of the stable intermolecular interactions. Earlier studies have demonstrated that Arg123, Arg124, Arg149, and Arg159 of VHBD are the major amino acid residues that interact with the heparin^{38,39}. The model structure of the VHBD-LHT7 complex showed that the main chain of LHT7, corresponding to the LMWH polysaccharide, was located near the cluster of the arginine residues that were mentioned above (**Fig. 2.1C**). Intriguingly, this model structure showed two

additional binding residues on the VHBD that are interacting with the conjugated sodium taurocholate moieties of LHT7: the additional electrostatic interactions occurred between the terminal sulfate groups of the two conjugated sodium taurocholate moieties and the two arginine residues of VHBD, which are Arg112 and Arg165; however, such interactions were not found in the VHBD-LMWH complex. These results suggested that the additional favorable interactions between the terminal sulfate groups of the conjugated sodium taurocholate moieties of LHT7 and the VHBD would have led to the reduction of the intermolecular potential energy, thus further stabilizing the complex structure.

2.3.4. VEGF binding affinities of LHT7 and its structural analogs

The basis of the enhanced binding of LHT7 to VEGF was further evaluated by comparing the VEGF binding affinities of LMWH, LHT7, and the LHT7 structural analogs – cholic acid conjugated and taurine conjugated LMWH (**Fig. 2.1B**) – that were determined using SPR analysis (**Table 2.1**). The result showed that binding affinities of the cholic acid conjugated LMWH ($K_D = 22.4 \mu\text{M}$), which shares an identical sterane core with LHT7 but lacks the terminal sulfate groups, and the LMWH ($K_D = 39.3 \mu\text{M}$) to VEGF were almost similar. This indicated that the sterane core had no contribution to the increased binding affinity of LHT7. By contrast, the taurine conjugated LMWH ($K_D = 2.37 \mu\text{M}$) showed about ten-fold higher binding affinity to VEGF when compared to that of the LMWH and the cholic acid conjugated LMWH, reflecting the importance of the overall degree of sulfation in the interaction with VEGF. However, despite the similar degree of sulfation of the taurine conjugated LMWH to LHT7, the taurine conjugated LMWH showed lower binding affinity than the LHT7 ($K_D = 0.21 \mu\text{M}$). This implied the existence of other potential factor that is contributing to the enhanced binding of LHT7 to VEGF. Considering the VHBD-LHT7 complex model shown in the molecular dynamic simulation, this result strongly substantiate the notion that having a certain distance between the additional sulfate groups and the heparin core chain is critical in developing

new interactions between of LHT7 with VEGF that are significant for the increased binding affinity.

2.3.5. Effect of LHT7 on tumor angiogenesis in vivo

Degree of angiogenesis inside the grafted tumor tissue was directly visualized and quantified by using X-ray μ CT (**Fig. 2.2A**). The SCC7-grafted animal model was prepared and received one of the saline, LMWH, and LHT7 for two weeks every other day at a dose of 5 mg/kg. Then, the animals were sacrificed and blood was replaced with radiopaque polymer solution via heart perfusion. The tumors, which contain polymerized radiopaque material inside their blood vessels, were isolated and subjected to the X-ray μ CT. The mean blood vessel volume of the LHT7-treated group was 41.65 mm³, while control and LMWH-treated group were 1116.98 mm³ and 446.34 mm³, respectively. This was 96.4% and 80.8% decrease for LHT7-treated group when compared to the control and the LMWH-treated group, respectively (**Fig. 2.2B**).

Since the absolute volume of the total blood vessels is largely dependent to the size of the tumor, density of the blood vessel within the tumor tissue was also calculated. The mean blood vessel volume fraction was calculated by dividing the mean blood vessel volume by the mean tumor tissue volume. The mean vessel fraction of the LHT7-treated group was 6.03%, while the control and the LMWH-treated group were 24.53% and 15.68%, respectively. This was 75.5% and 61.8% decrease of the blood vessel density in LHT7-treated group when compared to the control and the LMWH-treated group, respectively (**Fig. 2.2B**). This result clearly showed the inhibition of neovascularization in the tumors when the animals were treated with LHT7. Moreover, it showed that LHT7 had superior anti-angiogenic activity than LMWH, agreeing with the result that demonstrated higher binding affinity of LHT7 to VEGF than that of LMWH.

2.3.6. Anticancer effects of LHT7 on distinct types of carcinoma xenografts

The therapeutic potential of LHT7 in tumor growth was evaluated on three distinct types of carcinomas, A549, HT-29, and AMC-HN9, which differ in their angiogenic property. When compared to the control, LHT7 showed marked suppression of A549 and HT-29 tumor growth: a dosage of 1 mg/kg of LHT7 inhibited cancer growth by 35% and 48%, respectively; and a dosage of 5 mg/kg of LHT7 inhibited the growth by 9% and 31%, respectively (**Fig. 2.3A and B**). The histological assessments of the tumor types responding to LHT7, which are A549 and HT-29 in particular, showed significant amount of endothelium and smooth muscle cells exist within the tissue represented by the immunostaining of CD34 and α SMA, respectively (**Fig. 2.3C**). This indicated an active formation of vasculatures in those tumors.

On the other hand, the histological assessment of the AMC-HN9 tumor, which did not respond to LHT7 in any of the tested doses (**Fig. 2.4A**), showed few immunostained CD34 and α SMA in the tissue (**Fig. 2.4B**), indicating very weak angiogenic capability of the AMC-HN9 tumor. However, despite the absence of typical blood vessels in the AMC-HN9 tumor, substantial number of red blood cells was found in the extracellular space of the sectioned tissue (**Fig. 2.4C**). This implied that the growth of the AMC-HN9 tumor is independent to conventional angiogenesis, but rather relies on the formation of abnormal blood flow channels, which the phenomenon is termed as vascular mimicry.

These results showed that the distinct types of carcinomas displayed different susceptibility to LHT7 depending on the angiogenic activity of the tumor. The angiogenic tumors, which are A549 and HT-29, were very sensitive to LHT7. By contrast, non-angiogenic tumor, which is AMC-HN9, was insensitive to that. This manifested that LHT7 shows its anticancer effect through its ability to suppress tumor angiogenesis *in vivo*.

2.3.7. Intratumor localization of LHT7

The whole-body distribution of LHT7 was determined by an *ex vivo* observation on MDA-MB-231 xenograft animal models after intravenous administration of fluorescent-labeled LHT7 via tail vein (**Fig. 2.5A**). When the animal was observed after an hour of the administration, LHT7 was distributed to the every part of the body by blood circulation. However, when observed after four hours, the drug was mainly observed in the tumor site in high concentration, which the measured intensity was almost similar to that observed at one-hour time point, and the was eliminated in the other body parts. The LHT7 observed in the site other than the tumor was almost eliminated at 24 hours of post-administration. The selective accumulation of LHT7 in the tumor lasted for at least 48 hours.

To determine more specific site of the LHT7 localization inside the tumor, the tumor tissue was sectioned and immunostained for microscopic observations (**Fig. 2.5B**). The animals received fluorescent-labeled LHT7 by intravenous route in advance of tissue sectioning, followed by the immunostaining of CD31 to distinguish the endothelium of the tumor vasculatures. The observations showed that the LHT7 was mainly located in the tumor vasculatures rather than in the extravascular extracellular space of tumor tissue. These results collectively suggest the existence of certain driving force that mediates LHT7 to be selectively accumulated in the tumor vasculatures.

2.3.8. LHT7 uptake by platelets

Human platelets were incubated with fluorescent-labeled LHT7 at varying concentrations ranging up to 20 $\mu\text{g/ml}$ in order to investigate whether LHT7 could be taken up by platelets.

The flow cytometry analysis showed that the LHT7 was taken up into the platelets in a dose-dependent manner as shown by the right shift of the histogram following the increased concentration of the treated LHT7 (**Fig.**

2.6A). However, this result did not clearly showed whether the LHT7 was taken up inside the granules of platelet or simply bound on the surface.

To determine whether LHT7 was bound on the surface or taken up inside the platelets, the platelets that were incubated with the fluorescent-labeled LHT7 in varying concentrations were further activated with thrombin. The activated platelets could be separated into two compartments by centrifugation: the granular substances remain in the supernatant, and the membrane and membrane bound substances are collected as a pellet. After activation of the platelets, fluorescent-labeled LHT7 was completely released out to the supernatant and not remained on the platelet pellets. This clearly indicated that the LHT7 was taken up by platelets in a dose-dependent manner rather than adhering on the surface (**Fig. 2.6B**).

The immunocytochemical observation of the platelets further supported the uptake of LHT7 in their granules. When the platelets were incubated with the fluorescent-labeled LHT7 and immunostained with P-selectin antibody, the platelets showed a double staining pattern, in which the fluorescent-labeled LHT7 (green) was surrounded by the stained P-selectin (red) marking the boundary of the α -granule (**Fig. 2.6C**). This result further supported the observation that LHT7 was taken up into the platelet, especially inside the α -granules.

Table 2.1. Characteristics of LHT7 and its analogs

	LMWH	Cholic acid conjugated LMWH	Taurine conjugated LMWH	LHT7
Anti-FXa (%)	100	1.95 ± 0.56	86.61 ± 5.14	4.18 ± 1.47
K _D (μM)	39.3 ± 3.7	22.4 ± 2.9	2.37 ± 0.40	0.21 ± 0.06

Data expressed as means ± s.d.

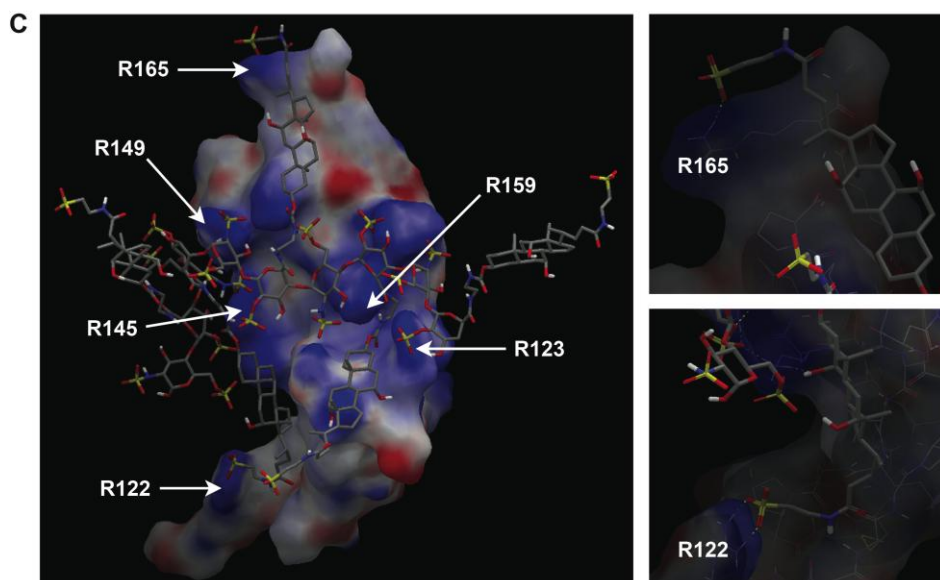
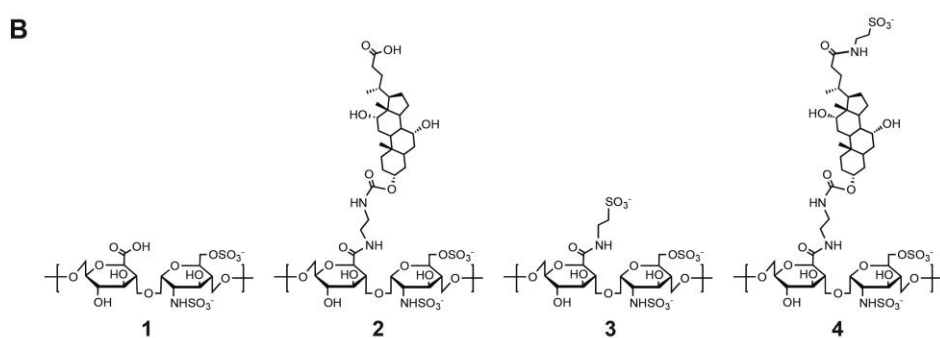
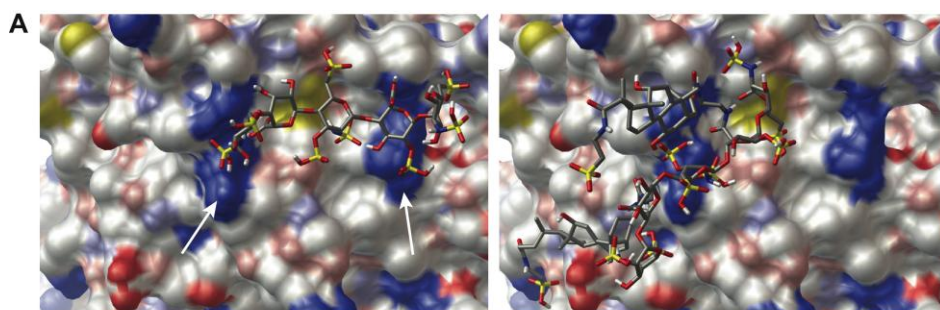


Figure 2.1. (A) Computerized molecular docking of LMWH (left) and LHT7 (right) on the ATIII heparin binding site (arrow). The pairs were allowed to reach the minimum intermolecular energy level and the final appearances were examined. (B) Representative chemical structures of LMWH **1**, cholic acid conjugated LMWH **2**, taurine conjugated LMWH **3**, and LHT7 **4**. (C) The model structure of LHT7 and VEGF-HBD complex when the intermolecular energy level has reached the minimum during molecular dynamics.

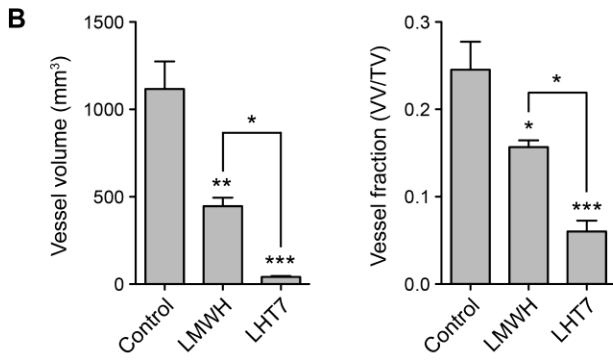
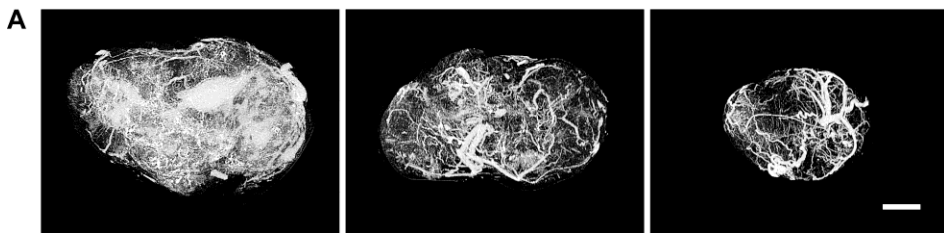


Figure 2.2. (A) Representative images of saline (control), LMWH, and LHT7 treated SCC7 tumors obtained by X-ray μ CT. Scale bar, 5 mm. (B) Tumor vessel volumes (left) and vessel fractions (right) calculated through reconstruction of vasculatures followed by computed calculation of the volumes. $*P < 0.05$, $**P < 0.005$, and $***P < 0.001$ versus control. Data are expressed as mean \pm s.e.m.

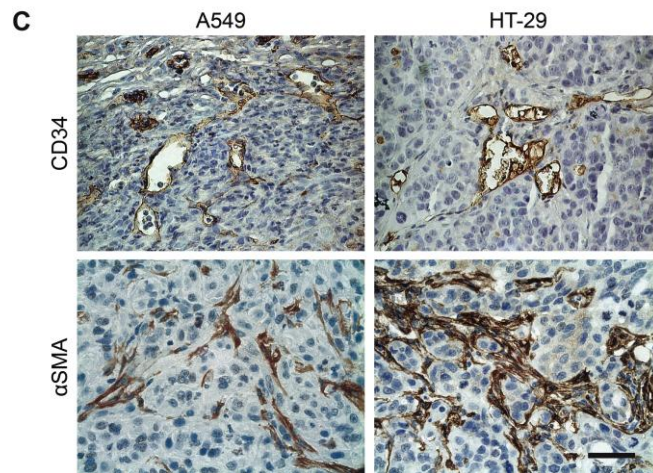
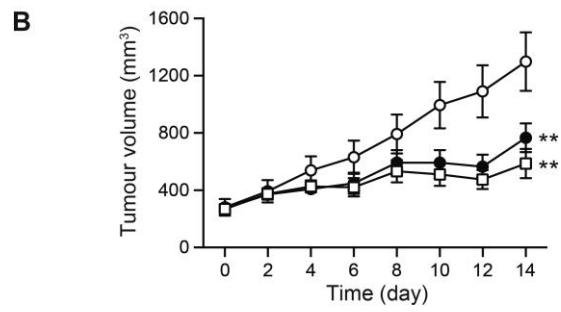
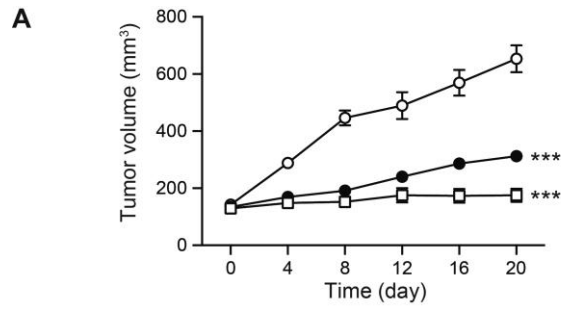


Figure 2.3. Tumor growth suppression on A549 (A) and HT-29 (B) xenografts. The three groups received either saline as control (○) or LHT7 in two different doses: 1 mg/kg (●) and 5 mg/kg (□) administered intravenously every other day. n = 9. Data presented as mean ± s.e.m. (C) Histological analysis of A549 (left) and HT-29 (right) tumor sections. Immunostaining of the upper and lower panels indicates CD34 and αSMA, respectively. Scale bar, 50 μm.

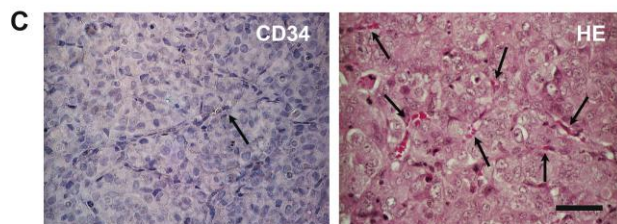
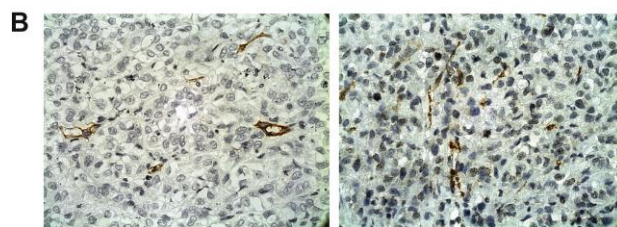
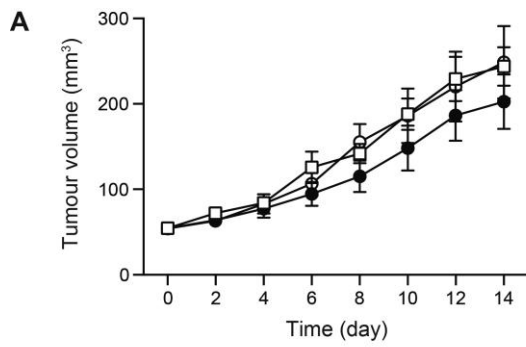


Figure 2.4. (A) Tumor growth suppression of AMC-HN9 xenografts. Mice received either saline as control (○) or LHT7 in different doses: 1 mg/kg (●) and 5 mg/kg (□) administered every other day. n = 9. (B) Histological analysis of AMC-HN9 tumor sections. Immunostaining of the left and right panels indicates CD34 and α SMA, respectively. Scale bar, 50 μ m. (C) CD34 (left) and HE (right) staining of the tumor specimens. Arrows depict a subset of red blood cells. Scale bar, 50 μ m.

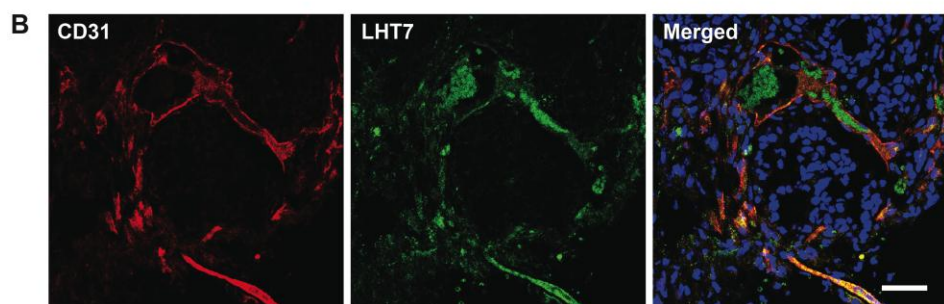
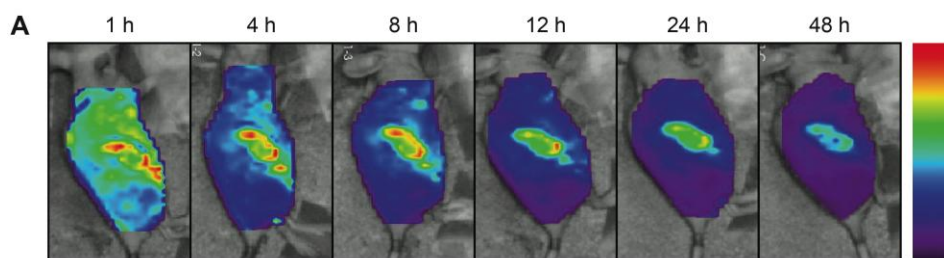


Figure 2.5. (A) *Ex vivo* biodistribution observations of the fluorescent-labeled LHT7 after intravenous administration in mice. (B) Immunostaining of tumor specimens at post-administration of LHT7. Red and green color represents CD31 and LHT7, respectively. Scale bar, 50 μ m.

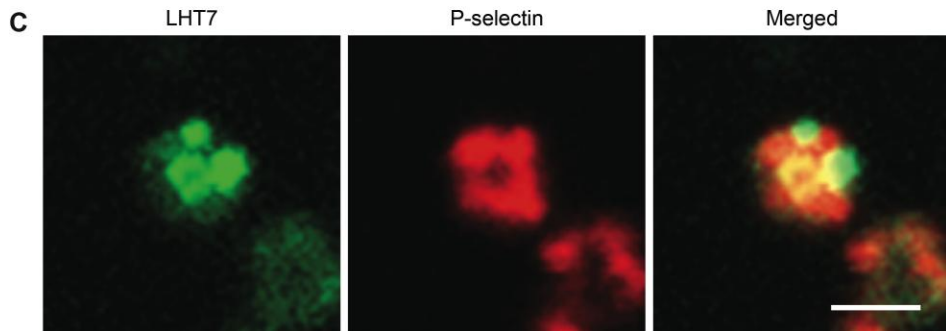
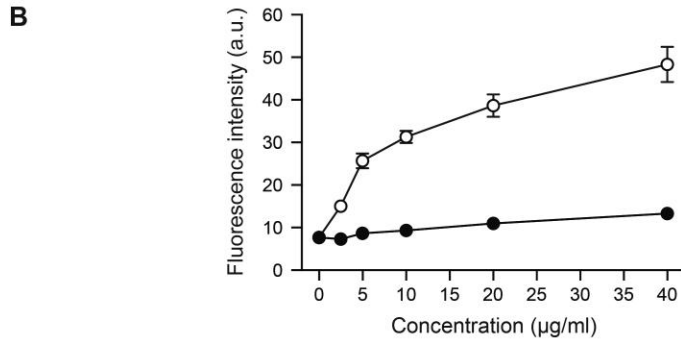
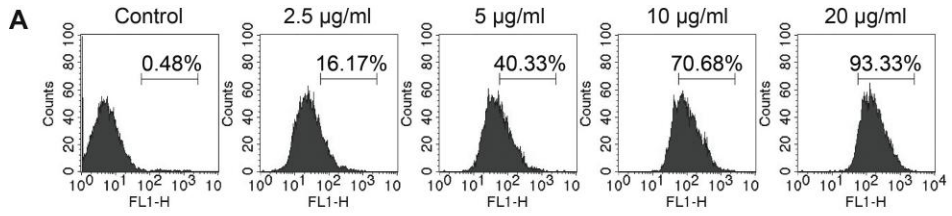


Figure 2.6. (A) FACS analysis of platelets that have taken up LHT7 after incubation with a series of concentrations of fluorescent-labeled LHT7. Numbers represent the gated percentage in the assigned range. (B) Quantitative analysis of released (○) and bound (●) LHT7 on the pellet of the platelets after activation of platelets incubated with fluorescent-labeled LHT7. Data are expressed as means \pm s.d. (C) Immunocytochemical staining of platelets incubated with fluorescent-labeled LHT7. Green and red represents LHT7 and P-selectin in α -granules of platelets, respectively. Scale bar, 2 μ m.

2.4. Discussion

The preceded study of LHT7 showed that the conjugation of sodium taurocholate on LMWH resulted in decreased anticoagulant activity and increased anti-angiogenic effect, particularly showing increased binding affinity to VEGF²⁶. It was questioned how such chemical modification of LMWH altered the two distinct biological activities – anticoagulant and anti-angiogenic activity – in differential manner at the same time. To address this question, the binding properties of LHT7 to ATIII and VEGF were determined using various approaches.

The interaction of heparin with ATIII, which is the main principle of the anticoagulant activity of LMWH, is mediated by a specific non-variable pentasaccharide sequence within the heparin^{40,41}. On the other hand, the interaction with many other proteins including the diverse range of the pro-angiogenic factors is mediated through electrostatic attractions via polyanionic dispersion from the sulfate groups⁴¹. In particular, it was reported that the interaction of heparin with VEGF strongly depends on the *N*- and 6-*O*-sulfation, and with FGF depends on the 2-*O*-sulfation of the heparin polysaccharide chain⁴². The specific pentasaccharide unit that plays crucial role in the interaction with ATIII was demonstrated not to be important in the interaction with VEGF⁴³. The distinct binding mechanisms of heparin on ATIII and VEGF eventually allowed the sodium taurocholate conjugation to act in differential manner as would be discussed in detail further.

The preceding study have demonstrated that the conjugation of sodium taurocholate on LMWH gradually decreased its anticoagulant activity following the increasing number of conjugated sodium taurocholate²⁶. The anticoagulant activities were determined using chromogenic factor Xa assay³⁷. The principle of this assay is as the followings: a functional heparin binds to and induces conformational change of ATIII; then the activated ATIII further forms a complex with factor Xa; the chromogenic substrate of factor Xa reacts with the remaining unbound factor Xa and allows the colorimetric quantification.

Therefore, the results obtained by using this methodology indirectly show whether the heparin (or heparin derivative) was properly bound to the ATIII, which triggers the conformational change and further binding with factor Xa.

According to the principle of the chromogenic factor Xa assay, it was hypothesized that the conjugated sodium taurocholates in LHT7 interfered the proper binding of the specific non-variable pentasaccharide sequence of the comprised LMWH chain to the ATIII, which eventually led to the decreased anti-factor Xa activity. The computerized simulation results showed that the transient energy, when designated to bind to the heparin-binding site of ATIII, was notably higher for LHT7 than that for LMWH. As a result, LHT7 preferred binding on the location other than the defined heparin-binding site of ATIII, while LMWH preferred binding on the heparin-binding site. This indicated that conjugation of sodium taurocholates on LMWH impeded its proper binding on the heparin-binding site of ATIII; therefore, did not induce an appropriate conformational change of ATIII that is required for the inhibition of factor Xa activity. This was further supported by the varying anti-factor Xa activities of LHT7 and its structural analogs. The cholic acid conjugated LMWH, which the conjugated cholic acid share the identical steroidal structure with the sodium taurocholate in LHT7, showed very low anti-factor Xa activity similar to LHT7. By contrast, taurine conjugated LMWH showed only slightly reduced anti-factor Xa activity when compared to LHT7. These results indicated that the steroidal structure of the conjugated sodium taurocholate played the key role in impeding the proper binding of the pentasaccharide unit to the heparin-binding site of the ATIII. Considering that the steroidal structure is relatively bulky and rigid, this would have generated steric hindrance that veils the non-variable pentasaccharide sequence of LMWH to contact with the heparin-binding site of the ATIII, ultimately leading to the decreased anticoagulant activity.

On the other hand, LHT7 showed stronger anticancer and anti-angiogenic activity when compared to the non-modified LMWH. This was demonstrated to be partly due to the increased binding affinity against VEGF when sodium taurocholates were conjugated on LMWH in the preceding study²⁶. In the

current study, it was investigated more thoroughly how the conjugated sodium taurocholate moieties on LMWH could actually enhanced the binding affinity against VEGF rather than interfering with it as observed in the binding against ATIII. Two distinct experiments were performed: *in silico* molecular dynamics modeling of binding between the LHT7 and the VEGF-heparin binding domain (VHBD), and the SPR binding analysis of LHT7 and the structural analogs of LHT7 with VEGF. The *in silico* molecular dynamics modeling showed that when the intermolecular potential energy reached the minimum during the dynamic interaction between LHT7 and VHBD, two distinct arginine residues on the VHBD – Arg122 and Arg165 – strongly interacted with terminal sulfate group of the conjugated sodium taurocholate moieties, while the core heparin chain of the LHT7 was properly located on the heparin-binding site of VHBD, still interacting with the four arginine residues that are known to have significant role in binding with heparin – Arg123, Arg124, Arg149, and Arg159^{38,39}. This suggested that the additional interactions with Arg122 and Arg165 on the VHBD produced by the sodium taurocholate moieties have potentially contributed to the more stabilized binding of LHT7 to VEGF, resulting in the improved anti-angiogenic activity when compared to that of the LMWH.

The SPR binding studies with LHT7 and its structural analogs further manifested the role of the conjugated sodium taurocholate in the improved binding affinity to VEGF. The conjugated sodium taurocholate was defined as a molecule comprising a steroidal structure and a strong anionic charge originated from the sulfate group; its structure was separated into cholic acid and taurine, each of which was chemically conjugated to LMWH to produce cholic acid conjugated LMWH and taurine conjugated LMWH, respectively. The results showed that cholic acid conjugated LMWH had no improvement in the binding affinity compared to the native LMWH, implying that steroidal structure of the conjugated sodium taurocholate itself did not have any directly positive effect on improving the binding of LMWH on VEGF. On the other hand, taurine conjugated LMWH showed increased binding affinity, implying that the

increased number of sulfate groups, which resulted in the increased amount of net negative charge on the molecule, positively affected the binding affinity of the LMWH towards VEGF. The influence of the degree of sulfation on heparin on binding with proteins including VEGF was already well demonstrated in the previous reports⁴².

However, the taurine conjugated LMWH still had lower binding affinity on VEGF than that of LHT7 despite the identical overall anionic charge density, which implied the existence of other underlying factors contributing to the enhanced VEGF binding. According to the result obtained by *in silico* molecular dynamics modeling, there were two additional arginine residues – Arg112 and Arg165 – participating in the interaction between LHT7 and VEGF that were not found in the interaction between LMWH and VEGF. These two residues were interacting with the sulfate groups of the taurocholate moiety rather than the heparin chain and were located far apart from the typical heparin binding residues, the cluster of Arg123, Arg124, Arg149 and Arg159, within the VHBD. The distance between the traditional heparin binding residues and the newly generated binding residues in the VHBD corresponds to the length of the sterane core of the sodium taurocholate.

On the other hand, since taurine is a very small and short molecule, the taurine conjugated LMWH has the additional sulfate groups originating from the conjugated taurine molecules near the other pre-existing sulfate groups of LMWH. Therefore, although the conjugated taurines increased the net anionic charge of the molecule and contributed to the increased binding affinity towards VEGF, their sulfate groups are likely to compete with the pre-existing sulfate groups of the heparin core chain in the interaction with the cluster of the arginine residues in the VHBD heparin-binding site. Therefore, the electrostatic attraction of the individual sulfate groups to the heparin-binding arginine residues of VHBD would be attenuated. In contrast, additional sulfate groups of LHT7 on the terminal end of the conjugated sodium taurocholate could retain their entire potential of electrical attraction because they are located in distance from the sulfate groups of the core heparin chain, thereby free from the

competition. According to the result obtained from the SPR binding study of the cholic acid conjugated LMWH, the sterane core of the conjugated sodium taurocholate solely had no direct effect in enhancing the binding strength of LHT7 on VEGF. Rather, it indirectly affected the binding by efficiently delivering the additional sulfate groups to the distant location from the general heparin-binding site of VHBD through its rigid chemical structure, resulting in highly improved VEGF binding than merely increasing the degree of sulfation.

As mentioned earlier, the binding of heparin on ATIII depends on a specific pentasaccharide unit of the polysaccharide chain, while the binding on other proteins including VEGF mainly depends on the polyanionic charge dispersion and does not require any specific sequence⁴⁴. The distinct binding characteristics of heparin on two different proteins, ATIII and VEGF, allowed the differential effect of sodium taurocholate conjugation. The conjugation of sodium taurocholate on LMWH blocked the proper binding to ATIII by concealing the ATIII-binding pentasaccharide unit by its bulky steroidal structure, whereas it improved the binding to VEGF by adding fully functional electrostatic interactions via the sulfate group.

The therapeutic implication of the VEGF binding of LHT7 was evaluated *in vivo* through direct observation of intratumor angiogenesis and tumor growth of distinct types of carcinomas that differ in their degree of angiogenic potential when treated with LHT7. The results showed significant reduction in both absolute intratumor blood vessel volume and vessel density in the tumor tissue when the animal model was treated with LHT7. This indicated that the suppression of tumor growth when treated with LHT7 was mainly caused by the inhibition of tumor angiogenesis rather than any possible direct cytotoxic effect to the tumor cells. The anti-angiogenic effect of LHT7 is considered to be the consequence of VEGF signaling pathway blockade. In addition, the fact that only the tumors that are strongly angiogenic responded to the LHT7 treatment further supported that anti-angiogenic activity including the blockade of VEGF signaling pathway is the main mechanism of action in the *in vivo* anticancer effect of the LHT7.

It was also found that LHT7 was selectively localized in the tumor, especially accumulated inside the tumor blood vessels for more than 48 hours. This phenomenon is interesting because accumulation of therapeutic molecules specifically to a pathological site could increase the therapeutic potential with fewer side effects. Therefore, the tumor accumulation of LHT7 was considered to be another important factor contributing to its potent anticancer effect examined in various types of xenograft animal models.

Although the reason for the selective intratumor accumulation of LHT7 is not completely understood so far, the uptake by platelets shown in the experimental results was suggested to be one of the important factor contributing to the phenomenon. Verheul et al. have demonstrated that platelets can take up and store bevacizumab, trastuzumab, and cetuximab in their granules apparently in a non-specific manner⁴⁵. LHT7 may have been taken up by platelets into their granules in a similar manner. Platelets are generally activated in the tumor tissue to release granular contents since tumor is regarded as a persistent wound⁴⁶. The platelets are also well recognized to release substantial amount of VEGF and other pro-angiogenic factors to promote angiogenesis⁴⁷. Thus, the platelets could act as the vehicles that could continuously deliver LHT7 to the tumor after taking up the molecules inside their granules. This would eventually increase the local concentration of LHT7 within the tumor tissue. Moreover, LHT7 could bind and neutralize the VEGF either inside the platelet granule or at the site of the release, thereby more efficiently blocking the VEGF that was supposed to act in the tumor tissue.

Another factor to be considered in the tumor accumulation of LHT7 is the presence of overexpressed integrins in the tumor tissue. Heparin is capable in binding with a diverse range of integrins including P-selectin, L-selectin, PECAM-1, and MAC-1, which are generally expressed on activated endothelial and inflammatory cells¹⁵. These integrins are also upregulated in the tumor, managing many crucial steps of tumor progression⁴⁸. Hence, LHT7, which is originated from heparin, may bind with integrins expressed on the tumor

endothelium. However, integrin-binding capability of LHT7 remains to be elucidated in the further studies.

2.5. Conclusion

The findings in this study suggest that appropriate modification of heparin could potentiate its intrinsic property of suppressing angiogenesis while eliminating anticoagulant activity at the same time. Current study suggest that such modifications could be accomplished by blocking the ATIII-interacting pentasaccharide unit of heparin by a bulky molecule, in this case, the sterane core, to inhibit the binding on ATIII, and increasing the net anionic charge by adding more sulfate groups that could enhance binding to VEGF. Interestingly, it was also shown that not only the quantitative amount of the anionic charge density is important but also the charge distribution within the molecules is crucial for enhanced binding to the VEGF. The heparin-based anti-angiogenic agent, LHT7, had sodium taurocholates conjugated on the LMWH. The conjugated sodium taurocholate satisfied the properties that are required for the above-mentioned appropriate modification for the ideal alteration of heparin activity. As a result, LHT7 showed excellent anticancer and anti-angiogenic effect with no noticeable anticoagulant activity.

References

- 1 Hanahan, D. & Weinberg, R. A. The hallmarks of cancer. *Cell* **100**, 57-70 (2000).
- 2 Ferrara, N., Hillan, K. J., Gerber, H. P. & Novotny, W. Discovery and development of bevacizumab, an anti-VEGF antibody for treating cancer. *Nat Rev Drug Discov* **3**, 391-400 (2004).
- 3 Saltz, L. B., Lenz, H. J., Kindler, H. L., Hochster, H. S., Wadler, S., Hoff, P. M., Kemeny, N. E., Hollywood, E. M., Gonen, M., Quinones, M., Morse, M. & Chen, H. X. Randomized phase II trial of cetuximab, bevacizumab, and irinotecan compared with cetuximab and bevacizumab alone in irinotecan-refractory colorectal cancer: the BOND-2 study. *J Clin Oncol* **25**, 4557-4561 (2007).
- 4 Kindler, H. L., Niedzwiecki, D., Hollis, D., Sutherland, S., Schrag, D., Hurwitz, H., Innocenti, F., Mulcahy, M. F., O'Reilly, E., Wozniak, T. F., Picus, J., Bhargava, P.,

- Mayer, R. J., Schilsky, R. L. & Goldberg, R. M. Gemcitabine plus bevacizumab compared with gemcitabine plus placebo in patients with advanced pancreatic cancer: phase III trial of the Cancer and Leukemia Group B (CALGB 80303). *J Clin Oncol* **28**, 3617-3622 (2010).
- 5 Bergers, G. & Hanahan, D. Modes of resistance to anti-angiogenic therapy. *Nat Rev Cancer* **8**, 592-603 (2008).
 - 6 Casanovas, O., Hicklin, D. J., Bergers, G. & Hanahan, D. Drug resistance by evasion of antiangiogenic targeting of VEGF signaling in late-stage pancreatic islet tumors. *Cancer Cell* **8**, 299-309 (2005).
 - 7 Fernando, N. T., Koch, M., Rothrock, C., Gollogly, L. K., D'Amore, P. A., Ryeom, S. & Yoon, S. S. Tumor escape from endogenous, extracellular matrix-associated angiogenesis inhibitors by up-regulation of multiple proangiogenic factors. *Clin Cancer Res* **14**, 1529-1539 (2008).
 - 8 Hamdan, R., Zhou, Z. & Kleinerman, E. S. SDF-1alpha induces PDGF-B expression and the differentiation of bone marrow cells into pericytes. *Mol Cancer Res* **9**, 1462-1470 (2011).
 - 9 Bergers, G. & Song, S. The role of pericytes in blood-vessel formation and maintenance. *Neuro Oncol* **7**, 452-464 (2005).
 - 10 Benjamin, L. E., Hemo, I. & Keshet, E. A plasticity window for blood vessel remodelling is defined by pericyte coverage of the preformed endothelial network and is regulated by PDGF-B and VEGF. *Development* **125**, 1591-1598 (1998).
 - 11 Bergers, G., Song, S., Meyer-Morse, N., Bergsland, E. & Hanahan, D. Benefits of targeting both pericytes and endothelial cells in the tumor vasculature with kinase inhibitors. *J Clin Invest* **111**, 1287-1295 (2003).
 - 12 Orlidge, A. & D'Amore, P. A. Inhibition of capillary endothelial cell growth by pericytes and smooth muscle cells. *J Cell Biol* **105**, 1455-1462 (1987).
 - 13 Hirschi, K. K. & D'Amore, P. A. Control of angiogenesis by the pericyte: molecular mechanisms and significance. *EXS* **79**, 419-428 (1997).
 - 14 Capila, I. & Linhardt, R. J. Heparin-protein interactions. *Angew Chem Int Ed Engl* **41**, 391-412 (2002).
 - 15 Lever, R. & Page, C. P. Novel drug development opportunities for heparin. *Nat Rev Drug Discov* **1**, 140-148 (2002).
 - 16 Sasisekharan, R., Shriver, Z., Venkataraman, G. & Narayanasami, U. Roles of heparan-sulphate glycosaminoglycans in cancer. *Nat Rev Cancer* **2**, 521-528 (2002).
 - 17 Mousa, S. A., Linhardt, R., Francis, J. L. & Amirkhosravi, A. Anti-metastatic effect of a non-anticoagulant low-molecular-weight heparin versus the standard low-molecular-weight heparin, enoxaparin. *Thromb Haemost* **96**, 816-821 (2006).

- 18 Pisano, C., Aulicino, C., Vesci, L., Casu, B., Naggi, A., Torri, G., Ribatti, D., Belleri, M., Rusnati, M. & Presta, M. Undersulfated, low-molecular-weight glycol-split heparin as an antiangiogenic VEGF antagonist. *Glycobiology* **15**, 1C-6C (2005).
- 19 Ritchie, J. P., Ramani, V. C., Ren, Y., Naggi, A., Torri, G., Casu, B., Penco, S., Pisano, C., Carminati, P., Tortoreto, M., Zunino, F., Vlodaysky, I., Sanderson, R. D. & Yang, Y. SST0001, a chemically modified heparin, inhibits myeloma growth and angiogenesis via disruption of the heparanase/syndecan-1 axis. *Clin Cancer Res* **17**, 1382-1393 (2011).
- 20 Kudchadkar, R., Gonzalez, R. & Lewis, K. D. PI-88: a novel inhibitor of angiogenesis. *Expert opinion on investigational drugs* **17**, 1769-1776 (2008).
- 21 Dredge, K., Hammond, E., Handley, P., Gonda, T. J., Smith, M. T., Vincent, C., Brandt, R., Ferro, V. & Bytheway, I. PG545, a dual heparanase and angiogenesis inhibitor, induces potent anti-tumour and anti-metastatic efficacy in preclinical models. *Br J Cancer* **104**, 635-642 (2011).
- 22 Lee, G. Y., Kim, S. K. & Byun, Y. Glucosylated heparin derivatives as non-toxic anti-cancer drugs. *J Control Release* **123**, 46-55 (2007).
- 23 Park, K., Kim, Y. S., Lee, G. Y., Nam, J. O., Lee, S. K., Park, R. W., Kim, S. Y., Kim, I. S. & Byun, Y. Antiangiogenic effect of bile acid acylated heparin derivative. *Pharm Res* **24**, 176-185 (2007).
- 24 Yu, M. K., Lee, D. Y., Kim, Y. S., Park, K., Park, S. A., Son, D. H., Lee, G. Y., Nam, J. H., Kim, S. Y., Kim, I. S., Park, R. W. & Byun, Y. Antiangiogenic and apoptotic properties of a novel amphiphilic folate-heparin-lithocholate derivative having cellular internality for cancer therapy. *Pharm Res* **24**, 705-714 (2007).
- 25 Park, J. W., Jeon, O. C., Kim, S. K., Al-Hilal, T. A., Jin, S. J., Moon, H. T., Yang, V. C., Kim, S. Y. & Byun, Y. High antiangiogenic and low anticoagulant efficacy of orally active low molecular weight heparin derivatives. *J Control Release* **148**, 317-326 (2010).
- 26 Lee, E., Kim, Y. S., Bae, S. M., Kim, S. K., Jin, S., Chung, S. W., Lee, M., Moon, H. T., Jeon, O. C., Park, R. W., Kim, I. S., Byun, Y. & Kim, S. Y. Polyproline-type helical-structured low-molecular weight heparin (LMWH)-taurocholate conjugate as a new angiogenesis inhibitor. *Int J Cancer* **124**, 2755-2765 (2009).
- 27 Fini, A., Fazio, G., Roda, A., Bellini, A. M., Mencini, E. & Guarneri, M. Basic cholane derivatives. XI: Comparison between acid and basic derivatives. *J Pharm Sci* **81**, 726-730 (1992).
- 28 Silvestri, L. J., Hurst, R. E., Simpson, L. & Settine, J. M. Analysis of sulfate in complex carbohydrates. *Anal Biochem* **123**, 303-309 (1982).

- 29 Jorgensen, W. L., Chandrasekhar, J., Madura, J. D., Impey, R. W. & Klein, M. L. Comparison of simple potential functions for simulating liquid water. *The Journal of Chemical Physics* **79**, 926-935 (1983).
- 30 Morris, G. M., Goodsell, D. S., Halliday, R. S., Huey, R., Hart, W. E., Belew, R. K. & Olson, A. J. Automated docking using a Lamarckian genetic algorithm and an empirical binding free energy function. *J Comput Chem* **19**, 1639-1662 (1998).
- 31 Skinner, R., Abrahams, J. P., Whisstock, J. C., Lesk, A. M., Carrell, R. W. & Wardell, M. R. The 2.6 Å structure of antithrombin indicates a conformational change at the heparin binding site. *J Mol Biol* **266**, 601-609 (1997).
- 32 Gasteiger, J. & Marsili, M. Iterative partial equalization of orbital electronegativity—a rapid access to atomic charges. *Tetrahedron* **36**, 3219-3228 (1980).
- 33 Ersdal-Badju, E., Lu, A., Zuo, Y., Picard, V. & Bock, S. C. Identification of the antithrombin III heparin binding site. *J Biol Chem* **272**, 19393-19400 (1997).
- 34 Garcia-Sanz, A., Rodriguez-Barbero, A., Bentley, M. D., Ritman, E. L. & Romero, J. C. Three-dimensional microcomputed tomography of renal vasculature in rats. *Hypertension* **31**, 440-444 (1998).
- 35 Maehara, N. Experimental microcomputed tomography study of the 3D microangioarchitecture of tumors. *Eur Radiol* **13**, 1559-1565 (2003).
- 36 Ferreira, I. A., Mocking, A. I., Urbanus, R. T., Varlack, S., Wnuk, M. & Akkerman, J. W. Glucose uptake via glucose transporter 3 by human platelets is regulated by protein kinase B. *J Biol Chem* **280**, 32625-32633 (2005).
- 37 ten Cate, H., Lamping, R. J., Henny, C. P., Prins, A. & ten Cate, J. W. Automated amidolytic method for determining heparin, a heparinoid, and a low-Mr heparin fragment, based on their anti-Xa activity. *Clin Chem* **30**, 860-864 (1984).
- 38 Robinson, C. J., Mulloy, B., Gallagher, J. T. & Stringer, S. E. VEGF165-binding sites within heparan sulfate encompass two highly sulfated domains and can be liberated by K5 lyase. *J Biol Chem* **281**, 1731-1740 (2006).
- 39 Krilleke, D., DeErkenez, A., Schubert, W., Giri, I., Robinson, G. S., Ng, Y. S. & Shima, D. T. Molecular mapping and functional characterization of the VEGF164 heparin-binding domain. *J Biol Chem* **282**, 28045-28056 (2007).
- 40 Lindahl, U., Backstrom, G., Hook, M., Thunberg, L., Fransson, L. A. & Linker, A. Structure of the antithrombin-binding site in heparin. *Proc Natl Acad Sci U S A* **76**, 3198-3202 (1979).
- 41 Bishop, J. R., Schuksz, M. & Esko, J. D. Heparan sulphate proteoglycans fine-tune mammalian physiology. *Nature* **446**, 1030-1037 (2007).
- 42 Ono, K., Hattori, H., Takeshita, S., Kurita, A. & Ishihara, M. Structural features in heparin that interact with VEGF165 and modulate its biological activity. *Glycobiology* **9**, 705-711 (1999).

- 43 Zhao, W., McCallum, S. A., Xiao, Z., Zhang, F. & Linhardt, R. J. Binding affinities of vascular endothelial growth factor (VEGF) for heparin-derived oligosaccharides. *Biosci Rep* **32**, 71-81 (2012).
- 44 Esko, J. D. & Selleck, S. B. Order out of chaos: assembly of ligand binding sites in heparan sulfate. *Annu Rev Biochem* **71**, 435-471 (2002).
- 45 Verheul, H. M., Lolkema, M. P., Qian, D. Z., Hilkes, Y. H., Liapi, E., Akkerman, J. W., Pili, R. & Voest, E. E. Platelets take up the monoclonal antibody bevacizumab. *Clin Cancer Res* **13**, 5341-5347 (2007).
- 46 Verheul, H. M., Hoekman, K., Luykx-de Bakker, S., Eekman, C. A., Folman, C. C., Broxterman, H. J. & Pinedo, H. M. Platelet: transporter of vascular endothelial growth factor. *Clin Cancer Res* **3**, 2187-2190 (1997).
- 47 Weltermann, A., Wolzt, M., Petersmann, K., Czerni, C., Graselli, U., Lechner, K. & Kyrle, P. A. Large amounts of vascular endothelial growth factor at the site of hemostatic plug formation in vivo. *Arterioscler Thromb Vasc Biol* **19**, 1757-1760 (1999).
- 48 Desgrosellier, J. S. & Cheresh, D. A. Integrins in cancer: biological implications and therapeutic opportunities. *Nat Rev Cancer* **10**, 9-22 (2010).

Chapter 3

Multiple-stage angiogenesis inhibition of LHT7 by blocking VEGF, FGF2, and PDGF-B

Despite the therapeutic benefits of the angiogenesis inhibitors shown in the clinics, they have encountered an unexpected limitation by the occurrence of acquired resistance. Although the mechanism of the resistance is not clear so far, the upregulation of alternative pro-angiogenic pathways and stabilization of endothelium by mural cells were reported to be responsible. Therefore, blocking multiple pro-angiogenic pathways that are crucial in tumor angiogenesis has been highlighted to overcome such limitations. To develop an angiogenesis inhibitor that could block multiple pro-angiogenic factors, heparin is an excellent lead compound since wide array of pro-angiogenic factors are heparin-binding proteins. In the previous section, LHT7, a heparin-derived angiogenesis inhibitor, was demonstrated as a potent angiogenesis inhibitor and showed that it blocked VEGF signaling pathway. Here it is shown that LHT7 could block the FGF2 and PDGF-B in addition to VEGF. Simultaneous blockade of these pro-angiogenic factors resulted in inhibition of multiple stages of the angiogenic process, including initial angiogenic response to maturation of the endothelium by pericyte coverage *in vitro*. In addition, the treatment of LHT7 *in vivo* did not show any sign of vascular normalization and directly led to decreased blood perfusion throughout the tumor. Current findings show that LHT7 could effectively inhibit tumor angiogenesis by blocking multiple stages of the angiogenesis, and could potentially be used to overcome the resistance.

3.1. Introduction

Tumor angiogenesis plays a critical role in mass growth and metastasis of tumor¹. Tumors that have inadequate vasculatures turns necrotic or apoptotic due to the insufficient supply of oxygen and nutrient for their survival². Therefore, blocking angiogenesis has been proposed as a distinct strategy for treatment of cancer. Since the development of bevacizumab, the first angiogenesis inhibitor to be approved by FDA, angiogenesis inhibitor has been one of the major class agents in modern cancer therapeutics, especially that blocks VEGF (now known as VEGF-A) signaling pathway³.

Angiogenesis inhibitors were initially expected to be free from the drug resistance issues that were typically shown in conventional chemotherapeutics, since the angiogenesis inhibitors target endothelial cells rather than genetically instable tumor cells⁴. In the clinic, angiogenesis inhibitors successfully arrested tumor growth during the initial treatment, but failed to produce constant clinical responses and eventually tumor relapsed. Although the underlying mechanisms of the acquired resistance against angiogenesis inhibitors are not entirely understood so far, several distinct mechanisms have been suggested. Unlike the conventional means of resistance against chemotherapeutic agents, which involves mutational alteration of the gene encoding a therapeutic target or the uptake and efflux of a drug^{5,6}, the adaptive resistance against angiogenesis inhibitors is acquired in tumors by variously employing evasive pathways during therapeutic blockade of angiogenesis⁷⁻¹¹.

Among the suggested mechanisms of the acquired resistance, the overexpression of alternative pro-angiogenic factors in the refractory tumor was considered significant^{8,11}. Many reports have demonstrated upregulation of pro-angiogenic factors including FGF1, FGF2, PDGF-A, PDGF-B, and PIGF when VEGF signaling pathway was blocked, which eventually led to regrowth of the tumors^{8,9,12}. Although VEGF plays the most predominant role in the tumor angiogenesis, many other pro-angiogenic factors are also involved¹. Therefore, the alternative pro-angiogenic factors upregulated from hypoxic tumor cells

could compensate the depleted VEGF signaling and provide evasive pathways for angiogenesis, resulting in regrowth of the tumor.

The coverage of tumor vasculatures by mural cells was also reported to be responsible for the resistance against angiogenesis inhibitors. The survival of the endothelium covered with pericytes is independent of VEGF, thus not affected by the depletion of VEGF¹¹. By contrast, the tumor vessels with inadequate pericyte coverage are more vulnerable to depletion of VEGF signaling^{13,14}. It has been demonstrated that pericytes support the endothelial survival in juxtacrine manner by expressing appreciable amount of VEGF and other factors crucial in the survival of the contacting endothelial cells^{15,16}. Moreover, pericytes attenuate the proliferation rate of endothelial cells and reduce their necessity of VEGF as a part of vessel stabilization process^{17,18}. Therefore, blocking only the VEGF signaling pathway is insufficient for an effective and enduring inhibition of tumor angiogenesis. Instead, blocking multiple factors involved in multiple stages of angiogenesis, from the initial robust angiogenic response to the maturation of the primitive vascular network, is deemed necessary to overcome the resistance and to inhibit tumor angiogenesis effectively.

To develop an angiogenesis inhibitor that could block multiple pro-angiogenic factors simultaneously, heparin is a promising lead compound, since it could intrinsically interact with various endogenous proteins including a broad range of pro-angiogenic factors¹⁹. For this purpose, a novel heparin-based anti-angiogenic agent, LHT7, was developed, which sodium taurocholates are chemically conjugated to LMWH²⁰. Such chemical modification of LMWH decreased binding affinity against ATIII but increased that against VEGF, resulting in a potent inhibition of tumor angiogenesis without any anticoagulant activity as discussed in the previous chapter.

This study shows that LHT7 could block FGF2 and PDGF-B in addition to VEGF. Both VEGF and FGF2 play significant roles in the initial angiogenic response, and PDGF-B is a key player of stabilizing primitive vascular network by recruiting mural cells to the endothelium^{1,11}. In purpose to evaluate the

multi-targeting effect of LHT7, various *in vitro* experiments that represent each stage of the angiogenic process were carried out. Also, the inhibitory effect of LHT7 on the multiple angiogenic signaling pathways was assessed at the molecular level shown by the reduction of receptor tyrosine phosphorylation of VEGFR2, FGFR1 and PDGFR β . Furthermore, since vascular normalization shown in tumors that were treated with VEGF blockers is closely related to stabilization of blood vessels by mural cells, it was evaluated whether vascular normalization also occurs when the tumor was treated with LHT7, which is a multi-targeted agent.

3.2. Materials and Methods

3.2.1. Cell lines

Human umbilical vein endothelial cells (HUVEC), human dermal microvascular endothelial cells (HDMEC) and human pericytes from placenta were purchased from PromoCell (Heidelberg, Germany). MDA-MB-231 cells were obtained from the American Type Culture Collection (ATCC; Manassas, VA). HUVECs and HDMECs were cultured in Endothelial Cell Growth Medium MV2 (ECGM; PromoCell). Pericytes and MDA-MB-231 cells were grown in Pericyte Growth Medium (PromoCell) and high-glucose Dulbecco's modified eagle medium (Gibco, Carlsbad, CA) supplemented with 10% fetal bovine serum (Gibco), respectively. The cells were maintained in a humidified 5% CO₂ atmosphere at 37°C.

3.2.2. Transwell chemotactic migration assay

To determine the effect of LHT7 on the migration of HUVECs, a cell migration assay was carried out as described previously²¹. Briefly, HUVECs were seeded on the 96-well transwell insert with 8- μ m pores (Corning, Tewksbury, MA) at 5×10^4 cells in 50 μ l of serum-free endothelial basal medium (EBM; PromoCell). VEGF₁₆₅ or FGF2 (R&D Systems, Minneapolis, MN) was prepared at a concentration of 100 ng/ml in serum-free EBM and were added to the receiver

plate at final volume of 150 μ l. LHT7 was added at a final concentration of 100 μ g/ml to the treatment group, and then the transwell insert was combined with the receiver plate. After 12 h of incubation, the receiver plate was replaced with another black receiver plate containing 100 μ l of cell dissociation solution (Trevigen, Gaithersburg, MD) containing Calcein AM (Molecular Probes, Eugene, OR) at final concentration of 2 μ g/ml to detach and stain. The combined plate was incubated for 1 h at 37°C and then the transwell insert was removed. The migrated cells were quantified with a microplate reader (Synergy HT; BioTek Instruments, Winooski, VT) through fluorescent top reading (485/520 nm).

3.2.3. MTT cytotoxicity assay

To evaluate the cytotoxicity of LHT7 on HUVECs and pericytes, MTT cytotoxicity assay was performed according to the standard procedure. MTT cell proliferation assay kit was purchased from Trevigen. HUVECs or pericytes were plated in 96-well culture plates at 5×10^4 cells per well in 100 μ l of ECGM or pericyte growth medium, respectively. After the incubation of the cells with various concentrations of LHT7 (0, 0.01, 0.1, and 1 mg/ml) for 24 h, 10 μ l of MTT reagent was added to each well, and the cells were further incubated for 3 h. When the purple precipitate was visible inside the cells, 100 μ l of detergent reagent was added to each well and kept in the dark for 2 h at room temperature. The absorbance was measured at 570 nm using a microplate reader (Synergy HT; BioTek Instruments) to measure the amount of viable cells.

3.2.4. HUVEC spheroid sprouting assay

To assess the effect of LHT7 on angiogenic sprouting, HUVEC spheroids were prepared as described previously²², and evaluated the sprouting from the spheroids with or without LHT7. Briefly, methocel solution was prepared by adding methylcellulose (Sigma-Aldrich) in ECGM at a final concentration of 1.2% w/v. Then the HUVECs were harvested, and resuspended at 1×10^7 cell/ml in ECGM. The cell suspension (100 μ l) was transferred to 20 ml of the

culture medium and well suspended. Then 5 ml of the prepared methocel solution was added to the cell suspension and mixed thoroughly. The cell suspension containing methocel solution was placed on a non-adherent square dish as droplets (25 μ l per droplet) and incubated upside down as hanging drops at 37°C for overnight in 100% humidity. The spheroids were collected by washing the dishes with the culture medium followed by centrifugation (3000 rpm, 15 min, 4°C), and resuspended in the collagen matrix, which was prepared as described elsewhere²³. The collagen matrix containing HUVEC spheroids was added to 96-well culture plate (50 μ l per well) and incubated at 37°C for 1 h to allow collagen to polymerize. Feeding medium containing 100 ng/ml of VEGF₁₆₅, FGF2, or a mixture of VEGF₁₆₅ and FGF2 (50 ng/ml each) in EBM was added to each well (200 μ l per well). For the treatment group, LHT7 was added to the feeding medium at a final concentration of 100 μ g/ml. After 48 h incubation, the spheroids were stained with Calcein AM (8 μ g/ml in EBM) according to the manufacturer's instruction. The spheroids were observed under fluorescence microscope (Eclipse TE2000-S; Nikon Instruments, Tokyo, Japan).

3.5.5. Endothelial tube formation assay

To determine the effect of LHT7 on HUVEC differentiation *in vitro*, a tube formation assay was performed as described previously²⁴. Briefly, Matrigel (BD Bioscience, San Jose, CA) was coated onto a 96-well culture plate by adding 48 μ l of chilled Matrigel to each well and incubating for 90 min at 37°C. The cultured HUVECs were harvested and resuspended at 1×10^6 cell/ml in EBM and plated on the matrigel coated dish at a density of 5×10^4 cells per well (50 μ l). VEGF₁₆₅, FGF2 (100 ng/ml), or a mixture of VEGF₁₆₅ and FGF2 (50 ng/ml each) was treated with or without LHT7 (100 μ g/ml), and incubated for 24 h at 37°C. Then the cells were stained by replacing the medium with HBSS containing Calcein AM (8 μ g/ml) followed by 30 min incubation, and observed under fluorescence microscope (Eclipse TE2000-S). The acquired images were analyzed with ImageJ angiogenesis analyzer for the quantification of degree of tube formation according to the earlier literature²⁵.

3.2.6. Matrigel plug angiogenesis assay

To assess the inhibitory effect of LHT7 on angiogenesis *in vivo*, a matrigel plug assay was performed as described elsewhere²⁶. Briefly, 500 μ l of Matrigel supplemented with VEGF₁₆₅, FGF2, or PDGF-B (500 ng/ml; R&D Systems) and with or without LHT7 (500 μ g/ml) was injected subcutaneously into the ventral side of a 6 week-old male C3H/HeN mice (n = 6). Matrigel supplemented with VEGF₁₆₅, FGF2, or PDGF-B containing anti-VEGF antibody (Bevacizumab; Roche), anti-FGF2 antibody (Abcam), or anti-PDGF-B antibody (Abcam), respectively, at final concentration of 100 μ g/ml, was implanted as inhibitor controls. For the FGF2 and PDGF-B combination group, 250 ng/ml of each growth factor was added to the matrigel. Matrigel without any growth factor or drug was implanted as a control. After 10 days, the matrigel plugs were isolated from the mice and observed.

3.2.7. Receptor tyrosine kinase phosphorylation studies

The tyrosine kinase phosphorylation level of VEGFR2, FGFR1, and PDGFR β was evaluated to determine the inhibitory effect of LHT7 at the molecular level. The effect of LHT7 on VEGFR2 or FGFR1 tyrosine phosphorylation stimulated by VEGF₁₆₅ or FGF2, respectively, was evaluated on HUVECs and HDMECs. The effect of LHT7 on PDGFR β tyrosine phosphorylation stimulated by PDGF-B was evaluated on pericytes. When at 80% confluence, the cells were starved for 24 h in a serum-free culture medium. Then, LHT7 or neutralizing antibodies were treated 30 min prior to the addition of the growth factor at a final concentration of 100 μ g/ml. The cells were then treated with the corresponding growth factor at a final concentration of 100 ng/ml and incubated for 5 min. The cells were immediately washed with ice-cold PBS and lysed with RIPA buffer containing protease and phosphatase inhibitors (Pierce, Rockford, IL). The samples were then subjected to Western blot analysis according to the standard procedure. Antibodies for pVEGFR2 (1:2000) and pPDGFR β (1:2000) were purchased from R&D Systems. Antibodies for VEGFR2 (1:1000), FGFR1

(1:1000), pFGFR1 (1:2000), and PDGFR β (1:1000) were from Cell Signaling Technology (Danvers, MA). The blotted membranes were developed using ImageQuant LAS 4000 imaging system (GE Healthcare Life Sciences, Uppsala, Sweden).

3.2.8. *In vitro* pericyte migration to endothelial tube

To determine the effect of LHT7 in pericyte coverage of endothelium *in vitro*, HUVECs were labeled with red CellTracker (Molecular Probes) according to the manufacturer's instructions. Then, endothelium tubes on a matrigel-coated 96-well culture plate were prepared as described earlier with the exception of using complete ECGM as the feeding medium. When endothelial tubes were completely formed after 24 h of the HUVEC seeding, the cells were washed gently with pre-warmed HBSS. Then pericytes were harvested, labeled with green CellTracker (Molecular Probes), and resuspended in serum-free EBM at 5×10^4 cell/ml. The pericyte suspension was transferred to each well at a density of 5×10^3 cells per well (100 μ l of the cell suspension). LHT7 or bevacizumab was treated at a final concentration of 100 μ g/ml for the drug treatment group. The cells were further incubated at 37°C and observed under fluorescence microscope (Eclipse TE2000-S) at 2 and 18 h of post-pericyte seeding.

3.2.9. *In vitro* pericyte-endothelium adhesion assay

To evaluate the effect of LHT7 on pericyte adhesion on endothelium, an *in vitro* adhesion assay was performed. HUVECs were plated on a 96-well culture plate 1×10^5 cells per well in 100 μ l ECGM and grown until the cells formed a confluent monolayer. The medium was replaced with serum-free EBM (50 μ l) with or without LHT7 (200 μ g/ml) and incubated for 30 min. Then, pericytes were labeled with green CellTracker (Molecular Probes) according to the manufacturer's instruction and adjusted to 1×10^5 cell/ml in the serum-free EBM. The pericyte suspension (50 μ l) was added to each well containing the endothelial monolayer, and further incubated for 3 h. Finally the wells were washed twice with pre-warmed PBS and fixed with 4% PFA. The samples were

observed under fluorescence microscope (Eclipse TE2000-S). The fluorescent image of the cell was acquired in the center of the well at $\times 40$ magnification for each well and the number of pericytes (red fluorescence) was counted using ImageJ software ($n = 3$ for each group).

3.2.10. Surface plasmon resonance (SPR) analysis

Biacore T100 (GE Healthcare, Waukesha, WI) was used for the SPR analysis. LHT7 was immobilized, which was adjusted to a level of 1,000 RU, on a sensor chip CM5 (GE Healthcare) by using the amide-coupling method. Recombinant human VEGF₁₆₅, FGF2, and PDGF-B were prepared at concentrations ranging from 0.001 to 10 $\mu\text{g/ml}$ in HBS-EP plus buffer (GE Healthcare), which was also used as a running buffer. The flow rate for the overall analysis was adjusted to 10 $\mu\text{l/min}$ and 50 mM NaOH was used for the regeneration of the sensor chip surface after each cycle of analysis. The analysis was done in triplicate and the data were processed using the BIAevaluation software (GE Healthcare).

3.2.11. Dynamic contrast enhanced magnetic resonance imaging

In 6 to 7-week-old female BALB/cSlc-nu mice, MDA-MB-231 cells (1×10^7) were inoculated subcutaneously into the bilateral flank of each mouse. When the tumor diameter reached 5 mm, LHT7 ($n = 3$, 5 mg/kg) or saline ($n = 3$, control) was administered daily intravenously. Dynamic contrast-enhanced magnetic resonance images (DCE-MRI) were obtained using a 3.0-T MR imaging system (Achieva; Philips Healthcare, Best, Netherlands) with the following parameters: TR, 20 ms; TE, 2.1 ms; flip angle, 30° ; FOV, $4.0 \times 4.0 \text{ cm}^2$; matrix size, 128×128 ; and number of repetition, 400. A contrast agent, Gd-DOTA (Guerbet, Villepinte, France), was injected as a bolus into the tail vein at a dose of 0.1 mmol/kg for 30 sec following the start of image acquisition. Based on DCE-MRI, a two-compartment model of Buckley was used for the analysis to measure the rate constants of Gd-DOTA from the extravascular extracellular space (EES) to plasma compartments (K_{ep}) and the elimination of

Gd-DOTA by the plasma (K_{ep}). The plasma concentration of Gd-DOTA was not directly measured in this pharmacokinetic model because the clearance rate (K_{el}) can be estimated from the measured tissue curve. Accordingly, a time-intensity curve was fitted with the following equation:

$$\frac{S(t)}{S(0)} = 1 + A^H K_{ep} \left(\frac{e^{-K_{ep}t} - e^{-K_{el}t}}{K_{el} - K_{ep}} \right)$$

,where $S(0)$ is the signal intensity before contrast injection and $S(t)$ is the signal intensity at a certain time t . From this fitting, four perfusion-related parameters were estimated as follows: K_{ep} , which is the efflux rate constant from extravascular extracellular space to blood plasma indicating the permeability; K_{el} , which indicates the first-order rate constant for the elimination of contrast agent from the blood plasma; initial slope, which indicates the differential at the onset of the exponential curve; and K^{trans} , which is a volume transfer constant of contrast agent between blood plasma and the extravascular extracellular space, to determine vascular permeability.

3.2.12. Statistical analysis

Data were analyzed using unpaired one-tailed Mann-Whitney test or Kruskal-Wallis non-parametric ANOVA followed by the Dunn's multiple comparisons test. The GraphPad Prism version 6.0c (GraphPad Software, San Diego, CA) was used for the statistical calculations. P value less than 0.05 was considered statistically significant.

3.3. Results

3.3.1. HUVEC migration inhibitory effect and cytotoxicity evaluation of LHT7

A set of *in vitro* experiments that represent several phases of the initial angiogenic response was carried out on HUVECs. The inhibitory effect of LHT7 on the chemotactic migration of HUVECs stimulated by VEGF or FGF2 was evaluated through a transwell chemotactic migration assay (also known as modified Boyden chamber assay). Both VEGF and FGF2 stimulated the

migration of HUVECs, whereas VEGF was a more potent stimulator than FGF2. In the presence of LHT7, the cell migration induced by VEGF or FGF2 was significantly inhibited and the number of the migrated cells was decreased by 46% and 29%, respectively, compared to the control (**Fig. 3.1A**). To clarify that the inhibition of cell migration by LHT7 was not associated with any cytotoxicity of LHT7, MTT cytotoxicity assay of LHT7 was performed on HUVECs. The result showed no significant cytotoxic effect of LHT7 on HUVECs at concentrations up to 1 mg/ml, which was ten-fold higher concentration than that used throughout the *in vitro* studies (**Fig. 3.1B**). This manifested that LHT7 inhibited the migration of HUVECs by suppressing the chemotaxis stimulated by VEGF and/or FGF2, not by affecting the cell viability.

3.3.2. Inhibitory effect of LHT7 in endothelial sproutings

The HUVEC spheroids were prepared to determine the effect of LHT7 in angiogenic sprouting from the spheroids in 3D culture environment *in vitro*, which mimics the vessel sprouting from the pre-existing vasculatures during the initial robust angiogenic response (**Fig. 3.1C**). Both VEGF and FGF2 induced marked endothelial sprouting from the spheroids at 48 hour of post-treatment, showing intensive branching of endothelium from the spheroid cores. However, simultaneous treatment of LHT7 significantly inhibited the sprouting stimulated by VEGF or FGF2, and almost no branching of the endothelium was observed. Since simultaneous treatment of VEGF and FGF2 have been reported to show an angiogenic synergism²⁷, it was further assessed whether LHT7 could also suppress the angiogenic sprouting stimulated by the treatment of the both pro-angiogenic factors. Indeed, when VEGF and FGF2 were treated at the same time, the HUVEC spheroids showed the most robust sprouting among all of the tested groups. Nevertheless, treatment of LHT7 effectively inhibited the sprouting induced by the both pro-angiogenic factors and showed that LHT7 could suppress the activity of VEGF and FGF2 at the same time.

3.3.3. Inhibitory effect of LHT7 in endothelial tubular differentiation

Endothelial tube formation assay with HUVECs was carried out, which represents the endothelial differentiation *in vitro*. VEGF and FGF2 were used as the stimulators for the endothelial tube formation. As shown in **Fig. 3.2A**, the two pro-angiogenic factors strongly stimulated the tube formation individually or together. In particular, the simultaneous treatment of the both pro-angiogenic factors induced the highest degree of the tube formation. However, LHT7 treatment to the HUVECs significantly inhibited the tube formation induced by VEGF, FGF2, and combination of the both pro-angiogenic factors, showing 91%, 88%, and 87% decreased number of nodes compared to the positive controls, respectively. The tubular structure of each group was quantified using ImageJ (**Fig. 3.2B**).

3.3.4. Inhibitory effect of LHT7 in the angiogenesis induced by VEGF and FGF2 in matrigel plugs

The inhibitory effect of LHT7 in the angiogenesis induced by VEGF and FGF2 was evaluated *in vivo* by matrigel plug angiogenesis assay (**Fig. 3.3A**). When isolated after two weeks of implantation, the matrigel plugs supplemented with VEGF or FGF2 showed high degree of angiogenesis represented by the bloody red color of the plugs, while non-supplemented matrigel plugs showed no occurrence of the angiogenesis. However, addition of LHT7 to the matrigel plugs significantly inhibited angiogenesis that were induced by supplementation of the either of VEGF and FGF2. The inhibitory effect shown by LHT7 was similar to that shown by the neutralizing antibodies to the corresponding pro-angiogenic factors, showing only pale red color in the plugs. This result showed that LHT7 effectively suppressed the VEGF and FGF2-mediated angiogenesis *in vivo*.

3.3.5. VEGF-VEGFR2 and FGF2-FGFR1 signaling pathway blockade by LHT7

The inhibition of VEGF-VEGFR2 and FGF2-FGFR1 signaling pathway by LHT7 was evaluated at molecular level by determining the level of the receptor tyrosine phosphorylation of VEGFR2 and FGFR1, which are the major receptors involved in the initial stage of angiogenesis mediated by VEGF and FGF2, respectively. Two different types of endothelial cells – HUVECs and HDMECs – were used. The cells were initially exposed to LHT7 followed by addition of VEGF or FGF2, and then subjected to a standard procedure of western blot.

The treatment of VEGF without pretreatment of LHT7 resulted in potent stimulation of VEGFR2 tyrosine phosphorylation in both HUVEC and HDMEC cells. However, when the cells were treated with LHT7 in advance of VEGF stimulation, significantly lower degree of VEGFR2 phosphorylation was detected, indicating evident inhibition of the tyrosine phosphorylation by LHT7. The inhibitory effect shown by LHT7 treatment was comparable to that of anti-VEGF antibody (**Fig. 3.3B**).

Similar inhibitory effect was shown in the FGF2-FGFR1 signaling axis when the cells were treated with LHT7. When the cells were stimulated with FGF2, there were significant amount of phosphorylated FGFR1 detected. However, treatment of LHT7 effectively inhibited the FGFR1 tyrosine phosphorylation stimulated by FGF2 in the both cells. The inhibitory effect of LHT7 in the FGFR1 tyrosine phosphorylation was similar to that of anti-FGF2 antibody (**Fig. 3.3C**). These results clearly showed that the inhibitory effect of LHT7 on initial angiogenic responses that were described above was due to the blockade of VEGF and FGF2 signaling pathways.

The interaction studies between LHT7 and VEGF or FGF2 using surface plasmon resonance (SPR) showed that LHT7 bound to the both pro-angiogenic factors at nano- to micromolar range of binding affinity (**Table 3.1**), suggesting that LHT7 blocked the downstream signaling of the VEGF and FGF2 signaling pathway by binding to the VEGF and FGF2.

3.3.6. Inhibitory effect of LHT7 on pericyte recruitment to endothelium linings

To determine whether LHT7 could block the maturation of the primitive blood vessels, an *in vitro* experiment that mimics the vascular maturation was designed and carried out as follows: first, well-formed endothelial tubes were prepared on matrigel, which represent the primitive vessel network; the culture medium was then replaced with serum-free medium; the human pericytes from placenta (hereafter, pericytes) were added with or without LHT7 (**Fig. 3.4A**).

In the control group, most of the seeded pericytes were recruited around the established endothelial tubes within two hours. After 18 hours, although the appearance of the endothelial tube network was altered, the tubular structures were well maintained with the pericytes adhered to the tubes.

In the presence of LHT7, however, the number of pericytes recruited around the endothelial tubes was significantly decreased and the pericytes were randomly distributed within the observed frame when observed after two hours from the pericyte addition. After 18 hours, most of the endothelial tubes were collapsed and few tubes remained. In contrast, anti-VEGF monoclonal antibody showed no influence in the migration of pericytes towards the endothelial tubes when observed at two hours of post-pericyte addition, and showed random distribution of the pericytes similar to that of the control group. Consequently, after 18 hours, higher extent of the tubes remained when compared to the LHT7-treated group. The endothelial tubes of the each group after 18 hours of pericyte addition were quantified using the ImageJ angiogenesis analyzer and the number of nodes and branches was calculated (**Fig. 3.4B**). The results showed that the LHT7-treated group had the calculated mean number of nodes and branches of the endothelial tubes decreased by 67% and 54%, whereas the anti-VEGF antibody-treated group decreased by 15% and 8% compared to control, respectively. According to the results, blocking only the VEGF had no significant effect in the regression of the endothelial tubes that are accompanied

by pericytes. On the other hand, treatment of LHT7 effectively regressed the tubes.

3.3.7. Determination of cytotoxicity on pericytes and possible effects in the endothelial cell and pericyte adhesion of LHT7

The cytotoxic effect of LHT7 was evaluated on pericytes to determine whether the inhibition of the pericyte recruitment to the endothelial tubes was possibly due to the cytotoxic effect of LHT7. In the MTT cytotoxicity assay, LHT7 did not affect the viability of the pericytes at concentrations up to 1 mg/ml, which was ten-fold higher concentration than that used in the study described above (**Fig. 3.4C**). This result supported that the inhibition of pericyte recruitment to endothelial tubes was not related to the viability of the pericytes when LHT7 was treated.

Since heparin has been recognized to affect cell-to-cell adhesion by modulating the activity of integrin²⁸, it was further determined whether LHT7 affected the direct cell-to-cell interaction between HUVECs and pericytes. The experiment was carried out by establishing a HUVEC monolayer on the cell culture dish followed by addition of pericytes with or without LHT7. The adhesion assay showed no significant difference in the number of pericytes adhered to the HUVEC monolayer between the control and LHT7-treated group (**Fig. 3.4D**), implying that LHT7 inhibited the migration, rather than affecting the adherence of pericytes to the endothelium.

3.3.8. Inhibitory effect of LHT7 on PDGF-B-induced angiogenesis in matrigel plugs

PDGF-B is one of the major chemotactic driving forces for pericytes to recruit around the established endothelial vessels²⁹. To determine the effect of LHT7 on PDGF-B signaling pathway, an *in vivo* matrigel plug assay was performed using PDGF-B as a stimulant. PDGF-B induced moderate angiogenesis in the matrigel, whereas treatment of LHT7 in the matrigel significantly inhibited angiogenesis in the gel (**Fig. 3.5A**). The inhibitory effect of LHT7 in PDGF-B-induced angiogenesis in the matrigel was comparable to that of the neutralizing

antibody of PDGF-B. However, PDGF-B is not an initiator of angiogenesis and the potency of stimulating angiogenesis is relatively weaker than other major pro-angiogenic factors, such as VEGF or FGF2. Previous study has reported that combination of PDGF-B and FGF2 could synergistically induce a strong angiogenic response and form stable vascular networks³⁰. In this reason, the inhibitory effect of LHT7 on angiogenesis that was stimulated by combination of PDGF-B and FGF2 was determined. When matrigel plugs containing both PDGF-B and FGF2 were implanted in mice, an intensive angiogenic response was observed in the plugs. The treatment of LHT7, however, effectively inhibited the angiogenesis that was induced by the combination of PDGF-B and FGF2.

3.3.9. PDGFB-PDGFR β signaling pathway blockade by LHT7

The inhibition of PDGFB-PDGFR β signaling pathway by LHT7 was evaluated at molecular level by determining the level of the receptor tyrosine phosphorylation of PDGFR β , which are the major receptors involved in the late stage of angiogenesis mediated by PDGF-B (**Fig. 3.5B**). PDGFR β is abundantly expressed on pericytes, which surround the capillary endothelium and have been recognized to play a pivotal role in stabilizing the primitive vascular networks³¹. Treatment of pericytes with PDGF-B resulted in potent stimulation of PDGFR β tyrosine phosphorylation. However, treatment of the cells with LHT7 in advance of PDGF-B stimulation showed evident inhibition of the tyrosine phosphorylation of PDGFR β . The inhibitory effect shown in the result was similar to that of the neutralizing antibody of PDGF-B. The interaction studies between LHT7 and PDGF-B using surface plasmon resonance (SPR) showed micromolar range of binding affinity (**Table 3.1**), indicating that LHT7 bound to the PDGF-B.

3.3.10. Characterization of tumor vasculatures in LHT7-treated tumor-bearing animals using DCE-MRI

The tumor blood vessels were characterized *in vivo* after treatment of LHT7 to the animals. Four different kinetic parameters were derived from the DCE-MRI results: K^{trans} is the volume transfer constant between blood plasma and extravascular extracellular space (EES); K_{ep} is the rate constant between EES and blood plasma; initial slope is the differential at the onset of the exponential curve of contrast agents in the tissue of interest; K_{el} is the first-order rate constant for the elimination of contrast agents from the tissue of interest.

The tumor growth was effectively suppressed by the LHT7 treatment (**Fig. 3.6A**) without any decrease in body weight (**Fig. 3.6B**) in the current experimental animal models that were subjected to the DCE-MRI, indicating successful tumor angiogenesis inhibition without any significant toxic effects to the animals. K^{trans} (**Fig. 3.6C**) and K_{ep} (**Fig. 3.6D**), which represent the permeability of the vessel wall, showed no significant difference between the control and the LHT7-treated group. This indicated that the LHT7 treatment did not affect the property of the tumor vessel wall in terms of the permeability.

On the other hand, the initial slope, which represents the influx of the blood into the tumor, was higher in the control group than the LHT7-treated group at the last day of the observation, indicating retarded blood influx in the treatment group (**Fig. 3.6E**). This result was further supported by the gradual decrease of the K_{el} , which represents the blood perfusion, during the treatment of LHT7, which the decrease was not observed in the control group (**Fig. 3.6F**).

Table 3.1. Dissociation constants of LHT7 on VEGF, FGF2 or PDGF-B

	VEGF	FGF2	PDGF-B
K_D (μM)	0.412 ± 0.106	1.53 ± 0.43	0.971 ± 0.231

Data presented as means \pm s.d.

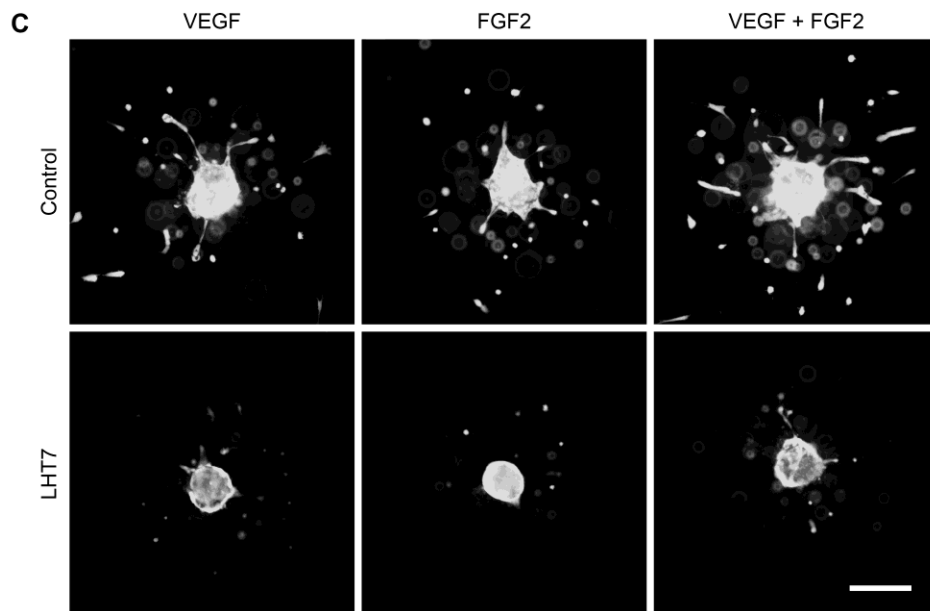
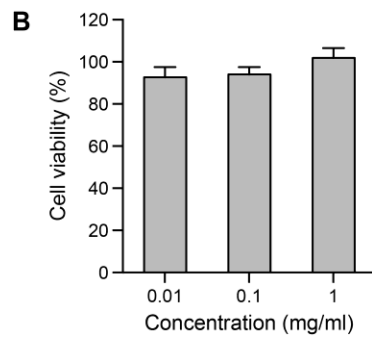
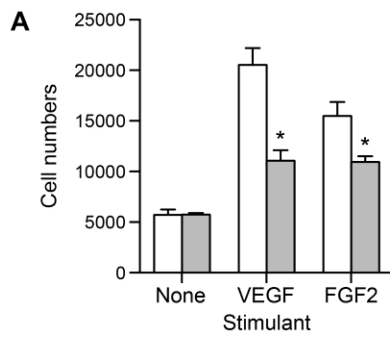


Figure 3.1. (A) Transwell chemotactic cell migration of HUVECs induced by VEGF or FGF2. Degree of migration in control (white) and LHT7-treated group (black) was assessed. (B) Cytotoxicity evaluation of LHT7 on HUVECs by using MTT cell proliferation assay at a concentration range of 0.01 to 1 mg/ml. (C) Representative images of VEGF and/or FGF2-induced angiogenic sprouting of HUVEC spheroid of control and LHT7-treated groups. Scale bar, 50 μ m.

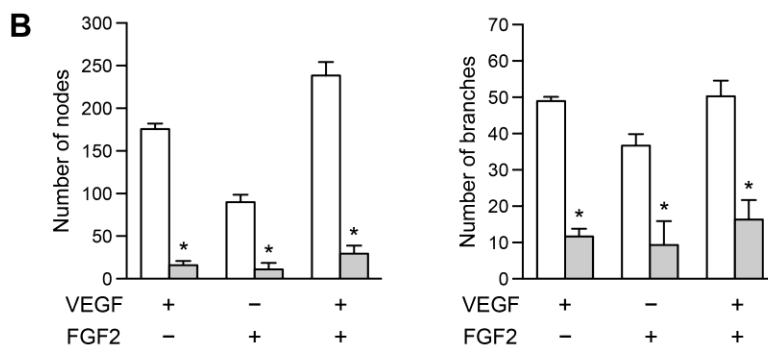
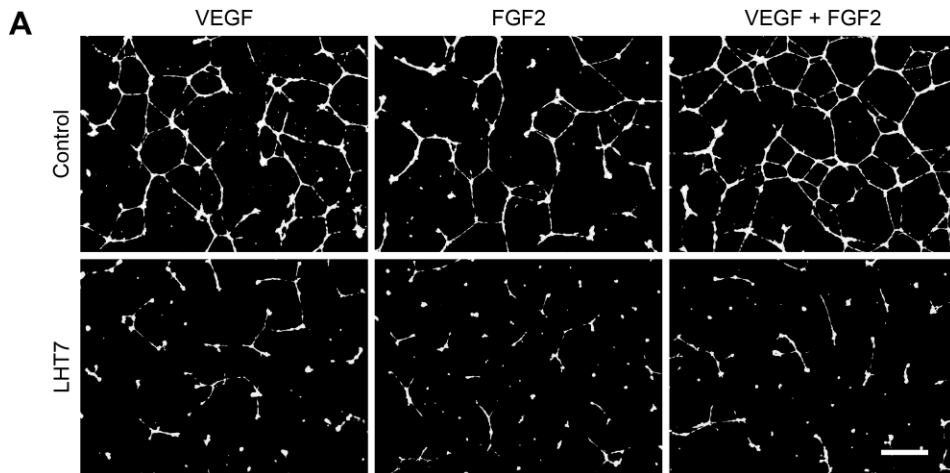


Figure 3.2. (A) HUVEC tube formation induced by VEGF and/or FGF2. HUVECs were stained in green fluorescence. Scale bar, 500 μm . (B) Quantitative analysis of HUVEC tubes by ImageJ angiogenesis analyzer. Number of nodes (left panel) and branches (right panel) of control (empty column) and LHT7 treated group (filled column) were calculated. $*P < 0.05$ versus control. Data are presented as mean \pm s.d.

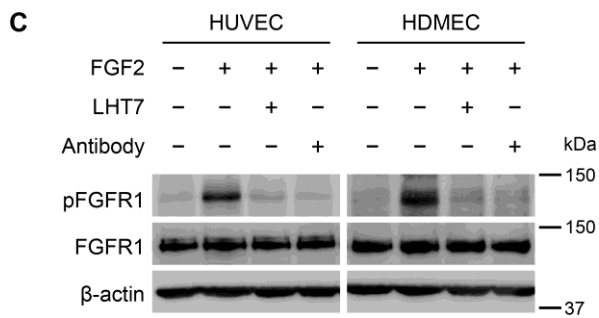
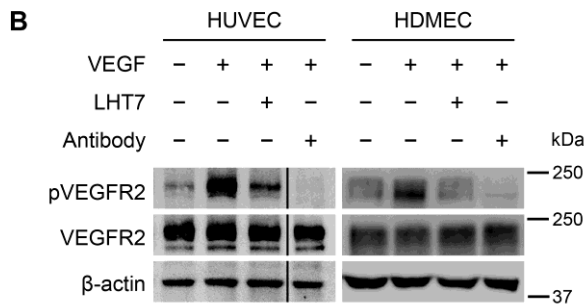
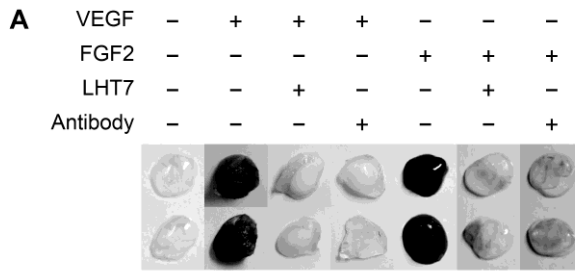


Figure 3.3. (A) *In vivo* matrigel plug angiogenesis assay using VEGF or FGF2 as an angiogenic stimulator. The inhibition of phosphotyrosine level of VEGFR2 stimulated by VEGF (B) and FGFR1 stimulated by FGF2 (C) on HUVECs (left) and HDMECs (right) by LHT7 are shown by immunoblots.

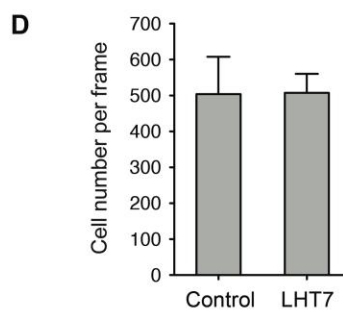
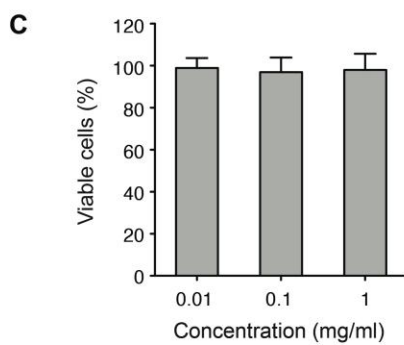
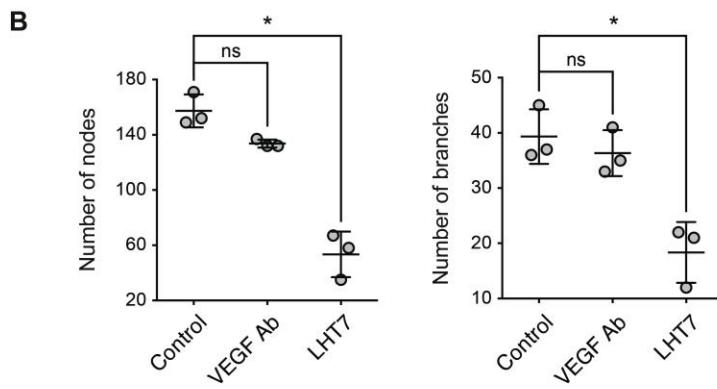
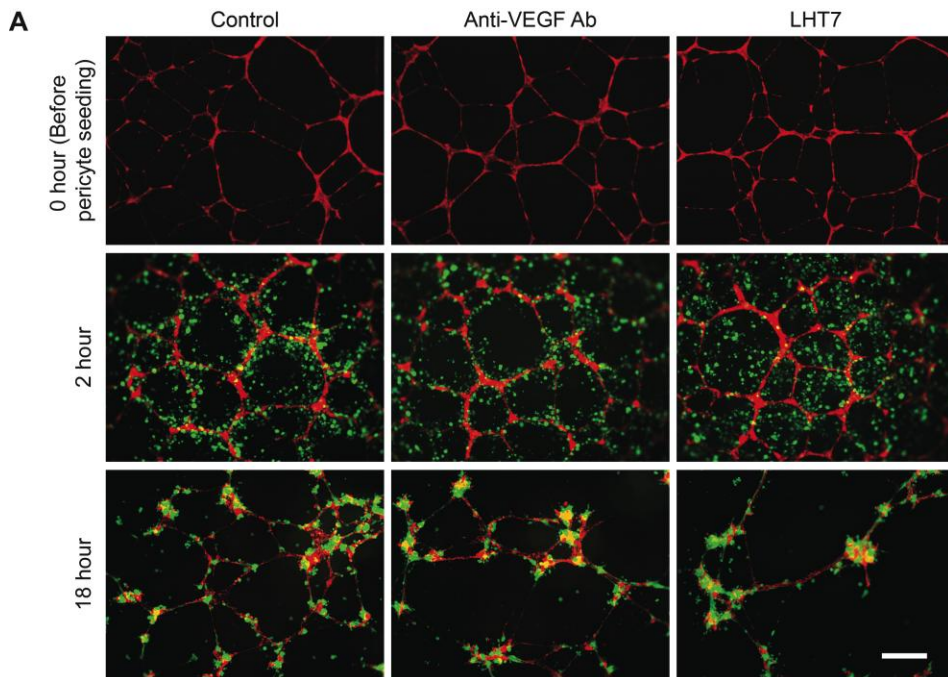


Figure. 3.4. Representative images of HUVECs (red) and pericytes (green) coculture system *in vitro*. (A) Pericytes were seeded after endothelial tubes were formed. Recruitment of pericytes to HUVEC tubes in control, anti-VEGF mAb, and LHT7-treated groups were observed after 2 h and 18 h of pericyte addition. Scale bars, 500 μ m. (B) Quantitative analysis of remaining endothelial tubes after 18 h of pericyte addition by ImageJ angiogenesis analyzer. Number of nodes (left panel) and branches (right panel) were calculated and shown as means \pm s.d. with individual plot. * $P < 0.05$ versus control. (C) Cytotoxic effect of LHT7 evaluated by MTT assay at a concentration range of 0.01 to 1 mg/ml. (D) Pericytes adhesion on confluent HUVEC monolayer. Single image was obtained in the center of the each well (n = 3) at 40x magnification and number of the adhered pericytes were counted and averaged. Data are expressed as means \pm s.d.

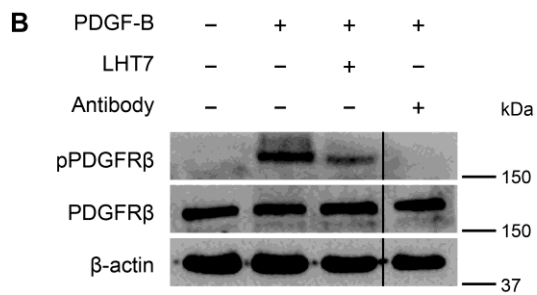
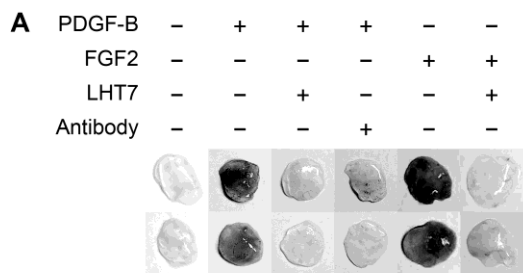


Figure 3.5. (A) *In vivo* matrigel plug angiogenesis assay using PDGF-B and PDGF-B/FGF2 mixture as angiogenic stimulators. (B) Western blots of phosphotyrosine level of PDGFR β on pericytes stimulated by PDGF-B in the presence or absence of LHT7 or neutralizing antibody.

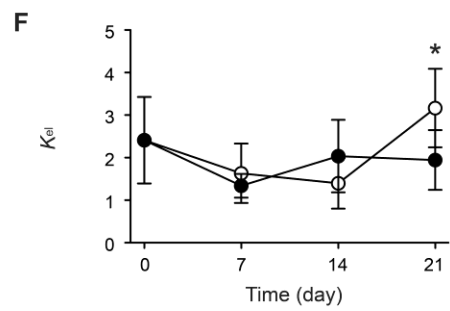
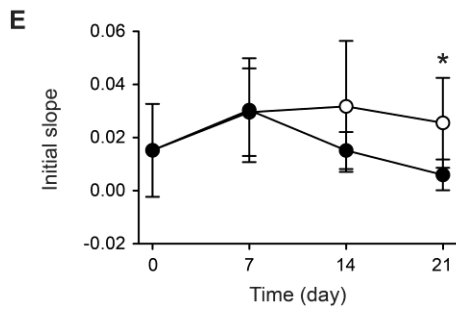
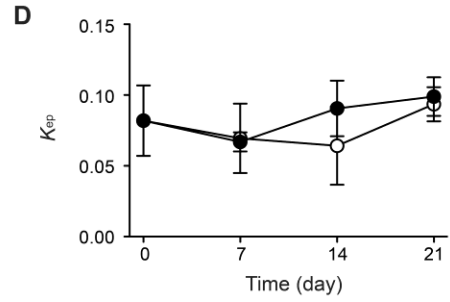
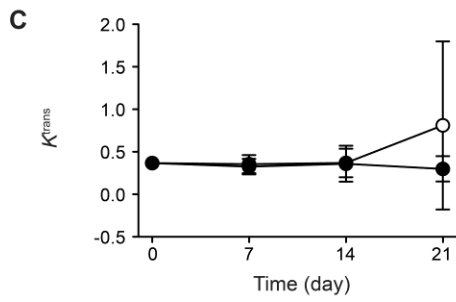
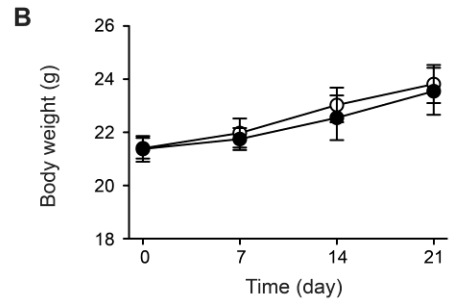
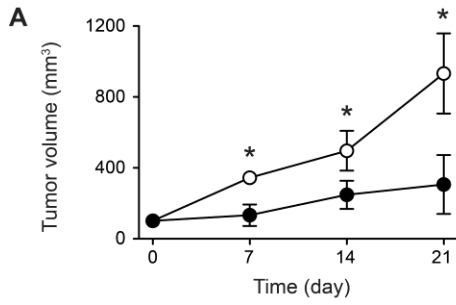


Figure 3.6. MDA-MB-231 tumor-bearing mice were treated with LHT7 at a dose of 5 mg/kg intravenously daily for three weeks (●) and compared with control (○). Tumor growth (A) and body weight (B) change were measured. DCE-MRI parameters were measured during the treatment at day 0, 7, 14 and 21. The values of K_{trans} (C), K_{ep} (D), initial slope (E), and K_{el} (F) were calculated. $n = 3$. Data are expressed as mean \pm s.d. * $P < 0.05$ versus control.

3.4. Discussion

The present study demonstrates that LHT7 could inhibit multiple stages of angiogenesis by blocking the pro-angiogenic factors that are involved in the initial robust angiogenesis (i.e. VEGF and FGF2) as well as the stabilization of the primitive endothelial vessel network (i.e. PDGF-B), ultimately leading to a potent suppression of tumor growth in xenograft animal models.

The early stage angiogenesis, which produces immature endothelial vascular networks, is accomplished by recruitment, migration, differentiation of progenitor endothelial cells, and angiogenic sprouting from the pre-existing blood vessels³². LHT7 significantly inhibited these processes that were stimulated by VEGF and FGF2 *in vitro*. Inhibitory effects of LHT7 on VEGF and FGF2 were further supported at the molecular level: western blot results showed that LHT7 blocked the tyrosine kinase phosphorylation of VEGFR2 and FGFR1 stimulated by VEGF and FGF2, respectively. SPR binding analysis showed that LHT7 bound to VEGF and FGF2, indicating that LHT7 blocked the two pro-angiogenic factors and inhibited their downstream signalings. Previous study has reported that these pro-angiogenic factors have synergistic effect on stimulating angiogenesis²⁷, which was also observed in our *in vitro* studies. Moreover, FGF2 is reported to induce VEGF expression in endothelial cells through autocrine and paracrine manner³³. Therefore, blocking FGF2 in addition to VEGF is essential to disrupt the interconnection between these two pro-angiogenic factors and effectively inhibit the early stage angiogenesis.

It was also shown that LHT7 blocked the maturation of primitive endothelial vessels *in vitro*. Pericytes promote endothelial cell survival by producing VEGF that acts in a juxtacrine manner¹⁶ and by inducing anti-apoptotic protein Bcl-w in the endothelial cells³⁴. The blockade of VEGF did not affect the pericyte recruitment to the endothelial tubes. LHT7, however, inhibited the migration of pericytes towards the tubes, thereby blocking the juxtacrine crosstalk between pericytes and HUVECs, leading to regression of the endothelial tubes.

The paracrine signaling via PDGF-B, which is expressed by endothelial cells, plays a central role in the recruitment of pericytes to the endothelium³⁵. Therefore, the effect of LHT7 on PDGF-B signaling pathway was further investigated. The *in vivo* matrigel plug assay showed that PDGF-B-induced angiogenesis was significantly inhibited in the presence of LHT7. Moreover, LHT7 was also capable of inhibiting the angiogenesis in matrigel that was stimulated by combination of PDGF-B and FGF2, which showed more intensive angiogenesis than by PDGF-B alone. These results were further supported by the decreased tyrosine kinase phosphorylation level of PDGFR β stimulated by PDGF-B in the presence of LHT7.

The intimate interconnection among VEGF, FGF2, and PDGF-B postulates the significance of blocking PDGF-B signaling pathway besides VEGF and FGF2. PDGF-B synergistically stimulates angiogenesis with FGF2³⁰ and also upregulates the expression of FGF2 and VEGF³⁶. For this reason, blocking of PDGF-B is not only critical for inhibiting late stage angiogenesis, but also for early stage angiogenesis. Moreover, VEGF is reported as a negative regulator of vessel maturation, hence blockade of VEGF could facilitate the maturation of vessels, which in turn become insensitive to VEGF inhibition^{11,37}. Therefore, VEGF blockade should be accompanied by PDGF-B blockade to suppress vessel maturation and inhibit tumor angiogenesis effectively. The benefit of blocking VEGF and PDGF-B simultaneously was also demonstrated in a previous study¹³.

Our findings also showed that LHT7 did not induce vascular normalization in tumor blood vessels. Many studies have reported vascular normalization, defined as a structural and functional improvement of the generally abnormal tumor vasculatures during VEGF blockade, which shares lot of similarities with the vascular maturation³⁸. Because PDGF-B is a key regulator in the vascular maturation³², it was hypothesized that treatment of LHT7 would not induce vascular normalization unlike VEGF blockers. To address this question, the tumor vasculatures were observed via DCE-MRI *in vivo*. During three-week treatment of LHT7, permeability of the blood vessels showed no difference,

whereas perfusion throughout the tumor was significantly decreased when compared to the control. The results showed that LHT7 regressed blood vessels in the tumor without going through vascular normalization, implying that LHT7 negatively affected vascular maturation *in vivo*.

Collectively, it was shown that LHT7 could block not only VEGF, but also FGF2 and PDGF-B signaling pathways. It is indisputable that VEGF is a key regulator of angiogenesis³⁹. However, because the aforementioned three pro-angiogenic factors are intimately interconnected to each other, simultaneous inhibition of the three pro-angiogenic factors is likely to inhibit angiogenesis more effectively than blocking only one or two of those. In addition, tumor vasculatures are heterogeneous and presented in various stages of angiogenesis in a single tumor tissue. Therefore, blocking pro-angiogenic factors that are involved in the different stages of angiogenesis is crucial for successful and enduring angiogenesis inhibition. Previous studies have also reported on the efficacy of multiple signaling pathway inhibition by using single or multiple small molecule kinase inhibitors^{13,40}. Despite the therapeutic efficacy of the small molecule kinase inhibitors, however, they exhibited limitations including off-target effect such as cardiotoxicity⁴¹. In addition, since a single pro-angiogenic factor could interact with several receptors (e.g. VEGF on VEGFR1 and VEGFR2), blocking the pro-angiogenic factors could be more effective than blocking the receptor kinases.

Besides the therapeutic benefits of inhibiting multiple pro-angiogenic pathways, there is another advantage that is critical for successful anti-angiogenic therapy. Recent studies have shown that the clinical benefits of VEGF blockers are only transient in many patients. Many reports have demonstrated substantial number of evidences that the evasion of VEGF blockade is due to the upregulation of other pro-angiogenic factors such as FGF2 or PDGF-B, providing alternative pathways to stimulate angiogenesis. Moreover, maturation of primitive vasculatures by pericyte coverage has been also recognized to contribute to the resistance against angiogenesis inhibitors¹¹. Therefore, simultaneous inhibition of angiogenic pathways that are involved in

multiple-stages of angiogenesis would potentially overcome such resistance issue.

3.5. Conclusion

In the aspect of increasing therapeutic efficacy and overcoming the acquired resistance, targeting VEGF, FGF2 and PDGF-B at the same time is critical for successful inhibition of tumor angiogenesis. Despite the chemical modification of heparin, LHT7 retained the capacity of heparin to bind with VEGF, FGF2 and PDGF-B, and showed excellent inhibitory effect on their signaling pathways. Thus, LHT7 would potentially overcome the resistance and effectively inhibit angiogenesis as well as tumorigenesis. It was also confirmed that heparin is an excellent lead compound to develop multi-targeted agent due to its inherent capability to interact with broad range of pro-angiogenic factors.

References

- 1 Carmeliet, P. & Jain, R. K. Angiogenesis in cancer and other diseases. *Nature* **407**, 249-257 (2000).
- 2 Hanahan, D. & Weinberg, R. A. The hallmarks of cancer. *Cell* **100**, 57-70 (2000).
- 3 Folkman, J. Angiogenesis: an organizing principle for drug discovery? *Nat Rev Drug Discov* **6**, 273-286 (2007).
- 4 Boehm, T., Folkman, J., Browder, T. & O'Reilly, M. S. Antiangiogenic therapy of experimental cancer does not induce acquired drug resistance. *Nature* **390**, 404-407 (1997).
- 5 Gorre, M. E. & Sawyers, C. L. Molecular mechanisms of resistance to STI571 in chronic myeloid leukemia. *Curr Opin Hematol* **9**, 303-307 (2002).
- 6 O'Connor, R., Clynes, M., Dowling, P., O'Donovan, N. & O'Driscoll, L. Drug resistance in cancer - searching for mechanisms, markers and therapeutic agents. *Expert Opin Drug Metab Toxicol* **3**, 805-817 (2007).
- 7 Kerbel, R. S., Yu, J., Tran, J., Man, S., Vilorio-Petit, A., Klement, G., Coomber, B. L. & Rak, J. Possible mechanisms of acquired resistance to anti-angiogenic drugs: implications for the use of combination therapy approaches. *Cancer Metastasis Rev* **20**, 79-86 (2001).

- 8 Casanovas, O., Hicklin, D. J., Bergers, G. & Hanahan, D. Drug resistance by evasion of antiangiogenic targeting of VEGF signaling in late-stage pancreatic islet tumors. *Cancer Cell* **8**, 299-309 (2005).
- 9 Kerbel, R. S. Therapeutic implications of intrinsic or induced angiogenic growth factor redundancy in tumors revealed. *Cancer Cell* **8**, 269-271 (2005).
- 10 Shojaei, F., Wu, X., Malik, A. K., Zhong, C., Baldwin, M. E., Schanz, S., Fuh, G., Gerber, H. P. & Ferrara, N. Tumor refractoriness to anti-VEGF treatment is mediated by CD11b+Gr1+ myeloid cells. *Nat Biotechnol* **25**, 911-920 (2007).
- 11 Bergers, G. & Hanahan, D. Modes of resistance to anti-angiogenic therapy. *Nat Rev Cancer* **8**, 592-603 (2008).
- 12 Fernando, N. T., Koch, M., Rothrock, C., Gollogly, L. K., D'Amore, P. A., Ryeom, S. & Yoon, S. S. Tumor escape from endogenous, extracellular matrix-associated angiogenesis inhibitors by up-regulation of multiple proangiogenic factors. *Clin Cancer Res* **14**, 1529-1539 (2008).
- 13 Bergers, G., Song, S., Meyer-Morse, N., Bergsland, E. & Hanahan, D. Benefits of targeting both pericytes and endothelial cells in the tumor vasculature with kinase inhibitors. *J Clin Invest* **111**, 1287-1295 (2003).
- 14 Benjamin, L. E., Hemo, I. & Keshet, E. A plasticity window for blood vessel remodelling is defined by pericyte coverage of the preformed endothelial network and is regulated by PDGF-B and VEGF. *Development* **125**, 1591-1598 (1998).
- 15 Song, S., Ewald, A. J., Stallcup, W., Werb, Z. & Bergers, G. PDGFRbeta+ perivascular progenitor cells in tumours regulate pericyte differentiation and vascular survival. *Nat Cell Biol* **7**, 870-879 (2005).
- 16 Darland, D. C., Massingham, L. J., Smith, S. R., Piek, E., Saint-Geniez, M. & D'Amore, P. A. Pericyte production of cell-associated VEGF is differentiation-dependent and is associated with endothelial survival. *Dev Biol* **264**, 275-288 (2003).
- 17 Orlidge, A. & D'Amore, P. A. Inhibition of capillary endothelial cell growth by pericytes and smooth muscle cells. *J Cell Biol* **105**, 1455-1462 (1987).
- 18 Hirschi, K. K. & D'Amore, P. A. Control of angiogenesis by the pericyte: molecular mechanisms and significance. *EXS* **79**, 419-428 (1997).
- 19 Sasisekharan, R., Shriver, Z., Venkataraman, G. & Narayanasami, U. Roles of heparan-sulphate glycosaminoglycans in cancer. *Nat Rev Cancer* **2**, 521-528 (2002).
- 20 Lee, E., Kim, Y. S., Bae, S. M., Kim, S. K., Jin, S., Chung, S. W., Lee, M., Moon, H. T., Jeon, O. C., Park, R. W., Kim, I. S., Byun, Y. & Kim, S. Y. Polyproline-type helical-structured low-molecular weight heparin (LMWH)-taurocholate conjugate as a new angiogenesis inhibitor. *Int J Cancer* **124**, 2755-2765 (2009).

- 21 Senger, D. R., Perruzzi, C. A., Streit, M., Koteliansky, V. E., de Fougères, A. R. & Detmar, M. The $\alpha 1\beta 1$ and $\alpha 2\beta 1$ Integrins Provide Critical Support for Vascular Endothelial Growth Factor Signaling, Endothelial Cell Migration, and Tumor Angiogenesis. *Am J Pathol* **160**, 195-204 (2002).
- 22 Laib, A. M., Bartol, A., Alajati, A., Korff, T., Weber, H. & Augustin, H. G. Spheroid-based human endothelial cell microvessel formation in vivo. *Nat Protoc* **4**, 1202-1215 (2009).
- 23 Bayless, K. J., Kwak, H. I. & Su, S. C. Investigating endothelial invasion and sprouting behavior in three-dimensional collagen matrices. *Nat Protoc* **4**, 1888-1898 (2009).
- 24 Arnaoutova, I. & Kleinman, H. K. In vitro angiogenesis: endothelial cell tube formation on gelled basement membrane extract. *Nat Protoc* **5**, 628-635 (2010).
- 25 Carpentier, G. Contribution: angiogenesis analyzer. *ImageJ News* (2012).
- 26 Prewett, M., Huber, J., Li, Y., Santiago, A., O'Connor, W., King, K., Overholser, J., Hooper, A., Pytowski, B., Witte, L., Bohlen, P. & Hicklin, D. J. Antivascular endothelial growth factor receptor (fetal liver kinase 1) monoclonal antibody inhibits tumor angiogenesis and growth of several mouse and human tumors. *Cancer Res* **59**, 5209-5218 (1999).
- 27 Pepper, M. S., Ferrara, N., Orci, L. & Montesano, R. Potent synergism between vascular endothelial growth factor and basic fibroblast growth factor in the induction of angiogenesis in vitro. *Biochem Biophys Res Commun* **189**, 824-831 (1992).
- 28 Lever, R. & Page, C. P. Novel drug development opportunities for heparin. *Nat Rev Drug Discov* **1**, 140-148 (2002).
- 29 Abramsson, A., Lindblom, P. & Betsholtz, C. Endothelial and nonendothelial sources of PDGF-B regulate pericyte recruitment and influence vascular pattern formation in tumors. *J Clin Invest* **112**, 1142-1151 (2003).
- 30 Cao, R., Brakenhielm, E., Pawliuk, R., Wariaro, D., Post, M. J., Wahlberg, E., Lebourch, P. & Cao, Y. Angiogenic synergism, vascular stability and improvement of hind-limb ischemia by a combination of PDGF-BB and FGF-2. *Nat Med* **9**, 604-613 (2003).
- 31 Pietras, K., Sjöblom, T., Rubin, K., Heldin, C. H. & Ostman, A. PDGF receptors as cancer drug targets. *Cancer Cell* **3**, 439-443 (2003).
- 32 Carmeliet, P. Mechanisms of angiogenesis and arteriogenesis. *Nat Med* **6**, 389-395 (2000).
- 33 Seghezzi, G., Patel, S., Ren, C. J., Gualandris, A., Pintucci, G., Robbins, E. S., Shapiro, R. L., Galloway, A. C., Rifkin, D. B. & Mignatti, P. Fibroblast growth factor-2 (FGF-2) induces vascular endothelial growth factor (VEGF) expression in the

- endothelial cells of forming capillaries: an autocrine mechanism contributing to angiogenesis. *J Cell Biol* **141**, 1659-1673 (1998).
- 34 Franco, M., Roswall, P., Cortez, E., Hanahan, D. & Pietras, K. Pericytes promote endothelial cell survival through induction of autocrine VEGF-A signaling and Bcl-w expression. *Blood* **118**, 2906-2917 (2011).
- 35 Hellstrom, M., Gerhardt, H., Kalen, M., Li, X., Eriksson, U., Wolburg, H. & Betsholtz, C. Lack of pericytes leads to endothelial hyperplasia and abnormal vascular morphogenesis. *J Cell Biol* **153**, 543-553 (2001).
- 36 Brogi, E., Wu, T., Namiki, A. & Isner, J. M. Indirect angiogenic cytokines upregulate VEGF and bFGF gene expression in vascular smooth muscle cells, whereas hypoxia upregulates VEGF expression only. *Circulation* **90**, 649-652 (1994).
- 37 Greenberg, J. I., Shields, D. J., Barillas, S. G., Acevedo, L. M., Murphy, E., Huang, J., Scheppke, L., Stockmann, C., Johnson, R. S., Angle, N. & Cheresch, D. A. A role for VEGF as a negative regulator of pericyte function and vessel maturation. *Nature* **456**, 809-813 (2008).
- 38 Jain, R. K. Normalization of tumor vasculature: an emerging concept in antiangiogenic therapy. *Science* **307**, 58-62 (2005).
- 39 Ferrara, N., Gerber, H. P. & LeCouter, J. The biology of VEGF and its receptors. *Nat Med* **9**, 669-676 (2003).
- 40 Taeger, J., Moser, C., Hellerbrand, C., Mycielska, M. E., Glockzin, G., Schlitt, H. J., Geissler, E. K., Stoeltzing, O. & Lang, S. A. Targeting FGFR/PDGFR/VEGFR impairs tumor growth, angiogenesis, and metastasis by effects on tumor cells, endothelial cells, and pericytes in pancreatic cancer. *Mol Cancer Ther* **10**, 2157-2167 (2011).
- 41 Force, T. & Kolaja, K. L. Cardiotoxicity of kinase inhibitors: the prediction and translation of preclinical models to clinical outcomes. *Nat Rev Drug Discov* **10**, 111-126 (2011).

Part II

**Novel strategy for site-specific delivery
system and development of doxorubicin
prodrugs**

Chapter 4

General Introduction

4.1. Tumor heterogeneity

Recent studies have revealed extensive genomic and phenotypic variations between tumors (intertumor heterogeneity) and within individual tumors (intratumor heterogeneity)¹. Since the modern cancer therapy has largely shifted to the molecular targeted therapy from the conventional chemotherapy, the inter- and intratumor heterogeneity have produced significant implications in the choice of biomarkers for the guidance of clinical decision-making in cancer treatment.

The diversity of the tumor is mainly caused by the genomic instability, which produces variable cell populations that could adapt to given microenvironments or to exposure of therapies^{2,3}. The genomic instability could arise by various mechanisms and leaves distinct genomic footprints, which then differentially affects tumor progression and patient outcome.

4.1.1. Intertumor heterogeneity

It is not surprising that genomic and functional diversities exist among tumors. Tumors that originate from different tissues and cell types vary in terms of their genomic landscape, since the genetic events of transformation are largely determined by intrinsic biological properties of the cell¹. For this reason, originated organ of the primary tumor is generally considered important in the treatment decisions for cancer patients. However, variations in genomic aberrations and drug sensitivity also exist within tumors that originated from an identical tissue⁴. The clinical complications from to the diversities of tumors have obligated to classify the tumors into subgroups on the basis of mutations,

copy number changes, proteins or mRNA expression profiles, or patterns of genomic instability, thereby making the therapy more predictable in terms of patient outcomes or drug sensitivity⁵⁻⁷. For instance, breast cancers are generally classified according to the expression of HER2 (also known as ErbB2) and treated with different regimen of medication⁷. Also, around 15% of patients with NSCLC in the US and 35% in the East Asia have tumor associated EGFR mutations: this resulted in approval and clinical use of EGFR tyrosine kinase inhibitor (erlotinib, Tarceva[®], Roche) specifically to the NSCLC patients with the EGFR mutations⁸.

Recent advances in next-generation sequencing have revealed greater genomic variations of the tumor than that recognized in the past⁴. In addition, within a cohort of tumors, identical gene could be altered by point mutation, DNA methylation, and copy number alteration, emphasizing the demand for integrative approaches in analyzing somatic aberrations in the cancer genome. The efforts to define tumor subgroups based on specific mutations may be confounded by epistasis, which involves the action of one gene on another. For example, in acute myeloid leukemia (AML), NPM1 mutations confer a favorable prognosis only in the presence of a co-occurring IDH1 or IDH2 mutation⁹.

4.1.2. Intratumor heterogeneity

Not only among tumors, but there also exist significant variations at genomic and epigenomic levels among the tumor cells in a single tumor mass^{10,11}. This diversity poses challenges in revealing the genomic landscape of the tumor as well as validating the biomarker through the traditional sampling bias. The genomically diverse subclonal populations in the tumor appear through the genomic instability of the tumor cells, followed by adaptive selection and outgrowth of the clones that have phenotypic advantage in the given microenvironment during disease progression or therapy¹²⁻¹⁴. There was also a suggestion that genetically heterogeneous subclonal populations in tumors could be maintained by distinct cancer stem cells¹⁵.

Branched tumor evolutions, in which discrete subclones of tumor cells evolve in parallel, followed by the spatial separation of the subclones have been described recently. Multiple region sampling in the primary tumor of renal cell carcinoma and glioblastoma revealed the spatially separated subclones that had heterogeneous somatic mutations and copy number events¹⁶. The clonal multiplicity between primary and metastatic tumor has also been observed in other types of cancer including breast cancer¹⁷, pancreatic cancer¹², and medulloblastoma¹⁸. The diversity of the spatially separated subclones in a single tumor could be so profound that the genomic profiles of the tumor biopsy samples may more closely resemble in tumors from different patients than those of adjacent regions in a single tumor¹⁹.

Different genomic profiles between primary and metastatic tumors could be explained by the different microenvironment of the metastatic site followed by the adaptation and selection of the tumor cells during metastatic processes²⁰. On the other hand, it is difficult to explain how spatial separation of the genomically distinct clones are generated in the primary tumors¹⁶. Distinct microenvironmental niches might exist in the primary tumor, hence the subclones that are occupying each niche could evolve in different manner²¹. Also, there may be physical barriers between different subclones, such as blood vessels or tissue planes, which could prevent incorporation of the tumor subclones¹.

Nevertheless, intermingled heterogeneous subclones are also observed within single biopsies, which neighboring cells display expression of different receptor tyrosine kinases²²⁻²⁴. It is hard to imagine distinct microenvironment scattered around the intermingled subclones of tumor cells. The observation of the intermingled subclones of the tumor cells suggested that genomic instability of tumor cells might be the most crucial factor in the enhanced genomic diversity²⁵. This genomic heterogeneity increases phenotypic diversity, thus expanding the pool of cells that could be subjected to the selection, ultimately leading to emergence of the complex subclonal tumor architecture.

The subclonal mutations directly result in phenotypic variations. In renal cell carcinoma, for example, a heterogeneous *MTOR* mutation resulting in constitutive mTOR kinase activity was strongly associated with distinct mTOR signaling pathway activation after mTOR inhibitor therapy¹⁶. In a heterogeneous glioblastoma multiforme cell population with mosaic amplification of *EGFR* and *PDGFRA*, simultaneous blockade of both kinases was necessary to inhibit PI3K pathway activity²⁶. Observation of intermingling tumor cells with distinct receptor kinase amplification suggested functional codependency between the two cell populations²⁶⁻²⁸. Indeed, it has been found that *EGFR* mutant cells release interleukin 6 (IL6) and leukemia inhibitory factor (LIF), which facilitate the growth of adjacent subclones by activation of wild-type *EGFR*²⁹. This finding provided evidence of possible codependency between distinct subclones within tumor¹.

The phenotypic variations could also occur in the genomically homogeneous subclones by functionally distinct behavior and patterns of proliferation after exposure to therapy³⁰. The phenotypic heterogeneity arises not only through genomic differences between subclones, but also through stochastic events in gene expression and protein stability, epigenetic divergence and microenvironmental alteration^{11,30,31}.

4.2. Apoptosis targeted prodrug system

Despite the emergence of targeted therapy in the modern cancer therapeutics, chemotherapeutic agents are still widely used for the treatment of broad array of tumors in the first-line therapy as a single agent or in combination with other targeted therapies. Their clinical application, however, is often limited due to the dose-dependent toxicities³². These side effects are closely related to the non-selective distribution of doxorubicin throughout the body after administration³³. Therefore, many efforts have been made to deliver the chemotherapeutic agents selectively to the tumor tissue by introducing certain targeting moieties that could recognize tumor-specific ligands^{34,35}. These strategies, however, produced

only limited improvements due to the intertumor and intratumor heterogeneities, which were described in the previous section. Especially, finding of the intratumor heterogeneity posed challenges in the modern cancer therapeutics, which has relied on a single needle biopsy or the surgical excision of an extremely small portion of a tumor to overview its entire genomic landscape¹⁶. Therefore, efforts to deliver chemotherapeutic agents specifically to a tumor by relying on a target ligand expression have been ineffective thus far.

For an effective and reliable delivery of the chemotherapeutic agents to the tumor, a strategy of targeting an induced apoptosis of tumor cells is proposed for the drug delivery. In particular, caspase-3 is selected as the molecular target, which is a family of cysteine proteases and is upregulated during apoptotic events³⁶. The major advantage of utilizing caspase-3 as the molecular target is that the target site of the drug could be actively controlled by exogenous stimuli (i.e. radiation) rather than passively relying on the genotypic ligand expression of the tumor. Moreover, many chemotherapeutic agents trigger apoptosis by activation of caspase-3^{37,38}; therefore, the delivered agents could further upregulate the caspase-3 in the site where the apoptosis was initially induced. For this reason, the caspase-3 could sustain its local concentration within the site of the interest.

4.2.1. Caspase in apoptosis

Apoptosis is a term for the programmed cell death, which plays a central role in the development and homeostasis of metazoans³⁹. Either excessive or insufficient apoptosis could result in severe pathological consequences. For instance, suppression of the normal apoptotic pathways could cause autoimmune diseases and cancer. By contrast, abnormal upregulation of apoptosis contributes to neurological disorders. Since the concept of apoptosis was defined in 1972, hundreds of genes that regulate this event have been identified and showed that the mechanism of apoptosis is evolutionarily conserved^{40,41}.

Among the various components that participate in the apoptotic response, caspases play central role⁴¹. Caspases are a conserved family of cysteine proteases – peptidases that use a cysteine residue as the catalytic nucleophile and hydrolysis the amide bond after an aspartic acid residue of their substrates⁴² – that irreversibly induce cell death. Until now, at least 14 distinct mammalian caspases have been identified, and 11 of those are also found in humans⁴³. Among them, at least seven are known to play a key role in apoptosis. The apoptotic caspases are generally classified into two groups, initiator and executioner caspases, depending on their point of entry into the apoptotic cascade. The initiator caspases include caspase-2, -8, -9, and -10; the executioner caspases include caspase-3, -6, and -7⁴³. The initiator caspases are first activated through a particular apoptotic pathway and initiate the downstream signaling cascade by activating the executioner caspases⁴⁴.

All the caspases are produced and stored in cells as latent precursors that are catalytically inactive zymogens. These procaspases require proteolytic activation for the outbreak of their inherent enzymatic activity during apoptosis. The activation mechanisms of the initiator and executioner caspases totally differ to each other. The activation of the executioner caspases is mediated by the initiator caspases, which cleave the specific internal aspartic acid residue and separate the large (~p20) and small (~p10) subunits of the executioner caspases. On the other hand, the initiator caspases do not require cleavage for their enzymatic activation. Instead, they are activated by dimerization of the inactive monomeric zymogens – the zymogens of the initiator caspases that exist in the cell – through the assembly of a multi-component complex under apoptotic conditions^{45,46}. For instance, the activation of procaspases-9 is facilitated by the apoptosome, which is a ~1.4 MDa complex that includes APAF1 and cytochrome *c*^{47,48}. As the activation of the initiator caspases triggers the downstream apoptotic signalings, they are tightly regulated in the cells. Once activated, the downstream executioner caspases induce proteolytic cleavage of a wide array of cellular targets and ultimately lead to cell death⁴⁹.

In mammalian cells, the apoptosis occurs through either intrinsic or extrinsic pathway depending on the origin of death stimuli. The intrinsic pathway is triggered in response to apoptotic stimuli such as oncogene activation, DNA damage, and exposure to chemotherapeutic agents as well as ionizing radiation⁴⁴. Therefore, inactivation of the intrinsic pathway is generally considered as a hallmark of cancer⁵⁰. Following the apoptotic stimuli, mitochondria mediate the intrinsic pathway by releasing several proteins including cytochrome *c*, SMAC/DIABLO, AIF, EndoG, and OMI/HTRA2 from their intermembrane space to cytoplasm⁵¹. Particularly, the cytochrome *c* binds to APAF1, followed by the conformational change that allows the APAF1 to further bind ATP/dATP and eventually form the apoptosome. The apoptosome mediates the activation of caspase-9, which in turn cleaves and activates the executioner caspases, caspase-3 and -7^{52,53}.

The extrinsic pathway is initiated by the ligation of transmembrane death receptors such as Fas (also known as CD95 or APO-1)⁵⁴. When death ligands such as FasL bind on their receptors and form ligand-receptor complexes on the cell surface, adaptor molecule FADD (Fas-associated protein with death domain) and caspase-8 are recruited subsequently to the cytosolic tail of the complexes by a multi-step mechanism to form an oligomeric death-inducing signaling complex (DISC)⁵⁵. Formation of the DISC leads to the activation of the caspase-8, an initiator caspase, which then activates caspase-3 and -7, an executioner caspase. Caspase-8 activation by the TNF pathway is also demonstrated: the caspase-8 is activated by association with a cytosolic complex rather than at a membrane-associated signaling complex during TNF-induced apoptosis^{56,57}. The extrinsic pathway can crosstalk to the intrinsic pathway through the caspase-8-mediated cleavage of BID, a Bcl-2 interacting protein, which then triggers the release of the mitochondrial proteins^{58,59}.

4.2.2. Substrate recognition by caspases

Caspases recognize specific four continuous amino acid residues represented as P4-P3-P2-P1 within in their substrates, and hydrolytically cleave after the C-

terminus of P1 residue, which is usually an Asp. It has been widely accepted that the preferred amino acid residue in the P3 position is Glu for every caspases that have been examined⁴³. The preference in the P4 position varies among different groups of caspases and determines the substrate specificity. In the early study, Thornberry et al. demonstrated the peptide substrate specificities for the caspases using a positional scanning synthetic combinatorial library⁶⁰. This technique takes advantage of caspases enzymatically hydrolyzing the synthetic tetrapeptides that have C-terminal aminomethylcoumarin (AMC) as a fluorescently active leaving group. They examined nine human caspase family members (caspase-1 to caspase-9) and classified the caspases into three groups based on their substrate specificity. The members of group I (caspase-1, -4, and -5) preferentially recognized the tetrapeptide sequence WEHD. On the other hand, the members of group II (caspase-2, -3, and -7) preferred DEXD for their optimal recognition sequence, where the amino acid residue in P2 position could vary. In particular, the substrate specificity profiles shown between caspase-3 and caspase-7 were practically indistinguishable. The group III caspases (caspase-6, -8, and -9) preferred the sequence (L/V)EXD, where Leu and Val are interchangeable in the P4 position. The substrate specificity of the caspases is directly correlated with their physiological role. The group I caspases are involved in the inflammatory pathway, whereas the group II and III caspases are involved in the apoptotic pathway. Particularly, the group II caspases are executioner caspases and the group III caspases act as initiator caspases.

The comparison of the substrate specificities of caspases revealed the strict requirement of Asp in the P1 position of the substrate for every examined caspases. In addition, although not as strict as the preference of Asp in the P1 position, the caspases preferred Glu in P3 position in their substrates in varying degrees. Also, with only exception of caspase-9, which showed strong preference of His, liberal substitution in P2 position was also well tolerated for most of the caspases. As mentioned above, P4 position was the most critical determinant of the substrate specificity for caspases. The group I caspases was

Table 4.1. Optimal substrate sequences for caspases

Group	I			II			III		
Caspase	1	4	5	2	3	7	6	8	9
Sequence	WEHD	LEHD	LEHD	DEHD	DEVD	DEVD	VEHD	LETD	LEHD

able to accommodate large aromatic or hydrophobic amino acids in this position. On the other hand, the group II caspases strongly preferred Asp for efficient catalytic cleavage. The group III caspases generally allowed variable amino acids in this position, but preferred those with large aliphatic side chains. The optimal sequences for each caspase are shown in **Table 4.1**⁶⁰.

The recognition sequences for the each group of caspases are found in many proteins that are involved in the apoptotic signaling cascade⁶⁰. The optimal recognition motif of the group II caspases (DEXD) is found in cleavage sites of several cell maintenance and repair proteins that participate in the apoptotic event, including SREBPs⁶¹, D4-GDI⁶², PARP⁶³, SNRNP70⁶⁴, DNA-PKcs⁶⁴, and PRKCD⁶⁵. Some of these are endogenous substrates for the caspase-3^{64,66}.

On the other hand, the recognition sequence for the group III caspases are found in zymogens of several executioner caspases, particularly in caspase-3 and caspase-7. This indicated that the group III caspases indeed act as an initiator of the apoptotic cue by proteolytically activating the executioner caspases⁶⁰. Interestingly, initiator caspases have an extended N-terminal region that has specificity similar to their substrate sequences. This N-terminal region plays a crucial role in mediating dimerization of the monomeric initiator procaspases, resulting in their autocatalytic activation^{44,60}.

Although the optimal recognition sequences for each caspases have been identified and widely accepted by the remarkable study of Thornberry et al. in 1997⁶⁰, further studies have demonstrated divergent sequences for several caspases^{36,67,68}. As mentioned earlier in this section, caspase-3 and caspase-7 was shown to have their substrate specificity in DEXD, especially DEVD, identified by positional scanning synthetic combinatorial library (PS-SCL)⁶⁰. However, substrate-phage display library – the substrate is presented as a

proteolytically accessible-linker between two protein domains, making the context more akin to that of the natural substrate – showed that the optimal substrate preference of caspase-3 was DXVD rather than previously proposed DEXD. This study demonstrated that DLVD was 1.7-fold more rapidly hydrolyzed by caspase-3 than the canonical DEVD peptide, disputing the sequence preference of the group III caspases of the early report. Moreover, the amino acid residue in the P4 position within the substrates for caspase-3 were not as strictly limited to Asp as demonstrated earlier, and the enzyme also cleaved substrates with substitutions at the P4 position selected by phage display, albeit at a lower rate. The preferred sequence selection for caspase-8 showed that Glu was predominantly preferred in the P3 position of the substrate, agreeing with the previous reports. However, based on substitutions observed through the phage display in the P4 position, AETD showed 1.6-fold faster proteolysis than the canonical LETD sequence by caspase-8⁶⁷, which contradicts with the preferred requirement of Leu or Val at the P4 position for the group III caspases that was reported previously⁶⁰. Moreover, computational screening based on the amino acid positional fitness (APF) scores predicted DNLD and DFPD as potent inhibitors for caspase-3 and caspase-7, respectively⁶⁸. Requirement of Glu in the P3 position of the substrate for caspase-7 was further challenged by the study in crystal structures of caspase-7 complexed with the peptide analog of DMQD, DQMD, DNLD, IEPD, ESMD, or WEHD. The crystal structures showed that the S2 pocket of caspase-7 could accommodate with diverse amino acid residues. DMQD, DQMD, and DNLD, which varies in their P3 residue, interacted with caspase-7 as strongly as that of the canonical DEVD sequence, suggesting that Glu in the P3 position is not mandatory³⁶.

Caspases recognize their substrates through the four active-site loops, named L1, L2, L3, and L4, which constitute the substrate-binding groove. The L1 and L4 loops constitute the each flank of the groove, whereas L2 is located at the base. L2 loop, which harbors the catalytic residue Cys, is located at one end of the groove and is critical for binding and catalytic hydrolysis of the substrates.

The structural composition of the L1 and L3 loops is conserved among all mammalian caspases, whereas the L2 and L4 loops are highly divergent. These four loops are the determinant of the substrate sequence specificity. The binding pockets for the P4-P3-P2-P1 of the substrate are defined as the S4-S3-S2-S1 subsites, respectively. The pockets are mainly located between the base (L3) and the two flanks (L1 and L4) of the substrate-binding groove. The S1 and S3 subsites show slight variance among caspases, whereas the S2 and S4 subsites are conserved⁴³. The P1 residue of the substrate is coordinated by three invariant residues at the S1 subsite, an Arg residue of L1, a Gln residue at the beginning of L2, and an Arg residue at the end of L3⁶⁹. The Arg residue of L3 also coordinates the P3 residue of substrate. The S2 and S4 subsites map mainly to the L3 and L4 loops, thus the P2 and P4 residues exhibit greater sequence variation.

4.3. Tumor targeting strategies

4.3.1. Passive tumor targeting

Particulate carrier systems and macromolecules have been extensively studied and exploited in purpose to deliver chemotherapeutic agents selectively to tumor in passive manner. The passive targeting of macromolecules takes advantage of abnormal vascular architecture and physiological properties of tumor that results in enhanced permeation and retention (EPR) effect. The fundamental basis of the EPR effect is that tumor vasculatures are fenestrated and leaky, whereas normal vasculatures are tight and well-organized, thereby allowing macromolecules to escape from the circulation only in the tumor tissue⁷⁰. Drug delivery based on the EPR effect is applicable for most of the rapidly growing solid tumors with the exception of hypovascular tumors such as prostate cancer or pancreatic cancer⁷¹. Therefore, consideration of EPR effect is now the gold standard in designing drug carrier for tumor-targeted delivery.

The EPR effect of macromolecules in tumor was first suggested by Matsumura and Maeda in 1986⁷². They demonstrated that most of the solid

tumors have highly defective vasculatures and produce extensive amounts of vascular permeability factors such as VEGF, resulting in enhanced vascular permeability of the macromolecules. Moreover, tumors are highly vascularized showing relatively higher vascular density in comparison with normal tissues⁷³. The vascular dependency of the EPR effect was demonstrated by an experimental study involving a complex of Evans blue and albumin⁷⁴. When administered intravenously, the dye was exclusively found in the tumor, but not in the normal tissues. Interestingly, in the experimentally induced tumors with a diameter larger than 3 cm, the dye was found predominantly in the tumor periphery, where the functional blood vessels were mainly distributed. Considering that central regions of tumors are generally necrotic or hypovascular, these experimental results strongly supported that EPR effect is closely related to the presence of tumor vasculatures⁷³.

Among several characteristics of the tumor vasculatures, the defective and porous vessel wall is the major cause of the facilitated transportation of macromolecules or particles into the tumor. The EPR effect is largely dependent to the molecular weight of the macromolecules. Substances larger than 40 kDa, which is the threshold of renal clearance, have prolonged plasma half-life (increased plasma half-life) and very slow clearance, resulting in higher AUC (area under the concentration-time curve). They are also capable of leaking out through the tumor vessels and accumulating in tumor tissue, but not in normal tissues^{72,73}. It was reported that the accumulation of polymeric or macromolecular substances in tumor tissues was more than 10-200 fold higher than that in normal tissues and organs, such as skin, muscle, heart, and kidney⁷⁵⁻⁷⁹. The selective accumulation of the macromolecules in the tumor tissue is strongly correlated to the pore size of the fenestrae that exist on the tumor vasculatures. The pore size of the fenestrae varies from 100-1200 nm in diameter⁸⁰. Since the macromolecules that are generally employed as a tumor-targeted delivery vehicle typically have hydrodynamic radii in the range of 2-10 nm, they are capable of selectively extravasating in tumor tissue.

However, facilitated extravasation of macromolecules through the leaky tumor vasculatures only partly explains the enhanced accumulation, since the small molecules could also act in a similar manner. It has been widely accepted that macromolecules remain for prolonged time than small molecules when penetrated into the tumor tissue. The clearance rate from the tumor interstitium is dependent to the size of the accumulated molecules⁸¹. Small molecules were rapidly removed, whereas large molecules that exceeded 40 kDa in their molecular weight retained high intratumor concentration even after 100 hours of post application. The enhanced retention of the macromolecules in tumor is primarily caused by the lack of effective lymphatic drainage due to an impaired or absent lymphatic system in the tissue. Generally in normal tissues, the lymphatic system can effectively remove the penetrated macromolecules from the interstitial space. By contrast, the macromolecules in the tumor tissue cannot be removed by lymphatic drainage due to the defective lymphatic system, thereby they remain in the tissue for prolonged time⁷³. The EPR effect was observed in various substances including proteins, drug-polymer conjugates, micelles, liposomes, nanoparticles, DNA polyplexes, and lipid particles⁷³. Although the size of the macromolecules or particles is considered to be critical, the particle shape and surface characteristics are also important in determining the degree of EPR effect⁷⁰.

Because of the capability of allowing selective accumulation in many solid tumors, EPR effect has been considered to be one of the most practical principles in tumor targeting and regarded as highly promising paradigm for improving the therapeutic index of chemotherapeutic agents. Doxil[®], a PEGylated liposomal formulation of doxorubicin, is a representative example of an anticancer agent that is approved and successfully used clinically in the basis of the EPR effect. Many other drugs employing the passive targeting are also in clinical evaluations⁸²⁻⁸⁴. These drugs showed superior pharmacokinetic profile (i.e. extended plasma half-life) and more importantly, significantly higher tumor selectivity. Therefore, they produced improved anticancer effects with appreciably less adverse reactions than the conventional chemotherapeutic

agents. Despite the delivery of chemotherapeutic agents using the passive targeting have been proven effective in cancer therapy, there are still some hurdles to be surmounted. The passive targeting often results in low amount of drug delivered to the tumor, resulting in insufficient therapeutic efficacy^{85,86}. Moreover, the passive targeting some times disappointing selectivity, thereby producing insignificant improvement in the therapeutic index⁷⁰.

4.3.1.1. Albumin as a carrier for tumor targeting

Albumin is recognized as a versatile protein carrier molecule for the passively targeted drug delivery that could improve pharmacokinetic profile of drugs. It is the most abundant plasma protein accounting for more than half of the total plasma protein with a concentration of 35-50 mg/ml in human serum, and distributed throughout the body including blood circulation, lymphatic system, and extracellular as well as intracellular compartments⁸⁷. Albumin is one of the smallest proteins that present in plasma with molecular weight of 65 kDa. It is produced in the liver at a rate of approximately 0.7 mg/h per gram of liver tissue (10-15 g per day) with a very long plasma half-life, showing average 19-21 days in human.

The diverse physiological functions of albumin are partly from its distinct ability to bind with many substances in the biological fluid. It acts as a transport vehicle for long chain fatty acids (e.g., oleic acid, stearic acid, and palmitic acid) and metal ions (e.g., Cu^{2+} , Ni^{2+} , Ca^{2+} , and Zn^{2+}) in the blood, and also aids their uptake into the cells. It also binds with bilirubin, which is a degraded product of heme, and various kinds of hormones. Furthermore, it is capable of binding with broad range of pharmaceutical agents such as penicillins, sulfonamides, indoles, and benzodiazepines to name just few, thereby significantly affecting their pharmacokinetic properties. Regarding the abundance of the albumin in plasma, it is apparent that many metabolic substances and therapeutic agents could be affected and transported by this protein. Albumin also has some other physiological roles that are not related to its capability of binding with other biological substances. It is the protein that is most responsible for regulation of

the colloidal osmotic pressure in blood. Moreover, it is also a major source of amino acids for the peripheral tissue^{88,89}.

Human serum albumin is used for many purposes, mainly as a blood substitute, for treatment of certain pathological conditions (e.g., severe burns, nephritic syndrome, cardiopulmonary bypass, acute respiratory distress), and for compensating hypoalbuminemia as well as cachexia in cancer patients^{87,90}. As an alternative to the blood derived albumin, recombinant human albumin (Recombunin[®], Novozymes Biopharma) was developed and has shown comparable safety, tolerability, pharmacokinetics, and pharmacodynamics to the native human serum albumin⁹¹.

Besides the therapeutic applications, albumin has also been extensively studied for the potential as a drug carrier molecule. Albumin is a very soluble protein and generally regarded to be extremely robust, since it is stable in very broad range of pH (pH 4-9) and remains intact without any deleterious effect up to 40% ethanol and at 60°C for 10 hours. The physicochemical stability, long plasma half-life, preferential uptake in tumor and inflamed tissue, availability, biodegradability, and lack of toxicity and immunogenicity make it an attractive carrier molecule in the drug delivery field⁸⁹.

Albumin accumulates in malignant or inflamed tissue through EPR effect like other macromolecules. The first literature demonstrating that tumors could trap plasma proteins and use the metabolized products for their survival and proliferation appeared was reported in 1954⁹². This was further supported by an important study that was reported in 1986, which demonstrated the tumor accumulation of plasma proteins depending on their sizes⁷². The accumulation rate of the proteins ranging from 12-150 kDa in their molecular weight was closely related to their pharmacokinetic profile: the long circulation time was essential for the facilitated tumor accumulation. The plasma proteins that lie above the renal threshold (40 kDa) in terms of molecular weight have similarly long plasma half-life, hence accumulate in the malignant tissue due to the EPR effect⁹³. In fact, similar degree of tumor accumulation was observed between albumin and immunoglobulin, which have molecular weight of 66.5 and 150

kDa, respectively⁷². As described above (see section 5.3 for more detail), EPR effect in tumor is produced by the leaky vasculatures that allow the penetration of macromolecules through the fenestrae on the vessels^{72,94}. The pore size of the fenestrae varies from 100-1200 nm in diameter. Therefore, albumin, which has an effective diameter of 7.2 nm, could freely penetrate through the pores^{80,89,95}. Many experimental studies concerning the uptake of either radio- or chemical dye-labeled albumin showed that 3-25% of the total dose applied to the animal was found in the grafted tumor⁹⁶.

Besides EPR effect, which is a common feature of macromolecules for their tumor selective accumulation, there is also an albumin-specific tumor accumulation mechanism. On endothelial cell surface, 60 kDa glycoprotein gp60 (also known as albondin) is expressed, which mediates the albumin transportation pathway⁹⁷⁻⁹⁹. When albumin is bound to the gp60, it is internalized via caveolin-mediated endocytosis and transcytosed across the endothelium. Interestingly, some tumors secrete SPARC (secreted protein acidic and rich in cysteine), a gp60 homologous 43 kDa extracellular glycoprotein with high binding affinity to albumin. This protein binds to the transcytosed albumin in the tumor interstitium and prolong the residence time, and also contribute to the deep tumor penetration¹⁰⁰⁻¹⁰³. Clinical studies suggested that the overexpression of SPARC might be an important principle for the improved therapeutic efficacy of Abraxane[®] (albumin-paclitaxel nanoparticle) in comparison to the conventional formulation of paclitaxel. Sub-analysis of the overall SPARC levels in the metastatic pancreatic cancer patients treated with Abraxane[®] during phase I/II clinical trials showed that high SPARC levels correlated with improved overall survival (n = 20; median survival 13.6 months, *P* = 0.02) in comparison to the patients with low SPARC levels (n = 16; median survival 8.1 months)¹⁰⁰. Similar result was also shown in a retrospective analysis of 16 head and neck cancer patients¹⁰⁴.

In addition, to explain the high albumin turnover in tumors, Stehle et al. have proposed that tumor cells continuously and actively uptake the circulating albumins as their major energy and nutrition source¹⁰⁵. Their report was based

on the observation of the excessive plasma protein catabolism by tumor cells in demand for their aberrant metabolism and rapid proliferation. It has been also suggested that this continuous demand for albumin by tumor cells could contribute to the accumulation of albumin or albumin-bound pharmaceutical agents in the tumor¹⁰⁶.

Using albumin as a drug carrier has another advantage besides the tumor targeting capability. As mentioned earlier, serum albumin has the half-life of more than 19 days in human¹⁰⁰. Due to the long half-life of albumin, conjugating therapeutic agents such as peptides and cytokines is an attractive approach in improving their pharmacokinetic properties. The molecular weight of albumin (66.5 kDa), which exceeds the renal clearance threshold (40 kDa), is suggested to be one reason for the long half-life. However, recent studies demonstrated that binding of albumin to the neonatal Fc receptor (FcRn) could be the major reason for the extremely long plasma half-life of albumin. The FcRn, which is a membrane-bound receptor on the endothelial cell surface, is responsible for the long plasma half-life IgGs and related antibodies, which is also in the range from 2-3 weeks in human. It was suggested that the FcRn extend the half-life of albumin in a similar way that does to IgGs: an FcRn-mediated recycling in vascular endothelial cells, which protects IgGs or albumins from degradation^{107,108}.

4.3.1.2. Exploiting endogenous albumin for albumin-bound agents

More than a decade ago, Kratz et al. have proposed a concept of directly exploiting endogenous circulating serum albumin as a carrier for drug *in situ* instead of preparing an albumin-drug conjugate prior to administration¹⁰⁹. The therapeutic strategy according to the literature demonstrated the chemically engineered form of active compound binding rapidly and selectively to the circulating serum albumin in the blood after intravenous administration, thereby producing albumin-conjugated form of the compound *in situ*.

There are several significant advantages of exploiting circulating serum albumin as a drug carrier over preparing synthesized albumin-drug conjugates *ex vivo*. The advantages are as follows: the use of possibly pathogenic exogenous albumin could be avoided; the final form of the drug before administration is a chemical drug, thereby the substance could be easily defined; the production of the drug is relatively simple and inexpensive due to the straightforward organic chemistry; the analytical requirements for defining and managing the pharmaceutical products are comparable to the other chemical drugs; and the final product is relatively more stable, thereby allowing better storage and handling¹¹⁰.

The unique feature of the circulating albumin allows the chemically engineered compound to selectively react with the albumin among numerous other plasma substances. The *in situ* albumin binding involves Cys34 residue, which is located in subdomain IA of human serum albumin. This residue is highly conserved in all of the mammalian species that have been yet studied^{88,111}. The defatted albumin structure (PDB code 1ao6) revealed by X-ray crystallography showed that Cys34 is located in a hydrophobic crevice on the surface of the protein in 10-12 Å depths. However, binding of five molecules of myristic acids to albumin (PDB code 1bj5) induced conformational change and opened the crevice, thereby exposing the Cys34 to the surface¹¹².

Generally in the plasma, serum albumins are bound with one to three molecules of long-chain fatty acids. Therefore, most of the serum albumins have Cys34 exposed on the surface⁹⁶. Around 70% of the circulating albumins in the bloodstream contain an accessible Cys34 with free thiol group that is not blocked by endogenous thiol-bearing compounds such as cysteine, homocysteine, cysteinylglycine, glutathione, and nitric oxide. Physiologically, the thiol group on Cys34 was reported to play a role as scavenger for endogenous thiols, oxidants, and heavy metals (e.g., Cd²⁺, Au²⁺, Hg²⁺, Ag²⁺).

The free thiol exposed on the surface of albumin is a very unique feature regarding that only three other serum proteins have cysteine residues without interchain disulfide bond. One of them is apolipoprotein B-100, which has two

cysteine residues (Cys3734 and 4190) at the C-terminal end of the protein¹¹³. Another is fibronectin, which has two cryptic free thiol groups that have no reactivity under physiological condition¹¹⁴. Last is α_1 -antitrypsin, which has a single cysteine residue (Cys232) that is generally connected to either cysteine or glutathione by disulfide linkage in the plasma¹¹⁵. Despite that there are also many other small molecules containing thiols, the free thiol on the serum albumin accounts for 80-90% of the total free thiol concentration (400-500 μM) in the blood. Most of the thiol groups in the other blood substances exist as an oxidized form. The overall concentration of free thiols on the small molecules hardly exceeds 20 μM (i.e., cysteine 10-12 μM , homocysteine 0.15-0.25 μM , cysteinylglycine 3-4 μM , glutathione 4-5 μM) in human plasma, which is significantly lower amount than that of the circulating albumin¹¹⁰.

Moreover, the free thiol of Cys34 in serum albumin has the highest reactivity among the thiol groups in the substances that present in human plasma. In fact, the pK_{SH} (pK value of the thiol group) of cysteine and glutathione, which are the most abundant thiol-containing molecules besides the serum album, are 8.5 and 8.9, respectively. On the other hand, the pK_{SH} of the Cys34 in serum albumin is around 7, hence most reactive¹¹¹. Considering that the accessible thiol group on Cys34 of the serum albumin possesses the major portion of total free thiols in the plasma with the highest reactivity, it is an ideal target for the *in situ* selective coupling with a thiol-reactive compound after entering the bloodstream.

The first drug to employ the concept of the *in situ* albumin binding is aldoxorubicin (formerly INNO-206 or DOXO-EMCH; CytRX corporation), which is a doxorubicin derivative that could bind to the Cys34 of albumin via maleimide functional group. The drug is currently in phase II/III clinical investigation on patients with soft tissue sarcoma, glioblastoma, Kaposi's sarcoma, or small cell lung cancer. The aldoxorubicin has been proved to be as effective as doxorubicin with significantly less adverse effects. During the clinical trials, the administered dose of the aldoxorubicin were up to four times of the standard dose of doxorubicin, but showed no increase in the observed

side effects with superior therapeutic efficacy^{116,117}. There are also several other drugs in the preclinical investigations that employ the *in situ* albumin binding strategy, such as doxorubicin prodrug activated by urokinase-type-plasminogen activator (uPA)¹¹⁸, prodrugs of camptothecin and doxorubicin that are activated by cathepsin B¹¹⁹, and prodrug of zosuquidar¹²⁰, and showed successful binding to the circulating albumins.

4.3.2. Active tumor targeting strategy

Active targeting takes advantage of molecular recognition such as ligand-receptor and antigen-antibody, which could specifically bind to certain molecules that are overexpressed in a target tissue¹²¹. For the active tumor targeting, targeting ligands are attached at the surface of particulate carriers or directly conjugated to chemotherapeutic agents to deliver them to the tumor. The enhanced selectivity towards the tumor tissue produced increased therapeutic efficacy and reduced adverse effects⁸⁶.

The selectivity of the active targeting largely depends on the expression pattern of target molecule and the binding affinity of targeting ligand. An ideal target molecule should be exclusively and abundantly expressed on the tumor cells. In addition, they should be expressed homogeneously throughout the entire population of the tumor cells. Such a target molecule would allow the active targeting to affect the tumor cells potently and uniformly, but not the normal cells⁷¹.

The targeting ligand is also important for the successful active targeting. When a target molecule is determined, an appropriate targeting ligand should be selected and employed to the drug or carrier. An ideal targeting ligand should have very high affinity against the target molecule, but have very low or no affinity against any other molecules, thereby allowing it to specifically bind to the target molecule in the body. Many classes of substances such as aptamers, antibodies, peptides, and several ligand molecules (e.g., folate and transferrin) that are capable in high-affinity binding to a number of tumor-specific molecular targets have been investigated and proved useful⁷⁰. In particular,

antibodies and peptides have been extensively studied for their relative ease of developing high-affinity ligands for wide array of the known and newly discovered molecular targets.

Antibodies target specific antigens presented on the cell membrane or secreted from the cells. However, when using antibodies as the vehicle for targeted delivery of chemotherapeutic agents, the antigens on the cell membrane are mainly considered as the target. The application of antibodies in molecular targeted therapies has been extensively investigated over the past decades, resulting in development of numerous clinically available drugs. The therapeutic antibodies have been proven to be clinically beneficial in broad range of tumors such as chronic lymphocytic leukemia, colorectal cancer, metastatic lung cancer, advanced non-small cell lung cancer, non-hodgkin's lymphoma, advanced melanoma, and metastatic breast cancer^{86,122-125}. They function by binding to a specific antigen expressed on the tumor cells. The interaction between antibody and antigen results in alteration of the antigen function that may be critical in tumor growth and survival, thereby inducing antitumor effects by multiple mechanisms¹²⁶. EGFR is one of the most investigated molecular targets in clinical oncology. It is overexpressed in many tumors and plays significant role in proliferation and survival of the tumor cells, leading to development of monoclonal antibody against EGFR as an anticancer agent (cetuximab, Erbitux®, Bristol-Myers Squibb)¹²⁷. Other monoclonal antibodies have been developed such as ibritumomab tiuxetan (anti-CD20 mAb for radioimmunotherapy), panitumumab (anti-EGFR), rituximab (anti-CD20), tositumomab (anti-CD20), and trastuzumab (anti-HER2), which targets many cell surface antigens¹²²⁻¹²⁵.

Although antibodies have significant therapeutic activity by themselves in the cancer therapy, they have been also proved to be useful as vehicles for the tumor selective delivery of chemotherapeutic agents and particulate carrier systems. The nanoparticles conjugated with trastuzumab or rituximab were found at the frequency of 10-fold higher than the non-conjugated nanoparticles in the cells expressing the respective antigens¹²⁸. Antibody-drug conjugates

(ADCs), which cytotoxic agents are directly conjugated to an antibody, have recently gained much interest in the drug discovery field. The idea of combining antibody and cytotoxic agent for the selective delivery of the cytotoxic agent to the tumor dates back to the 1980s. However, due to the technological limitations in the past, the clinically practical products were only recently developed and approved¹²⁹. Owing to the discovery of appropriate targets and advances in bioconjugate technology, the development and clinical application of ADCs are accelerating rapidly. Indeed, as a pioneer of the new generation ADCs, brentuximab vedotin (Adcetris[®], Seattle Genetics), a monomethyl auristatin E (MMAE) conjugated CD30-specific monoclonal antibody, was approved by the US FDA in August 2011 for treatment of Hodgkin's lymphoma and systemic anaplastic large cell lymphoma. Another ADC, ado-trastuzumab emtansine (Kadcyla[®], Genentech), gained approval by the FDA in February 2013 for patients with HER2 (also known as ErbB2)-positive metastatic breast cancer. A number of ADCs, including inotuzumab ozogamicin (calicheamicin conjugated CD22 mAb; Pfizer), lorvotuzumab mertansine (DM1 conjugated CD56 mAb; ImmunoGen), and glembatumumab vedotin (MMAE conjugated GPNMB mAb; Seattle Genetics), are also in clinical investigation. Due to the highly selective targeting to tumor cells, the ADCs showed potent clinical efficacy with impressive safety and tolerability profiles¹³⁰.

Peptides have also been frequently used as targeting ligands for delivering chemotherapeutic agents to tumor. Screening and selection of the peptide sequence that could potentially bind to specific molecular targeted is typically achieved through combinatorial phage display technique. This approach produces peptide ligands ranging from 10-15 amino acids in length that selectively bind to target molecules in high affinity^{86,131,132}.

Integrin $\alpha v \beta 3$, which is overexpressed in several kinds of tumors and also on tumor endothelial cells, is one of the representative target molecule that has high affinity peptide ligands¹³³. It is specifically recognized by a tripeptide sequence, Arg-Gly-Asp (RGD)¹³⁴. Further investigation in RGD sequence has

led to discovery of several linear or cyclic peptides comprising RGD motif with improved affinity and selectivity towards integrin $\alpha\beta 3$ ¹³⁵. Another widely investigated peptide is angiopep-2, a 19 amino acid long peptide, which is capable of binding to the low-density lipoprotein receptor-related protein 1 (LRP1). LRP1 is upregulated in the blood-brain barrier (BBB), glioblastoma multiforme (GBM), and glioma. Angiopep-2 facilitates penetration through the BBB and delivers the payloads to the GBM or glioma at sufficient concentration⁷⁰.

Folate and transferrin are also promising ligand molecules that target tumor through ligand-receptor interaction⁷⁰. Folate is one of the most extensively studied ligands for targeted delivery of drugs or particulate carriers to tumor. It binds to folate receptor (FR) and membrane-bound high affinity folate binding protein in extremely high affinity ($K_D \sim 10^{-9}$)^{136,137}. Since folate is essential for the synthesis of nucleotide bases, FRs are upregulated in many kinds of tumors including ovarian carcinomas, choriocarcinomas, meningiomas, uterine sarcomas, osteosarcomas, and non-Hodgkin's lymphomas, owing to their rapid proliferation. Folate receptor 1 (FR1; also known as folate receptor α), an isoform of folate receptor, is overexpressed in 40% of human cancer. Folate receptor 2 (FR2; also known as folate receptor β) is overexpressed on activated macrophages as well as on the surfaces of malignant cells of hematopoietic origin¹³⁸. Therefore, folate is useful in delivering chemotherapeutic agents to those tumors with high selectivity¹³⁹.

Transferrin has also been investigated in plethora of studies for tumor targeting applications as another distinct ligand-receptor pair. Transferrin is an iron-binding blood plasma glycoprotein that controls the cellular uptake of irons in order to maintain the cellular iron homeostasis by interacting with transferrin receptor (TfR)¹⁴⁰. Physiologically, transferrin forms complex with iron, which is then internalized into the cells through transferrin receptor-mediated endocytosis¹⁴¹. The TfR is expressed up to 100-fold higher in tumor cells than on normal cells, making it an attractive target for delivery of chemotherapeutic agents^{142,143}.

4.3.2.1. Integrins

Cell adhesion molecules (CAMs) are glycoproteins presented on the cell surface that play significant roles in various cellular events such as locomotion, mitosis, cytokinesis, and phagocytosis¹⁴⁴⁻¹⁴⁶. In particular, they function as receptors for cell-to-cell and cell-ECM interactions during the cellular events¹⁴⁷⁻¹⁴⁹. CAMs are also involved in many pathological conditions such as cancer¹⁵⁰⁻¹⁵², thrombosis¹⁵³, rheumatoid arthritis¹⁵⁴, and diabetes¹⁵⁵. This group of molecules are generally divided into four classes: integrins, selectins, cadherins, and the immunoglobulin superfamily¹³⁵.

Integrins are a family of heterodimeric transmembrane glycoproteins. They promote interaction with other cells as well as broad range of endogenous substances such as ECM proteins, immunoglobulin, growth factors, cytokines, and matrix proteases¹⁵⁶⁻¹⁵⁸. Each member of integrins is composed of non-covalently associated transmembrane polypeptide α and β subunits. Each subunit has an extracellular domain, a single transmembrane region, and a cytoplasmic region¹⁵⁹. In mammalian species, 18 distinct α subunits and 8 distinct β subunits assemble into at least 24 different heterodimeric integrins¹⁶⁰. The binding specificity and signaling property of integrins are determined by the composition of α and β subunits within the heterodimer structure¹⁶¹. Integrins generally bind to their respective ECM proteins by recognizing short peptide sequences such as Arg-Gly-Asp (RGD), Glu-Ile-Leu-Asp-Val (EILDV), and Arg-Glu-Asp-Val (REDV)¹⁵⁸. Integrin ligation promotes the formation of integrin clusters at the cell membrane that are associated with cytoskeletal complex, and induce actin filament assembly^{162,163}. Consequently, the reorganization of actin filaments into large stress fibers facilitates the further clustering of integrins, resulting in enhanced binding affinity with ECM proteins¹⁶⁴.

Many integrins are critically involved in various stages of cancer progression including malignant transformation, invasion, metastasis, and angiogenesis. Among them, integrin $\alpha\beta3$ has been comprehensively studied,

since it is abundantly expressed on angiogenic tumor endothelial cells as well as on various malignant cells including late stage glioblastoma, melanoma, ovarian cancer, breast cancer, pancreatic cancer, and prostate cancer, whereas rarely expressed on the normal quiescent endothelial cells or and other normal cells^{158,165-167}.

The expression of integrin $\alpha\beta3$ on tumor endothelial cell is stimulated by pro-angiogenic factors such as fibroblast growth factor-2 (FGF2), tumor necrosis factor- α (TNF α), or interleukin-8 (IL8)^{156,159}. Integrin $\alpha\beta3$ regulates angiogenesis by several mechanisms. It stimulates cell-mediated collagen degradation in surrounding extracellular matrix (ECM) by inducing local secretion of proteolytically active matrix metalloproteinase-2 (MMP2), leading to rearrangement of the ECM. Through this mechanism, endothelial cell migration is facilitated when the integrin $\alpha\beta3$ binds to fibronectin, fibrinogen, or osteopontin. Moreover, the activation of integrin $\alpha\beta3$ increases the cyclooxygenase-2 (COX-2) level, which is necessary during the endothelial cell spreading and migration. It also acts as a survival factor and improves the survival of endothelial cells when bound to fibronectin¹⁶⁸. In addition, integrin $\alpha\beta3$ stimulates angiogenesis by interacting with other pro-angiogenic factors. Early reports showed that the interaction between integrin $\alpha\beta3$ and FGFR or VEGFR2 enhanced the FGF or VEGF-induced angiogenesis, respectively¹⁶⁹. These distinct angiogenic pathways showed that integrins regulate ECM and pro-angiogenic factors to induce specific intracellular signaling events that are critical in angiogenesis. Indeed, the inhibitors against integrin $\alpha\beta3$ or $\alpha\beta5$ suppressed pathological angiogenesis in animal models¹⁷⁰.

Integrin $\alpha\beta3$ also plays significant roles in the progression of various types of tumors. The overexpression of integrin $\alpha\beta3$ is associated with facilitated growth, invasion, and bone metastasis of breast cancer^{171,172}. It is also correlated with the sensitivity of breast cancer cells against chemotherapy, thereby suggested as a biomarker for chemosensitivity¹⁷³. In glioblastoma, integrin $\alpha\beta3$ was abundantly found at the invasive margins of the tumor with increased levels of fibronectin, which was closely related with enhanced cell motility and

survival¹⁷⁴. In other types of cancer including pancreatic cancer and prostate carcinoma, increased metastasis was also observed when integrin $\alpha v \beta 3$ was upregulated^{174,175}.

4.3.2.2. RGD peptide sequence for targeting integrin $\alpha v \beta 3$

Integrin $\alpha v \beta 3$ is consisted of 125 kDa αv subunit and 105 kDa $\beta 1$ subunit, and binds with broad array of ECM proteins that contains Arg-Gly-Asp (RGD) sequence in high affinity¹⁷⁶. The crystal structures of integrin $\alpha v \beta 3$ and RGD ligand complexes revealed that RGD motif binds at an interface between α and β subunits, where arginine residue fitting into a cleft of the β -propeller fold, and aspartic acid residue coordinating with the von Willebrand factor type A domain in the β subunit by cationic interaction¹⁷⁷. The RGD tripeptide sequence was first found in fibronectin as a cell adhesion residue in the early 1970s by E. Ruoslahti¹⁷⁶. This sequence was further found in other ECM proteins that bind with integrin $\alpha v \beta 3$ such as fibrinogen, vitronectin, plasminogen, prothrombin, MMP2, laminin, osteopontin, and thrombospondin^{174,178-180}. More than half of the identified integrins recognize this tripeptide sequence including all five αv integrins, $\alpha 5 \beta 1$, $\alpha 8 \beta 1$, and $\alpha I I \beta 3$ integrins¹⁸¹. According to these findings, many compounds including linear and cyclic peptides, and peptidomimetics that preferentially bind to integrin $\alpha v \beta 3$ were developed, employing RGD sequence as a basic module for targeted therapy in cancer treatment¹⁸². The binding affinity of the RGD peptides is largely governed by the steric conformations and the flanking residues¹⁸³.

Cyclization of RGD peptide is frequently used to improve the binding properties. Conformational rigidity that is provided by the cyclization could significantly increase the binding affinity and the selectivity against specific integrin subtype. The cyclization is also preferred in purpose to increase the chemical stability. Generally, linear RGD peptides are susceptible to chemical degradation as the Asp can cause a hydrolytic peptide cleavage when paired with Gly¹⁸⁴. The cyclization of the peptide could prevent such hydrolysis by producing rigid structure, which limits the movement of the Asp. Non-natural

peptide modifications such as inserting D-amino acids or replacing with peptidomimetic molecules have also been frequently used to improve the binding properties¹⁸⁵. The flanking residues of the linear or cyclic RGD sequences were also concerned, since they could also influence the affinity and selectivity against integrins¹⁸³.

The most representative RGD peptide that targets integrin $\alpha v\beta 3$ is c(RGDf-N(Me)-V), which is also known as cilengitide. Cilengitide exhibits highly preferential binding to integrin $\alpha v\beta 3$, displaying 1000-fold higher affinity over integrin $\alpha IIb\beta 3$ due to the cyclic structure and the presence of D-amino acid (i.e., D-Phe) next to the RGD sequence¹⁸⁶. Among the several derivatives of this compound, c(RGDfK) and c(RGDyK) are frequently used for targeted delivery of therapeutics due to the ease of chemical conjugation through the primary amine group on Lys side chain¹⁸². Several RGD peptides with high affinity and specificity against integrin $\alpha v\beta 3$ were further identified using the phage display technique. Among them, RGD4C (ACDCRGDCFCG) and RGD10 (DGARYCRGDCFDG) have been appreciated for their outstanding binding properties. RGD4C and RGD10 have two and one intramolecule disulfide bond to form stable cyclic structures, thereby producing high binding affinity. Since these peptides do not involve any non-natural amino acids or chemical modifications, they are preferred when introducing to a protein by recombinant engineering^{182,187}.

Peptidomimetics of RGD have also been reported to show improved binding to αv integrins¹⁸⁵. Most of the peptidomimetics have Arg and Asp residues respectively substituted with guanidine mimetic and carboxylic acid, which are connected to each other by various tethers and constraints, thereby producing compounds with nano- or even picomolar binding affinities to integrin $\alpha v\beta 3$.

Not only the individual characteristics of the peptide determine the binding properties. Multivalency of RGD peptides also significantly increases the binding affinity. For instance, Kok et al. have demonstrated that their multivalent RGD-protein conjugates showed subnanomolar affinity for integrin $\alpha v\beta 3$ overexpressing human umbilical cord endothelial cells (HUVECs), which

was a 250-fold increase compared to the single RGD peptide¹⁸⁸. Additionally, the multivalency also facilitates the internalization of the conjugated substances by endocytosis^{189,190}. Particulate carriers and macromolecules such as liposomes, nanoparticles, proteins, and other polymers bearing multiple RGD peptides are, therefore, more likely to be internalized via receptor-mediated endocytosis than the single peptide constructs.

4.4. Rationale of the research

Despite that the targeted therapy gained the most interest from many researchers and clinicians in the modern cancer therapeutics, chemotherapeutic agents are still widely used for the treatment of broad array of tumors in the first-line therapy solely or in combination with the targeted therapies. However, the clinical application of the chemotherapy is often limited due to the severe systemic toxicities, which are even sometimes lethal. These adverse effects are closely related to the systemically non-selective distribution as well as the non-specific mechanisms of action of the chemotherapeutic. Therefore, many efforts have been made to deliver these agents selectively to the tumor by introducing tumor-targeting moieties that could recognize certain tumor-specific surface antigens, so called as active tumor targeted delivery (see section 4.3.2). The traditional targeted delivery strategies, however, produced only limited improvements in the preclinical models, mainly due to the intratumor heterogeneity (see section 4.1.2). Considering the existence of many different cell populations in the tumor mass, the strategy to deliver chemotherapeutic agents specifically to a tumor by relying on a target antigen expression is fundamentally challenged.

For an effective and reliable delivery of chemotherapeutics (i.e. doxorubicin) to the tumor regardless of the intratumor heterogeneity, we have previously proposed a strategy of targeting radiation-induced apoptosis to deliver chemotherapeutic agents to the tumor. In particular, it involves caspase-3, which is upregulated during apoptotic events, for the targeted delivery system

(see section 4.2.1 for detailed description of caspase-3). The major advantage of utilizing caspase-3 as an activator of a prodrug is that the site of the activation could be controlled actively by exogenous stimuli (i.e. radiation), rather than passively relying on the genotype of the tumor. Therefore, this strategy could be a resolution for the obstacles in the current targeted delivery systems.

References

- 1 Burrell, R. A., McGranahan, N., Bartek, J. & Swanton, C. The causes and consequences of genetic heterogeneity in cancer evolution. *Nature* **501**, 338-345 (2013).
- 2 Merlo, L. M., Pepper, J. W., Reid, B. J. & Maley, C. C. Cancer as an evolutionary and ecological process. *Nat Rev Cancer* **6**, 924-935 (2006).
- 3 Greaves, M. & Maley, C. C. Clonal evolution in cancer. *Nature* **481**, 306-313 (2012).
- 4 Vogelstein, B., Papadopoulos, N., Velculescu, V. E., Zhou, S., Diaz, L. A., Jr. & Kinzler, K. W. Cancer genome landscapes. *Science* **339**, 1546-1558 (2013).
- 5 Lengauer, C., Kinzler, K. W. & Vogelstein, B. Genetic instability in colorectal cancers. *Nature* **386**, 623-627 (1997).
- 6 Popat, S., Hubner, R. & Houlston, R. S. Systematic review of microsatellite instability and colorectal cancer prognosis. *J Clin Oncol* **23**, 609-618 (2005).
- 7 Weigelt, B. & Reis-Filho, J. S. Histological and molecular types of breast cancer: is there a unifying taxonomy? *Nat Rev Clin Oncol* **6**, 718-730 (2009).
- 8 Pao, W. & Chmielecki, J. Rational, biologically based treatment of EGFR-mutant non-small-cell lung cancer. *Nat Rev Cancer* **10**, 760-774 (2010).
- 9 Patel, J. P., Gonen, M., Figueroa, M. E., Fernandez, H., Sun, Z., Racevskis, J., Van Vlierberghe, P., Dolgalev, I., Thomas, S., Aminova, O., Huberman, K., Cheng, J., Viale, A., Socci, N. D., Heguy, A., Cherry, A., Vance, G., Higgins, R. R., Ketterling, R. P., Gallagher, R. E., Litzow, M., van den Brink, M. R., Lazarus, H. M., Rowe, J. M., Luger, S., Ferrando, A., Paietta, E., Tallman, M. S., Melnick, A., Abdel-Wahab, O. & Levine, R. L. Prognostic relevance of integrated genetic profiling in acute myeloid leukemia. *N Engl J Med* **366**, 1079-1089 (2012).
- 10 Swanton, C. Intratumor heterogeneity: evolution through space and time. *Cancer Res* **72**, 4875-4882 (2012).
- 11 Marusyk, A., Almendro, V. & Polyak, K. Intra-tumour heterogeneity: a looking glass for cancer? *Nat Rev Cancer* **12**, 323-334 (2012).
- 12 Campbell, P. J., Yachida, S., Mudie, L. J., Stephens, P. J., Pleasance, E. D., Stebbings, L. A., Morsberger, L. A., Latimer, C., McLaren, S., Lin, M. L., McBride, D.

- J., Varela, I., Nik-Zainal, S. A., Leroy, C., Jia, M., Menzies, A., Butler, A. P., Teague, J. W., Griffin, C. A., Burton, J., Swerdlow, H., Quail, M. A., Stratton, M. R., Iacobuzio-Donahue, C. & Futreal, P. A. The patterns and dynamics of genomic instability in metastatic pancreatic cancer. *Nature* **467**, 1109-1113 (2010).
- 13 Ding, L., Ley, T. J., Larson, D. E., Miller, C. A., Koboldt, D. C., Welch, J. S., Ritchey, J. K., Young, M. A., Lamprecht, T., McLellan, M. D., McMichael, J. F., Wallis, J. W., Lu, C., Shen, D., Harris, C. C., Dooling, D. J., Fulton, R. S., Fulton, L. L., Chen, K., Schmidt, H., Kalicki-Veizer, J., Magrini, V. J., Cook, L., McGrath, S. D., Vickery, T. L., Wendl, M. C., Heath, S., Watson, M. A., Link, D. C., Tomasson, M. H., Shannon, W. D., Payton, J. E., Kulkarni, S., Westervelt, P., Walter, M. J., Graubert, T. A., Mardis, E. R., Wilson, R. K. & DiPersio, J. F. Clonal evolution in relapsed acute myeloid leukaemia revealed by whole-genome sequencing. *Nature* **481**, 506-510 (2012).
- 14 Landau, D. A., Carter, S. L., Stojanov, P., McKenna, A., Stevenson, K., Lawrence, M. S., Sougnez, C., Stewart, C., Sivachenko, A., Wang, L., Wan, Y., Zhang, W., Shukla, S. A., Vartanov, A., Fernandes, S. M., Saksena, G., Cibulskis, K., Tesar, B., Gabriel, S., Hacohen, N., Meyerson, M., Lander, E. S., Neuber, D., Brown, J. R., Getz, G. & Wu, C. J. Evolution and impact of subclonal mutations in chronic lymphocytic leukemia. *Cell* **152**, 714-726 (2013).
- 15 Meacham, C. E. & Morrison, S. J. Tumour heterogeneity and cancer cell plasticity. *Nature* **501**, 328-337 (2013).
- 16 Gerlinger, M., Rowan, A. J., Horswell, S., Larkin, J., Endesfelder, D., Gronroos, E., Martinez, P., Matthews, N., Stewart, A., Tarpey, P., Varela, I., Phillimore, B., Begum, S., McDonald, N. Q., Butler, A., Jones, D., Raine, K., Latimer, C., Santos, C. R., Nohadani, M., Eklund, A. C., Spencer-Dene, B., Clark, G., Pickering, L., Stamp, G., Gore, M., Szallasi, Z., Downward, J., Futreal, P. A. & Swanton, C. Intratumor heterogeneity and branched evolution revealed by multiregion sequencing. *N Engl J Med* **366**, 883-892 (2012).
- 17 Shah, S. P., Morin, R. D., Khattra, J., Prentice, L., Pugh, T., Burleigh, A., Delaney, A., Gelmon, K., Guliany, R., Senz, J., Steidl, C., Holt, R. A., Jones, S., Sun, M., Leung, G., Moore, R., Severson, T., Taylor, G. A., Teschendorff, A. E., Tse, K., Turashvili, G., Varhol, R., Warren, R. L., Watson, P., Zhao, Y., Caldas, C., Huntsman, D., Hirst, M., Marra, M. A. & Aparicio, S. Mutational evolution in a lobular breast tumour profiled at single nucleotide resolution. *Nature* **461**, 809-813 (2009).
- 18 Wu, X., Northcott, P. A., Dubuc, A., Dupuy, A. J., Shih, D. J., Witt, H., Croul, S., Bouffet, E., Fults, D. W., Eberhart, C. G., Garzia, L., Van Meter, T., Zagzag, D., Jabado, N., Schwartzentruber, J., Majewski, J., Scheetz, T. E., Pfister, S. M.,

- Korshunov, A., Li, X. N., Scherer, S. W., Cho, Y. J., Akagi, K., MacDonald, T. J., Koster, J., McCabe, M. G., Sarver, A. L., Collins, V. P., Weiss, W. A., Largaespada, D. A., Collier, L. S. & Taylor, M. D. Clonal selection drives genetic divergence of metastatic medulloblastoma. *Nature* **482**, 529-533 (2012).
- 19 Martinez, P., Birkbak, N. J., Gerlinger, M., McGranahan, N., Burrell, R. A., Rowan, A. J., Joshi, T., Fisher, R., Larkin, J., Szallasi, Z. & Swanton, C. Parallel evolution of tumour subclones mimics diversity between tumours. *J Pathol* **230**, 356-364 (2013).
- 20 Yates, L. R. & Campbell, P. J. Evolution of the cancer genome. *Nat Rev Genet* **13**, 795-806 (2012).
- 21 Junttila, M. R. & de Sauvage, F. J. Influence of tumour micro-environment heterogeneity on therapeutic response. *Nature* **501**, 346-354 (2013).
- 22 Navin, N., Kendall, J., Troge, J., Andrews, P., Rodgers, L., McIndoo, J., Cook, K., Stepansky, A., Levy, D., Esposito, D., Muthuswamy, L., Krasnitz, A., McCombie, W. R., Hicks, J. & Wigler, M. Tumour evolution inferred by single-cell sequencing. *Nature* **472**, 90-94 (2011).
- 23 Govindan, R., Ding, L., Griffith, M., Subramanian, J., Dees, N. D., Kanchi, K. L., Maher, C. A., Fulton, R., Fulton, L., Wallis, J., Chen, K., Walker, J., McDonald, S., Bose, R., Ornitz, D., Xiong, D., You, M., Dooling, D. J., Watson, M., Mardis, E. R. & Wilson, R. K. Genomic landscape of non-small cell lung cancer in smokers and never-smokers. *Cell* **150**, 1121-1134 (2012).
- 24 Nik-Zainal, S., Van Loo, P., Wedge, D. C., Alexandrov, L. B., Greenman, C. D., Lau, K. W., Raine, K., Jones, D., Marshall, J., Ramakrishna, M., Shlien, A., Cooke, S. L., Hinton, J., Menzies, A., Stebbings, L. A., Leroy, C., Jia, M., Rance, R., Mudie, L. J., Gamble, S. J., Stephens, P. J., McLaren, S., Tarpey, P. S., Papaemmanuil, E., Davies, H. R., Varela, I., McBride, D. J., Bignell, G. R., Leung, K., Butler, A. P., Teague, J. W., Martin, S., Jonsson, G., Mariani, O., Boyault, S., Miron, P., Fatima, A., Langerod, A., Aparicio, S. A., Tutt, A., Sieuwerts, A. M., Borg, A., Thomas, G., Salomon, A. V., Richardson, A. L., Borresen-Dale, A. L., Futreal, P. A., Stratton, M. R., Campbell, P. J. & Breast Cancer Working Group of the International Cancer Genome, C. The life history of 21 breast cancers. *Cell* **149**, 994-1007 (2012).
- 25 Cahill, D. P., Kinzler, K. W., Vogelstein, B. & Lengauer, C. Genetic instability and darwinian selection in tumours. *Trends Cell Biol* **9**, M57-60 (1999).
- 26 Szerlip, N. J., Pedraza, A., Chakravarty, D., Azim, M., McGuire, J., Fang, Y., Ozawa, T., Holland, E. C., Huse, J. T., Jhanwar, S., Leversha, M. A., Mikkelsen, T. & Brennan, C. W. Intratumoral heterogeneity of receptor tyrosine kinases EGFR and PDGFRA amplification in glioblastoma defines subpopulations with distinct growth factor response. *Proc Natl Acad Sci U S A* **109**, 3041-3046 (2012).

- 27 Wu, M., Pastor-Pareja, J. C. & Xu, T. Interaction between Ras(V12) and scribbled clones induces tumour growth and invasion. *Nature* **463**, 545-548 (2010).
- 28 Snuderl, M., Fazlollahi, L., Le, L. P., Nitta, M., Zhelyazkova, B. H., Davidson, C. J., Akhavanfard, S., Cahill, D. P., Aldape, K. D., Betensky, R. A., Louis, D. N. & Iafrate, A. J. Mosaic amplification of multiple receptor tyrosine kinase genes in glioblastoma. *Cancer Cell* **20**, 810-817 (2011).
- 29 Inda, M. M., Bonavia, R., Mukasa, A., Narita, Y., Sah, D. W., Vandenberg, S., Brennan, C., Johns, T. G., Bachoo, R., Hadwiger, P., Tan, P., Depinho, R. A., Cavenee, W. & Furnari, F. Tumor heterogeneity is an active process maintained by a mutant EGFR-induced cytokine circuit in glioblastoma. *Genes Dev* **24**, 1731-1745 (2010).
- 30 Kreso, A., O'Brien, C. A., van Galen, P., Gan, O. I., Notta, F., Brown, A. M., Ng, K., Ma, J., Wienholds, E., Dunant, C., Pollett, A., Gallinger, S., McPherson, J., Mullighan, C. G., Shibata, D. & Dick, J. E. Variable clonal repopulation dynamics influence chemotherapy response in colorectal cancer. *Science* **339**, 543-548 (2013).
- 31 Meads, M. B., Gatenby, R. A. & Dalton, W. S. Environment-mediated drug resistance: a major contributor to minimal residual disease. *Nat Rev Cancer* **9**, 665-674 (2009).
- 32 Zhang, S., Liu, X., Bawa-Khalife, T., Lu, L. S., Lyu, Y. L., Liu, L. F. & Yeh, E. T. Identification of the molecular basis of doxorubicin-induced cardiotoxicity. *Nat Med* **18**, 1639-1642 (2012).
- 33 Assumpção, J. U., Campos, M. L., Ferraz Nogueira Filho, M. A., Pestana, K. C., Baldan, H. M., Formariz Pilon, T. P., de Oliveira, A. G. & Peccinini, R. G. Biocompatible microemulsion modifies the pharmacokinetic profile and cardiotoxicity of doxorubicin. *J Pharm Sci* **102**, 289-296 (2013).
- 34 DiPaola, R. S., Rinehart, J., Nemunaitis, J., Ebbinghaus, S., Rubin, E., Capanna, T., Ciardella, M., Doyle-Lindrud, S., Goodwin, S., Fontaine, M., Adams, N., Williams, A., Schwartz, M., Winchell, G., Wickersham, K., Deutsch, P. & Yao, S. L. Characterization of a novel prostate-specific antigen-activated peptide-doxorubicin conjugate in patients with prostate cancer. *J Clin Oncol* **20**, 1874-1879 (2002).
- 35 Sapro, P., Stein, R., Pickett, J., Qu, Z., Govindan, S. V., Cardillo, T. M., Hansen, H. J., Horak, I. D., Griffiths, G. L. & Goldenberg, D. M. Anti-CD74 antibody-doxorubicin conjugate, IMMU-110, in a human multiple myeloma xenograft and in monkeys. *Clin Cancer Res* **11**, 5257-5264 (2005).
- 36 Agniswamy, J., Fang, B. & Weber, I. T. Plasticity of S2-S4 specificity pockets of executioner caspase-7 revealed by structural and kinetic analysis. *FEBS J* **274**, 4752-4765 (2007).

- 37 Asakura, T., Sawai, T., Hashidume, Y., Ohkawa, Y., Yokoyama, S. & Ohkawa, K. Caspase-3 activation during apoptosis caused by glutathione-doxorubicin conjugate. *Br J Cancer* **80**, 711-715 (1999).
- 38 Ueno, M., Kakinuma, Y., Yuhki, K., Murakoshi, N., Iemitsu, M., Miyauchi, T. & Yamaguchi, I. Doxorubicin induces apoptosis by activation of caspase-3 in cultured cardiomyocytes in vitro and rat cardiac ventricles in vivo. *J Pharmacol Sci* **101**, 151-158 (2006).
- 39 Jacobson, M. D., Weil, M. & Raff, M. C. Programmed cell death in animal development. *Cell* **88**, 347-354 (1997).
- 40 Kerr, J. F., Wyllie, A. H. & Currie, A. R. Apoptosis: a basic biological phenomenon with wide-ranging implications in tissue kinetics. *Br J Cancer* **26**, 239-257 (1972).
- 41 Danial, N. N. & Korsmeyer, S. J. Cell death: critical control points. *Cell* **116**, 205-219 (2004).
- 42 Alnemri, E. S., Livingston, D. J., Nicholson, D. W., Salvesen, G., Thornberry, N. A., Wong, W. W. & Yuan, J. Human ICE/CED-3 protease nomenclature. *Cell* **87**, 171 (1996).
- 43 Shi, Y. Mechanisms of caspase activation and inhibition during apoptosis. *Mol Cell* **9**, 459-470 (2002).
- 44 Boatright, K. M. & Salvesen, G. S. Mechanisms of caspase activation. *Curr Opin Cell Biol* **15**, 725-731 (2003).
- 45 Stennicke, H. R., Deveraux, Q. L., Humke, E. W., Reed, J. C., Dixit, V. M. & Salvesen, G. S. Caspase-9 can be activated without proteolytic processing. *J Biol Chem* **274**, 8359-8362 (1999).
- 46 Donepudi, M., Mac Sweeney, A., Briand, C. & Grutter, M. G. Insights into the regulatory mechanism for caspase-8 activation. *Mol Cell* **11**, 543-549 (2003).
- 47 Adams, J. M. & Cory, S. Apoptosomes: engines for caspase activation. *Curr Opin Cell Biol* **14**, 715-720 (2002).
- 48 Shi, Y. Apoptosome: the cellular engine for the activation of caspase-9. *Structure* **10**, 285-288 (2002).
- 49 Riedl, S. J. & Shi, Y. Molecular mechanisms of caspase regulation during apoptosis. *Nat Rev Mol Cell Biol* **5**, 897-907 (2004).
- 50 Hanahan, D. & Weinberg, R. A. The hallmarks of cancer. *Cell* **100**, 57-70 (2000).
- 51 Wang, X. The expanding role of mitochondria in apoptosis. *Genes Dev* **15**, 2922-2933 (2001).
- 52 Zou, H., Li, Y., Liu, X. & Wang, X. An APAF-1.cytochrome c multimeric complex is a functional apoptosome that activates procaspase-9. *J Biol Chem* **274**, 11549-11556 (1999).

- 53 Saleh, A., Srinivasula, S. M., Acharya, S., Fishel, R. & Alnemri, E. S. Cytochrome c and dATP-mediated oligomerization of Apaf-1 is a prerequisite for procaspase-9 activation. *J Biol Chem* **274**, 17941-17945 (1999).
- 54 Ashkenazi, A. & Dixit, V. M. Death receptors: signaling and modulation. *Science* **281**, 1305-1308 (1998).
- 55 Peter, M. E. & Krammer, P. H. The CD95(APO-1/Fas) DISC and beyond. *Cell Death Differ* **10**, 26-35 (2003).
- 56 Harper, N., Hughes, M., MacFarlane, M. & Cohen, G. M. Fas-associated death domain protein and caspase-8 are not recruited to the tumor necrosis factor receptor 1 signaling complex during tumor necrosis factor-induced apoptosis. *J Biol Chem* **278**, 25534-25541 (2003).
- 57 Micheau, O. & Tschopp, J. Induction of TNF receptor I-mediated apoptosis via two sequential signaling complexes. *Cell* **114**, 181-190 (2003).
- 58 Luo, X., Budihardjo, I., Zou, H., Slaughter, C. & Wang, X. Bid, a Bcl2 interacting protein, mediates cytochrome c release from mitochondria in response to activation of cell surface death receptors. *Cell* **94**, 481-490 (1998).
- 59 Li, H., Zhu, H., Xu, C. J. & Yuan, J. Cleavage of BID by caspase 8 mediates the mitochondrial damage in the Fas pathway of apoptosis. *Cell* **94**, 491-501 (1998).
- 60 Thornberry, N. A., Rano, T. A., Peterson, E. P., Rasper, D. M., Timkey, T., Garcia-Calvo, M., Houtzager, V. M., Nordstrom, P. A., Roy, S., Vaillancourt, J. P., Chapman, K. T. & Nicholson, D. W. A combinatorial approach defines specificities of members of the caspase family and granzyme B. Functional relationships established for key mediators of apoptosis. *J Biol Chem* **272**, 17907-17911 (1997).
- 61 Wang, X., Pai, J. T., Wiedenfeld, E. A., Medina, J. C., Slaughter, C. A., Goldstein, J. L. & Brown, M. S. Purification of an interleukin-1 beta converting enzyme-related cysteine protease that cleaves sterol regulatory element-binding proteins between the leucine zipper and transmembrane domains. *J Biol Chem* **270**, 18044-18050 (1995).
- 62 Na, S., Chuang, T. H., Cunningham, A., Turi, T. G., Hanke, J. H., Bokoch, G. M. & Danley, D. E. D4-GDI, a substrate of CPP32, is proteolyzed during Fas-induced apoptosis. *J Biol Chem* **271**, 11209-11213 (1996).
- 63 Lazebnik, Y. A., Kaufmann, S. H., Desnoyers, S., Poirier, G. G. & Earnshaw, W. C. Cleavage of poly(ADP-ribose) polymerase by a proteinase with properties like ICE. *Nature* **371**, 346-347 (1994).
- 64 Casciola-Rosen, L., Nicholson, D. W., Chong, T., Rowan, K. R., Thornberry, N. A., Miller, D. K. & Rosen, A. Apopain/CPP32 cleaves proteins that are essential for cellular repair: a fundamental principle of apoptotic death. *J Exp Med* **183**, 1957-1964 (1996).

- 65 Emoto, Y., Manome, Y., Meinhardt, G., Kisaki, H., Kharbanda, S., Robertson, M., Ghayur, T., Wong, W. W., Kamen, R., Weichselbaum, R. & et al. Proteolytic activation of protein kinase C delta by an ICE-like protease in apoptotic cells. *EMBO J* **14**, 6148-6156 (1995).
- 66 Nicholson, D. W., Ali, A., Thornberry, N. A., Vaillancourt, J. P., Ding, C. K., Gallant, M., Gareau, Y., Griffin, P. R., Labelle, M., Lazebnik, Y. A. & et al. Identification and inhibition of the ICE/CED-3 protease necessary for mammalian apoptosis. *Nature* **376**, 37-43 (1995).
- 67 Lien, S., Pastor, R., Sutherlin, D. & Lowman, H. B. A substrate-phage approach for investigating caspase specificity. *Protein J* **23**, 413-425 (2004).
- 68 Yoshimori, A., Takasawa, R. & Tanuma, S. A novel method for evaluation and screening of caspase inhibitory peptides by the amino acid positional fitness score. *BMC Pharmacol* **4**, 7 (2004).
- 69 Earnshaw, W. C., Martins, L. M. & Kaufmann, S. H. Mammalian caspases: structure, activation, substrates, and functions during apoptosis. *Annu Rev Biochem* **68**, 383-424 (1999).
- 70 Steichen, S. D., Caldorera-Moore, M. & Peppas, N. A. A review of current nanoparticle and targeting moieties for the delivery of cancer therapeutics. *Eur J Pharm Sci* **48**, 416-427 (2013).
- 71 Danhier, F., Feron, O. & Preat, V. To exploit the tumor microenvironment: Passive and active tumor targeting of nanocarriers for anti-cancer drug delivery. *J Control Release* **148**, 135-146 (2010).
- 72 Matsumura, Y. & Maeda, H. A new concept for macromolecular therapeutics in cancer chemotherapy: mechanism of tumorotropic accumulation of proteins and the antitumor agent smancs. *Cancer Res* **46**, 6387-6392 (1986).
- 73 Fang, J., Nakamura, H. & Maeda, H. The EPR effect: Unique features of tumor blood vessels for drug delivery, factors involved, and limitations and augmentation of the effect. *Adv Drug Deliv Rev* **63**, 136-151 (2011).
- 74 Maeda, H. Tumor-selective delivery of macromolecular drugs via the EPR effect: background and future prospects. *Bioconjug Chem* **21**, 797-802 (2010).
- 75 Fang, J., Sawa, T., Akaike, T. & Maeda, H. Tumor-targeted delivery of polyethylene glycol-conjugated D-amino acid oxidase for antitumor therapy via enzymatic generation of hydrogen peroxide. *Cancer Res* **62**, 3138-3143 (2002).
- 76 Fang, J., Sawa, T., Akaike, T., Akuta, T., Sahoo, S. K., Khaled, G., Hamada, A. & Maeda, H. In vivo antitumor activity of pegylated zinc protoporphyrin: targeted inhibition of heme oxygenase in solid tumor. *Cancer Res* **63**, 3567-3574 (2003).

- 77 Greish, K., Sawa, T., Fang, J., Akaike, T. & Maeda, H. SMA-doxorubicin, a new polymeric micellar drug for effective targeting to solid tumours. *J Control Release* **97**, 219-230 (2004).
- 78 Greish, K., Nagamitsu, A., Fang, J. & Maeda, H. Copoly(styrene-maleic acid)-pirarubicin micelles: high tumor-targeting efficiency with little toxicity. *Bioconjug Chem* **16**, 230-236 (2005).
- 79 Iyer, A. K., Greish, K., Fang, J., Murakami, R. & Maeda, H. High-loading nanosized micelles of copoly(styrene-maleic acid)-zinc protoporphyrin for targeted delivery of a potent heme oxygenase inhibitor. *Biomaterials* **28**, 1871-1881 (2007).
- 80 Yuan, F., Dellian, M., Fukumura, D., Leunig, M., Berk, D. A., Torchilin, V. P. & Jain, R. K. Vascular permeability in a human tumor xenograft: molecular size dependence and cutoff size. *Cancer Res* **55**, 3752-3756 (1995).
- 81 Noguchi, Y., Wu, J., Duncan, R., Strohmalm, J., Ulbrich, K., Akaike, T. & Maeda, H. Early phase tumor accumulation of macromolecules: a great difference in clearance rate between tumor and normal tissues. *Jpn J Cancer Res* **89**, 307-314 (1998).
- 82 Duncan, R. The dawning era of polymer therapeutics. *Nat Rev Drug Discov* **2**, 347-360 (2003).
- 83 Vicent, M. J., Ringsdorf, H. & Duncan, R. Polymer therapeutics: clinical applications and challenges for development. *Adv Drug Deliv Rev* **61**, 1117-1120 (2009).
- 84 Matsumura, Y. & Kataoka, K. Preclinical and clinical studies of anticancer agent-incorporating polymer micelles. *Cancer Sci* **100**, 572-579 (2009).
- 85 Brigger, I., Dubernet, C. & Couvreur, P. Nanoparticles in cancer therapy and diagnosis. *Adv Drug Deliv Rev* **54**, 631-651 (2002).
- 86 Gu, F. X., Karnik, R., Wang, A. Z., Alexis, F., Levy-Nissenbaum, E., Hong, S., Langer, R. S. & Farokhzad, O. C. Targeted nanoparticles for cancer therapy. *Nano Today* **2**, 14-21 (2007).
- 87 Kratz, F. & Elsakdeh, B. Clinical impact of serum proteins on drug delivery. *J Control Release* **161**, 429-445 (2012).
- 88 Peters, T., Jr. Serum albumin. *Adv Protein Chem* **37**, 161-245 (1985).
- 89 Kratz, F. Albumin as a drug carrier: design of prodrugs, drug conjugates and nanoparticles. *J Control Release* **132**, 171-183 (2008).
- 90 Mendez, C. M., McClain, C. J. & Marsano, L. S. Albumin therapy in clinical practice. *Nutr Clin Pract* **20**, 314-320 (2005).
- 91 Bosse, D., Praus, M., Kiessling, P., Nyman, L., Andresen, C., Waters, J. & Schindel, F. Phase I comparability of recombinant human albumin and human serum albumin. *J Clin Pharmacol* **45**, 57-67 (2005).
- 92 Babson, A. L. & Winnick, T. Protein transfer in tumor-bearing rats. *Cancer Res* **14**, 606-611 (1954).

- 93 Bazak, R., Houri, M., Achy, S. E., Hussein, W. & Refaat, T. Passive targeting of nanoparticles to cancer: A comprehensive review of the literature. *Molecular and clinical oncology* **2**, 904-908 (2014).
- 94 Jain, R. K. A new target for tumor therapy. *N Engl J Med* **360**, 2669-2671 (2009).
- 95 Hobbs, S. K., Monsky, W. L., Yuan, F., Roberts, W. G., Griffith, L., Torchilin, V. P. & Jain, R. K. Regulation of transport pathways in tumor vessels: role of tumor type and microenvironment. *Proc Natl Acad Sci U S A* **95**, 4607-4612 (1998).
- 96 Kratz, F. & Beyer, U. Serum proteins as drug carriers of anticancer agents: a review. *Drug Deliv* **5**, 281-299 (1998).
- 97 Schnitzer, J. E. gp60 is an albumin-binding glycoprotein expressed by continuous endothelium involved in albumin transcytosis. *Am J Physiol* **262**, H246-254 (1992).
- 98 Tiruppathi, C., Song, W., Bergenfeldt, M., Sass, P. & Malik, A. B. Gp60 activation mediates albumin transcytosis in endothelial cells by tyrosine kinase-dependent pathway. *J Biol Chem* **272**, 25968-25975 (1997).
- 99 Wang, Z., Tiruppathi, C., Minshall, R. D. & Malik, A. B. Size and dynamics of caveolae studied using nanoparticles in living endothelial cells. *ACS nano* **3**, 4110-4116 (2009).
- 100 Elsadek, B. & Kratz, F. Impact of albumin on drug delivery--new applications on the horizon. *J Control Release* **157**, 4-28 (2012).
- 101 Sage, H., Johnson, C. & Bornstein, P. Characterization of a novel serum albumin-binding glycoprotein secreted by endothelial cells in culture. *J Biol Chem* **259**, 3993-4007 (1984).
- 102 Tiruppathi, C., Finnegan, A. & Malik, A. B. Isolation and characterization of a cell surface albumin-binding protein from vascular endothelial cells. *Proc Natl Acad Sci U S A* **93**, 250-254 (1996).
- 103 Podhajcer, O. L., Benedetti, L. G., Girotti, M. R., Prada, F., Salvatierra, E. & Llera, A. S. The role of the matricellular protein SPARC in the dynamic interaction between the tumor and the host. *Cancer Metastasis Rev* **27**, 691-705 (2008).
- 104 Desai, N., Trieu, V., Damascelli, B. & Soon-Shiong, P. SPARC Expression Correlates with Tumor Response to Albumin-Bound Paclitaxel in Head and Neck Cancer Patients. *Transl Oncol* **2**, 59-64 (2009).
- 105 Stehle, G., Sinn, H., Wunder, A., Schrenk, H. H., Stewart, J. C., Hartung, G., Maier-Borst, W. & Heene, D. L. Plasma protein (albumin) catabolism by the tumor itself--implications for tumor metabolism and the genesis of cachexia. *Crit Rev Oncol Hematol* **26**, 77-100 (1997).
- 106 Kratz, F., Fichtner, I. & Graeser, R. Combination therapy with the albumin-binding prodrug of doxorubicin (INNO-206) and doxorubicin achieves complete remissions

- and improves tolerability in an ovarian A2780 xenograft model. *Invest New Drugs* **30**, 1743-1749 (2012).
- 107 Chaudhury, C., Mehnaz, S., Robinson, J. M., Hayton, W. L., Pearl, D. K., Roopenian, D. C. & Anderson, C. L. The major histocompatibility complex-related Fc receptor for IgG (FcRn) binds albumin and prolongs its lifespan. *J Exp Med* **197**, 315-322 (2003).
- 108 Chaudhury, C., Brooks, C. L., Carter, D. C., Robinson, J. M. & Anderson, C. L. Albumin binding to FcRn: distinct from the FcRn-IgG interaction. *Biochemistry* **45**, 4983-4990 (2006).
- 109 Kratz, F., Muller-Driver, R., Hofmann, I., Dreves, J. & Unger, C. A novel macromolecular prodrug concept exploiting endogenous serum albumin as a drug carrier for cancer chemotherapy. *J Med Chem* **43**, 1253-1256 (2000).
- 110 Kratz, F. DOXO-EMCH (INNO-206): the first albumin-binding prodrug of doxorubicin to enter clinical trials. *Expert opinion on investigational drugs* **16**, 855-866 (2007).
- 111 Carter, D. C. & Ho, J. X. Structure of serum albumin. *Adv Protein Chem* **45**, 153-203 (1994).
- 112 Kratz, F., Warnecke, A., Scheuermann, K., Stockmar, C., Schwab, J., Lazar, P., Druckes, P., Esser, N., Dreves, J., Rognan, D., Bissantz, C., Hinderling, C., Folkers, G., Fichtner, I. & Unger, C. Probing the cysteine-34 position of endogenous serum albumin with thiol-binding doxorubicin derivatives. Improved efficacy of an acid-sensitive doxorubicin derivative with specific albumin-binding properties compared to that of the parent compound. *J Med Chem* **45**, 5523-5533 (2002).
- 113 Ferguson, E., Singh, R. J., Hogg, N. & Kalyanaraman, B. The mechanism of apolipoprotein B-100 thiol depletion during oxidative modification of low-density lipoprotein. *Arch Biochem Biophys* **341**, 287-294 (1997).
- 114 Smith, D. E., Mosher, D. F., Johnson, R. B. & Furcht, L. T. Immunological identification of two sulfhydryl-containing fragments of human plasma fibronectin. *J Biol Chem* **257**, 5831-5838 (1982).
- 115 Shimokawa, Y., Abe, O. & Kuromizu, K. Fluorescence labeling of a single sulfhydryl group in human plasma alpha 1-proteinase inhibitor and characterization of the labeled inhibitor. *J Biochem* **100**, 563-570 (1986).
- 116 Chawla, S. P., Chua, V. S., Hendifar, A. F., Quon, D. V., Soman, N., Sankhala, K. K., Wieland, D. S. & Levitt, D. J. A phase 1B/2 study of aldodoxorubicin in patients with soft tissue sarcoma. *Cancer*, 1-10 (2014).
- 117 Kratz, F. INNO-206 (DOXO-EMCH), an albumin-binding prodrug of doxorubicin under development for phase II studies. *Curr Bioact Compd* **7**, 33-38 (2011).

- 118 Chung, D. E. & Kratz, F. Development of a novel albumin-binding prodrug that is cleaved by urokinase-type-plasminogen activator (uPA). *Bioorg Med Chem Lett* **16**, 5157-5163 (2006).
- 119 Schmid, B., Chung, D. E., Warnecke, A., Fichtner, I. & Kratz, F. Albumin-binding prodrugs of camptothecin and doxorubicin with an Ala-Leu-Ala-Leu-linker that are cleaved by cathepsin B: synthesis and antitumor efficacy. *Bioconjug Chem* **18**, 702-716 (2007).
- 120 Abu Ajaj, K., Graeser, R. & Kratz, F. Zosuquidar and an albumin-binding prodrug of zosuquidar reverse multidrug resistance in breast cancer cells of doxorubicin and an albumin-binding prodrug of doxorubicin. *Breast Cancer Res Treat* **134**, 117-129 (2012).
- 121 Haley, B. & Frenkel, E. Nanoparticles for drug delivery in cancer treatment. *Urol Oncol* **26**, 57-64 (2008).
- 122 Adams, G. P. & Weiner, L. M. Monoclonal antibody therapy of cancer. *Nat Biotechnol* **23**, 1147-1157 (2005).
- 123 Brannon-Peppas, L. & Blanchette, J. O. Nanoparticle and targeted systems for cancer therapy. *Adv Drug Deliv Rev* **56**, 1649-1659 (2004).
- 124 Weber, J. Review: anti-CTLA-4 antibody ipilimumab: case studies of clinical response and immune-related adverse events. *Oncologist* **12**, 864-872 (2007).
- 125 Weiner, L. M., Surana, R. & Wang, S. Monoclonal antibodies: versatile platforms for cancer immunotherapy. *Nat Rev Immunol* **10**, 317-327 (2010).
- 126 von Mehren, M., Adams, G. P. & Weiner, L. M. Monoclonal antibody therapy for cancer. *Annu Rev Med* **54**, 343-369 (2003).
- 127 Mendelsohn, J. Epidermal growth factor receptor inhibition by a monoclonal antibody as anticancer therapy. *Clin Cancer Res* **3**, 2703-2707 (1997).
- 128 Nobs, L., Buchegger, F., Gurny, R. & Allemann, E. Biodegradable nanoparticles for direct or two-step tumor immunotargeting. *Bioconjug Chem* **17**, 139-145 (2006).
- 129 Hughes, B. Antibody-drug conjugates for cancer: poised to deliver? *Nat Rev Drug Discov* **9**, 665-667 (2010).
- 130 Zolot, R. S., Basu, S. & Million, R. P. Antibody-drug conjugates. *Nat Rev Drug Discov* **12**, 259-260 (2013).
- 131 Brissette, R., Prendergast, J. K. & Goldstein, N. I. Identification of cancer targets and therapeutics using phage display. *Current opinion in drug discovery & development* **9**, 363-369 (2006).
- 132 Krag, D. N., Shukla, G. S., Shen, G. P., Pero, S., Ashikaga, T., Fuller, S., Weaver, D. L., Burdette-Radoux, S. & Thomas, C. Selection of tumor-binding ligands in cancer patients with phage display libraries. *Cancer Res* **66**, 7724-7733 (2006).

- 133 Brooks, P. C., Montgomery, A. M., Rosenfeld, M., Reisfeld, R. A., Hu, T., Klier, G. & Cheresch, D. A. Integrin alpha v beta 3 antagonists promote tumor regression by inducing apoptosis of angiogenic blood vessels. *Cell* **79**, 1157-1164 (1994).
- 134 Byrne, J. D., Betancourt, T. & Brannon-Peppas, L. Active targeting schemes for nanoparticle systems in cancer therapeutics. *Adv Drug Deliv Rev* **60**, 1615-1626 (2008).
- 135 Chen, K. & Chen, X. Integrin targeted delivery of chemotherapeutics. *Theranostics* **1**, 189-200 (2011).
- 136 Henderson, G. B. Folate-binding proteins. *Annu Rev Nutr* **10**, 319-335 (1990).
- 137 Hilgenbrink, A. R. & Low, P. S. Folate receptor-mediated drug targeting: from therapeutics to diagnostics. *J Pharm Sci* **94**, 2135-2146 (2005).
- 138 Low, P. S. & Kularatne, S. A. Folate-targeted therapeutic and imaging agents for cancer. *Curr Opin Chem Biol* **13**, 256-262 (2009).
- 139 Sudimack, J. & Lee, R. J. Targeted drug delivery via the folate receptor. *Adv Drug Deliv Rev* **41**, 147-162 (2000).
- 140 Ponka, P. & Lok, C. N. The transferrin receptor: role in health and disease. *Int J Biochem Cell Biol* **31**, 1111-1137 (1999).
- 141 Qian, Z. M., Li, H., Sun, H. & Ho, K. Targeted drug delivery via the transferrin receptor-mediated endocytosis pathway. *Pharmacol Rev* **54**, 561-587 (2002).
- 142 Sahoo, S. K., Ma, W. & Labhasetwar, V. Efficacy of transferrin-conjugated paclitaxel-loaded nanoparticles in a murine model of prostate cancer. *Int J Cancer* **112**, 335-340 (2004).
- 143 Daniels, T. R., Delgado, T., Helguera, G. & Penichet, M. L. The transferrin receptor part II: targeted delivery of therapeutic agents into cancer cells. *Clin Immunol* **121**, 159-176 (2006).
- 144 Pavalko, F. M. & Otey, C. A. Role of adhesion molecule cytoplasmic domains in mediating interactions with the cytoskeleton. *Proc Soc Exp Biol Med* **205**, 282-293 (1994).
- 145 Haass, N. K., Smalley, K. S., Li, L. & Herlyn, M. Adhesion, migration and communication in melanocytes and melanoma. *Pigment Cell Res* **18**, 150-159 (2005).
- 146 Turowski, P., Adamson, P. & Greenwood, J. Pharmacological targeting of ICAM-1 signaling in brain endothelial cells: potential for treating neuroinflammation. *Cell Mol Neurobiol* **25**, 153-170 (2005).
- 147 Ruoslahti, E. Fibronectin and its integrin receptors in cancer. *Adv Cancer Res* **76**, 1-20 (1999).
- 148 Hynes, R. O. & Zhao, Q. The evolution of cell adhesion. *J Cell Biol* **150**, F89-96 (2000).

- 149 Hynes, R. O. A reevaluation of integrins as regulators of angiogenesis. *Nat Med* **8**, 918-921 (2002).
- 150 Maaser, K., Wolf, K., Klein, C. E., Niggemann, B., Zanker, K. S., Brocker, E. B. & Friedl, P. Functional hierarchy of simultaneously expressed adhesion receptors: integrin alpha2beta1 but not CD44 mediates MV3 melanoma cell migration and matrix reorganization within three-dimensional hyaluronan-containing collagen matrices. *Mol Biol Cell* **10**, 3067-3079 (1999).
- 151 Ruoslahti, E. Specialization of tumour vasculature. *Nat Rev Cancer* **2**, 83-90 (2002).
- 152 Christofori, G. Changing neighbours, changing behaviour: cell adhesion molecule-mediated signalling during tumour progression. *EMBO J* **22**, 2318-2323 (2003).
- 153 Andrews, R. K. & Berndt, M. C. Platelet physiology and thrombosis. *Thromb Res* **114**, 447-453 (2004).
- 154 Banquy, X., Leclair, G., Rabanel, J. M., Argaw, A., Bouchard, J. F., Hildgen, P. & Giasson, S. Selectins ligand decorated drug carriers for activated endothelial cell targeting. *Bioconjug Chem* **19**, 2030-2039 (2008).
- 155 Ichinose, K., Kawasaki, E. & Eguchi, K. Recent advancement of understanding pathogenesis of type 1 diabetes and potential relevance to diabetic nephropathy. *Am J Nephrol* **27**, 554-564 (2007).
- 156 Brooks, P. C., Clark, R. A. & Cheresh, D. A. Requirement of vascular integrin alpha v beta 3 for angiogenesis. *Science* **264**, 569-571 (1994).
- 157 Hood, J. D. & Cheresh, D. A. Role of integrins in cell invasion and migration. *Nat Rev Cancer* **2**, 91-100 (2002).
- 158 Danhier, F., Le Breton, A. & Preat, V. RGD-based strategies to target alpha(v) beta(3) integrin in cancer therapy and diagnosis. *Mol Pharm* **9**, 2961-2973 (2012).
- 159 Avraamides, C. J., Garmy-Susini, B. & Varnier, J. A. Integrins in angiogenesis and lymphangiogenesis. *Nat Rev Cancer* **8**, 604-617 (2008).
- 160 Hynes, R. O. Integrins: bidirectional, allosteric signaling machines. *Cell* **110**, 673-687 (2002).
- 161 Barczyk, M., Carracedo, S. & Gullberg, D. Integrins. *Cell Tissue Res* **339**, 269-280 (2010).
- 162 Burridge, K. & Chrzanowska-Wodnicka, M. Focal adhesions, contractility, and signaling. *Annu Rev Cell Dev Biol* **12**, 463-518 (1996).
- 163 Takagi, J., Erickson, H. P. & Springer, T. A. C-terminal opening mimics 'inside-out' activation of integrin alpha5beta1. *Nat Struct Biol* **8**, 412-416 (2001).
- 164 Dunehoo, A. L., Anderson, M., Majumdar, S., Kobayashi, N., Berkland, C. & Siahaan, T. J. Cell adhesion molecules for targeted drug delivery. *J Pharm Sci* **95**, 1856-1872 (2006).

- 165 Cai, W. & Chen, X. Anti-angiogenic cancer therapy based on integrin alphavbeta3 antagonism. *Anticancer Agents Med Chem* **6**, 407-428 (2006).
- 166 Mizejewski, G. J. Role of integrins in cancer: survey of expression patterns. *Proc Soc Exp Biol Med* **222**, 124-138 (1999).
- 167 Jin, H. & Varner, J. Integrins: roles in cancer development and as treatment targets. *Br J Cancer* **90**, 561-565 (2004).
- 168 Francavilla, C., Maddaluno, L. & Cavallaro, U. The functional role of cell adhesion molecules in tumor angiogenesis. *Semin Cancer Biol* **19**, 298-309 (2009).
- 169 Desgrosellier, J. S. & Cheresch, D. A. Integrins in cancer: biological implications and therapeutic opportunities. *Nat Rev Cancer* **10**, 9-22 (2010).
- 170 Reynolds, A. R., Hart, I. R., Watson, A. R., Welti, J. C., Silva, R. G., Robinson, S. D., Da Violante, G., Gourlaouen, M., Salih, M., Jones, M. C., Jones, D. T., Saunders, G., Kostourou, V., Perron-Sierra, F., Norman, J. C., Tucker, G. C. & Hodivala-Dilke, K. M. Stimulation of tumor growth and angiogenesis by low concentrations of RGD-mimetic integrin inhibitors. *Nat Med* **15**, 392-400 (2009).
- 171 Furger, K. A., Allan, A. L., Wilson, S. M., Hota, C., Vantyghem, S. A., Postenka, C. O., Al-Katib, W., Chambers, A. F. & Tuck, A. B. Beta(3) integrin expression increases breast carcinoma cell responsiveness to the malignancy-enhancing effects of osteopontin. *Mol Cancer Res* **1**, 810-819 (2003).
- 172 Takayama, S., Ishii, S., Ikeda, T., Masamura, S., Doi, M. & Kitajima, M. The relationship between bone metastasis from human breast cancer and integrin alpha(v)beta3 expression. *Anticancer Res* **25**, 79-83 (2005).
- 173 Vellon, L., Menendez, J. A., Liu, H. & Lupu, R. Up-regulation of alphavbeta3 integrin expression is a novel molecular response to chemotherapy-induced cell damage in a heregulin-dependent manner. *Differentiation* **75**, 819-830 (2007).
- 174 Sheldrake, H. M. & Patterson, L. H. Function and antagonism of beta3 integrins in the development of cancer therapy. *Curr Cancer Drug Targets* **9**, 519-540 (2009).
- 175 Hosotani, R., Kawaguchi, M., Masui, T., Koshiba, T., Ida, J., Fujimoto, K., Wada, M., Doi, R. & Imamura, M. Expression of integrin alphaVbeta3 in pancreatic carcinoma: relation to MMP-2 activation and lymph node metastasis. *Pancreas* **25**, e30-35 (2002).
- 176 Ruoslahti, E. & Pierschbacher, M. D. New perspectives in cell adhesion: RGD and integrins. *Science* **238**, 491-497 (1987).
- 177 Xiong, J. P., Stehle, T., Zhang, R., Joachimiak, A., Frech, M., Goodman, S. L. & Arnaout, M. A. Crystal structure of the extracellular segment of integrin alpha Vbeta3 in complex with an Arg-Gly-Asp ligand. *Science* **296**, 151-155 (2002).

- 178 Grant, D. S., Tashiro, K., Segui-Real, B., Yamada, Y., Martin, G. R. & Kleinman, H. K. Two different laminin domains mediate the differentiation of human endothelial cells into capillary-like structures in vitro. *Cell* **58**, 933-943 (1989).
- 179 Miyachi, A., Alvarez, J., Greenfield, E. M., Teti, A., Grano, M., Colucci, S., Zamboni-Zallone, A., Ross, F. P., Teitelbaum, S. L., Cheresch, D. & et al. Recognition of osteopontin and related peptides by an alpha v beta 3 integrin stimulates immediate cell signals in osteoclasts. *J Biol Chem* **266**, 20369-20374 (1991).
- 180 Lawler, J., Weinstein, R. & Hynes, R. O. Cell attachment to thrombospondin: the role of ARG-GLY-ASP, calcium, and integrin receptors. *J Cell Biol* **107**, 2351-2361 (1988).
- 181 Ruoslahti, E. RGD and other recognition sequences for integrins. *Annu Rev Cell Dev Biol* **12**, 697-715 (1996).
- 182 Temming, K., Schiffelers, R. M., Molema, G. & Kok, R. J. RGD-based strategies for selective delivery of therapeutics and imaging agents to the tumour vasculature. *Drug resistance updates : reviews and commentaries in antimicrobial and anticancer chemotherapy* **8**, 381-402 (2005).
- 183 Liu, S. Radiolabeled multimeric cyclic RGD peptides as integrin alphavbeta3 targeted radiotracers for tumor imaging. *Mol Pharm* **3**, 472-487 (2006).
- 184 Bogdanowich-Knipp, S. J., Chakrabarti, S., Williams, T. D., Dillman, R. K. & Siahaan, T. J. Solution stability of linear vs. cyclic RGD peptides. *J Pept Res* **53**, 530-541 (1999).
- 185 Goodman, S. L., Holzemann, G., Sulyok, G. A. & Kessler, H. Nanomolar small molecule inhibitors for alphav(beta)6, alphav(beta)5, and alphav(beta)3 integrins. *J Med Chem* **45**, 1045-1051 (2002).
- 186 Dechantsreiter, M. A., Planker, E., Matha, B., Lohof, E., Holzemann, G., Jonczyk, A., Goodman, S. L. & Kessler, H. N-Methylated cyclic RGD peptides as highly active and selective alpha(V)beta(3) integrin antagonists. *J Med Chem* **42**, 3033-3040 (1999).
- 187 Holig, P., Bach, M., Volkel, T., Nahde, T., Hoffmann, S., Muller, R. & Kontermann, R. E. Novel RGD lipopeptides for the targeting of liposomes to integrin-expressing endothelial and melanoma cells. *Protein Eng Des Sel* **17**, 433-441 (2004).
- 188 Kok, R. J., Schraa, A. J., Bos, E. J., Moorlag, H. E., Asgeirsdottir, S. A., Everts, M., Meijer, D. K. & Molema, G. Preparation and functional evaluation of RGD-modified proteins as alpha(v)beta(3) integrin directed therapeutics. *Bioconjug Chem* **13**, 128-135 (2002).
- 189 Schraa, A. J., Kok, R. J., Berendsen, A. D., Moorlag, H. E., Bos, E. J., Meijer, D. K., de Leij, L. F. & Molema, G. Endothelial cells internalize and degrade RGD-modified

proteins developed for tumor vasculature targeting. *J Control Release* **83**, 241-251 (2002).

- 190 Boturyn, D., Coll, J. L., Garanger, E., Favrot, M. C. & Dumy, P. Template assembled cyclopeptides as multimeric system for integrin targeting and endocytosis. *J Am Chem Soc* **126**, 5730-5739 (2004).

Chapter 5

Albumin-binding radiation-induced apoptosis targeted doxorubicin prodrug

Despite potent anticancer effect of doxorubicin, its clinical use is often limited due to the dose-dependent toxicities. In purpose to improve the therapeutic index of doxorubicin, a novel drug delivery technology was employed that fundamentally differs with the conventional tumor-targeting approaches. The prepared doxorubicin prodrug includes two distinct features for an effective tumor targeting: EPR effect-mediated passive targeting of tumor and extended plasma half-life by *in situ* albumin binding, and radiation-induced apoptosis targeting. For these properties, the prodrug – EMC-DEVD-S-DOX – comprises two important functional molecules. One is a maleimide group that allows *in situ* binding of the prodrug to the circulating albumin after intravenous administration. Second is a DEVD motif that plays crucial role in the activation of the prodrug through caspase-3-mediated cleavage in the apoptotic tumor cells that are exposed to radiation. As a result, EMC-DEVD-S-DOX showed prolonged plasma half-life with selective accumulation within tumor tissue, and was only activated and released free doxorubicin when combined with radiotherapy, thereby showing excellent synergistic effect.

The currently suggested drug delivery strategy completely relies on the anatomical feature of tumor vasculatures and the upregulated caspase-3 after exposure to radiation. Therefore, the genomic diversity of tumor cells could hardly influence the efficacy of the prodrug. Considering that the conventional molecular targeted approach in cancer therapy is seriously challenged by the intratumor heterogeneity, EMC-DEVD-S-DOX could be an outstanding alternative for an effective cancer treatment.

5.1. Introduction

Although targeted therapies have gained considerable interests in the modern cancer therapeutics, chemotherapeutic agents still possess the most important status in the clinical oncology due to their potent anticancer effect and availability in broad spectrum of tumors. However, the dose-dependent toxicities of the chemotherapeutic agents limit both their dosage and frequency of administration, which are insufficient to achieve an effective cancer treatment. The toxicities of the chemotherapeutic agents are fundamentally caused by their lack of selectivity between tumor cells and normal cells in terms of mechanisms of action. In order to improve their selectivity, researchers have proposed many delivery systems that could selectively deliver the chemotherapeutics to a malignant tissue, thus generating site-selectivity to the agents.

One of the popular strategies to deliver chemotherapeutics selectively to a tumor is to introduce a tumor-targeting moiety that could recognize certain tumor-specific biomarkers^{1,2}. However, this strategy is fundamentally challenged by the recent findings that tumor cells differ in terms of their genotype, even within a single tumor mass, so called as intratumor heterogeneity³. The use of the aforementioned drug delivery strategy requires genomic analysis of the subject tumor in order to predict the feasibility. This is generally performed on the tissue samples that are obtained by single needle biopsy or surgical excision, where the samples only represent a small portion of the tumor tissue. However, the finding of intratumor heterogeneity indicated that such genomic analysis is inappropriate to overview the genomic landscape of the entire tumor, which may lead to wrong interpretation of determining the target biomarker in high possibility. Moreover, considering that a single tumor could have several different subtypes of tumor cells, the above mentioned tumor-targeting is likely to affect only a limited population of tumor cells and leave others unaffected, which could eventually result in regrowth of tumor. To overcome the limitations of the conventional targeted delivery of

chemotherapeutic agents, a strategy of targeting an induced-phenotype, radiation-induced apoptosis in particular, rather than targeting genotype of the tumor cells was proposed for more predictable and reliable targeted delivery of chemotherapeutic agents across all of the tumor cells in a malignant tissue⁴. When tumor cells are exposed to radiation, they undergo apoptosis and upregulate caspase-3, which is a cysteine protease^{5,6}. The major advantages of targeting the radiation-induced apoptotic tumor cells for selective delivery of chemotherapeutic agents are as follows: (i) the site of target could be controlled actively by exogenous stimuli (e.g. stereotactic radiotherapy); (ii) the amount of target molecule, which is caspase-3, increases as the therapy goes on, since the delivered drugs consequently induce tumor cell apoptosis and continuously upregulate the caspase-3. This is contrary to the conventional targeted therapy, which results in gradual decrease of target molecules due to the elimination of the tumor cells that are expressing them. Moreover, considering that radiotherapy is already used to treat approximately 50% of the cancer patients⁷, coupling the prodrug with a radiotherapy is a perfect match.

Another approach to selectively deposit chemotherapeutic agents in a malignant tissue is passively targeting the anatomical anomalies of tumor vasculatures. Due to the leaky vasculatures and lack of lymphatic drainage, macromolecules accumulate in the tumor tissue, which the phenomenon is termed as EPR (enhanced permeability and retention) effect. Albumin, a 65 kDa serum protein, also takes advantage of EPR effect and accumulates in the tumor tissue⁸. Therefore, albumin has been recognized as a promising macromolecular carrier in delivering chemotherapeutic agents to the tumor. In addition, serum albumin has a very long plasma half-life, which is more than 19 days in human⁹. Therefore, exploiting albumin as a carrier for drugs is also advantageous to prolong their circulation time. Previously, Kratz et al. proposed an interesting strategy that exploits endogenous albumin as a carrier of chemotherapeutic agents^{10,11}. Albumin is the most abundant protein in the plasma. It presents at about 35-50 mg/ml, which the amount is more than half of the total plasma proteins^{9,10}. Intriguingly, about 70% of the human serum albumin (HSA) has an

accessible free thiol group on the Cys34. This is a very unique feature among the plasma compartments regarding that thiols mostly do not exist in free form (or reduced form) in the plasma. In fact, the free thiols on the albumins account for more than 80% of the total free thiols in the blood. Moreover, they are most reactive among the thiols that exist in the plasma substances. Therefore, thiol-reactive molecules could selectively bind to the Cys34 of the HSA in the blood.

In this study, the radiation-induced apoptosis targeting and the endogenous albumin-mediated passive targeting were combined to achieve highly selective delivery of doxorubicin to the tumor (**Fig. 5.1A**). As a representative agent, EMC-DEVD-S-DOX was prepared, which the albumin-binding moiety (ϵ -maleimidocaproylamide; EMC) and doxorubicin are connected to each other via DEVD peptide spacer to produce a prodrug of doxorubicin (**Fig. 5.1B**).

The maleimide group in the EMC moiety could selectively react with thiol in physiological pH by Michael addition. Therefore, EMC-DEVD-S-DOX could bind with the Cys34 on the circulating albumins, producing a stable conjugate. The *in situ* binding of EMC-DEVD-S-DOX on albumin was confirmed using commercially available HSA in PBS (pH 7.4), human plasma, and mouse plasma.

The DEVD peptide, which acts as a spacer between EMC (or potentially albumin) and doxorubicin, is a well-known cleavable substrate of caspase-3. The caspase-3 recognizes the DEVD sequence within a peptide and enzymatically hydrolyzes the amide bond following the second Asp of the tetrapeptide sequence. Therefore, free doxorubicin could be released from the bound albumin when reached at the apoptotic site that is exposed to radiation. The release of doxorubicin in the presence of caspase-3 was confirmed through several *in vitro* studies. Pharmacokinetic and tumor regression studies were also carried out in preclinical models.

5.2. Materials and methods

5.2.1. Cell lines

SCC7 and MDA-MB-231 cells were obtained from the American Type Culture Collection (ATCC; Manassas, VA). The cells were grown in high-glucose Dulbecco's modified eagle medium (DMEM; Gibco, Carlsbad, CA) supplemented with 10% fetal bovine serum (FBS; Gibco). The cells were maintained in a humidified 5% CO₂ atmosphere at 37°C.

5.2.2. Synthesis

Ac-Lys(OAloc)-Gly-Asp(OAll)-Glu(OAll)-Val-Asp(OAll)-OH (344 mg, 0.38 mmol; AnyGen, Jeollanam-do, South Korea), 4-aminobenzyl alcohol (2 eq; Sigma-Aldrich, St. Louis, MO), and EEDQ (2 eq; Sigma-Aldrich) were dissolved in anhydrous DMF (11 ml; Sigma-Aldrich) and the reaction mixture was stirred at room temperature for 24 h under inert atmosphere. The solution was concentrated under reduced pressure, and 10 volume of diethyl ether (Burdick & Jackson, Muskegon, MI) was added. The precipitate was collected by filtration and dried *in vacuo* to obtain Ac-Lys(OAloc)-Gly-Asp(OAll)-Glu(OAll)-Val-Asp(OAll)-PABOH (322 mg, 84%). ESI-MS (m/z): 1035.7 [M + Na]⁺.

Ac-Lys(OAloc)-Gly-Asp(OAll)-Glu(OAll)-Val-Asp(OAll)-PABOH (322 mg, 0.318 mmol) and 4-nitrophenyl chloroformate (1.2 eq; Sigma-Aldrich) were dissolved in anhydrous CH₂Cl₂ (10 ml; Ducksan, Seoul, South Korea) under inert atmosphere. Then 2,6-lutidine (3 eq; Sigma-Aldrich) was added to the reaction mixture and stirred at room temperature for 2 h. Anhydrous DMF (2 ml) and additional 2,6-lutidine (2 eq) was again added to the reaction mixture. After 24, 27, and 46 h, 2,6-lutidine (4.75 eq) and 4-nitrophenyl chloroformate (1 eq) were further added to the reaction mixture. After 84 h, aqueous NaHCO₃ was added to the reaction mixture and extracted with ethyl acetate (100 ml x 3; Ducksan). The organic layer was washed with 0.5 M citric acid (Sigma-

Aldrich), aqueous NaHCO₃, and brine, subsequently. The obtained organic layer was dried by addition of anhydrous MgSO₄, filtered, and concentrated *in vacuo*. The concentrate was further purified with semi-preparative HPLC using C18 reverse phase column (250 mm × 22 mm) in a gradient system (Water and CH₃CN with 0.1% TFA as an additive, CH₃CN 20-53% over 30 min, 10 ml/min) to obtain Ac-Lys(OAloc)-Gly-Asp(OAll)-Glu(OAll)-Val-Asp(OAll)-PABC (77 mg, 20.5%). ESI-MS (m/z): 1200.54 [M + Na]⁺.

Ac-Lys(OAloc)-Gly-Asp(OAll)-Glu(OAll)-Val-Asp(OAll)-PABC (77 mg, 0.065 mmol) and doxorubicin HCl (1.2 eq; Korea United Pharm., Seoul, South Korea) were dissolved in anhydrous DMF (8 ml). DIEA (5.4 eq; Sigma-Aldrich) was added to the reaction mixture and stirred at room temperature for 16 h under inert atmosphere. The solution was concentrated *in vacuo* and further purified with semi-preparative HPLC using C18 reverse phase column (250 mm × 22 mm) in a gradient system (Water and CH₃CN with 0.1% TFA as an additive, CH₃CN 20-100% over 50 min, 10 ml/min) to obtain Ac-Lys(OAloc)-Gly-Asp(OAll)-Glu(OAll)-Val-Asp(OAll)-PABC-DOX (red amorphous solid, 50 mg, 50%). ESI-MS (m/z): 1605.06 [M + Na]⁺.

Ac-Lys(OAloc)-Gly-Asp(OAll)-Glu(OAll)-Val-Asp(OAll)-PABC-DOX (50 mg, 0.032 mmol) and Pd(PPh₃)₄ (0.2 eq; Sigma-Aldrich) were dissolved in anhydrous DMF (4 ml) under inert gas and degassed over 5 min. Then tributyltin hydride (17.3 eq; Sigma-Aldrich) and acetic acid (20 eq; Sigma-Aldrich) were added to the reaction mixture, and stirred at room temperature for 1 h. The product was then purified with semi-preparative HPLC using C18 reverse phase column (250 mm × 22 mm) in a gradient system (Water and CH₃CN with 0.1% TFA as an additive, CH₃CN 20-41% over 41 min, 10 ml/min) to obtain deprotected Ac-Lys-Gly-Asp-Glu-Val-Asp-PABC-DOX (red amorphous solid, 6 mg, 13.6%). ESI-MS (m/z): 1378.4 [M + Na]⁺.

Ac-Lys-Gly-Asp-Glu-Val-Asp-PABC-DOX (named as DEVD-S-DOX; 20 mg, 0.013 mmol) and *N*-(ε-maleimidocaproyloxy)succinimide ester (EMCS; 8.26 mg, 26.8 μmol, 2 eq; Pierce, Rockford, IL) were dissolved in anhydrous DMF (1.5 ml) under inert gas. Then TEA (4.64 μl, 2.5 eq; Sigma-Aldrich) was

added to the reaction mixture and stirred at room temperature for 2 h. The final product was purified with semi-preparative HPLC (Shimadzu, Kyoto, Japan) using ODS-A 5 μm reverse phase semi-preparative column (150 mm \times 20 mm) in a gradient system (Water and CH_3CN with 0.05% TFA as an additive, CH_3CN 20-50% over 50 min, 8 ml/min) to obtain Ac-Lys(EMC)-Gly-Asp-Glu-Val-Asp-PABC-DOX (named as EMC-DEVD-S-DOX; red amorphous solid, 16.7 mg, 73.6%). The peaks were monitored at 280 nm. The purity of the final products was confirmed by analytical HPLC (Agilent 1300 series, Agilent Technologies, Santa Clara, CA) using ODS-A 5 μm analytical column (150 mm \times 3 mm; YMC) in a gradient system (DW and CH_3CN with 0.1% TFA as an additive, CH_3CN 5-95%/5-30 min, 1 ml/min). The peaks were monitored under UV detector (214 nm) and fluorescent detector (excitation 470nm, emission 580 nm). The purity of the final compound was determined to be $\geq 95\%$. ESI-MS (m/z): 1593.3 $[\text{M} + \text{Na}]^+$.

5.2.3. EMC-DEVD-S-DOX binding study with HSA

A human serum albumin (HSA; Sigma-Aldrich) solution was prepared in PBS at a final concentration of 700 μM (46.5 mg/ml). To the solution of HSA, EMC-DEVD-S-DOX was added at a final concentration of 100 μM and incubated at room temperature for 3 min and 60 min. For blocking study, the HSA solution was preincubated with excess amount of 4-maleimidobutyric acid (Santa Cruz) for 1 h before addition of EMC-DEVD-S-DOX. The samples were subjected to analytical HPLC. HPLC analysis: Flow rate 1 ml/min, mobile phase A: DW with 0.1% TFA; mobile phase B: CH_3CN with 0.1% TFA; gradient 0-5 min 30% mobile phase B; 5-25 min increase to 50% mobile phase B; 25-30 min 50% mobile phase B.

5.2.4. HSA-DEVD-S-DOX analysis by SDS-PAGE

HSA (70 μM , 4.6 mg/ml) solution was prepared in PBS. EMC-DEVD-S-DOX (100 μM) or DEVD-S-DOX (100 μM) was incubated for 1 h in the HSA solution at room temperature. Same volume of EMC-DEVD-S-DOX in HSA

solution, DEVD-S-DOX in HSA solution, and HSA solution was subjected to a native SDS-PAGE using 12% polyacrylamide gel. The gel was visualized by trans-UV under ImageQuant LAS 4000 imaging system (GE Healthcare Life Sciences, Uppsala, Sweden). The albumin bands were stained with coomassie blue (Pierce, Rockford, IL).

5.2.5. Determination of thiol concentration of HSA using Ellman's test

Ellman's reagent (DTNB; Sigma-Aldrich) working solution was prepared at 80 $\mu\text{g/ml}$ in reaction buffer (0.1 M sodium phosphate buffer, pH 8.0, 1 mM EDTA). Cysteine standard was prepared at concentration of 0, 0.25, 0.5, 0.75 and 1 mM in the reaction buffer. HSA (Sigma-Aldrich) was prepared at 1 mM (66.5 mg/ml) in the reaction buffer. The standard and sample solution was transferred to a 96-well microplate at 20 μl and then, 200 μl of Ellman's reagent working solution was added. The mixture was incubated for 15 min at room temperature and the absorbance was measured using a microplate reader (Synergy HT; BioTek Instruments, Winooski, VT) at 412 nm. The thiol concentration of HSA was determined based on the standard curve and the percentage of mercaptalbumin was calculated.

5.2.6. Preparation and characterization of HSA-DEVD-S-DOX

To prepare HSA-DEVD-S-DOX, EMC-DEVD-S-DOX (100 μM) was incubated with HSA (70 μM , 4.6 mg/ml; Sigma-Aldrich) in pH 7.4 PBS for 1 h. Then the solution was transferred to an Amicon Ultra-4 centrifugal unit (MW cutoff 10 kDa; EMD Millipore, Billerica, MA) and centrifuged for 15 min at 3000 rpm to remove the excess amount of unreacted EMC-DEVD-S-DOX. The flow-through was discarded, distilled water was added to the concentrated substance, and centrifuged subsequently to wash the product. The solution in the insert was collected and lyophilized to obtain HSA-DEVD-S-DOX as a powder. The mass of the final product and HSA were analyzed using MALDI-TOF MS (Voyager-DE STR Biospectrometry Workstation, Applied Biosystems).

5.2.7. EMC-DEVD-S-DOX incubation study in plasma

Human plasma was obtained from a healthy volunteer and the blood was stabilized immediately with EDTA after withdrawal. Mouse plasma was obtained from C3H/HeN mice. EMC-DEVD-S-DOX was incubated with the plasma at a final concentration of 100 μ M at room temperature. For blocking study, excess amount of 4-maleimidobutyric acid (Santa Cruz) was preincubated with the plasma for 1 h, and then EMC-DEVD-S-DOX (100 μ M) was added, subsequently. The samples were diluted ten-fold in PBS and subjected to an analytical HPLC. Fresh plasma and EMC-DEVD-S-DOX in PBS were also analyzed. HPLC analysis: Flow rate 1 ml/min, mobile phase A: DW with 0.1% TFA; mobile phase B: CH₃CN with 0.1% TFA; gradient 0-5 min 30% mobile phase B; 5-25 min increase to 50% mobile phase B; 25-30 min 50% mobile phase B.

5.2.8. Western blot

EMC-DEVD-S-DOX (100 μ M) was incubated with HSA (500 μ M) in pH 7.4 PBS (1 ml) for 30 min at room temperature to produce an albumin-bound EMC-DEVD-S-DOX (HSA-DEVD-S-DOX). Then, 500 μ l of the solution was incubated with recombinant human caspase-3 (R&D Systems, Minneapolis, MN) at a final concentration of 500 ng/ml. SCC7 and MDA-MB-231 cells were cultured in 60 mm dishes until 80 - 90% confluence. The cells were treated with 0.1, 1, and 10 μ M of the previously prepared HSA-DEVD-S-DOX or HSA-DEVD-S-DOX preincubated with caspase-3, and incubated for 48 h at 37°C. The cells were washed with cold PBS and lysed with RIPA buffer (Pierce) supplemented with protease inhibitor cocktail (Pierce). The preparation of the samples and western blot were performed according to the standard protocol. For immunoblotting, anti-Caspase-3 antibody (1:1000) and anti-cleaved Caspase-3 antibody (1:1000) from Cell Signaling Technology (Danvers, MA) were used as primary antibodies. HRP-conjugated anti-rabbit IgG (1:2000;

R&D Systems) was used as secondary antibody. The blotted membranes were developed using ImageQuant LAS 4000 imaging system.

5.2.9. MTT cytotoxicity assay

MTT assay kit was purchased from Trevigen (Gaithersburg, MD). The assay was performed following the standard procedure. Briefly, SCC7 and MDA-MB-231 cells were plated at a density of 5×10^4 cell per well in 96 well culture plates (Corning, Tewksbury, MA). After 24 h incubation in DMEM supplemented with 10% FBS, doxorubicin, HSA-DEVD-S-DOX, or HSA-DEVD-S-DOX preincubated with caspase-3 (500 ng/ml) was treated at a concentration range of 0.01 to 100 μ M to the cells and further incubated for 48 h. Then MTT reagent (10 μ l) was added, and incubated for 2 h at 37°C. When purple formazan precipitates were observed clearly in the cells, detergent agent (100 μ l) was further added and incubated for 4 h at room temperature. The absorbance was measured at 570 nm using a microplate reader (Synergy HT).

5.2.10. Cellular uptake imaging

Cellular uptake of doxorubicin, DEVD-S-DOX, HSA-DEVD-S-DOX, and HSA-DEVD-S-DOX preincubated with caspase-3 was observed to determine the intracellular distribution. SCC7 or MDA-MB-231 cells were seeded on 35 mm cover glass-bottom dishes (SPL Life Sciences, Pocheon, Korea) at a density of 5×10^5 cells per dish and allowed to grow until 70-80% confluence. Prepared materials were treated to the cells at 10 μ M of final concentration and incubated for 2 h. The cells were carefully washed with cold PBS and fixed with 4% PFA (Sigma-Aldrich). The cell nucleus was stained using DAPI (Molecular Probes, Eugene, OR) and mounted with mounting medium. The cells were observed under confocal laser scanning microscopy (LSM 710; Carl Zeiss, Oberkochen, Germany).

5.2.11. HPLC determination of caspase-mediated activation

To determine the release of doxorubicin from HSA-DEVD-S-DOX by caspase-3, the EMC-DEVD-S-DOX (1 mM) was incubated with HSA (7 mM) in pH 7.4 PBS, diluted ten-fold in the caspase assay buffer (50 mM HEPES, pH 7.4, 100 mM NaCl, 0.1% CHAPS, 10 mM DTT, 1 mM EDTA, 10% glycerol; Enzo Life Sciences, Farmingdale, NY), and incubated with recombinant human caspase-3 (500 ng/ml; R&D Systems, Minneapolis, MN) at room temperature, subsequently. The solution was subjected to an analytical HPLC (Agilent 1300 series, Agilent Technologies) using ODS-A 5 μ m analytical column (150 mm \times 3 mm; YMC, Dinslaken, Germany) with a gradient system (DW and CH₃CN with 0.1% TFA as an additive, CH₃CN 30-50%/5-25 min) at a flow rate of 1 ml/min. The chromatograms were monitored using fluorescence detector at Ex 470 nm/Em 580 nm. Additionally, HSA-DEVD-S-DOX without caspase-3, and with caspase-3 (500 ng/ml) pretreated with caspase-3 inhibitor (Ac-DEVD-CHO, 10 μ M; Enzo Life Sciences) were incubated for 60 min at room temperature in the caspase assay buffer, and then subjected to an analytical HPLC. HPLC analysis: Flow rate 1 ml/min, mobile phase A: DW with 0.1% TFA; mobile phase B: CH₃CN with 0.1% TFA; gradient 0-5 min 30% mobile phase B; 5-25 min increase to 50% mobile phase B; 25-30 min 50% mobile phase B.

5.2.12. Pharmacokinetic study

To Spraque Dawley (SD) rats, EMC-DEVD-S-DOX or DEVD-S-DOX was administered at a dose of 2.89 or 2.54 mg/kg (equivalent to 1 mg/kg of doxorubicin), respectively, via tail vein (n = 3). The blood was withdrawn (500 μ l per each time point) at 5, 15, 30, 60, 90 min, and 2, 4, 8, 12, 24, 48, 72, 96 h of post-injection. The collected bloods stabilized immediately with sodium citrate and centrifuged for 15 min at 2000 \times g in a refrigerated centrifuge to separate the plasma. The plasma samples (200 μ l) were transferred to a 96-well black microplate and the intrinsic fluorescence of doxorubicin was read at

at Ex 485 nm/Em 590 nm. The standard was prepared in fresh plasma and the fluorescence was read as described above. All experimental procedures were approved by the Institutional Animal Care and Use Committee of the Seoul National University.

5.2.13. *Ex vivo* biodistribution imaging

SCC7 cells were suspended at 1×10^7 cell/ml in HBSS, and inoculated subcutaneously (100 μ l) into the thigh of 6 week-old male BALB/cSlc-nu mice. When the tumor volume reached 500 mm³, the mice received EMC-DEVD-Cy5.5, which the doxorubicin in EMC-DEVD-S-DOX was substituted with Cy5.5 for the *ex vivo* imaging, at a single dose of 1 mg/kg molar equivalent to doxorubicin through tail vein. The whole-body fluorescent imaging was taken at 1, 24, 48, 72, 96, and 120 h of post-administration under Optix MX3 imaging system (Advanced Research Technologies, Montreal, Canada). The intensity map of the acquired images in different time points were normalized. All experimental procedures were approved by the Institutional Animal Care and Use Committee of the Seoul National University.

5.2.14. Tumor growth suppression

SCC7 cells were suspended at 1×10^7 cell/ml in HBSS, and inoculated subcutaneously (100 μ l) into the dorsal flank of 6 week-old male C3H/HeN mice. When the tumor volume reached 50 mm³, the mice were randomized (n = 5), and received one of follows: normal saline, EMC-DEVD-S-DOX (2.89 mg/kg; equivalent to 1 mg/kg of doxorubicin) or DEVD-S-DOX (2.54 mg/kg; equivalent to 1 mg/kg of doxorubicin) for seven days daily via tail vein. For radiation-treated groups, 4 Gy of X-ray (6 MV, 300 cGy/min; Clinac 21EX, Varian, Palo Alto, CA) was given once to the tumor at the first day of the drug treatment. The tumor length and width were measured by caliper and the volume was calculated using the modified ellipsoid formula ($L \times W^2/2$). At the last day of observation, the tumors were isolated and weighed. All experimental

procedures were approved by the Institutional Animal Care and Use Committee of the Seoul National University.

5.3. Results

5.3.1. Synthesis of EMC-DEVD-S-DOX

Scheme 5.1 depicts the synthesis of maleimidocaproyl-AcKGDEVD-PABC-doxorubicin (EMC-DEVD-S-DOX). The carboxyl side chains of the AcKGDEVD-COOH peptide were protected with allyl ester in order to deprotect them in a mild condition that doxorubicin could remain stable. The protected AcKGDEVD-COOH peptide was conjugated to the 3'-NH₂ of doxorubicin via a self-immolative spacer (*p*-aminobenzyl carbamate; PABC) to avoid steric hindrance by bulky doxorubicin molecule interfering the interaction of DEVD moiety with caspase-3. When the amide bond between the peptide and PABC spacer is hydrolyzed by caspase-3, the self-immolative spacer releases itself from doxorubicin, thereby liberating the free drug.

The allyl ester groups that were protecting the side chains of Asp and Glu were deprotected using Pd(PPh₃)₄ catalyst to obtain AcKGDEVD-PABC-doxorubicin. Conventional protection and deprotection methods for carboxyl groups (e.g. *tert*-butyl ester protection) were avoided because doxorubicin is very labile in highly acidic or basic environment, which is generally used during deprotection of the carboxyl groups.

Finally, the amino group of Lys side chain was reacted with *N*-(ϵ -maleimidocaproyloxy)succinimide ester (EMCS) in the presence of Et₃N to afford the final product, EMC-DEVD-S-DOX. The purity was confirmed to be more than 95% using analytical HPLC (**Fig. 5.2A**). The mass was determined using ESI-MS (**Fig. 5.2B**).

5.3.2. Albumin-binding of EMC-DEVD-S-DOX

The plasma albumin-binding capability of EMC-DEVD-S-DOX was determined through various *in vitro* studies. Firstly, the albumin binding of

EMC-DEVD-S-DOX was determined on a commercially available human serum albumin (HSA). EMC-DEVD-S-DOX (100 μ M) was incubated with the HSA (700 μ M) and analyzed by HPLC (**Fig. 5.3A**). Binding of the EMC-DEVD-S-DOX to the HSA was presented by disappearance of the EMC-DEVD-S-DOX peak at 11.3 min and appearance of a broad peak between 15-20 min detected through the intrinsic fluorescence of the doxorubicin moiety (Ex 470/Em 580 nm). The binding of the EMC-DEVD-S-DOX to the HSA was accomplished within 3 min and only trace amount of the unbound substance was detected. However, when HSA was pre-incubated with 4-maleimidobutyric acid, which is a small molecule containing a maleimide group, EMC-DEVD-S-DOX did not bind to the HSA even after 1 h incubation. This clearly proved that the maleimide group on the EMC-DEVD-S-DOX was indeed the mediator of the HSA binding.

The HSA binding of the EMC-DEVD-S-DOX was further confirmed by SDS-PAGE (**Fig. 5.3B**). The EMC-DEVD-S-DOX and HSA were detected using the absorbance of the doxorubicin moiety and coomassie blue staining, respectively. EMC-DEVD-S-DOX band was observed below 15 kDa on the gel after electrophoresis. By contrast, when EMC-DEVD-S-DOX (100 μ M) was incubated with HSA (70 μ M), the band from the doxorubicin moiety was observed between 50-75 kDa, which the position was identical with the band from the intact HSA (MW 66.5 kDa). Also, the band from the unbound EMC-DEVD-S-DOX (shown below 15 kDa) was decreased when compared to the other lanes. However, when the HSA was blocked with 4-maleimidobutyric acid, the band from the EMC-DEVD-S-DOX was only visible below 15 kDa. This indicated that EMC-DEVD-S-DOX was unable to bind to HSA when the thiol of HSA is blocked, agreeing with the aforementioned HPLC result. The fact that the HSA binding was mediated through the maleimide group was further supported by the result that showed DEVD-S-DOX, which has no maleimide functional group in the molecule, did bind to the HSA represented by the band only shown below 15 kDa.

The molecular weight shift of the HSA-bound EMC-DEVD-S-DOX (hereafter, HSA-DEVD-S-DOX) from the commercially available HSA was evaluated using MALDI-TOF mass spectrometry (**Fig. 5.3C**). The maximum intensity mass of the HSA was determined to be 66383.4219, whereas the maximum intensity mass of the HSA-DEVD-S-DOX was shifted to 67940.3726, showing mass difference of 1556.9507. This value is similar to the mass of the EMC-DEVD-S-DOX (m/z 1570.59), indicating that a single molecule of EMC-DEVD-S-DOX was bound to a molecule of HSA.

Finally, a selective albumin binding of EMC-DEVD-S-DOX was confirmed in the human plasma. EMC-DEVD-S-DOX (100 μ M) was incubated in the human plasma and analyzed by HPLC (**Fig. 5.3D**). Binding of the EMC-DEVD-S-DOX to the serum albumin in the plasma was represented by the disappearance of EMC-DEVD-S-DOX peak at 11.3 min and the appearance of a broad peak between 16-20 min detected by the intrinsic fluorescence of doxorubicin moiety (Ex 470/Em 580 nm). The binding of EMC-DEVD-S-DOX to the serum albumin was rapid, which was accomplished within 3 min and only trace amount of the unbound substance was detected. However, when the plasma was pre-incubated with 4-maleimidobutyric acid (GMB) in advance of the EMC-DEVD-S-DOX addition, the height of the EMC-DEVD-S-DOX peak was unchanged even after 1 h incubation.

5.3.3. Caspase-3-mediated cleavage of HSA-DEVD-S-DOX

The therapeutic efficacy of the currently proposed system relies on its ability to release doxorubicin when recognized by caspase-3. Since the presence of a macromolecule (i.e. albumin) adjacent to the DEVD moiety might interfere such process, the major concern was whether caspase-3 could recognize and cleave the DEVD moiety when EMC-DEVD-S-DOX is bound to HSA. To address this question, HSA-DEVD-S-DOX was incubated with purified caspase-3 and subjected to HPLC analysis (**Fig. 5.4A**). The intensity of the broad peak from the HSA-DEVD-S-DOX was decreased to the ground level within an hour accompanied with the appearance of new sharp peak at 2.2 min.

The retention time of doxorubicin was identical with the new peak, indicating that the caspase-3 had indeed triggered the release of free doxorubicin from HSA-DEVD-S-DOX.

5.3.4. *In vitro* efficacy of HSA-DEVD-S-DOX

The cytotoxic effect of HSA-DEVD-S-DOX in the absence or presence of caspase-3 was determined. HSA-DEVD-S-DOX did not show any noticeable cytotoxic effect up to 100 μM in both SCC7 and MDA-MB-231 cells when evaluated through MTT assay. However, when the HSA-DEVD-S-DOX was pre-incubated with purified caspase-3 in advance of addition to the cells, it showed similar degree of cytotoxicity ($\text{IC}_{50} = 0.49$ and $4.17 \mu\text{M}$) with doxorubicin ($\text{IC}_{50} = 0.30$ and $2.04 \mu\text{M}$) on SCC7 and MDA-MB-231, respectively (**Fig. 5.4B**). These results were supported by the observation of the cells incubated with HSA-DEVD-S-DOX in the absence or presence of caspase-3 under confocal microscopy. The cells incubated with HSA-DEVD-S-DOX showed very small amount of the substances taken up into the cells with no accumulation in the cell nucleus. By contrast, when HSA-DEVD-S-DOX was pre-incubated with a purified caspase-3, the substance was clearly accumulated inside the cell nucleus in similar degree to that shown in the cells incubated with doxorubicin (**Fig. 5.4C**).

5.3.5. Caspase-3 upregulation induced by activated HSA-DEVD-S-DOX

For the current drug delivery strategy to be valid, the HSA-DEVD-S-DOX should upregulate the caspase-3 in the cells after it is activated. Therefore, the upregulation of caspase-3 in SCC7 and MDA-MB231 cells were examined after treatment of HSA-DEVD-S-DOX or activated HSA-DEVD-S-DOX by western blot. The results showed that HSA-DEVD-S-DOX itself did not upregulate the caspase-3 up to 10 μM . On the other hand, when HSA-DEVD-S-DOX was pre-incubated with a purified caspase-3 and treated to the cells, dose-dependent decrease of procaspase-3 and increase of cleaved (or active) caspase-3 were observed in the both cells (**Fig. 5.4D**). Procaspase-3 is a zymogen of caspase-3,

which is activated when cleaved into 17 and 19 kDa subunits. The results clearly showed that the caspase-3-mediated activation of HSA-DEVD-S-DOX is followed by the further upregulation of caspase-3 due to the released doxorubicin stimulating the cellular apoptosis.

5.3.6. Pharmacokinetic study

The pharmacokinetic profiles of the EMC-DEVD-S-DOX and DEVD-S-DOX were obtained after intravenous administration of the drugs to Sprague-Dawley rats at a dose of molar equivalent to 1 mg/kg of doxorubicin (2.89 and 2.54 mg/kg, respectively) (**Fig 5.5A**). The DEVD-S-DOX showed half-life of 30 min and the plasma concentration decreased below the detection limit (10 ng/ml) within 4 hours. However, EMC-DEVD-S-DOX showed significantly extended half-life with more than 19 hours, which is 38-fold longer than DEVD-S-DOX, and lasted more than 6 days in plasma after the administration, resulting in 157-fold higher AUC (**Table 5.1**).

5.3.7. Tumor accumulation of EMC-DEVD-Cy5.5

The whole-body distribution of EMC-DEVD-S-DOX after intravenous administration was determined indirectly by substituting doxorubicin to near-infrared dye Cy5.5 for *ex vivo* observation (**Fig 5.5B**). At one hour post-administration, the fluorescence from the substance was distributed throughout the entire body with no noticeable accumulation in any major organs or in tumor. However, when the animals were observed at 24 hour post-administration, significant accumulation of the substance in the tumor tissue was observed. The fluorescence intensity level in the tumor was even higher than the previously observed time-point, whereas the intensity level in other part of the body was decreased noticeably. This clearly showed that the selective accumulation of the administered agent occurred in the tumor. The fluorescent intensity in the tumor was unchanged up to 48 hour post-administration, while the intensity in other part of the body was continuously decreased. The relatively higher amount of the fluorescence in the tumor was

maintained for 120 hours, which was the last time of observation. Moreover, current observations also showed that the detectable amount of the substances remained for more than 120 hours in the body albeit lower than that observed in the tumor. This showed that the agent maintained their level in the circulation for very long time, agreeing with the findings in the pharmacokinetic study.

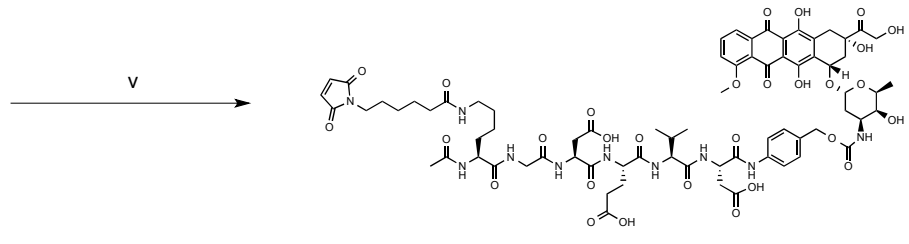
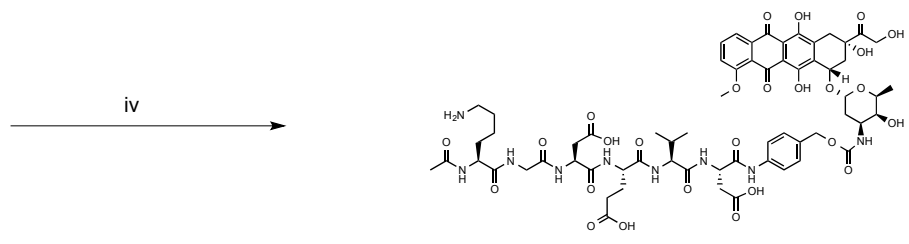
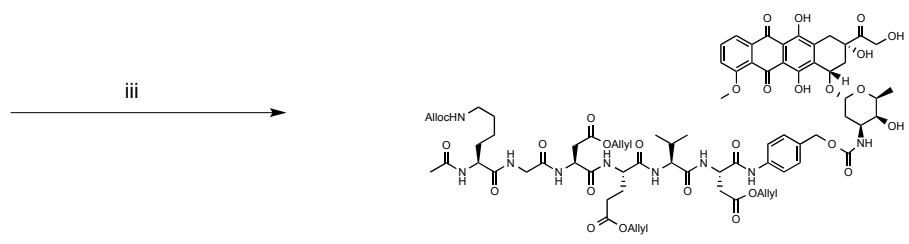
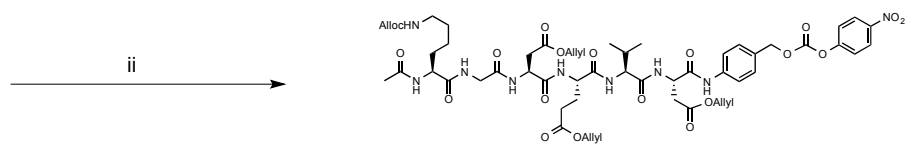
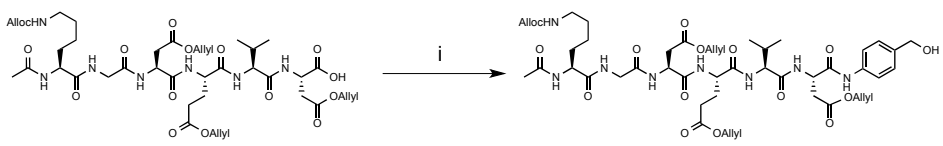
5.3.8. Tumor growth suppression of EMC-DEVD-S-DOX

Tumor growth suppression by EMC-DEVD-S-DOX was evaluated on SCC7-bearing C3H/HeN mice (**Fig 5.6A**). EMC-DEVD-S-DOX or DEVD-S-DOX was administered intravenously at a dose of molar equivalent to 1 mg/kg of doxorubicin daily for seven days daily observed for two weeks. For radiation treated groups, the tumors were exposed to a single dose of 4 Gy linear X-ray at the first day of the drug administration. Similar to the previous report that DEVD-S-DOX had no evident anticancer activity when used alone⁴, EMC-DEVD-S-DOX also showed negligible tumor suppression effect as shown by similar tumor growth in comparison to the control group. On the other hand, when EMC-DEVD-S-DOX was combined the radiation, the tumor volume was decreased by 77% ($P < 0.01$). The tumor suppression effect of EMC-DEVD-S-DOX was superior to that of DEVD-S-DOX. When combined with radiation, the tumor volume of EMC-DEVD-S-DOX treated group decreased by 65% when compared to the radiation only treated group, while that of DEVD-S-DOX treated group decreased by 29%. During the course of the study, noticeable body weight changes were not observed in any experimental group, indicating that there was no severe toxicity in all of the tested groups (**Fig. 5.6B**).

Table 5.1. Pharmacokinetic parameters in SD rats (1 mg/kg dox molar eq.)

	DEVD-S-DOX	EMC-DEVD-S-DOX
C_{\max} ($\mu\text{g/ml}$)	7.335 ± 1.175	14.49 ± 0.6180
$t_{1/2}$ (hr)	0.5002 ± 0.09237	19.13 ± 2.171
V_d (ml/kg)	464.2 ± 24.20	116.4 ± 10.09
CL (ml/kg/h)	655.2 ± 97.92	4.224 ± 0.1136
AUC_{last} (hr· $\mu\text{g/ml}$)	1.500 ± 0.2215	234.8 ± 7.064
AUC_{INF} (hr· $\mu\text{g/ml}$)	1.551 ± 0.2440	236.8 ± 6.370

Data presented as mean \pm s.d.



Scheme 5.1. Chemical synthesis of EMC-DEVD-S-DOX^a

^aReagents and conditions: (i) 4-aminobenzyl alcohol, EEDQ, DMF, rt. (ii) 4-NPC, 2,6-lutidine, DCM, DMF, rt. (iii) Doxorubicin HCl, DIEA, DMF, rt. (iv) Pd(PPh₃)₄, DMF, tributyltin hydride, acetic acid, rt. (v) EMCS, TEA, rt.

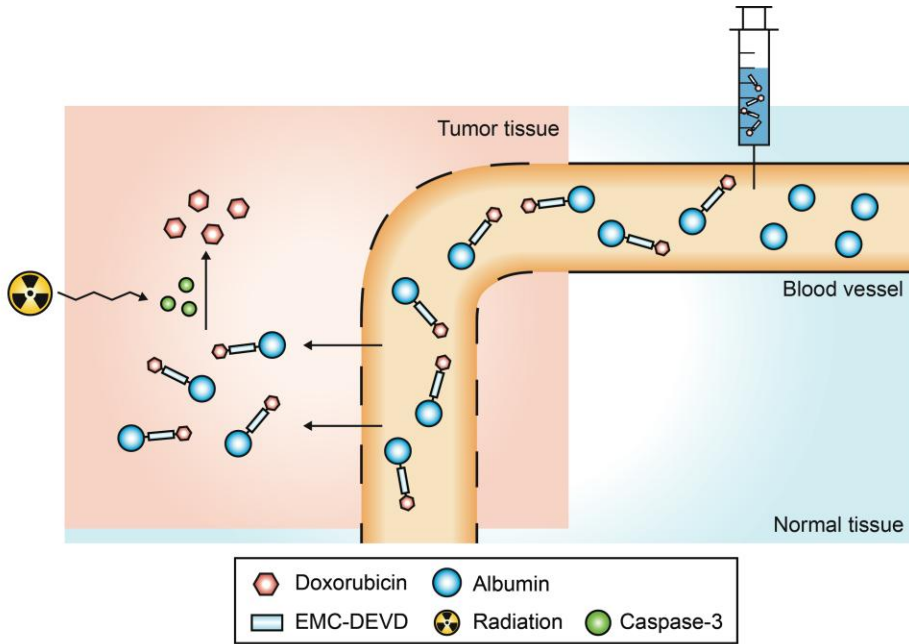
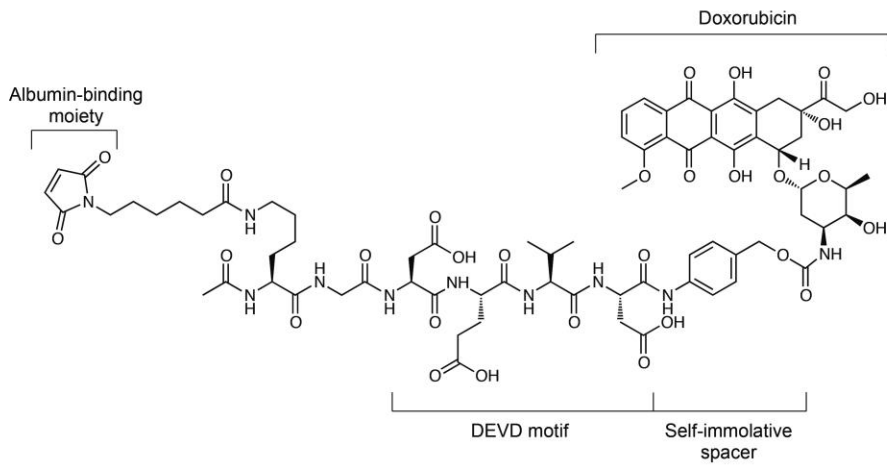
A**B**

Figure 5.1. (A) Schematic diagram of EMC-DEVD-S-DOX therapeutic strategy.
(B) Chemical structure of EMC-DEVD-S-DOX.

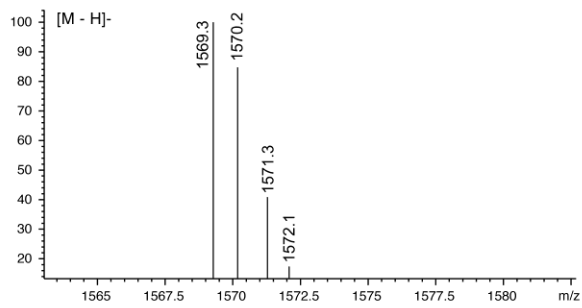
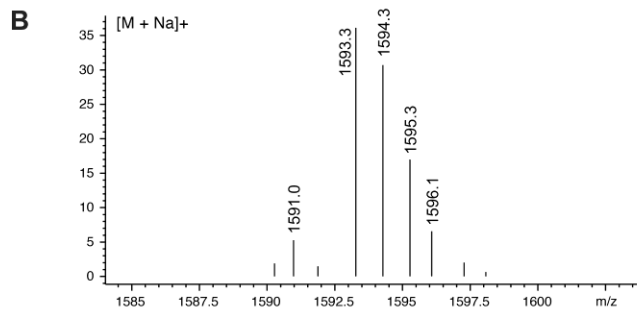
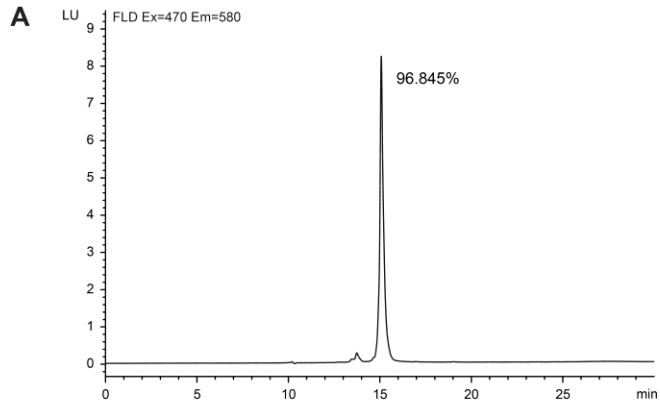


Figure 5.2. (A) Analytical HPLC chromatogram of the final product detected under fluorescence detector (470/580 nm). (B) Mass spectrum of the final product determined by LC/ESI-MS.

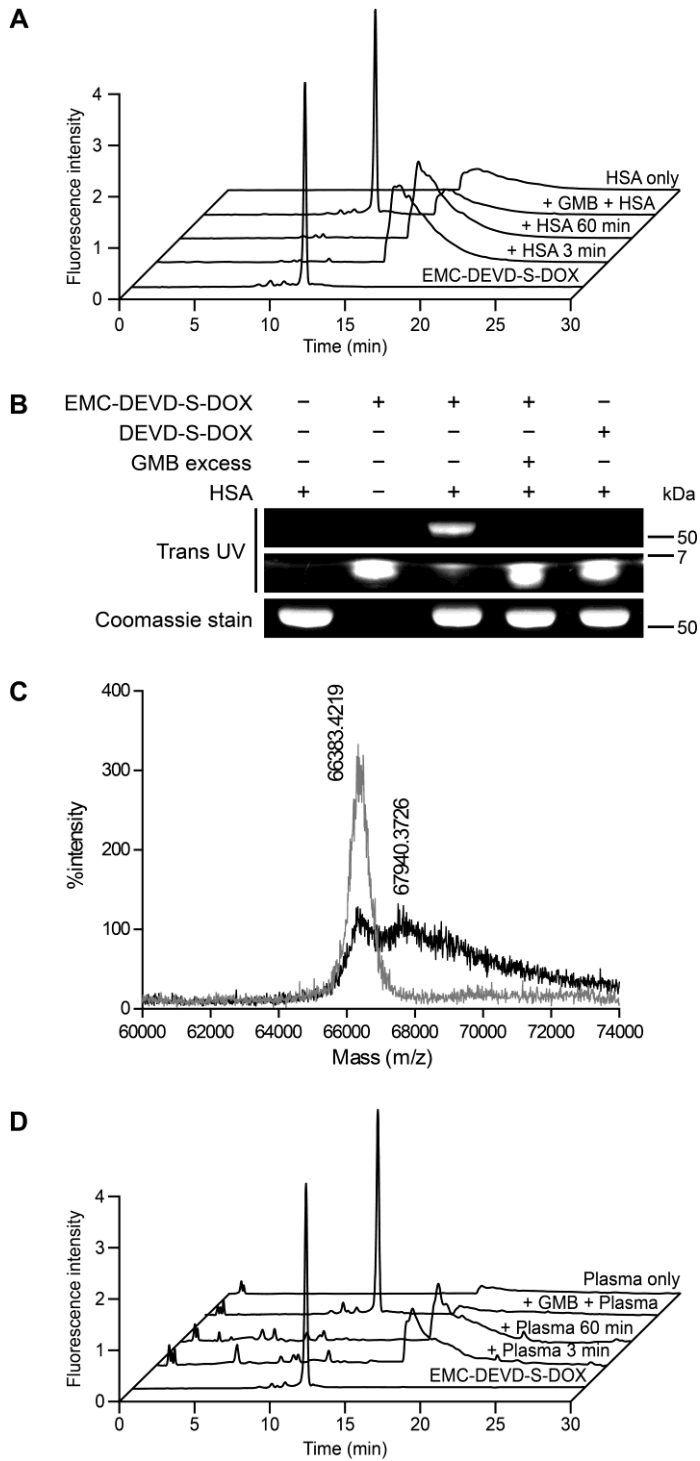


Figure 5.3. (A) HPLC chromatograms of EMC-DEVD-S-DOX and that incubated with commercially available HSA (3, 60 min), EMC-DEVD-S-DOX incubated with HSA blocked with excess GMB (60 min), and only HSA. (B) SDS-PAGE of EMC-DEVD-S-DOX or DEVD-S-DOX incubated with HSA or HSA blocked with excess GMB. (C) MALDI-TOF MS results of commercially available HSA (grey), and that incubated with EMC-DEVD-S-DOX in PBS (pH 7.4; black). (D) HPLC chromatograms of EMC-DEVD-S-DOX and that incubated in human plasma (3, 60 min), EMC-DEVD-S-DOX incubated with the plasma blocked with excess GMB (60 min), and only plasma.

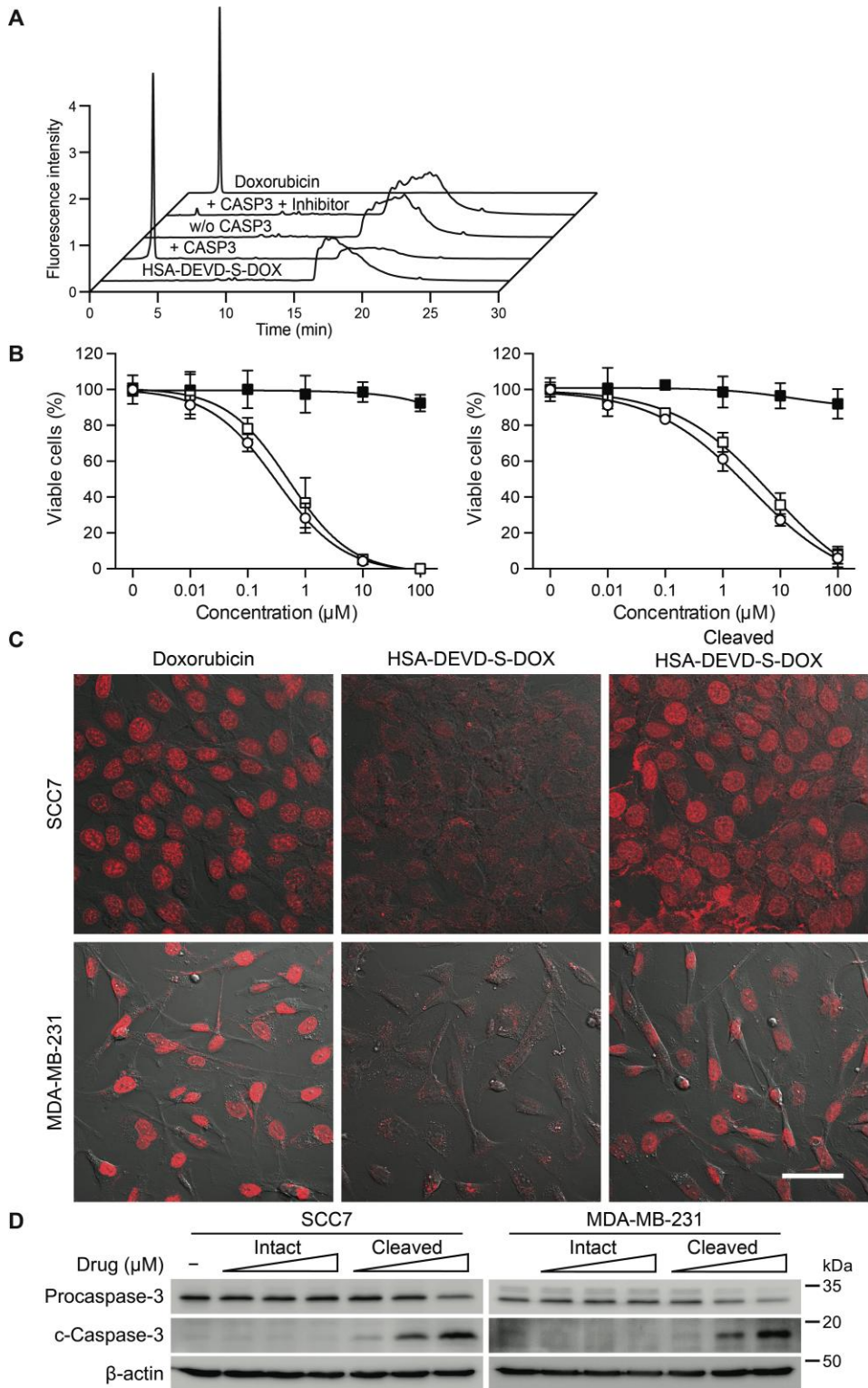


Figure 5.4. (A) HPLC chromatograms of HSA-DEVD-S-DOX and that incubated in the presence or absence of caspase-3, HSA-DEVD-S-DOX incubated with the caspase-3 pretreated with caspase inhibitor, and doxorubicin. (B) Concentration-dependent cytotoxicity of doxorubicin (○), HSA-DEVD-S-DOX (■), and HSA-DEVD-S-DOX incubated with recombinant human caspase-3 (□) on SCC7 (left) and MDA-MB-231 (right) cells determined by MTT assay. (C) Cellular uptake and intracellular distribution of doxorubicin (left), HSA-DEVD-S-DOX (center), and HSA-DEVD-S-DOX incubated with caspase-3 (right) in SCC7 (upper) and MDA-MB-231 (lower) cells observed under confocal microscopy. The substances were detected through intrinsic fluorescence of doxorubicin and represented as red color. Scale bar, 50 μm. (D) Western blots of SCC7 (upper) or MDA-MB-231 (lower) cells treated with HSA-DEVD-S-DOX or HSA-DEVD-S-DOX incubated with recombinant human caspase-3 (Cleaved HSA-DEVD-S-DOX) at a concentration of 1, 5, and 10 μM. The immunoblots were carried out using procaspase-3 (upper), cleaved caspase-3 (center), and β-actin (lower) antibodies.

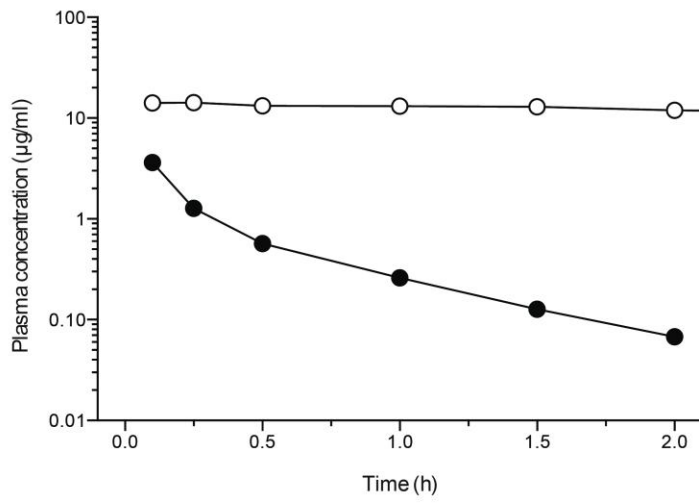
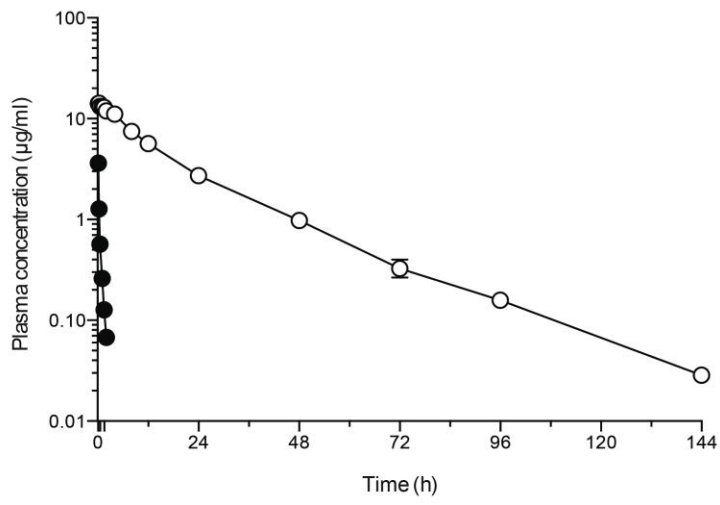
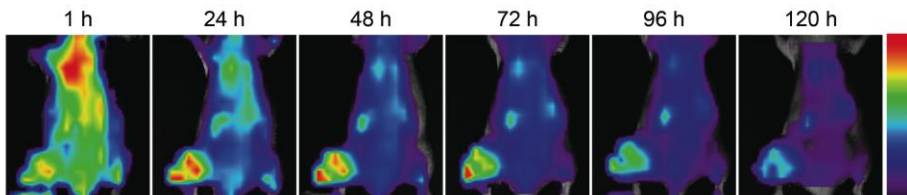
A**B**

Figure 5.5. (A) Logarithmic plasma concentration for time profiles of EMC-DEVD-S-DOX (○) and DEVD-S-DOX (●) administered to SD rats (n = 3) via intravenous route at a dose of 1 mg/kg molar equivalent to doxorubicin. The plasma concentration was calculated based on the mass concentration of doxorubicin content. Lower graph depicts enlarged plasma concentration profile showing until 2 h. (B) Ex vivo imaging of whole body distribution of EMC-DEVD-Cy5.5 in U87 MG tumor-bearing mice.

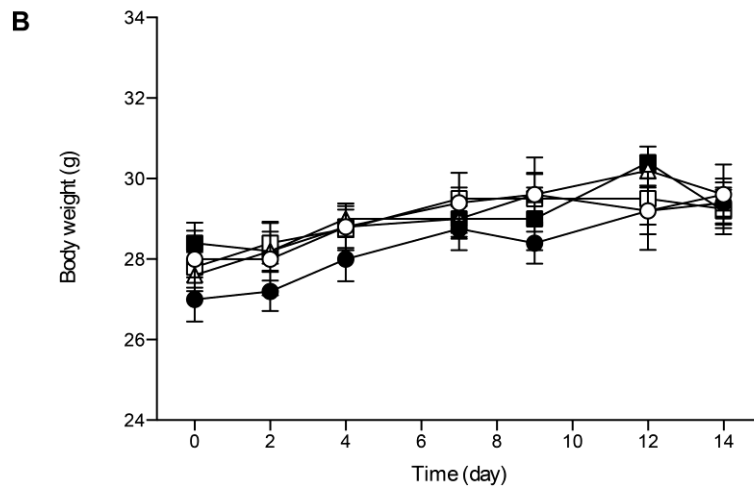
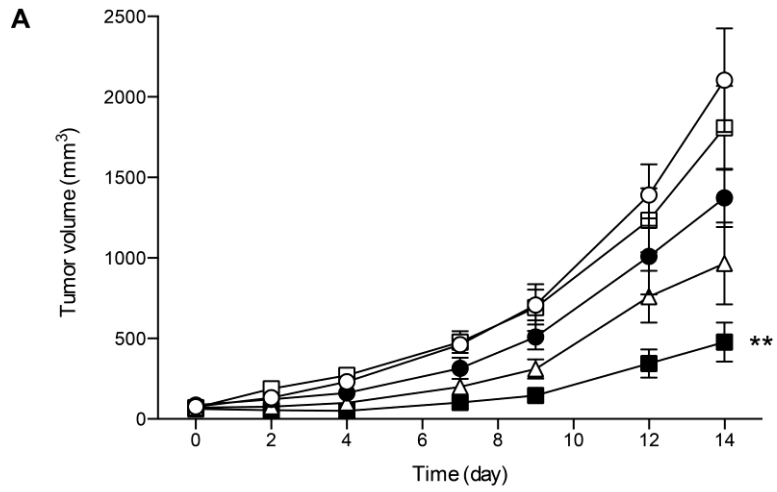


Figure 5.6. Animal study result of SCC7-tumor bearing C3H/HeN mice that received normal saline (○), radiation (●), DEVD-S-DOX accompanied by radiation (Δ), EMC-DEVD-S-DOX (□), or EMC-DEVD-S-DOX accompanied by radiation (■). EMC-DEVD-S-DOX or DEVD-S-DOX was intravenously administered daily for 7 days at 1 mg/kg molar equivalent to doxorubicin from day 0 (n = 5). Radiation was given at a dose of 4 Gy single time at day 0. Tumor growth profile (A) and body weight profile (B) are shown. Data are presented as mean ± s.e.m.

5.4. Discussion

The present study demonstrates about a prodrug comprising an *in situ* albumin-binding moiety (i.e. maleimide group), caspase-specific cleavable peptide, and doxorubicin as an active ingredient. The principle of the proposed prodrug system is as follows: (i) the prodrug instantly binds to an endogenous albumin, which acts as carrier molecule, in the blood stream after intravenous administration, (ii) the albumin-bound prodrug is delivered to the tumor that is exposed to a therapeutic radiation, (iii) caspase-3 that are upregulated in the irradiated tumor cells cleave the DEVD peptide spacer between albumin and doxorubicin, resulting in the release of free doxorubicin, (iv) the released free doxorubicin triggers apoptosis of the neighboring tumor cells, which again upregulate caspase-3, thereby repeatedly forcing the step (iii) and (iv). Hence, the activation of prodrug could be amplified in the site where apoptosis was first initiated by an exposure to radiation therapy.

The fundamental concept of the prodrug was recently proposed by our coworkers. The prodrug (DEVD-S-DOX) was prepared by conjugating a DEVD peptide to a doxorubicin via self-immolative spacer (*p*-aminobenzylcarbamate; PABC) and proved to be effective when combined with radiotherapy, so called as radiation-induced apoptosis-targeted chemotherapy (RIATC)⁴. However, hydrophilic peptides have very short plasma half-life with rapid renal excretion, which was also observed in the DEVD-S-DOX that had plasma half-life of 30 minutes in rats. Regarding that doxorubicin has a terminal half-life of 16.5 hours in SD rats¹², the significantly reduced plasma half-life is very disadvantageous in terms of therapeutic effect. Also, the previously prepared prodrug lacks tumor targeting capability that could selectively increase the local concentration of the agent within tumor

In order to overcome the aforementioned limitations, maleimide group, which acts as albumin-binding moiety, was introduced to the prodrug. Albumin has been recognized to be an excellent carrier for tumor targeting, and it was reported that maleimide group selectively reacts with the Cys34 of endogenous

albumin. EMC-DEVD-S-DOX, which was produced by simple modification of DEVD-S-DOX, was indeed capable in binding with the commercially available HSA as well as the albumins in plasma. The reaction was rapid, implying that the albumin binding of the EMC-DEVD-S-DOX would be immediate after entering the blood stream. The major concern was that the bound albumin might sterically hinder the caspase-3 recognizing the DEVD motif of EMC-DEVD-S-DOX. However, the results showed that the EMC-DEVD-S-DOX was well cleaved in the presence of caspase-3 regardless of HSA binding. As a result of the caspase-3-mediated cleavage, doxorubicin was liberated.

Our observations showed that albumin-bound form of EMC-DEVD-S-DOX (termed as HSA-DEVD-S-DOX) had almost no cytotoxic effect (or anticancer effect) *in vitro* as well as *in vivo*. The main reason of the inactivity is thought to be two-fold. One is the site of conjugation where the extra molecules are bound to the doxorubicin. The 3'-NH₂ group of the daunosamine sugar moiety plays critical role in stabilizing the DNA-doxorubicin complex when the doxorubicin is intercalated in the DNA. Therefore, this functional group is very important for the biological activity of doxorubicin¹³. As it could be seen in the chemical structure of EMC-DEVD-S-DOX, the DEVD peptide is conjugated to the 3'-NH₂ of doxorubicin via PABC spacer. Since the 3'-NH₂ is blocked by an amide bond, the conjugated doxorubicin loose its intrinsic anticancer effect. This was indeed proved in the previous study that showed loss of cytotoxic activity when KGDEVD-PABC was conjugated to 3'-NH₂ of doxorubicin. This was also supported by other study in our research group that screened the cytotoxic activity of doxorubicin with different molecule conjugated to the 3'-NH₂ (data not published). Another reason is the decreased cell penetration due to the bound albumin. There are no argument that doxorubicin should go into the cell to exert its anticancer effect. Since doxorubicin is a relatively hydrophobic and small molecule, it penetrates into the cell very easily as shown in the cellular uptake study. This is also supported by the fact that doxorubicin has a very large volume of distribution in pharmacokinetic study¹². In contrast, HSA-DEVD-S-DOX showed very low penetration into the cell. Since albumin is a

very hydrophilic macromolecule, it is obvious that the albumin interfered the penetration through the cell membrane. Consequently, EMC-DEVD-S-DOX had no observable cytotoxic effect. However, caspase-3 successfully cleaved the prodrug and allowed the recovery of the intrinsic biological activity of the doxorubicin, thereby proving its excellent property as a prodrug.

As a result of EMC-DEVD-S-DOX binding to the endogenous albumins, the plasma half-life of the agent increased 38-fold in comparison to DEVD-S-DOX (19 h versus 30 min), which is a non-albumin binding form of the prodrug. Especially for the chronic diseases, longer half-life of drugs is preferred for the ease of maintaining the plasma concentration in the therapeutic window and better patient compliance due to the less frequent dosing, leading to improved therapeutic outcomes. Apart from these typical benefits of the prolonged drug circulation time, there is an important advantage that is specific for the currently proposed prodrug system. Caspase-3, which is the principal molecular target, is expressed only temporarily unlike traditional molecular targets. However, it is difficult to estimate its time of maximum expression after stimulation (e.g. radiotherapy) and the duration of expression for every patient. Therefore, the prolonged circulation time of the prodrug is necessary to increase the possibility of encountering caspase-3 that would result in larger portion of the administered agent to be activated. The albumin-binding of EMC-DEVD-S-DOX also contributed in the selective accumulation of the prodrug in tumor. The elevated local concentration of the prodrug in the site of interest could further increase the chance of encountering the upregulated caspase-3.

5.5. Conclusion

EMC-DEVD-S-DOX is a novel anticancer drug that involves conventional approach of delivering drugs to tumor and our novel strategy of targeting the radiation-induced apoptosis. The prodrug system allows the comprised chemotherapeutic agent to act in highly selective manner in the tumor with very long plasma half-life, thereby greatly improving the therapeutic index.

Considering that the severe toxicities of the chemotherapeutic agents are one of the major limitations in the clinical oncology, this prodrug system is expected to contribute in overcoming those problems.

References

- 1 DiPaola, R. S., Rinehart, J., Nemunaitis, J., Ebbinghaus, S., Rubin, E., Capanna, T., Ciardella, M., Doyle-Lindrud, S., Goodwin, S., Fontaine, M., Adams, N., Williams, A., Schwartz, M., Winchell, G., Wickersham, K., Deutsch, P. & Yao, S. L. Characterization of a novel prostate-specific antigen-activated peptide-doxorubicin conjugate in patients with prostate cancer. *J Clin Oncol* **20**, 1874-1879 (2002).
- 2 Sapra, P., Stein, R., Pickett, J., Qu, Z., Govindan, S. V., Cardillo, T. M., Hansen, H. J., Horak, I. D., Griffiths, G. L. & Goldenberg, D. M. Anti-CD74 antibody-doxorubicin conjugate, IMMU-110, in a human multiple myeloma xenograft and in monkeys. *Clin Cancer Res* **11**, 5257-5264 (2005).
- 3 Gerlinger, M., Rowan, A. J., Horswell, S., Larkin, J., Endesfelder, D., Gronroos, E., Martinez, P., Matthews, N., Stewart, A., Tarpey, P., Varela, I., Phillimore, B., Begum, S., McDonald, N. Q., Butler, A., Jones, D., Raine, K., Latimer, C., Santos, C. R., Nohadani, M., Eklund, A. C., Spencer-Dene, B., Clark, G., Pickering, L., Stamp, G., Gore, M., Szallasi, Z., Downward, J., Futreal, P. A. & Swanton, C. Intratumor heterogeneity and branched evolution revealed by multiregion sequencing. *N Engl J Med* **366**, 883-892 (2012).
- 4 Lee, B. S., Cho, Y. W., Kim, G. C., Lee do, H., Kim, C. J., Kil, H. S., Chi, D. Y., Byun, Y., Yuk, S. H., Kim, K., Kim, I. S., Kwon, I. C. & Kim, S. Y. Induced phenotype targeted therapy: radiation-induced apoptosis-targeted chemotherapy. *J Natl Cancer Inst* **107** (2015).
- 5 Bucci, B., Misiti, S., Cannizzaro, A., Marchese, R., Raza, G. H., Miceli, R., Stigliano, A., Amendola, D., Monti, O., Biancolella, M., Amati, F., Novelli, G., Vecchione, A., Brunetti, E. & De Paula, U. Fractionated ionizing radiation exposure induces apoptosis through caspase-3 activation and reactive oxygen species generation. *Anticancer Res* **26**, 4549-4557 (2006).
- 6 Huang, Q., Li, F., Liu, X., Li, W., Shi, W., Liu, F. F., O'Sullivan, B., He, Z., Peng, Y., Tan, A. C., Zhou, L., Shen, J., Han, G., Wang, X. J., Thorburn, J., Thorburn, A., Jimeno, A., Raben, D., Bedford, J. S. & Li, C. Y. Caspase 3-mediated stimulation of tumor cell repopulation during cancer radiotherapy. *Nat Med* **17**, 860-866 (2011).

- 7 Delaney, G., Jacob, S., Featherstone, C. & Barton, M. The role of radiotherapy in cancer treatment: estimating optimal utilization from a review of evidence-based clinical guidelines. *Cancer* **104**, 1129-1137 (2005).
- 8 Kratz, F. Albumin as a drug carrier: design of prodrugs, drug conjugates and nanoparticles. *J Control Release* **132**, 171-183 (2008).
- 9 Dennis, M. S., Zhang, M., Meng, Y. G., Kadkhodayan, M., Kirchofer, D., Combs, D. & Damico, L. A. Albumin binding as a general strategy for improving the pharmacokinetics of proteins. *J Biol Chem* **277**, 35035-35043 (2002).
- 10 Kratz, F. & Beyer, U. Serum proteins as drug carriers of anticancer agents: a review. *Drug Deliv* **5**, 281-299 (1998).
- 11 Kratz, F., Muller-Driver, R., Hofmann, I., Dreves, J. & Unger, C. A novel macromolecular prodrug concept exploiting endogenous serum albumin as a drug carrier for cancer chemotherapy. *J Med Chem* **43**, 1253-1256 (2000).
- 12 Assumpção, J. U., Campos, M. L., Ferraz Nogueira Filho, M. A., Pestana, K. C., Baldan, H. M., Formariz Pilon, T. P., de Oliveira, A. G. & Peccinini, R. G. Biocompatible microemulsion modifies the pharmacokinetic profile and cardiotoxicity of doxorubicin. *J Pharm Sci* **102**, 289-296 (2013).
- 13 Jain, M., Barthwal, S. K., Barthwal, R., & Govil, G. Restrained molecular dynamics studies on complex of adriamycin with DNA hexamer sequence d-CGATCG. *Arch Biochem Biophys* **439**, 12-24 (2005).

Chapter 6

Integrin $\alpha\beta3$ targeted caspase-3-dependently activated doxorubicin prodrug

There have been numerous studies to deliver chemotherapeutic agents selectively to the tumor in attempt to increase their therapeutic index. One of the most popular approaches is to introduce an active targeting ligand that could recognize certain tumor-specific surface antigens. However, such approach has encountered a fundamental challenge due to the finding of intratumor heterogeneity, which conveyed the presence of distinct subclones of tumor cells in a single tumor mass. Paradoxically, specificity provided to the chemotherapeutic agents by conventional drug delivery approaches limit their therapeutic activity to only few subclones of tumor cells, potentially allowing tumor regrowth from the unaffected populations. In this study, a drug delivery strategy that could overcome such limitation of the conventional active targeting approach is proposed. As a model drug, RGDEV-D-DOX was prepared, which comprises integrin $\alpha\beta3$ recognizing sequence (RGD), caspase-3 cleavable sequence (DEV-D), and doxorubicin. The distinct feature of the proposed system is the presence of DEV-D sequence between the traditional targeting moiety (i.e., RGD) and the cytotoxic agent (i.e., doxorubicin). The RGD moiety selectively delivers the cytotoxic agent to the tumor and induces tumor cell apoptosis, leading to upregulation of caspase-3. The caspase-3 further activates other prodrug molecules, triggering the release of more hydrophobic form of the active compound that penetrates faster into the cell regardless of integrin $\alpha\beta3$ expression. Therefore, it could affect broader range of tumor cells in the tumor tissue, resulting in improved therapeutic outcome.

6.1. Introduction

Although newly developed drugs for clinical oncology are mostly focused in the targeted therapies, cytotoxic chemotherapeutic agents are still widely used in first-line therapy for their potent anticancer effect and availability in broad range of tumors. Their use, however, are often limited by the dose-dependent toxicities, which are sometimes even lethal¹. Therefore, many efforts have been made to deliver chemotherapeutic agents selectively to the tumor and minimize the distribution to the normal tissue. One of the most popular approaches is to introduce a molecular targeting moiety to the drugs, such as monoclonal antibodies or peptides that could selectively bind to tumor specific ligands, thereby alter the systemic pharmacokinetic properties and allow selective delivery of the agents to the tumor²⁻⁵. However, such an approach is fundamentally challenged by the intratumoral heterogeneity, which refers to the existence of genetically heterogeneous tumor cell population in a single tumor mass⁶. This finding implied that targeting a specific ligand would possibility affect only small portion of the tumor cells. Hence, there is a high possibility of tumor relapse from the unaffected subclones that do not express the target ligands. Moreover, the tumor growth is also aided by the tumor-associated stromal cells⁷, which are definitely not affected by the therapy. Therefore, effective cancer treatment demands delivery of chemotherapeutic agents to every tumor cells and the associated stromal cells, which differ in their genomic profiles. But targeting those cells that differ in their ligand expression pattern through the conventional approach is practically impossible.

In attempt to overcome the aforementioned limitations, it was hypothesized that the drug should approach to the site of interest in a selective manner, and then become non-selective, thereby allow the drug to affect every cell regardless of their genomic profile. To achieve such purpose, a peptide was prepared by which RGD and DEVD motif is combined, which is recognized by integrin $\alpha\beta3$ and caspase-3, respectively. In this peptide, RGD motif plays central role as an initial homing moiety to the tumor, since integrin $\alpha\beta3$ is

abundantly expressed on tumor endothelium as well as several types of tumor cells including late-stage glioblastoma, melanoma, ovarian, breast and prostate cancer^{8,9}. Moreover, RGD sequence could facilitate the cellular uptake of the RGD-bearing substance when bound to the integrins⁹. Many studies have, therefore, used RGD-containing peptides to deliver chemotherapeutic agents or particulate carrier systems to tumor¹⁰⁻¹².

The distinct property of the currently proposed system from the other studies that used RGD for tumor targeting comes from the insertion of the DEVD motif between the RGD moiety and the chemotherapeutic agent. The DEVD motif is the principal compartment in converting the drug from selective to non-selective drug. Caspase-3, which is activated as an executioner caspase during an apoptotic event, recognizes and enzymatically cleaves the DEVD sequence¹³. Therefore, when a sufficient number of cells that express integrin $\alpha\beta3$ are dead by the RGD-mediated delivery of chemotherapeutic agents, they could be liberated from the targeting moiety by the upregulated caspase-3 in the tumor. Generally, most of the chemotherapeutic agents lack selectivity. Therefore, the liberated drugs could diffuse into the nearby cells regardless of their integrin $\alpha\beta3$ expression and again induce cell death. After such event is initiated, the local concentration of caspase-3 is increased in the tumor by the apoptotic cells. Then the chemotherapeutic agents that are conjugated to the peptide could be continuously released in the tumor by the upregulated caspase-3 even after the cells that express integrin $\alpha\beta3$ are eliminated and kill the remaining integrin $\alpha\beta3$ -nonexpressing tumor cells, which would again increase caspase-3 (**Fig 6.1A**). Due to the cycling process, the concentration of the target molecule (i.e. caspase-3) would be sustained or even increased in the tumor as the therapy goes on, whereas the conventional targeted approach would eventually deplete the target molecule and become ineffective (**Fig. 6.1B**).

To prove the hypothesis, a model drug was synthesized. A peptide that has RGD and DEVD motif at the same time was prepared by addition of Arg-Gly sequence at the N-terminus of the DEVD, so that an Asp participating in RGD and DEVD motif. This pentapeptide is the shortest possible sequence that could

have both RGD and DEVD sequence. To the prepared peptide, doxorubicin was conjugated to produce a model prodrug for proof-of-concept in the current novel drug delivery strategy (**Fig. 6.1C**). This prodrug could be selectively delivered to the integrin $\alpha\beta3$ overexpressing cells including tumor endothelial cells and some types of tumor cells, and induce their apoptosis. Then by the upregulated caspase-3 in the tumor tissue, the further delivered prodrug could be cleaved and recover the non-selective and rapid penetrating characteristic of the doxorubicin, thus inducing further apoptosis of the tumor cell and the tumor-associated cells that does not express integrin $\alpha\beta3$.

6.2. Materials and Methods

6.2.1. Cell lines

Human umbilical vein endothelial cells (HUVEC) and human dermal microvascular endothelial cells (HDMEC) were purchased from PromoCell (Heidelberg, Germany). U87 MG and HT-29 cells were obtained from the American Type Culture Collection (ATCC; Manassas, VA). HUVECs and HDMECs were cultured in Endothelial Cell Growth Medium MV2 (ECGM; PromoCell). U87 MG and HT-29 cells were grown in high-glucose Dulbecco's modified eagle medium (Gibco, Carlsbad, CA) supplemented with 10% fetal bovine serum (Gibco). The cells were maintained in a humidified 5% CO₂ atmosphere at 37°C.

6.2.2. Synthesis

AcRGDEVDC-NH₂ and AcRDEVDC-NH₂ peptide was purchased from Pepton (Daejeon, South Korea). Daunorubicin hydrochloride was obtained from US Pharmacia (Rockville, MD). 1,4-Dioxane, anhydrous methanol, trimethyl orthoformate, propylene oxide, 48% hydrobromic acid and 1 M potassium butoxide in tetrahydrofuran were purchased from Sigma-Aldrich (St. Louis, MO). Bromine was obtained from Junsei Chemical (Tokyo, Japan). 4-Maleimidobutyric acid was from Santa Cruz Biotechnology (Dallas, TX). Cy5.5

maleimide was from Lumiprobe (Hallandale Beach, FL). All the other solvents were from Burdick & Jackson (Seoul, South Korea).

14-Doxorubicinyl maleimidobutyrate ester was synthesized according to Meyer-Losic et al. for conjugation with the prepared peptides¹⁴. Daunorubicin hydrochloride (100 mg, 177.3 μmol) was dissolved in a mixture of anhydrous methanol (3 ml) and anhydrous 1,4-dioxane (2.5 ml). Trimethyl orthoformate (89.2 μl , 815.6 μmol , 4.6 eq) was added followed by addition of bromine (15.7 μl , 306.8 μmol , 1.73 eq) at 11°C and reacted for 2 h under nitrogen. Propylene oxide (31.9 μl , 455.7 μmol , 2.57 eq) was added at 4°C and reacted for 75 min. Then mixture of acetone (8.6 ml) and 0.25 M hydrobromic acid (3 ml), and reacted for 48 h at room temperature. When the reaction was completed, the solution was diluted with distilled water (5 ml) and extracted with chloroform (10 ml \times 2). Saturated brine (5 ml) was added to the aqueous layer and the product was extracted into n-butanol until the aqueous layer was colorless. The collected n-butanol layer was concentrated at 35°C *in vacuo* and precipitated in 10 volume of n-hexane to obtain 14-halodaunorubicin as red solid. *m/z* (ESI-MS): 562.0 [M + H]⁺ for 14-chlorodaunorubicin, 605.9 [M + H]⁺ for 14-bromodaunorubicin.

Suspension of 4-maleimidobutyric acid was prepared and 0.1 M sodium bicarbonate was slowly added during stirring. The resulting solution was stirred for 20 min and concentrated at 30°C *in vacuo*. The concentrated solution was lyophilized to obtain sodium 4-maleimidobutyrate. The sodium 4-maleimidobutyrate (263 mg, 1.28 mmol) and 14-halodaunorubicin (138 mg, 237.2 μmol) were dissolved in acetone and refluxed under nitrogen for 4 h. The solution was cooled and filtered. The remaining solid was washed with acetone and the filtrate was evaporated under vacuum. The red residue was dissolved in water with 0.1% trifluoroacetic acid (TFA) and subjected to semi-preparative reverse-phase HPLC (Shimadzu, Kyoto, Japan) using ODS-A 5 μm semi-preparative column (150 mm \times 20 mm; YMC, Dinslaken, Germany) for further purification to obtain highly purified 14-doxorubicinyl maleimidobutyrate ester. A gradient system (Water and acetonitrile with 0.05% TFA as an additive) was

used with a flow rate of 8 mL/min. Each step of the reaction was monitored using normal phase TLC (CH₂Cl₂ : MeOH, 8 : 2). *m/z* (ESI-MS): 709.0 [M + H]⁺.

The 14-doxorubicinyl maleimidobutyrate ester and AcRGDEVDC-NH₂ was dissolved in anhydrous DMF and reacted overnight at 4°C. The solution was precipitated in diisopropyl ether and the precipitate was collected by filtration. The precipitate was washed three times with diisopropyl ether and dried *in vacuo*. The red solid was redissolved in water and subjected to a semi-preparative reverse-phase HPLC as mentioned above for further purification. Collected fractions were concentrated in reduced pressure and lyophilized to obtain final product RGDEVDC-DOX as red powder. The purity was confirmed by analytical HPLC with UV detection at 214 nm and was determined to be ≥ 95%. *m/z* (ESI-MS): 1542.0 [M + H]⁺.

AcRGDEVDC-NH₂ and AcRDEVDC-NH₂ peptides were fluorescently labeled using Cy5.5-maleimide with simple chemistry. The peptide (1 eq) and Cy5.5 maleimide (1.3 eq) was dissolved in DMF and reacted in dark at 4°C for 16 h. Then, 10 volume of dichloromethane was added to the solution and formed precipitate was recovered by filtration or centrifugation. The precipitate was dried *in vacuo* to obtain dark blue crude product. The solid was redissolved in small volume of DMF and subjected to a semi-preparative reverse-phase HPLC in purpose to remove any impurities, especially the unreacted Cy5.5 maleimide. The purity of the obtained AcRGDEVDC-Cy5.5 and AcRDEVDC-Cy5.5 was confirmed by analytical HPLC with UV detection at 214 nm and was determined to be ≥ 95%. In particular, no peak corresponding to Cy5.5-maleimide was detected, indicating the complete removal of unreacted Cy5.5-maleimide.

6.2.2. Integrin αvβ3 dependent cellular uptake imaging

HUVECs, HDMECs, and U87 MG cells were seeded on a cover-glass bottom dishes (SPL Life science, Pocheon, South Korea) at 3 × 10⁵ cells per dish and maintained for 48 h. When cells were at 80% confluence, AcRGDEVDC-Cy5.5

or AcRDEVDC-Cy5.5 were treated to the cells at final concentration of 1 μM and incubated for 5 min at 37°C. Then the cells were washed with cold PBS three times and fixed with 4% paraformaldehyde (Sigma-Aldrich, St. Louis, MO). The cell nucleus was stained with DAPI (Molecular Probes, Eugene, OR) and mounted with Slowfade gold anti-fade reagent (Molecular Probes). The cells were observed under a confocal laser-scanning microscope (LSM 710; Carl Zeiss, Oberkochen, Germany). Similar experiment using only AcRGDEVDC-Dy5.5 was carried out on HDMECs and U87 MG cells transfected with ITGAV siRNA (10 nM). The procedure was identical with above. The detailed description of siRNA transfection is shown below.

Another set of experiment was done using doxorubicin conjugated peptides. U87 MG cells were seeded on a cover-glass bottom dishes at 3×10^5 cells per dish and maintained for 48 h. When cells were at 80% confluence, RGDEVDDOX or RDEVDDOX were treated to the cells at final concentration of 10 μM and incubated for 30 min at 37°C. Then the cells were processed as described above and observed under a confocal laser-scanning microscope (LSM 710; Carl Zeiss, Oberkochen, Germany).

6.2.3. siRNA transfection.

Transient gene knockdown of HDMEC and U87 MG cells was carried out using Trilencer-27 siRNA duplexes against ITGAV (Cat. No. SR302468, ITGAV Trilencer-27 human siRNA; OriGene, Rockville, MD) or a scrambled control siRNA (OriGene). When the cells were at 80% confluency in 30 mm culture dish, the siRNA duplexes or the scrambled control siRNA were diluted at a concentration of 5 μM in siRNA dilution buffer (OriGene). Prepared siRNA solution (5 μl) was transferred to Opti-MEM (140 μl). Another set of solution containing transfection agent was prepared by addition of siTran1.0 (20 μl ; OriGene) to Opti-MEM (120 μl). The prepared solutions were combined and incubated 15 min at room temperature. The siRNA/siTrans complex solution was added to cells in complete medium (final volume 2.5 ml) to gain final concentration of 10 nM siRNA. The ratio between siRNA and siTran1.0 was

maintained in other concentrations of siRNA transfection. After 72 h incubation, the cells were applied for further experiments. The RNAi efficiency was confirmed through standard western blot using anti-integrin α v antibody (1:1000; Cell Signaling Technology, Danvers, MA).

6.2.4. Flow cytometry

U87 MG cells were cultured in 60 mm culture dishes. The cells were transfected with ITGAV or scrambled siRNA to produce integrin α v knock down or mock cells, respectively. The detailed siRNA transfection procedure is demonstrated above. When the transfection was completed, RGDEVDC-Cy5.5 was treated at a final concentration of 1 μ M for 5 min and washed twice with cold PBS. The cells were then detached with Trypsin/EDTA and collected by centrifuge at $400 \times g$ for 5 min. The cells were then fixed in 2% paraformaldehyde for 10 min at room temperature. After fixation, the cells were washed twice with and resuspended in 100 μ l of PBS containing 0.5% BSA. Then, Alexa 488-conjugated integrin α v β 3 antibody was added (1:100; R&D Systems, Minneapolis, MN) and incubated for 1 h at 4°C. The antibody-labeled cells were washed twice, resuspended in PBS containing 0.5% BSA, and subjected to flow cytometry (BD FACSCalibur, BD Biosciences, San Jose, CA) according to standard procedure.

6.2.5. HPLC determination of caspase-mediated activation

This experiment was carried out in purpose to determine the cleavage of RGDEVDC-DOX in presence of caspase-3. The RGDEVDC-DOX (100 μ M) was incubated with recombinant human caspase-3 (500 ng/mL; R&D Systems, Minneapolis, MN) in the caspase assay buffer (50 mM HEPES, pH 7.4, 100 mM NaCl, 0.1% CHAPS, 10 mM DTT, 1 mM EDTA, 10% glycerol; Enzo Life Sciences, Farmingdale, NY) at room temperature. Small portion of the solution was withdrawn at 15, 30, 60 min time point and quenched by addition of equal volume of DMSO to prevent the further reaction of the withdrawn samples. The samples were subjected to an analytical HPLC (Agilent 1300 series, Agilent

Technologies, Santa Clara, CA) using ODS-A 5 μm analytical column (150 mm \times 3 mm; YMC, Dinslaken, Germany). A gradient system (Water and ACN with 0.1% TFA as an additive, ACN 20-30%/5-25 min) was applied at a flow rate of 0.8 mL/min. The peaks were monitored under fluorescence detector at 470/580 nm. The ratio of the remaining RGDEVD-DOX and the released compound was determined in the basis of peak area. Additionally, the RGDEVD-DOX without caspase-3, and with caspase-3 (500 ng/ml) pretreated with caspase-3 inhibitor (Ac-DEVD-CHO, 10 μM ; Enzo Life Sciences), were incubated for 60 min at room temperature in the caspase assay buffer, and subjected to analytical HPLC using the identical experimental condition described above.

6.2.6. MTT cytotoxicity assay

The cytotoxicity of the prepared doxorubicin conjugates against cancer cells was examined on U87 MG and HT-29 cells. The cells were seeded in 96-well cell culture cluster plate (Corning, Tewksbury, MA) at 5×10^4 cells per well and incubated for 24 h in high-glucose Dulbecco's modified eagle medium with 10% FBS (Gibco). The medium was replaced with 100 μl of fresh medium containing the test compounds at final concentration of 0.1, 1, 10, and 100 μM and incubated for 1 h. The medium was then replaced with fresh medium and further incubated for 72 h at 37°C. Then 10 μl of MTT reagent (Trevigen, Gaithersburg, MD) was added to each well and incubated for 2 h at 37°C. When blue precipitate was clearly visualized inside the cells, 100 μl of detergent agent (Trevigen, Gaithersburg, MD) was added and further incubated for 4 h at room temperature. The absorbance was measured using microplate reader (Synergy HT, BioTek Instruments, Winooski, VT) at 570 nm. $n = 8$.

6.2.7. Western blots

U87 MG cells were treated with 0.1, 1, and 10 μM of the substance and incubated for 48 h. The cells were washed with cold PBS and lysed with RIPA buffer (Pierce, Rockford, IL) containing protease inhibitor cocktail (Pierce). The preparation of the samples and western blot were performed according to

the standard protocol. For immunoblotting, anti-Caspase-3 antibody (1:1000) and anti-cleaved Caspase-3 antibody (1:1000) from Cell Signaling Technology (Danvers, MA) were used as primary antibodies. HRP-conjugated anti-rabbit IgG (1:2000; R&D Systems) was used as secondary antibody. The blotted membranes were developed under ImageQuant LAS 4000 imaging system (GE Healthcare Life Sciences, Uppsala, Sweden).

6.2.8. Caspase-3 cellular activity assay

To determine the caspase-3 activity in the cells, the Calbiochem caspase-3 cellular activity assay kit (EMD Millipore, Darmstadt, Germany) was used following to the manufacturer's instruction. Briefly, U87 MG cells were treated with 0.1, 1, and 10 μM of RGDEVD-DOX with or without pretreatment of recombinant human caspase-3, and incubated for 48 h. The cells were washed once with cold PBS and lysed with CHAPS cell lysis buffer (50 mM HEPES, 5 mM DTT, 0.1 mM EDTA, 0.1% CHAPS, pH 7.4) without any addition of protease inhibitors, which may potentially inhibit the activity of caspase-3. The lysates were centrifuged in 14,000 rpm at 4°C for 15 min, and the supernatant was collected. The protein concentration was determined by BCA protein assay (Pierce) and all samples were diluted to equal concentration. The diluted cell lysate (10 μl), caspase substrate (10 μl , final concentration 200 μM ; Ac-DEVD-pNA), and assay buffer (80 μl ; 100 mM NaCl, 50 mM HEPES, 10 mM DTT, 1 mM EDTA, 10% glycerol 0.1% CHAPS, pH 7.4) were combined in half-area 96-well microplate in triplicate. Purified caspase-3 at final concentration 30 IU was used as control. The absorbance at 405 nm was measured at 10 min interval in microplate reader (Synergy HT, BioTek Instruments, Winooski, VT) for 60 min, and the slope ($\Delta\text{Abs}/\text{min}$) was calculated and averaged. The slope of the samples were divided by the slope of the purified caspase-3 and multiplied by 30 to calculate the specific activity (IU) of the samples. The values were further normalized by the amount of protein.

6.2.9. Cellular caspase-3 stain

U87 MG cells were seeded in 8-well cover glass chamber (Nalge Nunc, Rochester NY) at seeding density of 1×10^5 cells per well and grown until 80% confluence. RGDEVD-DOX or that preincubated with 500 ng/ml of recombinant human caspase-3 was treated to the cells at a final concentration of 1 μ M and incubated for 48 h. The activated caspase-3 within the cells was stained using Image-iT™ LIVE Green Caspase-3 Detection Kit (Molecular Probes, Eugene, OR) according to the manufacturer's instruction. The kit is based on a fluorescent inhibitor of caspases (FLICA) methodology, essentially an affinity label. Briefly, FAM-DEVD-FMK reagent was added to the cells and incubated for 60 min. Then, the cells were further stained with Hoechst 33342 (included in the kit). The cells were washed twice with the provided wash buffer and fixed with 4% paraformaldehyde. The fixed cells were then observed under a confocal laser-scanning microscope (LSM 710; Carl Zeiss, Oberkochen, Germany).

6.2.10. Animal study

U87 MG cells were suspended at 1×10^8 cell/ml in HBSS, and inoculated subcutaneously (100 μ l) into the thigh of 6 week-old male C3H/HeN mice. When the tumor volume reached 50-100 mm³, the mice were randomized and received saline (control), doxorubicin HCl (3 mg/kg), RDEVD-DOX (3 mg/kg doxorubicin equivalent), and RGDEVD-DOX (1, 3, 5 mg/kg doxorubicin equivalent) intravenously through tail vein for seven days daily. The mice were maintained for additional seven days after the last drug administration and sacrificed. The tumor length and width were measured by caliper and the volume was calculated using the modified ellipsoid formula ($L \times W^2/2$). Implanted tumors were isolated and weighed when sacrificed. All experimental procedures were approved by the Institutional Animal Care and Use Committee of the Seoul National University.

6.2.11. Statistical analysis

Data are presented as means \pm s.e.m. To test the differences between groups, the Mann-Whitney *U* test, which is a non-parametric statistics, was used. One-tailed test was performed. The GraphPad Prism version 6.0 (GraphPad Software, San Diego, CA) software was used for the statistical calculations. *P* values less than 0.05 were considered significant when compared to control and indicated with asterisks on the graphs.

6.3. Results

6.3.1. Synthesis of RGDEVD-DOX

Scheme 6.1 depicts the synthesis of RGDEVD-DOX. In order to retain the activity of doxorubicin when conjugated with the peptide, a location other than 3'-NH₂ was preferred as the conjugation site. In particular, the peptide was conjugated to the 14-OH of doxorubicin. For this, 14-doxorubicinyl maleimidobutyrate ester was first prepared according to Meyer-Losic et al., by using daunorubicin as a starting material¹⁴. This doxorubicin derivative allows conjugation of peptides that has sulfhydryl group in very mild condition via its maleimide group. Since RGDEVD peptide does not contain any sulfhydryl group, Cys was added to the C-terminus. The reaction was carried out in DMF by simply mixing the 14-doxorubicinyl maleimidobutyrate ester and AcRGDEVDC-NH₂. The final product was purified by semi-preparative HPLC. The purity was confirmed to be more than 95% using analytical HPLC (**Fig. 6.2A**). The mass was determined using ESI-MS (**Fig. 6.2B**).

6.3.2. Integrin $\alpha\beta3$ dependent cellular uptake of RGDEVD peptide

The facilitated cellular uptake of the RGDEVD peptide mediated by the RGD motif was determined in three different cell lines, U87 MG, HDMECs, and HUVECs, which overexpress integrin $\alpha\beta3$. RDEVDC peptide, which has defective RGD motif, was used as a control. The peptides that were labeled

with a fluorescent dye were used in the experimental studies. The labeled peptides – RGDEVD and RDEVD – were treated to the each cell line at 1 μ M for 5 minutes, which is a relatively short incubation time to avoid non-selective diffusion into the cells. When the cells were observed under confocal microscopy, RGDEVD peptide showed significantly higher accumulation than RDEVD peptide (**Fig. 6.3A**). Considering that the both peptides has almost identical structure except in the presence of one Gly residue, this result suggested that RGD motif within the RGDEVD peptide was involved in the facilitated cellular uptake in the integrin $\alpha\beta 3$ overexpressing cell lines.

This result was further supported with experiments on integrin αv siRNA transfected U87 MG and HDMECs (**Fig. 6.3B**) When RGDEVD peptide was treated to the cells, significant difference in the amount of that taken up between mock and siRNA transfected cells was found. The cells observed under confocal microscopy showed that integrin αv knocked down cells had drastically decreased uptake of the peptide than that in the mock cells. This was shown in both U87 MG cells and HDMECs (**Fig 6.3C**).

For U87 MG cells, their difference of the RGDEVD peptide uptake between siRNA transfected and mock cells were also determined by flow cytometry (**Fig. 6.3D**). After the treatment of RGDEVD peptide on the cells, both cells were also immunostained with fluorescent-labeled integrin $\alpha\beta 3$ antibody to confirm the integrin downregulation by siRNA transfection. The histogram plot showed a left shift of the integrin $\alpha\beta 3$ staining in the transfected cells, indicating a successful knock down of integrin αv in the U87 MG cells. Similar pattern of histogram was shown with the detector corresponding to the signal from RGDEVD peptide. The siRNA transfected U87 MG cells, which showed left shift of integrin $\alpha\beta 3$, also showed left shift of RGDEVD peptide uptake. This result manifested the correlation between the expression of integrin $\alpha\beta 3$ and uptake of RGDEVD peptide in the cells.

Same result was also shown in RGDEVD-DOX. When U87 MG cell was treated with RGDEVD-DOX or RDEVD-DOX, a facilitate drug uptake was

shown in RGDEVD-DOX, which has the RGD motif that interacts with integrin $\alpha\text{v}\beta\text{3}$ (**Fig. 6.3E**).

6.3.2. Caspase-3-mediated cleavage of RGDEVD-DOX

Cleavage of RGDEVD-DOX by caspase-3 was determined by HPLC analysis after incubation of RGDEVD-DOX (100 μM) with recombinant human caspase-3 (500 ng/ml) (**Fig. 6.4A**). When RGDEVD-DOX was subjected to HPLC analysis, the retention time of the peak showed 22.1 min. However, the incubation of the RGDEVD-DOX with the caspase-3 prior to the HPLC analysis shifted the retention time of the peak to 20.2 minute. The peak located at 22.1 min gradually decreased and that located at 20.2 minute gradually increased by time, showing more than 80% of the RGDEVD-DOX was cleaved within 30 minutes in the presence of the caspase-3. The peak of RGDEVD-DOX was undetectable when measure at 60 min time point, indicating the amount of uncleaved RGDEVD-DOX was decreased below the level of detection limit within 60 minutes. The mass spectrometry showed m/z value of 829.1 in the newly appeared peak, and the determined molecular weight was identical to the molecular weight of the anticipated cleaved product from RGDEVD-DOX. Also, m/z 732.2 was found, which corresponds to the mass of the peptide moiety after cleavage.

6.3.3. *In vitro* efficacy of RGDEVD-DOX

Therapeutic efficacy difference between RGDEVD-DOX and the active compound – RGDEVD-DOX pre-incubated with caspase-3 – was determined. The major difference between the two compounds was their influx rate into the cell regardless of the integrin $\alpha\text{v}\beta\text{3}$ expression. Initially, the U87 MG and HT-29 cells were incubated with doxorubicin, RGDEVD-DOX, or the active compound for 0.5, 1, 2, or 4 hours and observed under confocal microscopy. The acquired images were subjected to fluorescence intensity analysis to compare the cellular uptake as well as the influx rate into the cells (**Fig. 6.4B**). Not surprisingly, doxorubicin showed the most rapid accumulation in the cell

nuclei, whereas RGDEVD-DOX was significantly slower. However, the activation of RGDEVD-DOX by caspase-3 recovered its influx rate to that similar to doxorubicin. In the present observation, the cell influx rate of the active compound was slightly slower than doxorubicin, but the difference was insignificant. The representative images of compound accumulated into the two cell lines are shown in **Fig. 6.4C**.

The influx rate difference among the compounds was directly correlated with the cytotoxicity of the compounds. When U87 MG cells were exposed to doxorubicin, RGDEVD-DOX, and the active compound for two hours and further incubated for 72 hours, IC_{50} values were shown 0.104, 3.16, and 0.135 μM , respectively (**Fig. 6.5A**). The IC_{50} value of RGDEVD-DOX was significantly higher than doxorubicin, which was an agreement with the observation in cellular uptake. However, when the prodrug was cleaved by caspase-3, IC_{50} value was recovered to the level similar to that of doxorubicin.

Additionally, alteration of IC_{50} values according to the varying drug exposure time was determined (**Fig. 6.5B**). The doxorubicin, RGDEVD-DOX, or active compound was exposed to the U87 MG cells for 1, 2, or 4 hours with various concentration and the IC_{50} values were calculated. As it was reflecting the result shown in the cellular uptake study, longer exposure time resulted in decreased IC_{50} value. However, in the case of RGDEVD-DOX, it needed more than 3 hours of exposure to the cells to obtain similar IC_{50} value to an hour exposure of doxorubicin or active compound.

6.3.4. Caspase-3 upregulation induced by RGDEVD-DOX

For the concept of RGDEVD-DOX to be valid, the RGDEVD-DOX as well as the cleaved product of the prodrug should upregulate the active caspase-3 in the cells. To determine the upregulation of the active caspase-3 induced by the agents, three independent *in vitro* experiments were carried out: western blot, caspase activity assay, and cellular caspase staining. All these experiments were performed with U87 MG cells that were exposed for 48 hours to RGDEVD-DOX or to that pre-incubated with recombinant human caspase-3.

Western blot showed dose-dependently decreased procaspase-3 and increased cleaved (or active) caspase-3 for both compound treatments (**Fig. 6.6A**). Procaspase-3 is a zymogen of caspase-3, which is activated when cleaved into 17 and 19 kDa subunits. Hence, this result clearly shows activation of caspase-3 by both RGDEVD-DOX and cleaved RGDEVD-DOX. However, the amount the activate caspase-3 was shown more when treated with the cleaved RGDEVD-DOX.

Caspase-3 activation was further confirmed by cellular activity assay (**Fig. 6.6B**). This assay measures quantitative activity of the cellular caspase-3 rather than the amount of the protein itself, which is more important since the current prodrug strategy attempts to utilize the proteolytic feature of the caspase-3. The principle of the assay is based on the caspase-3-mediated cleavage of fluorometric substrate Ac-DEVD-AMC (7-amino-4-methylcoumarin), which in turn generates highly fluorescent AMC. Since the assay substrate comprises DEVD motif, which is also the peptide sequence adopted in current prodrug, the assay result could not only show the total activity of caspase-3 within cells, but also could indirectly reflect the potential of these apoptotic cells to further cleave the prodrug.

In a healthy U87 MG, which was not exposed to any cytotoxic agents, showed negligible caspase-3 activity in their cell lysate, whereas the cells treated with the RGDEVD-DOX or the cleaved RGDEVD-DOX had dose-dependent upregulation of caspase-3 activity. When RGDEVD-DOX and cleaved RGDEVD-DOX were treated to the cells at a concentration of 10 μ M, more than 99- and 128-fold increased caspase-3 activity was observed respectively when compared to the normal state cells. Also, similar to the western blot result, treatment of cleaved RGDEVD-DOX showed about 1.3-fold increased caspase-3 activity than when intact RGDEVD-DOX was treated.

Following study determined the cellular distribution of caspase-3 when the U87 MG cells were stimulated with the prodrug and the active compound (**Fig. 6.6C**). The caspase-3 staining method adopted in this study employs DEVD-FMK (fluoromethyl ketone), which is a fluorescent inhibitor of caspase-3.

DEVD peptide moiety of the compound is recognized by caspase-3 in specific manner followed by FMK irreversibly binding with a Cys residue within the protein. The FMK also acts as a fluorescent reporter for visualization. Thus this staining method could show the location within cell where the recognition of DEVD motif by caspase-3 actually occurs. As mentioned earlier, since the DEVD sequence is also an essential component of the currently suggested prodrug system, this method of caspase-3 staining could suggest where the caspase-3 mediated cleavage of the prodrug takes place in the cells. The cells treated with RGDEVD-DOX and the active compound showed high level of caspase-3 expression (green fluorescence) with highly accumulated doxorubicin moiety (red fluorescence) in the cell nuclei (nuclei were not properly stained with DAPI due to the competitive binding with the DNA-bound doxorubicin), whereas the untreated cells had almost no detectable staining of active caspase-3 within the cells (nuclei well stained with DAPI). The presence of the DEVD recognizing caspase-3 was observed throughout the cells regardless of any cell compartment.

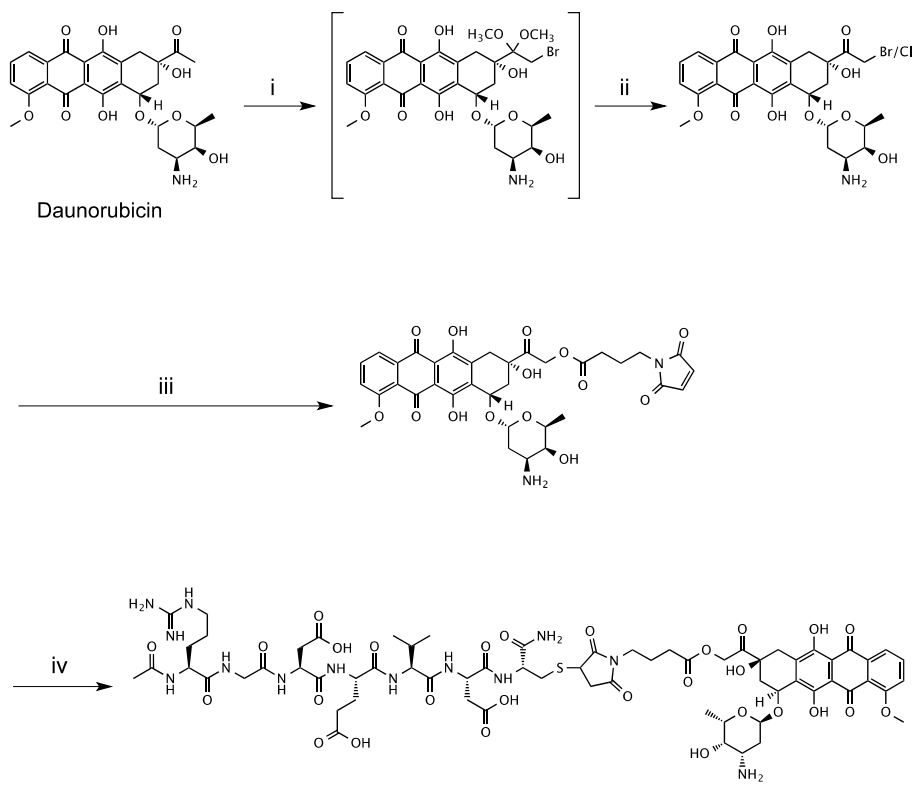
6.3.5. Tumor growth suppression of RGDEVD-DOX

Tumor growth suppression efficacy of RGDEVD-DOX was assessed in U87 MG tumor-bearing preclinical model (**Fig. 6.7**). The therapeutic efficacy of saline (control), doxorubicin, RDEVD-DOX, and RGDEVD-DOX were compared. When doxorubicin, RDEVD-DOX, and RGDEVD-DOX were administered to mice in identical dose (7×3 mg/kg molar equivalent to doxorubicin) the tumor growth rates of doxorubicin and RGDEVD-DOX received mice were similar, showing no noticeable increase in the tumor volumes during the course of study (8% decrease and 9% increase in final tumor volume compared to the initial volume, respectively), whereas the RDEVD-DOX received mice showed significantly increased tumor volume (4-fold increase) although smaller than the saline received control (5-fold increase). The average weight of the isolated tumors from doxorubicin, RDEVD-DOX, and RGDEVD-DOX treated groups at the last day of the study were reduced by

47.2, 83.2, and 85.0% compared to the control, respectively. Despite the similar therapeutic effect of doxorubicin and RGDEVD-DOX when administered in same dose, significant body weight loss was observed only in the doxorubicin received animals showing more than 30% decrease in their body weight. Moreover, three out of five examined mice were dead during the study in the doxorubicin treated group, but not in the other tested groups, indicating severe toxic effect of doxorubicin.

The systemic toxicity shown by the treatment of doxorubicin was even more severe than when RGDEVD-DOX was administered in higher dose (7×5 mg/kg molar equivalent to doxorubicin) despite the superior therapeutic efficacy of RGDEVD-DOX: 8% versus 70% reduction from the initial tumor volume in doxorubicin (7×3 mg/kg) and RGDEVD-DOX (7×5 mg/kg) received animal, respectively. As mentioned above, doxorubicin received animals showed more than 30% decreased average body weight in the last day of examination with 60% of the mice being dead. However, RGDEVD-DOX received animal showed maximum of 17% reduced body weight at day 12 and 14% reduced body weight at the end of examination. Also, in contrast to doxorubicin treated group, no mice were dead.

The therapeutic supremacy of RGDEVD-DOX over RDEVD-DOX in the same dose was already well described above. However, current study also showed RGDEVD-DOX had superior therapeutic effect even in a lower dose. While RDEVD-DOX (7×3 mg/kg) treated mice showed more than three-fold increase in their tumor volume during the course of the study, the mice received RGDEVD-DOX in 3 times lower dose (7×1 mg/kg) showed only 1.6-fold increase in that. The average weight of the isolated tumor from the RGDEVD-DOX treated animals were less than half of that from the RDEVD-DOX treated animals. Regarding that the physicochemical properties of these two compounds are nearly identical, the higher anticancer effect of RGDEVD-DOX clearly indicated the *in vivo* tumor targeting effect of RGD motif within the peptide.



Scheme 6.1. Chemical synthesis of RGDEVDC-DOX^a

^aReagents and conditions: (i) Trimethyl orthoformate, MeOH, 1,4-dioxane, Br₂, rt, and then propylene oxide, 2°C. (ii) 0.25 M HBr, acetone. (iii) sodium 4-maleimidobutyrate, acetone, refluxed. (iv) AcRGDEVDC-NH₂, DMF, rt.

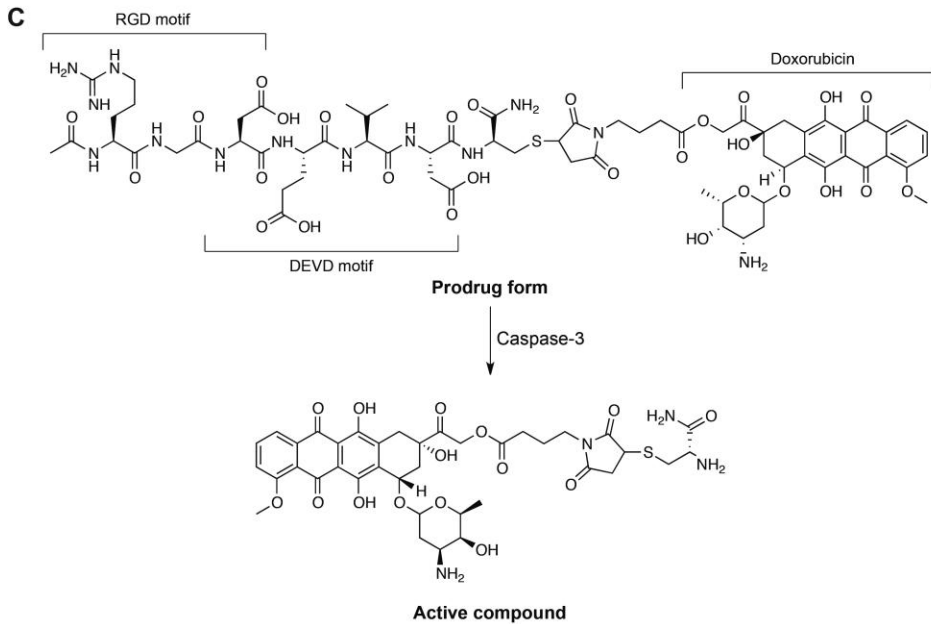
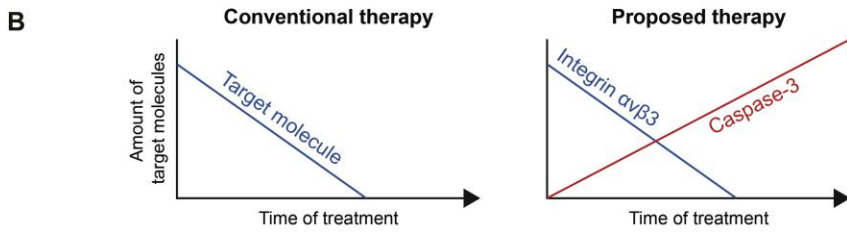
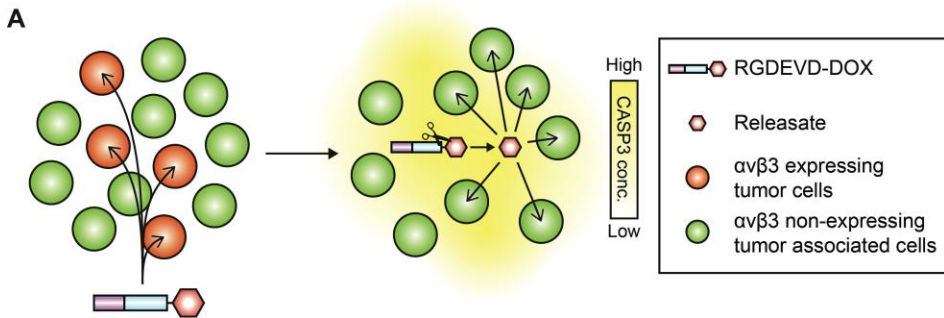


Figure 6.1. (A) Schematic diagram of the suggested prodrug strategy. (B) The major difference of the conventional targeted delivery system and the currently proposed targeted delivery system. (C) Chemical structure and compartment of the RGDEVD-DOX prodrug and its active compound.

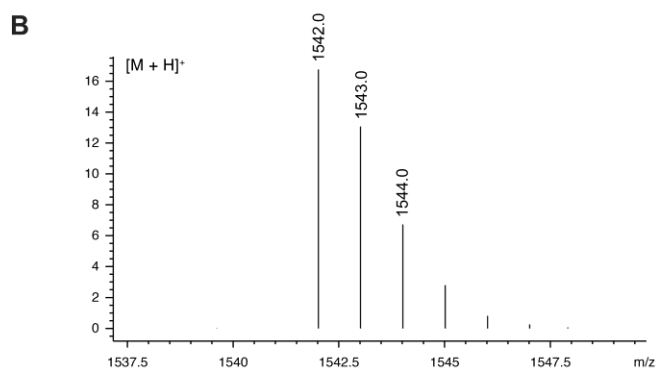
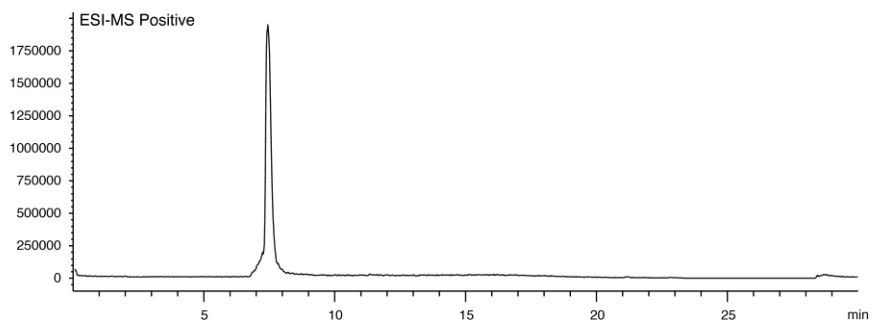
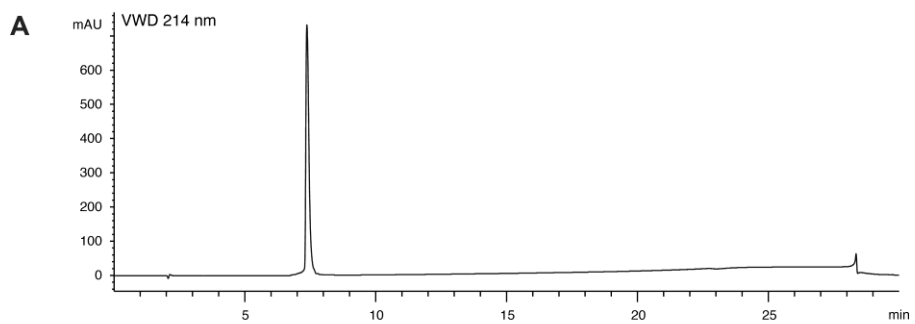


Figure 5.2. (A) Analytical HPLC chromatogram of the final product detected under UV detector (214 nm) and ESI-MS. (B) Mass spectrum of the final product determined by LC/ESI-MS.

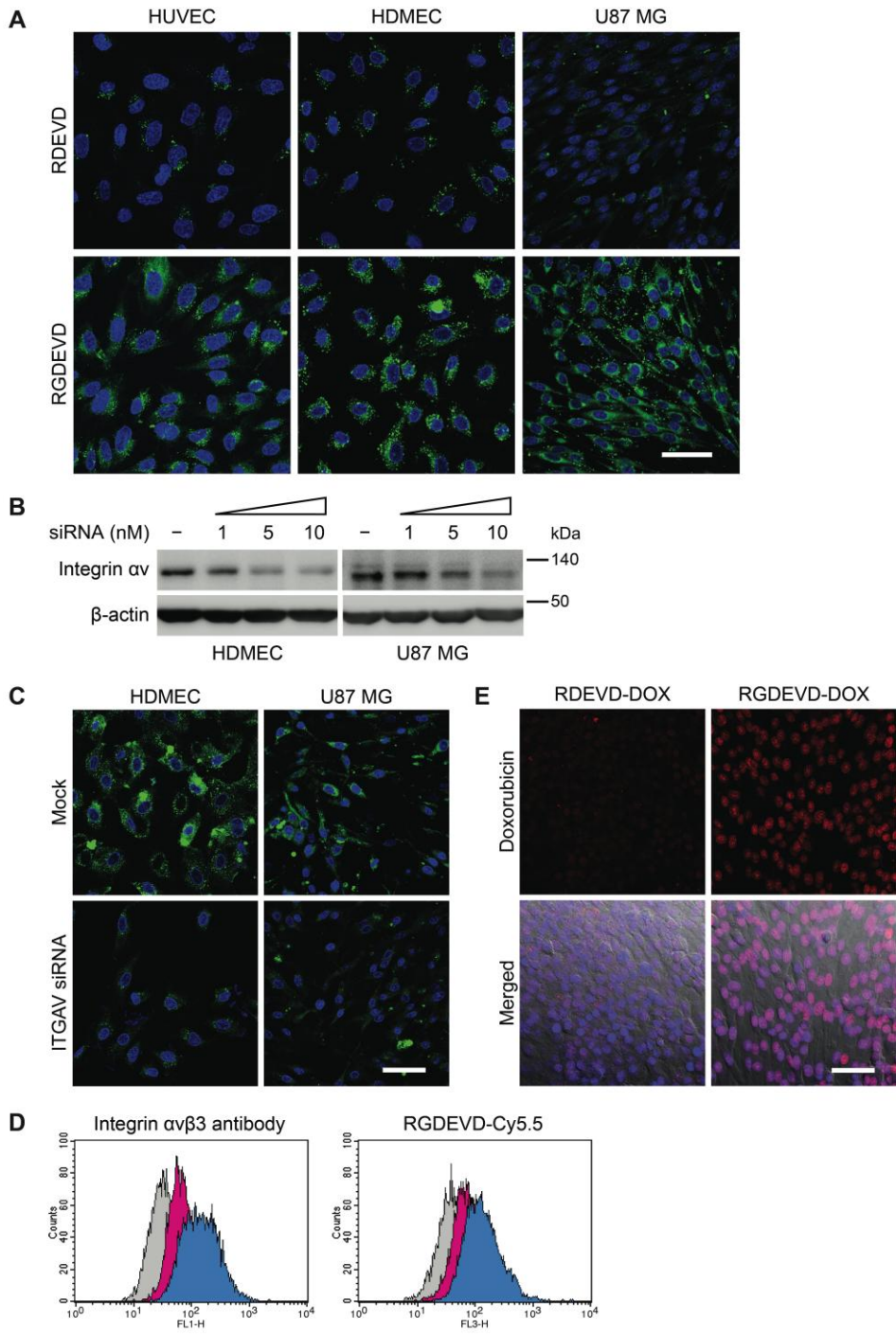


Figure 6.3. (A) Confocal microscopy images of HUVECs (left), HDMEC (center), and U87 MG cells (right) exposed to RDEVVD (upper panel) or RGDEVVD peptide (lower panel) labeled with Cy5.5. Green fluorescence represents the peptides. Cell nuclei are stained with DAPI (blue). Scale bar, 50 μ m. (B) Western blots of integrin α v after ITGAV siRNA transfection of HDMECs and U87 MG cells. (C) Confocal microscopy images of Cy5.5-labeled RGDEVVD peptide given to HDMECs (left) and U87 MG cells (right) that were mock-transfected (upper) or ITGAV siRNA transfected (lower). Green fluorescence represents the peptides. Cell nuclei are stained with DAPI (blue). Scale bar, 50 μ m. (D) Histograms of flow cytometry analysis. Mock-transfected (blue) and ITGAV siRNA transfected (pink) U87 MG cells were analyzed after RGDEVVD peptide treatment and integrin α v β 3 immunostaining. The cells were detected against Alexa488-labeled integrin α v β 3 antibody (left) and Cy5.5-labeled RGDEVVD peptide (right). Non-stained non-treated U87 MG cells were also analyzed (grey). (E) Confocal microscopy images of U87 MG cells exposed to RDEVVD-DOX (left) or RGDEVVD-DOX (right). The red fluorescence represents the doxorubicin moiety. The cells are also stained with DAPI (blue). All the acquired channels (red, blue, and DIC) were merged and shown in the lower panel. Scale bar, 50 μ m.

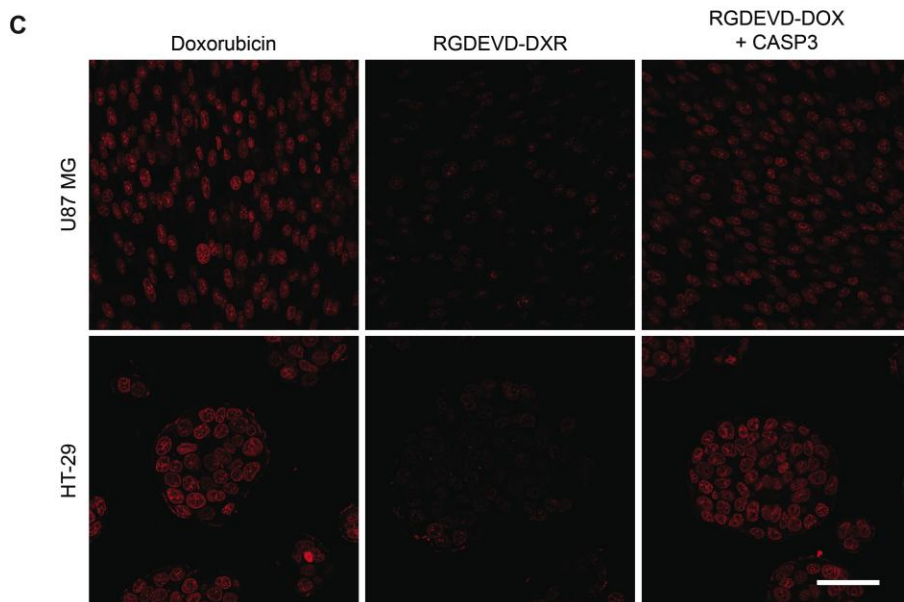
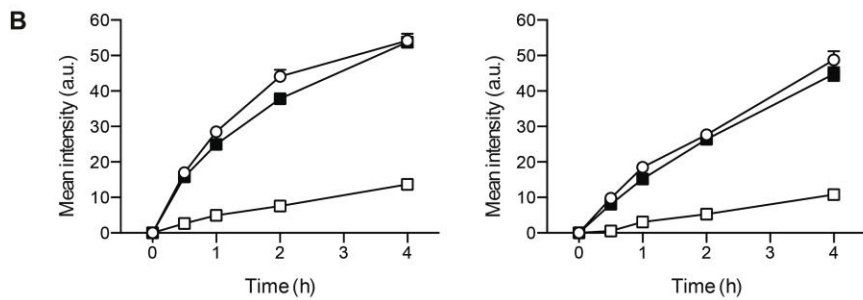
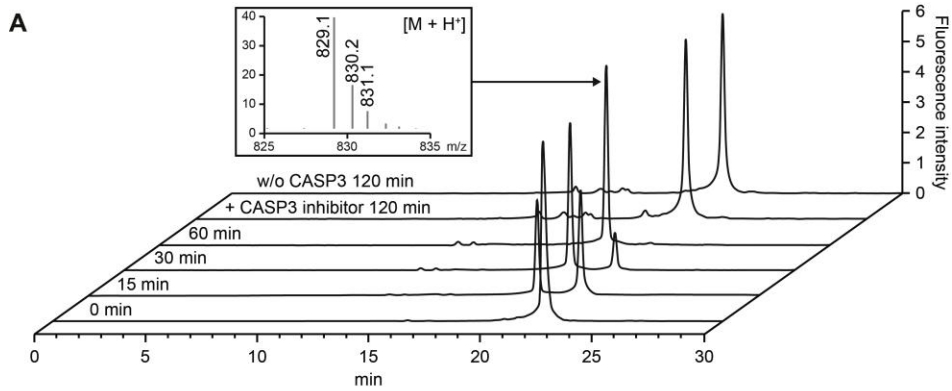


Figure 6.4. (A) HPLC chromatograms of RGDEVD-DOX incubated in the presence of recombinant human caspase-3 for 0, 15, 30, and 60 min. Chromatograms of RGDEVD-DOX incubated for 120 min with the caspase-3 pretreated with caspase inhibitor, and RGDEVD-DOX incubated for 120 min without addition of caspase-3 were also shown. (B) Mean intensity of doxorubicin fluorescence in the cell nuclei quantified depending on the drug exposure time. Doxorubicin (○), RGDEVD-DOX (□), or cleaved RGDEVD-DOX (■) was treated on U87 MG (left) and HT-29 (right) cells. Data are presented as mean ± s.e.m. (C) Representative images of doxorubicin (left), RGDEVD-DOX (center), and cleaved RGDEVD-DOX (right) treated on U87 MG (upper) and HT-29 (lower) cells for 1 h. Scale bar, 50 μm.

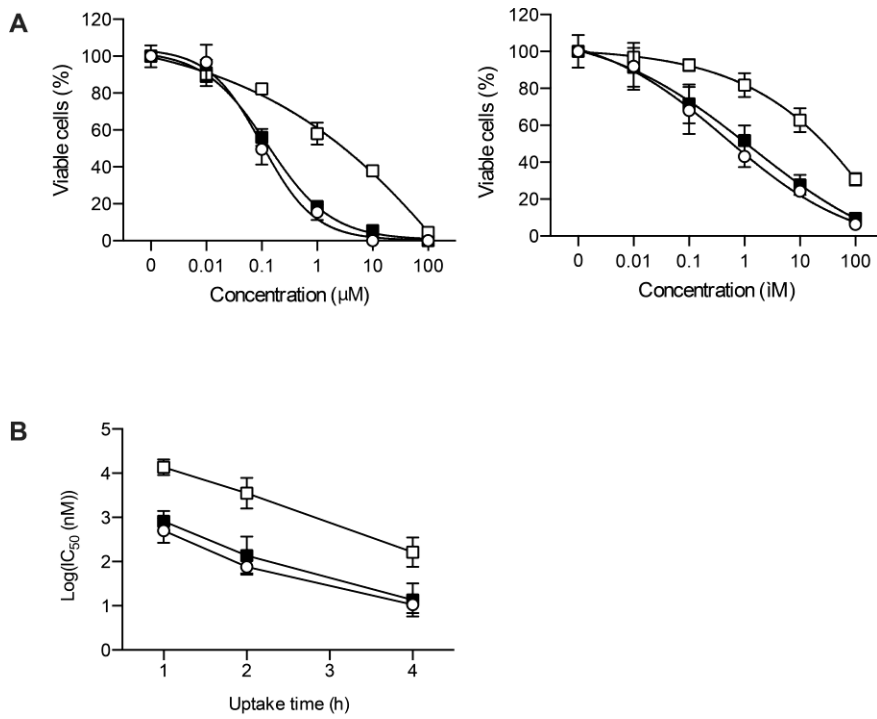


Figure 6.5. (A) Concentration-dependent cytotoxicity of doxorubicin (○), RGDEVD-DOX (□), and RGDEVD-DOX incubated with recombinant human caspase-3 (cleaved RGDEVD-DOX; ■) on U87 MG (left) and HT-29 (right) cells when exposed 2 h determined by MTT assay. (B) Exposure time-dependent IC50 values of the drugs on U87 MG cells. Data are presented as mean ± s.e.m.

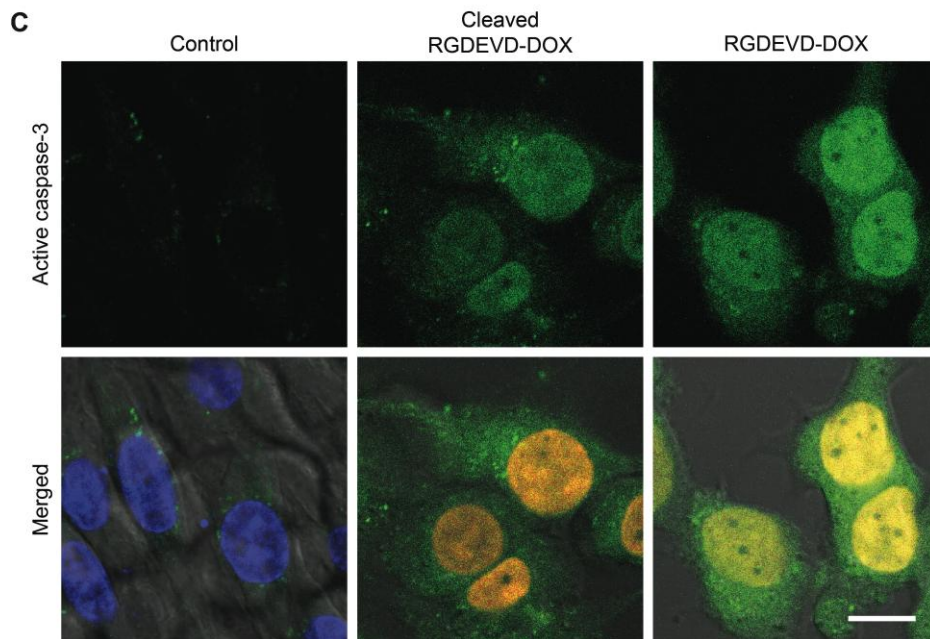
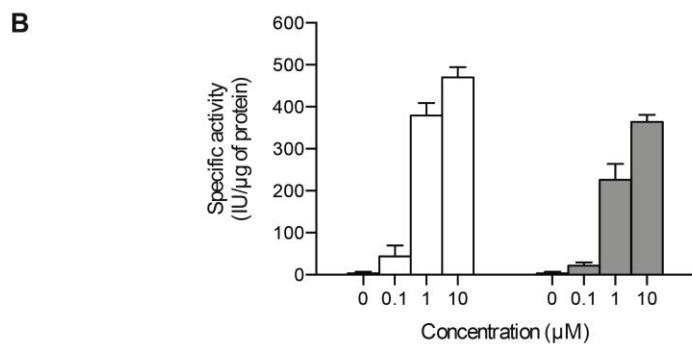
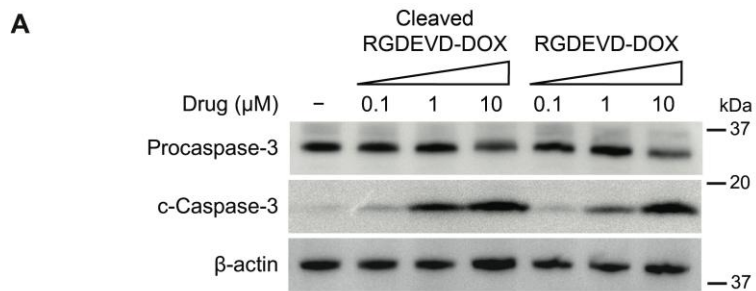


Figure 6.6. (A) Western blots of U87 MG cells treated with RGDEVD -DOX or RGDEVD-DOX incubated with recombinant human caspase-3 (cleaved RGDEVD-DOX) at a concentration of 0.1, 1, and 10 μ M. The immunoblots were carried out using procaspase-3 (upper), cleaved caspase-3 (center), and beta-actin (lower) antibodies. (B) Cellular caspase activities of U87 MG cells treated with cleaved RGDEVD-DOX (white) or RGDEVD-DOX (grey) at a concentration of 0, 0.1, 1, and 10 μ M. Data are presented as mean \pm s.e.m. (C) Cellular caspase-3 staining of U87 MG cells after 48 h exposure to cleaved RGDEVD-DOX (center) and RGDEVD-DOX (right). Control cells that have not been treated with any drugs were also shown (left). Green fluorescence represents the active caspase-3. Nuclei of control cells were stained with DAPI (blue). Nuclei of drug treated cells were accumulated with the drug (red) and were not stained with DAPI. Scale bar, 10 μ m.

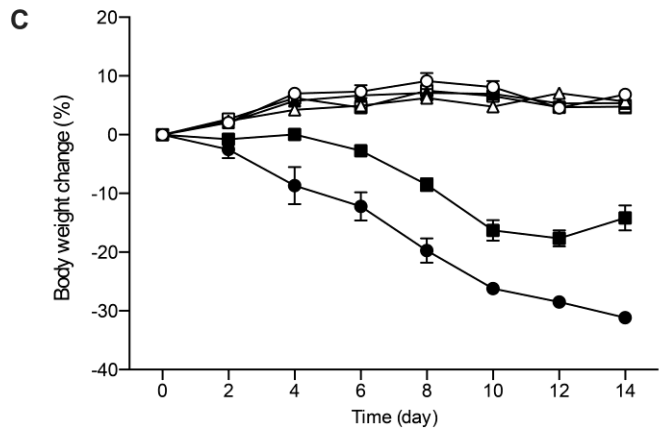
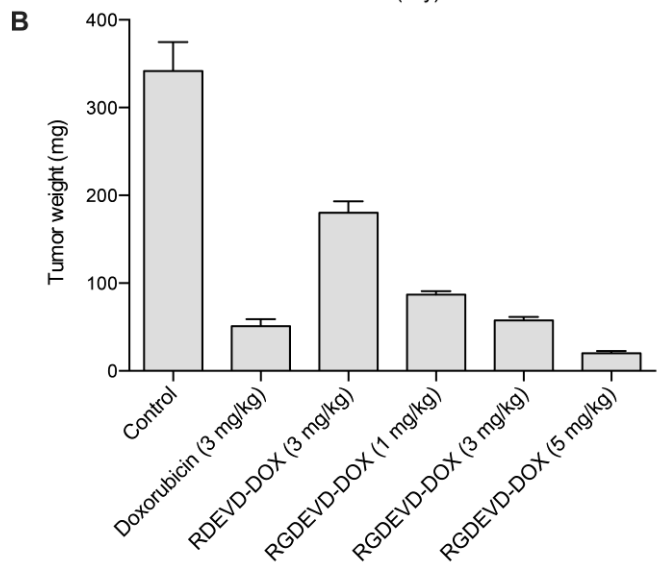
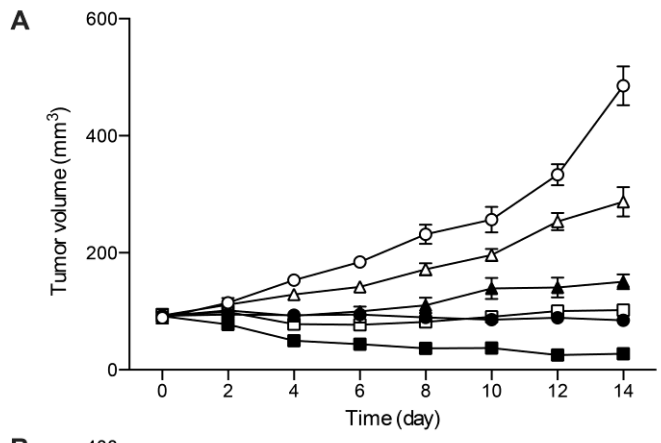


Figure 6.7. Animal study result of U87 MG-tumor bearing BALB/cSlc-nu mice that received normal saline (\circ), doxorubicin (7×3 mg/kg, \bullet), RDEV-D-DOX (7×3 mg/kg, Δ), and RGDEV-D-DOX in three different doses (7×1 mg/kg, \blacktriangle ; 7×3 mg/kg, \square ; 7×5 mg/kg, \blacksquare). The animals received the agents intravenously daily for 7 days. The doses are expressed at molar equivalent of doxorubicin. Tumor growth profiles (A), isolated tumor weights (C), and body weight profiles (B) are shown. Data are presented as mean \pm s.e.m.

6.4. Discussion

The present study demonstrates about the prodrug comprising an integrin $\alpha\beta3$ binding moiety, caspase-specific cleavable peptide, and a doxorubicin as an active cytotoxic compound. The principle of action of the current prodrug system are as followings: (i) the prodrug selectively targets integrin $\alpha\beta3$ overexpressing cells including certain tumor cells as well as endothelial cells constituting the angiogenic tumor blood vessels, and triggers apoptosis in those cells, (ii) due to the apoptosis induced in the integrin $\alpha\beta3$ overexpressing cell, local concentration of active caspase-3 increases within the tumor tissue, (iii) increased level of active caspase-3 cleave the prodrug and separate the peptide and doxorubicin compartment, (iv) since the peptide moiety is the one that provides the overall selectivity of the prodrug, the released doxorubicin compartment is non-selective with facilitated penetration into the cells due to its hydrophobicity, thus inducing cell death in the nearby cells regardless of their expression in integrin $\alpha\beta3$, and again upregulate caspase-3, which repeatedly force step (iii) and (iv) to occur. To put it shortly, during the initial phase of therapy, integrin $\alpha\beta3$ overexpressing cells are affected, and in the later phase, other tumor-associated cells are affected, potentially leading to complete remission of the tumor growth. A schematic illustration depicting this mode of action is shown in **Fig 6.1A**.

The importance of selectivity in development of anticancer agent has been always emphasized. However, this common sense is challenged by the finding of intratumor heterogeneity, which revealed the existence of different subclones of tumor cells in a single tumor mass. Moreover, many stromal cells constituting the tumor microenvironment also largely contribute to the growth of tumor. The selective targeting generally focuses on single molecule, which is likely to be expressed in the limited population of tumor cells according to the intratumor heterogeneity. Thus, such approach would be effective initially, but would soon be impotent by the regrowth of the unaffected tumor cells and the tumor-associated stromal cells.

In contrast, currently proposed strategy considers the selective delivery of chemotherapeutic agents to the tumor tissue, which in turn becomes non-selective within the tumor tissue. Therefore, it could possibly affect broad populations of tumor cells that differ in their biomarker expression pattern and also the tumor-associated stromal cells. This resembles intratumor injection of cytotoxic agents, which is generally not applicable for clinical use. Another significant difference between the current drug delivery strategy and the conventional one is that the target molecule increases as the therapy sustains, which is opposite in the conventional targeted therapies (see **Fig 6.2**).

As a model drug, RGDEVD-DOX was synthesized, which contains RGD and DEVD motif for targeting integrin $\alpha\beta3$ and caspase-3, respectively. These two amino acid sequences share one Asp and form fully functional single pentapeptide. This peptide was conjugated to the 14-OH position of doxorubicin to produce RGDEVD-DOX prodrug. This prodrug proved satisfactory integrin $\alpha\beta3$ targeting capability in various *in vitro* studies. It was also shown that RGDEVD-DOX was more potent than RDEVD-DOX in the U87 MG tumor-bearing preclinical model, indicating the benefit of the RGD motif *in vivo*.

The synthesized prodrug was rapidly cleaved in the presence of caspase-3, releasing a doxorubicin derivative. The cleavage of the prodrug significantly facilitated the penetration into the cell and nucleus of the active ingredient, similar to that of intact doxorubicin. It was considered that attachment of the very hydrophilic and negatively charged RGDEVD peptide on the doxorubicin had significantly delayed the cell and nucleus membrane penetration. Since cell surfaces are negatively charged due to the abundant phosphatidylserine, phosphatidylinositol¹⁵ and sialoglycoproteins¹⁶ on the membrane, negatively charged substances are difficult to penetrate through the cell membrane. Thus, detachment of this peptide from the doxorubicin compartment recovered the lipophilicity as well as the intrinsic rapid cell penetration capability. Hydrophilic molecules prefer their residence in the blood or plasma, whereas hydrophobic molecules prefer distribution in the tissue or cells. Therefore, the

conversion of the prodrug from hydrophilic form to hydrophobic form within the tumor tissue would consequently 'anchor' the conjugated doxorubicin in that location.

Not surprisingly, cell deaths induced by RGDEVD-DOX or the active form occurred through caspase-3-mediated pathway, hence showed upregulated caspase-3. The active caspase-3 was distributed evenly throughout the cells. In addition, caspases also leak out of the apoptotic cells¹⁷. Therefore, another molecules of RGDEVD-DOX reached to the tumor tissue could be further cleaved and activated by the easily accessible upregulated caspase-3.

6.5. Conclusion

RGDEVD-DOX has proven its efficacy for the proof-of-concept in the currently proposed drug delivery strategy as a model drug. This prodrug could selectively deliver the cytotoxic agent to the tumor tissue by the employed RGD motif, which could recognize tumor and tumor endothelial cells that overexpress integrin $\alpha v \beta 3$, during the initial phase of the therapy. Then the upregulated caspase-3 caused by the initially delivered cytotoxic agents could activate another molecule of the prodrug and facilitate their distribution into the nearby cells in non-selective manner.

As long as the DEVD moiety or other caspase-3-cleavable sequence is conserved in the prodrug, targeting moiety other than RGD and also other cytotoxic agents could be possibly adopted to achieve the same purposed delivery strategy. Therefore, current delivery strategy could be largely expanded and lead to development of various new prodrugs.

References

- 1 Allen, T. M. Ligand-targeted therapeutics in anticancer therapy. *Nat Rev Cancer* **2**, 750-763 (2002).
- 2 DiPaola, R. S., Rinehart, J., Nemunaitis, J., Ebbinghaus, S., Rubin, E., Capanna, T., Ciardella, M., Doyle-Lindrud, S., Goodwin, S., Fontaine, M., Adams, N., Williams, A., Schwartz, M., Winchell, G., Wickersham, K., Deutsch, P. & Yao, S. L.

- Characterization of a novel prostate-specific antigen-activated peptide-doxorubicin conjugate in patients with prostate cancer. *J Clin Oncol* **20**, 1874-1879 (2002).
- 3 Sapa, P., Stein, R., Pickett, J., Qu, Z., Govindan, S. V., Cardillo, T. M., Hansen, H. J., Horak, I. D., Griffiths, G. L. & Goldenberg, D. M. Anti-CD74 antibody-doxorubicin conjugate, IMMU-110, in a human multiple myeloma xenograft and in monkeys. *Clin Cancer Res* **11**, 5257-5264 (2005).
 - 4 Breij, E. C., de Goeij, B. E., Verploegen, S., Schuurhuis, D. H., Amirkhosravi, A., Francis, J. L., Breinholt Miller, V., Houtkamp, M., Bleeker, W. K., Satijn, D. & Parren, P. W. An antibody-drug conjugate that targets tissue factor exhibits potent therapeutic activity against a broad range of solid tumors. *Cancer Res* (2013).
 - 5 Deckert, J., Park, P. U., Chicklas, S., Yi, Y., Li, M., Lai, K. C., Mayo, M. F., Carrigan, C. N., Erickson, H. K., Pinkas, J., Lutz, R. J., Chittenden, T. & Lambert, J. M. A novel anti-CD37 antibody-drug conjugate with multiple anti-tumor mechanisms for the treatment of B-cell malignancies. *Blood* **122**, 3500-3510 (2013).
 - 6 Gerlinger, M., Rowan, A. J., Horswell, S., Larkin, J., Endesfelder, D., Gronroos, E., Martinez, P., Matthews, N., Stewart, A., Tarpey, P., Varela, I., Phillimore, B., Begum, S., McDonald, N. Q., Butler, A., Jones, D., Raine, K., Latimer, C., Santos, C. R., Nohadani, M., Eklund, A. C., Spencer-Dene, B., Clark, G., Pickering, L., Stamp, G., Gore, M., Szallasi, Z., Downward, J., Futreal, P. A. & Swanton, C. Intratumor heterogeneity and branched evolution revealed by multiregion sequencing. *N Engl J Med* **366**, 883-892 (2012).
 - 7 Wiseman, B. S. & Werb, Z. Stromal effects on mammary gland development and breast cancer. *Science* **296**, 1046-1049 (2002).
 - 8 Zitzmann, S., Ehemann, V. & Schwab, M. Arginine-glycine-aspartic acid (RGD)-peptide binds to both tumor and tumor-endothelial cells in vivo. *Cancer Res* **62**, 5139-5143 (2002).
 - 9 Chen, K. & Chen, X. Integrin targeted delivery of chemotherapeutics. *Theranostics* **1**, 189-200 (2011).
 - 10 Zhan, C., Gu, B., Xie, C., Li, J., Liu, Y. & Lu, W. Cyclic RGD conjugated poly(ethylene glycol)-co-poly(lactic acid) micelle enhances paclitaxel anti-glioblastoma effect. *J Control Release* **143**, 136-142 (2010).
 - 11 Xu, Q., Liu, Y., Su, S., Li, W., Chen, C. & Wu, Y. Anti-tumor activity of paclitaxel through dual-targeting carrier of cyclic RGD and transferrin conjugated hyperbranched copolymer nanoparticles. *Biomaterials* **33**, 1627-1639 (2012).
 - 12 Miura, Y., Takenaka, T., Toh, K., Wu, S., Nishihara, H., Kano, M. R., Ino, Y., Nomoto, T., Matsumoto, Y., Koyama, H., Cabral, H., Nishiyama, N. & Kataoka, K. Cyclic RGD-linked polymeric micelles for targeted delivery of platinum anticancer

- drugs to glioblastoma through the blood-brain tumor barrier. *ACS nano* **7**, 8583-8592 (2013).
- 13 Lien, S., Pastor, R., Sutherlin, D. & Lowman, H. B. A substrate-phage approach for investigating caspase specificity. *Protein J* **23**, 413-425 (2004).
 - 14 Meyer-Losic, F., Quinonero, J., Dubois, V., Alluis, B., Dechambre, M., Michel, M., Cailler, F., Fernandez, A. M., Trouet, A. & Kearsley, J. Improved therapeutic efficacy of doxorubicin through conjugation with a novel peptide drug delivery technology (Vectocell). *J Med Chem* **49**, 6908-6916 (2006).
 - 15 Goldenberg, N. M. & Steinberg, B. E. Surface charge: a key determinant of protein localization and function. *Cancer Res* **70**, 1277-1280 (2010).
 - 16 Wang, B. & Brand-Miller, J. The role and potential of sialic acid in human nutrition. *Eur J Clin Nutr* **57**, 1351-1369 (2003).
 - 17 Hentze, H., Schwoebel, F., Lund, S., Keel, M., Ertel, W., Wendel, A., Jaattela, M. & Leist, M. In vivo and in vitro evidence for extracellular caspase activity released from apoptotic cells. *Biochem Biophys Res Commun* **283**, 1111-1117 (2001).

Concluding remarks

Although heparin has been only approved and used clinically for its anticoagulant activity, it has been regarded as an interesting molecule for its capability to interact with broad range of endogenous molecules and regulatory effects in diverse pathophysiological states. This study was particularly focused in its potential role in tumor progression and angiogenesis. Regarding that angiogenesis inhibitors have recently encountered a problematic issue, in which showing adaptive resistance by upregulation of alternative pro-angiogenic factors, heparin could be an excellent lead compound for developing a novel angiogenesis inhibitor, since diverse pro-angiogenic factors are heparin-binding proteins. However, due to the potent anticoagulant activity of heparin, it cannot be directly applied clinically for use in indication other than venous thromboembolism.

In purpose to utilize heparin for treatment of cancer as an angiogenesis inhibitor, LMWH was chemically modified by introducing sodium taurocholates on the polysaccharide chain. Appropriate modification of LMWH allowed potentiation of anti-angiogenic activity while eliminating its anti-coagulant activity. It was found that such modifications resulted in blocking the ATIII-interacting pentasaccharide unit of heparin by a bulky molecule, in this case, the sterane core, and increasing the net anionic electrical charge by adding more sulfate groups that could enhance binding to VEGF. In addition, LHT7 retained the intrinsic capacity of heparin to bind with other pro-angiogenic molecules including FGF2 and PDGF-B, despite the chemical modification. In the aspect of increasing therapeutic efficacy and overcoming the acquired resistance, targeting VEGF, FGF2 and PDGF-B at the same time is critical for angiogenesis inhibition. Thus, LHT7 would potentially overcome the resistance and effectively inhibit angiogenesis as well as tumorigenesis. It was also confirmed that heparin is an excellent lead compound to develop multi-targeted agent due to its inherent capability to interact with broad range of pro-angiogenic factors.

Apart from development of heparin-based multitargeted angiogenesis inhibitor, two doxorubicin prodrugs were also developed according to a novel drug delivery strategy. Traditionally, one of the most popular approaches to deliver cytotoxic agents to the tumor tissue is by introducing tumor specific surface antigen recognition ligand to the drug. However, such approach has been severely challenged by the discovery of intratumor heterogeneity, which makes aware of presence of distinct subclones of cell populations within single mass of tumor. Ironically, due to the highly selective or specific nature of the employed ligand, the cytotoxic agents are conveyed to only limited subpopulations of tumor, ultimately resulting in regrowth of tumor by the unaffected tumor cells. Two different doxorubicin prodrugs, EMC-DEVD-S-DOX and RGDEVD-DOX, were synthesized that shares DEVD peptide sequence, an essential functional molecule for the currently suggested drug delivery strategy.

Firstly, the EMC-DEVD-S-DOX is delivered to the tumor tissue through the conventional passive targeting with long circulation time by the *in situ* albumin-binding capability. It is then specifically activated and recovers the cytotoxic activity by releasing free doxorubicin from the inactive form of the prodrug upon presence of caspase-3 induced by radiation exposure. Unlike the traditional target of tumor targeting, which the target molecules are invariably expressed on their cell surface unless there are significant changes in their environment, upregulation of caspase-3 is relatively a transitory event that occurs only during cell apoptosis. Therefore, long circulation and tumor accumulation capability provided by albumin binding significantly increases the possibility of prodrug to contact with the upregulated caspase-3 in the tumor tissue. Hence, the capabilities for albumin binding and radiation-stimulated prodrug activation are inseparable to achieve the purposed drug delivery strategy ideally. The major advantage of this strategy is that the site of drug action could be controlled more actively by determining the location of radiation exposure. Since there was a huge advance in stereotactic radiotherapy, the site where the prodrug is activated could be controlled very precisely, thus

leaving minimum sequelae to the patients. Already about half of the entire cancer patients commonly receive radiotherapy. Therefore, EMC-DEVD-S-DOX, which shows a perfect synergy with radiation, would be very attractive and ideal form of drug to treat the cancer patients.

By comparison with the EMC-DEVD-S-DOX, the RGDEVD-DOX comprises conventional active targeting moiety rather than the passive one. Although this drug delivery system employs the identical active targeting moiety with the conventional targeted delivery system, the insertion of DEVD sequence between the active ingredient and the targeting moiety totally differentiates the characteristics of the delivery mechanism. While the conventional active targeting strategy could affect only the limited subpopulation of the tumor, RGDEVD-DOX could affect broader range of tumor subpopulations that differ in their genomic profile within the site where integrin $\alpha\beta3$ overexpressing cells are located. The RGD moiety of the prodrug selectively delivers the cytotoxic agent to the tumor during the initial phase of administration and induces apoptosis in certain subclone of tumor cells as well as tumor endothelial cells that overexpress integrin $\alpha\beta3$, leading to upregulation of caspase-3. Then the caspase-3 further activates the other molecules of the prodrug, triggering to release more hydrophobic form of the active compound with facilitated penetration into the cell, regardless of their integrin $\alpha\beta3$ expression.

Since the upregulation of the caspase-3, which is a key event in the proposed drug delivery strategy, is common during the apoptosis of mammalian cells, the genomic diversity of tumor cells would hardly influence the efficacy of the currently developed prodrugs. Considering that conventional molecular targeted approach in any aspect of tumor therapy is seriously challenged by tumor heterogeneity, these two doxorubicin prodrugs could be outstanding alternatives. Also, current delivery strategy could be largely expanded and lead to development of various new prodrugs.

국문초록

현대의학에서 종양학의 비약적인 발전에도 불구하고 암은 여전히 난치병으로 간주된다. 이에 따라 많은 임상의를 및 연구자들이 암을 효과적으로 치료하기 위한 연구를 활발히 전개하고 있다. 하지만 현재까지 개발된 항암제들은 암의 유전적 다양성과 복잡성으로 인해 기대에 못 미치는 치료효과를 보이고 있으며 심각한 부작용과 같은 여러 문제점들 또한 갖고 있다. 따라서 보다 혁신적인 항암제가 요구되는 상황에서 기존 항암제와는 차별되는 신개념의 항암제를 연구 개발하였다.

본 학위논문에서는 크게 분류하여 두 종류의 항암제를 제시하였다. 첫 번째는 신개념의 혈관신생억제제로 헤파린을 기반으로 개발하였다. 혈관신생작용은 암의 성장에 있어서 필수적인 요소 중 하나이다. 종양이 어느 정도 이상의 크기로 성장하려면 이미 존재하고 있던 주변 혈관으로부터의 확산작용만으로는 조직 내의 모든 세포로 영양소나 산소를 공급받을 수가 없게 된다. 따라서 암 조직은 자가 생존을 위해 조직 내외로 새로운 혈관을 발생시키는데 이를 혈관신생작용이라고 한다. 일반적으로 저산소 상태에 처해진 암세포들은 이를 극복하고 생존하기 위해 여러 혈관신생성장인자들은 발현하여 혈관신생작용을 일으키게 되는데 이들 중 하나 이상의 신호전달과정을 차단하는 약물을 혈관신생억제제라고 한다. 본 연구에서 개발된 헤파린 기반의 혈관신생억제제(LHT7)는 VEGF와 FGF2, PDGF-B 등의 활성을 차단함으로써 종양 내 혈관신생작용 과정의 여러 단계에 동시에 억제작용이 있음을 확인하였다. 현재 임상적으로 사용되거나 개발되고 있는 혈관신생억제제 중 혈관신생인자를 다중으로 표적하는 약물은 찾아볼 수 없어 매우 획기적이다. 특히 여러 혈관신생인자에 대한 수용체의 티로신키나아제를 비특이적으로 억제하는 소분자

티로신키나아제 억제제에 비해 더 상위체계의 인자를 다중으로 표적하기 때문에 더 효과적인 혈관신생억제작용을 기대할 수 있다.

다른 하나는 세포사멸에 의해 활성화되는 독소루비신의 프로드럭이다. 일반적으로 세포독성 항암제의 가장 큰 문제점은 용량의존적으로 나타나는 심각한 독성 및 부작용이다. 이를 개선하기 위한 방편으로 세포독성 항암제를 선택적으로 암 조직에 전달하고 정상조직에서의 분포를 줄이기 위한 여러 시도들이 있어왔다. 본 연구에서는 널리 사용되고 있는 세포독성 화학요법제인 독소루비신을 기존 약물전달시스템과는 근본적으로 다른 이론적 배경으로 암조직에 보다 선택적으로 전달할 수 있도록 하였다. 이러한 약물전달시스템의 개발을 가능하게 할 방법으로 유도표현형질표적요법을 제안하였다. 유도표현형질표적요법이란 표적물질의 전달에 있어서 기존 방식의 암세포의 유전형질에 의존하는 것이 아닌 인위적으로 특정 표현형질을 유도시켜 그것을 표적하는 약물전달 방법이다. 본 연구에서는 특히 세포사멸을 유도시켜 이것을 표적하는 방법을 제안하였다. 종양 내 이질성에 의해 하나의 암을 유전형질에 기반을 두어 특정 지을 수 없으므로 유전형질에 의존하는 것보다 세포사멸을 외부자극으로 유도한 뒤 이것에 의존하여 세포독성 항암제를 전달하는 것이 보다 신뢰도가 높다. 특히 기존 약물전달시스템에 응용되는 수동적 수송과 능동적 수송 기술들 또한 접목하여 암조직에 매우 선택적으로 독소루비신이 수송될 수 있도록 하였다.

주요어 : 헤파린; 항암제; 혈관신생억제제; 다중표적형 치료제; VEGF; FGF; PDGF; 독소루비신; 프로드럭; 카스파제; DEVD; 알부민; RGD; 인테그린

학 번 : 2010-31129



저작자표시-비영리-변경금지 2.0 대한민국

이용자는 아래의 조건을 따르는 경우에 한하여 자유롭게

- 이 저작물을 복제, 배포, 전송, 전시, 공연 및 방송할 수 있습니다.

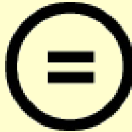
다음과 같은 조건을 따라야 합니다:



저작자표시. 귀하는 원저작자를 표시하여야 합니다.



비영리. 귀하는 이 저작물을 영리 목적으로 이용할 수 없습니다.



변경금지. 귀하는 이 저작물을 개작, 변형 또는 가공할 수 없습니다.

- 귀하는, 이 저작물의 재이용이나 배포의 경우, 이 저작물에 적용된 이용허락조건을 명확하게 나타내어야 합니다.
- 저작권자로부터 별도의 허가를 받으면 이러한 조건들은 적용되지 않습니다.

저작권법에 따른 이용자의 권리는 위의 내용에 의하여 영향을 받지 않습니다.

이것은 [이용허락규약\(Legal Code\)](#)을 이해하기 쉽게 요약한 것입니다.

[Disclaimer](#)

약학박사학위논문

Design and development of multi-targeted
anticancer agents for anti-angiogenic therapy
or tumor tissue-selective delivery

혈관신생억제 및 종양선택적 전달을 위한
다중표적형 항암제의 설계와 개발

2015년 2월

서울대학교 대학원
약학과 약제과학전공
정 성 우

ABSTRACT

Despite the rapid advances of cancer research, cancer is still one of the leading causes of mortality worldwide. During the past decades, research of anticancer agents mostly focused on selective targeting of tumor-specific antigens in the context of molecular targeted therapy as well as targeted drug delivery to improve the therapeutic index of the traditional chemotherapy. However, due to the intrinsic genetic diversity and complexity of tumors, the targeted therapeutics showed only limited improvements. Therefore, a breakthrough of the fundamental concept in cancer treatment has been deemed necessary. In this dissertation, novel therapeutic alternatives are proposed and evaluated that could contribute to the further advance in the cancer therapeutics.

Part one concerns development of a heparin-based anti-angiogenic agent LHT7 – a sodium taurocholate conjugated LMWH – that inhibits multiple stages of angiogenesis, and investigation of its mode of action. This study showed that the conjugation of sodium taurocholates abolished the intrinsic capability of LMWH to interact with ATIII while enhancing the binding property on VEGF, resulting in decreased anticoagulant activity and enhanced anti-angiogenic activity. The differential effects of sodium taurocholate conjugation to LMWH on its interaction between ATIII and VEGF were attributable to the unique structure of sodium taurocholate: the bulky and rigid sterane core of taurocholate sterically concealed the ATIII-binding pentasaccharide unit of LMWH, while the terminal sulfate group generated additional interactions with VEGF leading to a stronger binding.

The major advantage of exploiting heparin as a lead compound for the development of novel anti-angiogenic agents comes from the intrinsic capability of interacting and regulating wide array of pro-angiogenic factors. LHT7 was speculated to block FGF2 and PDGF-B in addition to VEGF. Since these three pro-angiogenic factors play key roles in multiple stages of angiogenesis, simultaneous blockade of these factors resulted in potent suppression of tumor angiogenesis as well as tumor growth. The results of this

study suggested that LHT7 would potentially overcome the resistance issue shown in the conventional anti-angiogenic agents.

Part two discusses development of doxorubicin prodrugs that target induced-apoptosis for effective delivery of chemotherapeutics to the tumor regardless of its genomic property. The first doxorubicin prodrug involves two distinct features for an effective tumor targeting: EPR effect-mediated tumor accumulation with extended plasma half-life, and radiation-induced apoptosis targeting. This prodrug – EMC-DEVD-S-DOX – comprises a maleimide group, which binds to the circulating albumin after intravenous administration, and a DEVD motif, which is cleaved by caspase-3 upregulated in the tumor cells that are exposed to radiation. The EMC-DEVD-S-DOX showed a prolonged plasma half-life with selective accumulation within tumor tissue, and released free doxorubicin only when combined with radiotherapy.

The second doxorubicin prodrug – RGDEVD-DOX – comprises an integrin $\alpha\beta3$ recognizing RGD sequence and a DEVD sequence. The RGD moiety selectively delivers the prodrug to the tumor during the initial phase of administration and induces apoptosis in certain subclone of tumor cells as well as tumor endothelial cells that overexpress integrin $\alpha\beta3$. The caspase-3 from the apoptotic cells further activates other molecules of the prodrug, forcing those to release hydrophobic active compound with facilitated cell penetration regardless of integrin $\alpha\beta3$ expression. Therefore, it could affect broader range of tumor cells within the tumor tissue, thereby providing more effective therapeutic outcomes. Since the upregulation of the caspase-3, which is the key event of the proposed drug delivery strategy, is common during the apoptosis, the genomic diversity of tumor cells hardly influences the efficacy of the currently developed prodrugs.

Keywords: Heparin; anticancer agent; angiogenesis inhibitor, multi-targeting; VEGF; FGF; PDGF; doxorubicin; prodrug; caspase-3; DEVD; albumin; RGD; integrin $\alpha\beta3$.

Student number: 2010-31129

Table of Contents

ABSTRACT	i
Table of Contents	iii
List of Tables	ix
List of Figures	ix
Abbreviations	xvi
Introduction	1
References	3
Part I. Study of mode of action and multiple pathway inhibitory capability in tumor angiogenesis of heparin-based agent LHT7	5
1. General Introduction	7
1.1. Tumor angiogenesis	7
1.1.1. Physiology of tumor angiogenesis	7
1.1.2. Angiogenesis inhibition	10
1.1.3. Resistance to angiogenesis inhibitors	13
1.2. Heparin	17
1.2.1. Structural Characteristics of Heparin	18
1.2.2. Anticoagulant Activity of Heparin	19
1.2.2. Heparin in Cancer	20
1.3. Rationale of the research	22
References	23
2. Potentiation of anti-angiogenic activity of heparin by blocking the ATIII- interacting pentasaccharide unit and increasing net anionic charge	35
2.1. Introduction	36
2.2. Materials and Methods	38
2.2.1. Cell lines	38
2.2.2. Synthesis	38
2.2.3. Characterization of the synthesized LMWH-derivatives	41
2.2.4. Surface plasmon resonance (SPR) analysis	43
2.2.5. Molecular dynamics	43
2.2.6. Computer simulated molecular docking	44

2.2.7. X-ray μ CT angiography	45
2.2.8. Tumor growth suppression	46
2.2.9. Histological analysis	46
2.2.10. Ex vivo imaging of whole-body distribution.....	46
2.2.11. Immunofluorescence	47
2.2.12. Platelet uptake study of fluorescent-labeled LHT7.....	47
2.2.13. Statistical analysis	48
2.3. Results.....	48
2.3.1. Effects of the conjugated sodium taurocholate between the interaction of LMWH and ATIII determined by computerized docking simulation.....	48
2.3.2. Anticoagulant activities of LHT7 and its structural analogs	49
2.3.3. Effects of the conjugated sodium taurocholate between the interaction of LMWH and VEGF determined by computerized molecular dynamics	50
2.3.4. VEGF binding affinities of LHT7 and its structural analogs.....	51
2.3.5. Effect of LHT7 on tumor angiogenesis in vivo	52
2.3.6. Anticancer effects of LHT7 on distinct types of carcinoma xenografts.....	53
2.3.7. Intratumor localization of LHT7.....	54
2.3.8. LHT7 uptake by platelets	54
2.4. Discussion	70
2.5. Conclusion.....	76
References.....	76
3. Multiple-stage angiogenesis inhibition of LHT7 by blocking VEGF, FGF2, and PDGF-B	81
3.1. Introduction	82
3.2. Materials and Methods.....	84
3.2.1. Cell lines.....	84
3.2.2. Transwell chemotactic migration assay	84
3.2.3. MTT cytotoxicity assay.....	85
3.2.4. HUVEC spheroid sprouting assay	85
3.5.5. Endothelial tube formation assay.....	86

3.2.6. Matrigel plug angiogenesis assay	87
3.2.7. Receptor tyrosine kinase phosphorylation studies	87
3.2.8. In vitro pericyte migration to endothelial tube	88
3.2.9. In vitro pericyte-endothelium adhesion assay	88
3.2.10. Surface plasmon resonance (SPR) analysis.....	89
3.2.11. Dynamic contrast enhanced magnetic resonance imaging.....	89
3.2.12. Statistical analysis.....	90
3.3. Results	90
3.3.1. HUVEC migration inhibitory effect and cytotoxicity evaluation of LHT7	90
3.3.2. Inhibitory effect of LHT7 in endothelial sproutings	91
3.3.3. Inhibitory effect of LHT7 in endothelial tubular differentiation ...	92
3.3.4. Inhibitory effect of LHT7 in the angiogenesis induced by VEGF and FGF2 in matrigel plugs	92
3.3.5. VEGF-VEGFR2 and FGF2-FGFR1 signaling pathway blockade by LHT7	93
3.3.6. Inhibitory effect of LHT7 on pericyte recruitment to endothelium linings	94
3.3.7. Determination of cytotoxicity on pericytes and possible effects in the endothelial cell and pericyte adhesion of LHT7.....	95
3.3.8. Inhibitory effect of LHT7 on PDGF-B-induced angiogenesis in matrigel plugs	95
3.3.9. PDGFB-PDGFR β signaling pathway blockade by LHT7	96
3.3.10. Characterization of tumor vasculatures in LHT7-treated tumor-bearing animals using DCE-MRI.....	97
3.4. Discussion.....	112
3.5. Conclusion	115
References	115
Part II. Novel strategy for site-specific delivery system and development of doxorubicin prodrugs	119
4. General Introduction	121
4.1. Tumor heterogeneity	121
4.1.1. Intertumor heterogeneity.....	121
4.1.2. Intratumor heterogeneity.....	122

4.2. Apoptosis targeted prodrug system.....	124
4.2.1. Caspase in apoptosis	125
4.2.2. Substrate recognition by caspases.....	127
4.3. Tumor targeting strategies.....	131
4.3.1. Passive tumor targeting	131
4.3.1.1. Albumin as a carrier for tumor targeting	134
4.3.1.2. Exploiting endogenous albumin for albumin-bound agents	137
4.3.2. Active tumor targeting strategy	140
4.3.2.1. Integrins.....	144
4.3.2.2. RGD peptide sequence for targeting integrin $\alpha\beta3$	146
4.4. Rationale of the research.....	148
References.....	149
5. Albumin-binding radiation-induced apoptosis targeted doxorubicin prodrug .	165
5.1. Introduction	166
5.2. Materials and methods	169
5.2.1. Cell lines.....	169
5.2.2. Synthesis.....	169
5.2.3. EMC-DEVD-S-DOX binding study with HSA	171
5.2.4. HSA-DEVD-S-DOX analysis by SDS-PAGE	171
5.2.5. Determination of thiol concentration of HSA using Ellman’s test	
.....	172
5.2.6. Preparation and characterization of HSA-DEVD-S-DOX	172
5.2.7. EMC-DEVD-S-DOX incubation study in plasma	173
5.2.8. Western blot.....	173
5.2.9. MTT cytotoxicity assay.....	174
5.2.10. Cellular uptake imaging	174
5.2.11. HPLC determination of caspase-mediated activation	175
5.2.12. Pharmacokinetic study	175
5.2.13. Ex vivo biodistribution imaging	176
5.2.14. Tumor growth suppression	176
5.3. Results.....	177
5.3.1. Synthesis of EMC-DEVD-S-DOX	177

5.3.2. Albumin-binding of EMC-DEVD-S-DOX	177
5.3.3. Caspase-3-mediated cleavage of HSA-DEVD-S-DOX	179
5.3.4. In vitro efficacy of HSA-DEVD-S-DOX.....	180
5.3.5. Caspase-3 upregulation induced by activated HSA-DEVD-S-DOX	180
5.3.6. Pharmacokinetic study	181
5.3.7. Tumor accumulation of EMC-DEVD-Cy5.5	181
5.3.8. Tumor growth suppression of EMC-DEVD-S-DOX.....	182
5.4. Discussion	198
5.5. Conclusion	200
References	201
6. Integrin $\alpha\beta 3$ targeted caspase-3-dependently activated doxorubicin prodrug	203
6.1. Introduction.....	204
6.2. Materials and Methods	206
6.2.1. Cell lines	206
6.2.2. Synthesis	206
6.2.2. Integrin $\alpha\beta 3$ dependent cellular uptake imaging	208
6.2.3. siRNA transfection.	209
6.2.4. Flow cytometry.....	210
6.2.5. HPLC determination of caspase-mediated activation.....	210
6.2.6. MTT cytotoxicity assay	211
6.2.7. Western blots.....	211
6.2.8. Caspase-3 cellular activity assay	212
6.2.9. Cellular caspase-3 stain.....	213
6.2.10. Animal study	213
6.2.11. Statistical analysis.....	214
6.3. Results	214
6.3.1. Synthesis of RGDEVD-DOX.....	214
6.3.2. Integrin $\alpha\beta 3$ dependent cellular uptake of RGDEVD peptide... 214	
6.3.2. Caspase-3-mediated cleavage of RGDEVD-DOX	216
6.3.3. In vitro efficacy of RGDEVD-DOX.....	216
6.3.4. Caspase-3 upregulation induced by RGDEVD-DOX.....	217

6.3.5. Tumor growth suppression of RGDEVD-DOX	219
6.4. Discussion	238
6.5. Conclusion.....	240
References.....	240
Concluding remarks	243

List of Tables

Table 2.1. Characteristics of LHT7 and its analogs	57
Table 3.1. Dissociation constants of LHT7 on VEGF, FGF2 or PDGF-B	99
Table 4.1. Optimal substrate sequences for caspases	129
Table 5.1. Pharmacokinetic parameters in SD rats (1 mg/kg dox molar eq.) .	183

List of Schemes

Scheme 5.1. Chemical synthesis of EMC-DEVD-S-DOX	185
Scheme 6.1. Chemical synthesis of RGDEVD-DOX	223

List of Figures

Figure 2.1. (A) Computerized molecular docking of LMWH (left) and LHT7 (right) on the ATIII heparin binding site (arrow). The pairs were allowed to reach the minimum intermolecular energy level and the final appearances were examined. (B) Representative chemical structures of LMWH **1**, cholic acid conjugated LMWH **2**, taurine conjugated LMWH **3**, and LHT7 **4**. (C) The model structure of LHT7 and VEGF-HBD complex when the intermolecular energy level has reached the minimum during molecular dynamics. 59

Figure 2.2. (A) Representative images of saline (control), LMWH, and LHT7 treated SCC7 tumors obtained by X-ray μ CT. Scale bar, 5 mm. (B) Tumor vessel volumes (left) and vessel fractions (right) calculated through reconstruction of vasculatures followed by computed calculation of the volumes. * $P < 0.05$, ** $P < 0.005$, and *** $P < 0.001$ versus control. Data are expressed as mean \pm s.e.m. 61

Figure 2.3. Tumor growth suppression on A549 (A) and HT-29 (B) xenografts. The three groups received either saline as control (\circ) or LHT7 in two different doses: 1 mg/kg (\bullet) and 5 mg/kg (\square) administered intravenously every other day.

n = 9. Data presented as mean \pm s.e.m. (C) Histological analysis of A549 (left) and HT-29 (right) tumor sections. Immunostaining of the upper and lower panels indicates CD34 and α SMA, respectively. Scale bar, 50 μ m. 63

Figure 2.4. (A) Tumor growth suppression of AMC-HN9 xenografts. Mice received either saline as control (\circ) or LHT7 in different doses: 1 mg/kg (\bullet) and 5 mg/kg (\square) administered every other day. n = 9. (B) Histological analysis of AMC-HN9 tumor sections. Immunostaining of the left and right panels indicates CD34 and α SMA, respectively. Scale bar, 50 μ m. (C) CD34 (left) and HE (right) staining of the tumor specimens. Arrows depict a subset of red blood cells. Scale bar, 50 μ m. 65

Figure 2.5. (A) *Ex vivo* biodistribution observations of the fluorescent-labeled LHT7 after intravenous administration in mice. (B) Immunostaining of tumor specimens at post-administration of LHT7. Red and green color represents CD31 and LHT7, respectively. Scale bar, 50 μ m. 67

Figure 2.6. (A) FACS analysis of platelets that have taken up LHT7 after incubation with a series of concentrations of fluorescent-labeled LHT7. Numbers represent the gated percentage in the assigned range. (B) Quantitative analysis of released (\circ) and bound (\bullet) LHT7 on the pellet of the platelets after activation of platelets incubated with fluorescent-labeled LHT7. Data are expressed as means \pm s.d. (C) Immunocytochemical staining of platelets incubated with fluorescent-labeled LHT7. Green and red represents LHT7 and P-selectin in α -granules of platelets, respectively. Scale bar, 2 μ m. 69

Figure 3.1. (A) Transwell chemotactic cell migration of HUVECs induced by VEGF or FGF2. Degree of migration in control (white) and LHT7-treated group (black) was assessed. (B) Cytotoxicity evaluation of LHT7 on HUVECs by using MTT cell proliferation assay at a concentration range of 0.01 to 1 mg/ml. (C) Representative images of VEGF and/or FGF2-induced angiogenic sprouting of HUVEC spheroid of control and LHT7-treated groups. Scale bar, 50 μ m. 101

Figure 3.2. (A) HUVEC tube formation induced by VEGF and/or FGF2. HUVECs were stained in green fluorescence. Scale bar, 500 μ m. (B) Quantitative analysis of HUVEC tubes by ImageJ angiogenesis analyzer. Number of nodes (left panel) and branches (right panel) of control (empty column) and LHT7 treated group (filled column) were calculated. * $P < 0.05$ versus control. Data are presented as mean \pm s.d. 103

Figure 3.3. (A) *In vivo* matrigel plug angiogenesis assay using VEGF or FGF2 as an angiogenic stimulator. The inhibition of phosphotyrosine level of VEGFR2 stimulated by VEGF (B) and FGFR1 stimulated by FGF2 (C) on HUVECs (left) and HDMECs (right) by LHT7 are shown by immunoblots. . 105

Figure. 3.4. Representative images of HUVECs (red) and pericytes (green) coculture system *in vitro*. (A) Pericytes were seeded after endothelial tubes were formed. Recruitment of pericytes to HUVEC tubes in control, anti-VEGF mAb, and LHT7-treated groups were observed after 2 h and 18 h of pericyte addition. Scale bars, 500 μ m. (B) Quantitative analysis of remaining endothelial tubes after 18 h of pericyte addition by ImageJ angiogenesis analyzer. Number of nodes (left panel) and branches (right panel) were calculated and shown as means \pm s.d. with individual plot. * $P < 0.05$ versus control. (C) Cytotoxic effect of LHT7 evaluated by MTT assay at a concentration range of 0.01 to 1 mg/ml. (D) Pericytes adhesion on confluent HUVEC monolayer. Single image was obtained in the center of the each well (n = 3) at 40x magnification and number of the adhered pericytes were counted and averaged. Data are expressed as means \pm s.d. 107

Figure 3.5. (A) *In vivo* matrigel plug angiogenesis assay using PDGF-B and PDGF-B/FGF2 mixture as angiogenic stimulators. (B) Western blots of phosphotyrosine level of PDGFR β on pericytes stimulated by PDGF-B in the presence or absence of LHT7 or neutralizing antibody. 109

Figure 3.6. MDA-MB-231 tumor-bearing mice were treated with LHT7 at a dose of 5 mg/kg intravenously daily for three weeks (●) and compared with

control (○). Tumor growth (A) and body weight (B) change were measured. DCE-MRI parameters were measured during the treatment at day 0, 7, 14 and 21. The values of K_{trans} (C), K_{ep} (D), initial slope (E), and K_{el} (F) were calculated. $n = 3$. Data are expressed as mean \pm s.d. * $P < 0.05$ versus control.

..... 111

Figure 5.1. (A) Schematic diagram of EMC-DEVD-S-DOX therapeutic strategy. (B) Chemical structure of EMC-DEVD-S-DOX. 187

Figure 5.2. (A) Analytical HPLC chromatogram of the final product detected under fluorescence detector (470/580 nm). (B) Mass spectrum of the final product determined by LC/ESI-MS..... 189

Figure 5.3. (A) HPLC chromatograms of EMC-DEVD-S-DOX and that incubated with commercially available HSA (3, 60 min), EMC-DEVD-S-DOX incubated with HSA blocked with excess GMB (60 min), and only HSA. (B) SDS-PAGE of EMC-DEVD-S-DOX or DEVD-S-DOX incubated with HSA or HSA blocked with excess GMB. (C) MALDI-TOF MS results of commercially available HSA (grey), and that incubated with EMC-DEVD-S-DOX in PBS (pH 7.4; black). (D) HPLC chromatograms of EMC-DEVD-S-DOX and that incubated in human plasma (3, 60 min), EMC-DEVD-S-DOX incubated with the plasma blocked with excess GMB (60 min), and only plasma..... 191

Figure 5.4. (A) HPLC chromatograms of HSA-DEVD-S-DOX and that incubated in the presence or absence of caspase-3, HSA-DEVD-S-DOX incubated with the caspase-3 pretreated with caspase inhibitor, and doxorubicin. (B) Concentration-dependent cytotoxicity of doxorubicin (○), HSA-DEVD-S-DOX (■), and HSA-DEVD-S-DOX incubated with recombinant human caspase-3 (□) on SCC7 (left) and MDA-MB-231 (right) cells determined by MTT assay. (C) Cellular uptake and intracellular distribution of doxorubicin (left), HSA-DEVD-S-DOX (center), and HSA-DEVD-S-DOX incubated with caspase-3 (right) in SCC7 (upper) and MDA-MB-231 (lower) cells observed under confocal microscopy. The substances were detected through intrinsic

fluorescence of doxorubicin and represented as red color. Scale bar, 50 μm . (D) Western blots of SCC7 (upper) or MDA-MB-231 (lower) cells treated with HSA-DEVD-S-DOX or HSA-DEVD-S-DOX incubated with recombinant human caspase-3 (Cleaved HSA-DEVD-S-DOX) at a concentration of 1, 5, and 10 μM . The immunoblots were carried out using procaspase-3 (upper), cleaved caspase-3 (center), and β -actin (lower) antibodies. 193

Figure 5.5. (A) Logarithmic plasma concentration for time profiles of EMC-DEVD-S-DOX (\circ) and DEVD-S-DOX (\bullet) administered to SD rats ($n = 3$) via intravenous route at a dose of 1 mg/kg molar equivalent to doxorubicin. The plasma concentration was calculated based on the mass concentration of doxorubicin content. Lower graph depicts enlarged plasma concentration profile showing until 2 h. (B) Ex vivo imaging of whole body distribution of EMC-DEVD-Cy5.5 in U87 MG tumor-bearing mice. 195

Figure 5.6. Animal study result of SCC7-tumor bearing C3H/HeN mice that received normal saline (\circ), radiation (\bullet), DEVD-S-DOX accompanied by radiation (Δ), EMC-DEVD-S-DOX (\square), or EMC-DEVD-S-DOX accompanied by radiation (\blacksquare). EMC-DEVD-S-DOX or DEVD-S-DOX was intravenously administered daily for 7 days at 1 mg/kg molar equivalent to doxorubicin from day 0 ($n = 5$). Radiation was given at a dose of 4 Gy single time at day 0. Tumor growth profile (A) and body weight profile (B) are shown. Data are presented as mean \pm s.e.m. 197

Figure 6.1. (A) Schematic diagram of the suggested prodrug strategy. (B) The major difference of the conventional targeted delivery system and the currently proposed targeted delivery system. (C) Chemical structure and compartment of the RGDEVD-DOX prodrug and its active compound. 225

Figure 5.2. (A) Analytical HPLC chromatogram of the final product detected under UV detector (214 nm) and ESI-MS. (B) Mass spectrum of the final product determined by LC/ESI-MS. 227

Figure 6.3. (A) Confocal microscopy images of HUVECs (left), HDMEC (center), and U87 MG cells (right) exposed to RDEV D (upper panel) or RGDEV D peptide (lower panel) labeled with Cy5.5. Green fluorescence represents the peptides. Cell nuclei are stained with DAPI (blue). Scale bar, 50 μ m. (B) Western blots of integrin α v after ITGAV siRNA transfection of HDMECs and U87 MG cells. (C) Confocal microscopy images of Cy5.5-labeled RGDEV D peptide given to HDMECs (left) and U87 MG cells (right) that were mock-transfected (upper) or ITGAV siRNA transfected (lower). Green fluorescence represents the peptides. Cell nuclei are stained with DAPI (blue). Scale bar, 50 μ m. (D) Histograms of flow cytometry analysis. Mock-transfected (blue) and ITGAV siRNA transfected (pink) U87 MG cells were analyzed after RGDEV D peptide treatment and integrin α v β 3 immunostaining. The cells were detected against Alexa488-labeled integrin α v β 3 antibody (left) and Cy5.5-labeled RGDEV D peptide (right). Non-stained non-treated U87 MG cells were also analyzed (grey). (E) Confocal microscopy images of U87 MG cells exposed to RDEV D-DOX (left) or RGDEV D-DOX (right). The red fluorescence represents the doxorubicin moiety. The cells are also stained with DAPI (blue). All the acquired channels (red, blue, and DIC) were merged and shown in the lower panel. Scale bar, 50 μ m. 229

Figure 6.4. (A) HPLC chromatograms of RGDEV D-DOX incubated in the presence of recombinant human caspase-3 for 0, 15, 30, and 60 min. Chromatograms of RGDEV D-DOX incubated for 120 min with the caspase-3 pretreated with caspase inhibitor, and RGDEV D-DOX incubated for 120 min without addition of caspase-3 were also shown. (B) Mean intensity of doxorubicin fluorescence in the cell nuclei quantified depending on the drug exposure time. Doxorubicin (\circ), RGDEV D-DOX (\square), or cleaved RGDEV D-DOX (\blacksquare) was treated on U87 MG (left) and HT-29 (right) cells. Data are presented as mean \pm s.e.m. (C) Representative images of doxorubicin (left), RGDEV D-DOX (center), and cleaved RGDEV D-DOX (right) treated on U87 MG (upper) and HT-29 (lower) cells for 1 h. Scale bar, 50 μ m. 231

Figure 6.5. (A) Concentration-dependent cytotoxicity of doxorubicin (○), RGDEVD-DOX (□), and RGDEVD-DOX incubated with recombinant human caspase-3 (cleaved RGDEVD-DOX; ■) on U87 MG (left) and HT-29 (right) cells when exposed 2 h determined by MTT assay. (B) Exposure time-dependent IC50 values of the drugs on U87 MG cells. Data are presented as mean ± s.e.m.233

Figure 6.6. (A) Western blots of U87 MG cells treated with RGDEVD -DOX or RGDEVD-DOX incubated with recombinant human caspase-3 (cleaved RGDEVD-DOX) at a concentration of 0.1, 1, and 10 μM. The immunoblots were carried out using procaspase-3 (upper), cleaved caspase-3 (center), and beta-actin (lower) antibodies. (B) Cellular caspase activities of U87 MG cells treated with cleaved RGDEVD-DOX (white) or RGDEVD-DOX (grey) at a concentration of 0, 0.1, 1, and 10 μM. Data are presented as mean ± s.e.m. (C) Cellular caspase-3 staining of U87 MG cells after 48 h exposure to cleaved RGDEVD-DOX (center) and RGDEVD-DOX (right). Control cells that have not been treated with any drugs were also shown (left). Green fluorescence represents the active caspase-3. Nuclei of control cells were stained with DAPI (blue). Nuclei of drug treated cells were accumulated with the drug (red) and were not stained with DAPI. Scale bar, 10 μm.235

Figure 6.7. Animal study result of U87 MG-tumor bearing BALC/cSlc-nu mice that received normal saline (○), doxorubicin (7 × 3 mg/kg, ●), RDEVD-DOX (7 × 3 mg/kg, Δ), and RGDEVD-DOX in three different doses (7 × 1 mg/kg, ▲; 7 × 3 mg/kg, □; 7 × 5 mg/kg, ■). The animals received the agents intravenously daily for 7 days. The doses are expressed at molar equivalent of doxorubicin. Tumor growth profiles (A), isolated tumor weights (C), and body weight profiles (B) are shown. Data are presented as mean ± s.e.m.237

Abbreviations

A

Ab	Antibody
ADC	Antibody-drug conjugate
AIF	Apoptosis-inducing factor
AMC	7-amino-4-methylcoumarin (not for AMC-HN9)
AML	Acute myeloid leukemia
Ang	Angiopoietin
ANOVA	Analysis of variance
APAF1	Apoptotic-proteases-activating factor-1
APF	Amino acid positional fitness
APO-1	Apoptosis antigen 1
AT	Antithrombin
ATP	Adenosine triphosphate
AUC	Area under the concentration-time curve

B

BBB	Blood-brain barrier
BCA	Bicinchoninic acid
Bcl	B-cell lymphoma
BID	BH3 interacting-domain death agonist
BMDC	Bone marrow-derived cell
BSA	Bovine serum albumin

C

CAF	Carcinoma-activated fibroblast
CAM	Cell adhesion molecule
CD	Cluster of differentiation protein
CHAPS	3-[(3-Cholamidopropyl)dimethylammonio]-1-propanesulfonate
CL	Clearance
C_{max}	Maximum concentration
COX-2	Cyclooxygenase-2
CT	Computed tomography
CXCL	C-X-C chemokine ligand
CXCR	C-X-C chemokine receptor
Cy	Cyanine

D

D4-GDI	D4 GDP dissociation inhibitor
Da	Dalton
DAB	Diaminobenzidine
DAPI	4',6-Diamidino-2-phenylindole

DCE-MRI	Dynamic contrast enhanced magnetic resonance imaging
DIABLO	Direct inhibitor of apoptosis (IAP)-binding protein with low pi
DIEA	<i>N,N</i> -diisopropylethylamine
DISC	Death-inducing signaling complex
DLL	Delta-like ligand
DMEM	Dulbecco's modified eagle medium
DMF	Dimethyl formamide
DNA	Deoxyribonucleic acid
DNA-PKcs	DNA-dependent protein kinase catalytic subunit
DOX	Doxorubicin
DTT	Dithiothreitol
DVT	Deep vein thrombosis
DW	Distilled water
E	
EBM	Endothelial basal medium
ECGM	Endothelial cell growth medium
ECM	Extracellular matrix
EDC	<i>N</i> -(3-dimethylaminopropyl)- <i>N</i> '-ethylcarbodiimide
EDTA	Ethylenediaminetetraacetic acid
EEDQ	<i>N</i> -Ethoxycarbonyl-2-ethoxy-1,2-dihydroquinoline
EGF	Epidermal growth factor
EGFR	Epidermal growth factor receptor
EMC	ϵ -maleimidocaproylamide
EMCS	ϵ -maleimidocaproyl succinimide
EMT	Epithelial-mesenchymal transition
EndoG	Endonuclease G
EPC	Endothelial progenitor cells
EPR	Enhanced permeation and retention
ErbB	Erythroblastosis oncogene B
ESI-MS	Electrospray ionization mass spectrometry
EtSTC	Ethylamine sodium taurocholate
F	
FACS	Fluorescence-activated cell sorting
FADD	Fas-associated protein with death domain
FAM	Carboxyfluorescein
FasL	Fas ligand
FBS	Fetal bovine serum
FcRn	Neonatal Fc receptor
FDA	Food and drug administration
FGF	Fibroblast growth factor
FGFR	Fibroblast growth factor receptor

FITC	Fluorescein isothiocyanate
FLICA	Fluorescent-Labeled Inhibitors of Caspases
FMK	Fluoromethyl ketone
FR	Folate receptor
FXa	Factor Xa
G	
GBM	Glioblastoma multiforme
GCSF	Granulocyte colony-stimulating factor
Gd-DOTA	Gadolinium- tetraazacyclododecanetetraacetic acid
Glc	Glucosamine
GMB	γ -maleimidobutyric acid
gp60	60 kDa glycoprotein
GPNMB	Transmembrane glycoprotein NMB
H	
HB-EGF	Heparin-binding epidermal growth factor
HBSS	Hank's balanced salt solution
HDMEC	Human dermal microvascular endothelial cell
HE	Hematoxylin and eosin
HEPES	4-(2-hydroxyethyl)-1-piperazineethanesulfonic acid
HER	Human epidermal growth factor receptor
HGF	Hepatocyte growth factor
HIF	Hypoxia-inducible factor
HPLC	High performance liquid chromatography
HRMS	High resolution mass spectrometry
HRP	Horseradish peroxidase
HSA	Human serum albumin
HSGAG	Heparan sulfate glycosaminoglycan
HTRA2	High-temperature-requirement protein A2
HUVEC	Human umbilical vein endothelial cell
I	
IDH	Isocitrate dehydrogenase
IdoA	Iduronic acid
IgG	Immunoglobulin G
IL	Interleukin
IPTT	Induced-phenotype targeted therapy
ITGAV	Integrin α v
L	
LIF	Leukemia inhibitory factor
LMWH	Low-molecular-weight heparin
LRP1	Lipoprotein receptor-related protein 1
M	

mAb	Monoclonal antibody
MAC-1	Macrophage-1 antigen
MALDI-TOF MS	Matrix-assisted laser desorption/ionization time-of-flight mass spectrometry
MAPK	Mitogen-activated protein kinase
MDR	Multidrug resistance
MMAE	Monomethyl auristatin E
MMP	Matrix metalloproteinase
MRI	Magnetic resonance imaging
mRNA	Messenger ribonucleic acid
MT1-MMP	Membrane type 1 matrix metalloproteinase
mTOR	Mechanistic target of rapamycin
MTT	3-(4,5-Dimethylthiazol-2-yl)-2,5-diphenyltetrazolium bromide
N	
NG2	Neural/glial antigen 2
NHS	<i>N</i> -hydroxysuccinimide
NMR	Nuclear magnetic resonance
NPC	Nitrophenyl chloroformate
NPM	Nucleophosmin
NRP	Neuropilin
NSCLC	Non-small-cell lung cancer
O	
OAlI	Allyl ester
ODS	Octadecylsilane
OMI	Oocyte maturation inhibitor
OPLS	Optimized Potentials for Liquid Simulations
P	
PABC	<i>para</i> -aminobenzylcarbamate
PARP	Poly(ADP-ribose) polymerase
PBS	Phosphate buffered saline
PDB	Protein data bank
PDGF	Platelet-derived growth factor
PDGFR	Platelet-derived growth factor receptor
PE	Pulmonary embolism
PECAM	Platelet endothelial cell adhesion molecule
PEG	Polyethylene glycol
PFA	Paraformaldehyde
PGI	Prostaglandin I
PI3K	Phosphoinositide 3-kinase
PKC	Protein kinase C
PIGF	Placental growth factor

<i>p</i> NA	<i>para</i> -Nitroaniline
PRKCD	Protein kinase C δ
PS-SCL	Positional scanning synthetic combinatorial library
R	
RESPA	Reversible reference system propagator algorithm
RIATC	Radiation-induced apoptosis targeted chemotherapy
RIPA	Radioimmunoprecipitation assay
RNA	Ribonucleic acid
RNAi	RNA interference
RNS	Reactive nitrogen species
ROS	Reactive oxygen species
RTKI	Receptor tyrosine kinase inhibitors
RU	Response unit
S	
SCF	Stem cell factor
SDF	Stromal cell-derived factor
SDS-PAGE	Sodium dodecyl sulfate polyacrylamide gel electrophoresis
siRNA	Small interference RNA
SMA	Smooth muscle actin
SMAC	Second mitochondria-derived activator of caspase
SNRNP70	Small nuclear ribonucleoprotein 70kda (U1)
SPARC	Secreted protein acidic and rich in cysteine
SPR	Surface plasmon resonance
SREBP	Sterol regulatory element-binding proteins
STC	Sodium taurocholate
T	
$t_{1/2}$	Half-life
TEA	Triethylamine
TFA	Trifluoroacetic acid
TfR	Transferrin receptor
TIE	Tyrosine kinase with immunoglobulin-like and EGF-like domains
TIP3P	Transferable intermolecular potential 3P
TNF	Tumor necrosis factor
U	
UFH	Unfractionated heparin
uPA	Urokinase-type-plasminogen activator
UV	Ultraviolet
V	
VEGF	Vascular endothelial growth factor
VEGFR	Vascular endothelial growth factor receptor
VHBD	VEGF-heparin binding domain

VHL
VTE

von Hippel Lindau
Venous thromboembolism

Introduction

Since Paul Ehrlich proposed a concept of “magic bullet” more than a century ago, there was an enormous advance in the cancer therapeutics towards development of more selective anticancer agents¹. The early generation of anticancer agents was developed based on the practical knowledge that cancer cells proliferate at a higher rate than normal cells. These agents including alkylating agents, topoisomerase inhibitors, antimetabolites, and vinca alkaloids arrest cell division by inhibiting various pathways required for the DNA replication or cell mitosis, ultimately leading to cell death². Therefore, cells with higher proliferation rate are more prone to these cytotoxic agents, which is the fundamental basis for their tumor cell selectivity over normal cells in the therapeutic aspect¹.

Although cancer cells are more susceptible to the cytotoxic agents, normal cells are also affected since they too proliferate albeit in slower rate³. Moreover, the cytotoxic agents distribute to the cells in non-selective manner since their target molecules such as DNA or topoisomerases exist in similar quantity in both tumor and normal cells². Therefore, despite the potent anticancer effect, they also showed severe toxicities on the normal tissues and organs that were some times even lethal.

The increased understandings of the molecular biology involved in tumor progression have led to the idea of the molecular targeted therapy in aim to develop more selective anticancer agents with reduced risk of adverse effects⁴. Many new molecular targets were revealed that are specifically expressed or biologically significant only in tumor cells, those including several kinds of growth factors, signaling molecules, cell-cycle proteins, modulators of apoptosis, and pro-angiogenic factors⁵. The advances in biotechnology and combinatorial chemistry allowed the development of molecular targeted agents such as monoclonal antibodies and small molecule tyrosine kinase inhibitors (smTKIs) that could selectively block the downstream signaling pathways of their target molecules or deliver cytotoxic agents to the tumor cells expressing

the target molecules on their cell surface^{6,7}. Especially, antibody-drug conjugates (ADCs), which could deliver the cytotoxic agents selectively to the tumor cells, gained increasing interests after the recent clinical approval of two new agents, brentuximab vedotin and ado-trastuzumab emtansine⁷. As a result of the highly selective property of the molecular targeted agents to the target molecules, they showed favorable toxicity profile at the therapeutically effective doses.

However, the clinical outcomes of the molecular targeted agents were disappointing than have been expected, showing only limited improvements in the overall survival of the patients³. The inherent genomic instability and complexity of the tumor cells largely contribute to their resistance against the anticancer therapies⁸. Due to the high frequency of mutations, tumor cells easily adapt to the therapy and acquire an evasive pathway for their survival. Moreover, molecular and genomic heterogeneities of the tumor lead to only partial response to the targeted therapies, resulting in regrowth from the unaffected population of the tumor subclones. There are still a lot of endeavors to discover new molecular targets in a belief that there exists a critical cellular signaling pathway that is irreplaceable and specifically occurs only in tumor in order to overcome the many known issues shown in the modern molecular targeted therapies. However, when considering the genomic instability and the heterogeneity of the tumors, that effort seems to be not that much promising.

The major hurdles in using molecular targeted agents, such as limited therapeutic effect and easily acquired resistance, are ironically due to the highly selective property of those agents. As much as the narrowed target reduced the adverse effects in the normal tissues, it also limited the actions in the tumors, which has a dynamic and complex nature. The well refined targeting capability towards the limited number of molecular targets of the targeted agents allows tumor cells to easily evade the therapy by acquiring alternative pathways. Also, regarding that many distinct subclones of tumor cells exist in a tumor mass, the highly selective property of the targeted therapy limits the number of therapeutically affected tumor cell subclones, thus leaving many tumor cells

unaffected. But according to the past experience, the selectivity of the anticancer agent between the normal tissue and the tumor tissue cannot be renounced to avoid any toxic adverse effects during therapy. Therefore, an ideal anticancer agent should selectively act to the tumor, but act in a non-selective manner among the distinct subclones of tumor cells or molecular targets that are associated with the given pathological condition. In other words, selective and non-selective natures should coexist, but in differential aspects, in the anticancer agents for effective and enduring cancer treatment.

This dissertation discusses about two different strategies that concern the coexistence of selectivity and non-selectivity in a single therapeutic agent. Part one demonstrates development of heparin-based anti-angiogenic agent LHT7 that inhibits multiple stages of pathological angiogenesis by blocking VEGF, FGF2, and PDGF-B at the same time, and stresses its mode of action. This shows the benefit of blocking broad range of pro-angiogenic factors associated in tumor angiogenesis than simply blocking single pro-angiogenic factor. Part two discusses about the development of doxorubicin prodrugs that employ two distinct targeted delivery strategies for an effective delivery of chemotherapeutics to the tumor. Basically, these prodrugs involve traditional targeted delivery system and induced-phenotype targeted prodrug system, allowing the doxorubicin to be selectively delivered to the tumor tissue regardless of the genomic profiles of the tumor cells, followed by non-selective distribution of the active compound to the tumor cells.

References

- 1 Strebhardt, K. & Ullrich, A. Paul Ehrlich's magic bullet concept: 100 years of progress. *Nat Rev Cancer* **8**, 473-480 (2008).
- 2 Gerber, D. E. Targeted therapies: a new generation of cancer treatments. *Am Fam Physician* **77**, 311-319 (2008).
- 3 Holohan, C., Van Schaeybroeck, S., Longley, D. B. & Johnston, P. G. Cancer drug resistance: an evolving paradigm. *Nat Rev Cancer* **13**, 714-726 (2013).
- 4 Schrama, D., Reisfeld, R. A. & Becker, J. C. Antibody targeted drugs as cancer therapeutics. *Nat Rev Drug Discov* **5**, 147-159 (2006).

- 5 Hanahan, D. & Weinberg, R. A. The hallmarks of cancer. *Cell* **100**, 57-70 (2000).
- 6 Imai, K. & Takaoka, A. Comparing antibody and small-molecule therapies for cancer. *Nat Rev Cancer* **6**, 714-727 (2006).
- 7 Hughes, B. Antibody-drug conjugates for cancer: poised to deliver? *Nat Rev Drug Discov* **9**, 665-667 (2010).
- 8 Burrell, R. A., McGranahan, N., Bartek, J. & Swanton, C. The causes and consequences of genetic heterogeneity in cancer evolution. *Nature* **501**, 338-345 (2013).

Part I

**Study of mode of action and multiple pathway
inhibitory capability in tumor angiogenesis of
heparin-based agent LHT7**

Chapter 1

General Introduction

1.1. Tumor angiogenesis

Tumor angiogenesis refers to a new blood vessel formation within tumor, which plays a critical role in mass growth and metastasis of tumor¹. Since the diffusion limit of the oxygen and nutrients from the blood vessel is ranged within 100-200 μm , tumors demand their own blood vessels for the survival and to grow beyond certain size¹. The observations of angiogenesis in the tumor were reported decades ago, which led to an establishment of hypothesis that the tumors may express some driving forces that could recruit blood vessels around themselves². Following studies suggested that tumor cells secrete diffusible substances that could stimulate angiogenesis rather than require direct contact to the nearby endothelium^{3,4}, which eventually guided to the discovery and isolation of several pro-angiogenic factors⁵. In the basis of extensive study about the critical role of angiogenesis in tumor progression combined with the identification of pro-angiogenic factors, Judah Folkman proposed a novel strategy for treatment of cancer through inhibition of angiogenesis by blocking the pro-angiogenic factors in 1971⁶.

1.1.1. Physiology of tumor angiogenesis

Large quantity of studies in angiogenesis have revealed a number of angiogenic factors that are secreted by tumor cells as well as stromal cells, endothelial cells, and blood cells, which indicated complex interplay of tumor and host stroma during the angiogenic process⁷. The past studies not only identified pro-angiogenic factors, but also discovered numbers of endogenous anti-angiogenic factors. In normal condition, the balance of pro-angiogenic and anti-angiogenic

factors tightly regulates physiological angiogenesis. However, in certain pathological condition, such as in malignancy or inflammation, the balance between the pro-angiogenic and anti-angiogenic factors is collapsed by the excessive production of pro-angiogenic factors. This phenomenon is termed as ‘angiogenic switch’, and leads to stimulation of angiogenesis¹. The normal blood vessels are developed in the well-balanced pro-angiogenic and anti-angiogenic signaling, which generates well-organized endothelial cell linings tightly surrounded by vascular smooth muscle cells and basement membranes in order to ensure their optimal function. In contrast, due to the highly leaned balance toward the pro-angiogenic signaling during tumor progression, tumor vasculatures have irregular and disorganized structure with tortuous and dilated vessels. In addition, the endothelial cell that constitutes the vessel wall does not form homogenous layer, and the vessels lack functional mural cells, which plays role in stabilization of the vasculatures⁸.

Multiple steps are involved in the angiogenesis⁹. The sprouting from pre-existing vessels to the avascular region of the tissue requires the opening of the vessels and degradation of the surrounding extracellular matrix (ECM), which allows infiltration of the endothelial cells. Hypoxic conditions in the microenvironment induce endothelial cells to express hypoxia-inducible factor-1 α (HIF-1 α), leading to expression of vascular endothelial growth factor A (VEGF-A) and vascular endothelial growth factor receptor 2 (VEGFR2)¹⁰. VEGF-A is the most predominant pro-angiogenic factor that guides endothelial cells into the avascular regions, mainly through the interaction with the VEGFR2 expressed on the surface of endothelial cells¹¹. The concentration gradient of VEGF-A induces formation of ‘tip cells’, which could proteolytically degrade the basement membrane and guide the direction of sprouting, and stimulates the proliferation of trailing stalk cells for the successful endothelial sprout formations¹². During the sprouting, the tip cells secrete membrane type 1-matrix metalloproteinase (MT1-MMP), which degrades and opens the surrounding ECM. The MT1-MMP is downregulated in the late stage of angiogenesis when the stalks cells contact with the recruited

mural cells¹³. The tip cells also express delta-like ligand 4 (DLL4), which binds to Notch 1 and Notch 4 expressed on the adjacent stalk cells when exposed to VEGF-A. The DLL4-Notch signaling restricts the angiogenic potential of the nearby stalk cells by downregulating the VEGFR2 expression; hence prevent the participation of the nearby cells in developing sprout and promote orderly development of the new vessels¹⁴.

The maturation and stabilization of the nascent vessels involve mural cells. When the primitive vascular network is established, the endothelial cells secrete platelet-derived growth factor B (PDGF-B): this promotes migration, recruitment, and proliferation of mural cells such as pericytes and vascular smooth muscle cells¹⁵. The secreted PDGF-B binds to the heparan sulfate proteoglycans that present in the ECM surrounding the endothelium through the carboxyl-terminal retention motif, generating a concentration gradient that acts as a guidance cue for the migration of the mural cells¹⁵. Recent studies suggested that sonic hedgehog (Shh) is involved in the PDGF-B-mediated migration of mural cells by inducing ERK1/2 and Akt phosphorylation¹⁶. In addition, SDF-1 α is also reported to regulate PDGF-B-mediated-differentiation of bone-marrow derived pericytes¹⁷. These mural cells are essential for nascent vessels to be matured into functional blood vessels¹⁸. The recruited mural cells express angiopoietin 1 (Ang1) on their surface that interacts with the tyrosine kinase with immunoglobulin-like and EGF-like domains 2 (TIE2) on the endothelial cells, which the downstream signalings contribute to the stabilization of the blood vessels¹⁹. The Ang1/TIE2 signal also stimulates the expression of heparin-binding EGF-like growth factor (HB-EGF) by endothelial cells, which facilitates the migration of mural cells via the epidermal growth factor receptors (EGFRs)²⁰. Recent studies suggested that PDGF-C and PDGF-D could also facilitate the coverage of the nascent vessels by mural cells^{21,22}. FGF2 was also demonstrated to stimulate the migration and proliferation of pericytes, and increased the pericyte coverage²³. When the fully functional blood vessels are developed in the tumor, VEGF level decreases as the local concentration of oxygen increases, thereby terminating the angiogenesis²⁴.

Generally, hypoxic microenvironment stimulates the activation of angiogenesis through expression of hypoxia-inducible factors (HIFs)²⁵. In tumor, however, other pathways can aberrantly upregulate the expression of HIF-1 α under normoxic conditions, which is known as hypoxic mimicry²⁶. Mutations in the tumor suppressor gene von Hippel Lindau (*VHL*) enhance the activity of HIF-1 α by preventing its polyubiquitylation and proteasomal degradation²⁷. Moreover, mutations in several oncogenes that results in the activation of mitogen-activated protein kinase (MAPK), phosphoinositide 3-kinase (PI3K) or protein kinase C (PKC) pathways can also increase the activation or the synthesis of HIF-1 α ²⁸. Other factors including reactive oxygen species (ROS) and reactive nitrogen species (RNS), loss of a tumor suppressor gene function, or the expression of viral oncogenes can also induce the upregulation of HIF-1 α ²⁶. As a result of these environmental cues, VEGF-A expression is upregulated in tumors²⁹. VEGF-A secreted from tumors functions not only as a paracrine mediator for stimulating angiogenesis via endothelial cells, but also as an autocrine signal directly to the tumor cells: it promotes the survival, proliferation, and invasiveness of tumor cells independent of angiogenesis³⁰⁻³². It is recognized that in addition to VEGFRs, neuropilins (NRPs) play central role as crucial effectors in the autocrine VEGF signaling in tumors. Recent finding also suggested that VEGF-A contributes to the epithelial-mesenchymal transition (EMT) and the cancer stemness of the tumor cells, which could initiate tumor propagation and metastatic spread from the primary tumor^{33,34}.

1.1.2. Angiogenesis inhibition

Over the past decades, intensive efforts have been undertaken to develop angiogenesis inhibitors for use in the clinical oncology. Among many pro-angiogenic factors identified so far, VEGF has been considered as the most attractive target molecule for its critical role in angiogenesis³⁵. The pioneer of the clinical proof-of-concept as an angiogenesis inhibitor as well as the first VEGF inhibitor to be approved for the clinical use is the humanized monoclonal VEGF antibody, bevacizumab (Avastin[®], Genentech/Roche). Since the FDA

approval in 2004 for treatment of metastatic colorectal cancer, bevacizumab was further approved for the clinical use in treating patients with recurrent or metastatic non-squamous non-small-cell lung cancer (NSCLC), metastatic human epidermal growth factor receptor 2 (HER2, also known as ErbB2)-negative breast cancer (the approval has been withdrawn in 2011), glioblastoma, metastatic renal cell carcinoma, and most recently approved for recurrent or late-stage (metastatic) cervical cancer (FDA approval in August 2014) with combination of chemotherapy³⁶. Additional compounds targeting VEGF signaling axis including VEGF aptamer (Pegaptanib, Macugen[®], Eyetech/Pfizer), VEGF trap (VEGFR fusion protein; Aflibercept, Eylea[®], Regeneron/Bayer), humanized monoclonal VEGFR2 antibody (Ramucirumab, Cyramza[®], ImClone/Eli Lilly), and receptor tyrosine kinase inhibitors (RTKIs) that target VEGFR, such as sorafenib (Nexavar[®], Bayer) and sunitinib (Sutent[®], Pfizer), were developed and clinically approved to treat various types of cancers as well as other pathological conditions related to angiogenesis³⁷.

The VEGF inhibitors arrest proliferation of the endothelial cells and suppress mobilization of the endothelial progenitor cells (EPCs) from the bone marrow, thus prevent growth of the blood vessels in tumor. They could also regress the immature blood vessels, which are predominant in tumor vasculatures, since the immature vessels are susceptible to depletion of VEGF signaling required for their maintenance. Moreover, although yet controversial, VEGF inhibitors are suggested to improve delivery of chemotherapeutic agents to the tumor by normalizing the disorganized and abnormal architecture of tumor vasculatures, which improves chaotic blood flow, reduces vascular permeability and interstitial fluid pressure³⁸.

Angiogenesis inhibitors that target cells other than the endothelial cells are also investigated. Although not as tightly covered as the normal vessels, tumor vessels are also covered by mural cells³⁸. These mural cells are differentiated from the bone marrow-derived mural progenitor cells, which are recruited in the response to PDGF-B that is secreted by endothelial cells³⁹. The mural cells covering the endothelium promote the endothelial cell survival by producing

VEGF that acts in a juxtacrine manner, and by inducing anti-apoptotic protein Bcl-w in the endothelial cells^{40,41}. Therefore, the survival of the endothelium covered with mural cells is independent of the external VEGF. For this reason, depletion of VEGF does not affect the integrity of the blood vessels that are already covered and stabilized by the mural cells³⁶.

The overexpression of PDGF-B by tumor facilitates the stabilization of the blood vessels by mural cells, leading to an accelerated growth of the tumor⁴². Conversely, inhibition of PDGF-B signaling axis by using the PDGF receptor β (PDGFR β) inhibitor results in loss of mural cells on the endothelium and increased apoptosis of the endothelial cells. Such destabilization of the matured vessels transforms the tumor vessels to be more susceptible to the VEGF inhibitors. Indeed, previous study has demonstrated that simultaneous treatment of RTKIs that target VEGFRs and PDGFR β synergistically enhanced the angiogenesis inhibition even in the late-stage solid tumors, which are often resistant to the VEGF inhibitors³⁶. Blockade of stromal cell-derived factor 1 α (SDF-1 α ; also known as CXCL12 α)/C-X-C chemokine receptor type 4 (CXCR4) axis was also recently reported to downregulate PDGF-B, and inhibited the bone marrow-derived pericyte differentiation and tumor vascular expansion⁴³.

Carcinoma-activated fibroblasts (CAFs) are another kind of the stromal cells that are highlighted for their significant role in the progression of tumor. CAFs are reported to accelerate tumor growth, increase malignancy, and affect tumor angiogenesis. CAFs express PDGFR β , and in response to PDGF-B, they are recruited to the tumor and release several pro-angiogenic factors including VEGF and placental growth factor (PIGF)⁴². Stromal fibroblasts are also involved in angiogenesis as they recruit EPCs by releasing SDF-1 α . Inhibition of this chemokine was also effective in the tumor growth suppression⁴⁴.

1.1.3. Resistance to angiogenesis inhibitors

Angiogenesis inhibitors including bevacizumab, sunitinib, and sorafenib have proven their therapeutic benefits in many aggressive tumors. However, the angiogenesis inhibitors, particularly the inhibitors of VEGF pathway, failed to produce enduring clinical responses and showed only transient improvements in most patients^{45,46}. Clinical use of chemotherapeutic agents often suffers in the occurrence of multidrug resistance (MDR), which makes the efficacy of the agent significantly decrease. The MDR is fundamentally caused by the genetically unstable nature of tumor cells. Considering that the angiogenesis inhibitors target majorly endothelial cells, which is genetically stable unlike tumor cells, those were initially regarded to be an ideal therapeutic strategy having no resistant issues³⁷. Therefore, the occurrence of the acquired resistance against angiogenesis inhibitors was unexpected to many researchers and clinicians. Even though the mechanisms of resistance are not fully understood, several mechanisms have been suggested in many studies. Contrary to the traditional means of resistance against chemotherapeutic agents, which involves mutational alteration of the gene encoding a drug target or by alterations in drug uptake and efflux^{47,48}, the resistance against the angiogenesis inhibitors is largely indirect by variously acquiring evasive pathways during the therapeutic blockade of angiogenesis^{49,50}. The observations showed that the specific therapeutic target of the angiogenesis inhibitor still remained inhibited when the tumors acquired resistance, but the alternative pathways were activated to evade the therapy and sustain the tumor growth^{49,51,52}. There are at least four distinct adaptive mechanisms suggested in the evasive resistance to the anti-angiogenic therapies: first, upregulation of alternative pro-angiogenic signaling pathways in the tumor; second, recruitment of bone marrow-derived pro-angiogenic cells that could surmount the depletion of VEGF signaling; third, coverage of tumor vessels by mural cells, which improves the stability of the vessels and attenuate the demand for VEGF signaling for the survival of endothelial cells; and fourth,

facilitated invasion and metastasis of tumor cells to access to the distant normal vasculatures³⁶.

Upregulation of alternative pro-angiogenic factors during blockade of VEGF signaling pathway was demonstrated by several preclinical studies. When genetically engineered mice with pancreatic neuroendocrine cancer (*Rip1-Tag2* mice) were treated with a monoclonal antibody against VEGFR2 (DC101; now ramucirumab or Cyramza[®]), the tumor only showed transient response (10-14 days) followed by regrowth that was accompanied by restoration of the tumor vasculatures⁴⁹. The relapsing tumors had increased levels of the mRNAs of fibroblast growth factor 1 (FGF1), fibroblast growth factor 2 (FGF2), ephrin A1, ephrin A2, and Ang1. The upregulation of these mRNAs was closely associated with the hypoxia induced by the initial regression of vasculature by the DC101 treatment. When the animals were treated with the DC101 followed by the treatment of FGF trap (FGFR-Fc fusion protein), the revascularization and the tumor growth were significantly delayed. This indicated that FGF signaling induced the restoration of angiogenesis that occurred after blockade of the VEGF signaling. Other studies have also demonstrated upregulation of interleukin 8 (IL8) and PDGF-A in the refractory tumors that were initially treated with the anti-angiogenic therapy^{51,53}. The evasive resistance by upregulation of FGF2 was also shown in the clinical observations involving a study of glioblastoma patients being treated with VEGFR inhibitor (Cediranib, Recentin[®], Astra Zeneca)⁵⁴. During the treatment, plasma levels of FGF2 were elevated in the patients during the relapsing phase than in the response phase. Concurrent study showed that the tumor relapse of the glioma patients treated with the cediranib was accompanied by re-initiation of the tumor angiogenesis and loss of the vascular normalization revealed by vascular imaging, which could be highly related to the upregulated FGF2 level in the plasma. Other clinical studies have demonstrated transiently increased plasma levels of VEGF and PlGF in the patients treated with receptor tyrosine kinase inhibitors^{55,56}. The upregulation of the alternative pro-angiogenic factors induced by the host was also observed. The increased levels of the pro-angiogenic factors including

granulocyte colony-stimulating factor (G-CSF), SDF-1 α , stem cell factor (SCF; also known as c-kit ligand), and osteopontin were observed in the non-tumor bearing mice that received sunitinib, implicating a systemic endocrine response to inhibition of VEGF and PDGF signaling in the host tissue⁵⁷. Recent report demonstrated that the upregulation of SDF-1 α could induce the expression of PDGF-B in the VEGF inhibited Ewing's sarcoma. The secreted PDGF-B increased infiltration and differentiation of PDGFR β ⁺ bone marrow-derived cells (BMDCs) into desmin and NG2 expressing matured pericytes, thereby re-initiating the tumor growth¹⁷.

Hypoxia caused by the vessel regression by the anti-angiogenic therapy also stimulates the recruitment of BMDCs that are capable to elicit neovasculatures in the tumor tissues³⁶. The BMDCs consist of vascular progenitors and vascular modulatory cells. Endothelial and pericyte progenitor cells are the vascular progenitor cells, which eventually become the physical compositions of the blood vessels^{39,58}. TAMs (tumor-associated macrophages)⁵⁹, TIE2⁺ (also known as TEK⁺) monocytes⁶⁰, VEGFR1⁺ hemangiocytes⁶¹, and CD11b⁺ (also known as ITGAM⁺) myeloid cells⁶² play role as the vascular modulators by expressing various cytokines, growth factors, and proteases during angiogenesis⁶³. In the experimentally induced ischemic tissue, endothelial progenitor cells and other CXCR4⁺ BMDCs were recruited through increased HIF-1 α , SDF-1 α , and VEGF⁶⁴⁻⁶⁶. Recruitment of various bone marrow-derived CD45⁺ (also known as PTPRC⁺) myeloid cells, mature F4/80⁺ tumor-associated macrophages, as well as the endothelial and the pericyte progenitor cells mediated by HIF-1 α were also observed during neovascularization of glioblastoma multiforme (GBM), which is characterized as a highly hypoxic and necrotic tumor⁶³. Conversely, GBMs deficient in HIF-1 α had few BMDCs recruited, and the vascularization and the mass growth was severely impaired. These results collectively suggested that hypoxia induced by anti-angiogenic therapy recruited BMDCs that facilitated the revascularization of the tumor. Experimental study showed that vascular disrupting agent, which induces acute hypoxia and necrosis within tumor, triggered the accumulation of the endothelial progenitor cells that were

sufficient for the revascularization at the tumor margins⁶⁷. By contrast, untreated tumor showed no significant infiltration of the BMDCs, indicating that the recruitment of the BMDCs contributes to the adaptive response to the anti-angiogenic therapy.

Number of evidences have also suggested that the coverage of endothelial vessels by pericytes protected the vessels from the anti-angiogenic therapy⁶⁸. Several studies have reported that distinctive functional vessels that were tightly covered with pericytes remained after the substantial reduction of the tumor vasculatures by the VEGF inhibition⁶⁹⁻⁷¹. These vessels from the refractory tumors were distinguishable from the typical vessels in the untreated tumors, which are, by contrast, sporadically covered with less closely associated pericytes⁷². These reports collectively indicated that the pericyte coverage of the tumor blood vessels contribute to the resistance to anti-angiogenic therapy. Experimental study showed that the tumor vessels with inadequate pericyte coverage were more vulnerable to the depletion of VEGF signaling⁷³, and this was further elucidated by the fact that pericytes support the endothelial survival in juxtacrine manner by expressing appreciable amount of VEGF and other factors that are critical in survival of endothelial cells^{39,40}. Moreover, the pericytes attenuate the proliferation rate of the endothelial cells as a part of the vessel stabilization process, which reduces the necessity of the VEGF in the endothelial cells⁷⁴.

The increased invasiveness of the tumor cells has been suggested as another mechanism of the evasive resistance to the anti-angiogenic therapy. Preclinical studies in orthotopic GBM mouse model demonstrated an aggressive invasion of the malignant cells and the continuous growth of tumor, albeit more slowly, when angiogenesis was impeded by genetically deleting pro-angiogenic factors such as VEGF, HIF-1 α , and matrix metalloproteinase 9 (MMP-9). Similar result was shown when the angiogenesis was inhibited pharmacologically with the VEGFR tyrosine kinase inhibitor SU5416 (sunitinib). The glioblastoma cells invaded to the normal tissue and co-opt with the normal blood vessels, using those vessels as channels to penetrated deep into the brain. This perivascular

tumor invasion allowed the tumor cells to evade the vascular deficiency in a dispersed fashion⁷⁵. The pro-invasive adaptation of tumor was also observed in clinical studies in a subset of GBM patients who had developed multifocal recurrence of tumors during the course of bevacizumab treatment^{76,77}. The increased incidence of the metastasis during the anti-angiogenic therapy was also reported in several other tumors. The adaptive mechanisms for the increased tumor invasiveness by the anti-angiogenic therapy were suggested as the follows: firstly, tumors may increase the activity of the pre-existing invasion program in compensation to their loss of angiogenic capability; secondly, tumors might switch on an invasion program that is distinct to that occurs spontaneously during progression; thirdly, VEGF might have a potential role in restricting the tumor cell invasion, thus inhibition of VEGF signaling initiating the intrinsic invasiveness of tumor cells. In fact, a recent study revealed that the VEGF directly inhibit the tumor cell invasiveness by facilitating the protein tyrosine phosphatase 1B (PTP1B) to a MET/VEGFR2 heterocomplex, thereby suppressing the MET-dependent tumor cell migration. The VEGF blockade resulted in increased MET activity in GBM cells in a hypoxia-independent manner and induction of epithelial-mesenchymal transition (EMT)⁷⁸.

Although the transitory clinical outcome of the angiogenesis inhibitors might be construed disappointing, they still possess an important status in the modern cancer therapeutics and are becoming components of gold standard regimens. The growing evidence and knowledge about the mechanistic basis for adaptive evasive resistance provides affirmative opportunities for improving the anti-angiogenic therapy.

1.2. Heparin

Heparin is a naturally occurring highly sulfated glycosaminoglycan that is commonly used as an injectable anticoagulant agent for prevention and treatment of venous thromboembolism (VTE)⁷⁹. About a century ago, Jay McLean and William H. Howard at Johns Hopkins University found that an

extract of canine liver prolonged the plasma clotting time, and isolated an anticoagulant, which the substance was termed as 'heparin' (hepar or ήπαρ means liver in Greek)⁸⁰. Although the heparin was initially extract from the canine liver, pharmaceutical grade of heparin is currently obtained from mucosal tissues, such as porcine intestines or bovine lungs⁸¹. Since the discovery in 1916, heparin still remains one of the most important anticoagulant agents in clinical use⁸². Despite that heparin is only approved for anticoagulation in clinical use, large quantities of studies revealed its regulatory effects in diverse pathophysiological processes, thereby attracting researchers for its potential to be used in other pathological conditions⁸³.

1.2.1. Structural Characteristics of Heparin

Heparin is a linear polysaccharide consisting of alternative disaccharide units with molecular weight range of 5-40 kDa and average molecular weight of 15 kDa⁸⁴. The most common disaccharide unit within the heparin is composed of a 2-*O*-sulfated iduronic acid, and 6-*O*- and *N*-sulfated glucosamine (IdoA(2S)-GlcNS(6S)), which accounts for about 85% and 75% of the heparin composition extracted from bovine lung and porcine intestinal mucosa, respectively⁸⁵. Although IdoA(2S)-GlcNS(6S) unit is the major component, a number of structural variation in the disaccharide unit exists, contributing to the microheterogeneity of the heparin. Another important characteristic of the heparin is the strong anionic charge within the molecule. The IdoA(2S)-GlcNS(6S) disaccharide unit contains three sulfate groups, which provides significant amount of anionic charge to the heparin molecule. In fact, the disaccharide units that compose heparin have average 2.7 sulfate groups. Due to the high content of sulfate and carboxyl groups, heparin is recognized to have the highest anionic charge density among any of the known biological macromolecules, which attributes to its diverse biological activity by interacting with wide-array of endogenous proteins⁸⁴.

1.2.2. Anticoagulant Activity of Heparin

The most relevant activity of heparin is anticoagulation. The heparin shows its anticoagulant activity by binding to antithrombin III (ATIII), a serine protease inhibitor. When heparin is bound, the ATIII undergoes conformational change that initiates its enzymatic activity by the increased flexibility of the reactive center loop sequence⁸⁶. The activation of the ATIII leads to the inhibition of thrombin and other proteases that are crucially involved in blood coagulation cascade. The activation of ATIII through heparin binding increased the inactivation rate of the associated proteases up to 1000-fold⁸⁷. The ATIII binds to a specific pentasaccharide within the heparin polysaccharide, which is identified as GlcNAc/NS(6S)-GlcA-GlcNS(3S,6S)-IdoA(2S)-GlcNS(6S)^{88,89}. The inhibition of factor Xa only needs binding of ATIII to the heparin pentasaccharide unit. However, inactivation of thrombin requires additional binding of the thrombin to the heparin polysaccharide at the site near the pentasaccharide unit, which results in the formation of a ternary complex of ATIII, thrombin, and heparin. The activity of heparin against thrombin is dependent to the length of the heparin oligosaccharide, since the formation of the ternary complex requires at least 18 saccharide units^{90,91}. The different mode of actions in the inhibition of coagulation cascade of heparin depending in its chain length has led to the development of low-molecular-weight heparin (LMWH). The LMWH consists of low-molecular weight fragments of heparin with an average molecular weight of approximately 5,000 Da, and it is obtained by fractionation or by controlled enzymatic or chemical depolymerization of heparin by various methods⁸¹. Because of the relatively shorter oligosaccharide chain, LMWH preferably targets factor Xa than thrombin. The LMWH has more predictable anticoagulant response and longer plasma half-life than the unfractionated heparin (UFH), thereby produces improved therapeutic index with fewer side effects⁹²⁻⁹⁴. For this reason, LMWH is preferred over UFH in patients with VTE, such as pulmonary embolism (PE) and deep vein thrombosis (DVT)^{95,96}.

1.2.2. Heparin in Cancer

Although heparin has been clinically used as an anticoagulant agent, other potential functions in physiological or pathological conditions was reported in number of studies^{82,97}. Among many suggested biological roles of heparin, the regulatory effect in tumor progression was mainly focused. Especially, LMWH was preferably studied than UFH. In fact, the retrospective analysis of cancer patients who received LMWH demonstrated significantly improved survival as compared to UFH recipients^{98,99}, and according to the recent international guidelines, LMWH is the recommended regimen for the cancer patients^{100,101}. Many experimental studies showed that the heparin affected tumor progression by regulating various pathways besides coagulation cascade. It was demonstrated that heparin could induce cell apoptosis^{102,103}, inhibit cell proliferation^{104,105}, metastasis¹⁰⁶⁻¹⁰⁹, and angiogenesis¹¹⁰⁻¹¹², and also modulate immune systems⁸³. The diverse physiological roles of heparin are attributable to the polyanionic groups on the glycosaminoglycan chain, which allows the electrostatic interactions with broad range of endogenous proteins other than ATIII, including cytokines, chemokines, growth factors, and pro-angiogenic factors. Among these heparin-binding proteins, many proteins such as VEGF, FGF, PDGF, HB-EGF, heparanase, MMPs, selectins, and integrins are crucially involved in various stages of tumor progression⁸²⁻⁸⁴. The binding properties of heparin are determined by its saccharide sequence composition, sulfation pattern, charge distribution, overall anionic charge density, and the size of the oligosaccharide^{84,113}.

Among many regulatory roles in tumor progression, the effect of heparin in tumor angiogenesis has been an area of a great interest^{113,114}. Many experimental studies showed anti-angiogenic effect of heparin in both *in vitro* and *in vivo*, which eventually led to suppression of tumor growth in the animal models¹¹⁰⁻¹¹². Considering that the angiogenesis significantly contributes not only to the mass growth of tumor, but also to the metastasis, the anti-angiogenic activity of heparin possesses a great importance in the clinical oncology¹¹⁵.

Tumor cells release various pro-angiogenic factors, which many are heparin-binding proteins, during tumor progression to stimulate angiogenesis within tumor tissue for further growth^{116,117}. The secreted pro-angiogenic factors stimulate angiogenic responses via interactions with their receptors expressed on the endothelial cells. Interestingly, effective interaction between pro-angiogenic factors and their corresponding receptors requires preceded binding of the pro-angiogenic factors on the cell surface heparan sulfate glycosaminoglycans (HSGAGs), which are related substances of heparin.

The HSGAGs are expressed on the surface of every eukaryotic cells including tumor cells and their related cells, and are crucially involved in the tumor progression such as cellular transformation, mass growth, metastasis, and angiogenesis⁸³. Similar to heparin, the HSGAGs interact with broad range of extracellular signaling molecules including the pro-angiogenic factors and allow them to regulate the pathological processes. The HSGAGs prevents diffusion, proteolytic degradation, and inactivation of the bound pro-angiogenic factors in the microenvironment, thus storing and stabilizing those proteins before their action^{116,118-120}. In addition, the HSGAGs act as a cofactor and potentiate the interaction between the pro-angiogenic factors and their receptors, and enhance the downstream angiogenic signals¹²¹⁻¹²⁴. Therefore, it has been suggested that heparin modulate the angiogenesis by interfering the interaction between the pro-angiogenic factors and the HSGAGs by competitive binding, thereby disrupting the proper angiogenic signalings^{125,126}.

Heparin has shown differential regulatory effects in angiogenesis depending in their size¹¹⁴. Many reports have demonstrated that LMWH effectively inhibited angiogenesis, whereas UFH was significantly less effective or even stimulated the angiogenesis^{111,127-132}. In particular, the angiogenesis induced by VEGF or FGF2 was inhibited by the heparin oligosaccharides with less than 20 or 12 saccharide units *in vitro*, respectively^{104,111}. In fact, Soker et al. demonstrated that heparin fragments of 16-18 saccharide units inhibited the binding of VEGF-A to VEGFRs, while the fragments larger than 22 saccharide units enhanced the binding¹¹¹. Other studies have also showed the inhibitory

effects of the small fragment of heparin in VEGF and FGF2-mediated angiogenesis *in vivo*^{129,133}. However, recent study has demonstrated that heparin requires at least eight saccharide units for an efficient binding to VEGF¹³⁴, indicating that there exist a minimum threshold of the polysaccharide size for the heparin to express its regulatory roles.

1.3. Rationale of the research

In the modern cancer therapeutics, molecular targeted therapies gained the most interest by the increased understandings of the molecular basis of cancer progression. As a part of the molecular targeted therapy, a number of angiogenesis inhibitors, especially blocking VEGF signaling pathway, have been developed and approved for many types of tumor³⁵. However, regardless of the initial response, these agents failed to produce enduring clinical benefit in the cancer patients. Since the overexpression of alternative pro-angiogenic factors besides VEGF was found to be substantially responsible to the resistance against angiogenesis inhibitors, simultaneous blockade of the multiple angiogenic signaling pathways has been deemed necessary for effective and enduring inhibition of tumor angiogenesis³⁶.

Currently, the major classes constituting the molecular targeted agents including angiogenesis inhibitors are humanized monoclonal antibodies and small molecule tyrosine kinase inhibitors (smTKIs). The monoclonal antibodies are intrinsically specific to a target molecule and are difficult to be developed as multi-targeted agent. By contrast, smTKIs are relatively non-specific and targets several receptor kinases at the same time, therefore, generally regarded as multi-targeted agents¹³⁵. However, considering that single pro-angiogenic factor acts as a ligand for more than one receptor – for example, VEGF-A interacts with VEGFR1 and VEGFR2 – blocking multiple receptor kinases could only partly block the angiogenic signals from each pro-angiogenic factor. Therefore, blocking multiple pro-angiogenic factors instead of the receptors

could be more effective in practical means of inhibiting the multiple angiogenic signaling pathways³⁶.

Many pro-angiogenic factors including VEGF, FGF, PDGF, HB-EGF, heparanase, and MMPs are inherently heparin-binding proteins and their activities could be inhibited by heparin^{82,84}. Therefore, an appropriate modification of heparin that could retain its capability to interact with broad array of pro-angiogenic factors and eliminate its anticoagulant activity at the same time would produce an ideal multi-targeted angiogenesis inhibitor.

References

- 1 Carmeliet, P. & Jain, R. K. Angiogenesis in cancer and other diseases. *Nature* **407**, 249-257 (2000).
- 2 Goldmann, E. The Growth of Malignant Disease in Man and the Lower Animals, with special reference to the Vascular System. *Proc R Soc Med* **1**, 1-13 (1908).
- 3 Greenblatt, M. & Shubi, P. Tumor angiogenesis: transfilter diffusion studies in the hamster by the transparent chamber technique. *J Natl Cancer Inst* **41**, 111-124 (1968).
- 4 Ehrmann, R. L. & Knoth, M. Choriocarcinoma. Transfilter stimulation of vasoproliferation in the hamster cheek pouch. Studied by light and electron microscopy. *J Natl Cancer Inst* **41**, 1329-1341 (1968).
- 5 Folkman, J. & Klagsbrun, M. Angiogenic factors. *Science* **235**, 442-447 (1987).
- 6 Folkman, J., Merler, E., Abernathy, C. & Williams, G. Isolation of a tumor factor responsible for angiogenesis. *J Exp Med* **133**, 275-288 (1971).
- 7 Fukumura, D., Xavier, R., Sugiura, T., Chen, Y., Park, E. C., Lu, N., Selig, M., Nielsen, G., Taksir, T., Jain, R. K. & Seed, B. Tumor induction of VEGF promoter activity in stromal cells. *Cell* **94**, 715-725 (1998).
- 8 Jain, R. K. A new target for tumor therapy. *N Engl J Med* **360**, 2669-2671 (2009).
- 9 Carmeliet, P. Angiogenesis in health and disease. *Nat Med* **9**, 653-660 (2003).
- 10 Tang, N., Wang, L., Esko, J., Giordano, F. J., Huang, Y., Gerber, H. P., Ferrara, N. & Johnson, R. S. Loss of HIF-1alpha in endothelial cells disrupts a hypoxia-driven VEGF autocrine loop necessary for tumorigenesis. *Cancer Cell* **6**, 485-495 (2004).
- 11 Ferrara, N., Gerber, H. P. & LeCouter, J. The biology of VEGF and its receptors. *Nat Med* **9**, 669-676 (2003).
- 12 Gerhardt, H., Golding, M., Fruttiger, M., Ruhrberg, C., Lundkvist, A., Abramsson, A., Jeltsch, M., Mitchell, C., Alitalo, K., Shima, D. & Betsholtz, C. VEGF guides

- angiogenic sprouting utilizing endothelial tip cell filopodia. *J Cell Biol* **161**, 1163-1177 (2003).
- 13 Chung, A. S., Lee, J. & Ferrara, N. Targeting the tumour vasculature: insights from physiological angiogenesis. *Nat Rev Cancer* **10**, 505-514 (2010).
 - 14 Hellstrom, M., Phng, L. K., Hofmann, J. J., Wallgard, E., Coultas, L., Lindblom, P., Alva, J., Nilsson, A. K., Karlsson, L., Gaiano, N., Yoon, K., Rossant, J., Iruela-Arispe, M. L., Kalen, M., Gerhardt, H. & Betsholtz, C. Dll4 signalling through Notch1 regulates formation of tip cells during angiogenesis. *Nature* **445**, 776-780 (2007).
 - 15 Lindblom, P., Gerhardt, H., Liebner, S., Abramsson, A., Enge, M., Hellstrom, M., Backstrom, G., Fredriksson, S., Landegren, U., Nystrom, H. C., Bergstrom, G., Dejana, E., Ostman, A., Lindahl, P. & Betsholtz, C. Endothelial PDGF-B retention is required for proper investment of pericytes in the microvessel wall. *Genes Dev* **17**, 1835-1840 (2003).
 - 16 Yao, Q., Renault, M. A., Chapouly, C., Vandierdonck, S., Belloc, I., Jaspard-Vinassa, B., Daniel-Lamaziere, J. M., Laffargue, M., Merched, A., Desgranges, C. & Gadeau, A. P. Sonic hedgehog mediates a novel pathway of PDGF-BB-dependent vessel maturation. *Blood* **123**, 2429-2437 (2014).
 - 17 Hamdan, R., Zhou, Z. & Kleinerman, E. S. SDF-1alpha induces PDGF-B expression and the differentiation of bone marrow cells into pericytes. *Mol Cancer Res* **9**, 1462-1470 (2011).
 - 18 Hellstrom, M., Gerhardt, H., Kalen, M., Li, X., Eriksson, U., Wolburg, H. & Betsholtz, C. Lack of pericytes leads to endothelial hyperplasia and abnormal vascular morphogenesis. *J Cell Biol* **153**, 543-553 (2001).
 - 19 Hawighorst, T., Skobe, M., Streit, M., Hong, Y. K., Velasco, P., Brown, L. F., Riccardi, L., Lange-Asschenfeldt, B. & Detmar, M. Activation of the tie2 receptor by angiopoietin-1 enhances tumor vessel maturation and impairs squamous cell carcinoma growth. *Am J Pathol* **160**, 1381-1392 (2002).
 - 20 Iivanainen, E., Nelimarkka, L., Elenius, V., Heikkinen, S. M., Junttila, T. T., Sihombing, L., Sundvall, M., Maatta, J. A., Laine, V. J., Yla-Herttuala, S., Higashiyama, S., Alitalo, K. & Elenius, K. Angiopoietin-regulated recruitment of vascular smooth muscle cells by endothelial-derived heparin binding EGF-like growth factor. *FASEB J* **17**, 1609-1621 (2003).
 - 21 di Tomaso, E., London, N., Fuja, D., Logie, J., Tyrrell, J. A., Kamoun, W., Munn, L. L. & Jain, R. K. PDGF-C induces maturation of blood vessels in a model of glioblastoma and attenuates the response to anti-VEGF treatment. *PLoS One* **4**, e5123 (2009).
 - 22 Liu, J., Liao, S., Huang, Y., Samuel, R., Shi, T., Naxerova, K., Huang, P., Kamoun, W., Jain, R. K., Fukumura, D. & Xu, L. PDGF-D improves drug delivery and efficacy

- via vascular normalization, but promotes lymphatic metastasis by activating CXCR4 in breast cancer. *Clin Cancer Res* **17**, 3638-3648 (2011).
- 23 Ricard, N., Tu, L., Le Hirsch, M., Huertas, A., Phan, C., Thuillet, R., Sattler, C., Fadel, E., Seferian, A., Montani, D., Dorfmüller, P., Humbert, M. & Guignabert, C. Increased pericyte coverage mediated by endothelial-derived fibroblast growth factor-2 and interleukin-6 is a source of smooth muscle-like cells in pulmonary hypertension. *Circulation* **129**, 1586-1597 (2014).
 - 24 Darland, D. C. & D'Amore, P. A. Blood vessel maturation: vascular development comes of age. *J Clin Invest* **103**, 157-158 (1999).
 - 25 Dayan, F., Mazure, N. M., Brahimi-Horn, M. C. & Pouyssegur, J. A dialogue between the hypoxia-inducible factor and the tumor microenvironment. *Cancer Microenviron* **1**, 53-68 (2008).
 - 26 Semenza, G. L. Oxygen homeostasis. *Wiley Interdiscip Rev Syst Biol Med* **2**, 336-361 (2010).
 - 27 Pugh, C. W. & Ratcliffe, P. J. Regulation of angiogenesis by hypoxia: role of the HIF system. *Nat Med* **9**, 677-684 (2003).
 - 28 Liao, D. & Johnson, R. S. Hypoxia: a key regulator of angiogenesis in cancer. *Cancer Metastasis Rev* **26**, 281-290 (2007).
 - 29 Kerbel, R. S. Tumor angiogenesis. *N Engl J Med* **358**, 2039-2049 (2008).
 - 30 Mercurio, A. M., Bachelder, R. E., Bates, R. C. & Chung, J. Autocrine signaling in carcinoma: VEGF and the $\alpha 6 \beta 4$ integrin. *Semin Cancer Biol* **14**, 115-122 (2004).
 - 31 Lichtenberger, B. M., Tan, P. K., Niederleithner, H., Ferrara, N., Petzelbauer, P. & Sibilio, M. Autocrine VEGF signaling synergizes with EGFR in tumor cells to promote epithelial cancer development. *Cell* **140**, 268-279 (2010).
 - 32 Cao, Y., E, G., Wang, E., Pal, K., Dutta, S. K., Bar-Sagi, D. & Mukhopadhyay, D. VEGF exerts an angiogenesis-independent function in cancer cells to promote their malignant progression. *Cancer Res* **72**, 3912-3918 (2012).
 - 33 Beck, B., Driessens, G., Goossens, S., Youssef, K. K., Kuchnio, A., Caauwe, A., Sotiropoulou, P. A., Loges, S., Lapouge, G., Candi, A., Mascré, G., Drogat, B., Dekoninck, S., Haigh, J. J., Carmeliet, P. & Blanpain, C. A vascular niche and a VEGF-Nrp1 loop regulate the initiation and stemness of skin tumours. *Nature* **478**, 399-403 (2011).
 - 34 Fantozzi, A., Gruber, D. C., Pisarsky, L., Heck, C., Kunita, A., Yilmaz, M., Meyer-Schaller, N., Cornille, K., Hopfer, U., Bentires-Alj, M. & Christofori, G. VEGF-mediated angiogenesis links EMT-induced cancer stemness to tumor initiation. *Cancer Res* **74**, 1566-1575 (2014).

- 35 Ellis, L. M. & Hicklin, D. J. VEGF-targeted therapy: mechanisms of anti-tumour activity. *Nat Rev Cancer* **8**, 579-591 (2008).
- 36 Bergers, G. & Hanahan, D. Modes of resistance to anti-angiogenic therapy. *Nat Rev Cancer* **8**, 592-603 (2008).
- 37 Carmeliet, P. Angiogenesis in life, disease and medicine. *Nature* **438**, 932-936 (2005).
- 38 Jain, R. K. Normalization of tumor vasculature: an emerging concept in antiangiogenic therapy. *Science* **307**, 58-62 (2005).
- 39 Song, S., Ewald, A. J., Stallcup, W., Werb, Z. & Bergers, G. PDGFRbeta+ perivascular progenitor cells in tumours regulate pericyte differentiation and vascular survival. *Nat Cell Biol* **7**, 870-879 (2005).
- 40 Darland, D. C., Massingham, L. J., Smith, S. R., Piek, E., Saint-Geniez, M. & D'Amore, P. A. Pericyte production of cell-associated VEGF is differentiation-dependent and is associated with endothelial survival. *Dev Biol* **264**, 275-288 (2003).
- 41 Franco, M., Roswall, P., Cortez, E., Hanahan, D. & Pietras, K. Pericytes promote endothelial cell survival through induction of autocrine VEGF-A signaling and Bcl-w expression. *Blood* **118**, 2906-2917 (2011).
- 42 Ostman, A. PDGF receptors-mediators of autocrine tumor growth and regulators of tumor vasculature and stroma. *Cytokine Growth Factor Rev* **15**, 275-286 (2004).
- 43 Hamdan, R., Zhou, Z. & Kleinerman, E. S. Blocking SDF-1alpha/CXCR4 downregulates PDGF-B and inhibits bone marrow-derived pericyte differentiation and tumor vascular expansion in Ewing tumors. *Mol Cancer Ther* **13**, 483-491 (2014).
- 44 Orimo, A., Gupta, P. B., Sgroi, D. C., Arenzana-Seisdedos, F., Delaunay, T., Naeem, R., Carey, V. J., Richardson, A. L. & Weinberg, R. A. Stromal fibroblasts present in invasive human breast carcinomas promote tumor growth and angiogenesis through elevated SDF-1/CXCL12 secretion. *Cell* **121**, 335-348 (2005).
- 45 Saltz, L. B., Lenz, H. J., Kindler, H. L., Hochster, H. S., Wadler, S., Hoff, P. M., Kemeny, N. E., Hollywood, E. M., Gonen, M., Quinones, M., Morse, M. & Chen, H. X. Randomized phase II trial of cetuximab, bevacizumab, and irinotecan compared with cetuximab and bevacizumab alone in irinotecan-refractory colorectal cancer: the BOND-2 study. *J Clin Oncol* **25**, 4557-4561 (2007).
- 46 Kindler, H. L., Niedzwiecki, D., Hollis, D., Sutherland, S., Schrag, D., Hurwitz, H., Innocenti, F., Mulcahy, M. F., O'Reilly, E., Wozniak, T. F., Picus, J., Bhargava, P., Mayer, R. J., Schilsky, R. L. & Goldberg, R. M. Gemcitabine plus bevacizumab compared with gemcitabine plus placebo in patients with advanced pancreatic

- cancer: phase III trial of the Cancer and Leukemia Group B (CALGB 80303). *J Clin Oncol* **28**, 3617-3622 (2010).
- 47 Gorre, M. E. & Sawyers, C. L. Molecular mechanisms of resistance to STI571 in chronic myeloid leukemia. *Curr Opin Hematol* **9**, 303-307 (2002).
- 48 O'Connor, R., Clynes, M., Dowling, P., O'Donovan, N. & O'Driscoll, L. Drug resistance in cancer - searching for mechanisms, markers and therapeutic agents. *Expert Opin Drug Metab Toxicol* **3**, 805-817 (2007).
- 49 Casanovas, O., Hicklin, D. J., Bergers, G. & Hanahan, D. Drug resistance by evasion of antiangiogenic targeting of VEGF signaling in late-stage pancreatic islet tumors. *Cancer Cell* **8**, 299-309 (2005).
- 50 Shojaei, F., Wu, X., Malik, A. K., Zhong, C., Baldwin, M. E., Schanz, S., Fuh, G., Gerber, H. P. & Ferrara, N. Tumor refractoriness to anti-VEGF treatment is mediated by CD11b+Gr1+ myeloid cells. *Nat Biotechnol* **25**, 911-920 (2007).
- 51 Fernando, N. T., Koch, M., Rothrock, C., Gollogly, L. K., D'Amore, P. A., Ryeom, S. & Yoon, S. S. Tumor escape from endogenous, extracellular matrix-associated angiogenesis inhibitors by up-regulation of multiple proangiogenic factors. *Clin Cancer Res* **14**, 1529-1539 (2008).
- 52 Kadenhe-Chiweshe, A., Papa, J., McCrudden, K. W., Frischer, J., Bae, J. O., Huang, J., Fisher, J., Lefkowitz, J. H., Feirt, N., Rudge, J., Holash, J., Yancopoulos, G. D., Kandel, J. J. & Yamashiro, D. J. Sustained VEGF blockade results in microenvironmental sequestration of VEGF by tumors and persistent VEGF receptor-2 activation. *Mol Cancer Res* **6**, 1-9 (2008).
- 53 Mizukami, Y., Jo, W. S., Duerr, E. M., Gala, M., Li, J., Zhang, X., Zimmer, M. A., Iliopoulos, O., Zukerberg, L. R., Kohgo, Y., Lynch, M. P., Rueda, B. R. & Chung, D. C. Induction of interleukin-8 preserves the angiogenic response in HIF-1alpha-deficient colon cancer cells. *Nat Med* **11**, 992-997 (2005).
- 54 Batchelor, T. T., Sorensen, A. G., di Tomaso, E., Zhang, W. T., Duda, D. G., Cohen, K. S., Kozak, K. R., Cahill, D. P., Chen, P. J., Zhu, M., Ancukiewicz, M., Mrugala, M. M., Plotkin, S., Drappatz, J., Louis, D. N., Ivy, P., Scadden, D. T., Benner, T., Loeffler, J. S., Wen, P. Y. & Jain, R. K. AZD2171, a pan-VEGF receptor tyrosine kinase inhibitor, normalizes tumor vasculature and alleviates edema in glioblastoma patients. *Cancer Cell* **11**, 83-95 (2007).
- 55 Bocci, G., Man, S., Green, S. K., Francia, G., Ebos, J. M., du Manoir, J. M., Weinerman, A., Emmenegger, U., Ma, L., Thorpe, P., Davidoff, A., Huber, J., Hicklin, D. J. & Kerbel, R. S. Increased plasma vascular endothelial growth factor (VEGF) as a surrogate marker for optimal therapeutic dosing of VEGF receptor-2 monoclonal antibodies. *Cancer Res* **64**, 6616-6625 (2004).

- 56 Motzer, R. J., Michaelson, M. D., Redman, B. G., Hudes, G. R., Wilding, G., Figlin, R. A., Ginsberg, M. S., Kim, S. T., Baum, C. M., DePrimo, S. E., Li, J. Z., Bello, C. L., Theuer, C. P., George, D. J. & Rini, B. I. Activity of SU11248, a multitargeted inhibitor of vascular endothelial growth factor receptor and platelet-derived growth factor receptor, in patients with metastatic renal cell carcinoma. *J Clin Oncol* **24**, 16-24 (2006).
- 57 Ebos, J. M., Lee, C. R., Christensen, J. G., Mutsaers, A. J. & Kerbel, R. S. Multiple circulating proangiogenic factors induced by sunitinib malate are tumor-independent and correlate with antitumor efficacy. *Proc Natl Acad Sci U S A* **104**, 17069-17074 (2007).
- 58 Asahara, T., Murohara, T., Sullivan, A., Silver, M., van der Zee, R., Li, T., Witzenbichler, B., Schatteman, G. & Isner, J. M. Isolation of putative progenitor endothelial cells for angiogenesis. *Science* **275**, 964-967 (1997).
- 59 Pollard, J. W. Tumour-educated macrophages promote tumour progression and metastasis. *Nat Rev Cancer* **4**, 71-78 (2004).
- 60 De Palma, M., Venneri, M. A., Galli, R., Sergi Sergi, L., Politi, L. S., Sampaolesi, M. & Naldini, L. Tie2 identifies a hematopoietic lineage of proangiogenic monocytes required for tumor vessel formation and a mesenchymal population of pericyte progenitors. *Cancer Cell* **8**, 211-226 (2005).
- 61 Kaplan, R. N., Riba, R. D., Zacharoulis, S., Bramley, A. H., Vincent, L., Costa, C., MacDonald, D. D., Jin, D. K., Shido, K., Kerns, S. A., Zhu, Z., Hicklin, D., Wu, Y., Port, J. L., Altorki, N., Port, E. R., Ruggero, D., Shmelkov, S. V., Jensen, K. K., Rafii, S. & Lyden, D. VEGFR1-positive haematopoietic bone marrow progenitors initiate the pre-metastatic niche. *Nature* **438**, 820-827 (2005).
- 62 Yang, L., DeBusk, L. M., Fukuda, K., Fingleton, B., Green-Jarvis, B., Shyr, Y., Matrisian, L. M., Carbone, D. P. & Lin, P. C. Expansion of myeloid immune suppressor Gr⁺CD11b⁺ cells in tumor-bearing host directly promotes tumor angiogenesis. *Cancer Cell* **6**, 409-421 (2004).
- 63 Du, R., Lu, K. V., Petritsch, C., Liu, P., Ganss, R., Passegue, E., Song, H., Vandenberg, S., Johnson, R. S., Werb, Z. & Bergers, G. HIF1 α induces the recruitment of bone marrow-derived vascular modulatory cells to regulate tumor angiogenesis and invasion. *Cancer Cell* **13**, 206-220 (2008).
- 64 Ceradini, D. J., Kulkarni, A. R., Callaghan, M. J., Tepper, O. M., Bastidas, N., Kleinman, M. E., Capla, J. M., Galiano, R. D., Levine, J. P. & Gurtner, G. C. Progenitor cell trafficking is regulated by hypoxic gradients through HIF-1 induction of SDF-1. *Nat Med* **10**, 858-864 (2004).
- 65 De Falco, E., Porcelli, D., Torella, A. R., Straino, S., Iachininoto, M. G., Orlandi, A., Truffa, S., Biglioli, P., Napolitano, M., Capogrossi, M. C. & Pesce, M. SDF-1

- involvement in endothelial phenotype and ischemia-induced recruitment of bone marrow progenitor cells. *Blood* **104**, 3472-3482 (2004).
- 66 Petit, I., Jin, D. & Rafii, S. The SDF-1-CXCR4 signaling pathway: a molecular hub modulating neo-angiogenesis. *Trends Immunol* **28**, 299-307 (2007).
- 67 Shaked, Y., Ciarrocchi, A., Franco, M., Lee, C. R., Man, S., Cheung, A. M., Hicklin, D. J., Chaplin, D., Foster, F. S., Benezra, R. & Kerbel, R. S. Therapy-induced acute recruitment of circulating endothelial progenitor cells to tumors. *Science* **313**, 1785-1787 (2006).
- 68 Bergers, G. & Song, S. The role of pericytes in blood-vessel formation and maintenance. *Neuro Oncol* **7**, 452-464 (2005).
- 69 Tong, R. T., Boucher, Y., Kozin, S. V., Winkler, F., Hicklin, D. J. & Jain, R. K. Vascular normalization by vascular endothelial growth factor receptor 2 blockade induces a pressure gradient across the vasculature and improves drug penetration in tumors. *Cancer Res* **64**, 3731-3736 (2004).
- 70 Winkler, F., Kozin, S. V., Tong, R. T., Chae, S. S., Booth, M. F., Garkavtsev, I., Xu, L., Hicklin, D. J., Fukumura, D., di Tomaso, E., Munn, L. L. & Jain, R. K. Kinetics of vascular normalization by VEGFR2 blockade governs brain tumor response to radiation: role of oxygenation, angiotensin-1, and matrix metalloproteinases. *Cancer Cell* **6**, 553-563 (2004).
- 71 Mancuso, M. R., Davis, R., Norberg, S. M., O'Brien, S., Sennino, B., Nakahara, T., Yao, V. J., Inai, T., Brooks, P., Freimark, B., Shalinsky, D. R., Hu-Lowe, D. D. & McDonald, D. M. Rapid vascular regrowth in tumors after reversal of VEGF inhibition. *J Clin Invest* **116**, 2610-2621 (2006).
- 72 Baluk, P., Hashizume, H. & McDonald, D. M. Cellular abnormalities of blood vessels as targets in cancer. *Curr Opin Genet Dev* **15**, 102-111 (2005).
- 73 Bergers, G., Song, S., Meyer-Morse, N., Bergsland, E. & Hanahan, D. Benefits of targeting both pericytes and endothelial cells in the tumor vasculature with kinase inhibitors. *J Clin Invest* **111**, 1287-1295 (2003).
- 74 Orlidge, A. & D'Amore, P. A. Inhibition of capillary endothelial cell growth by pericytes and smooth muscle cells. *J Cell Biol* **105**, 1455-1462 (1987).
- 75 Rubenstein, J. L., Kim, J., Ozawa, T., Zhang, M., Westphal, M., Deen, D. F. & Shuman, M. A. Anti-VEGF antibody treatment of glioblastoma prolongs survival but results in increased vascular cooption. *Neoplasia* **2**, 306-314 (2000).
- 76 Norden, A. D., Young, G. S., Setayesh, K., Muzikansky, A., Klufas, R., Ross, G. L., Ciampa, A. S., Ebbeling, L. G., Levy, B., Drappatz, J., Kesari, S. & Wen, P. Y. Bevacizumab for recurrent malignant gliomas: efficacy, toxicity, and patterns of recurrence. *Neurology* **70**, 779-787 (2008).

- 77 Narayana, A., Kelly, P., Golfinos, J., Parker, E., Johnson, G., Knopp, E., Zagzag, D., Fischer, I., Raza, S., Medabalmi, P., Eagan, P. & Gruber, M. L. Antiangiogenic therapy using bevacizumab in recurrent high-grade glioma: impact on local control and patient survival. *J Neurosurg* **110**, 173-180 (2009).
- 78 Lu, K. V., Chang, J. P., Parachoniak, C. A., Pandika, M. M., Aghi, M. K., Meyronet, D., Isachenko, N., Fouse, S. D., Phillips, J. J., Cheresch, D. A., Park, M. & Bergers, G. VEGF inhibits tumor cell invasion and mesenchymal transition through a MET/VEGFR2 complex. *Cancer Cell* **22**, 21-35 (2012).
- 79 Turchini, J. & Khau Van Kien, L. [Heparin and basophil granulations]. *Montp Med* **41-42**, 967-970 (1952).
- 80 Mc, L. J. The discovery of heparin. *Circulation* **19**, 75-78 (1959).
- 81 Linhardt, R. J. & Gunay, N. S. Production and chemical processing of low molecular weight heparins. *Semin Thromb Hemost* **25 Suppl 3**, 5-16 (1999).
- 82 Lever, R. & Page, C. P. Novel drug development opportunities for heparin. *Nat Rev Drug Discov* **1**, 140-148 (2002).
- 83 Sasisekharan, R., Shriver, Z., Venkataraman, G. & Narayanasami, U. Roles of heparan-sulphate glycosaminoglycans in cancer. *Nat Rev Cancer* **2**, 521-528 (2002).
- 84 Capila, I. & Linhardt, R. J. Heparin-protein interactions. *Angew Chem Int Ed Engl* **41**, 391-412 (2002).
- 85 Gatti, G., Casu, B. & Perlin, A. S. Conformations of the major residues in heparin. H-NMR spectroscopic studies. *Biochem Biophys Res Commun* **85**, 14-20 (1978).
- 86 Chuang, Y. J., Swanson, R., Raja, S. M. & Olson, S. T. Heparin enhances the specificity of antithrombin for thrombin and factor Xa independent of the reactive center loop sequence. Evidence for an exosite determinant of factor Xa specificity in heparin-activated antithrombin. *J Biol Chem* **276**, 14961-14971 (2001).
- 87 Bjork, I. & Lindahl, U. Mechanism of the anticoagulant action of heparin. *Mol Cell Biochem* **48**, 161-182 (1982).
- 88 Lindahl, U., Backstrom, G., Hook, M., Thunberg, L., Fransson, L. A. & Linker, A. Structure of the antithrombin-binding site in heparin. *Proc Natl Acad Sci U S A* **76**, 3198-3202 (1979).
- 89 Jin, L., Abrahams, J. P., Skinner, R., Petitou, M., Pike, R. N. & Carrell, R. W. The anticoagulant activation of antithrombin by heparin. *Proc Natl Acad Sci U S A* **94**, 14683-14688 (1997).
- 90 Petitou, M., Duchaussoy, P., Driguez, P. A., Herault, J. P., Lormeau, J. C. & Herbert, J. M. New synthetic heparin mimetics able to inhibit thrombin and factor Xa. *Bioorg Med Chem Lett* **9**, 1155-1160 (1999).

- 91 Petitou, M., Herault, J. P., Bernat, A., Driguez, P. A., Duchaussoy, P., Lormeau, J. C. & Herbert, J. M. Synthesis of thrombin-inhibiting heparin mimetics without side effects. *Nature* **398**, 417-422 (1999).
- 92 Bara, L., Billaud, E., Kher, A. & Samama, M. Increased anti-Xa bioavailability for a low molecular weight heparin (PK 10169) compared with unfractionated heparin. *Semin Thromb Hemost* **11**, 316-317 (1985).
- 93 Boneu, B., Caranobe, C., Cadroy, Y., Dol, F., Gabaig, A. M., Dupouy, D. & Sie, P. Pharmacokinetic studies of standard unfractionated heparin, and low molecular weight heparins in the rabbit. *Semin Thromb Hemost* **14**, 18-27 (1988).
- 94 Young, E., Prins, M., Levine, M. N. & Hirsh, J. Heparin binding to plasma proteins, an important mechanism for heparin resistance. *Thromb Haemost* **67**, 639-643 (1992).
- 95 Hull, R. D. Treatment of pulmonary embolism: The use of low-molecular-weight heparin in the inpatient and outpatient settings. *Thromb Haemost* **99**, 502-510 (2008).
- 96 Snow, V., Qaseem, A., Barry, P., Hornbake, E. R., Rodnick, J. E., Tobolic, T., Ireland, B., Segal, J. B., Bass, E. B., Weiss, K. B., Green, L., Owens, D. K., American College of, P. & American Academy of Family Physicians Panel on Deep Venous Thrombosis/Pulmonary, E. Management of venous thromboembolism: a clinical practice guideline from the American College of Physicians and the American Academy of Family Physicians. *Ann Intern Med* **146**, 204-210 (2007).
- 97 Mousa, S. A. & Petersen, L. J. Anti-cancer properties of low-molecular-weight heparin: preclinical evidence. *Thromb Haemost* **102**, 258-267 (2009).
- 98 Hull, R. D., Raskob, G. E., Pineo, G. F., Green, D., Trowbridge, A. A., Elliott, C. G., Lerner, R. G., Hall, J., Sparling, T., Brettell, H. R. & et al. Subcutaneous low-molecular-weight heparin compared with continuous intravenous heparin in the treatment of proximal-vein thrombosis. *N Engl J Med* **326**, 975-982 (1992).
- 99 Prandoni, P., Lensing, A. W., Buller, H. R., Carta, M., Cogo, A., Vigo, M., Casara, D., Ruol, A. & ten Cate, J. W. Comparison of subcutaneous low-molecular-weight heparin with intravenous standard heparin in proximal deep-vein thrombosis. *Lancet* **339**, 441-445 (1992).
- 100 Mandala, M., Falanga, A., Piccioli, A., Prandoni, P., Pogliani, E. M., Labianca, R., Barni, S. & working group, A. Venous thromboembolism and cancer: guidelines of the Italian Association of Medical Oncology (AIOM). *Crit Rev Oncol Hematol* **59**, 194-204 (2006).
- 101 Lyman, G. H., Khorana, A. A., Falanga, A., Clarke-Pearson, D., Flowers, C., Jahanzeb, M., Kakkar, A., Kuderer, N. M., Levine, M. N., Liebman, H., Mendelson, D., Raskob, G., Somerfield, M. R., Thodiyil, P., Trent, D., Francis, C. W. &

- American Society of Clinical, O. American Society of Clinical Oncology guideline: recommendations for venous thromboembolism prophylaxis and treatment in patients with cancer. *J Clin Oncol* **25**, 5490-5505 (2007).
- 102 Li, H. L., Ye, K. H., Zhang, H. W., Luo, Y. R., Ren, X. D., Xiong, A. H. & Situ, R. Effect of heparin on apoptosis in human nasopharyngeal carcinoma CNE2 cells. *Cell Res* **11**, 311-315 (2001).
- 103 Berry, D., Lynn, D. M., Sasisekharan, R. & Langer, R. Poly(beta-amino ester)s promote cellular uptake of heparin and cancer cell death. *Chem Biol* **11**, 487-498 (2004).
- 104 Jayson, G. C. & Gallagher, J. T. Heparin oligosaccharides: inhibitors of the biological activity of bFGF on Caco-2 cells. *Br J Cancer* **75**, 9-16 (1997).
- 105 Karti, S. S., Ovali, E., Ozgur, O., Yilmaz, M., Sonmez, M., Ratip, S. & Ozdemir, F. Induction of apoptosis and inhibition of growth of human hepatoma HepG2 cells by heparin. *Hepatogastroenterology* **50**, 1864-1866 (2003).
- 106 Saiki, I., Murata, J., Nakajima, M., Tokura, S. & Azuma, I. Inhibition by sulfated chitin derivatives of invasion through extracellular matrix and enzymatic degradation by metastatic melanoma cells. *Cancer Res* **50**, 3631-3637 (1990).
- 107 Vlodaysky, I., Mohsen, M., Lider, O., Svahn, C. M., Ekre, H. P., Vigoda, M., Ishai-Michaeli, R. & Peretz, T. Inhibition of tumor metastasis by heparanase inhibiting species of heparin. *Invasion Metastasis* **14**, 290-302 (1994).
- 108 Antachopoulos, C. T., Iliopoulos, D. C., Gagos, S., Agapitos, M. V., Karayannacos, P. E., Roboli, S. K. & Skalkas, G. D. In vitro effects of heparin on SW480 tumor cell-matrix interaction. *Anticancer Res* **15**, 1411-1416 (1995).
- 109 Bertozzi, C. R. & Kiessling, L. L. Chemical glycobiology. *Science* **291**, 2357-2364 (2001).
- 110 Folkman, J., Langer, R., Linhardt, R. J., Haudenschild, C. & Taylor, S. Angiogenesis inhibition and tumor regression caused by heparin or a heparin fragment in the presence of cortisone. *Science* **221**, 719-725 (1983).
- 111 Soker, S., Goldstaub, D., Svahn, C. M., Vlodaysky, I., Levi, B. Z. & Neufeld, G. Variations in the size and sulfation of heparin modulate the effect of heparin on the binding of VEGF165 to its receptors. *Biochem Biophys Res Commun* **203**, 1339-1347 (1994).
- 112 Takahashi, H., Ebihara, S., Okazaki, T., Asada, M., Sasaki, H. & Yamaya, M. A comparison of the effects of unfractionated heparin, dalteparin and danaparoid on vascular endothelial growth factor-induced tumour angiogenesis and heparanase activity. *Br J Pharmacol* **146**, 333-343 (2005).

- 113 Smorenburg, S. M. & Van Noorden, C. J. The complex effects of heparins on cancer progression and metastasis in experimental studies. *Pharmacol Rev* **53**, 93-105 (2001).
- 114 Norrby, K. Low-molecular-weight heparins and angiogenesis. *APMIS* **114**, 79-102 (2006).
- 115 Ebos, J. M. & Kerbel, R. S. Antiangiogenic therapy: impact on invasion, disease progression, and metastasis. *Nat Rev Clin Oncol* **8**, 210-221 (2011).
- 116 Ruoslahti, E. & Yamaguchi, Y. Proteoglycans as modulators of growth factor activities. *Cell* **64**, 867-869 (1991).
- 117 Folkman, J. Angiogenesis in cancer, vascular, rheumatoid and other disease. *Nat Med* **1**, 27-31 (1995).
- 118 Colin, S., Jeanny, J. C., Mascarelli, F., Vienet, R., Al-Mahmood, S., Courtois, Y. & Labarre, J. In vivo involvement of heparan sulfate proteoglycan in the bioavailability, internalization, and catabolism of exogenous basic fibroblast growth factor. *Mol Pharmacol* **55**, 74-82 (1999).
- 119 Saksela, O., Moscatelli, D., Sommer, A. & Rifkin, D. B. Endothelial cell-derived heparan sulfate binds basic fibroblast growth factor and protects it from proteolytic degradation. *J Cell Biol* **107**, 743-751 (1988).
- 120 Rusnati, M. & Presta, M. Interaction of angiogenic basic fibroblast growth factor with endothelial cell heparan sulfate proteoglycans. Biological implications in neovascularization. *Int J Clin Lab Res* **26**, 15-23 (1996).
- 121 Spivak-Kroizman, T., Lemmon, M. A., Dikic, I., Ladbury, J. E., Pinchasi, D., Huang, J., Jaye, M., Crumley, G., Schlessinger, J. & Lax, I. Heparin-induced oligomerization of FGF molecules is responsible for FGF receptor dimerization, activation, and cell proliferation. *Cell* **79**, 1015-1024 (1994).
- 122 Mason, I. J. The ins and outs of fibroblast growth factors. *Cell* **78**, 547-552 (1994).
- 123 Tessler, S., Rockwell, P., Hicklin, D., Cohen, T., Levi, B. Z., Witte, L., Lemischka, I. R. & Neufeld, G. Heparin modulates the interaction of VEGF165 with soluble and cell associated flk-1 receptors. *J Biol Chem* **269**, 12456-12461 (1994).
- 124 Schlessinger, J., Lax, I. & Lemmon, M. Regulation of growth factor activation by proteoglycans: what is the role of the low affinity receptors? *Cell* **83**, 357-360 (1995).
- 125 Folkman, J., Klagsbrun, M., Sasse, J., Wadzinski, M., Ingber, D. & Vlodavsky, I. A heparin-binding angiogenic protein--basic fibroblast growth factor--is stored within basement membrane. *Am J Pathol* **130**, 393-400 (1988).
- 126 Vlodavsky, I., Ishai-Michaeli, R., Mohsen, M., Bar-Shavit, R., Catane, R., Ekre, H. P. & Svahn, C. M. Modulation of neovascularization and metastasis by species of heparin. *Adv Exp Med Biol* **313**, 317-327 (1992).

- 127 Norrby, K. & Sorbo, J. Heparin enhances angiogenesis by a systemic mode of action. *Int J Exp Pathol* **73**, 147-155 (1992).
- 128 Norrby, K. Heparin and angiogenesis: a low-molecular-weight fraction inhibits and a high-molecular-weight fraction stimulates angiogenesis systemically. *Haemostasis* **23 Suppl 1**, 141-149 (1993).
- 129 Norrby, K. & Ostergaard, P. Basic-fibroblast-growth-factor-mediated de novo angiogenesis is more effectively suppressed by low-molecular-weight than by high-molecular-weight heparin. *Int J Microcirc Clin Exp* **16**, 8-15 (1996).
- 130 Collen, A., Smorenburg, S. M., Peters, E., Lupu, F., Koolwijk, P., Van Noorden, C. & van Hinsbergh, V. W. Unfractionated and low molecular weight heparin affect fibrin structure and angiogenesis in vitro. *Cancer Res* **60**, 6196-6200 (2000).
- 131 Khorana, A. A., Sahni, A., Altland, O. D. & Francis, C. W. Heparin inhibition of endothelial cell proliferation and organization is dependent on molecular weight. *Arterioscler Thromb Vasc Biol* **23**, 2110-2115 (2003).
- 132 Marchetti, M., Vignoli, A., Russo, L., Balducci, D., Pagnoncelli, M., Barbui, T. & Falanga, A. Endothelial capillary tube formation and cell proliferation induced by tumor cells are affected by low molecular weight heparins and unfractionated heparin. *Thromb Res* **121**, 637-645 (2008).
- 133 Norrby, K. & Ostergaard, P. A 5.0-kD heparin fraction systemically suppresses VEGF165-mediated angiogenesis. *Int J Microcirc Clin Exp* **17**, 314-321 (1997).
- 134 Zhao, W., McCallum, S. A., Xiao, Z., Zhang, F. & Linhardt, R. J. Binding affinities of vascular endothelial growth factor (VEGF) for heparin-derived oligosaccharides. *Biosci Rep* **32**, 71-81 (2012).
- 135 Imai, K. & Takaoka, A. Comparing antibody and small-molecule therapies for cancer. *Nat Rev Cancer* **6**, 714-727 (2006).

Chapter 2

Potentialiation of anti-angiogenic activity of heparin by blocking the ATIII-interacting pentasaccharide unit and increasing net anionic charge

Heparin, a potent anticoagulant agent used for the prevention of venous thromboembolism, has been also recognized to inhibit angiogenesis in tumor. However, its clinical application for cancer therapy is limited due to the anticoagulant activity, which may cause the bleeding-associated adverse effects. The current study shows the structural correlation of LHT7, a heparin-based angiogenesis inhibitor, with enhanced anti-angiogenic activity and decreased anticoagulant activity when compared to LMWH. LHT7 is characterized as having average seven molecules of sodium taurocholates conjugated per one molecule of LMWH. The results showed that the sodium taurocholate conjugation distorted the proper binding of LMWH chain to ATIII, while improving the binding to VEGF. The differential effect of sodium taurocholate conjugation was attributable to its unique structure. The bulky and rigid sterane core of the sodium taurocholate hindered the proper interaction between the specific pentasaccharide unit of LMWH and ATIII. By contrast, the terminal sulfate group generated an additional interaction site on VEGF, thereby improving the binding property. The anti-angiogenic activity of LHT7 was further confirmed *in vivo* using three distinct tumor models that differ in their angiogenic potential. The decreased amount of tumor vasculature in tumor tissue after LHT7 administration was also visualized and quantified.

2.1. Introduction

Angiogenesis is a crucial step in tumor progression by which tumor grows and survives beyond the certain size; on the other hand, tumor that has inadequate blood supply turns necrotic or apoptotic¹. When tumor cells become hypoxic, they secrete pro-angiogenic factors to induce angiogenesis. Among the secreted pro-angiogenic factors, VEGF (now known as VEGF-A) is the key regulator in the initial robust angiogenic responses, affecting survival, migration, proliferation, and differentiation of endothelial cells². Therefore, it has been regarded as the most attractive therapeutic target in the inhibition of tumor angiogenesis, leading to development of several angiogenesis inhibitors that block VEGF signaling pathway. However, these angiogenesis inhibitors failed to produce enduring clinical responses by the occurrence of acquired resistance^{3,4}.

Several adaptive mechanisms of the acquired resistance to the angiogenesis inhibitors have been proposed⁵. Among those, the upregulation of alternative pro-angiogenic factors have been suggested as one of the predominant cause of the resistance. Indeed, overexpression of FGF1, FGF2, PDGF-A, PDGF-B, and other pro-angiogenic factors in refractory tumors after the pharmacological blockade of VEGF signaling pathway was observed in many pre-clinical and clinical studies⁶⁻⁸. In addition, the maturation of tumor vasculatures by pericytes were also suggested to be responsible to the resistance, in which the pericyte coverage protecting the blood vessel from the anti-angiogenic therapy⁹. The experimental studies showed that the tumor vessels with inadequate pericyte coverage were more vulnerable to the depletion of VEGF signaling^{10,11}, and this was further elucidated by the fact that the pericytes stabilize the endothelium in juxtacrine manner by expressing appreciable amount of VEGF and other proteins that are critical in the survival of endothelial cells^{12,13}. For this reason, blockade of multiple angiogenic pathways, especially that are involved in the initial angiogenic response as well as the late-stage of angiogenesis, has been suggested for effective and enduring angiogenesis inhibition⁵.

In this context, heparin is a promising lead compound for developing the broad-spectrum angiogenesis inhibitor. Although heparin is clinically approved for use as a potent anticoagulant agent, its other physiological functions mediated by the capability to regulate various endogenous proteins are demonstrated by a number of studies. The heparin-binding proteins include VEGF, FGF, PDGF, HB-EGF, heparanase, MMPs, and selectins, which are crucially involved in many stages of tumor progression¹⁴⁻¹⁶. However, direct clinical application of heparin in the cancer therapy is limited due to its potent anticoagulant activity and relatively insufficient anticancer activity. Therefore, many efforts have been made to develop heparin-based anticancer agents by various approaches including the use of non-anticoagulant fractions of heparin¹⁷, chemical modification of heparin^{18,19} or synthesizing heparin mimetic by oversulfation of oligosaccharides^{20,21}, which demonstrated applicable efficacy in preclinical models, especially focusing on the inhibition of metastasis and angiogenesis.

In our research group, a series of chemically modified heparin has been previously prepared by conjugating different bile acids including deoxycholic acid, lithocholic acid, and taurocholic acid on the carboxylic groups of heparin as heparin-based anticancer therapeutics; they have been demonstrated to have good anticancer effect *in vivo* with very low anticoagulant activity²²⁻²⁵. Among the prepared bile acid-heparin conjugates, LHT7, which was characterized as average seven molecules of sodium taurocholates conjugated on carboxylic groups of low-molecular weight heparin (LMWH), showed the most potent anticancer and anti-angiogenic activity with negligible anticoagulation activity. A preceded study demonstrated that LHT7 had relatively stronger binding affinity against VEGF when compared to the non-modified LMWH²⁶. The chromogenic factor Xa assay showed a gradual decrease in the anticoagulant activity as more sodium taurocholates were conjugated to LMWH, indicating that the conjugated sodium taurocholate could interfere with LMWH from properly interacting with antithrombin III (ATIII).

In order to provide an insight in designing heparin-based anticancer therapeutics, the structural correlation of the LHT7 to the ATIII and VEGF bindings, which are strongly correlated to the respective anticoagulant and anti-angiogenic activity of LMWH, was carried out. In particular, computerized simulated binding studies were performed to determine the binding configuration of LHT7 to ATIII and VEGF. The binding affinities against VEGF and also the anticoagulant activities of LHT7 and its structural analogs were further evaluated. The *in vivo* tumor growth inhibitory effect of LHT7 on various kinds of carcinomas depending on their degree of angiogenesis was evaluated. In addition, the biodistribution of LHT7 in a tumor xenografted animal model was assessed in both macroscopic and microscopic scale.

2.2. Materials and Methods

2.2.1. Cell lines

A549, HT-29, and MDA-MB-231 cells were obtained from the American Type Culture Collection (ATCC; Manassas, VA). AMC-HN9 cells (head and neck carcinoma) were kindly provided from Asan Medical Center, Korea. The cells were grown in high-glucose DMEM (Gibco, Carlsbad, CA) supplemented with 10% FBS (Gibco). The cells were maintained in a humidified 5% CO₂ atmosphere at 37°C.

2.2.2. Synthesis

LHT7 was synthesized by conjugating LMWH with sodium taurocholate as the follows: To conjugate LMWH with sodium taurocholate, 3-OH of the sodium taurocholate was first converted into primary amine group through several synthetic steps in purpose to react it with the carboxylic group of LMWH. Firstly, sodium taurocholate (500 mg, 0.93 mmol; Sigma-Aldrich, St. Louis, MO) was dissolved in anhydrous DMF (4.6 ml; Sigma-Aldrich) and cooled to 4°C. Then triethylamine (778 µl, 5.58 mmol; Sigma-Aldrich) and 4-NPC (937 mg, 4.65 mmol; Sigma-Aldrich) were added to the solution and reacted for an

hour at 4°C, and 6 hours at room temperature. When the reaction was completed, the solution was diluted with 10 ml of DW and extracted with ethyl acetate (10 ml × 3). The remaining aqueous layer was collected and lyophilized to obtain a yellowish powder of carbonate-taurocholate derivative (NPC-STC). The NPC-STC (500 mg, 0.71 mmol) was dissolved in anhydrous DMF (5 ml), 4-methylmorpholine (157 µl, 1.42 mmol; Sigma-Aldrich) was added to the solution, and stirred for an hour at 50°C. Then the solution was dropped slowly to the solution of excess amount of ethylenediamine (5 ml in 10 ml of anhydrous DMF; Sigma-Aldrich) and reacted for 16 hours at room temperature. When the reaction was completed, the solution was transferred to a 10 volume of acetone to precipitate the product. The precipitate was collect by filtration and dried *in vacuo* to obtain EtSTC as a yellowish powder.

The final product, LHT7, was prepared by conjugating LMWH with the synthesized EtSTC. LMWH (100 mg, 22 µmol; Fraxiparin[®], GlaxoSmithKline, Genval, Belgium) was dissolved in 10 ml of 20 mM acetate buffer (pH 4.5) and *N*-(3-dimethylaminopropyl)-*N*'-ethylcarbodiimide HCl (EDC; 56 mg, 294 µmol; Sigma-Aldrich) was added followed by the addition of *N*-hydroxysuccinimide (NHS; 34 mg, 294 µmol; Sigma-Aldrich) on ice bath, and stirred for 30 min. Then, EtSTC (166 mg, 245 µmol) was added, and the solution was reacted further overnight at room temperature. After reaction was completed, unreacted EDC, NHS, and EtSTC were removed by dialysis (molecular weight cutoff 2,000; dialysis membrane obtained from Spectrum Laboratories, Rancho Dominguez, CA) in DW. The solution in the enclosed membrane was collected and lyophilized to obtain white powder of LHT7.

Cholic acid conjugated LMWH was synthesized as follows: Cholic acid (500 mg, 1.22 mmol; Sigma-Aldrich) and *p*-toluenesulfonic acid monohydrate (4.7 mg, 24.7 µmol; Sigma-Aldrich) was dissolved in methanol (10 ml) and refluxed overnight. The solution concentrated to half of its initial volume and cooled to on ice bath for recrystallization. The solid was collected, washed with methanol, and dried *in vacuo* to obtain methylated cholic acid (MeCA) as yellow solid. The obtained MeCA (200 mg, 473 µmol) was dissolved in

dichloromethane (5 ml) and 4-methylmorpholine (65 μ l, 591 μ mol) was added. The solution was heated to 40°C, and then solution of 4-NPC (130 mg, 645 μ mol) in dichloromethane (5 ml) was added slowly and reacted for 3 hours. The solution was cooled to room temperature and extracted with DW (10 ml \times 3). The organic layer was collected, dried by addition of anhydrous MgSO₄ (Sigma-Aldrich), and filtered. The filtrate was evaporated in reduced pressure to remove all the solvents. Then, ethyl acetate (5 ml) was added to the residue and heated to 60°C until the residue was completely dissolved. The concentrated solution was added to 10 volume of n-hexane to form precipitate. The precipitate was collected by filtration and dried in reduced pressure to obtain NPC-MeCA as a yellow solid. Then, the obtained NPC-MeCA (200 mg, 341 μ mol) was dissolved in dichloromethane (5 ml), and 4-methylmorpholine (56 μ l, 509 μ mol) was added slowly and stirred for an hour. The NPC-MeCA solution was slowly added to a solution of ethylenediamine (1 ml) in dichloromethane (2 ml), and reacted for overnight at room temperature. When the reaction was completed, the solution was extracted with DW (10 ml \times 3) and the organic layer was collected, and evaporated to remove the solvent. The residue was redissolved in ethyl acetate (5 ml) and precipitated in 10 volume of n-hexane. The precipitate was collected, washed with n-hexane, and dried *in vacuo* to obtain Et-MeCA. The obtained Et-MeCA (150 mg, 295 μ mol) was dissolved in mixture of methanol (8 ml) and water (2 ml) containing NaOH (120 mg, 3 mmol), and refluxed for 2 hours. The solution was cooled to room temperature and acidified with equal volume of 1N HCl, and then extracted with ethyl acetate (100 ml \times 3). The organic layer was collected and evaporated. The residue was redissolved in methanol (5 ml) and precipitated in 10 volume of DW. The precipitate was collected by filtration and dried *in vacuo* to obtain EtCA.

LMWH (100 mg, 22 μ mol) was dissolved in formamide (5 ml; Sigma-Aldrich) at 70°C, and cooled on ice bath. EDC (103 mg, 588 μ mol) was added to the LMWH solution followed by addition of NHS (68 mg, 588 μ mol), and reacted for 30 min. To the solution of LMWH, EtCA (226 mg, 457 μ mol) in

anhydrous DMF (5 ml) was added, and reacted overnight at room temperature. After reaction was completed, the solution was concentrated under reduced pressure and precipitated in methanol. The precipitate was collected by filtration and washed three times with methanol, and dried. The obtained solid was dissolved in DW and further purified by dialysis (molecular weight cutoff 2,000) in DW. The solution in the enclosed membrane was collected and lyophilized to obtain white powder of cholic acid conjugated LMWH.

Taurine conjugated LMWH was synthesized as follows: LMWH (100 mg, 22 μmol) was dissolved in 10 ml of 20 mM acetate buffer (pH 4.5) and EDC (56 mg, 294 μmol) was added followed by the addition of NHS (34 mg, 294 μmol) on ice bath, and stirred for 30 min. Then, taurine (30 mg, 245 μmol) was added, and the solution was reacted further overnight at room temperature. After reaction was completed, unreacted EDC, NHS, and taurine were removed by dialysis (molecular weight cutoff 2,000) in DW. The solution in the enclosed membrane was collected and lyophilized to obtain white powder of taurine conjugated LMWH.

2.2.3. Characterization of the synthesized LMWH-derivatives

The synthesized products were subjected to $^1\text{H-NMR}$ (Avance III, Bruker, Billerica, MA) and elemental analysis (Flash1112, Thermo Fischer Scientific, Waltham, MA). The coupling ratio of the conjugated bile acids on the LHT7 and cholic acid conjugated LMWH was determined by using the quantitative detection method for bile acids, which will be detailed below²⁷. The anticoagulant activities of the synthesized products were determined using the chromogenic factor Xa assay (Coatest Heparin; Chromogenix, Milan, Italy) according to the manufacturer's instruction. The content of sulfate in the synthesized substances was also quantified according to the previous article²⁸. The detailed procedure is also described below.

The coupling ratio of the conjugated bile acids was determined as follows: The sample solution was prepared in DW at a concentration of 5 mg/ml. The standard solutions of EtSTC (or EtCA) and LMWH were prepared at a

concentration of 2.937, 3.566, 4.093, 4.539, 4.924 mg/ml and 7.0621, 6.4322, 5.9055, 5.4605, 5.0761 mg/ml, respectively, in DW. The final standard solution was prepared by combining the EtSTC (or EtCA) standard solution (100 µl) and LMWH standard solution (100 µl) in a same order described above. The final concentration of EtSTC (or EtCA) of each standard solution is 0.0734, 0.0892, 0.1023, 0.1135, and 0.1231 mg/ml. Then, 50 µl of standard and sample solutions were transferred to microtubes and diluted to 280 µl with DW, and placed on ice. Pre-chilled sulfuric acid (720 µl) was transferred and incubated 5 min at 80°C. The solutions were then cooled in ice bath and the absorbance was measured at 420 nm. The concentration of the sample was calculated based on the standard curve. The conjugation ratio was calculated according to the following equation:

$$\text{Conjugation ratio} = \frac{[\text{BA concentration}] \times [\text{LMWH molecular weight}]}{(0.25 - [\text{BA concentration}]) \times [\text{BA molecular weight}]}$$

,where BA represents conjugated bile acid.

The sulfate content of the synthesized LMWH derivatives was determined as follows: When barium ion is in complex with rhodizonate ion, the complex shows color. However, when barium ion binds with inorganic sulfate to form BaSO₄ and dissociate from rhodizonate ion, the color disappears. The content of sulfate in glycosaminoglycans including heparin and heparin derivatives can be determined by measuring the intensity of the color from the barium-rhodizonate complex. Firstly, barium buffer was prepared from 2 M acetic acid (5 ml), 0.01 M BaCl₂ (1 ml) and 0.02 M NaHCO₃ (4 ml), which were adjusted to 150 ml with ethanol. Rhodizonate reagent was prepared by dissolving rhodizonate (5 mg) and L-ascorbic acid (100 mg) in 20 ml of DW, and adjusted to 100 ml with ethanol. The standard solution was prepared from 0.01 M sulfuric acid. The sample solution (1 ml, 10 nmol) and 0.1 M NaOH (20 µl) were combined and lyophilized. The dried residues were pyrolyzed by heating for 10 sec, and then dissolved in 0.5 ml of DW. The prepared barium buffer (3 ml) and rhodizonate reagent (1.5 ml) were added, and the solution was agitated. The absorbance of the samples was read at 520 nm.

2.2.4. Surface plasmon resonance (SPR) analysis

Biacore T100 (GE Healthcare, Waukesha, WI) was used for the SPR analysis. The sample analytes, LMWH, LHT7, cholic acid conjugated LMWH, and taurine conjugated LMWH, were prepared at concentrations ranging from 50-1000 ng/ml in HBS-EP buffer (GE Healthcare), which the buffer was also used as a running buffer. Recombinant human VEGF₁₆₅ (Peprotech, Rocky Hill, NJ) was immobilized on a sensor chip CM5 (GE Healthcare) by using EDC/NHS amide coupling method, adjusting the level of immobilization to approach 2,000 RU. The flow rate of the overall analysis was 30 μ l/min, and 50 mM of NaOH was used for regeneration of the chip surface after each cycle of analysis. The experiments were done in triplicate at each concentration. Obtained data were globally fitted and calculated for kinetics by BIAevaluation software (GE healthcare).

2.2.5. Molecular dynamics

For molecular dynamics modeling, the coordinates of VEGF-heparin binding domain (VHBD) and heparin were obtained from the RCSB Protein Data Bank (PDB; www.pdb.org). The coordinates of VHBD were obtained from the NMR structure of amino acids 111-165 from VEGF (PDB code 2VGH). The coordinates of heparin were obtained from the crystal structure of a ternary FGF1-FGFR2-heparin complex (PDB code 1E0O). Sodium taurocholate grafts were added at every 6-carboxylic position of the coordinates of heparin in order to build the structure of LHT7. To generate the initial structures for VHBD-LMWH and VHBD-LHT7 complexes, heparin or LHT7 was positioned near Arg124, Lys140, Arg149 and Arg156. In the case of LHT7, some dihedral angles in the structure were adjusted to avoid atom clashes between VHBD and LHT7. The initial structures for VHBD-LMWH and VHBD-LHT7 complexes were oriented in the orthorhombic simulation boxes. The dimensions of the boxes were calculated by using 10 Å buffer distances between any atom and the simulation box boundary. Each system was solvated in a TIP3P water model²⁹.

Sodium and chloride ions were added to maintain physiological salinity (150 μM) and neutral total charge of the systems. All molecular dynamics simulations were performed using the Desmond program. The OPLS-2005 force field was used for simulations and the energy calculation for trajectories. RESPA time step scheduling was used as the simulation integrator with parameters of 2.0 fs, 2.0 fs and 6.0 fs for bonded forces, non-bonded near forces, and non-bonded far forces, respectively. The Nosé-Hoover thermostat and the Martyna-Tobias-Klein barostat were utilized for the NPT ensemble simulations. Long-range electrostatics was treated by the smooth particle-mesh-Ewald method. The SHAKE algorithm was used to constrain heavy atom-hydrogen bonds. Each system was relaxed before the production run. This relaxation process consisted of a series of minimization and short molecular dynamics simulations. After relaxation, each system was simulated for 50 ns at constant temperature (300 K) and pressure (1 bar). Trajectories were saved every 10 ps for analysis. When the intermolecular energy level had reached the minimum, the corresponding structure was commenced with the Truncated Newton Conjugate Gradient minimization algorithm using the derivative convergence criterion of 0.05 kJ/Å/mol.

2.2.6. Computer simulated molecular docking

To investigate the binding of LMWH and LHT7 on ATIII, the ATII-binding pentasaccharide coordinate was used since it is the critical part among entire heparin chain in the interaction with the heparin-binding site of ATIII. The docking of pentasaccharide was simulated using the AutoDock Lamarckian GA version 4.2³⁰. The coordinates of rigid receptor protein ATIII were obtained for the crystal structure of a dimeric form of intact antithrombin III (PDB code 2ANT)³¹. In the structure of ATIII, all hydrogens were added and Gasteiger charges were assigned³². ATIII has the heparin binding residues including Arg13, Arg47, Arg125, and Arg129³³. A grid, with regular cubes of 50 Å per side, was placed on the map to indicate the heparin-binding site (x.y.z = 2.12.105).

2.2.7. X-ray μ CT angiography

X-ray μ CT for the macroscopic analysis of tumor vasculature was carried out as described elsewhere^{34,35}. The animal models were established in a 6-7 weeks old male C3H/HeN mice (Orient Bio, Seongnam, Korea) by dorsal flank subcutaneous inoculation of 1×10^7 SCC7 cells per mouse and allowed to grow. When the tumor volume reached 50-100 mm³, the mice were randomized into three groups and received normal saline, LMWH (5 mg/kg), or LHT7 (5 mg/kg) via intravenous route every other day for 14 days. After the treatment, the mice received a 50 μ l intraperitoneal injection of heparin prior to sacrificing by CO₂ inhalation. The thoracic cavity was opened and an incision was made on the apex of the heart. A polyethylene tube (i.d. 0.58 mm; o.d. 0.96 mm) was cannulated through the left ventricle and secured in the ascending aorta using surgical suture. Nitroprusside (Sigma-Aldrich) in a normal saline solution (0.1 mM, 30 ml) was perfused at a rate of 0.7 ml/min in purpose to replace the blood and vasodilate. Microfil[®] (Flow Tech, Carver, MA), which is a radiopaque polymer solution, was prepared as instructed by the manufacturer. Then 15 ml of the Microfil[®] solution was perfused at a rate of 0.2 ml/min through the cannulated tube. Microfil[®] perfused into the vasculature was allowed to polymerize at room temperature for 2 h and the tumor was dissected, followed by immersion in 4% PFA. Dissected and fixed tumors were scanned and observed using Skyscan 1076 (Bruker, Kontich, Belgium) X-ray micro-computed tomography system at a voxel resolution of $18 \times 18 \times 18 \mu\text{m}$ with the following scanning parameters: 45 kV, 180 μA , 0.5 mm aluminum filter, 590 ms exposure time and 0.5° rotation step. The vessel volume was measured by generating 3D models of the tumor vasculature reconstructed from the acquired cross-section images by Mimics 13.1 software (Materialise, Leuven, Belgium). The vessel volume divided by the tissue volume was presented as the vessel volume fraction.

2.2.8. Tumor growth suppression

The xenograft animal models of A549, HT-29, and AMC-HN9 were established in 6-7 weeks old male BALB/cSlc-nu mice (Orient Bio) by dorsal flank subcutaneous inoculation of 1×10^7 cells per mouse and allowed to grow. When tumors reached the volume of 150 mm³ for A549, 300 mm³ for HT-29 and 50 mm³ for AMC-HN9 xenografts, mice were randomized into three groups (n = 9) and received one of the followings: normal saline as control; 1 or 5 mg/kg of LHT7 every other day. All experimental and surgical procedures were carried out according to the guidelines of the Institute of Laboratory Animal Resources, Seoul National University (IACUC no. SNU-070822-5).

2.2.9. Histological analysis

The xenograft animal models of A549, HT-29, and AMC-HN9 were prepared as described above. At day 16, tumors were isolated, and prepared as FFPE blocks. The specimens were sectioned in 4 µm thicknesses and immunostained with anti-human CD34 antibody (1:50; Dako, Carpinteria, CA) or anti-human αSMA antibody (1:50; Dako). HRP visualization system (Dako) in combination with DAB was used for detection of the primary antibody. The sections were then counterstained with Hematoxylin. Hematoxylin and Eosin (HE) stained sections were additionally prepared for the AMC-HN9 tumor specimens.

2.2.10. Ex vivo imaging of whole-body distribution

Cy7.5 (Amersham Biosciences, Piscataway, NJ) labeled LHT7 were intravenously administered to MDA-MB-231 xenografted 7-week-old female BALB/cSlc-nu mice (Orient Bio) in a dose of 5 mg/kg. Lateral images for tumors were acquired at 15 min, 1, 4, 8, 12, 18, 24, 36, and 48 h after injection using the eXplore Optix imaging system (GE Medical Systems, Milwaukee, WI). Laser power and count time settings on the instrument were adjusted to 8 µW and 0.3 per point, respectively. Excitation and emission spots were raster-scanned in 1 mm steps.

2.2.11. Immunofluorescence

For the microscopic analysis of the tumor vasculatures, mice received Cy7.5-LHT7 intravenously 6 h prior to heart perfusion with 4% PFA, followed by preparation of 10 μm sections from the tumors. Sections were incubated with rat anti-mouse CD31 antibody (1:20; BD Pharmingen, San Diego, CA) and FITC-conjugated secondary antibody (1:200; Jackson ImmunoResearch Laboratories, West Grove, PA), subsequently. The sections were washed with PBS, and the nuclei of cells were stained with DAPI (1:1000; Invitrogen, Carlsbad, CA). The photomicrographs were acquired under confocal laser scanning microscopy (LSM 510, Carl Zeiss, Thornwood, NY).

2.2.12. Platelet uptake study of fluorescent-labeled LHT7

Human blood was obtained from a healthy volunteer and the blood was stabilized with EDTA immediately after withdrawal. Platelets were prepared from the blood as described elsewhere³⁶. The Prepared platelets were washed twice and resuspended carefully in the glucose HEPES-Tryodes buffer (pH 6.5 during washing, pH 7.3 for resuspension) in the presence of prostacyclin (Sigma-Aldrich) at a final concentration of 10 ng/ml. Platelets (4×10^8 PLTs per ml) were incubated with varying concentrations of FITC-labeled LHT7. The flow cytometry analysis and the immunofluorescence microscopic observation were carried out after complete washing of platelets. For the microscopic observation, the platelets were fixed and permeabilized with 4% PFA (Sigma-Aldrich), followed by 0.1% Triton X-100 (Sigma-Aldrich). The α -granules of the platelets were immunostained with Alexa 647 labeled P-selectin mAb (Biolegend, San Diego, CA). The relative amount of the taken up LHT7 was measured by activating the platelets with 5 IU/ml of thrombin (Sigma-Aldrich) at 37°C. Fluorescence intensity was each measured in the supernatant and the platelet pellets.

2.2.13. Statistical analysis

Data were analyzed using unpaired one-way ANOVA followed by the Dunnett's multiple comparisons test. The GraphPad Prism version 5.01 (GraphPad Software, San Diego, CA) was used for the statistical calculations. *P* value less than 0.05 was considered statistically significant.

2.3. Results

2.3.1. Effects of the conjugated sodium taurocholate between the interaction of LMWH and ATIII determined by computerized docking simulation

Previous study have demonstrated that conjugation of sodium taurocholates on LMWH significantly reduced the anticoagulant activity, indicating attenuation of the interaction between LMWH and ATIII²⁶. The anticoagulant activities of the LMWH-taurocholate conjugates were inversely proportional to the number of the conjugated sodium taurocholate on LMWH, showing gradual decrease of the anticoagulant activity following the increased number of the conjugated sodium taurocholate. The anticoagulant activities were determined by the chromogenic factor Xa assay. This assay determines the anticoagulant activity by quantitatively measuring the amount of remaining factor Xa that did not form complex with ATIII in the presence of heparin³⁷. Considering that appropriate binding of heparin to the ATIII triggers the further complex formation with the factor Xa, the decreased anticoagulant activity as a result of sodium taurocholate conjugation implied that the conjugated sodium taurocholate hindered the proper interaction between the ATIII-binding pentasaccharide unit of LMWH and the heparin-binding site of ATIII.

For deeper understanding of such phenomenon, the binding between ATIII and LHT7 were observed through a computerized docking simulation study using AutoDock Lamarckian GA 4.2 software. Since the specific pentasaccharide unit within the heparin plays the predominant role in the interaction with ATIII, the pentasaccharide coordinate was used in the

simulation as a representative molecule of LMWH. Similarly, the same pentasaccharide coordinate that has two molecules of sodium taurocholate conjugated was used for the representative molecule of LHT7.

The simulation results showed that when LHT7 was docked on the designated area around the heparin-binding moiety of ATIII, which comprises Arg13, Arg47, Arg125, and Arg129³³, it did not preferentially bind to the heparin-binding moiety, but rather stabilized on the other location. By contrast, LMWH was properly stabilized on the heparin-binding moiety (**Fig. 2.1A**). The energy transitions that occurred during the binding of LMWH and LHT7 on the ATIII were -1.39 and 7.48 kcal/mol, respectively, indicating relatively more unstable binding of LHT7 to ATIII when compared to that of LMWH: this ultimately led to the decreased anticoagulant activity in LHT7.

2.3.2. Anticoagulant activities of LHT7 and its structural analogs

The results were further supported by the comparison of the anticoagulant activities of the LHT7 and its structural analogs. Since the conjugated sodium taurocholate was considered to be entirely responsible to the altered activities of LHT7, the analogous compounds were prepared by conjugating each of the distinguishing compartment of this molecule – cholic acid and taurine – to LMWH (**1**), thereby producing two distinct LHT7 (**4**) analogs, cholic acid conjugated LMWH (**2**) and taurine conjugated LMWH (**3**), respectively (**Fig. 2.1B**). The rationale of separating the compartment of the sodium taurocholate to cholic acid and taurine is from the idea that the significant characteristics of the sodium taurocholate are the steroidal structure (also called as sterane core) and the strong anionic charge from the sulfate group. The prepared cholic acid conjugated LMWH shares the identical sterane core, and the taurine conjugated LMWH has the same overall charge density with LHT7. Therefore, the comparison of the LHT7 analogs and the LHT7 as well as the LMWH could provide important information in which compartment of the conjugated sodium taurocholate contributed to the altered biological activities.

Similar to LHT7, cholic acid conjugated LMWH showed very low anticoagulant activity; however, taurine conjugated LMWH showed only slight decrease of the activity (**Table 2.1**). As mentioned above, the LHT7 and the cholic acid conjugated LMWH share the same sterane core in their conjugated bile acid moieties. This clearly suggested that the sterane core of the conjugated sodium taurocholate, which has rigid and bulky chemical structure, is mainly responsible to the improper binding of the pentasaccharide unit in the LHT7 to the heparin-binding moiety of ATIII through steric hindrance.

2.3.3. Effects of the conjugated sodium taurocholate between the interaction of LMWH and VEGF determined by computerized molecular dynamics

Preceding study has demonstrated that conjugation of sodium taurocholates on LMWH significantly increased binding affinity against VEGF₁₆₅ (hereafter, VEGF)²⁶. A computerized molecular dynamics simulation was carried out to thoroughly investigate the configuration when LHT7 is bound to VEGF. Intermolecular potential energy, defined as a sum of van der Waals and electrostatic interaction energies, was calculated during the binding simulation between VEGF-heparin binding domain (VHBD) and LMWH or LHT7. The final results showed that VHBD-LHT7 complex had a significantly lower energy state (-2,228 kcal/mol) than that shown in VHBD-LMWH complex (-1,865 kcal/mol) in their respective lowest intermolecular potential energy states. The more stable complex formation of LHT7 than LMWH with the VHBD indicated a stronger binding of LHT7 to the VHBD. The structure that was obtained at the lowest intermolecular energy states of VHBD-LHT7 complex was used as the model structure to describe the origin of the stable intermolecular interactions. Earlier studies have demonstrated that Arg123, Arg124, Arg149, and Arg159 of VHBD are the major amino acid residues that interact with the heparin^{38,39}. The model structure of the VHBD-LHT7 complex showed that the main chain of LHT7, corresponding to the LMWH polysaccharide, was located near the cluster of the arginine residues that were mentioned above (**Fig. 2.1C**). Intriguingly, this model structure showed two

additional binding residues on the VHBD that are interacting with the conjugated sodium taurocholate moieties of LHT7: the additional electrostatic interactions occurred between the terminal sulfate groups of the two conjugated sodium taurocholate moieties and the two arginine residues of VHBD, which are Arg112 and Arg165; however, such interactions were not found in the VHBD-LMWH complex. These results suggested that the additional favorable interactions between the terminal sulfate groups of the conjugated sodium taurocholate moieties of LHT7 and the VHBD would have led to the reduction of the intermolecular potential energy, thus further stabilizing the complex structure.

2.3.4. VEGF binding affinities of LHT7 and its structural analogs

The basis of the enhanced binding of LHT7 to VEGF was further evaluated by comparing the VEGF binding affinities of LMWH, LHT7, and the LHT7 structural analogs – cholic acid conjugated and taurine conjugated LMWH (**Fig. 2.1B**) – that were determined using SPR analysis (**Table 2.1**). The result showed that binding affinities of the cholic acid conjugated LMWH ($K_D = 22.4 \mu\text{M}$), which shares an identical sterane core with LHT7 but lacks the terminal sulfate groups, and the LMWH ($K_D = 39.3 \mu\text{M}$) to VEGF were almost similar. This indicated that the sterane core had no contribution to the increased binding affinity of LHT7. By contrast, the taurine conjugated LMWH ($K_D = 2.37 \mu\text{M}$) showed about ten-fold higher binding affinity to VEGF when compared to that of the LMWH and the cholic acid conjugated LMWH, reflecting the importance of the overall degree of sulfation in the interaction with VEGF. However, despite the similar degree of sulfation of the taurine conjugated LMWH to LHT7, the taurine conjugated LMWH showed lower binding affinity than the LHT7 ($K_D = 0.21 \mu\text{M}$). This implied the existence of other potential factor that is contributing to the enhanced binding of LHT7 to VEGF. Considering the VHBD-LHT7 complex model shown in the molecular dynamic simulation, this result strongly substantiate the notion that having a certain distance between the additional sulfate groups and the heparin core chain is critical in developing

new interactions between of LHT7 with VEGF that are significant for the increased binding affinity.

2.3.5. Effect of LHT7 on tumor angiogenesis in vivo

Degree of angiogenesis inside the grafted tumor tissue was directly visualized and quantified by using X-ray μ CT (**Fig. 2.2A**). The SCC7-grafted animal model was prepared and received one of the saline, LMWH, and LHT7 for two weeks every other day at a dose of 5 mg/kg. Then, the animals were sacrificed and blood was replaced with radiopaque polymer solution via heart perfusion. The tumors, which contain polymerized radiopaque material inside their blood vessels, were isolated and subjected to the X-ray μ CT. The mean blood vessel volume of the LHT7-treated group was 41.65 mm³, while control and LMWH-treated group were 1116.98 mm³ and 446.34 mm³, respectively. This was 96.4% and 80.8% decrease for LHT7-treated group when compared to the control and the LMWH-treated group, respectively (**Fig. 2.2B**).

Since the absolute volume of the total blood vessels is largely dependent to the size of the tumor, density of the blood vessel within the tumor tissue was also calculated. The mean blood vessel volume fraction was calculated by dividing the mean blood vessel volume by the mean tumor tissue volume. The mean vessel fraction of the LHT7-treated group was 6.03%, while the control and the LMWH-treated group were 24.53% and 15.68%, respectively. This was 75.5% and 61.8% decrease of the blood vessel density in LHT7-treated group when compared to the control and the LMWH-treated group, respectively (**Fig. 2.2B**). This result clearly showed the inhibition of neovascularization in the tumors when the animals were treated with LHT7. Moreover, it showed that LHT7 had superior anti-angiogenic activity than LMWH, agreeing with the result that demonstrated higher binding affinity of LHT7 to VEGF than that of LMWH.

2.3.6. Anticancer effects of LHT7 on distinct types of carcinoma xenografts

The therapeutic potential of LHT7 in tumor growth was evaluated on three distinct types of carcinomas, A549, HT-29, and AMC-HN9, which differ in their angiogenic property. When compared to the control, LHT7 showed marked suppression of A549 and HT-29 tumor growth: a dosage of 1 mg/kg of LHT7 inhibited cancer growth by 35% and 48%, respectively; and a dosage of 5 mg/kg of LHT7 inhibited the growth by 9% and 31%, respectively (**Fig. 2.3A and B**). The histological assessments of the tumor types responding to LHT7, which are A549 and HT-29 in particular, showed significant amount of endothelium and smooth muscle cells exist within the tissue represented by the immunostaining of CD34 and α SMA, respectively (**Fig. 2.3C**). This indicated an active formation of vasculatures in those tumors.

On the other hand, the histological assessment of the AMC-HN9 tumor, which did not respond to LHT7 in any of the tested doses (**Fig. 2.4A**), showed few immunostained CD34 and α SMA in the tissue (**Fig. 2.4B**), indicating very weak angiogenic capability of the AMC-HN9 tumor. However, despite the absence of typical blood vessels in the AMC-HN9 tumor, substantial number of red blood cells was found in the extracellular space of the sectioned tissue (**Fig. 2.4C**). This implied that the growth of the AMC-HN9 tumor is independent to conventional angiogenesis, but rather relies on the formation of abnormal blood flow channels, which the phenomenon is termed as vascular mimicry.

These results showed that the distinct types of carcinomas displayed different susceptibility to LHT7 depending on the angiogenic activity of the tumor. The angiogenic tumors, which are A549 and HT-29, were very sensitive to LHT7. By contrast, non-angiogenic tumor, which is AMC-HN9, was insensitive to that. This manifested that LHT7 shows its anticancer effect through its ability to suppress tumor angiogenesis *in vivo*.

2.3.7. Intratumor localization of LHT7

The whole-body distribution of LHT7 was determined by an *ex vivo* observation on MDA-MB-231 xenograft animal models after intravenous administration of fluorescent-labeled LHT7 via tail vein (**Fig. 2.5A**). When the animal was observed after an hour of the administration, LHT7 was distributed to the every part of the body by blood circulation. However, when observed after four hours, the drug was mainly observed in the tumor site in high concentration, which the measured intensity was almost similar to that observed at one-hour time point, and the was eliminated in the other body parts. The LHT7 observed in the site other than the tumor was almost eliminated at 24 hours of post-administration. The selective accumulation of LHT7 in the tumor lasted for at least 48 hours.

To determine more specific site of the LHT7 localization inside the tumor, the tumor tissue was sectioned and immunostained for microscopic observations (**Fig. 2.5B**). The animals received fluorescent-labeled LHT7 by intravenous route in advance of tissue sectioning, followed by the immunostaining of CD31 to distinguish the endothelium of the tumor vasculatures. The observations showed that the LHT7 was mainly located in the tumor vasculatures rather than in the extravascular extracellular space of tumor tissue. These results collectively suggest the existence of certain driving force that mediates LHT7 to be selectively accumulated in the tumor vasculatures.

2.3.8. LHT7 uptake by platelets

Human platelets were incubated with fluorescent-labeled LHT7 at varying concentrations ranging up to 20 $\mu\text{g/ml}$ in order to investigate whether LHT7 could be taken up by platelets.

The flow cytometry analysis showed that the LHT7 was taken up into the platelets in a dose-dependent manner as shown by the right shift of the histogram following the increased concentration of the treated LHT7 (**Fig.**

2.6A). However, this result did not clearly showed whether the LHT7 was taken up inside the granules of platelet or simply bound on the surface.

To determine whether LHT7 was bound on the surface or taken up inside the platelets, the platelets that were incubated with the fluorescent-labeled LHT7 in varying concentrations were further activated with thrombin. The activated platelets could be separated into two compartments by centrifugation: the granular substances remain in the supernatant, and the membrane and membrane bound substances are collected as a pellet. After activation of the platelets, fluorescent-labeled LHT7 was completely released out to the supernatant and not remained on the platelet pellets. This clearly indicated that the LHT7 was taken up by platelets in a dose-dependent manner rather than adhering on the surface (**Fig. 2.6B**).

The immunocytochemical observation of the platelets further supported the uptake of LHT7 in their granules. When the platelets were incubated with the fluorescent-labeled LHT7 and immunostained with P-selectin antibody, the platelets showed a double staining pattern, in which the fluorescent-labeled LHT7 (green) was surrounded by the stained P-selectin (red) marking the boundary of the α -granule (**Fig. 2.6C**). This result further supported the observation that LHT7 was taken up into the platelet, especially inside the α -granules.

Table 2.1. Characteristics of LHT7 and its analogs

	LMWH	Cholic acid conjugated LMWH	Taurine conjugated LMWH	LHT7
Anti-FXa (%)	100	1.95 ± 0.56	86.61 ± 5.14	4.18 ± 1.47
K _D (μM)	39.3 ± 3.7	22.4 ± 2.9	2.37 ± 0.40	0.21 ± 0.06

Data expressed as means ± s.d.

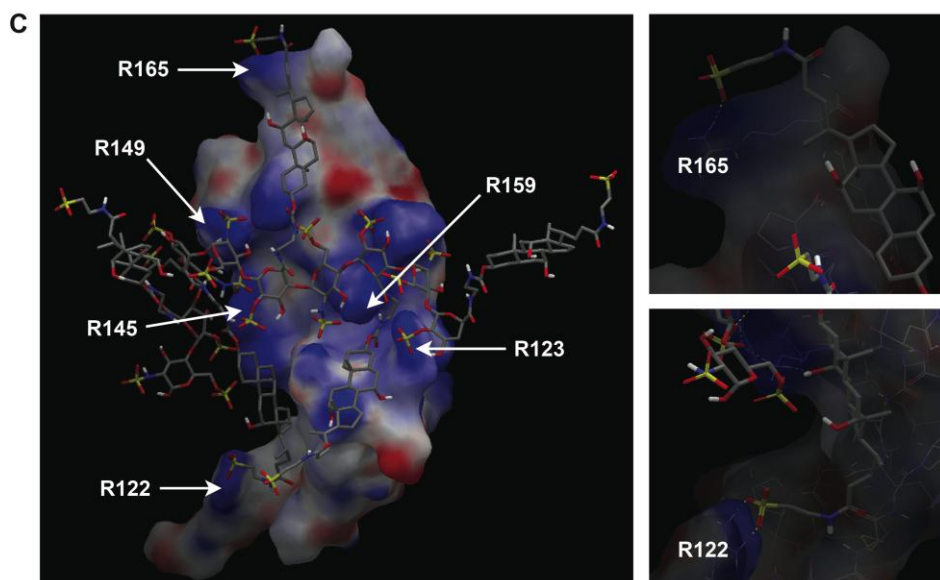
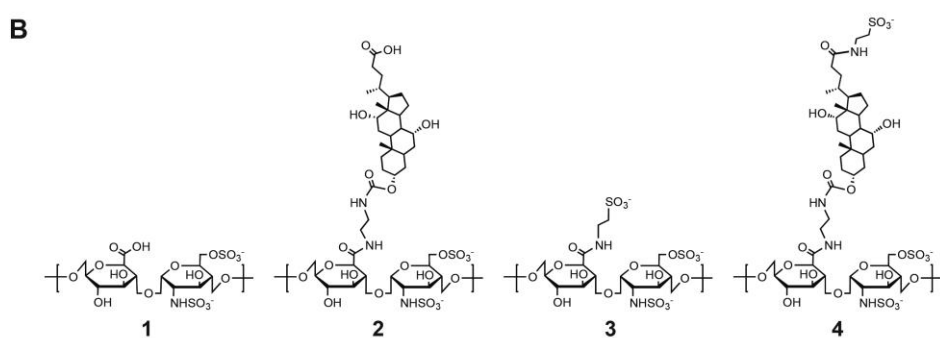
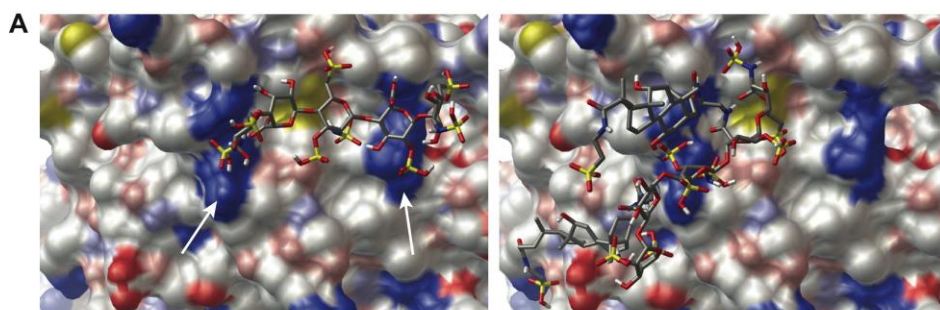


Figure 2.1. (A) Computerized molecular docking of LMWH (left) and LHT7 (right) on the ATIII heparin binding site (arrow). The pairs were allowed to reach the minimum intermolecular energy level and the final appearances were examined. (B) Representative chemical structures of LMWH **1**, cholic acid conjugated LMWH **2**, taurine conjugated LMWH **3**, and LHT7 **4**. (C) The model structure of LHT7 and VEGF-HBD complex when the intermolecular energy level has reached the minimum during molecular dynamics.

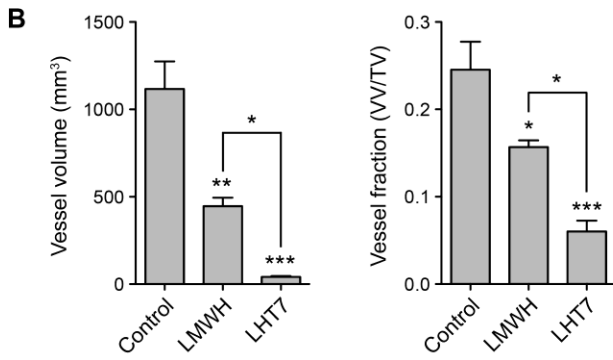
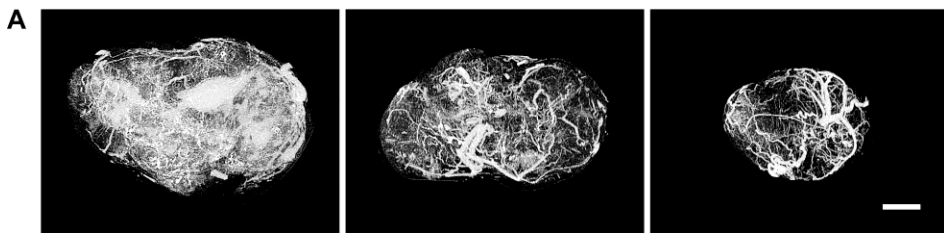


Figure 2.2. (A) Representative images of saline (control), LMWH, and LHT7 treated SCC7 tumors obtained by X-ray μ CT. Scale bar, 5 mm. (B) Tumor vessel volumes (left) and vessel fractions (right) calculated through reconstruction of vasculatures followed by computed calculation of the volumes. $*P < 0.05$, $**P < 0.005$, and $***P < 0.001$ versus control. Data are expressed as mean \pm s.e.m.

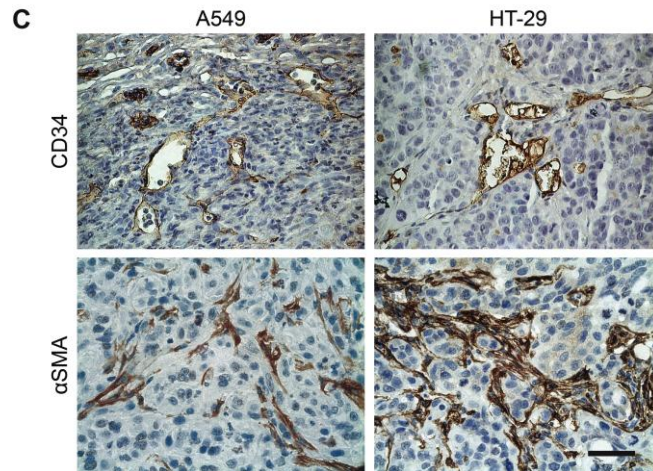
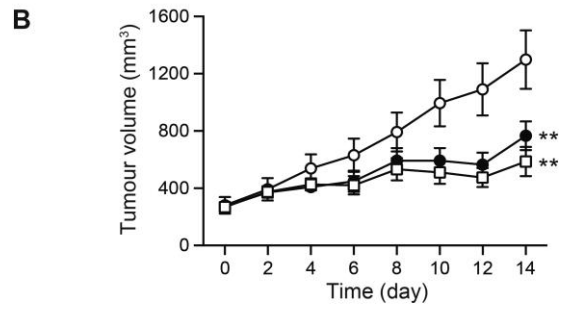
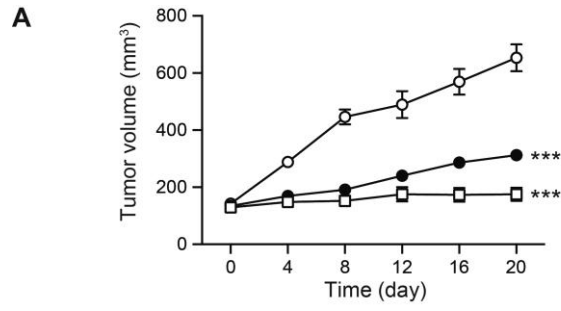


Figure 2.3. Tumor growth suppression on A549 (A) and HT-29 (B) xenografts. The three groups received either saline as control (○) or LHT7 in two different doses: 1 mg/kg (●) and 5 mg/kg (□) administered intravenously every other day. n = 9. Data presented as mean ± s.e.m. (C) Histological analysis of A549 (left) and HT-29 (right) tumor sections. Immunostaining of the upper and lower panels indicates CD34 and αSMA, respectively. Scale bar, 50 μm.

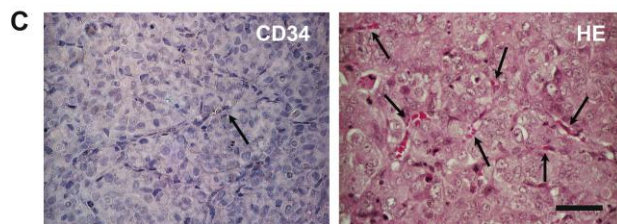
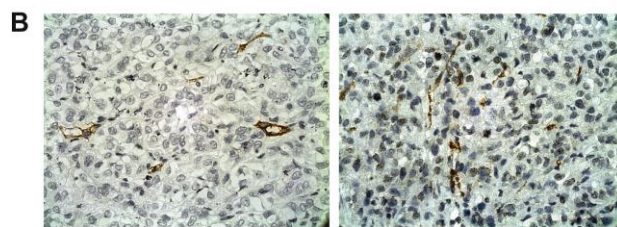
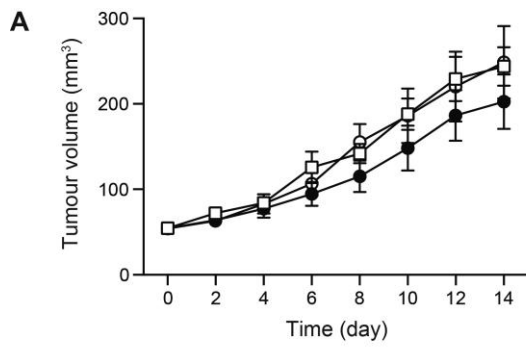


Figure 2.4. (A) Tumor growth suppression of AMC-HN9 xenografts. Mice received either saline as control (○) or LHT7 in different doses: 1 mg/kg (●) and 5 mg/kg (□) administered every other day. n = 9. (B) Histological analysis of AMC-HN9 tumor sections. Immunostaining of the left and right panels indicates CD34 and α SMA, respectively. Scale bar, 50 μ m. (C) CD34 (left) and HE (right) staining of the tumor specimens. Arrows depict a subset of red blood cells. Scale bar, 50 μ m.

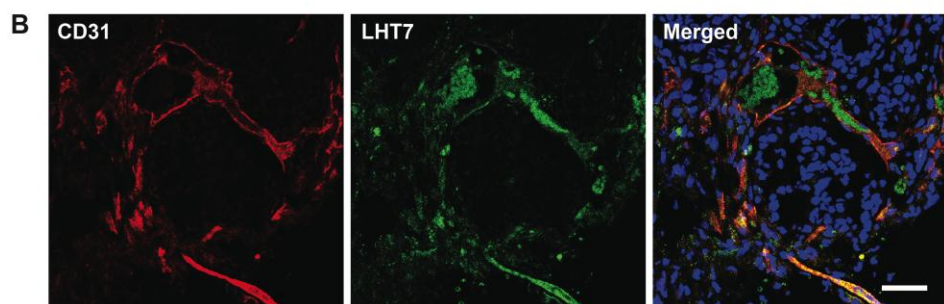
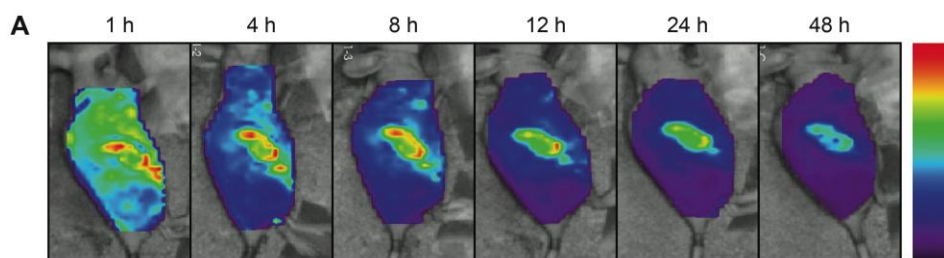


Figure 2.5. (A) *Ex vivo* biodistribution observations of the fluorescent-labeled LHT7 after intravenous administration in mice. (B) Immunostaining of tumor specimens at post-administration of LHT7. Red and green color represents CD31 and LHT7, respectively. Scale bar, 50 μm .

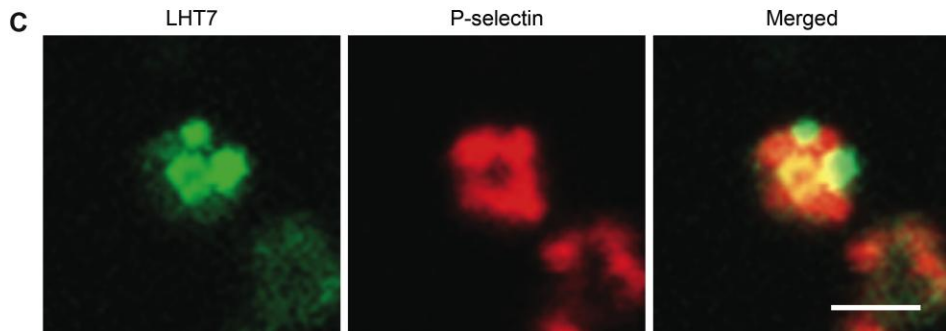
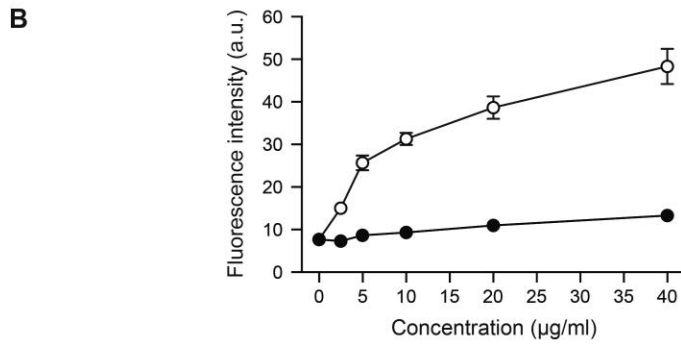
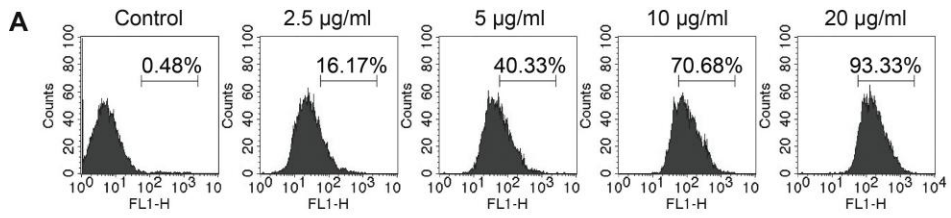


Figure 2.6. (A) FACS analysis of platelets that have taken up LHT7 after incubation with a series of concentrations of fluorescent-labeled LHT7. Numbers represent the gated percentage in the assigned range. (B) Quantitative analysis of released (○) and bound (●) LHT7 on the pellet of the platelets after activation of platelets incubated with fluorescent-labeled LHT7. Data are expressed as means \pm s.d. (C) Immunocytochemical staining of platelets incubated with fluorescent-labeled LHT7. Green and red represents LHT7 and P-selectin in α -granules of platelets, respectively. Scale bar, 2 μ m.

2.4. Discussion

The preceded study of LHT7 showed that the conjugation of sodium taurocholate on LMWH resulted in decreased anticoagulant activity and increased anti-angiogenic effect, particularly showing increased binding affinity to VEGF²⁶. It was questioned how such chemical modification of LMWH altered the two distinct biological activities – anticoagulant and anti-angiogenic activity – in differential manner at the same time. To address this question, the binding properties of LHT7 to ATIII and VEGF were determined using various approaches.

The interaction of heparin with ATIII, which is the main principle of the anticoagulant activity of LMWH, is mediated by a specific non-variable pentasaccharide sequence within the heparin^{40,41}. On the other hand, the interaction with many other proteins including the diverse range of the pro-angiogenic factors is mediated through electrostatic attractions via polyanionic dispersion from the sulfate groups⁴¹. In particular, it was reported that the interaction of heparin with VEGF strongly depends on the *N*- and 6-*O*-sulfation, and with FGF depends on the 2-*O*-sulfation of the heparin polysaccharide chain⁴². The specific pentasaccharide unit that plays crucial role in the interaction with ATIII was demonstrated not to be important in the interaction with VEGF⁴³. The distinct binding mechanisms of heparin on ATIII and VEGF eventually allowed the sodium taurocholate conjugation to act in differential manner as would be discussed in detail further.

The preceding study have demonstrated that the conjugation of sodium taurocholate on LMWH gradually decreased its anticoagulant activity following the increasing number of conjugated sodium taurocholate²⁶. The anticoagulant activities were determined using chromogenic factor Xa assay³⁷. The principle of this assay is as the followings: a functional heparin binds to and induces conformational change of ATIII; then the activated ATIII further forms a complex with factor Xa; the chromogenic substrate of factor Xa reacts with the remaining unbound factor Xa and allows the colorimetric quantification.

Therefore, the results obtained by using this methodology indirectly show whether the heparin (or heparin derivative) was properly bound to the ATIII, which triggers the conformational change and further binding with factor Xa.

According to the principle of the chromogenic factor Xa assay, it was hypothesized that the conjugated sodium taurocholates in LHT7 interfered the proper binding of the specific non-variable pentasaccharide sequence of the comprised LMWH chain to the ATIII, which eventually led to the decreased anti-factor Xa activity. The computerized simulation results showed that the transient energy, when designated to bind to the heparin-binding site of ATIII, was notably higher for LHT7 than that for LMWH. As a result, LHT7 preferred binding on the location other than the defined heparin-binding site of ATIII, while LMWH preferred binding on the heparin-binding site. This indicated that conjugation of sodium taurocholates on LMWH impeded its proper binding on the heparin-binding site of ATIII; therefore, did not induce an appropriate conformational change of ATIII that is required for the inhibition of factor Xa activity. This was further supported by the varying anti-factor Xa activities of LHT7 and its structural analogs. The cholic acid conjugated LMWH, which the conjugated cholic acid share the identical steroidal structure with the sodium taurocholate in LHT7, showed very low anti-factor Xa activity similar to LHT7. By contrast, taurine conjugated LMWH showed only slightly reduced anti-factor Xa activity when compared to LHT7. These results indicated that the steroidal structure of the conjugated sodium taurocholate played the key role in impeding the proper binding of the pentasaccharide unit to the heparin-binding site of the ATIII. Considering that the steroidal structure is relatively bulky and rigid, this would have generated steric hindrance that veils the non-variable pentasaccharide sequence of LMWH to contact with the heparin-binding site of the ATIII, ultimately leading to the decreased anticoagulant activity.

On the other hand, LHT7 showed stronger anticancer and anti-angiogenic activity when compared to the non-modified LMWH. This was demonstrated to be partly due to the increased binding affinity against VEGF when sodium taurocholates were conjugated on LMWH in the preceding study²⁶. In the

current study, it was investigated more thoroughly how the conjugated sodium taurocholate moieties on LMWH could actually enhanced the binding affinity against VEGF rather than interfering with it as observed in the binding against ATIII. Two distinct experiments were performed: *in silico* molecular dynamics modeling of binding between the LHT7 and the VEGF-heparin binding domain (VHBD), and the SPR binding analysis of LHT7 and the structural analogs of LHT7 with VEGF. The *in silico* molecular dynamics modeling showed that when the intermolecular potential energy reached the minimum during the dynamic interaction between LHT7 and VHBD, two distinct arginine residues on the VHBD – Arg122 and Arg165 – strongly interacted with terminal sulfate group of the conjugated sodium taurocholate moieties, while the core heparin chain of the LHT7 was properly located on the heparin-binding site of VHBD, still interacting with the four arginine residues that are known to have significant role in binding with heparin – Arg123, Arg124, Arg149, and Arg159^{38,39}. This suggested that the additional interactions with Arg122 and Arg165 on the VHBD produced by the sodium taurocholate moieties have potentially contributed to the more stabilized binding of LHT7 to VEGF, resulting in the improved anti-angiogenic activity when compared to that of the LMWH.

The SPR binding studies with LHT7 and its structural analogs further manifested the role of the conjugated sodium taurocholate in the improved binding affinity to VEGF. The conjugated sodium taurocholate was defined as a molecule comprising a steroidal structure and a strong anionic charge originated from the sulfate group; its structure was separated into cholic acid and taurine, each of which was chemically conjugated to LMWH to produce cholic acid conjugated LMWH and taurine conjugated LMWH, respectively. The results showed that cholic acid conjugated LMWH had no improvement in the binding affinity compared to the native LMWH, implying that steroidal structure of the conjugated sodium taurocholate itself did not have any directly positive effect on improving the binding of LMWH on VEGF. On the other hand, taurine conjugated LMWH showed increased binding affinity, implying that the

increased number of sulfate groups, which resulted in the increased amount of net negative charge on the molecule, positively affected the binding affinity of the LMWH towards VEGF. The influence of the degree of sulfation on heparin on binding with proteins including VEGF was already well demonstrated in the previous reports⁴².

However, the taurine conjugated LMWH still had lower binding affinity on VEGF than that of LHT7 despite the identical overall anionic charge density, which implied the existence of other underlying factors contributing to the enhanced VEGF binding. According to the result obtained by *in silico* molecular dynamics modeling, there were two additional arginine residues – Arg112 and Arg165 – participating in the interaction between LHT7 and VEGF that were not found in the interaction between LMWH and VEGF. These two residues were interacting with the sulfate groups of the taurocholate moiety rather than the heparin chain and were located far apart from the typical heparin binding residues, the cluster of Arg123, Arg124, Arg149 and Arg159, within the VHBD. The distance between the traditional heparin binding residues and the newly generated binding residues in the VHBD corresponds to the length of the sterane core of the sodium taurocholate.

On the other hand, since taurine is a very small and short molecule, the taurine conjugated LMWH has the additional sulfate groups originating from the conjugated taurine molecules near the other pre-existing sulfate groups of LMWH. Therefore, although the conjugated taurines increased the net anionic charge of the molecule and contributed to the increased binding affinity towards VEGF, their sulfate groups are likely to compete with the pre-existing sulfate groups of the heparin core chain in the interaction with the cluster of the arginine residues in the VHBD heparin-binding site. Therefore, the electrostatic attraction of the individual sulfate groups to the heparin-binding arginine residues of VHBD would be attenuated. In contrast, additional sulfate groups of LHT7 on the terminal end of the conjugated sodium taurocholate could retain their entire potential of electrical attraction because they are located in distance from the sulfate groups of the core heparin chain, thereby free from the

competition. According to the result obtained from the SPR binding study of the cholic acid conjugated LMWH, the sterane core of the conjugated sodium taurocholate solely had no direct effect in enhancing the binding strength of LHT7 on VEGF. Rather, it indirectly affected the binding by efficiently delivering the additional sulfate groups to the distant location from the general heparin-binding site of VHBD through its rigid chemical structure, resulting in highly improved VEGF binding than merely increasing the degree of sulfation.

As mentioned earlier, the binding of heparin on ATIII depends on a specific pentasaccharide unit of the polysaccharide chain, while the binding on other proteins including VEGF mainly depends on the polyanionic charge dispersion and does not require any specific sequence⁴⁴. The distinct binding characteristics of heparin on two different proteins, ATIII and VEGF, allowed the differential effect of sodium taurocholate conjugation. The conjugation of sodium taurocholate on LMWH blocked the proper binding to ATIII by concealing the ATIII-binding pentasaccharide unit by its bulky steroidal structure, whereas it improved the binding to VEGF by adding fully functional electrostatic interactions via the sulfate group.

The therapeutic implication of the VEGF binding of LHT7 was evaluated *in vivo* through direct observation of intratumor angiogenesis and tumor growth of distinct types of carcinomas that differ in their degree of angiogenic potential when treated with LHT7. The results showed significant reduction in both absolute intratumor blood vessel volume and vessel density in the tumor tissue when the animal model was treated with LHT7. This indicated that the suppression of tumor growth when treated with LHT7 was mainly caused by the inhibition of tumor angiogenesis rather than any possible direct cytotoxic effect to the tumor cells. The anti-angiogenic effect of LHT7 is considered to be the consequence of VEGF signaling pathway blockade. In addition, the fact that only the tumors that are strongly angiogenic responded to the LHT7 treatment further supported that anti-angiogenic activity including the blockade of VEGF signaling pathway is the main mechanism of action in the *in vivo* anticancer effect of the LHT7.

It was also found that LHT7 was selectively localized in the tumor, especially accumulated inside the tumor blood vessels for more than 48 hours. This phenomenon is interesting because accumulation of therapeutic molecules specifically to a pathological site could increase the therapeutic potential with fewer side effects. Therefore, the tumor accumulation of LHT7 was considered to be another important factor contributing to its potent anticancer effect examined in various types of xenograft animal models.

Although the reason for the selective intratumor accumulation of LHT7 is not completely understood so far, the uptake by platelets shown in the experimental results was suggested to be one of the important factor contributing to the phenomenon. Verheul et al. have demonstrated that platelets can take up and store bevacizumab, trastuzumab, and cetuximab in their granules apparently in a non-specific manner⁴⁵. LHT7 may have been taken up by platelets into their granules in a similar manner. Platelets are generally activated in the tumor tissue to release granular contents since tumor is regarded as a persistent wound⁴⁶. The platelets are also well recognized to release substantial amount of VEGF and other pro-angiogenic factors to promote angiogenesis⁴⁷. Thus, the platelets could act as the vehicles that could continuously deliver LHT7 to the tumor after taking up the molecules inside their granules. This would eventually increase the local concentration of LHT7 within the tumor tissue. Moreover, LHT7 could bind and neutralize the VEGF either inside the platelet granule or at the site of the release, thereby more efficiently blocking the VEGF that was supposed to act in the tumor tissue.

Another factor to be considered in the tumor accumulation of LHT7 is the presence of overexpressed integrins in the tumor tissue. Heparin is capable in binding with a diverse range of integrins including P-selectin, L-selectin, PECAM-1, and MAC-1, which are generally expressed on activated endothelial and inflammatory cells¹⁵. These integrins are also upregulated in the tumor, managing many crucial steps of tumor progression⁴⁸. Hence, LHT7, which is originated from heparin, may bind with integrins expressed on the tumor

endothelium. However, integrin-binding capability of LHT7 remains to be elucidated in the further studies.

2.5. Conclusion

The findings in this study suggest that appropriate modification of heparin could potentiate its intrinsic property of suppressing angiogenesis while eliminating anticoagulant activity at the same time. Current study suggest that such modifications could be accomplished by blocking the ATIII-interacting pentasaccharide unit of heparin by a bulky molecule, in this case, the sterane core, to inhibit the binding on ATIII, and increasing the net anionic charge by adding more sulfate groups that could enhance binding to VEGF. Interestingly, it was also shown that not only the quantitative amount of the anionic charge density is important but also the charge distribution within the molecules is crucial for enhanced binding to the VEGF. The heparin-based anti-angiogenic agent, LHT7, had sodium taurocholates conjugated on the LMWH. The conjugated sodium taurocholate satisfied the properties that are required for the above-mentioned appropriate modification for the ideal alteration of heparin activity. As a result, LHT7 showed excellent anticancer and anti-angiogenic effect with no noticeable anticoagulant activity.

References

- 1 Hanahan, D. & Weinberg, R. A. The hallmarks of cancer. *Cell* **100**, 57-70 (2000).
- 2 Ferrara, N., Hillan, K. J., Gerber, H. P. & Novotny, W. Discovery and development of bevacizumab, an anti-VEGF antibody for treating cancer. *Nat Rev Drug Discov* **3**, 391-400 (2004).
- 3 Saltz, L. B., Lenz, H. J., Kindler, H. L., Hochster, H. S., Wadler, S., Hoff, P. M., Kemeny, N. E., Hollywood, E. M., Gonen, M., Quinones, M., Morse, M. & Chen, H. X. Randomized phase II trial of cetuximab, bevacizumab, and irinotecan compared with cetuximab and bevacizumab alone in irinotecan-refractory colorectal cancer: the BOND-2 study. *J Clin Oncol* **25**, 4557-4561 (2007).
- 4 Kindler, H. L., Niedzwiecki, D., Hollis, D., Sutherland, S., Schrag, D., Hurwitz, H., Innocenti, F., Mulcahy, M. F., O'Reilly, E., Wozniak, T. F., Picus, J., Bhargava, P.,

- Mayer, R. J., Schilsky, R. L. & Goldberg, R. M. Gemcitabine plus bevacizumab compared with gemcitabine plus placebo in patients with advanced pancreatic cancer: phase III trial of the Cancer and Leukemia Group B (CALGB 80303). *J Clin Oncol* **28**, 3617-3622 (2010).
- 5 Bergers, G. & Hanahan, D. Modes of resistance to anti-angiogenic therapy. *Nat Rev Cancer* **8**, 592-603 (2008).
 - 6 Casanovas, O., Hicklin, D. J., Bergers, G. & Hanahan, D. Drug resistance by evasion of antiangiogenic targeting of VEGF signaling in late-stage pancreatic islet tumors. *Cancer Cell* **8**, 299-309 (2005).
 - 7 Fernando, N. T., Koch, M., Rothrock, C., Gollogly, L. K., D'Amore, P. A., Ryeom, S. & Yoon, S. S. Tumor escape from endogenous, extracellular matrix-associated angiogenesis inhibitors by up-regulation of multiple proangiogenic factors. *Clin Cancer Res* **14**, 1529-1539 (2008).
 - 8 Hamdan, R., Zhou, Z. & Kleinerman, E. S. SDF-1alpha induces PDGF-B expression and the differentiation of bone marrow cells into pericytes. *Mol Cancer Res* **9**, 1462-1470 (2011).
 - 9 Bergers, G. & Song, S. The role of pericytes in blood-vessel formation and maintenance. *Neuro Oncol* **7**, 452-464 (2005).
 - 10 Benjamin, L. E., Hemo, I. & Keshet, E. A plasticity window for blood vessel remodelling is defined by pericyte coverage of the preformed endothelial network and is regulated by PDGF-B and VEGF. *Development* **125**, 1591-1598 (1998).
 - 11 Bergers, G., Song, S., Meyer-Morse, N., Bergsland, E. & Hanahan, D. Benefits of targeting both pericytes and endothelial cells in the tumor vasculature with kinase inhibitors. *J Clin Invest* **111**, 1287-1295 (2003).
 - 12 Orledge, A. & D'Amore, P. A. Inhibition of capillary endothelial cell growth by pericytes and smooth muscle cells. *J Cell Biol* **105**, 1455-1462 (1987).
 - 13 Hirschi, K. K. & D'Amore, P. A. Control of angiogenesis by the pericyte: molecular mechanisms and significance. *EXS* **79**, 419-428 (1997).
 - 14 Capila, I. & Linhardt, R. J. Heparin-protein interactions. *Angew Chem Int Ed Engl* **41**, 391-412 (2002).
 - 15 Lever, R. & Page, C. P. Novel drug development opportunities for heparin. *Nat Rev Drug Discov* **1**, 140-148 (2002).
 - 16 Sasisekharan, R., Shriver, Z., Venkataraman, G. & Narayanasami, U. Roles of heparan-sulphate glycosaminoglycans in cancer. *Nat Rev Cancer* **2**, 521-528 (2002).
 - 17 Mousa, S. A., Linhardt, R., Francis, J. L. & Amirkhosravi, A. Anti-metastatic effect of a non-anticoagulant low-molecular-weight heparin versus the standard low-molecular-weight heparin, enoxaparin. *Thromb Haemost* **96**, 816-821 (2006).

- 18 Pisano, C., Alicino, C., Vesci, L., Casu, B., Naggi, A., Torri, G., Ribatti, D., Belleri, M., Rusnati, M. & Presta, M. Undersulfated, low-molecular-weight glycol-split heparin as an antiangiogenic VEGF antagonist. *Glycobiology* **15**, 1C-6C (2005).
- 19 Ritchie, J. P., Ramani, V. C., Ren, Y., Naggi, A., Torri, G., Casu, B., Penco, S., Pisano, C., Carminati, P., Tortoreto, M., Zunino, F., Vlodaysky, I., Sanderson, R. D. & Yang, Y. SST0001, a chemically modified heparin, inhibits myeloma growth and angiogenesis via disruption of the heparanase/syndecan-1 axis. *Clin Cancer Res* **17**, 1382-1393 (2011).
- 20 Kudchadkar, R., Gonzalez, R. & Lewis, K. D. PI-88: a novel inhibitor of angiogenesis. *Expert opinion on investigational drugs* **17**, 1769-1776 (2008).
- 21 Dredge, K., Hammond, E., Handley, P., Gonda, T. J., Smith, M. T., Vincent, C., Brandt, R., Ferro, V. & Bytheway, I. PG545, a dual heparanase and angiogenesis inhibitor, induces potent anti-tumour and anti-metastatic efficacy in preclinical models. *Br J Cancer* **104**, 635-642 (2011).
- 22 Lee, G. Y., Kim, S. K. & Byun, Y. Glucosylated heparin derivatives as non-toxic anti-cancer drugs. *J Control Release* **123**, 46-55 (2007).
- 23 Park, K., Kim, Y. S., Lee, G. Y., Nam, J. O., Lee, S. K., Park, R. W., Kim, S. Y., Kim, I. S. & Byun, Y. Antiangiogenic effect of bile acid acylated heparin derivative. *Pharm Res* **24**, 176-185 (2007).
- 24 Yu, M. K., Lee, D. Y., Kim, Y. S., Park, K., Park, S. A., Son, D. H., Lee, G. Y., Nam, J. H., Kim, S. Y., Kim, I. S., Park, R. W. & Byun, Y. Antiangiogenic and apoptotic properties of a novel amphiphilic folate-heparin-lithocholate derivative having cellular internality for cancer therapy. *Pharm Res* **24**, 705-714 (2007).
- 25 Park, J. W., Jeon, O. C., Kim, S. K., Al-Hilal, T. A., Jin, S. J., Moon, H. T., Yang, V. C., Kim, S. Y. & Byun, Y. High antiangiogenic and low anticoagulant efficacy of orally active low molecular weight heparin derivatives. *J Control Release* **148**, 317-326 (2010).
- 26 Lee, E., Kim, Y. S., Bae, S. M., Kim, S. K., Jin, S., Chung, S. W., Lee, M., Moon, H. T., Jeon, O. C., Park, R. W., Kim, I. S., Byun, Y. & Kim, S. Y. Polyproline-type helical-structured low-molecular weight heparin (LMWH)-taurocholate conjugate as a new angiogenesis inhibitor. *Int J Cancer* **124**, 2755-2765 (2009).
- 27 Fini, A., Fazio, G., Roda, A., Bellini, A. M., Mencini, E. & Guarneri, M. Basic cholane derivatives. XI: Comparison between acid and basic derivatives. *J Pharm Sci* **81**, 726-730 (1992).
- 28 Silvestri, L. J., Hurst, R. E., Simpson, L. & Settine, J. M. Analysis of sulfate in complex carbohydrates. *Anal Biochem* **123**, 303-309 (1982).

- 29 Jorgensen, W. L., Chandrasekhar, J., Madura, J. D., Impey, R. W. & Klein, M. L. Comparison of simple potential functions for simulating liquid water. *The Journal of Chemical Physics* **79**, 926-935 (1983).
- 30 Morris, G. M., Goodsell, D. S., Halliday, R. S., Huey, R., Hart, W. E., Belew, R. K. & Olson, A. J. Automated docking using a Lamarckian genetic algorithm and an empirical binding free energy function. *J Comput Chem* **19**, 1639-1662 (1998).
- 31 Skinner, R., Abrahams, J. P., Whisstock, J. C., Lesk, A. M., Carrell, R. W. & Wardell, M. R. The 2.6 Å structure of antithrombin indicates a conformational change at the heparin binding site. *J Mol Biol* **266**, 601-609 (1997).
- 32 Gasteiger, J. & Marsili, M. Iterative partial equalization of orbital electronegativity—a rapid access to atomic charges. *Tetrahedron* **36**, 3219-3228 (1980).
- 33 Ersdal-Badju, E., Lu, A., Zuo, Y., Picard, V. & Bock, S. C. Identification of the antithrombin III heparin binding site. *J Biol Chem* **272**, 19393-19400 (1997).
- 34 Garcia-Sanz, A., Rodriguez-Barbero, A., Bentley, M. D., Ritman, E. L. & Romero, J. C. Three-dimensional microcomputed tomography of renal vasculature in rats. *Hypertension* **31**, 440-444 (1998).
- 35 Maehara, N. Experimental microcomputed tomography study of the 3D microangioarchitecture of tumors. *Eur Radiol* **13**, 1559-1565 (2003).
- 36 Ferreira, I. A., Mocking, A. I., Urbanus, R. T., Varlack, S., Wnuk, M. & Akkerman, J. W. Glucose uptake via glucose transporter 3 by human platelets is regulated by protein kinase B. *J Biol Chem* **280**, 32625-32633 (2005).
- 37 ten Cate, H., Lamping, R. J., Henny, C. P., Prins, A. & ten Cate, J. W. Automated amidolytic method for determining heparin, a heparinoid, and a low-Mr heparin fragment, based on their anti-Xa activity. *Clin Chem* **30**, 860-864 (1984).
- 38 Robinson, C. J., Mulloy, B., Gallagher, J. T. & Stringer, S. E. VEGF165-binding sites within heparan sulfate encompass two highly sulfated domains and can be liberated by K5 lyase. *J Biol Chem* **281**, 1731-1740 (2006).
- 39 Krilleke, D., DeErkenez, A., Schubert, W., Giri, I., Robinson, G. S., Ng, Y. S. & Shima, D. T. Molecular mapping and functional characterization of the VEGF164 heparin-binding domain. *J Biol Chem* **282**, 28045-28056 (2007).
- 40 Lindahl, U., Backstrom, G., Hook, M., Thunberg, L., Fransson, L. A. & Linker, A. Structure of the antithrombin-binding site in heparin. *Proc Natl Acad Sci U S A* **76**, 3198-3202 (1979).
- 41 Bishop, J. R., Schuksz, M. & Esko, J. D. Heparan sulphate proteoglycans fine-tune mammalian physiology. *Nature* **446**, 1030-1037 (2007).
- 42 Ono, K., Hattori, H., Takeshita, S., Kurita, A. & Ishihara, M. Structural features in heparin that interact with VEGF165 and modulate its biological activity. *Glycobiology* **9**, 705-711 (1999).

- 43 Zhao, W., McCallum, S. A., Xiao, Z., Zhang, F. & Linhardt, R. J. Binding affinities of vascular endothelial growth factor (VEGF) for heparin-derived oligosaccharides. *Biosci Rep* **32**, 71-81 (2012).
- 44 Esko, J. D. & Selleck, S. B. Order out of chaos: assembly of ligand binding sites in heparan sulfate. *Annu Rev Biochem* **71**, 435-471 (2002).
- 45 Verheul, H. M., Lolkema, M. P., Qian, D. Z., Hilkes, Y. H., Liapi, E., Akkerman, J. W., Pili, R. & Voest, E. E. Platelets take up the monoclonal antibody bevacizumab. *Clin Cancer Res* **13**, 5341-5347 (2007).
- 46 Verheul, H. M., Hoekman, K., Luykx-de Bakker, S., Eekman, C. A., Folman, C. C., Broxterman, H. J. & Pinedo, H. M. Platelet: transporter of vascular endothelial growth factor. *Clin Cancer Res* **3**, 2187-2190 (1997).
- 47 Weltermann, A., Wolzt, M., Petersmann, K., Czerni, C., Graselli, U., Lechner, K. & Kyrle, P. A. Large amounts of vascular endothelial growth factor at the site of hemostatic plug formation in vivo. *Arterioscler Thromb Vasc Biol* **19**, 1757-1760 (1999).
- 48 Desgrosellier, J. S. & Cheresh, D. A. Integrins in cancer: biological implications and therapeutic opportunities. *Nat Rev Cancer* **10**, 9-22 (2010).

Chapter 3

Multiple-stage angiogenesis inhibition of LHT7 by blocking VEGF, FGF2, and PDGF-B

Despite the therapeutic benefits of the angiogenesis inhibitors shown in the clinics, they have encountered an unexpected limitation by the occurrence of acquired resistance. Although the mechanism of the resistance is not clear so far, the upregulation of alternative pro-angiogenic pathways and stabilization of endothelium by mural cells were reported to be responsible. Therefore, blocking multiple pro-angiogenic pathways that are crucial in tumor angiogenesis has been highlighted to overcome such limitations. To develop an angiogenesis inhibitor that could block multiple pro-angiogenic factors, heparin is an excellent lead compound since wide array of pro-angiogenic factors are heparin-binding proteins. In the previous section, LHT7, a heparin-derived angiogenesis inhibitor, was demonstrated as a potent angiogenesis inhibitor and showed that it blocked VEGF signaling pathway. Here it is shown that LHT7 could block the FGF2 and PDGF-B in addition to VEGF. Simultaneous blockade of these pro-angiogenic factors resulted in inhibition of multiple stages of the angiogenic process, including initial angiogenic response to maturation of the endothelium by pericyte coverage *in vitro*. In addition, the treatment of LHT7 *in vivo* did not show any sign of vascular normalization and directly led to decreased blood perfusion throughout the tumor. Current findings show that LHT7 could effectively inhibit tumor angiogenesis by blocking multiple stages of the angiogenesis, and could potentially be used to overcome the resistance.

3.1. Introduction

Tumor angiogenesis plays a critical role in mass growth and metastasis of tumor¹. Tumors that have inadequate vasculatures turns necrotic or apoptotic due to the insufficient supply of oxygen and nutrient for their survival². Therefore, blocking angiogenesis has been proposed as a distinct strategy for treatment of cancer. Since the development of bevacizumab, the first angiogenesis inhibitor to be approved by FDA, angiogenesis inhibitor has been one of the major class agents in modern cancer therapeutics, especially that blocks VEGF (now known as VEGF-A) signaling pathway³.

Angiogenesis inhibitors were initially expected to be free from the drug resistance issues that were typically shown in conventional chemotherapeutics, since the angiogenesis inhibitors target endothelial cells rather than genetically instable tumor cells⁴. In the clinic, angiogenesis inhibitors successfully arrested tumor growth during the initial treatment, but failed to produce constant clinical responses and eventually tumor relapsed. Although the underlying mechanisms of the acquired resistance against angiogenesis inhibitors are not entirely understood so far, several distinct mechanisms have been suggested. Unlike the conventional means of resistance against chemotherapeutic agents, which involves mutational alteration of the gene encoding a therapeutic target or the uptake and efflux of a drug^{5,6}, the adaptive resistance against angiogenesis inhibitors is acquired in tumors by variously employing evasive pathways during therapeutic blockade of angiogenesis⁷⁻¹¹.

Among the suggested mechanisms of the acquired resistance, the overexpression of alternative pro-angiogenic factors in the refractory tumor was considered significant^{8,11}. Many reports have demonstrated upregulation of pro-angiogenic factors including FGF1, FGF2, PDGF-A, PDGF-B, and PIGF when VEGF signaling pathway was blocked, which eventually led to regrowth of the tumors^{8,9,12}. Although VEGF plays the most predominant role in the tumor angiogenesis, many other pro-angiogenic factors are also involved¹. Therefore, the alternative pro-angiogenic factors upregulated from hypoxic tumor cells

could compensate the depleted VEGF signaling and provide evasive pathways for angiogenesis, resulting in regrowth of the tumor.

The coverage of tumor vasculatures by mural cells was also reported to be responsible for the resistance against angiogenesis inhibitors. The survival of the endothelium covered with pericytes is independent of VEGF, thus not affected by the depletion of VEGF¹¹. By contrast, the tumor vessels with inadequate pericyte coverage are more vulnerable to depletion of VEGF signaling^{13,14}. It has been demonstrated that pericytes support the endothelial survival in juxtacrine manner by expressing appreciable amount of VEGF and other factors crucial in the survival of the contacting endothelial cells^{15,16}. Moreover, pericytes attenuate the proliferation rate of endothelial cells and reduce their necessity of VEGF as a part of vessel stabilization process^{17,18}. Therefore, blocking only the VEGF signaling pathway is insufficient for an effective and enduring inhibition of tumor angiogenesis. Instead, blocking multiple factors involved in multiple stages of angiogenesis, from the initial robust angiogenic response to the maturation of the primitive vascular network, is deemed necessary to overcome the resistance and to inhibit tumor angiogenesis effectively.

To develop an angiogenesis inhibitor that could block multiple pro-angiogenic factors simultaneously, heparin is a promising lead compound, since it could intrinsically interact with various endogenous proteins including a broad range of pro-angiogenic factors¹⁹. For this purpose, a novel heparin-based anti-angiogenic agent, LHT7, was developed, which sodium taurocholates are chemically conjugated to LMWH²⁰. Such chemical modification of LMWH decreased binding affinity against ATIII but increased that against VEGF, resulting in a potent inhibition of tumor angiogenesis without any anticoagulant activity as discussed in the previous chapter.

This study shows that LHT7 could block FGF2 and PDGF-B in addition to VEGF. Both VEGF and FGF2 play significant roles in the initial angiogenic response, and PDGF-B is a key player of stabilizing primitive vascular network by recruiting mural cells to the endothelium^{1,11}. In purpose to evaluate the

multi-targeting effect of LHT7, various *in vitro* experiments that represent each stage of the angiogenic process were carried out. Also, the inhibitory effect of LHT7 on the multiple angiogenic signaling pathways was assessed at the molecular level shown by the reduction of receptor tyrosine phosphorylation of VEGFR2, FGFR1 and PDGFR β . Furthermore, since vascular normalization shown in tumors that were treated with VEGF blockers is closely related to stabilization of blood vessels by mural cells, it was evaluated whether vascular normalization also occurs when the tumor was treated with LHT7, which is a multi-targeted agent.

3.2. Materials and Methods

3.2.1. Cell lines

Human umbilical vein endothelial cells (HUVEC), human dermal microvascular endothelial cells (HDMEC) and human pericytes from placenta were purchased from PromoCell (Heidelberg, Germany). MDA-MB-231 cells were obtained from the American Type Culture Collection (ATCC; Manassas, VA). HUVECs and HDMECs were cultured in Endothelial Cell Growth Medium MV2 (ECGM; PromoCell). Pericytes and MDA-MB-231 cells were grown in Pericyte Growth Medium (PromoCell) and high-glucose Dulbecco's modified eagle medium (Gibco, Carlsbad, CA) supplemented with 10% fetal bovine serum (Gibco), respectively. The cells were maintained in a humidified 5% CO₂ atmosphere at 37°C.

3.2.2. Transwell chemotactic migration assay

To determine the effect of LHT7 on the migration of HUVECs, a cell migration assay was carried out as described previously²¹. Briefly, HUVECs were seeded on the 96-well transwell insert with 8- μ m pores (Corning, Tewksbury, MA) at 5×10^4 cells in 50 μ l of serum-free endothelial basal medium (EBM; PromoCell). VEGF₁₆₅ or FGF2 (R&D Systems, Minneapolis, MN) was prepared at a concentration of 100 ng/ml in serum-free EBM and were added to the receiver

plate at final volume of 150 μ l. LHT7 was added at a final concentration of 100 μ g/ml to the treatment group, and then the transwell insert was combined with the receiver plate. After 12 h of incubation, the receiver plate was replaced with another black receiver plate containing 100 μ l of cell dissociation solution (Trevigen, Gaithersburg, MD) containing Calcein AM (Molecular Probes, Eugene, OR) at final concentration of 2 μ g/ml to detach and stain. The combined plate was incubated for 1 h at 37°C and then the transwell insert was removed. The migrated cells were quantified with a microplate reader (Synergy HT; BioTek Instruments, Winooski, VT) through fluorescent top reading (485/520 nm).

3.2.3. MTT cytotoxicity assay

To evaluate the cytotoxicity of LHT7 on HUVECs and pericytes, MTT cytotoxicity assay was performed according to the standard procedure. MTT cell proliferation assay kit was purchased from Trevigen. HUVECs or pericytes were plated in 96-well culture plates at 5×10^4 cells per well in 100 μ l of ECGM or pericyte growth medium, respectively. After the incubation of the cells with various concentrations of LHT7 (0, 0.01, 0.1, and 1 mg/ml) for 24 h, 10 μ l of MTT reagent was added to each well, and the cells were further incubated for 3 h. When the purple precipitate was visible inside the cells, 100 μ l of detergent reagent was added to each well and kept in the dark for 2 h at room temperature. The absorbance was measured at 570 nm using a microplate reader (Synergy HT; BioTek Instruments) to measure the amount of viable cells.

3.2.4. HUVEC spheroid sprouting assay

To assess the effect of LHT7 on angiogenic sprouting, HUVEC spheroids were prepared as described previously²², and evaluated the sprouting from the spheroids with or without LHT7. Briefly, methocel solution was prepared by adding methylcellulose (Sigma-Aldrich) in ECGM at a final concentration of 1.2% w/v. Then the HUVECs were harvested, and resuspended at 1×10^7 cell/ml in ECGM. The cell suspension (100 μ l) was transferred to 20 ml of the

culture medium and well suspended. Then 5 ml of the prepared methocel solution was added to the cell suspension and mixed thoroughly. The cell suspension containing methocel solution was placed on a non-adherent square dish as droplets (25 μ l per droplet) and incubated upside down as hanging drops at 37°C for overnight in 100% humidity. The spheroids were collected by washing the dishes with the culture medium followed by centrifugation (3000 rpm, 15 min, 4°C), and resuspended in the collagen matrix, which was prepared as described elsewhere²³. The collagen matrix containing HUVEC spheroids was added to 96-well culture plate (50 μ l per well) and incubated at 37°C for 1 h to allow collagen to polymerize. Feeding medium containing 100 ng/ml of VEGF₁₆₅, FGF2, or a mixture of VEGF₁₆₅ and FGF2 (50 ng/ml each) in EBM was added to each well (200 μ l per well). For the treatment group, LHT7 was added to the feeding medium at a final concentration of 100 μ g/ml. After 48 h incubation, the spheroids were stained with Calcein AM (8 μ g/ml in EBM) according to the manufacturer's instruction. The spheroids were observed under fluorescence microscope (Eclipse TE2000-S; Nikon Instruments, Tokyo, Japan).

3.5.5. Endothelial tube formation assay

To determine the effect of LHT7 on HUVEC differentiation *in vitro*, a tube formation assay was performed as described previously²⁴. Briefly, Matrigel (BD Bioscience, San Jose, CA) was coated onto a 96-well culture plate by adding 48 μ l of chilled Matrigel to each well and incubating for 90 min at 37°C. The cultured HUVECs were harvested and resuspended at 1×10^6 cell/ml in EBM and plated on the matrigel coated dish at a density of 5×10^4 cells per well (50 μ l). VEGF₁₆₅, FGF2 (100 ng/ml), or a mixture of VEGF₁₆₅ and FGF2 (50 ng/ml each) was treated with or without LHT7 (100 μ g/ml), and incubated for 24 h at 37°C. Then the cells were stained by replacing the medium with HBSS containing Calcein AM (8 μ g/ml) followed by 30 min incubation, and observed under fluorescence microscope (Eclipse TE2000-S). The acquired images were analyzed with ImageJ angiogenesis analyzer for the quantification of degree of tube formation according to the earlier literature²⁵.

3.2.6. Matrigel plug angiogenesis assay

To assess the inhibitory effect of LHT7 on angiogenesis *in vivo*, a matrigel plug assay was performed as described elsewhere²⁶. Briefly, 500 μ l of Matrigel supplemented with VEGF₁₆₅, FGF2, or PDGF-B (500 ng/ml; R&D Systems) and with or without LHT7 (500 μ g/ml) was injected subcutaneously into the ventral side of a 6 week-old male C3H/HeN mice (n = 6). Matrigel supplemented with VEGF₁₆₅, FGF2, or PDGF-B containing anti-VEGF antibody (Bevacizumab; Roche), anti-FGF2 antibody (Abcam), or anti-PDGF-B antibody (Abcam), respectively, at final concentration of 100 μ g/ml, was implanted as inhibitor controls. For the FGF2 and PDGF-B combination group, 250 ng/ml of each growth factor was added to the matrigel. Matrigel without any growth factor or drug was implanted as a control. After 10 days, the matrigel plugs were isolated from the mice and observed.

3.2.7. Receptor tyrosine kinase phosphorylation studies

The tyrosine kinase phosphorylation level of VEGFR2, FGFR1, and PDGFR β was evaluated to determine the inhibitory effect of LHT7 at the molecular level. The effect of LHT7 on VEGFR2 or FGFR1 tyrosine phosphorylation stimulated by VEGF₁₆₅ or FGF2, respectively, was evaluated on HUVECs and HDMECs. The effect of LHT7 on PDGFR β tyrosine phosphorylation stimulated by PDGF-B was evaluated on pericytes. When at 80% confluence, the cells were starved for 24 h in a serum-free culture medium. Then, LHT7 or neutralizing antibodies were treated 30 min prior to the addition of the growth factor at a final concentration of 100 μ g/ml. The cells were then treated with the corresponding growth factor at a final concentration of 100 ng/ml and incubated for 5 min. The cells were immediately washed with ice-cold PBS and lysed with RIPA buffer containing protease and phosphatase inhibitors (Pierce, Rockford, IL). The samples were then subjected to Western blot analysis according to the standard procedure. Antibodies for pVEGFR2 (1:2000) and pPDGFR β (1:2000) were purchased from R&D Systems. Antibodies for VEGFR2 (1:1000), FGFR1

(1:1000), pFGFR1 (1:2000), and PDGFR β (1:1000) were from Cell Signaling Technology (Danvers, MA). The blotted membranes were developed using ImageQuant LAS 4000 imaging system (GE Healthcare Life Sciences, Uppsala, Sweden).

3.2.8. *In vitro* pericyte migration to endothelial tube

To determine the effect of LHT7 in pericyte coverage of endothelium *in vitro*, HUVECs were labeled with red CellTracker (Molecular Probes) according to the manufacturer's instructions. Then, endothelium tubes on a matrigel-coated 96-well culture plate were prepared as described earlier with the exception of using complete ECGM as the feeding medium. When endothelial tubes were completely formed after 24 h of the HUVEC seeding, the cells were washed gently with pre-warmed HBSS. Then pericytes were harvested, labeled with green CellTracker (Molecular Probes), and resuspended in serum-free EBM at 5×10^4 cell/ml. The pericyte suspension was transferred to each well at a density of 5×10^3 cells per well (100 μ l of the cell suspension). LHT7 or bevacizumab was treated at a final concentration of 100 μ g/ml for the drug treatment group. The cells were further incubated at 37°C and observed under fluorescence microscope (Eclipse TE2000-S) at 2 and 18 h of post-pericyte seeding.

3.2.9. *In vitro* pericyte-endothelium adhesion assay

To evaluate the effect of LHT7 on pericyte adhesion on endothelium, an *in vitro* adhesion assay was performed. HUVECs were plated on a 96-well culture plate 1×10^5 cells per well in 100 μ l ECGM and grown until the cells formed a confluent monolayer. The medium was replaced with serum-free EBM (50 μ l) with or without LHT7 (200 μ g/ml) and incubated for 30 min. Then, pericytes were labeled with green CellTracker (Molecular Probes) according to the manufacturer's instruction and adjusted to 1×10^5 cell/ml in the serum-free EBM. The pericyte suspension (50 μ l) was added to each well containing the endothelial monolayer, and further incubated for 3 h. Finally the wells were washed twice with pre-warmed PBS and fixed with 4% PFA. The samples were

observed under fluorescence microscope (Eclipse TE2000-S). The fluorescent image of the cell was acquired in the center of the well at $\times 40$ magnification for each well and the number of pericytes (red fluorescence) was counted using ImageJ software ($n = 3$ for each group).

3.2.10. Surface plasmon resonance (SPR) analysis

Biacore T100 (GE Healthcare, Waukesha, WI) was used for the SPR analysis. LHT7 was immobilized, which was adjusted to a level of 1,000 RU, on a sensor chip CM5 (GE Healthcare) by using the amide-coupling method. Recombinant human VEGF₁₆₅, FGF2, and PDGF-B were prepared at concentrations ranging from 0.001 to 10 $\mu\text{g/ml}$ in HBS-EP plus buffer (GE Healthcare), which was also used as a running buffer. The flow rate for the overall analysis was adjusted to 10 $\mu\text{l/min}$ and 50 mM NaOH was used for the regeneration of the sensor chip surface after each cycle of analysis. The analysis was done in triplicate and the data were processed using the BIAevaluation software (GE Healthcare).

3.2.11. Dynamic contrast enhanced magnetic resonance imaging

In 6 to 7-week-old female BALB/cSlc-nu mice, MDA-MB-231 cells (1×10^7) were inoculated subcutaneously into the bilateral flank of each mouse. When the tumor diameter reached 5 mm, LHT7 ($n = 3$, 5 mg/kg) or saline ($n = 3$, control) was administered daily intravenously. Dynamic contrast-enhanced magnetic resonance images (DCE-MRI) were obtained using a 3.0-T MR imaging system (Achieva; Philips Healthcare, Best, Netherlands) with the following parameters: TR, 20 ms; TE, 2.1 ms; flip angle, 30° ; FOV, $4.0 \times 4.0 \text{ cm}^2$; matrix size, 128×128 ; and number of repetition, 400. A contrast agent, Gd-DOTA (Guerbet, Villepinte, France), was injected as a bolus into the tail vein at a dose of 0.1 mmol/kg for 30 sec following the start of image acquisition. Based on DCE-MRI, a two-compartment model of Buckley was used for the analysis to measure the rate constants of Gd-DOTA from the extravascular extracellular space (EES) to plasma compartments (K_{ep}) and the elimination of

Gd-DOTA by the plasma (K_{ep}). The plasma concentration of Gd-DOTA was not directly measured in this pharmacokinetic model because the clearance rate (K_{el}) can be estimated from the measured tissue curve. Accordingly, a time-intensity curve was fitted with the following equation:

$$\frac{S(t)}{S(0)} = 1 + A^H K_{ep} \left(\frac{e^{-K_{ep}t} - e^{-K_{el}t}}{K_{el} - K_{ep}} \right)$$

,where $S(0)$ is the signal intensity before contrast injection and $S(t)$ is the signal intensity at a certain time t . From this fitting, four perfusion-related parameters were estimated as follows: K_{ep} , which is the efflux rate constant from extravascular extracellular space to blood plasma indicating the permeability; K_{el} , which indicates the first-order rate constant for the elimination of contrast agent from the blood plasma; initial slope, which indicates the differential at the onset of the exponential curve; and K^{trans} , which is a volume transfer constant of contrast agent between blood plasma and the extravascular extracellular space, to determine vascular permeability.

3.2.12. Statistical analysis

Data were analyzed using unpaired one-tailed Mann-Whitney test or Kruskal-Wallis non-parametric ANOVA followed by the Dunn's multiple comparisons test. The GraphPad Prism version 6.0c (GraphPad Software, San Diego, CA) was used for the statistical calculations. P value less than 0.05 was considered statistically significant.

3.3. Results

3.3.1. HUVEC migration inhibitory effect and cytotoxicity evaluation of LHT7

A set of *in vitro* experiments that represent several phases of the initial angiogenic response was carried out on HUVECs. The inhibitory effect of LHT7 on the chemotactic migration of HUVECs stimulated by VEGF or FGF2 was evaluated through a transwell chemotactic migration assay (also known as modified Boyden chamber assay). Both VEGF and FGF2 stimulated the

migration of HUVECs, whereas VEGF was a more potent stimulator than FGF2. In the presence of LHT7, the cell migration induced by VEGF or FGF2 was significantly inhibited and the number of the migrated cells was decreased by 46% and 29%, respectively, compared to the control (**Fig. 3.1A**). To clarify that the inhibition of cell migration by LHT7 was not associated with any cytotoxicity of LHT7, MTT cytotoxicity assay of LHT7 was performed on HUVECs. The result showed no significant cytotoxic effect of LHT7 on HUVECs at concentrations up to 1 mg/ml, which was ten-fold higher concentration than that used throughout the *in vitro* studies (**Fig. 3.1B**). This manifested that LHT7 inhibited the migration of HUVECs by suppressing the chemotaxis stimulated by VEGF and/or FGF2, not by affecting the cell viability.

3.3.2. Inhibitory effect of LHT7 in endothelial sproutings

The HUVEC spheroids were prepared to determine the effect of LHT7 in angiogenic sprouting from the spheroids in 3D culture environment *in vitro*, which mimics the vessel sprouting from the pre-existing vasculatures during the initial robust angiogenic response (**Fig. 3.1C**). Both VEGF and FGF2 induced marked endothelial sprouting from the spheroids at 48 hour of post-treatment, showing intensive branching of endothelium from the spheroid cores. However, simultaneous treatment of LHT7 significantly inhibited the sprouting stimulated by VEGF or FGF2, and almost no branching of the endothelium was observed. Since simultaneous treatment of VEGF and FGF2 have been reported to show an angiogenic synergism²⁷, it was further assessed whether LHT7 could also suppress the angiogenic sprouting stimulated by the treatment of the both pro-angiogenic factors. Indeed, when VEGF and FGF2 were treated at the same time, the HUVEC spheroids showed the most robust sprouting among all of the tested groups. Nevertheless, treatment of LHT7 effectively inhibited the sprouting induced by the both pro-angiogenic factors and showed that LHT7 could suppress the activity of VEGF and FGF2 at the same time.

3.3.3. Inhibitory effect of LHT7 in endothelial tubular differentiation

Endothelial tube formation assay with HUVECs was carried out, which represents the endothelial differentiation *in vitro*. VEGF and FGF2 were used as the stimulators for the endothelial tube formation. As shown in **Fig. 3.2A**, the two pro-angiogenic factors strongly stimulated the tube formation individually or together. In particular, the simultaneous treatment of the both pro-angiogenic factors induced the highest degree of the tube formation. However, LHT7 treatment to the HUVECs significantly inhibited the tube formation induced by VEGF, FGF2, and combination of the both pro-angiogenic factors, showing 91%, 88%, and 87% decreased number of nodes compared to the positive controls, respectively. The tubular structure of each group was quantified using ImageJ (**Fig. 3.2B**).

3.3.4. Inhibitory effect of LHT7 in the angiogenesis induced by VEGF and FGF2 in matrigel plugs

The inhibitory effect of LHT7 in the angiogenesis induced by VEGF and FGF2 was evaluated *in vivo* by matrigel plug angiogenesis assay (**Fig. 3.3A**). When isolated after two weeks of implantation, the matrigel plugs supplemented with VEGF or FGF2 showed high degree of angiogenesis represented by the bloody red color of the plugs, while non-supplemented matrigel plugs showed no occurrence of the angiogenesis. However, addition of LHT7 to the matrigel plugs significantly inhibited angiogenesis that were induced by supplementation of the either of VEGF and FGF2. The inhibitory effect shown by LHT7 was similar to that shown by the neutralizing antibodies to the corresponding pro-angiogenic factors, showing only pale red color in the plugs. This result showed that LHT7 effectively suppressed the VEGF and FGF2-mediated angiogenesis *in vivo*.

3.3.5. VEGF-VEGFR2 and FGF2-FGFR1 signaling pathway blockade by LHT7

The inhibition of VEGF-VEGFR2 and FGF2-FGFR1 signaling pathway by LHT7 was evaluated at molecular level by determining the level of the receptor tyrosine phosphorylation of VEGFR2 and FGFR1, which are the major receptors involved in the initial stage of angiogenesis mediated by VEGF and FGF2, respectively. Two different types of endothelial cells – HUVECs and HDMECs – were used. The cells were initially exposed to LHT7 followed by addition of VEGF or FGF2, and then subjected to a standard procedure of western blot.

The treatment of VEGF without pretreatment of LHT7 resulted in potent stimulation of VEGFR2 tyrosine phosphorylation in both HUVEC and HDMEC cells. However, when the cells were treated with LHT7 in advance of VEGF stimulation, significantly lower degree of VEGFR2 phosphorylation was detected, indicating evident inhibition of the tyrosine phosphorylation by LHT7. The inhibitory effect shown by LHT7 treatment was comparable to that of anti-VEGF antibody (**Fig. 3.3B**).

Similar inhibitory effect was shown in the FGF2-FGFR1 signaling axis when the cells were treated with LHT7. When the cells were stimulated with FGF2, there were significant amount of phosphorylated FGFR1 detected. However, treatment of LHT7 effectively inhibited the FGFR1 tyrosine phosphorylation stimulated by FGF2 in the both cells. The inhibitory effect of LHT7 in the FGFR1 tyrosine phosphorylation was similar to that of anti-FGF2 antibody (**Fig. 3.3C**). These results clearly showed that the inhibitory effect of LHT7 on initial angiogenic responses that were described above was due to the blockade of VEGF and FGF2 signaling pathways.

The interaction studies between LHT7 and VEGF or FGF2 using surface plasmon resonance (SPR) showed that LHT7 bound to the both pro-angiogenic factors at nano- to micromolar range of binding affinity (**Table 3.1**), suggesting that LHT7 blocked the downstream signaling of the VEGF and FGF2 signaling pathway by binding to the VEGF and FGF2.

3.3.6. Inhibitory effect of LHT7 on pericyte recruitment to endothelium linings

To determine whether LHT7 could block the maturation of the primitive blood vessels, an *in vitro* experiment that mimics the vascular maturation was designed and carried out as follows: first, well-formed endothelial tubes were prepared on matrigel, which represent the primitive vessel network; the culture medium was then replaced with serum-free medium; the human pericytes from placenta (hereafter, pericytes) were added with or without LHT7 (**Fig. 3.4A**).

In the control group, most of the seeded pericytes were recruited around the established endothelial tubes within two hours. After 18 hours, although the appearance of the endothelial tube network was altered, the tubular structures were well maintained with the pericytes adhered to the tubes.

In the presence of LHT7, however, the number of pericytes recruited around the endothelial tubes was significantly decreased and the pericytes were randomly distributed within the observed frame when observed after two hours from the pericyte addition. After 18 hours, most of the endothelial tubes were collapsed and few tubes remained. In contrast, anti-VEGF monoclonal antibody showed no influence in the migration of pericytes towards the endothelial tubes when observed at two hours of post-pericyte addition, and showed random distribution of the pericytes similar to that of the control group. Consequently, after 18 hours, higher extent of the tubes remained when compared to the LHT7-treated group. The endothelial tubes of the each group after 18 hours of pericyte addition were quantified using the ImageJ angiogenesis analyzer and the number of nodes and branches was calculated (**Fig. 3.4B**). The results showed that the LHT7-treated group had the calculated mean number of nodes and branches of the endothelial tubes decreased by 67% and 54%, whereas the anti-VEGF antibody-treated group decreased by 15% and 8% compared to control, respectively. According to the results, blocking only the VEGF had no significant effect in the regression of the endothelial tubes that are accompanied

by pericytes. On the other hand, treatment of LHT7 effectively regressed the tubes.

3.3.7. Determination of cytotoxicity on pericytes and possible effects in the endothelial cell and pericyte adhesion of LHT7

The cytotoxic effect of LHT7 was evaluated on pericytes to determine whether the inhibition of the pericyte recruitment to the endothelial tubes was possibly due to the cytotoxic effect of LHT7. In the MTT cytotoxicity assay, LHT7 did not affect the viability of the pericytes at concentrations up to 1 mg/ml, which was ten-fold higher concentration than that used in the study described above (**Fig. 3.4C**). This result supported that the inhibition of pericyte recruitment to endothelial tubes was not related to the viability of the pericytes when LHT7 was treated.

Since heparin has been recognized to affect cell-to-cell adhesion by modulating the activity of integrin²⁸, it was further determined whether LHT7 affected the direct cell-to-cell interaction between HUVECs and pericytes. The experiment was carried out by establishing a HUVEC monolayer on the cell culture dish followed by addition of pericytes with or without LHT7. The adhesion assay showed no significant difference in the number of pericytes adhered to the HUVEC monolayer between the control and LHT7-treated group (**Fig. 3.4D**), implying that LHT7 inhibited the migration, rather than affecting the adherence of pericytes to the endothelium.

3.3.8. Inhibitory effect of LHT7 on PDGF-B-induced angiogenesis in matrigel plugs

PDGF-B is one of the major chemotactic driving forces for pericytes to recruit around the established endothelial vessels²⁹. To determine the effect of LHT7 on PDGF-B signaling pathway, an *in vivo* matrigel plug assay was performed using PDGF-B as a stimulant. PDGF-B induced moderate angiogenesis in the matrigel, whereas treatment of LHT7 in the matrigel significantly inhibited angiogenesis in the gel (**Fig. 3.5A**). The inhibitory effect of LHT7 in PDGF-B-induced angiogenesis in the matrigel was comparable to that of the neutralizing

antibody of PDGF-B. However, PDGF-B is not an initiator of angiogenesis and the potency of stimulating angiogenesis is relatively weaker than other major pro-angiogenic factors, such as VEGF or FGF2. Previous study has reported that combination of PDGF-B and FGF2 could synergistically induce a strong angiogenic response and form stable vascular networks³⁰. In this reason, the inhibitory effect of LHT7 on angiogenesis that was stimulated by combination of PDGF-B and FGF2 was determined. When matrigel plugs containing both PDGF-B and FGF2 were implanted in mice, an intensive angiogenic response was observed in the plugs. The treatment of LHT7, however, effectively inhibited the angiogenesis that was induced by the combination of PDGF-B and FGF2.

3.3.9. PDGFB-PDGFR β signaling pathway blockade by LHT7

The inhibition of PDGFB-PDGFR β signaling pathway by LHT7 was evaluated at molecular level by determining the level of the receptor tyrosine phosphorylation of PDGFR β , which are the major receptors involved in the late stage of angiogenesis mediated by PDGF-B (**Fig. 3.5B**). PDGFR β is abundantly expressed on pericytes, which surround the capillary endothelium and have been recognized to play a pivotal role in stabilizing the primitive vascular networks³¹. Treatment of pericytes with PDGF-B resulted in potent stimulation of PDGFR β tyrosine phosphorylation. However, treatment of the cells with LHT7 in advance of PDGF-B stimulation showed evident inhibition of the tyrosine phosphorylation of PDGFR β . The inhibitory effect shown in the result was similar to that of the neutralizing antibody of PDGF-B. The interaction studies between LHT7 and PDGF-B using surface plasmon resonance (SPR) showed micromolar range of binding affinity (**Table 3.1**), indicating that LHT7 bound to the PDGF-B.

3.3.10. Characterization of tumor vasculatures in LHT7-treated tumor-bearing animals using DCE-MRI

The tumor blood vessels were characterized *in vivo* after treatment of LHT7 to the animals. Four different kinetic parameters were derived from the DCE-MRI results: K^{trans} is the volume transfer constant between blood plasma and extravascular extracellular space (EES); K_{ep} is the rate constant between EES and blood plasma; initial slope is the differential at the onset of the exponential curve of contrast agents in the tissue of interest; K_{el} is the first-order rate constant for the elimination of contrast agents from the tissue of interest.

The tumor growth was effectively suppressed by the LHT7 treatment (**Fig. 3.6A**) without any decrease in body weight (**Fig. 3.6B**) in the current experimental animal models that were subjected to the DCE-MRI, indicating successful tumor angiogenesis inhibition without any significant toxic effects to the animals. K^{trans} (**Fig. 3.6C**) and K_{ep} (**Fig. 3.6D**), which represent the permeability of the vessel wall, showed no significant difference between the control and the LHT7-treated group. This indicated that the LHT7 treatment did not affect the property of the tumor vessel wall in terms of the permeability.

On the other hand, the initial slope, which represents the influx of the blood into the tumor, was higher in the control group than the LHT7-treated group at the last day of the observation, indicating retarded blood influx in the treatment group (**Fig. 3.6E**). This result was further supported by the gradual decrease of the K_{el} , which represents the blood perfusion, during the treatment of LHT7, which the decrease was not observed in the control group (**Fig. 3.6F**).

Table 3.1. Dissociation constants of LHT7 on VEGF, FGF2 or PDGF-B

	VEGF	FGF2	PDGF-B
K_D (μM)	0.412 ± 0.106	1.53 ± 0.43	0.971 ± 0.231

Data presented as means \pm s.d.

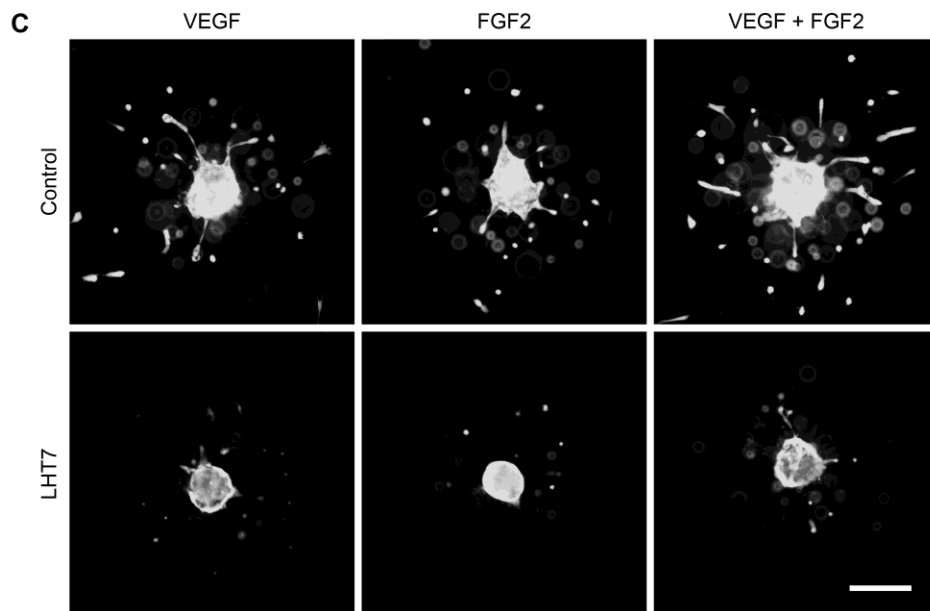
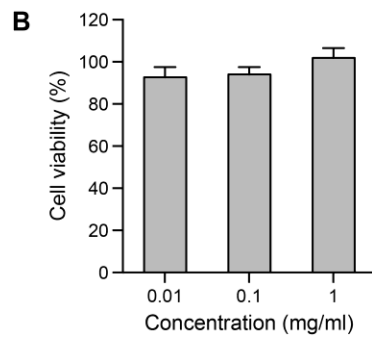
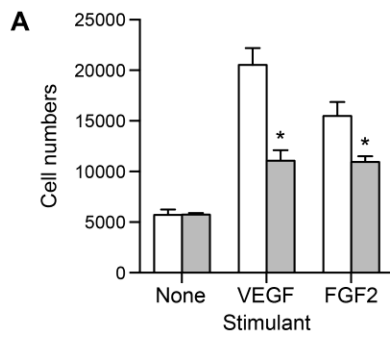


Figure 3.1. (A) Transwell chemotactic cell migration of HUVECs induced by VEGF or FGF2. Degree of migration in control (white) and LHT7-treated group (black) was assessed. (B) Cytotoxicity evaluation of LHT7 on HUVECs by using MTT cell proliferation assay at a concentration range of 0.01 to 1 mg/ml. (C) Representative images of VEGF and/or FGF2-induced angiogenic sprouting of HUVEC spheroid of control and LHT7-treated groups. Scale bar, 50 μ m.

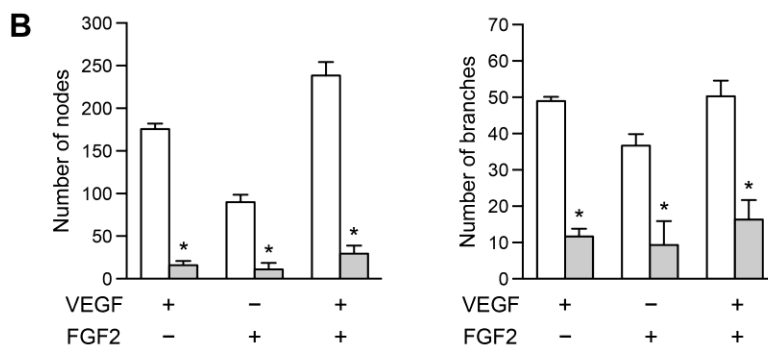
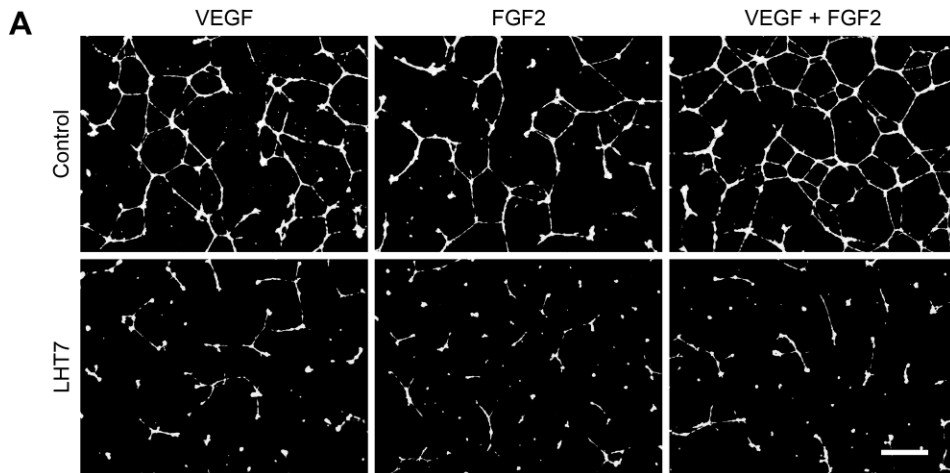


Figure 3.2. (A) HUVEC tube formation induced by VEGF and/or FGF2. HUVECs were stained in green fluorescence. Scale bar, 500 μm . (B) Quantitative analysis of HUVEC tubes by ImageJ angiogenesis analyzer. Number of nodes (left panel) and branches (right panel) of control (empty column) and LHT7 treated group (filled column) were calculated. $*P < 0.05$ versus control. Data are presented as mean \pm s.d.

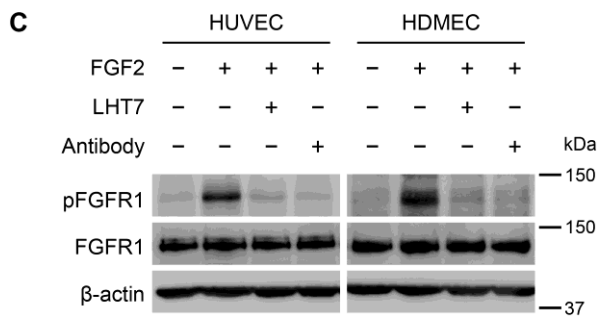
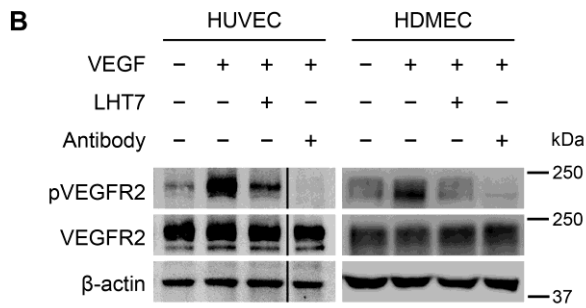
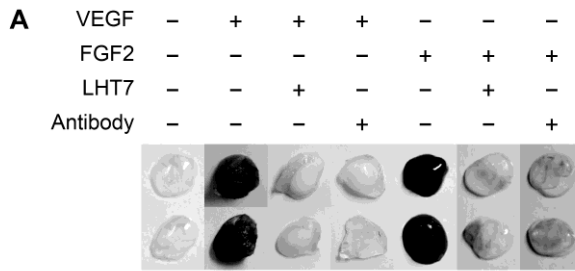


Figure 3.3. (A) *In vivo* matrigel plug angiogenesis assay using VEGF or FGF2 as an angiogenic stimulator. The inhibition of phosphotyrosine level of VEGFR2 stimulated by VEGF (B) and FGFR1 stimulated by FGF2 (C) on HUVECs (left) and HDMECs (right) by LHT7 are shown by immunoblots.

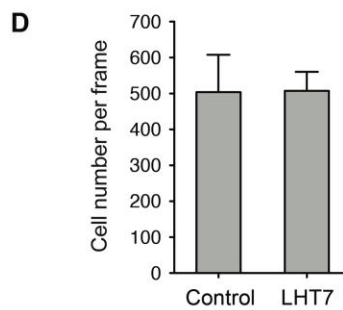
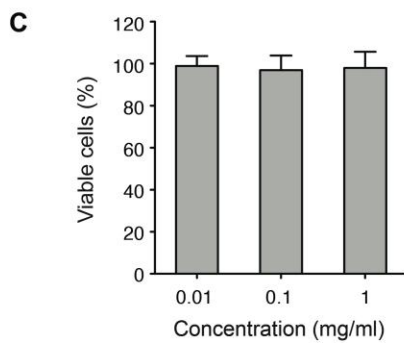
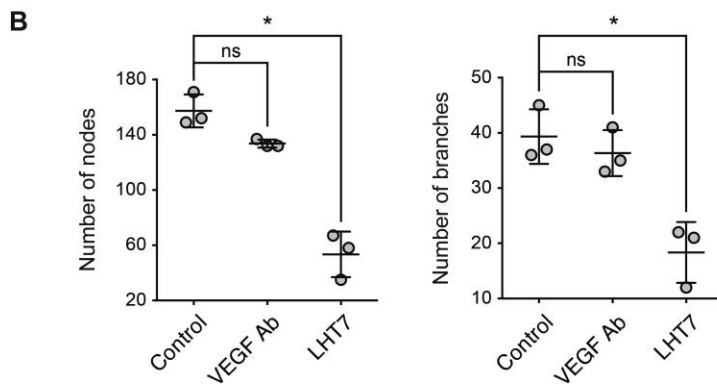
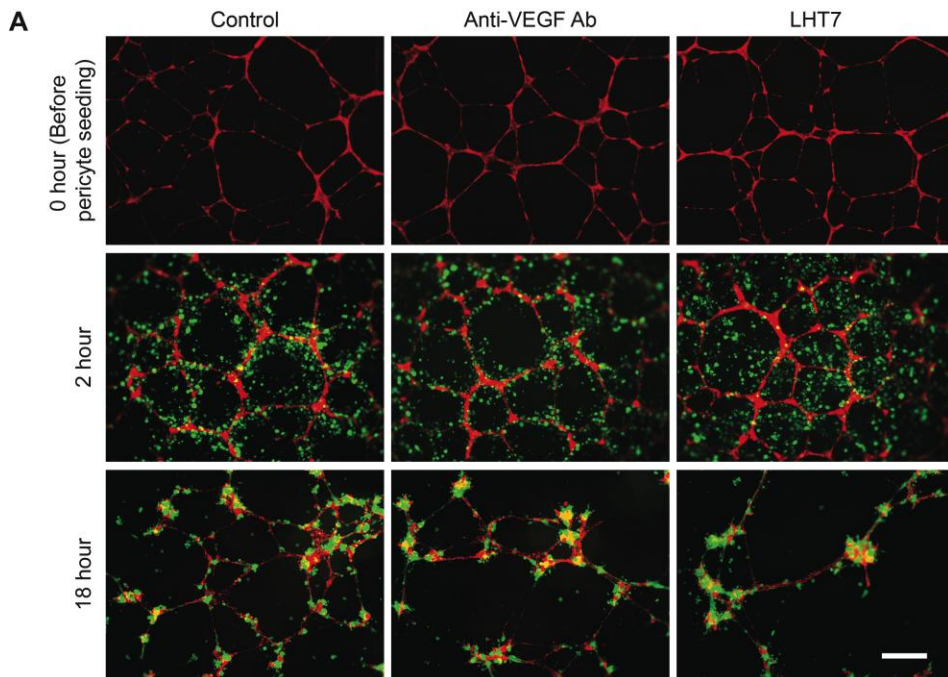


Figure. 3.4. Representative images of HUVECs (red) and pericytes (green) coculture system *in vitro*. (A) Pericytes were seeded after endothelial tubes were formed. Recruitment of pericytes to HUVEC tubes in control, anti-VEGF mAb, and LHT7-treated groups were observed after 2 h and 18 h of pericyte addition. Scale bars, 500 μ m. (B) Quantitative analysis of remaining endothelial tubes after 18 h of pericyte addition by ImageJ angiogenesis analyzer. Number of nodes (left panel) and branches (right panel) were calculated and shown as means \pm s.d. with individual plot. * $P < 0.05$ versus control. (C) Cytotoxic effect of LHT7 evaluated by MTT assay at a concentration range of 0.01 to 1 mg/ml. (D) Pericytes adhesion on confluent HUVEC monolayer. Single image was obtained in the center of the each well (n = 3) at 40x magnification and number of the adhered pericytes were counted and averaged. Data are expressed as means \pm s.d.

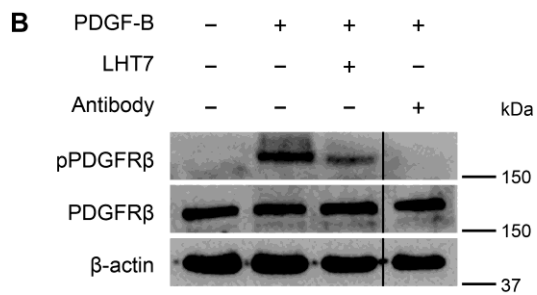
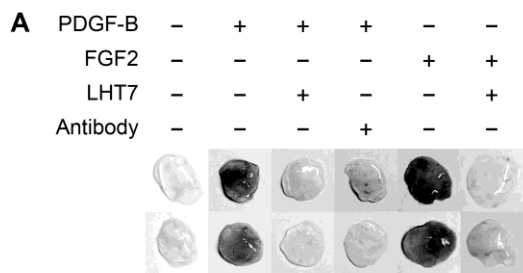


Figure 3.5. (A) *In vivo* matrigel plug angiogenesis assay using PDGF-B and PDGF-B/FGF2 mixture as angiogenic stimulators. (B) Western blots of phosphotyrosine level of PDGFR β on pericytes stimulated by PDGF-B in the presence or absence of LHT7 or neutralizing antibody.

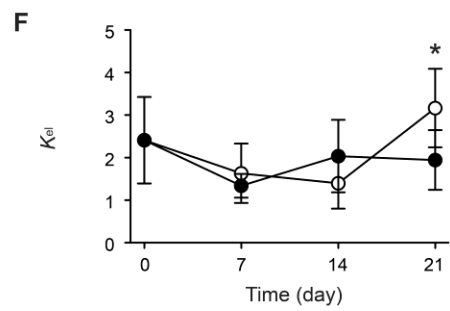
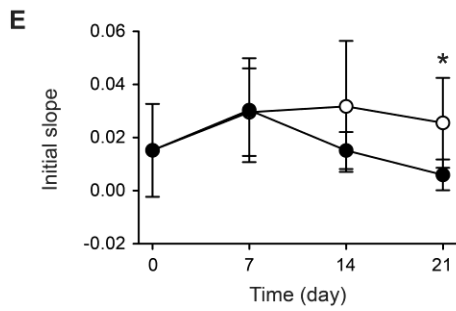
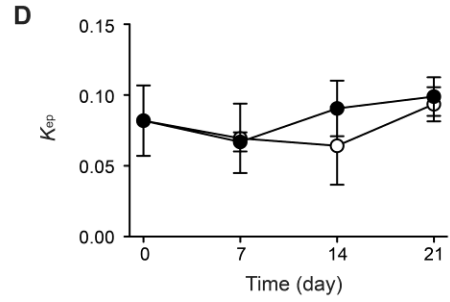
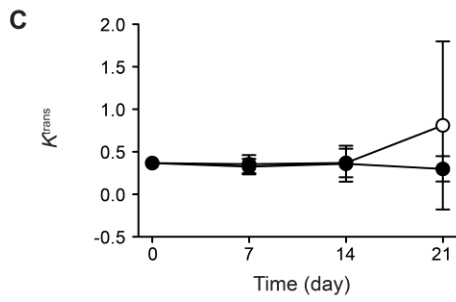
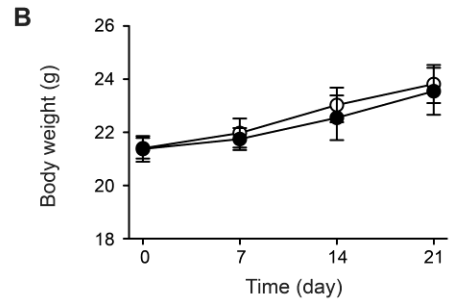
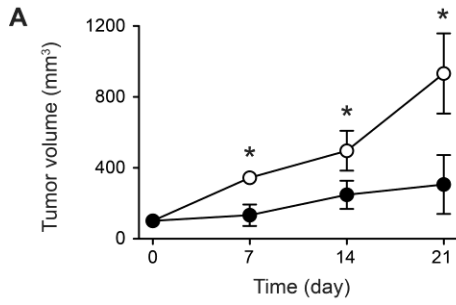


Figure 3.6. MDA-MB-231 tumor-bearing mice were treated with LHT7 at a dose of 5 mg/kg intravenously daily for three weeks (●) and compared with control (○). Tumor growth (A) and body weight (B) change were measured. DCE-MRI parameters were measured during the treatment at day 0, 7, 14 and 21. The values of K_{trans} (C), K_{ep} (D), initial slope (E), and K_{el} (F) were calculated. $n = 3$. Data are expressed as mean \pm s.d. * $P < 0.05$ versus control.

3.4. Discussion

The present study demonstrates that LHT7 could inhibit multiple stages of angiogenesis by blocking the pro-angiogenic factors that are involved in the initial robust angiogenesis (i.e. VEGF and FGF2) as well as the stabilization of the primitive endothelial vessel network (i.e. PDGF-B), ultimately leading to a potent suppression of tumor growth in xenograft animal models.

The early stage angiogenesis, which produces immature endothelial vascular networks, is accomplished by recruitment, migration, differentiation of progenitor endothelial cells, and angiogenic sprouting from the pre-existing blood vessels³². LHT7 significantly inhibited these processes that were stimulated by VEGF and FGF2 *in vitro*. Inhibitory effects of LHT7 on VEGF and FGF2 were further supported at the molecular level: western blot results showed that LHT7 blocked the tyrosine kinase phosphorylation of VEGFR2 and FGFR1 stimulated by VEGF and FGF2, respectively. SPR binding analysis showed that LHT7 bound to VEGF and FGF2, indicating that LHT7 blocked the two pro-angiogenic factors and inhibited their downstream signalings. Previous study has reported that these pro-angiogenic factors have synergistic effect on stimulating angiogenesis²⁷, which was also observed in our *in vitro* studies. Moreover, FGF2 is reported to induce VEGF expression in endothelial cells through autocrine and paracrine manner³³. Therefore, blocking FGF2 in addition to VEGF is essential to disrupt the interconnection between these two pro-angiogenic factors and effectively inhibit the early stage angiogenesis.

It was also shown that LHT7 blocked the maturation of primitive endothelial vessels *in vitro*. Pericytes promote endothelial cell survival by producing VEGF that acts in a juxtacrine manner¹⁶ and by inducing anti-apoptotic protein Bcl-w in the endothelial cells³⁴. The blockade of VEGF did not affect the pericyte recruitment to the endothelial tubes. LHT7, however, inhibited the migration of pericytes towards the tubes, thereby blocking the juxtacrine crosstalk between pericytes and HUVECs, leading to regression of the endothelial tubes.

The paracrine signaling via PDGF-B, which is expressed by endothelial cells, plays a central role in the recruitment of pericytes to the endothelium³⁵. Therefore, the effect of LHT7 on PDGF-B signaling pathway was further investigated. The *in vivo* matrigel plug assay showed that PDGF-B-induced angiogenesis was significantly inhibited in the presence of LHT7. Moreover, LHT7 was also capable of inhibiting the angiogenesis in matrigel that was stimulated by combination of PDGF-B and FGF2, which showed more intensive angiogenesis than by PDGF-B alone. These results were further supported by the decreased tyrosine kinase phosphorylation level of PDGFR β stimulated by PDGF-B in the presence of LHT7.

The intimate interconnection among VEGF, FGF2, and PDGF-B postulates the significance of blocking PDGF-B signaling pathway besides VEGF and FGF2. PDGF-B synergistically stimulates angiogenesis with FGF2³⁰ and also upregulates the expression of FGF2 and VEGF³⁶. For this reason, blocking of PDGF-B is not only critical for inhibiting late stage angiogenesis, but also for early stage angiogenesis. Moreover, VEGF is reported as a negative regulator of vessel maturation, hence blockade of VEGF could facilitate the maturation of vessels, which in turn become insensitive to VEGF inhibition^{11,37}. Therefore, VEGF blockade should be accompanied by PDGF-B blockade to suppress vessel maturation and inhibit tumor angiogenesis effectively. The benefit of blocking VEGF and PDGF-B simultaneously was also demonstrated in a previous study¹³.

Our findings also showed that LHT7 did not induce vascular normalization in tumor blood vessels. Many studies have reported vascular normalization, defined as a structural and functional improvement of the generally abnormal tumor vasculatures during VEGF blockade, which shares lot of similarities with the vascular maturation³⁸. Because PDGF-B is a key regulator in the vascular maturation³², it was hypothesized that treatment of LHT7 would not induce vascular normalization unlike VEGF blockers. To address this question, the tumor vasculatures were observed via DCE-MRI *in vivo*. During three-week treatment of LHT7, permeability of the blood vessels showed no difference,

whereas perfusion throughout the tumor was significantly decreased when compared to the control. The results showed that LHT7 regressed blood vessels in the tumor without going through vascular normalization, implying that LHT7 negatively affected vascular maturation *in vivo*.

Collectively, it was shown that LHT7 could block not only VEGF, but also FGF2 and PDGF-B signaling pathways. It is indisputable that VEGF is a key regulator of angiogenesis³⁹. However, because the aforementioned three pro-angiogenic factors are intimately interconnected to each other, simultaneous inhibition of the three pro-angiogenic factors is likely to inhibit angiogenesis more effectively than blocking only one or two of those. In addition, tumor vasculatures are heterogeneous and presented in various stages of angiogenesis in a single tumor tissue. Therefore, blocking pro-angiogenic factors that are involved in the different stages of angiogenesis is crucial for successful and enduring angiogenesis inhibition. Previous studies have also reported on the efficacy of multiple signaling pathway inhibition by using single or multiple small molecule kinase inhibitors^{13,40}. Despite the therapeutic efficacy of the small molecule kinase inhibitors, however, they exhibited limitations including off-target effect such as cardiotoxicity⁴¹. In addition, since a single pro-angiogenic factor could interact with several receptors (e.g. VEGF on VEGFR1 and VEGFR2), blocking the pro-angiogenic factors could be more effective than blocking the receptor kinases.

Besides the therapeutic benefits of inhibiting multiple pro-angiogenic pathways, there is another advantage that is critical for successful anti-angiogenic therapy. Recent studies have shown that the clinical benefits of VEGF blockers are only transient in many patients. Many reports have demonstrated substantial number of evidences that the evasion of VEGF blockade is due to the upregulation of other pro-angiogenic factors such as FGF2 or PDGF-B, providing alternative pathways to stimulate angiogenesis. Moreover, maturation of primitive vasculatures by pericyte coverage has been also recognized to contribute to the resistance against angiogenesis inhibitors¹¹. Therefore, simultaneous inhibition of angiogenic pathways that are involved in

multiple-stages of angiogenesis would potentially overcome such resistance issue.

3.5. Conclusion

In the aspect of increasing therapeutic efficacy and overcoming the acquired resistance, targeting VEGF, FGF2 and PDGF-B at the same time is critical for successful inhibition of tumor angiogenesis. Despite the chemical modification of heparin, LHT7 retained the capacity of heparin to bind with VEGF, FGF2 and PDGF-B, and showed excellent inhibitory effect on their signaling pathways. Thus, LHT7 would potentially overcome the resistance and effectively inhibit angiogenesis as well as tumorigenesis. It was also confirmed that heparin is an excellent lead compound to develop multi-targeted agent due to its inherent capability to interact with broad range of pro-angiogenic factors.

References

- 1 Carmeliet, P. & Jain, R. K. Angiogenesis in cancer and other diseases. *Nature* **407**, 249-257 (2000).
- 2 Hanahan, D. & Weinberg, R. A. The hallmarks of cancer. *Cell* **100**, 57-70 (2000).
- 3 Folkman, J. Angiogenesis: an organizing principle for drug discovery? *Nat Rev Drug Discov* **6**, 273-286 (2007).
- 4 Boehm, T., Folkman, J., Browder, T. & O'Reilly, M. S. Antiangiogenic therapy of experimental cancer does not induce acquired drug resistance. *Nature* **390**, 404-407 (1997).
- 5 Gorre, M. E. & Sawyers, C. L. Molecular mechanisms of resistance to STI571 in chronic myeloid leukemia. *Curr Opin Hematol* **9**, 303-307 (2002).
- 6 O'Connor, R., Clynes, M., Dowling, P., O'Donovan, N. & O'Driscoll, L. Drug resistance in cancer - searching for mechanisms, markers and therapeutic agents. *Expert Opin Drug Metab Toxicol* **3**, 805-817 (2007).
- 7 Kerbel, R. S., Yu, J., Tran, J., Man, S., Vilorio-Petit, A., Klement, G., Coomber, B. L. & Rak, J. Possible mechanisms of acquired resistance to anti-angiogenic drugs: implications for the use of combination therapy approaches. *Cancer Metastasis Rev* **20**, 79-86 (2001).

- 8 Casanovas, O., Hicklin, D. J., Bergers, G. & Hanahan, D. Drug resistance by evasion of antiangiogenic targeting of VEGF signaling in late-stage pancreatic islet tumors. *Cancer Cell* **8**, 299-309 (2005).
- 9 Kerbel, R. S. Therapeutic implications of intrinsic or induced angiogenic growth factor redundancy in tumors revealed. *Cancer Cell* **8**, 269-271 (2005).
- 10 Shojaei, F., Wu, X., Malik, A. K., Zhong, C., Baldwin, M. E., Schanz, S., Fuh, G., Gerber, H. P. & Ferrara, N. Tumor refractoriness to anti-VEGF treatment is mediated by CD11b+Gr1+ myeloid cells. *Nat Biotechnol* **25**, 911-920 (2007).
- 11 Bergers, G. & Hanahan, D. Modes of resistance to anti-angiogenic therapy. *Nat Rev Cancer* **8**, 592-603 (2008).
- 12 Fernando, N. T., Koch, M., Rothrock, C., Gollogly, L. K., D'Amore, P. A., Ryeom, S. & Yoon, S. S. Tumor escape from endogenous, extracellular matrix-associated angiogenesis inhibitors by up-regulation of multiple proangiogenic factors. *Clin Cancer Res* **14**, 1529-1539 (2008).
- 13 Bergers, G., Song, S., Meyer-Morse, N., Bergsland, E. & Hanahan, D. Benefits of targeting both pericytes and endothelial cells in the tumor vasculature with kinase inhibitors. *J Clin Invest* **111**, 1287-1295 (2003).
- 14 Benjamin, L. E., Hemo, I. & Keshet, E. A plasticity window for blood vessel remodelling is defined by pericyte coverage of the preformed endothelial network and is regulated by PDGF-B and VEGF. *Development* **125**, 1591-1598 (1998).
- 15 Song, S., Ewald, A. J., Stallcup, W., Werb, Z. & Bergers, G. PDGFRbeta+ perivascular progenitor cells in tumours regulate pericyte differentiation and vascular survival. *Nat Cell Biol* **7**, 870-879 (2005).
- 16 Darland, D. C., Massingham, L. J., Smith, S. R., Piek, E., Saint-Geniez, M. & D'Amore, P. A. Pericyte production of cell-associated VEGF is differentiation-dependent and is associated with endothelial survival. *Dev Biol* **264**, 275-288 (2003).
- 17 Orlidge, A. & D'Amore, P. A. Inhibition of capillary endothelial cell growth by pericytes and smooth muscle cells. *J Cell Biol* **105**, 1455-1462 (1987).
- 18 Hirschi, K. K. & D'Amore, P. A. Control of angiogenesis by the pericyte: molecular mechanisms and significance. *EXS* **79**, 419-428 (1997).
- 19 Sasisekharan, R., Shriver, Z., Venkataraman, G. & Narayanasami, U. Roles of heparan-sulphate glycosaminoglycans in cancer. *Nat Rev Cancer* **2**, 521-528 (2002).
- 20 Lee, E., Kim, Y. S., Bae, S. M., Kim, S. K., Jin, S., Chung, S. W., Lee, M., Moon, H. T., Jeon, O. C., Park, R. W., Kim, I. S., Byun, Y. & Kim, S. Y. Polyproline-type helical-structured low-molecular weight heparin (LMWH)-taurocholate conjugate as a new angiogenesis inhibitor. *Int J Cancer* **124**, 2755-2765 (2009).

- 21 Senger, D. R., Perruzzi, C. A., Streit, M., Koteliansky, V. E., de Fougères, A. R. & Detmar, M. The $\alpha 1\beta 1$ and $\alpha 2\beta 1$ Integrins Provide Critical Support for Vascular Endothelial Growth Factor Signaling, Endothelial Cell Migration, and Tumor Angiogenesis. *Am J Pathol* **160**, 195-204 (2002).
- 22 Laib, A. M., Bartol, A., Alajati, A., Korff, T., Weber, H. & Augustin, H. G. Spheroid-based human endothelial cell microvessel formation in vivo. *Nat Protoc* **4**, 1202-1215 (2009).
- 23 Bayless, K. J., Kwak, H. I. & Su, S. C. Investigating endothelial invasion and sprouting behavior in three-dimensional collagen matrices. *Nat Protoc* **4**, 1888-1898 (2009).
- 24 Arnaoutova, I. & Kleinman, H. K. In vitro angiogenesis: endothelial cell tube formation on gelled basement membrane extract. *Nat Protoc* **5**, 628-635 (2010).
- 25 Carpentier, G. Contribution: angiogenesis analyzer. *ImageJ News* (2012).
- 26 Prewett, M., Huber, J., Li, Y., Santiago, A., O'Connor, W., King, K., Overholser, J., Hooper, A., Pytowski, B., Witte, L., Bohlen, P. & Hicklin, D. J. Antivasular endothelial growth factor receptor (fetal liver kinase 1) monoclonal antibody inhibits tumor angiogenesis and growth of several mouse and human tumors. *Cancer Res* **59**, 5209-5218 (1999).
- 27 Pepper, M. S., Ferrara, N., Orci, L. & Montesano, R. Potent synergism between vascular endothelial growth factor and basic fibroblast growth factor in the induction of angiogenesis in vitro. *Biochem Biophys Res Commun* **189**, 824-831 (1992).
- 28 Lever, R. & Page, C. P. Novel drug development opportunities for heparin. *Nat Rev Drug Discov* **1**, 140-148 (2002).
- 29 Abramsson, A., Lindblom, P. & Betsholtz, C. Endothelial and nonendothelial sources of PDGF-B regulate pericyte recruitment and influence vascular pattern formation in tumors. *J Clin Invest* **112**, 1142-1151 (2003).
- 30 Cao, R., Brakenhielm, E., Pawliuk, R., Wariaro, D., Post, M. J., Wahlberg, E., Lebourch, P. & Cao, Y. Angiogenic synergism, vascular stability and improvement of hind-limb ischemia by a combination of PDGF-BB and FGF-2. *Nat Med* **9**, 604-613 (2003).
- 31 Pietras, K., Sjoblom, T., Rubin, K., Heldin, C. H. & Ostman, A. PDGF receptors as cancer drug targets. *Cancer Cell* **3**, 439-443 (2003).
- 32 Carmeliet, P. Mechanisms of angiogenesis and arteriogenesis. *Nat Med* **6**, 389-395 (2000).
- 33 Seghezzi, G., Patel, S., Ren, C. J., Gualandris, A., Pintucci, G., Robbins, E. S., Shapiro, R. L., Galloway, A. C., Rifkin, D. B. & Mignatti, P. Fibroblast growth factor-2 (FGF-2) induces vascular endothelial growth factor (VEGF) expression in the

- endothelial cells of forming capillaries: an autocrine mechanism contributing to angiogenesis. *J Cell Biol* **141**, 1659-1673 (1998).
- 34 Franco, M., Roswall, P., Cortez, E., Hanahan, D. & Pietras, K. Pericytes promote endothelial cell survival through induction of autocrine VEGF-A signaling and Bcl-w expression. *Blood* **118**, 2906-2917 (2011).
- 35 Hellstrom, M., Gerhardt, H., Kalen, M., Li, X., Eriksson, U., Wolburg, H. & Betsholtz, C. Lack of pericytes leads to endothelial hyperplasia and abnormal vascular morphogenesis. *J Cell Biol* **153**, 543-553 (2001).
- 36 Brogi, E., Wu, T., Namiki, A. & Isner, J. M. Indirect angiogenic cytokines upregulate VEGF and bFGF gene expression in vascular smooth muscle cells, whereas hypoxia upregulates VEGF expression only. *Circulation* **90**, 649-652 (1994).
- 37 Greenberg, J. I., Shields, D. J., Barillas, S. G., Acevedo, L. M., Murphy, E., Huang, J., Scheppke, L., Stockmann, C., Johnson, R. S., Angle, N. & Cheresch, D. A. A role for VEGF as a negative regulator of pericyte function and vessel maturation. *Nature* **456**, 809-813 (2008).
- 38 Jain, R. K. Normalization of tumor vasculature: an emerging concept in antiangiogenic therapy. *Science* **307**, 58-62 (2005).
- 39 Ferrara, N., Gerber, H. P. & LeCouter, J. The biology of VEGF and its receptors. *Nat Med* **9**, 669-676 (2003).
- 40 Taeger, J., Moser, C., Hellerbrand, C., Mycielska, M. E., Glockzin, G., Schlitt, H. J., Geissler, E. K., Stoeltzing, O. & Lang, S. A. Targeting FGFR/PDGFR/VEGFR impairs tumor growth, angiogenesis, and metastasis by effects on tumor cells, endothelial cells, and pericytes in pancreatic cancer. *Mol Cancer Ther* **10**, 2157-2167 (2011).
- 41 Force, T. & Kolaja, K. L. Cardiotoxicity of kinase inhibitors: the prediction and translation of preclinical models to clinical outcomes. *Nat Rev Drug Discov* **10**, 111-126 (2011).

Part II

**Novel strategy for site-specific delivery
system and development of doxorubicin
prodrugs**

Chapter 4

General Introduction

4.1. Tumor heterogeneity

Recent studies have revealed extensive genomic and phenotypic variations between tumors (intertumor heterogeneity) and within individual tumors (intratumor heterogeneity)¹. Since the modern cancer therapy has largely shifted to the molecular targeted therapy from the conventional chemotherapy, the inter- and intratumor heterogeneity have produced significant implications in the choice of biomarkers for the guidance of clinical decision-making in cancer treatment.

The diversity of the tumor is mainly caused by the genomic instability, which produces variable cell populations that could adapt to given microenvironments or to exposure of therapies^{2,3}. The genomic instability could arise by various mechanisms and leaves distinct genomic footprints, which then differentially affects tumor progression and patient outcome.

4.1.1. Intertumor heterogeneity

It is not surprising that genomic and functional diversities exist among tumors. Tumors that originate from different tissues and cell types vary in terms of their genomic landscape, since the genetic events of transformation are largely determined by intrinsic biological properties of the cell¹. For this reason, originated organ of the primary tumor is generally considered important in the treatment decisions for cancer patients. However, variations in genomic aberrations and drug sensitivity also exist within tumors that originated from an identical tissue⁴. The clinical complications from to the diversities of tumors have obligated to classify the tumors into subgroups on the basis of mutations,

copy number changes, proteins or mRNA expression profiles, or patterns of genomic instability, thereby making the therapy more predictable in terms of patient outcomes or drug sensitivity⁵⁻⁷. For instance, breast cancers are generally classified according to the expression of HER2 (also known as ErbB2) and treated with different regimen of medication⁷. Also, around 15% of patients with NSCLC in the US and 35% in the East Asia have tumor associated EGFR mutations: this resulted in approval and clinical use of EGFR tyrosine kinase inhibitor (erlotinib, Tarceva[®], Roche) specifically to the NSCLC patients with the EGFR mutations⁸.

Recent advances in next-generation sequencing have revealed greater genomic variations of the tumor than that recognized in the past⁴. In addition, within a cohort of tumors, identical gene could be altered by point mutation, DNA methylation, and copy number alteration, emphasizing the demand for integrative approaches in analyzing somatic aberrations in the cancer genome. The efforts to define tumor subgroups based on specific mutations may be confounded by epistasis, which involves the action of one gene on another. For example, in acute myeloid leukemia (AML), NPM1 mutations confer a favorable prognosis only in the presence of a co-occurring IDH1 or IDH2 mutation⁹.

4.1.2. Intratumor heterogeneity

Not only among tumors, but there also exist significant variations at genomic and epigenomic levels among the tumor cells in a single tumor mass^{10,11}. This diversity poses challenges in revealing the genomic landscape of the tumor as well as validating the biomarker through the traditional sampling bias. The genomically diverse subclonal populations in the tumor appear through the genomic instability of the tumor cells, followed by adaptive selection and outgrowth of the clones that have phenotypic advantage in the given microenvironment during disease progression or therapy¹²⁻¹⁴. There was also a suggestion that genetically heterogeneous subclonal populations in tumors could be maintained by distinct cancer stem cells¹⁵.

Branched tumor evolutions, in which discrete subclones of tumor cells evolve in parallel, followed by the spatial separation of the subclones have been described recently. Multiple region sampling in the primary tumor of renal cell carcinoma and glioblastoma revealed the spatially separated subclones that had heterogeneous somatic mutations and copy number events¹⁶. The clonal multiplicity between primary and metastatic tumor has also been observed in other types of cancer including breast cancer¹⁷, pancreatic cancer¹², and medulloblastoma¹⁸. The diversity of the spatially separated subclones in a single tumor could be so profound that the genomic profiles of the tumor biopsy samples may more closely resemble in tumors from different patients than those of adjacent regions in a single tumor¹⁹.

Different genomic profiles between primary and metastatic tumors could be explained by the different microenvironment of the metastatic site followed by the adaptation and selection of the tumor cells during metastatic processes²⁰. On the other hand, it is difficult to explain how spatial separation of the genomically distinct clones are generated in the primary tumors¹⁶. Distinct microenvironmental niches might exist in the primary tumor, hence the subclones that are occupying each niche could evolve in different manner²¹. Also, there may be physical barriers between different subclones, such as blood vessels or tissue planes, which could prevent incorporation of the tumor subclones¹.

Nevertheless, intermingled heterogeneous subclones are also observed within single biopsies, which neighboring cells display expression of different receptor tyrosine kinases²²⁻²⁴. It is hard to imagine distinct microenvironment scattered around the intermingled subclones of tumor cells. The observation of the intermingled subclones of the tumor cells suggested that genomic instability of tumor cells might be the most crucial factor in the enhanced genomic diversity²⁵. This genomic heterogeneity increases phenotypic diversity, thus expanding the pool of cells that could be subjected to the selection, ultimately leading to emergence of the complex subclonal tumor architecture.

The subclonal mutations directly result in phenotypic variations. In renal cell carcinoma, for example, a heterogeneous *MTOR* mutation resulting in constitutive mTOR kinase activity was strongly associated with distinct mTOR signaling pathway activation after mTOR inhibitor therapy¹⁶. In a heterogeneous glioblastoma multiforme cell population with mosaic amplification of *EGFR* and *PDGFRA*, simultaneous blockade of both kinases was necessary to inhibit PI3K pathway activity²⁶. Observation of intermingling tumor cells with distinct receptor kinase amplification suggested functional codependency between the two cell populations²⁶⁻²⁸. Indeed, it has been found that *EGFR* mutant cells release interleukin 6 (IL6) and leukemia inhibitory factor (LIF), which facilitate the growth of adjacent subclones by activation of wild-type *EGFR*²⁹. This finding provided evidence of possible codependency between distinct subclones within tumor¹.

The phenotypic variations could also occur in the genomically homogeneous subclones by functionally distinct behavior and patterns of proliferation after exposure to therapy³⁰. The phenotypic heterogeneity arises not only through genomic differences between subclones, but also through stochastic events in gene expression and protein stability, epigenetic divergence and microenvironmental alteration^{11,30,31}.

4.2. Apoptosis targeted prodrug system

Despite the emergence of targeted therapy in the modern cancer therapeutics, chemotherapeutic agents are still widely used for the treatment of broad array of tumors in the first-line therapy as a single agent or in combination with other targeted therapies. Their clinical application, however, is often limited due to the dose-dependent toxicities³². These side effects are closely related to the non-selective distribution of doxorubicin throughout the body after administration³³. Therefore, many efforts have been made to deliver the chemotherapeutic agents selectively to the tumor tissue by introducing certain targeting moieties that could recognize tumor-specific ligands^{34,35}. These strategies, however, produced

only limited improvements due to the intertumor and intratumor heterogeneities, which were described in the previous section. Especially, finding of the intratumor heterogeneity posed challenges in the modern cancer therapeutics, which has relied on a single needle biopsy or the surgical excision of an extremely small portion of a tumor to overview its entire genomic landscape¹⁶. Therefore, efforts to deliver chemotherapeutic agents specifically to a tumor by relying on a target ligand expression have been ineffective thus far.

For an effective and reliable delivery of the chemotherapeutic agents to the tumor, a strategy of targeting an induced apoptosis of tumor cells is proposed for the drug delivery. In particular, caspase-3 is selected as the molecular target, which is a family of cysteine proteases and is upregulated during apoptotic events³⁶. The major advantage of utilizing caspase-3 as the molecular target is that the target site of the drug could be actively controlled by exogenous stimuli (i.e. radiation) rather than passively relying on the genotypic ligand expression of the tumor. Moreover, many chemotherapeutic agents trigger apoptosis by activation of caspase-3^{37,38}; therefore, the delivered agents could further upregulate the caspase-3 in the site where the apoptosis was initially induced. For this reason, the caspase-3 could sustain its local concentration within the site of the interest.

4.2.1. Caspase in apoptosis

Apoptosis is a term for the programmed cell death, which plays a central role in the development and homeostasis of metazoans³⁹. Either excessive or insufficient apoptosis could result in severe pathological consequences. For instance, suppression of the normal apoptotic pathways could cause autoimmune diseases and cancer. By contrast, abnormal upregulation of apoptosis contributes to neurological disorders. Since the concept of apoptosis was defined in 1972, hundreds of genes that regulate this event have been identified and showed that the mechanism of apoptosis is evolutionarily conserved^{40,41}.

Among the various components that participate in the apoptotic response, caspases play central role⁴¹. Caspases are a conserved family of cysteine proteases – peptidases that use a cysteine residue as the catalytic nucleophile and hydrolysis the amide bond after an aspartic acid residue of their substrates⁴² – that irreversibly induce cell death. Until now, at least 14 distinct mammalian caspases have been identified, and 11 of those are also found in humans⁴³. Among them, at least seven are known to play a key role in apoptosis. The apoptotic caspases are generally classified into two groups, initiator and executioner caspases, depending on their point of entry into the apoptotic cascade. The initiator caspases include caspase-2, -8, -9, and -10; the executioner caspases include caspase-3, -6, and -7⁴³. The initiator caspases are first activated through a particular apoptotic pathway and initiate the downstream signaling cascade by activating the executioner caspases⁴⁴.

All the caspases are produced and stored in cells as latent precursors that are catalytically inactive zymogens. These procaspases require proteolytic activation for the outbreak of their inherent enzymatic activity during apoptosis. The activation mechanisms of the initiator and executioner caspases totally differ to each other. The activation of the executioner caspases is mediated by the initiator caspases, which cleave the specific internal aspartic acid residue and separate the large (~p20) and small (~p10) subunits of the executioner caspases. On the other hand, the initiator caspases do not require cleavage for their enzymatic activation. Instead, they are activated by dimerization of the inactive monomeric zymogens – the zymogens of the initiator caspases that exist in the cell – through the assembly of a multi-component complex under apoptotic conditions^{45,46}. For instance, the activation of procaspases-9 is facilitated by the apoptosome, which is a ~1.4 MDa complex that includes APAF1 and cytochrome *c*^{47,48}. As the activation of the initiator caspases triggers the downstream apoptotic signalings, they are tightly regulated in the cells. Once activated, the downstream executioner caspases induce proteolytic cleavage of a wide array of cellular targets and ultimately lead to cell death⁴⁹.

In mammalian cells, the apoptosis occurs through either intrinsic or extrinsic pathway depending on the origin of death stimuli. The intrinsic pathway is triggered in response to apoptotic stimuli such as oncogene activation, DNA damage, and exposure to chemotherapeutic agents as well as ionizing radiation⁴⁴. Therefore, inactivation of the intrinsic pathway is generally considered as a hallmark of cancer⁵⁰. Following the apoptotic stimuli, mitochondria mediate the intrinsic pathway by releasing several proteins including cytochrome *c*, SMAC/DIABLO, AIF, EndoG, and OMI/HTRA2 from their intermembrane space to cytoplasm⁵¹. Particularly, the cytochrome *c* binds to APAF1, followed by the conformational change that allows the APAF1 to further bind ATP/dATP and eventually form the apoptosome. The apoptosome mediates the activation of caspase-9, which in turn cleaves and activates the executioner caspases, caspase-3 and -7^{52,53}.

The extrinsic pathway is initiated by the ligation of transmembrane death receptors such as Fas (also known as CD95 or APO-1)⁵⁴. When death ligands such as FasL bind on their receptors and form ligand-receptor complexes on the cell surface, adaptor molecule FADD (Fas-associated protein with death domain) and caspase-8 are recruited subsequently to the cytosolic tail of the complexes by a multi-step mechanism to form an oligomeric death-inducing signaling complex (DISC)⁵⁵. Formation of the DISC leads to the activation of the caspase-8, an initiator caspase, which then activates caspase-3 and -7, an executioner caspase. Caspase-8 activation by the TNF pathway is also demonstrated: the caspase-8 is activated by association with a cytosolic complex rather than at a membrane-associated signaling complex during TNF-induced apoptosis^{56,57}. The extrinsic pathway can crosstalk to the intrinsic pathway through the caspase-8-mediated cleavage of BID, a Bcl-2 interacting protein, which then triggers the release of the mitochondrial proteins^{58,59}.

4.2.2. Substrate recognition by caspases

Caspases recognize specific four continuous amino acid residues represented as P4-P3-P2-P1 within in their substrates, and hydrolytically cleave after the C-

terminus of P1 residue, which is usually an Asp. It has been widely accepted that the preferred amino acid residue in the P3 position is Glu for every caspases that have been examined⁴³. The preference in the P4 position varies among different groups of caspases and determines the substrate specificity. In the early study, Thornberry et al. demonstrated the peptide substrate specificities for the caspases using a positional scanning synthetic combinatorial library⁶⁰. This technique takes advantage of caspases enzymatically hydrolyzing the synthetic tetrapeptides that have C-terminal aminomethylcoumarin (AMC) as a fluorescently active leaving group. They examined nine human caspase family members (caspase-1 to caspase-9) and classified the caspases into three groups based on their substrate specificity. The members of group I (caspase-1, -4, and -5) preferentially recognized the tetrapeptide sequence WEHD. On the other hand, the members of group II (caspase-2, -3, and -7) preferred DEXD for their optimal recognition sequence, where the amino acid residue in P2 position could vary. In particular, the substrate specificity profiles shown between caspase-3 and caspase-7 were practically indistinguishable. The group III caspases (caspase-6, -8, and -9) preferred the sequence (L/V)EXD, where Leu and Val are interchangeable in the P4 position. The substrate specificity of the caspases is directly correlated with their physiological role. The group I caspases are involved in the inflammatory pathway, whereas the group II and III caspases are involved in the apoptotic pathway. Particularly, the group II caspases are executioner caspases and the group III caspases act as initiator caspases.

The comparison of the substrate specificities of caspases revealed the strict requirement of Asp in the P1 position of the substrate for every examined caspases. In addition, although not as strict as the preference of Asp in the P1 position, the caspases preferred Glu in P3 position in their substrates in varying degrees. Also, with only exception of caspase-9, which showed strong preference of His, liberal substitution in P2 position was also well tolerated for most of the caspases. As mentioned above, P4 position was the most critical determinant of the substrate specificity for caspases. The group I caspases was

Table 4.1. Optimal substrate sequences for caspases

Group	I			II			III		
Caspase	1	4	5	2	3	7	6	8	9
Sequence	WEHD	LEHD	LEHD	DEHD	DEVD	DEVD	VEHD	LETD	LEHD

able to accommodate large aromatic or hydrophobic amino acids in this position. On the other hand, the group II caspases strongly preferred Asp for efficient catalytic cleavage. The group III caspases generally allowed variable amino acids in this position, but preferred those with large aliphatic side chains. The optimal sequences for each caspase are shown in **Table 4.1**⁶⁰.

The recognition sequences for the each group of caspases are found in many proteins that are involved in the apoptotic signaling cascade⁶⁰. The optimal recognition motif of the group II caspases (DEXD) is found in cleavage sites of several cell maintenance and repair proteins that participate in the apoptotic event, including SREBPs⁶¹, D4-GDI⁶², PARP⁶³, SNRNP70⁶⁴, DNA-PKcs⁶⁴, and PRKCD⁶⁵. Some of these are endogenous substrates for the caspase-3^{64,66}.

On the other hand, the recognition sequence for the group III caspases are found in zymogens of several executioner caspases, particularly in caspase-3 and caspase-7. This indicated that the group III caspases indeed act as an initiator of the apoptotic cue by proteolytically activating the executioner caspases⁶⁰. Interestingly, initiator caspases have an extended N-terminal region that has specificity similar to their substrate sequences. This N-terminal region plays a crucial role in mediating dimerization of the monomeric initiator procaspases, resulting in their autocatalytic activation^{44,60}.

Although the optimal recognition sequences for each caspases have been identified and widely accepted by the remarkable study of Thornberry et al. in 1997⁶⁰, further studies have demonstrated divergent sequences for several caspases^{36,67,68}. As mentioned earlier in this section, caspase-3 and caspase-7 was shown to have their substrate specificity in DEXD, especially DEVD, identified by positional scanning synthetic combinatorial library (PS-SCL)⁶⁰. However, substrate-phage display library – the substrate is presented as a

proteolytically accessible-linker between two protein domains, making the context more akin to that of the natural substrate – showed that the optimal substrate preference of caspase-3 was DXVD rather than previously proposed DEXD. This study demonstrated that DLVD was 1.7-fold more rapidly hydrolyzed by caspase-3 than the canonical DEVD peptide, disputing the sequence preference of the group III caspases of the early report. Moreover, the amino acid residue in the P4 position within the substrates for caspase-3 were not as strictly limited to Asp as demonstrated earlier, and the enzyme also cleaved substrates with substitutions at the P4 position selected by phage display, albeit at a lower rate. The preferred sequence selection for caspase-8 showed that Glu was predominantly preferred in the P3 position of the substrate, agreeing with the previous reports. However, based on substitutions observed through the phage display in the P4 position, AETD showed 1.6-fold faster proteolysis than the canonical LETD sequence by caspase-8⁶⁷, which contradicts with the preferred requirement of Leu or Val at the P4 position for the group III caspases that was reported previously⁶⁰. Moreover, computational screening based on the amino acid positional fitness (APF) scores predicted DNLD and DFPD as potent inhibitors for caspase-3 and caspase-7, respectively⁶⁸. Requirement of Glu in the P3 position of the substrate for caspase-7 was further challenged by the study in crystal structures of caspase-7 complexed with the peptide analog of DMQD, DQMD, DNLD, IEPD, ESMD, or WEHD. The crystal structures showed that the S2 pocket of caspase-7 could accommodate with diverse amino acid residues. DMQD, DQMD, and DNLD, which varies in their P3 residue, interacted with caspase-7 as strongly as that of the canonical DEVD sequence, suggesting that Glu in the P3 position is not mandatory³⁶.

Caspases recognize their substrates through the four active-site loops, named L1, L2, L3, and L4, which constitute the substrate-binding groove. The L1 and L4 loops constitute the each flank of the groove, whereas L2 is located at the base. L2 loop, which harbors the catalytic residue Cys, is located at one end of the groove and is critical for binding and catalytic hydrolysis of the substrates.

The structural composition of the L1 and L3 loops is conserved among all mammalian caspases, whereas the L2 and L4 loops are highly divergent. These four loops are the determinant of the substrate sequence specificity. The binding pockets for the P4-P3-P2-P1 of the substrate are defined as the S4-S3-S2-S1 subsites, respectively. The pockets are mainly located between the base (L3) and the two flanks (L1 and L4) of the substrate-binding groove. The S1 and S3 subsites show slight variance among caspases, whereas the S2 and S4 subsites are conserved⁴³. The P1 residue of the substrate is coordinated by three invariant residues at the S1 subsite, an Arg residue of L1, a Gln residue at the beginning of L2, and an Arg residue at the end of L3⁶⁹. The Arg residue of L3 also coordinates the P3 residue of substrate. The S2 and S4 subsites map mainly to the L3 and L4 loops, thus the P2 and P4 residues exhibit greater sequence variation.

4.3. Tumor targeting strategies

4.3.1. Passive tumor targeting

Particulate carrier systems and macromolecules have been extensively studied and exploited in purpose to deliver chemotherapeutic agents selectively to tumor in passive manner. The passive targeting of macromolecules takes advantage of abnormal vascular architecture and physiological properties of tumor that results in enhanced permeation and retention (EPR) effect. The fundamental basis of the EPR effect is that tumor vasculatures are fenestrated and leaky, whereas normal vasculatures are tight and well-organized, thereby allowing macromolecules to escape from the circulation only in the tumor tissue⁷⁰. Drug delivery based on the EPR effect is applicable for most of the rapidly growing solid tumors with the exception of hypovascular tumors such as prostate cancer or pancreatic cancer⁷¹. Therefore, consideration of EPR effect is now the gold standard in designing drug carrier for tumor-targeted delivery.

The EPR effect of macromolecules in tumor was first suggested by Matsumura and Maeda in 1986⁷². They demonstrated that most of the solid

tumors have highly defective vasculatures and produce extensive amounts of vascular permeability factors such as VEGF, resulting in enhanced vascular permeability of the macromolecules. Moreover, tumors are highly vascularized showing relatively higher vascular density in comparison with normal tissues⁷³. The vascular dependency of the EPR effect was demonstrated by an experimental study involving a complex of Evans blue and albumin⁷⁴. When administered intravenously, the dye was exclusively found in the tumor, but not in the normal tissues. Interestingly, in the experimentally induced tumors with a diameter larger than 3 cm, the dye was found predominantly in the tumor periphery, where the functional blood vessels were mainly distributed. Considering that central regions of tumors are generally necrotic or hypovascular, these experimental results strongly supported that EPR effect is closely related to the presence of tumor vasculatures⁷³.

Among several characteristics of the tumor vasculatures, the defective and porous vessel wall is the major cause of the facilitated transportation of macromolecules or particles into the tumor. The EPR effect is largely dependent to the molecular weight of the macromolecules. Substances larger than 40 kDa, which is the threshold of renal clearance, have prolonged plasma half-life (increased plasma half-life) and very slow clearance, resulting in higher AUC (area under the concentration-time curve). They are also capable of leaking out through the tumor vessels and accumulating in tumor tissue, but not in normal tissues^{72,73}. It was reported that the accumulation of polymeric or macromolecular substances in tumor tissues was more than 10-200 fold higher than that in normal tissues and organs, such as skin, muscle, heart, and kidney⁷⁵⁻⁷⁹. The selective accumulation of the macromolecules in the tumor tissue is strongly correlated to the pore size of the fenestrae that exist on the tumor vasculatures. The pore size of the fenestrae varies from 100-1200 nm in diameter⁸⁰. Since the macromolecules that are generally employed as a tumor-targeted delivery vehicle typically have hydrodynamic radii in the range of 2-10 nm, they are capable of selectively extravasating in tumor tissue.

However, facilitated extravasation of macromolecules through the leaky tumor vasculatures only partly explains the enhanced accumulation, since the small molecules could also act in a similar manner. It has been widely accepted that macromolecules remain for prolonged time than small molecules when penetrated into the tumor tissue. The clearance rate from the tumor interstitium is dependent to the size of the accumulated molecules⁸¹. Small molecules were rapidly removed, whereas large molecules that exceeded 40 kDa in their molecular weight retained high intratumor concentration even after 100 hours of post application. The enhanced retention of the macromolecules in tumor is primarily caused by the lack of effective lymphatic drainage due to an impaired or absent lymphatic system in the tissue. Generally in normal tissues, the lymphatic system can effectively remove the penetrated macromolecules from the interstitial space. By contrast, the macromolecules in the tumor tissue cannot be removed by lymphatic drainage due to the defective lymphatic system, thereby they remain in the tissue for prolonged time⁷³. The EPR effect was observed in various substances including proteins, drug-polymer conjugates, micelles, liposomes, nanoparticles, DNA polyplexes, and lipid particles⁷³. Although the size of the macromolecules or particles is considered to be critical, the particle shape and surface characteristics are also important in determining the degree of EPR effect⁷⁰.

Because of the capability of allowing selective accumulation in many solid tumors, EPR effect has been considered to be one of the most practical principles in tumor targeting and regarded as highly promising paradigm for improving the therapeutic index of chemotherapeutic agents. Doxil[®], a PEGylated liposomal formulation of doxorubicin, is a representative example of an anticancer agent that is approved and successfully used clinically in the basis of the EPR effect. Many other drugs employing the passive targeting are also in clinical evaluations⁸²⁻⁸⁴. These drugs showed superior pharmacokinetic profile (i.e. extended plasma half-life) and more importantly, significantly higher tumor selectivity. Therefore, they produced improved anticancer effects with appreciably less adverse reactions than the conventional chemotherapeutic

agents. Despite the delivery of chemotherapeutic agents using the passive targeting have been proven effective in cancer therapy, there are still some hurdles to be surmounted. The passive targeting often results in low amount of drug delivered to the tumor, resulting in insufficient therapeutic efficacy^{85,86}. Moreover, the passive targeting some times disappointing selectivity, thereby producing insignificant improvement in the therapeutic index⁷⁰.

4.3.1.1. Albumin as a carrier for tumor targeting

Albumin is recognized as a versatile protein carrier molecule for the passively targeted drug delivery that could improve pharmacokinetic profile of drugs. It is the most abundant plasma protein accounting for more than half of the total plasma protein with a concentration of 35-50 mg/ml in human serum, and distributed throughout the body including blood circulation, lymphatic system, and extracellular as well as intracellular compartments⁸⁷. Albumin is one of the smallest proteins that present in plasma with molecular weight of 65 kDa. It is produced in the liver at a rate of approximately 0.7 mg/h per gram of liver tissue (10-15 g per day) with a very long plasma half-life, showing average 19-21 days in human.

The diverse physiological functions of albumin are partly from its distinct ability to bind with many substances in the biological fluid. It acts as a transport vehicle for long chain fatty acids (e.g., oleic acid, stearic acid, and palmitic acid) and metal ions (e.g., Cu^{2+} , Ni^{2+} , Ca^{2+} , and Zn^{2+}) in the blood, and also aids their uptake into the cells. It also binds with bilirubin, which is a degraded product of heme, and various kinds of hormones. Furthermore, it is capable of binding with broad range of pharmaceutical agents such as penicillins, sulfonamides, indoles, and benzodiazepines to name just few, thereby significantly affecting their pharmacokinetic properties. Regarding the abundance of the albumin in plasma, it is apparent that many metabolic substances and therapeutic agents could be affected and transported by this protein. Albumin also has some other physiological roles that are not related to its capability of binding with other biological substances. It is the protein that is most responsible for regulation of

the colloidal osmotic pressure in blood. Moreover, it is also a major source of amino acids for the peripheral tissue^{88,89}.

Human serum albumin is used for many purposes, mainly as a blood substitute, for treatment of certain pathological conditions (e.g., severe burns, nephritic syndrome, cardiopulmonary bypass, acute respiratory distress), and for compensating hypoalbuminemia as well as cachexia in cancer patients^{87,90}. As an alternative to the blood derived albumin, recombinant human albumin (Recombunin[®], Novozymes Biopharma) was developed and has shown comparable safety, tolerability, pharmacokinetics, and pharmacodynamics to the native human serum albumin⁹¹.

Besides the therapeutic applications, albumin has also been extensively studied for the potential as a drug carrier molecule. Albumin is a very soluble protein and generally regarded to be extremely robust, since it is stable in very broad range of pH (pH 4-9) and remains intact without any deleterious effect up to 40% ethanol and at 60°C for 10 hours. The physicochemical stability, long plasma half-life, preferential uptake in tumor and inflamed tissue, availability, biodegradability, and lack of toxicity and immunogenicity make it an attractive carrier molecule in the drug delivery field⁸⁹.

Albumin accumulates in malignant or inflamed tissue through EPR effect like other macromolecules. The first literature demonstrating that tumors could trap plasma proteins and use the metabolized products for their survival and proliferation appeared was reported in 1954⁹². This was further supported by an important study that was reported in 1986, which demonstrated the tumor accumulation of plasma proteins depending on their sizes⁷². The accumulation rate of the proteins ranging from 12-150 kDa in their molecular weight was closely related to their pharmacokinetic profile: the long circulation time was essential for the facilitated tumor accumulation. The plasma proteins that lie above the renal threshold (40 kDa) in terms of molecular weight have similarly long plasma half-life, hence accumulate in the malignant tissue due to the EPR effect⁹³. In fact, similar degree of tumor accumulation was observed between albumin and immunoglobulin, which have molecular weight of 66.5 and 150

kDa, respectively⁷². As described above (see section 5.3 for more detail), EPR effect in tumor is produced by the leaky vasculatures that allow the penetration of macromolecules through the fenestrae on the vessels^{72,94}. The pore size of the fenestrae varies from 100-1200 nm in diameter. Therefore, albumin, which has an effective diameter of 7.2 nm, could freely penetrate through the pores^{80,89,95}. Many experimental studies concerning the uptake of either radio- or chemical dye-labeled albumin showed that 3-25% of the total dose applied to the animal was found in the grafted tumor⁹⁶.

Besides EPR effect, which is a common feature of macromolecules for their tumor selective accumulation, there is also an albumin-specific tumor accumulation mechanism. On endothelial cell surface, 60 kDa glycoprotein gp60 (also known as albondin) is expressed, which mediates the albumin transportation pathway⁹⁷⁻⁹⁹. When albumin is bound to the gp60, it is internalized via caveolin-mediated endocytosis and transcytosed across the endothelium. Interestingly, some tumors secrete SPARC (secreted protein acidic and rich in cysteine), a gp60 homologous 43 kDa extracellular glycoprotein with high binding affinity to albumin. This protein binds to the transcytosed albumin in the tumor interstitium and prolong the residence time, and also contribute to the deep tumor penetration¹⁰⁰⁻¹⁰³. Clinical studies suggested that the overexpression of SPARC might be an important principle for the improved therapeutic efficacy of Abraxane[®] (albumin-paclitaxel nanoparticle) in comparison to the conventional formulation of paclitaxel. Sub-analysis of the overall SPARC levels in the metastatic pancreatic cancer patients treated with Abraxane[®] during phase I/II clinical trials showed that high SPARC levels correlated with improved overall survival (n = 20; median survival 13.6 months, *P* = 0.02) in comparison to the patients with low SPARC levels (n = 16; median survival 8.1 months)¹⁰⁰. Similar result was also shown in a retrospective analysis of 16 head and neck cancer patients¹⁰⁴.

In addition, to explain the high albumin turnover in tumors, Stehle et al. have proposed that tumor cells continuously and actively uptake the circulating albumins as their major energy and nutrition source¹⁰⁵. Their report was based

on the observation of the excessive plasma protein catabolism by tumor cells in demand for their aberrant metabolism and rapid proliferation. It has been also suggested that this continuous demand for albumin by tumor cells could contribute to the accumulation of albumin or albumin-bound pharmaceutical agents in the tumor¹⁰⁶.

Using albumin as a drug carrier has another advantage besides the tumor targeting capability. As mentioned earlier, serum albumin has the half-life of more than 19 days in human¹⁰⁰. Due to the long half-life of albumin, conjugating therapeutic agents such as peptides and cytokines is an attractive approach in improving their pharmacokinetic properties. The molecular weight of albumin (66.5 kDa), which exceeds the renal clearance threshold (40 kDa), is suggested to be one reason for the long half-life. However, recent studies demonstrated that binding of albumin to the neonatal Fc receptor (FcRn) could be the major reason for the extremely long plasma half-life of albumin. The FcRn, which is a membrane-bound receptor on the endothelial cell surface, is responsible for the long plasma half-life IgGs and related antibodies, which is also in the range from 2-3 weeks in human. It was suggested that the FcRn extend the half-life of albumin in a similar way that does to IgGs: an FcRn-mediated recycling in vascular endothelial cells, which protects IgGs or albumins from degradation^{107,108}.

4.3.1.2. Exploiting endogenous albumin for albumin-bound agents

More than a decade ago, Kratz et al. have proposed a concept of directly exploiting endogenous circulating serum albumin as a carrier for drug *in situ* instead of preparing an albumin-drug conjugate prior to administration¹⁰⁹. The therapeutic strategy according to the literature demonstrated the chemically engineered form of active compound binding rapidly and selectively to the circulating serum albumin in the blood after intravenous administration, thereby producing albumin-conjugated form of the compound *in situ*.

There are several significant advantages of exploiting circulating serum albumin as a drug carrier over preparing synthesized albumin-drug conjugates *ex vivo*. The advantages are as follows: the use of possibly pathogenic exogenous albumin could be avoided; the final form of the drug before administration is a chemical drug, thereby the substance could be easily defined; the production of the drug is relatively simple and inexpensive due to the straightforward organic chemistry; the analytical requirements for defining and managing the pharmaceutical products are comparable to the other chemical drugs; and the final product is relatively more stable, thereby allowing better storage and handling¹¹⁰.

The unique feature of the circulating albumin allows the chemically engineered compound to selectively react with the albumin among numerous other plasma substances. The *in situ* albumin binding involves Cys34 residue, which is located in subdomain IA of human serum albumin. This residue is highly conserved in all of the mammalian species that have been yet studied^{88,111}. The defatted albumin structure (PDB code 1ao6) revealed by X-ray crystallography showed that Cys34 is located in a hydrophobic crevice on the surface of the protein in 10-12 Å depths. However, binding of five molecules of myristic acids to albumin (PDB code 1bj5) induced conformational change and opened the crevice, thereby exposing the Cys34 to the surface¹¹².

Generally in the plasma, serum albumins are bound with one to three molecules of long-chain fatty acids. Therefore, most of the serum albumins have Cys34 exposed on the surface⁹⁶. Around 70% of the circulating albumins in the bloodstream contain an accessible Cys34 with free thiol group that is not blocked by endogenous thiol-bearing compounds such as cysteine, homocysteine, cysteinylglycine, glutathione, and nitric oxide. Physiologically, the thiol group on Cys34 was reported to play a role as scavenger for endogenous thiols, oxidants, and heavy metals (e.g., Cd²⁺, Au²⁺, Hg²⁺, Ag²⁺).

The free thiol exposed on the surface of albumin is a very unique feature regarding that only three other serum proteins have cysteine residues without interchain disulfide bond. One of them is apolipoprotein B-100, which has two

cysteine residues (Cys3734 and 4190) at the C-terminal end of the protein¹¹³. Another is fibronectin, which has two cryptic free thiol groups that have no reactivity under physiological condition¹¹⁴. Last is α_1 -antitrypsin, which has a single cysteine residue (Cys232) that is generally connected to either cysteine or glutathione by disulfide linkage in the plasma¹¹⁵. Despite that there are also many other small molecules containing thiols, the free thiol on the serum albumin accounts for 80-90% of the total free thiol concentration (400-500 μM) in the blood. Most of the thiol groups in the other blood substances exist as an oxidized form. The overall concentration of free thiols on the small molecules hardly exceeds 20 μM (i.e., cysteine 10-12 μM , homocysteine 0.15-0.25 μM , cysteinylglycine 3-4 μM , glutathione 4-5 μM) in human plasma, which is significantly lower amount than that of the circulating albumin¹¹⁰.

Moreover, the free thiol of Cys34 in serum albumin has the highest reactivity among the thiol groups in the substances that present in human plasma. In fact, the pK_{SH} (pK value of the thiol group) of cysteine and glutathione, which are the most abundant thiol-containing molecules besides the serum albumin, are 8.5 and 8.9, respectively. On the other hand, the pK_{SH} of the Cys34 in serum albumin is around 7, hence most reactive¹¹¹. Considering that the accessible thiol group on Cys34 of the serum albumin possesses the major portion of total free thiols in the plasma with the highest reactivity, it is an ideal target for the *in situ* selective coupling with a thiol-reactive compound after entering the bloodstream.

The first drug to employ the concept of the *in situ* albumin binding is aldoxorubicin (formerly INNO-206 or DOXO-EMCH; CytRX corporation), which is a doxorubicin derivative that could bind to the Cys34 of albumin via maleimide functional group. The drug is currently in phase II/III clinical investigation on patients with soft tissue sarcoma, glioblastoma, Kaposi's sarcoma, or small cell lung cancer. The aldoxorubicin has been proved to be as effective as doxorubicin with significantly less adverse effects. During the clinical trials, the administered dose of the aldoxorubicin were up to four times of the standard dose of doxorubicin, but showed no increase in the observed

side effects with superior therapeutic efficacy^{116,117}. There are also several other drugs in the preclinical investigations that employ the *in situ* albumin binding strategy, such as doxorubicin prodrug activated by urokinase-type-plasminogen activator (uPA)¹¹⁸, prodrugs of camptothecin and doxorubicin that are activated by cathepsin B¹¹⁹, and prodrug of zosuquidar¹²⁰, and showed successful binding to the circulating albumins.

4.3.2. Active tumor targeting strategy

Active targeting takes advantage of molecular recognition such as ligand-receptor and antigen-antibody, which could specifically bind to certain molecules that are overexpressed in a target tissue¹²¹. For the active tumor targeting, targeting ligands are attached at the surface of particulate carriers or directly conjugated to chemotherapeutic agents to deliver them to the tumor. The enhanced selectivity towards the tumor tissue produced increased therapeutic efficacy and reduced adverse effects⁸⁶.

The selectivity of the active targeting largely depends on the expression pattern of target molecule and the binding affinity of targeting ligand. An ideal target molecule should be exclusively and abundantly expressed on the tumor cells. In addition, they should be expressed homogeneously throughout the entire population of the tumor cells. Such a target molecule would allow the active targeting to affect the tumor cells potently and uniformly, but not the normal cells⁷¹.

The targeting ligand is also important for the successful active targeting. When a target molecule is determined, an appropriate targeting ligand should be selected and employed to the drug or carrier. An ideal targeting ligand should have very high affinity against the target molecule, but have very low or no affinity against any other molecules, thereby allowing it to specifically bind to the target molecule in the body. Many classes of substances such as aptamers, antibodies, peptides, and several ligand molecules (e.g., folate and transferrin) that are capable in high-affinity binding to a number of tumor-specific molecular targets have been investigated and proved useful⁷⁰. In particular,

antibodies and peptides have been extensively studied for their relative ease of developing high-affinity ligands for wide array of the known and newly discovered molecular targets.

Antibodies target specific antigens presented on the cell membrane or secreted from the cells. However, when using antibodies as the vehicle for targeted delivery of chemotherapeutic agents, the antigens on the cell membrane are mainly considered as the target. The application of antibodies in molecular targeted therapies has been extensively investigated over the past decades, resulting in development of numerous clinically available drugs. The therapeutic antibodies have been proven to be clinically beneficial in broad range of tumors such as chronic lymphocytic leukemia, colorectal cancer, metastatic lung cancer, advanced non-small cell lung cancer, non-hodgkin's lymphoma, advanced melanoma, and metastatic breast cancer^{86,122-125}. They function by binding to a specific antigen expressed on the tumor cells. The interaction between antibody and antigen results in alteration of the antigen function that may be critical in tumor growth and survival, thereby inducing antitumor effects by multiple mechanisms¹²⁶. EGFR is one of the most investigated molecular targets in clinical oncology. It is overexpressed in many tumors and plays significant role in proliferation and survival of the tumor cells, leading to development of monoclonal antibody against EGFR as an anticancer agent (cetuximab, Erbitux®, Bristol-Myers Squibb)¹²⁷. Other monoclonal antibodies have been developed such as ibritumomab tiuxetan (anti-CD20 mAb for radioimmunotherapy), panitumumab (anti-EGFR), rituximab (anti-CD20), tositumomab (anti-CD20), and trastuzumab (anti-HER2), which targets many cell surface antigens¹²²⁻¹²⁵.

Although antibodies have significant therapeutic activity by themselves in the cancer therapy, they have been also proved to be useful as vehicles for the tumor selective delivery of chemotherapeutic agents and particulate carrier systems. The nanoparticles conjugated with trastuzumab or rituximab were found at the frequency of 10-fold higher than the non-conjugated nanoparticles in the cells expressing the respective antigens¹²⁸. Antibody-drug conjugates

(ADCs), which cytotoxic agents are directly conjugated to an antibody, have recently gained much interest in the drug discovery field. The idea of combining antibody and cytotoxic agent for the selective delivery of the cytotoxic agent to the tumor dates back to the 1980s. However, due to the technological limitations in the past, the clinically practical products were only recently developed and approved¹²⁹. Owing to the discovery of appropriate targets and advances in bioconjugate technology, the development and clinical application of ADCs are accelerating rapidly. Indeed, as a pioneer of the new generation ADCs, brentuximab vedotin (Adcetris[®], Seattle Genetics), a monomethyl auristatin E (MMAE) conjugated CD30-specific monoclonal antibody, was approved by the US FDA in August 2011 for treatment of Hodgkin's lymphoma and systemic anaplastic large cell lymphoma. Another ADC, ado-trastuzumab emtansine (Kadcyla[®], Genentech), gained approval by the FDA in February 2013 for patients with HER2 (also known as ErbB2)-positive metastatic breast cancer. A number of ADCs, including inotuzumab ozogamicin (calicheamicin conjugated CD22 mAb; Pfizer), lorvotuzumab mertansine (DM1 conjugated CD56 mAb; ImmunoGen), and glembatumumab vedotin (MMAE conjugated GPNMB mAb; Seattle Genetics), are also in clinical investigation. Due to the highly selective targeting to tumor cells, the ADCs showed potent clinical efficacy with impressive safety and tolerability profiles¹³⁰.

Peptides have also been frequently used as targeting ligands for delivering chemotherapeutic agents to tumor. Screening and selection of the peptide sequence that could potentially bind to specific molecular targeted is typically achieved through combinatorial phage display technique. This approach produces peptide ligands ranging from 10-15 amino acids in length that selectively bind to target molecules in high affinity^{86,131,132}.

Integrin $\alpha v \beta 3$, which is overexpressed in several kinds of tumors and also on tumor endothelial cells, is one of the representative target molecule that has high affinity peptide ligands¹³³. It is specifically recognized by a tripeptide sequence, Arg-Gly-Asp (RGD)¹³⁴. Further investigation in RGD sequence has

led to discovery of several linear or cyclic peptides comprising RGD motif with improved affinity and selectivity towards integrin $\alpha\beta3$ ¹³⁵. Another widely investigated peptide is angiopep-2, a 19 amino acid long peptide, which is capable of binding to the low-density lipoprotein receptor-related protein 1 (LRP1). LRP1 is upregulated in the blood-brain barrier (BBB), glioblastoma multiforme (GBM), and glioma. Angiopep-2 facilitates penetration through the BBB and delivers the payloads to the GBM or glioma at sufficient concentration⁷⁰.

Folate and transferrin are also promising ligand molecules that target tumor through ligand-receptor interaction⁷⁰. Folate is one of the most extensively studied ligands for targeted delivery of drugs or particulate carriers to tumor. It binds to folate receptor (FR) and membrane-bound high affinity folate binding protein in extremely high affinity ($K_D \sim 10^{-9}$)^{136,137}. Since folate is essential for the synthesis of nucleotide bases, FRs are upregulated in many kinds of tumors including ovarian carcinomas, choriocarcinomas, meningiomas, uterine sarcomas, osteosarcomas, and non-Hodgkin's lymphomas, owing to their rapid proliferation. Folate receptor 1 (FR1; also known as folate receptor α), an isoform of folate receptor, is overexpressed in 40% of human cancer. Folate receptor 2 (FR2; also known as folate receptor β) is overexpressed on activated macrophages as well as on the surfaces of malignant cells of hematopoietic origin¹³⁸. Therefore, folate is useful in delivering chemotherapeutic agents to those tumors with high selectivity¹³⁹.

Transferrin has also been investigated in plethora of studies for tumor targeting applications as another distinct ligand-receptor pair. Transferrin is an iron-binding blood plasma glycoprotein that controls the cellular uptake of irons in order to maintain the cellular iron homeostasis by interacting with transferrin receptor (TfR)¹⁴⁰. Physiologically, transferrin forms complex with iron, which is then internalized into the cells through transferrin receptor-mediated endocytosis¹⁴¹. The TfR is expressed up to 100-fold higher in tumor cells than on normal cells, making it an attractive target for delivery of chemotherapeutic agents^{142,143}.

4.3.2.1. Integrins

Cell adhesion molecules (CAMs) are glycoproteins presented on the cell surface that play significant roles in various cellular events such as locomotion, mitosis, cytokinesis, and phagocytosis¹⁴⁴⁻¹⁴⁶. In particular, they function as receptors for cell-to-cell and cell-ECM interactions during the cellular events¹⁴⁷⁻¹⁴⁹. CAMs are also involved in many pathological conditions such as cancer¹⁵⁰⁻¹⁵², thrombosis¹⁵³, rheumatoid arthritis¹⁵⁴, and diabetes¹⁵⁵. This group of molecules are generally divided into four classes: integrins, selectins, cadherins, and the immunoglobulin superfamily¹³⁵.

Integrins are a family of heterodimeric transmembrane glycoproteins. They promote interaction with other cells as well as broad range of endogenous substances such as ECM proteins, immunoglobulin, growth factors, cytokines, and matrix proteases¹⁵⁶⁻¹⁵⁸. Each member of integrins is composed of non-covalently associated transmembrane polypeptide α and β subunits. Each subunit has an extracellular domain, a single transmembrane region, and a cytoplasmic region¹⁵⁹. In mammalian species, 18 distinct α subunits and 8 distinct β subunits assemble into at least 24 different heterodimeric integrins¹⁶⁰. The binding specificity and signaling property of integrins are determined by the composition of α and β subunits within the heterodimer structure¹⁶¹. Integrins generally bind to their respective ECM proteins by recognizing short peptide sequences such as Arg-Gly-Asp (RGD), Glu-Ile-Leu-Asp-Val (EILDV), and Arg-Glu-Asp-Val (REDV)¹⁵⁸. Integrin ligation promotes the formation of integrin clusters at the cell membrane that are associated with cytoskeletal complex, and induce actin filament assembly^{162,163}. Consequently, the reorganization of actin filaments into large stress fibers facilitates the further clustering of integrins, resulting in enhanced binding affinity with ECM proteins¹⁶⁴.

Many integrins are critically involved in various stages of cancer progression including malignant transformation, invasion, metastasis, and angiogenesis. Among them, integrin $\alpha\beta3$ has been comprehensively studied,

since it is abundantly expressed on angiogenic tumor endothelial cells as well as on various malignant cells including late stage glioblastoma, melanoma, ovarian cancer, breast cancer, pancreatic cancer, and prostate cancer, whereas rarely expressed on the normal quiescent endothelial cells or and other normal cells^{158,165-167}.

The expression of integrin $\alpha\beta3$ on tumor endothelial cell is stimulated by pro-angiogenic factors such as fibroblast growth factor-2 (FGF2), tumor necrosis factor- α (TNF α), or interleukin-8 (IL8)^{156,159}. Integrin $\alpha\beta3$ regulates angiogenesis by several mechanisms. It stimulates cell-mediated collagen degradation in surrounding extracellular matrix (ECM) by inducing local secretion of proteolytically active matrix metalloproteinase-2 (MMP2), leading to rearrangement of the ECM. Through this mechanism, endothelial cell migration is facilitated when the integrin $\alpha\beta3$ binds to fibronectin, fibrinogen, or osteopontin. Moreover, the activation of integrin $\alpha\beta3$ increases the cyclooxygenase-2 (COX-2) level, which is necessary during the endothelial cell spreading and migration. It also acts as a survival factor and improves the survival of endothelial cells when bound to fibronectin¹⁶⁸. In addition, integrin $\alpha\beta3$ stimulates angiogenesis by interacting with other pro-angiogenic factors. Early reports showed that the interaction between integrin $\alpha\beta3$ and FGFR or VEGFR2 enhanced the FGF or VEGF-induced angiogenesis, respectively¹⁶⁹. These distinct angiogenic pathways showed that integrins regulate ECM and pro-angiogenic factors to induce specific intracellular signaling events that are critical in angiogenesis. Indeed, the inhibitors against integrin $\alpha\beta3$ or $\alpha\beta5$ suppressed pathological angiogenesis in animal models¹⁷⁰.

Integrin $\alpha\beta3$ also plays significant roles in the progression of various types of tumors. The overexpression of integrin $\alpha\beta3$ is associated with facilitated growth, invasion, and bone metastasis of breast cancer^{171,172}. It is also correlated with the sensitivity of breast cancer cells against chemotherapy, thereby suggested as a biomarker for chemosensitivity¹⁷³. In glioblastoma, integrin $\alpha\beta3$ was abundantly found at the invasive margins of the tumor with increased levels of fibronectin, which was closely related with enhanced cell motility and

survival¹⁷⁴. In other types of cancer including pancreatic cancer and prostate carcinoma, increased metastasis was also observed when integrin $\alpha v\beta 3$ was upregulated^{174,175}.

4.3.2.2. RGD peptide sequence for targeting integrin $\alpha v\beta 3$

Integrin $\alpha v\beta 3$ is consisted of 125 kDa αv subunit and 105 kDa $\beta 1$ subunit, and binds with broad array of ECM proteins that contains Arg-Gly-Asp (RGD) sequence in high affinity¹⁷⁶. The crystal structures of integrin $\alpha v\beta 3$ and RGD ligand complexes revealed that RGD motif binds at an interface between α and β subunits, where arginine residue fitting into a cleft of the β -propeller fold, and aspartic acid residue coordinating with the von Willebrand factor type A domain in the β subunit by cationic interaction¹⁷⁷. The RGD tripeptide sequence was first found in fibronectin as a cell adhesion residue in the early 1970s by E. Ruoslahti¹⁷⁶. This sequence was further found in other ECM proteins that bind with integrin $\alpha v\beta 3$ such as fibrinogen, vitronectin, plasminogen, prothrombin, MMP2, laminin, osteopontin, and thrombospondin^{174,178-180}. More than half of the identified integrins recognize this tripeptide sequence including all five αv integrins, $\alpha 5\beta 1$, $\alpha 8\beta 1$, and $\alpha IIb\beta 3$ integrins¹⁸¹. According to these findings, many compounds including linear and cyclic peptides, and peptidomimetics that preferentially bind to integrin $\alpha v\beta 3$ were developed, employing RGD sequence as a basic module for targeted therapy in cancer treatment¹⁸². The binding affinity of the RGD peptides is largely governed by the steric conformations and the flanking residues¹⁸³.

Cyclization of RGD peptide is frequently used to improve the binding properties. Conformational rigidity that is provided by the cyclization could significantly increase the binding affinity and the selectivity against specific integrin subtype. The cyclization is also preferred in purpose to increase the chemical stability. Generally, linear RGD peptides are susceptible to chemical degradation as the Asp can cause a hydrolytic peptide cleavage when paired with Gly¹⁸⁴. The cyclization of the peptide could prevent such hydrolysis by producing rigid structure, which limits the movement of the Asp. Non-natural

peptide modifications such as inserting D-amino acids or replacing with peptidomimetic molecules have also been frequently used to improve the binding properties¹⁸⁵. The flanking residues of the linear or cyclic RGD sequences were also concerned, since they could also influence the affinity and selectivity against integrins¹⁸³.

The most representative RGD peptide that targets integrin $\alpha v\beta 3$ is c(RGDf-N(Me)-V), which is also known as cilengitide. Cilengitide exhibits highly preferential binding to integrin $\alpha v\beta 3$, displaying 1000-fold higher affinity over integrin $\alpha IIb\beta 3$ due to the cyclic structure and the presence of D-amino acid (i.e., D-Phe) next to the RGD sequence¹⁸⁶. Among the several derivatives of this compound, c(RGDfK) and c(RGDyK) are frequently used for targeted delivery of therapeutics due to the ease of chemical conjugation through the primary amine group on Lys side chain¹⁸². Several RGD peptides with high affinity and specificity against integrin $\alpha v\beta 3$ were further identified using the phage display technique. Among them, RGD4C (ACDCRGDCFCG) and RGD10 (DGARYCRGDCFDG) have been appreciated for their outstanding binding properties. RGD4C and RGD10 have two and one intramolecule disulfide bond to form stable cyclic structures, thereby producing high binding affinity. Since these peptides do not involve any non-natural amino acids or chemical modifications, they are preferred when introducing to a protein by recombinant engineering^{182,187}.

Peptidomimetics of RGD have also been reported to show improved binding to αv integrins¹⁸⁵. Most of the peptidomimetics have Arg and Asp residues respectively substituted with guanidine mimetic and carboxylic acid, which are connected to each other by various tethers and constraints, thereby producing compounds with nano- or even picomolar binding affinities to integrin $\alpha v\beta 3$.

Not only the individual characteristics of the peptide determine the binding properties. Multivalency of RGD peptides also significantly increases the binding affinity. For instance, Kok et al. have demonstrated that their multivalent RGD-protein conjugates showed subnanomolar affinity for integrin $\alpha v\beta 3$ overexpressing human umbilical cord endothelial cells (HUVECs), which

was a 250-fold increase compared to the single RGD peptide¹⁸⁸. Additionally, the multivalency also facilitates the internalization of the conjugated substances by endocytosis^{189,190}. Particulate carriers and macromolecules such as liposomes, nanoparticles, proteins, and other polymers bearing multiple RGD peptides are, therefore, more likely to be internalized via receptor-mediated endocytosis than the single peptide constructs.

4.4. Rationale of the research

Despite that the targeted therapy gained the most interest from many researchers and clinicians in the modern cancer therapeutics, chemotherapeutic agents are still widely used for the treatment of broad array of tumors in the first-line therapy solely or in combination with the targeted therapies. However, the clinical application of the chemotherapy is often limited due to the severe systemic toxicities, which are even sometimes lethal. These adverse effects are closely related to the systemically non-selective distribution as well as the non-specific mechanisms of action of the chemotherapeutic. Therefore, many efforts have been made to deliver these agents selectively to the tumor by introducing tumor-targeting moieties that could recognize certain tumor-specific surface antigens, so called as active tumor targeted delivery (see section 4.3.2). The traditional targeted delivery strategies, however, produced only limited improvements in the preclinical models, mainly due to the intratumor heterogeneity (see section 4.1.2). Considering the existence of many different cell populations in the tumor mass, the strategy to deliver chemotherapeutic agents specifically to a tumor by relying on a target antigen expression is fundamentally challenged.

For an effective and reliable delivery of chemotherapeutics (i.e. doxorubicin) to the tumor regardless of the intratumor heterogeneity, we have previously proposed a strategy of targeting radiation-induced apoptosis to deliver chemotherapeutic agents to the tumor. In particular, it involves caspase-3, which is upregulated during apoptotic events, for the targeted delivery system

(see section 4.2.1 for detailed description of caspase-3). The major advantage of utilizing caspase-3 as an activator of a prodrug is that the site of the activation could be controlled actively by exogenous stimuli (i.e. radiation), rather than passively relying on the genotype of the tumor. Therefore, this strategy could be a resolution for the obstacles in the current targeted delivery systems.

References

- 1 Burrell, R. A., McGranahan, N., Bartek, J. & Swanton, C. The causes and consequences of genetic heterogeneity in cancer evolution. *Nature* **501**, 338-345 (2013).
- 2 Merlo, L. M., Pepper, J. W., Reid, B. J. & Maley, C. C. Cancer as an evolutionary and ecological process. *Nat Rev Cancer* **6**, 924-935 (2006).
- 3 Greaves, M. & Maley, C. C. Clonal evolution in cancer. *Nature* **481**, 306-313 (2012).
- 4 Vogelstein, B., Papadopoulos, N., Velculescu, V. E., Zhou, S., Diaz, L. A., Jr. & Kinzler, K. W. Cancer genome landscapes. *Science* **339**, 1546-1558 (2013).
- 5 Lengauer, C., Kinzler, K. W. & Vogelstein, B. Genetic instability in colorectal cancers. *Nature* **386**, 623-627 (1997).
- 6 Popat, S., Hubner, R. & Houlston, R. S. Systematic review of microsatellite instability and colorectal cancer prognosis. *J Clin Oncol* **23**, 609-618 (2005).
- 7 Weigelt, B. & Reis-Filho, J. S. Histological and molecular types of breast cancer: is there a unifying taxonomy? *Nat Rev Clin Oncol* **6**, 718-730 (2009).
- 8 Pao, W. & Chmielecki, J. Rational, biologically based treatment of EGFR-mutant non-small-cell lung cancer. *Nat Rev Cancer* **10**, 760-774 (2010).
- 9 Patel, J. P., Gonen, M., Figueroa, M. E., Fernandez, H., Sun, Z., Racevskis, J., Van Vlierberghe, P., Dolgalev, I., Thomas, S., Aminova, O., Huberman, K., Cheng, J., Viale, A., Socci, N. D., Heguy, A., Cherry, A., Vance, G., Higgins, R. R., Ketterling, R. P., Gallagher, R. E., Litzow, M., van den Brink, M. R., Lazarus, H. M., Rowe, J. M., Luger, S., Ferrando, A., Paietta, E., Tallman, M. S., Melnick, A., Abdel-Wahab, O. & Levine, R. L. Prognostic relevance of integrated genetic profiling in acute myeloid leukemia. *N Engl J Med* **366**, 1079-1089 (2012).
- 10 Swanton, C. Intratumor heterogeneity: evolution through space and time. *Cancer Res* **72**, 4875-4882 (2012).
- 11 Marusyk, A., Almendro, V. & Polyak, K. Intra-tumour heterogeneity: a looking glass for cancer? *Nat Rev Cancer* **12**, 323-334 (2012).
- 12 Campbell, P. J., Yachida, S., Mudie, L. J., Stephens, P. J., Pleasance, E. D., Stebbings, L. A., Morsberger, L. A., Latimer, C., McLaren, S., Lin, M. L., McBride, D.

- J., Varela, I., Nik-Zainal, S. A., Leroy, C., Jia, M., Menzies, A., Butler, A. P., Teague, J. W., Griffin, C. A., Burton, J., Swerdlow, H., Quail, M. A., Stratton, M. R., Iacobuzio-Donahue, C. & Futreal, P. A. The patterns and dynamics of genomic instability in metastatic pancreatic cancer. *Nature* **467**, 1109-1113 (2010).
- 13 Ding, L., Ley, T. J., Larson, D. E., Miller, C. A., Koboldt, D. C., Welch, J. S., Ritchey, J. K., Young, M. A., Lamprecht, T., McLellan, M. D., McMichael, J. F., Wallis, J. W., Lu, C., Shen, D., Harris, C. C., Dooling, D. J., Fulton, R. S., Fulton, L. L., Chen, K., Schmidt, H., Kalicki-Veizer, J., Magrini, V. J., Cook, L., McGrath, S. D., Vickery, T. L., Wendl, M. C., Heath, S., Watson, M. A., Link, D. C., Tomasson, M. H., Shannon, W. D., Payton, J. E., Kulkarni, S., Westervelt, P., Walter, M. J., Graubert, T. A., Mardis, E. R., Wilson, R. K. & DiPersio, J. F. Clonal evolution in relapsed acute myeloid leukaemia revealed by whole-genome sequencing. *Nature* **481**, 506-510 (2012).
- 14 Landau, D. A., Carter, S. L., Stojanov, P., McKenna, A., Stevenson, K., Lawrence, M. S., Sougnez, C., Stewart, C., Sivachenko, A., Wang, L., Wan, Y., Zhang, W., Shukla, S. A., Vartanov, A., Fernandes, S. M., Saksena, G., Cibulskis, K., Tesar, B., Gabriel, S., Hacohen, N., Meyerson, M., Lander, E. S., Neuber, D., Brown, J. R., Getz, G. & Wu, C. J. Evolution and impact of subclonal mutations in chronic lymphocytic leukemia. *Cell* **152**, 714-726 (2013).
- 15 Meacham, C. E. & Morrison, S. J. Tumour heterogeneity and cancer cell plasticity. *Nature* **501**, 328-337 (2013).
- 16 Gerlinger, M., Rowan, A. J., Horswell, S., Larkin, J., Endesfelder, D., Gronroos, E., Martinez, P., Matthews, N., Stewart, A., Tarpey, P., Varela, I., Phillimore, B., Begum, S., McDonald, N. Q., Butler, A., Jones, D., Raine, K., Latimer, C., Santos, C. R., Nohadani, M., Eklund, A. C., Spencer-Dene, B., Clark, G., Pickering, L., Stamp, G., Gore, M., Szallasi, Z., Downward, J., Futreal, P. A. & Swanton, C. Intratumor heterogeneity and branched evolution revealed by multiregion sequencing. *N Engl J Med* **366**, 883-892 (2012).
- 17 Shah, S. P., Morin, R. D., Khattra, J., Prentice, L., Pugh, T., Burleigh, A., Delaney, A., Gelmon, K., Guliany, R., Senz, J., Steidl, C., Holt, R. A., Jones, S., Sun, M., Leung, G., Moore, R., Severson, T., Taylor, G. A., Teschendorff, A. E., Tse, K., Turashvili, G., Varhol, R., Warren, R. L., Watson, P., Zhao, Y., Caldas, C., Huntsman, D., Hirst, M., Marra, M. A. & Aparicio, S. Mutational evolution in a lobular breast tumour profiled at single nucleotide resolution. *Nature* **461**, 809-813 (2009).
- 18 Wu, X., Northcott, P. A., Dubuc, A., Dupuy, A. J., Shih, D. J., Witt, H., Croul, S., Bouffet, E., Fu, D. W., Eberhart, C. G., Garzia, L., Van Meter, T., Zagzag, D., Jabado, N., Schwartzentruber, J., Majewski, J., Scheetz, T. E., Pfister, S. M.,

- Korshunov, A., Li, X. N., Scherer, S. W., Cho, Y. J., Akagi, K., MacDonald, T. J., Koster, J., McCabe, M. G., Sarver, A. L., Collins, V. P., Weiss, W. A., Largaespada, D. A., Collier, L. S. & Taylor, M. D. Clonal selection drives genetic divergence of metastatic medulloblastoma. *Nature* **482**, 529-533 (2012).
- 19 Martinez, P., Birkbak, N. J., Gerlinger, M., McGranahan, N., Burrell, R. A., Rowan, A. J., Joshi, T., Fisher, R., Larkin, J., Szallasi, Z. & Swanton, C. Parallel evolution of tumour subclones mimics diversity between tumours. *J Pathol* **230**, 356-364 (2013).
- 20 Yates, L. R. & Campbell, P. J. Evolution of the cancer genome. *Nat Rev Genet* **13**, 795-806 (2012).
- 21 Junttila, M. R. & de Sauvage, F. J. Influence of tumour micro-environment heterogeneity on therapeutic response. *Nature* **501**, 346-354 (2013).
- 22 Navin, N., Kendall, J., Troge, J., Andrews, P., Rodgers, L., McIndoo, J., Cook, K., Stepansky, A., Levy, D., Esposito, D., Muthuswamy, L., Krasnitz, A., McCombie, W. R., Hicks, J. & Wigler, M. Tumour evolution inferred by single-cell sequencing. *Nature* **472**, 90-94 (2011).
- 23 Govindan, R., Ding, L., Griffith, M., Subramanian, J., Dees, N. D., Kanchi, K. L., Maher, C. A., Fulton, R., Fulton, L., Wallis, J., Chen, K., Walker, J., McDonald, S., Bose, R., Ornitz, D., Xiong, D., You, M., Dooling, D. J., Watson, M., Mardis, E. R. & Wilson, R. K. Genomic landscape of non-small cell lung cancer in smokers and never-smokers. *Cell* **150**, 1121-1134 (2012).
- 24 Nik-Zainal, S., Van Loo, P., Wedge, D. C., Alexandrov, L. B., Greenman, C. D., Lau, K. W., Raine, K., Jones, D., Marshall, J., Ramakrishna, M., Shlien, A., Cooke, S. L., Hinton, J., Menzies, A., Stebbings, L. A., Leroy, C., Jia, M., Rance, R., Mudie, L. J., Gamble, S. J., Stephens, P. J., McLaren, S., Tarpey, P. S., Papaemmanuil, E., Davies, H. R., Varela, I., McBride, D. J., Bignell, G. R., Leung, K., Butler, A. P., Teague, J. W., Martin, S., Jonsson, G., Mariani, O., Boyault, S., Miron, P., Fatima, A., Langerod, A., Aparicio, S. A., Tutt, A., Sieuwerts, A. M., Borg, A., Thomas, G., Salomon, A. V., Richardson, A. L., Borresen-Dale, A. L., Futreal, P. A., Stratton, M. R., Campbell, P. J. & Breast Cancer Working Group of the International Cancer Genome, C. The life history of 21 breast cancers. *Cell* **149**, 994-1007 (2012).
- 25 Cahill, D. P., Kinzler, K. W., Vogelstein, B. & Lengauer, C. Genetic instability and darwinian selection in tumours. *Trends Cell Biol* **9**, M57-60 (1999).
- 26 Szerlip, N. J., Pedraza, A., Chakravarty, D., Azim, M., McGuire, J., Fang, Y., Ozawa, T., Holland, E. C., Huse, J. T., Jhanwar, S., Leversha, M. A., Mikkelsen, T. & Brennan, C. W. Intratumoral heterogeneity of receptor tyrosine kinases EGFR and PDGFRA amplification in glioblastoma defines subpopulations with distinct growth factor response. *Proc Natl Acad Sci U S A* **109**, 3041-3046 (2012).

- 27 Wu, M., Pastor-Pareja, J. C. & Xu, T. Interaction between Ras(V12) and scribbled clones induces tumour growth and invasion. *Nature* **463**, 545-548 (2010).
- 28 Snuderl, M., Fazlollahi, L., Le, L. P., Nitta, M., Zhelyazkova, B. H., Davidson, C. J., Akhavanfard, S., Cahill, D. P., Aldape, K. D., Betensky, R. A., Louis, D. N. & Iafrate, A. J. Mosaic amplification of multiple receptor tyrosine kinase genes in glioblastoma. *Cancer Cell* **20**, 810-817 (2011).
- 29 Inda, M. M., Bonavia, R., Mukasa, A., Narita, Y., Sah, D. W., Vandenberg, S., Brennan, C., Johns, T. G., Bachoo, R., Hadwiger, P., Tan, P., Depinho, R. A., Cavenee, W. & Furnari, F. Tumor heterogeneity is an active process maintained by a mutant EGFR-induced cytokine circuit in glioblastoma. *Genes Dev* **24**, 1731-1745 (2010).
- 30 Kreso, A., O'Brien, C. A., van Galen, P., Gan, O. I., Notta, F., Brown, A. M., Ng, K., Ma, J., Wienholds, E., Dunant, C., Pollett, A., Gallinger, S., McPherson, J., Mullighan, C. G., Shibata, D. & Dick, J. E. Variable clonal repopulation dynamics influence chemotherapy response in colorectal cancer. *Science* **339**, 543-548 (2013).
- 31 Meads, M. B., Gatenby, R. A. & Dalton, W. S. Environment-mediated drug resistance: a major contributor to minimal residual disease. *Nat Rev Cancer* **9**, 665-674 (2009).
- 32 Zhang, S., Liu, X., Bawa-Khalife, T., Lu, L. S., Lyu, Y. L., Liu, L. F. & Yeh, E. T. Identification of the molecular basis of doxorubicin-induced cardiotoxicity. *Nat Med* **18**, 1639-1642 (2012).
- 33 Assumpção, J. U., Campos, M. L., Ferraz Nogueira Filho, M. A., Pestana, K. C., Baldan, H. M., Formariz Pilon, T. P., de Oliveira, A. G. & Peccinini, R. G. Biocompatible microemulsion modifies the pharmacokinetic profile and cardiotoxicity of doxorubicin. *J Pharm Sci* **102**, 289-296 (2013).
- 34 DiPaola, R. S., Rinehart, J., Nemunaitis, J., Ebbinghaus, S., Rubin, E., Capanna, T., Ciardella, M., Doyle-Lindrud, S., Goodwin, S., Fontaine, M., Adams, N., Williams, A., Schwartz, M., Winchell, G., Wickersham, K., Deutsch, P. & Yao, S. L. Characterization of a novel prostate-specific antigen-activated peptide-doxorubicin conjugate in patients with prostate cancer. *J Clin Oncol* **20**, 1874-1879 (2002).
- 35 Sapro, P., Stein, R., Pickett, J., Qu, Z., Govindan, S. V., Cardillo, T. M., Hansen, H. J., Horak, I. D., Griffiths, G. L. & Goldenberg, D. M. Anti-CD74 antibody-doxorubicin conjugate, IMMU-110, in a human multiple myeloma xenograft and in monkeys. *Clin Cancer Res* **11**, 5257-5264 (2005).
- 36 Agniswamy, J., Fang, B. & Weber, I. T. Plasticity of S2-S4 specificity pockets of executioner caspase-7 revealed by structural and kinetic analysis. *FEBS J* **274**, 4752-4765 (2007).

- 37 Asakura, T., Sawai, T., Hashidume, Y., Ohkawa, Y., Yokoyama, S. & Ohkawa, K. Caspase-3 activation during apoptosis caused by glutathione-doxorubicin conjugate. *Br J Cancer* **80**, 711-715 (1999).
- 38 Ueno, M., Kakinuma, Y., Yuhki, K., Murakoshi, N., Iemitsu, M., Miyauchi, T. & Yamaguchi, I. Doxorubicin induces apoptosis by activation of caspase-3 in cultured cardiomyocytes in vitro and rat cardiac ventricles in vivo. *J Pharmacol Sci* **101**, 151-158 (2006).
- 39 Jacobson, M. D., Weil, M. & Raff, M. C. Programmed cell death in animal development. *Cell* **88**, 347-354 (1997).
- 40 Kerr, J. F., Wyllie, A. H. & Currie, A. R. Apoptosis: a basic biological phenomenon with wide-ranging implications in tissue kinetics. *Br J Cancer* **26**, 239-257 (1972).
- 41 Danial, N. N. & Korsmeyer, S. J. Cell death: critical control points. *Cell* **116**, 205-219 (2004).
- 42 Alnemri, E. S., Livingston, D. J., Nicholson, D. W., Salvesen, G., Thornberry, N. A., Wong, W. W. & Yuan, J. Human ICE/CED-3 protease nomenclature. *Cell* **87**, 171 (1996).
- 43 Shi, Y. Mechanisms of caspase activation and inhibition during apoptosis. *Mol Cell* **9**, 459-470 (2002).
- 44 Boatright, K. M. & Salvesen, G. S. Mechanisms of caspase activation. *Curr Opin Cell Biol* **15**, 725-731 (2003).
- 45 Stennicke, H. R., Deveraux, Q. L., Humke, E. W., Reed, J. C., Dixit, V. M. & Salvesen, G. S. Caspase-9 can be activated without proteolytic processing. *J Biol Chem* **274**, 8359-8362 (1999).
- 46 Donepudi, M., Mac Sweeney, A., Briand, C. & Grutter, M. G. Insights into the regulatory mechanism for caspase-8 activation. *Mol Cell* **11**, 543-549 (2003).
- 47 Adams, J. M. & Cory, S. Apoptosomes: engines for caspase activation. *Curr Opin Cell Biol* **14**, 715-720 (2002).
- 48 Shi, Y. Apoptosome: the cellular engine for the activation of caspase-9. *Structure* **10**, 285-288 (2002).
- 49 Riedl, S. J. & Shi, Y. Molecular mechanisms of caspase regulation during apoptosis. *Nat Rev Mol Cell Biol* **5**, 897-907 (2004).
- 50 Hanahan, D. & Weinberg, R. A. The hallmarks of cancer. *Cell* **100**, 57-70 (2000).
- 51 Wang, X. The expanding role of mitochondria in apoptosis. *Genes Dev* **15**, 2922-2933 (2001).
- 52 Zou, H., Li, Y., Liu, X. & Wang, X. An APAF-1.cytochrome c multimeric complex is a functional apoptosome that activates procaspase-9. *J Biol Chem* **274**, 11549-11556 (1999).

- 53 Saleh, A., Srinivasula, S. M., Acharya, S., Fishel, R. & Alnemri, E. S. Cytochrome c and dATP-mediated oligomerization of Apaf-1 is a prerequisite for procaspase-9 activation. *J Biol Chem* **274**, 17941-17945 (1999).
- 54 Ashkenazi, A. & Dixit, V. M. Death receptors: signaling and modulation. *Science* **281**, 1305-1308 (1998).
- 55 Peter, M. E. & Krammer, P. H. The CD95(APO-1/Fas) DISC and beyond. *Cell Death Differ* **10**, 26-35 (2003).
- 56 Harper, N., Hughes, M., MacFarlane, M. & Cohen, G. M. Fas-associated death domain protein and caspase-8 are not recruited to the tumor necrosis factor receptor 1 signaling complex during tumor necrosis factor-induced apoptosis. *J Biol Chem* **278**, 25534-25541 (2003).
- 57 Micheau, O. & Tschopp, J. Induction of TNF receptor I-mediated apoptosis via two sequential signaling complexes. *Cell* **114**, 181-190 (2003).
- 58 Luo, X., Budihardjo, I., Zou, H., Slaughter, C. & Wang, X. Bid, a Bcl2 interacting protein, mediates cytochrome c release from mitochondria in response to activation of cell surface death receptors. *Cell* **94**, 481-490 (1998).
- 59 Li, H., Zhu, H., Xu, C. J. & Yuan, J. Cleavage of BID by caspase 8 mediates the mitochondrial damage in the Fas pathway of apoptosis. *Cell* **94**, 491-501 (1998).
- 60 Thornberry, N. A., Rano, T. A., Peterson, E. P., Rasper, D. M., Timkey, T., Garcia-Calvo, M., Houtzager, V. M., Nordstrom, P. A., Roy, S., Vaillancourt, J. P., Chapman, K. T. & Nicholson, D. W. A combinatorial approach defines specificities of members of the caspase family and granzyme B. Functional relationships established for key mediators of apoptosis. *J Biol Chem* **272**, 17907-17911 (1997).
- 61 Wang, X., Pai, J. T., Wiedenfeld, E. A., Medina, J. C., Slaughter, C. A., Goldstein, J. L. & Brown, M. S. Purification of an interleukin-1 beta converting enzyme-related cysteine protease that cleaves sterol regulatory element-binding proteins between the leucine zipper and transmembrane domains. *J Biol Chem* **270**, 18044-18050 (1995).
- 62 Na, S., Chuang, T. H., Cunningham, A., Turi, T. G., Hanke, J. H., Bokoch, G. M. & Danley, D. E. D4-GDI, a substrate of CPP32, is proteolyzed during Fas-induced apoptosis. *J Biol Chem* **271**, 11209-11213 (1996).
- 63 Lazebnik, Y. A., Kaufmann, S. H., Desnoyers, S., Poirier, G. G. & Earnshaw, W. C. Cleavage of poly(ADP-ribose) polymerase by a proteinase with properties like ICE. *Nature* **371**, 346-347 (1994).
- 64 Casciola-Rosen, L., Nicholson, D. W., Chong, T., Rowan, K. R., Thornberry, N. A., Miller, D. K. & Rosen, A. Apopain/CPP32 cleaves proteins that are essential for cellular repair: a fundamental principle of apoptotic death. *J Exp Med* **183**, 1957-1964 (1996).

- 65 Emoto, Y., Manome, Y., Meinhardt, G., Kisaki, H., Kharbanda, S., Robertson, M., Ghayur, T., Wong, W. W., Kamen, R., Weichselbaum, R. & et al. Proteolytic activation of protein kinase C delta by an ICE-like protease in apoptotic cells. *EMBO J* **14**, 6148-6156 (1995).
- 66 Nicholson, D. W., Ali, A., Thornberry, N. A., Vaillancourt, J. P., Ding, C. K., Gallant, M., Gareau, Y., Griffin, P. R., Labelle, M., Lazebnik, Y. A. & et al. Identification and inhibition of the ICE/CED-3 protease necessary for mammalian apoptosis. *Nature* **376**, 37-43 (1995).
- 67 Lien, S., Pastor, R., Sutherlin, D. & Lowman, H. B. A substrate-phage approach for investigating caspase specificity. *Protein J* **23**, 413-425 (2004).
- 68 Yoshimori, A., Takasawa, R. & Tanuma, S. A novel method for evaluation and screening of caspase inhibitory peptides by the amino acid positional fitness score. *BMC Pharmacol* **4**, 7 (2004).
- 69 Earnshaw, W. C., Martins, L. M. & Kaufmann, S. H. Mammalian caspases: structure, activation, substrates, and functions during apoptosis. *Annu Rev Biochem* **68**, 383-424 (1999).
- 70 Steichen, S. D., Caldorera-Moore, M. & Peppas, N. A. A review of current nanoparticle and targeting moieties for the delivery of cancer therapeutics. *Eur J Pharm Sci* **48**, 416-427 (2013).
- 71 Danhier, F., Feron, O. & Preat, V. To exploit the tumor microenvironment: Passive and active tumor targeting of nanocarriers for anti-cancer drug delivery. *J Control Release* **148**, 135-146 (2010).
- 72 Matsumura, Y. & Maeda, H. A new concept for macromolecular therapeutics in cancer chemotherapy: mechanism of tumorotropic accumulation of proteins and the antitumor agent smancs. *Cancer Res* **46**, 6387-6392 (1986).
- 73 Fang, J., Nakamura, H. & Maeda, H. The EPR effect: Unique features of tumor blood vessels for drug delivery, factors involved, and limitations and augmentation of the effect. *Adv Drug Deliv Rev* **63**, 136-151 (2011).
- 74 Maeda, H. Tumor-selective delivery of macromolecular drugs via the EPR effect: background and future prospects. *Bioconjug Chem* **21**, 797-802 (2010).
- 75 Fang, J., Sawa, T., Akaike, T. & Maeda, H. Tumor-targeted delivery of polyethylene glycol-conjugated D-amino acid oxidase for antitumor therapy via enzymatic generation of hydrogen peroxide. *Cancer Res* **62**, 3138-3143 (2002).
- 76 Fang, J., Sawa, T., Akaike, T., Akuta, T., Sahoo, S. K., Khaled, G., Hamada, A. & Maeda, H. In vivo antitumor activity of pegylated zinc protoporphyrin: targeted inhibition of heme oxygenase in solid tumor. *Cancer Res* **63**, 3567-3574 (2003).

- 77 Greish, K., Sawa, T., Fang, J., Akaike, T. & Maeda, H. SMA-doxorubicin, a new polymeric micellar drug for effective targeting to solid tumours. *J Control Release* **97**, 219-230 (2004).
- 78 Greish, K., Nagamitsu, A., Fang, J. & Maeda, H. Copoly(styrene-maleic acid)-pirarubicin micelles: high tumor-targeting efficiency with little toxicity. *Bioconjug Chem* **16**, 230-236 (2005).
- 79 Iyer, A. K., Greish, K., Fang, J., Murakami, R. & Maeda, H. High-loading nanosized micelles of copoly(styrene-maleic acid)-zinc protoporphyrin for targeted delivery of a potent heme oxygenase inhibitor. *Biomaterials* **28**, 1871-1881 (2007).
- 80 Yuan, F., Dellian, M., Fukumura, D., Leunig, M., Berk, D. A., Torchilin, V. P. & Jain, R. K. Vascular permeability in a human tumor xenograft: molecular size dependence and cutoff size. *Cancer Res* **55**, 3752-3756 (1995).
- 81 Noguchi, Y., Wu, J., Duncan, R., Strohmalm, J., Ulbrich, K., Akaike, T. & Maeda, H. Early phase tumor accumulation of macromolecules: a great difference in clearance rate between tumor and normal tissues. *Jpn J Cancer Res* **89**, 307-314 (1998).
- 82 Duncan, R. The dawning era of polymer therapeutics. *Nat Rev Drug Discov* **2**, 347-360 (2003).
- 83 Vicent, M. J., Ringsdorf, H. & Duncan, R. Polymer therapeutics: clinical applications and challenges for development. *Adv Drug Deliv Rev* **61**, 1117-1120 (2009).
- 84 Matsumura, Y. & Kataoka, K. Preclinical and clinical studies of anticancer agent-incorporating polymer micelles. *Cancer Sci* **100**, 572-579 (2009).
- 85 Brigger, I., Dubernet, C. & Couvreur, P. Nanoparticles in cancer therapy and diagnosis. *Adv Drug Deliv Rev* **54**, 631-651 (2002).
- 86 Gu, F. X., Karnik, R., Wang, A. Z., Alexis, F., Levy-Nissenbaum, E., Hong, S., Langer, R. S. & Farokhzad, O. C. Targeted nanoparticles for cancer therapy. *Nano Today* **2**, 14-21 (2007).
- 87 Kratz, F. & Elsakdeh, B. Clinical impact of serum proteins on drug delivery. *J Control Release* **161**, 429-445 (2012).
- 88 Peters, T., Jr. Serum albumin. *Adv Protein Chem* **37**, 161-245 (1985).
- 89 Kratz, F. Albumin as a drug carrier: design of prodrugs, drug conjugates and nanoparticles. *J Control Release* **132**, 171-183 (2008).
- 90 Mendez, C. M., McClain, C. J. & Marsano, L. S. Albumin therapy in clinical practice. *Nutr Clin Pract* **20**, 314-320 (2005).
- 91 Bosse, D., Praus, M., Kiessling, P., Nyman, L., Andresen, C., Waters, J. & Schindel, F. Phase I comparability of recombinant human albumin and human serum albumin. *J Clin Pharmacol* **45**, 57-67 (2005).
- 92 Babson, A. L. & Winnick, T. Protein transfer in tumor-bearing rats. *Cancer Res* **14**, 606-611 (1954).

- 93 Bazak, R., Houri, M., Achy, S. E., Hussein, W. & Refaat, T. Passive targeting of nanoparticles to cancer: A comprehensive review of the literature. *Molecular and clinical oncology* **2**, 904-908 (2014).
- 94 Jain, R. K. A new target for tumor therapy. *N Engl J Med* **360**, 2669-2671 (2009).
- 95 Hobbs, S. K., Monsky, W. L., Yuan, F., Roberts, W. G., Griffith, L., Torchilin, V. P. & Jain, R. K. Regulation of transport pathways in tumor vessels: role of tumor type and microenvironment. *Proc Natl Acad Sci U S A* **95**, 4607-4612 (1998).
- 96 Kratz, F. & Beyer, U. Serum proteins as drug carriers of anticancer agents: a review. *Drug Deliv* **5**, 281-299 (1998).
- 97 Schnitzer, J. E. gp60 is an albumin-binding glycoprotein expressed by continuous endothelium involved in albumin transcytosis. *Am J Physiol* **262**, H246-254 (1992).
- 98 Tiruppathi, C., Song, W., Bergenfeldt, M., Sass, P. & Malik, A. B. Gp60 activation mediates albumin transcytosis in endothelial cells by tyrosine kinase-dependent pathway. *J Biol Chem* **272**, 25968-25975 (1997).
- 99 Wang, Z., Tiruppathi, C., Minshall, R. D. & Malik, A. B. Size and dynamics of caveolae studied using nanoparticles in living endothelial cells. *ACS nano* **3**, 4110-4116 (2009).
- 100 Elsadek, B. & Kratz, F. Impact of albumin on drug delivery--new applications on the horizon. *J Control Release* **157**, 4-28 (2012).
- 101 Sage, H., Johnson, C. & Bornstein, P. Characterization of a novel serum albumin-binding glycoprotein secreted by endothelial cells in culture. *J Biol Chem* **259**, 3993-4007 (1984).
- 102 Tiruppathi, C., Finnegan, A. & Malik, A. B. Isolation and characterization of a cell surface albumin-binding protein from vascular endothelial cells. *Proc Natl Acad Sci U S A* **93**, 250-254 (1996).
- 103 Podhajcer, O. L., Benedetti, L. G., Girotti, M. R., Prada, F., Salvatierra, E. & Llera, A. S. The role of the matricellular protein SPARC in the dynamic interaction between the tumor and the host. *Cancer Metastasis Rev* **27**, 691-705 (2008).
- 104 Desai, N., Trieu, V., Damascelli, B. & Soon-Shiong, P. SPARC Expression Correlates with Tumor Response to Albumin-Bound Paclitaxel in Head and Neck Cancer Patients. *Transl Oncol* **2**, 59-64 (2009).
- 105 Stehle, G., Sinn, H., Wunder, A., Schrenk, H. H., Stewart, J. C., Hartung, G., Maier-Borst, W. & Heene, D. L. Plasma protein (albumin) catabolism by the tumor itself--implications for tumor metabolism and the genesis of cachexia. *Crit Rev Oncol Hematol* **26**, 77-100 (1997).
- 106 Kratz, F., Fichtner, I. & Graeser, R. Combination therapy with the albumin-binding prodrug of doxorubicin (INNO-206) and doxorubicin achieves complete remissions

- and improves tolerability in an ovarian A2780 xenograft model. *Invest New Drugs* **30**, 1743-1749 (2012).
- 107 Chaudhury, C., Mehnaz, S., Robinson, J. M., Hayton, W. L., Pearl, D. K., Roopenian, D. C. & Anderson, C. L. The major histocompatibility complex-related Fc receptor for IgG (FcRn) binds albumin and prolongs its lifespan. *J Exp Med* **197**, 315-322 (2003).
- 108 Chaudhury, C., Brooks, C. L., Carter, D. C., Robinson, J. M. & Anderson, C. L. Albumin binding to FcRn: distinct from the FcRn-IgG interaction. *Biochemistry* **45**, 4983-4990 (2006).
- 109 Kratz, F., Muller-Driver, R., Hofmann, I., Dreves, J. & Unger, C. A novel macromolecular prodrug concept exploiting endogenous serum albumin as a drug carrier for cancer chemotherapy. *J Med Chem* **43**, 1253-1256 (2000).
- 110 Kratz, F. DOXO-EMCH (INNO-206): the first albumin-binding prodrug of doxorubicin to enter clinical trials. *Expert opinion on investigational drugs* **16**, 855-866 (2007).
- 111 Carter, D. C. & Ho, J. X. Structure of serum albumin. *Adv Protein Chem* **45**, 153-203 (1994).
- 112 Kratz, F., Warnecke, A., Scheuermann, K., Stockmar, C., Schwab, J., Lazar, P., Druckes, P., Esser, N., Dreves, J., Rognan, D., Bissantz, C., Hinderling, C., Folkers, G., Fichtner, I. & Unger, C. Probing the cysteine-34 position of endogenous serum albumin with thiol-binding doxorubicin derivatives. Improved efficacy of an acid-sensitive doxorubicin derivative with specific albumin-binding properties compared to that of the parent compound. *J Med Chem* **45**, 5523-5533 (2002).
- 113 Ferguson, E., Singh, R. J., Hogg, N. & Kalyanaraman, B. The mechanism of apolipoprotein B-100 thiol depletion during oxidative modification of low-density lipoprotein. *Arch Biochem Biophys* **341**, 287-294 (1997).
- 114 Smith, D. E., Mosher, D. F., Johnson, R. B. & Furcht, L. T. Immunological identification of two sulfhydryl-containing fragments of human plasma fibronectin. *J Biol Chem* **257**, 5831-5838 (1982).
- 115 Shimokawa, Y., Abe, O. & Kuromizu, K. Fluorescence labeling of a single sulfhydryl group in human plasma alpha 1-proteinase inhibitor and characterization of the labeled inhibitor. *J Biochem* **100**, 563-570 (1986).
- 116 Chawla, S. P., Chua, V. S., Hendifar, A. F., Quon, D. V., Soman, N., Sankhala, K. K., Wieland, D. S. & Levitt, D. J. A phase 1B/2 study of aldodoxorubicin in patients with soft tissue sarcoma. *Cancer*, 1-10 (2014).
- 117 Kratz, F. INNO-206 (DOXO-EMCH), an albumin-binding prodrug of doxorubicin under development for phase II studies. *Curr Bioact Compd* **7**, 33-38 (2011).

- 118 Chung, D. E. & Kratz, F. Development of a novel albumin-binding prodrug that is cleaved by urokinase-type-plasminogen activator (uPA). *Bioorg Med Chem Lett* **16**, 5157-5163 (2006).
- 119 Schmid, B., Chung, D. E., Warnecke, A., Fichtner, I. & Kratz, F. Albumin-binding prodrugs of camptothecin and doxorubicin with an Ala-Leu-Ala-Leu-linker that are cleaved by cathepsin B: synthesis and antitumor efficacy. *Bioconjug Chem* **18**, 702-716 (2007).
- 120 Abu Ajaj, K., Graeser, R. & Kratz, F. Zosuquidar and an albumin-binding prodrug of zosuquidar reverse multidrug resistance in breast cancer cells of doxorubicin and an albumin-binding prodrug of doxorubicin. *Breast Cancer Res Treat* **134**, 117-129 (2012).
- 121 Haley, B. & Frenkel, E. Nanoparticles for drug delivery in cancer treatment. *Urol Oncol* **26**, 57-64 (2008).
- 122 Adams, G. P. & Weiner, L. M. Monoclonal antibody therapy of cancer. *Nat Biotechnol* **23**, 1147-1157 (2005).
- 123 Brannon-Peppas, L. & Blanchette, J. O. Nanoparticle and targeted systems for cancer therapy. *Adv Drug Deliv Rev* **56**, 1649-1659 (2004).
- 124 Weber, J. Review: anti-CTLA-4 antibody ipilimumab: case studies of clinical response and immune-related adverse events. *Oncologist* **12**, 864-872 (2007).
- 125 Weiner, L. M., Surana, R. & Wang, S. Monoclonal antibodies: versatile platforms for cancer immunotherapy. *Nat Rev Immunol* **10**, 317-327 (2010).
- 126 von Mehren, M., Adams, G. P. & Weiner, L. M. Monoclonal antibody therapy for cancer. *Annu Rev Med* **54**, 343-369 (2003).
- 127 Mendelsohn, J. Epidermal growth factor receptor inhibition by a monoclonal antibody as anticancer therapy. *Clin Cancer Res* **3**, 2703-2707 (1997).
- 128 Nobs, L., Buchegger, F., Gurny, R. & Allemann, E. Biodegradable nanoparticles for direct or two-step tumor immunotargeting. *Bioconjug Chem* **17**, 139-145 (2006).
- 129 Hughes, B. Antibody-drug conjugates for cancer: poised to deliver? *Nat Rev Drug Discov* **9**, 665-667 (2010).
- 130 Zolot, R. S., Basu, S. & Million, R. P. Antibody-drug conjugates. *Nat Rev Drug Discov* **12**, 259-260 (2013).
- 131 Brissette, R., Prendergast, J. K. & Goldstein, N. I. Identification of cancer targets and therapeutics using phage display. *Current opinion in drug discovery & development* **9**, 363-369 (2006).
- 132 Krag, D. N., Shukla, G. S., Shen, G. P., Pero, S., Ashikaga, T., Fuller, S., Weaver, D. L., Burdette-Radoux, S. & Thomas, C. Selection of tumor-binding ligands in cancer patients with phage display libraries. *Cancer Res* **66**, 7724-7733 (2006).

- 133 Brooks, P. C., Montgomery, A. M., Rosenfeld, M., Reisfeld, R. A., Hu, T., Klier, G. & Cheresch, D. A. Integrin alpha v beta 3 antagonists promote tumor regression by inducing apoptosis of angiogenic blood vessels. *Cell* **79**, 1157-1164 (1994).
- 134 Byrne, J. D., Betancourt, T. & Brannon-Peppas, L. Active targeting schemes for nanoparticle systems in cancer therapeutics. *Adv Drug Deliv Rev* **60**, 1615-1626 (2008).
- 135 Chen, K. & Chen, X. Integrin targeted delivery of chemotherapeutics. *Theranostics* **1**, 189-200 (2011).
- 136 Henderson, G. B. Folate-binding proteins. *Annu Rev Nutr* **10**, 319-335 (1990).
- 137 Hilgenbrink, A. R. & Low, P. S. Folate receptor-mediated drug targeting: from therapeutics to diagnostics. *J Pharm Sci* **94**, 2135-2146 (2005).
- 138 Low, P. S. & Kularatne, S. A. Folate-targeted therapeutic and imaging agents for cancer. *Curr Opin Chem Biol* **13**, 256-262 (2009).
- 139 Sudimack, J. & Lee, R. J. Targeted drug delivery via the folate receptor. *Adv Drug Deliv Rev* **41**, 147-162 (2000).
- 140 Ponka, P. & Lok, C. N. The transferrin receptor: role in health and disease. *Int J Biochem Cell Biol* **31**, 1111-1137 (1999).
- 141 Qian, Z. M., Li, H., Sun, H. & Ho, K. Targeted drug delivery via the transferrin receptor-mediated endocytosis pathway. *Pharmacol Rev* **54**, 561-587 (2002).
- 142 Sahoo, S. K., Ma, W. & Labhasetwar, V. Efficacy of transferrin-conjugated paclitaxel-loaded nanoparticles in a murine model of prostate cancer. *Int J Cancer* **112**, 335-340 (2004).
- 143 Daniels, T. R., Delgado, T., Helguera, G. & Penichet, M. L. The transferrin receptor part II: targeted delivery of therapeutic agents into cancer cells. *Clin Immunol* **121**, 159-176 (2006).
- 144 Pavalko, F. M. & Otey, C. A. Role of adhesion molecule cytoplasmic domains in mediating interactions with the cytoskeleton. *Proc Soc Exp Biol Med* **205**, 282-293 (1994).
- 145 Haass, N. K., Smalley, K. S., Li, L. & Herlyn, M. Adhesion, migration and communication in melanocytes and melanoma. *Pigment Cell Res* **18**, 150-159 (2005).
- 146 Turowski, P., Adamson, P. & Greenwood, J. Pharmacological targeting of ICAM-1 signaling in brain endothelial cells: potential for treating neuroinflammation. *Cell Mol Neurobiol* **25**, 153-170 (2005).
- 147 Ruoslahti, E. Fibronectin and its integrin receptors in cancer. *Adv Cancer Res* **76**, 1-20 (1999).
- 148 Hynes, R. O. & Zhao, Q. The evolution of cell adhesion. *J Cell Biol* **150**, F89-96 (2000).

- 149 Hynes, R. O. A reevaluation of integrins as regulators of angiogenesis. *Nat Med* **8**, 918-921 (2002).
- 150 Maaser, K., Wolf, K., Klein, C. E., Niggemann, B., Zanker, K. S., Brocker, E. B. & Friedl, P. Functional hierarchy of simultaneously expressed adhesion receptors: integrin alpha2beta1 but not CD44 mediates MV3 melanoma cell migration and matrix reorganization within three-dimensional hyaluronan-containing collagen matrices. *Mol Biol Cell* **10**, 3067-3079 (1999).
- 151 Ruoslahti, E. Specialization of tumour vasculature. *Nat Rev Cancer* **2**, 83-90 (2002).
- 152 Christofori, G. Changing neighbours, changing behaviour: cell adhesion molecule-mediated signalling during tumour progression. *EMBO J* **22**, 2318-2323 (2003).
- 153 Andrews, R. K. & Berndt, M. C. Platelet physiology and thrombosis. *Thromb Res* **114**, 447-453 (2004).
- 154 Banquy, X., Leclair, G., Rabanel, J. M., Argaw, A., Bouchard, J. F., Hildgen, P. & Giasson, S. Selectins ligand decorated drug carriers for activated endothelial cell targeting. *Bioconjug Chem* **19**, 2030-2039 (2008).
- 155 Ichinose, K., Kawasaki, E. & Eguchi, K. Recent advancement of understanding pathogenesis of type 1 diabetes and potential relevance to diabetic nephropathy. *Am J Nephrol* **27**, 554-564 (2007).
- 156 Brooks, P. C., Clark, R. A. & Cheresh, D. A. Requirement of vascular integrin alpha v beta 3 for angiogenesis. *Science* **264**, 569-571 (1994).
- 157 Hood, J. D. & Cheresh, D. A. Role of integrins in cell invasion and migration. *Nat Rev Cancer* **2**, 91-100 (2002).
- 158 Danhier, F., Le Breton, A. & Preat, V. RGD-based strategies to target alpha(v) beta(3) integrin in cancer therapy and diagnosis. *Mol Pharm* **9**, 2961-2973 (2012).
- 159 Avraamides, C. J., Garmy-Susini, B. & Varnier, J. A. Integrins in angiogenesis and lymphangiogenesis. *Nat Rev Cancer* **8**, 604-617 (2008).
- 160 Hynes, R. O. Integrins: bidirectional, allosteric signaling machines. *Cell* **110**, 673-687 (2002).
- 161 Barczyk, M., Carracedo, S. & Gullberg, D. Integrins. *Cell Tissue Res* **339**, 269-280 (2010).
- 162 Burridge, K. & Chrzanowska-Wodnicka, M. Focal adhesions, contractility, and signaling. *Annu Rev Cell Dev Biol* **12**, 463-518 (1996).
- 163 Takagi, J., Erickson, H. P. & Springer, T. A. C-terminal opening mimics 'inside-out' activation of integrin alpha5beta1. *Nat Struct Biol* **8**, 412-416 (2001).
- 164 Dunehoo, A. L., Anderson, M., Majumdar, S., Kobayashi, N., Berkland, C. & Siahaan, T. J. Cell adhesion molecules for targeted drug delivery. *J Pharm Sci* **95**, 1856-1872 (2006).

- 165 Cai, W. & Chen, X. Anti-angiogenic cancer therapy based on integrin alphavbeta3 antagonism. *Anticancer Agents Med Chem* **6**, 407-428 (2006).
- 166 Mizejewski, G. J. Role of integrins in cancer: survey of expression patterns. *Proc Soc Exp Biol Med* **222**, 124-138 (1999).
- 167 Jin, H. & Varner, J. Integrins: roles in cancer development and as treatment targets. *Br J Cancer* **90**, 561-565 (2004).
- 168 Francavilla, C., Maddaluno, L. & Cavallaro, U. The functional role of cell adhesion molecules in tumor angiogenesis. *Semin Cancer Biol* **19**, 298-309 (2009).
- 169 Desgrosellier, J. S. & Cheresch, D. A. Integrins in cancer: biological implications and therapeutic opportunities. *Nat Rev Cancer* **10**, 9-22 (2010).
- 170 Reynolds, A. R., Hart, I. R., Watson, A. R., Welti, J. C., Silva, R. G., Robinson, S. D., Da Violante, G., Gourlaouen, M., Salih, M., Jones, M. C., Jones, D. T., Saunders, G., Kostourou, V., Perron-Sierra, F., Norman, J. C., Tucker, G. C. & Hodivala-Dilke, K. M. Stimulation of tumor growth and angiogenesis by low concentrations of RGD-mimetic integrin inhibitors. *Nat Med* **15**, 392-400 (2009).
- 171 Furger, K. A., Allan, A. L., Wilson, S. M., Hota, C., Vantyghem, S. A., Postenka, C. O., Al-Katib, W., Chambers, A. F. & Tuck, A. B. Beta(3) integrin expression increases breast carcinoma cell responsiveness to the malignancy-enhancing effects of osteopontin. *Mol Cancer Res* **1**, 810-819 (2003).
- 172 Takayama, S., Ishii, S., Ikeda, T., Masamura, S., Doi, M. & Kitajima, M. The relationship between bone metastasis from human breast cancer and integrin alpha(v)beta3 expression. *Anticancer Res* **25**, 79-83 (2005).
- 173 Vellon, L., Menendez, J. A., Liu, H. & Lupu, R. Up-regulation of alphavbeta3 integrin expression is a novel molecular response to chemotherapy-induced cell damage in a heregulin-dependent manner. *Differentiation* **75**, 819-830 (2007).
- 174 Sheldrake, H. M. & Patterson, L. H. Function and antagonism of beta3 integrins in the development of cancer therapy. *Curr Cancer Drug Targets* **9**, 519-540 (2009).
- 175 Hosotani, R., Kawaguchi, M., Masui, T., Koshiba, T., Ida, J., Fujimoto, K., Wada, M., Doi, R. & Imamura, M. Expression of integrin alphaVbeta3 in pancreatic carcinoma: relation to MMP-2 activation and lymph node metastasis. *Pancreas* **25**, e30-35 (2002).
- 176 Ruoslahti, E. & Pierschbacher, M. D. New perspectives in cell adhesion: RGD and integrins. *Science* **238**, 491-497 (1987).
- 177 Xiong, J. P., Stehle, T., Zhang, R., Joachimiak, A., Frech, M., Goodman, S. L. & Arnaout, M. A. Crystal structure of the extracellular segment of integrin alpha Vbeta3 in complex with an Arg-Gly-Asp ligand. *Science* **296**, 151-155 (2002).

- 178 Grant, D. S., Tashiro, K., Segui-Real, B., Yamada, Y., Martin, G. R. & Kleinman, H. K. Two different laminin domains mediate the differentiation of human endothelial cells into capillary-like structures in vitro. *Cell* **58**, 933-943 (1989).
- 179 Miyachi, A., Alvarez, J., Greenfield, E. M., Teti, A., Grano, M., Colucci, S., Zamboni-Zallone, A., Ross, F. P., Teitelbaum, S. L., Cheresch, D. & et al. Recognition of osteopontin and related peptides by an alpha v beta 3 integrin stimulates immediate cell signals in osteoclasts. *J Biol Chem* **266**, 20369-20374 (1991).
- 180 Lawler, J., Weinstein, R. & Hynes, R. O. Cell attachment to thrombospondin: the role of ARG-GLY-ASP, calcium, and integrin receptors. *J Cell Biol* **107**, 2351-2361 (1988).
- 181 Ruoslahti, E. RGD and other recognition sequences for integrins. *Annu Rev Cell Dev Biol* **12**, 697-715 (1996).
- 182 Temming, K., Schiffelers, R. M., Molema, G. & Kok, R. J. RGD-based strategies for selective delivery of therapeutics and imaging agents to the tumour vasculature. *Drug resistance updates : reviews and commentaries in antimicrobial and anticancer chemotherapy* **8**, 381-402 (2005).
- 183 Liu, S. Radiolabeled multimeric cyclic RGD peptides as integrin alphavbeta3 targeted radiotracers for tumor imaging. *Mol Pharm* **3**, 472-487 (2006).
- 184 Bogdanowich-Knipp, S. J., Chakrabarti, S., Williams, T. D., Dillman, R. K. & Siahaan, T. J. Solution stability of linear vs. cyclic RGD peptides. *J Pept Res* **53**, 530-541 (1999).
- 185 Goodman, S. L., Holzemann, G., Sulyok, G. A. & Kessler, H. Nanomolar small molecule inhibitors for alphav(beta)6, alphav(beta)5, and alphav(beta)3 integrins. *J Med Chem* **45**, 1045-1051 (2002).
- 186 Dechantsreiter, M. A., Planker, E., Matha, B., Lohof, E., Holzemann, G., Jonczyk, A., Goodman, S. L. & Kessler, H. N-Methylated cyclic RGD peptides as highly active and selective alpha(V)beta(3) integrin antagonists. *J Med Chem* **42**, 3033-3040 (1999).
- 187 Holig, P., Bach, M., Volkel, T., Nahde, T., Hoffmann, S., Muller, R. & Kontermann, R. E. Novel RGD lipopeptides for the targeting of liposomes to integrin-expressing endothelial and melanoma cells. *Protein Eng Des Sel* **17**, 433-441 (2004).
- 188 Kok, R. J., Schraa, A. J., Bos, E. J., Moorlag, H. E., Asgeirsdottir, S. A., Everts, M., Meijer, D. K. & Molema, G. Preparation and functional evaluation of RGD-modified proteins as alpha(v)beta(3) integrin directed therapeutics. *Bioconjug Chem* **13**, 128-135 (2002).
- 189 Schraa, A. J., Kok, R. J., Berendsen, A. D., Moorlag, H. E., Bos, E. J., Meijer, D. K., de Leij, L. F. & Molema, G. Endothelial cells internalize and degrade RGD-modified

proteins developed for tumor vasculature targeting. *J Control Release* **83**, 241-251 (2002).

- 190 Boturyn, D., Coll, J. L., Garanger, E., Favrot, M. C. & Dumy, P. Template assembled cyclopeptides as multimeric system for integrin targeting and endocytosis. *J Am Chem Soc* **126**, 5730-5739 (2004).

Chapter 5

Albumin-binding radiation-induced apoptosis targeted doxorubicin prodrug

Despite potent anticancer effect of doxorubicin, its clinical use is often limited due to the dose-dependent toxicities. In purpose to improve the therapeutic index of doxorubicin, a novel drug delivery technology was employed that fundamentally differs with the conventional tumor-targeting approaches. The prepared doxorubicin prodrug includes two distinct features for an effective tumor targeting: EPR effect-mediated passive targeting of tumor and extended plasma half-life by *in situ* albumin binding, and radiation-induced apoptosis targeting. For these properties, the prodrug – EMC-DEVD-S-DOX – comprises two important functional molecules. One is a maleimide group that allows *in situ* binding of the prodrug to the circulating albumin after intravenous administration. Second is a DEVD motif that plays crucial role in the activation of the prodrug through caspase-3-mediated cleavage in the apoptotic tumor cells that are exposed to radiation. As a result, EMC-DEVD-S-DOX showed prolonged plasma half-life with selective accumulation within tumor tissue, and was only activated and released free doxorubicin when combined with radiotherapy, thereby showing excellent synergistic effect.

The currently suggested drug delivery strategy completely relies on the anatomical feature of tumor vasculatures and the upregulated caspase-3 after exposure to radiation. Therefore, the genomic diversity of tumor cells could hardly influence the efficacy of the prodrug. Considering that the conventional molecular targeted approach in cancer therapy is seriously challenged by the intratumor heterogeneity, EMC-DEVD-S-DOX could be an outstanding alternative for an effective cancer treatment.

5.1. Introduction

Although targeted therapies have gained considerable interests in the modern cancer therapeutics, chemotherapeutic agents still possess the most important status in the clinical oncology due to their potent anticancer effect and availability in broad spectrum of tumors. However, the dose-dependent toxicities of the chemotherapeutic agents limit both their dosage and frequency of administration, which are insufficient to achieve an effective cancer treatment. The toxicities of the chemotherapeutic agents are fundamentally caused by their lack of selectivity between tumor cells and normal cells in terms of mechanisms of action. In order to improve their selectivity, researchers have proposed many delivery systems that could selectively deliver the chemotherapeutics to a malignant tissue, thus generating site-selectivity to the agents.

One of the popular strategies to deliver chemotherapeutics selectively to a tumor is to introduce a tumor-targeting moiety that could recognize certain tumor-specific biomarkers^{1,2}. However, this strategy is fundamentally challenged by the recent findings that tumor cells differ in terms of their genotype, even within a single tumor mass, so called as intratumor heterogeneity³. The use of the aforementioned drug delivery strategy requires genomic analysis of the subject tumor in order to predict the feasibility. This is generally performed on the tissue samples that are obtained by single needle biopsy or surgical excision, where the samples only represent a small portion of the tumor tissue. However, the finding of intratumor heterogeneity indicated that such genomic analysis is inappropriate to overview the genomic landscape of the entire tumor, which may lead to wrong interpretation of determining the target biomarker in high possibility. Moreover, considering that a single tumor could have several different subtypes of tumor cells, the above mentioned tumor-targeting is likely to affect only a limited population of tumor cells and leave others unaffected, which could eventually result in regrowth of tumor. To overcome the limitations of the conventional targeted delivery of

chemotherapeutic agents, a strategy of targeting an induced-phenotype, radiation-induced apoptosis in particular, rather than targeting genotype of the tumor cells was proposed for more predictable and reliable targeted delivery of chemotherapeutic agents across all of the tumor cells in a malignant tissue⁴. When tumor cells are exposed to radiation, they undergo apoptosis and upregulate caspase-3, which is a cysteine protease^{5,6}. The major advantages of targeting the radiation-induced apoptotic tumor cells for selective delivery of chemotherapeutic agents are as follows: (i) the site of target could be controlled actively by exogenous stimuli (e.g. stereotactic radiotherapy); (ii) the amount of target molecule, which is caspase-3, increases as the therapy goes on, since the delivered drugs consequently induce tumor cell apoptosis and continuously upregulate the caspase-3. This is contrary to the conventional targeted therapy, which results in gradual decrease of target molecules due to the elimination of the tumor cells that are expressing them. Moreover, considering that radiotherapy is already used to treat approximately 50% of the cancer patients⁷, coupling the prodrug with a radiotherapy is a perfect match.

Another approach to selectively deposit chemotherapeutic agents in a malignant tissue is passively targeting the anatomical anomalies of tumor vasculatures. Due to the leaky vasculatures and lack of lymphatic drainage, macromolecules accumulate in the tumor tissue, which the phenomenon is termed as EPR (enhanced permeability and retention) effect. Albumin, a 65 kDa serum protein, also takes advantage of EPR effect and accumulates in the tumor tissue⁸. Therefore, albumin has been recognized as a promising macromolecular carrier in delivering chemotherapeutic agents to the tumor. In addition, serum albumin has a very long plasma half-life, which is more than 19 days in human⁹. Therefore, exploiting albumin as a carrier for drugs is also advantageous to prolong their circulation time. Previously, Kratz et al. proposed an interesting strategy that exploits endogenous albumin as a carrier of chemotherapeutic agents^{10,11}. Albumin is the most abundant protein in the plasma. It presents at about 35-50 mg/ml, which the amount is more than half of the total plasma proteins^{9,10}. Intriguingly, about 70% of the human serum albumin (HSA) has an

accessible free thiol group on the Cys34. This is a very unique feature among the plasma compartments regarding that thiols mostly do not exist in free form (or reduced form) in the plasma. In fact, the free thiols on the albumins account for more than 80% of the total free thiols in the blood. Moreover, they are most reactive among the thiols that exist in the plasma substances. Therefore, thiol-reactive molecules could selectively bind to the Cys34 of the HSA in the blood.

In this study, the radiation-induced apoptosis targeting and the endogenous albumin-mediated passive targeting were combined to achieve highly selective delivery of doxorubicin to the tumor (**Fig. 5.1A**). As a representative agent, EMC-DEVD-S-DOX was prepared, which the albumin-binding moiety (ϵ -maleimidocaproylamide; EMC) and doxorubicin are connected to each other via DEVD peptide spacer to produce a prodrug of doxorubicin (**Fig. 5.1B**).

The maleimide group in the EMC moiety could selectively react with thiol in physiological pH by Michael addition. Therefore, EMC-DEVD-S-DOX could bind with the Cys34 on the circulating albumins, producing a stable conjugate. The *in situ* binding of EMC-DEVD-S-DOX on albumin was confirmed using commercially available HSA in PBS (pH 7.4), human plasma, and mouse plasma.

The DEVD peptide, which acts as a spacer between EMC (or potentially albumin) and doxorubicin, is a well-known cleavable substrate of caspase-3. The caspase-3 recognizes the DEVD sequence within a peptide and enzymatically hydrolyzes the amide bond following the second Asp of the tetrapeptide sequence. Therefore, free doxorubicin could be released from the bound albumin when reached at the apoptotic site that is exposed to radiation. The release of doxorubicin in the presence of caspase-3 was confirmed through several *in vitro* studies. Pharmacokinetic and tumor regression studies were also carried out in preclinical models.

5.2. Materials and methods

5.2.1. Cell lines

SCC7 and MDA-MB-231 cells were obtained from the American Type Culture Collection (ATCC; Manassas, VA). The cells were grown in high-glucose Dulbecco's modified eagle medium (DMEM; Gibco, Carlsbad, CA) supplemented with 10% fetal bovine serum (FBS; Gibco). The cells were maintained in a humidified 5% CO₂ atmosphere at 37°C.

5.2.2. Synthesis

Ac-Lys(OAloc)-Gly-Asp(OAll)-Glu(OAll)-Val-Asp(OAll)-OH (344 mg, 0.38 mmol; AnyGen, Jeollanam-do, South Korea), 4-aminobenzyl alcohol (2 eq; Sigma-Aldrich, St. Louis, MO), and EEDQ (2 eq; Sigma-Aldrich) were dissolved in anhydrous DMF (11 ml; Sigma-Aldrich) and the reaction mixture was stirred at room temperature for 24 h under inert atmosphere. The solution was concentrated under reduced pressure, and 10 volume of diethyl ether (Burdick & Jackson, Muskegon, MI) was added. The precipitate was collected by filtration and dried *in vacuo* to obtain Ac-Lys(OAloc)-Gly-Asp(OAll)-Glu(OAll)-Val-Asp(OAll)-PABOH (322 mg, 84%). ESI-MS (m/z): 1035.7 [M + Na]⁺.

Ac-Lys(OAloc)-Gly-Asp(OAll)-Glu(OAll)-Val-Asp(OAll)-PABOH (322 mg, 0.318 mmol) and 4-nitrophenyl chloroformate (1.2 eq; Sigma-Aldrich) were dissolved in anhydrous CH₂Cl₂ (10 ml; Ducksan, Seoul, South Korea) under inert atmosphere. Then 2,6-lutidine (3 eq; Sigma-Aldrich) was added to the reaction mixture and stirred at room temperature for 2 h. Anhydrous DMF (2 ml) and additional 2,6-lutidine (2 eq) was again added to the reaction mixture. After 24, 27, and 46 h, 2,6-lutidine (4.75 eq) and 4-nitrophenyl chloroformate (1 eq) were further added to the reaction mixture. After 84 h, aqueous NaHCO₃ was added to the reaction mixture and extracted with ethyl acetate (100 ml x 3; Ducksan). The organic layer was washed with 0.5 M citric acid (Sigma-

Aldrich), aqueous NaHCO₃, and brine, subsequently. The obtained organic layer was dried by addition of anhydrous MgSO₄, filtered, and concentrated *in vacuo*. The concentrate was further purified with semi-preparative HPLC using C18 reverse phase column (250 mm × 22 mm) in a gradient system (Water and CH₃CN with 0.1% TFA as an additive, CH₃CN 20-53% over 30 min, 10 ml/min) to obtain Ac-Lys(OAloc)-Gly-Asp(OAll)-Glu(OAll)-Val-Asp(OAll)-PABC (77 mg, 20.5%). ESI-MS (m/z): 1200.54 [M + Na]⁺.

Ac-Lys(OAloc)-Gly-Asp(OAll)-Glu(OAll)-Val-Asp(OAll)-PABC (77 mg, 0.065 mmol) and doxorubicin HCl (1.2 eq; Korea United Pharm., Seoul, South Korea) were dissolved in anhydrous DMF (8 ml). DIEA (5.4 eq; Sigma-Aldrich) was added to the reaction mixture and stirred at room temperature for 16 h under inert atmosphere. The solution was concentrated *in vacuo* and further purified with semi-preparative HPLC using C18 reverse phase column (250 mm × 22 mm) in a gradient system (Water and CH₃CN with 0.1% TFA as an additive, CH₃CN 20-100% over 50 min, 10 ml/min) to obtain Ac-Lys(OAloc)-Gly-Asp(OAll)-Glu(OAll)-Val-Asp(OAll)-PABC-DOX (red amorphous solid, 50 mg, 50%). ESI-MS (m/z): 1605.06 [M + Na]⁺.

Ac-Lys(OAloc)-Gly-Asp(OAll)-Glu(OAll)-Val-Asp(OAll)-PABC-DOX (50 mg, 0.032 mmol) and Pd(PPh₃)₄ (0.2 eq; Sigma-Aldrich) were dissolved in anhydrous DMF (4 ml) under inert gas and degassed over 5 min. Then tributyltin hydride (17.3 eq; Sigma-Aldrich) and acetic acid (20 eq; Sigma-Aldrich) were added to the reaction mixture, and stirred at room temperature for 1 h. The product was then purified with semi-preparative HPLC using C18 reverse phase column (250 mm × 22 mm) in a gradient system (Water and CH₃CN with 0.1% TFA as an additive, CH₃CN 20-41% over 41 min, 10 ml/min) to obtain deprotected Ac-Lys-Gly-Asp-Glu-Val-Asp-PABC-DOX (red amorphous solid, 6 mg, 13.6%). ESI-MS (m/z): 1378.4 [M + Na]⁺.

Ac-Lys-Gly-Asp-Glu-Val-Asp-PABC-DOX (named as DEVD-S-DOX; 20 mg, 0.013 mmol) and *N*-(ε-maleimidocaproyloxy)succinimide ester (EMCS; 8.26 mg, 26.8 μmol, 2 eq; Pierce, Rockford, IL) were dissolved in anhydrous DMF (1.5 ml) under inert gas. Then TEA (4.64 μl, 2.5 eq; Sigma-Aldrich) was

added to the reaction mixture and stirred at room temperature for 2 h. The final product was purified with semi-preparative HPLC (Shimadzu, Kyoto, Japan) using ODS-A 5 μm reverse phase semi-preparative column (150 mm \times 20 mm) in a gradient system (Water and CH_3CN with 0.05% TFA as an additive, CH_3CN 20-50% over 50 min, 8 ml/min) to obtain Ac-Lys(EMC)-Gly-Asp-Glu-Val-Asp-PABC-DOX (named as EMC-DEVD-S-DOX; red amorphous solid, 16.7 mg, 73.6%). The peaks were monitored at 280 nm. The purity of the final products was confirmed by analytical HPLC (Agilent 1300 series, Agilent Technologies, Santa Clara, CA) using ODS-A 5 μm analytical column (150 mm \times 3 mm; YMC) in a gradient system (DW and CH_3CN with 0.1% TFA as an additive, CH_3CN 5-95%/5-30 min, 1 ml/min). The peaks were monitored under UV detector (214 nm) and fluorescent detector (excitation 470nm, emission 580 nm). The purity of the final compound was determined to be $\geq 95\%$. ESI-MS (m/z): 1593.3 $[\text{M} + \text{Na}]^+$.

5.2.3. EMC-DEVD-S-DOX binding study with HSA

A human serum albumin (HSA; Sigma-Aldrich) solution was prepared in PBS at a final concentration of 700 μM (46.5 mg/ml). To the solution of HSA, EMC-DEVD-S-DOX was added at a final concentration of 100 μM and incubated at room temperature for 3 min and 60 min. For blocking study, the HSA solution was preincubated with excess amount of 4-maleimidobutyric acid (Santa Cruz) for 1 h before addition of EMC-DEVD-S-DOX. The samples were subjected to analytical HPLC. HPLC analysis: Flow rate 1 ml/min, mobile phase A: DW with 0.1% TFA; mobile phase B: CH_3CN with 0.1% TFA; gradient 0-5 min 30% mobile phase B; 5-25 min increase to 50% mobile phase B; 25-30 min 50% mobile phase B.

5.2.4. HSA-DEVD-S-DOX analysis by SDS-PAGE

HSA (70 μM , 4.6 mg/ml) solution was prepared in PBS. EMC-DEVD-S-DOX (100 μM) or DEVD-S-DOX (100 μM) was incubated for 1 h in the HSA solution at room temperature. Same volume of EMC-DEVD-S-DOX in HSA

solution, DEVD-S-DOX in HSA solution, and HSA solution was subjected to a native SDS-PAGE using 12% polyacrylamide gel. The gel was visualized by trans-UV under ImageQuant LAS 4000 imaging system (GE Healthcare Life Sciences, Uppsala, Sweden). The albumin bands were stained with coomassie blue (Pierce, Rockford, IL).

5.2.5. Determination of thiol concentration of HSA using Ellman's test

Ellman's reagent (DTNB; Sigma-Aldrich) working solution was prepared at 80 µg/ml in reaction buffer (0.1 M sodium phosphate buffer, pH 8.0, 1 mM EDTA). Cysteine standard was prepared at concentration of 0, 0.25, 0.5, 0.75 and 1 mM in the reaction buffer. HSA (Sigma-Aldrich) was prepared at 1 mM (66.5 mg/ml) in the reaction buffer. The standard and sample solution was transferred to a 96-well microplate at 20 µl and then, 200 µl of Ellman's reagent working solution was added. The mixture was incubated for 15 min at room temperature and the absorbance was measured using a microplate reader (Synergy HT; BioTek Instruments, Winooski, VT) at 412 nm. The thiol concentration of HSA was determined based on the standard curve and the percentage of mercaptalbumin was calculated.

5.2.6. Preparation and characterization of HSA-DEVD-S-DOX

To prepare HSA-DEVD-S-DOX, EMC-DEVD-S-DOX (100 µM) was incubated with HSA (70 µM, 4.6 mg/ml; Sigma-Aldrich) in pH 7.4 PBS for 1 h. Then the solution was transferred to an Amicon Ultra-4 centrifugal unit (MW cutoff 10 kDa; EMD Millipore, Billerica, MA) and centrifuged for 15 min at 3000 rpm to remove the excess amount of unreacted EMC-DEVD-S-DOX. The flow-through was discarded, distilled water was added to the concentrated substance, and centrifuged subsequently to wash the product. The solution in the insert was collected and lyophilized to obtain HSA-DEVD-S-DOX as a powder. The mass of the final product and HSA were analyzed using MALDI-TOF MS (Voyager-DE STR Biospectrometry Workstation, Applied Biosystems).

5.2.7. EMC-DEVD-S-DOX incubation study in plasma

Human plasma was obtained from a healthy volunteer and the blood was stabilized immediately with EDTA after withdrawal. Mouse plasma was obtained from C3H/HeN mice. EMC-DEVD-S-DOX was incubated with the plasma at a final concentration of 100 μ M at room temperature. For blocking study, excess amount of 4-maleimidobutyric acid (Santa Cruz) was preincubated with the plasma for 1 h, and then EMC-DEVD-S-DOX (100 μ M) was added, subsequently. The samples were diluted ten-fold in PBS and subjected to an analytical HPLC. Fresh plasma and EMC-DEVD-S-DOX in PBS were also analyzed. HPLC analysis: Flow rate 1 ml/min, mobile phase A: DW with 0.1% TFA; mobile phase B: CH₃CN with 0.1% TFA; gradient 0-5 min 30% mobile phase B; 5-25 min increase to 50% mobile phase B; 25-30 min 50% mobile phase B.

5.2.8. Western blot

EMC-DEVD-S-DOX (100 μ M) was incubated with HSA (500 μ M) in pH 7.4 PBS (1 ml) for 30 min at room temperature to produce an albumin-bound EMC-DEVD-S-DOX (HSA-DEVD-S-DOX). Then, 500 μ l of the solution was incubated with recombinant human caspase-3 (R&D Systems, Minneapolis, MN) at a final concentration of 500 ng/ml. SCC7 and MDA-MB-231 cells were cultured in 60 mm dishes until 80 - 90% confluence. The cells were treated with 0.1, 1, and 10 μ M of the previously prepared HSA-DEVD-S-DOX or HSA-DEVD-S-DOX preincubated with caspase-3, and incubated for 48 h at 37°C. The cells were washed with cold PBS and lysed with RIPA buffer (Pierce) supplemented with protease inhibitor cocktail (Pierce). The preparation of the samples and western blot were performed according to the standard protocol. For immunoblotting, anti-Caspase-3 antibody (1:1000) and anti-cleaved Caspase-3 antibody (1:1000) from Cell Signaling Technology (Danvers, MA) were used as primary antibodies. HRP-conjugated anti-rabbit IgG (1:2000;

R&D Systems) was used as secondary antibody. The blotted membranes were developed using ImageQuant LAS 4000 imaging system.

5.2.9. MTT cytotoxicity assay

MTT assay kit was purchased from Trevigen (Gaithersburg, MD). The assay was performed following the standard procedure. Briefly, SCC7 and MDA-MB-231 cells were plated at a density of 5×10^4 cell per well in 96 well culture plates (Corning, Tewksbury, MA). After 24 h incubation in DMEM supplemented with 10% FBS, doxorubicin, HSA-DEVD-S-DOX, or HSA-DEVD-S-DOX preincubated with caspase-3 (500 ng/ml) was treated at a concentration range of 0.01 to 100 μ M to the cells and further incubated for 48 h. Then MTT reagent (10 μ l) was added, and incubated for 2 h at 37°C. When purple formazan precipitates were observed clearly in the cells, detergent agent (100 μ l) was further added and incubated for 4 h at room temperature. The absorbance was measured at 570 nm using a microplate reader (Synergy HT).

5.2.10. Cellular uptake imaging

Cellular uptake of doxorubicin, DEVD-S-DOX, HSA-DEVD-S-DOX, and HSA-DEVD-S-DOX preincubated with caspase-3 was observed to determine the intracellular distribution. SCC7 or MDA-MB-231 cells were seeded on 35 mm cover glass-bottom dishes (SPL Life Sciences, Pocheon, Korea) at a density of 5×10^5 cells per dish and allowed to grow until 70-80% confluence. Prepared materials were treated to the cells at 10 μ M of final concentration and incubated for 2 h. The cells were carefully washed with cold PBS and fixed with 4% PFA (Sigma-Aldrich). The cell nucleus was stained using DAPI (Molecular Probes, Eugene, OR) and mounted with mounting medium. The cells were observed under confocal laser scanning microscopy (LSM 710; Carl Zeiss, Oberkochen, Germany).

5.2.11. HPLC determination of caspase-mediated activation

To determine the release of doxorubicin from HSA-DEVD-S-DOX by caspase-3, the EMC-DEVD-S-DOX (1 mM) was incubated with HSA (7 mM) in pH 7.4 PBS, diluted ten-fold in the caspase assay buffer (50 mM HEPES, pH 7.4, 100 mM NaCl, 0.1% CHAPS, 10 mM DTT, 1 mM EDTA, 10% glycerol; Enzo Life Sciences, Farmingdale, NY), and incubated with recombinant human caspase-3 (500 ng/ml; R&D Systems, Minneapolis, MN) at room temperature, subsequently. The solution was subjected to an analytical HPLC (Agilent 1300 series, Agilent Technologies) using ODS-A 5 μ m analytical column (150 mm \times 3 mm; YMC, Dinslaken, Germany) with a gradient system (DW and CH₃CN with 0.1% TFA as an additive, CH₃CN 30-50%/5-25 min) at a flow rate of 1 ml/min. The chromatograms were monitored using fluorescence detector at Ex 470 nm/Em 580 nm. Additionally, HSA-DEVD-S-DOX without caspase-3, and with caspase-3 (500 ng/ml) pretreated with caspase-3 inhibitor (Ac-DEVD-CHO, 10 μ M; Enzo Life Sciences) were incubated for 60 min at room temperature in the caspase assay buffer, and then subjected to an analytical HPLC. HPLC analysis: Flow rate 1 ml/min, mobile phase A: DW with 0.1% TFA; mobile phase B: CH₃CN with 0.1% TFA; gradient 0-5 min 30% mobile phase B; 5-25 min increase to 50% mobile phase B; 25-30 min 50% mobile phase B.

5.2.12. Pharmacokinetic study

To Spraque Dawley (SD) rats, EMC-DEVD-S-DOX or DEVD-S-DOX was administered at a dose of 2.89 or 2.54 mg/kg (equivalent to 1 mg/kg of doxorubicin), respectively, via tail vein (n = 3). The blood was withdrawn (500 μ l per each time point) at 5, 15, 30, 60, 90 min, and 2, 4, 8, 12, 24, 48, 72, 96 h of post-injection. The collected bloods stabilized immediately with sodium citrate and centrifuged for 15 min at 2000 \times g in a refrigerated centrifuge to separate the plasma. The plasma samples (200 μ l) were transferred to a 96-well black microplate and the intrinsic fluorescence of doxorubicin was read at

at Ex 485 nm/Em 590 nm. The standard was prepared in fresh plasma and the fluorescence was read as described above. All experimental procedures were approved by the Institutional Animal Care and Use Committee of the Seoul National University.

5.2.13. *Ex vivo* biodistribution imaging

SCC7 cells were suspended at 1×10^7 cell/ml in HBSS, and inoculated subcutaneously (100 μ l) into the thigh of 6 week-old male BALB/cSlc-nu mice. When the tumor volume reached 500 mm³, the mice received EMC-DEVD-Cy5.5, which the doxorubicin in EMC-DEVD-S-DOX was substituted with Cy5.5 for the *ex vivo* imaging, at a single dose of 1 mg/kg molar equivalent to doxorubicin through tail vein. The whole-body fluorescent imaging was taken at 1, 24, 48, 72, 96, and 120 h of post-administration under Optix MX3 imaging system (Advanced Research Technologies, Montreal, Canada). The intensity map of the acquired images in different time points were normalized. All experimental procedures were approved by the Institutional Animal Care and Use Committee of the Seoul National University.

5.2.14. Tumor growth suppression

SCC7 cells were suspended at 1×10^7 cell/ml in HBSS, and inoculated subcutaneously (100 μ l) into the dorsal flank of 6 week-old male C3H/HeN mice. When the tumor volume reached 50 mm³, the mice were randomized (n = 5), and received one of follows: normal saline, EMC-DEVD-S-DOX (2.89 mg/kg; equivalent to 1 mg/kg of doxorubicin) or DEVD-S-DOX (2.54 mg/kg; equivalent to 1 mg/kg of doxorubicin) for seven days daily via tail vein. For radiation-treated groups, 4 Gy of X-ray (6 MV, 300 cGy/min; Clinac 21EX, Varian, Palo Alto, CA) was given once to the tumor at the first day of the drug treatment. The tumor length and width were measured by caliper and the volume was calculated using the modified ellipsoid formula ($L \times W^2/2$). At the last day of observation, the tumors were isolated and weighed. All experimental

procedures were approved by the Institutional Animal Care and Use Committee of the Seoul National University.

5.3. Results

5.3.1. Synthesis of EMC-DEVD-S-DOX

Scheme 5.1 depicts the synthesis of maleimidocaproyl-AcKGDEVD-PABC-doxorubicin (EMC-DEVD-S-DOX). The carboxyl side chains of the AcKGDEVD-COOH peptide were protected with allyl ester in order to deprotect them in a mild condition that doxorubicin could remain stable. The protected AcKGDEVD-COOH peptide was conjugated to the 3'-NH₂ of doxorubicin via a self-immolative spacer (*p*-aminobenzyl carbamate; PABC) to avoid steric hindrance by bulky doxorubicin molecule interfering the interaction of DEVD moiety with caspase-3. When the amide bond between the peptide and PABC spacer is hydrolyzed by caspase-3, the self-immolative spacer releases itself from doxorubicin, thereby liberating the free drug.

The allyl ester groups that were protecting the side chains of Asp and Glu were deprotected using Pd(PPh₃)₄ catalyst to obtain AcKGDEVD-PABC-doxorubicin. Conventional protection and deprotection methods for carboxyl groups (e.g. *tert*-butyl ester protection) were avoided because doxorubicin is very labile in highly acidic or basic environment, which is generally used during deprotection of the carboxyl groups.

Finally, the amino group of Lys side chain was reacted with *N*-(ϵ -maleimidocaproyloxy)succinimide ester (EMCS) in the presence of Et₃N to afford the final product, EMC-DEVD-S-DOX. The purity was confirmed to be more than 95% using analytical HPLC (**Fig. 5.2A**). The mass was determined using ESI-MS (**Fig. 5.2B**).

5.3.2. Albumin-binding of EMC-DEVD-S-DOX

The plasma albumin-binding capability of EMC-DEVD-S-DOX was determined through various *in vitro* studies. Firstly, the albumin binding of

EMC-DEVD-S-DOX was determined on a commercially available human serum albumin (HSA). EMC-DEVD-S-DOX (100 μ M) was incubated with the HSA (700 μ M) and analyzed by HPLC (**Fig. 5.3A**). Binding of the EMC-DEVD-S-DOX to the HSA was presented by disappearance of the EMC-DEVD-S-DOX peak at 11.3 min and appearance of a broad peak between 15-20 min detected through the intrinsic fluorescence of the doxorubicin moiety (Ex 470/Em 580 nm). The binding of the EMC-DEVD-S-DOX to the HSA was accomplished within 3 min and only trace amount of the unbound substance was detected. However, when HSA was pre-incubated with 4-maleimidobutyric acid, which is a small molecule containing a maleimide group, EMC-DEVD-S-DOX did not bind to the HSA even after 1 h incubation. This clearly proved that the maleimide group on the EMC-DEVD-S-DOX was indeed the mediator of the HSA binding.

The HSA binding of the EMC-DEVD-S-DOX was further confirmed by SDS-PAGE (**Fig. 5.3B**). The EMC-DEVD-S-DOX and HSA were detected using the absorbance of the doxorubicin moiety and coomassie blue staining, respectively. EMC-DEVD-S-DOX band was observed below 15 kDa on the gel after electrophoresis. By contrast, when EMC-DEVD-S-DOX (100 μ M) was incubated with HSA (70 μ M), the band from the doxorubicin moiety was observed between 50-75 kDa, which the position was identical with the band from the intact HSA (MW 66.5 kDa). Also, the band from the unbound EMC-DEVD-S-DOX (shown below 15 kDa) was decreased when compared to the other lanes. However, when the HSA was blocked with 4-maleimidobutyric acid, the band from the EMC-DEVD-S-DOX was only visible below 15 kDa. This indicated that EMC-DEVD-S-DOX was unable to bind to HSA when the thiol of HSA is blocked, agreeing with the aforementioned HPLC result. The fact that the HSA binding was mediated through the maleimide group was further supported by the result that showed DEVD-S-DOX, which has no maleimide functional group in the molecule, did bind to the HSA represented by the band only shown below 15 kDa.

The molecular weight shift of the HSA-bound EMC-DEVD-S-DOX (hereafter, HSA-DEVD-S-DOX) from the commercially available HSA was evaluated using MALDI-TOF mass spectrometry (**Fig. 5.3C**). The maximum intensity mass of the HSA was determined to be 66383.4219, whereas the maximum intensity mass of the HSA-DEVD-S-DOX was shifted to 67940.3726, showing mass difference of 1556.9507. This value is similar to the mass of the EMC-DEVD-S-DOX (m/z 1570.59), indicating that a single molecule of EMC-DEVD-S-DOX was bound to a molecule of HSA.

Finally, a selective albumin binding of EMC-DEVD-S-DOX was confirmed in the human plasma. EMC-DEVD-S-DOX (100 μ M) was incubated in the human plasma and analyzed by HPLC (**Fig. 5.3D**). Binding of the EMC-DEVD-S-DOX to the serum albumin in the plasma was represented by the disappearance of EMC-DEVD-S-DOX peak at 11.3 min and the appearance of a broad peak between 16-20 min detected by the intrinsic fluorescence of doxorubicin moiety (Ex 470/Em 580 nm). The binding of EMC-DEVD-S-DOX to the serum albumin was rapid, which was accomplished within 3 min and only trace amount of the unbound substance was detected. However, when the plasma was pre-incubated with 4-maleimidobutyric acid (GMB) in advance of the EMC-DEVD-S-DOX addition, the height of the EMC-DEVD-S-DOX peak was unchanged even after 1 h incubation.

5.3.3. Caspase-3-mediated cleavage of HSA-DEVD-S-DOX

The therapeutic efficacy of the currently proposed system relies on its ability to release doxorubicin when recognized by caspase-3. Since the presence of a macromolecule (i.e. albumin) adjacent to the DEVD moiety might interfere such process, the major concern was whether caspase-3 could recognize and cleave the DEVD moiety when EMC-DEVD-S-DOX is bound to HSA. To address this question, HSA-DEVD-S-DOX was incubated with purified caspase-3 and subjected to HPLC analysis (**Fig. 5.4A**). The intensity of the broad peak from the HSA-DEVD-S-DOX was decreased to the ground level within an hour accompanied with the appearance of new sharp peak at 2.2 min.

The retention time of doxorubicin was identical with the new peak, indicating that the caspase-3 had indeed triggered the release of free doxorubicin from HSA-DEVD-S-DOX.

5.3.4. *In vitro* efficacy of HSA-DEVD-S-DOX

The cytotoxic effect of HSA-DEVD-S-DOX in the absence or presence of caspase-3 was determined. HSA-DEVD-S-DOX did not show any noticeable cytotoxic effect up to 100 μM in both SCC7 and MDA-MB-231 cells when evaluated through MTT assay. However, when the HSA-DEVD-S-DOX was pre-incubated with purified caspase-3 in advance of addition to the cells, it showed similar degree of cytotoxicity ($\text{IC}_{50} = 0.49$ and $4.17 \mu\text{M}$) with doxorubicin ($\text{IC}_{50} = 0.30$ and $2.04 \mu\text{M}$) on SCC7 and MDA-MB-231, respectively (**Fig. 5.4B**). These results were supported by the observation of the cells incubated with HSA-DEVD-S-DOX in the absence or presence of caspase-3 under confocal microscopy. The cells incubated with HSA-DEVD-S-DOX showed very small amount of the substances taken up into the cells with no accumulation in the cell nucleus. By contrast, when HSA-DEVD-S-DOX was pre-incubated with a purified caspase-3, the substance was clearly accumulated inside the cell nucleus in similar degree to that shown in the cells incubated with doxorubicin (**Fig. 5.4C**).

5.3.5. Caspase-3 upregulation induced by activated HSA-DEVD-S-DOX

For the current drug delivery strategy to be valid, the HSA-DEVD-S-DOX should upregulate the caspase-3 in the cells after it is activated. Therefore, the upregulation of caspase-3 in SCC7 and MDA-MB231 cells were examined after treatment of HSA-DEVD-S-DOX or activated HSA-DEVD-S-DOX by western blot. The results showed that HSA-DEVD-S-DOX itself did not upregulate the caspase-3 up to 10 μM . On the other hand, when HSA-DEVD-S-DOX was pre-incubated with a purified caspase-3 and treated to the cells, dose-dependent decrease of procaspase-3 and increase of cleaved (or active) caspase-3 were observed in the both cells (**Fig. 5.4D**). Procaspase-3 is a zymogen of caspase-3,

which is activated when cleaved into 17 and 19 kDa subunits. The results clearly showed that the caspase-3-mediated activation of HSA-DEVD-S-DOX is followed by the further upregulation of caspase-3 due to the released doxorubicin stimulating the cellular apoptosis.

5.3.6. Pharmacokinetic study

The pharmacokinetic profiles of the EMC-DEVD-S-DOX and DEVD-S-DOX were obtained after intravenous administration of the drugs to Sprague-Dawley rats at a dose of molar equivalent to 1 mg/kg of doxorubicin (2.89 and 2.54 mg/kg, respectively) (**Fig 5.5A**). The DEVD-S-DOX showed half-life of 30 min and the plasma concentration decreased below the detection limit (10 ng/ml) within 4 hours. However, EMC-DEVD-S-DOX showed significantly extended half-life with more than 19 hours, which is 38-fold longer than DEVD-S-DOX, and lasted more than 6 days in plasma after the administration, resulting in 157-fold higher AUC (**Table 5.1**).

5.3.7. Tumor accumulation of EMC-DEVD-Cy5.5

The whole-body distribution of EMC-DEVD-S-DOX after intravenous administration was determined indirectly by substituting doxorubicin to near-infrared dye Cy5.5 for *ex vivo* observation (**Fig 5.5B**). At one hour post-administration, the fluorescence from the substance was distributed throughout the entire body with no noticeable accumulation in any major organs or in tumor. However, when the animals were observed at 24 hour post-administration, significant accumulation of the substance in the tumor tissue was observed. The fluorescence intensity level in the tumor was even higher than the previously observed time-point, whereas the intensity level in other part of the body was decreased noticeably. This clearly showed that the selective accumulation of the administered agent occurred in the tumor. The fluorescent intensity in the tumor was unchanged up to 48 hour post-administration, while the intensity in other part of the body was continuously decreased. The relatively higher amount of the fluorescence in the tumor was

maintained for 120 hours, which was the last time of observation. Moreover, current observations also showed that the detectable amount of the substances remained for more than 120 hours in the body albeit lower than that observed in the tumor. This showed that the agent maintained their level in the circulation for very long time, agreeing with the findings in the pharmacokinetic study.

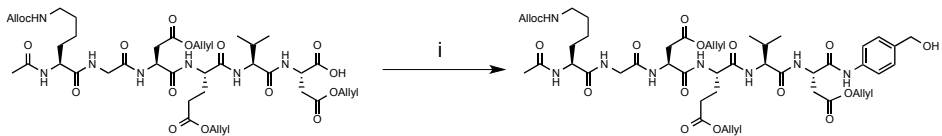
5.3.8. Tumor growth suppression of EMC-DEVD-S-DOX

Tumor growth suppression by EMC-DEVD-S-DOX was evaluated on SCC7-bearing C3H/HeN mice (**Fig 5.6A**). EMC-DEVD-S-DOX or DEVD-S-DOX was administered intravenously at a dose of molar equivalent to 1 mg/kg of doxorubicin daily for seven days daily observed for two weeks. For radiation treated groups, the tumors were exposed to a single dose of 4 Gy linear X-ray at the first day of the drug administration. Similar to the previous report that DEVD-S-DOX had no evident anticancer activity when used alone⁴, EMC-DEVD-S-DOX also showed negligible tumor suppression effect as shown by similar tumor growth in comparison to the control group. On the other hand, when EMC-DEVD-S-DOX was combined the radiation, the tumor volume was decreased by 77% ($P < 0.01$). The tumor suppression effect of EMC-DEVD-S-DOX was superior to that of DEVD-S-DOX. When combined with radiation, the tumor volume of EMC-DEVD-S-DOX treated group decreased by 65% when compared to the radiation only treated group, while that of DEVD-S-DOX treated group decreased by 29%. During the course of the study, noticeable body weight changes were not observed in any experimental group, indicating that there was no severe toxicity in all of the tested groups (**Fig. 5.6B**).

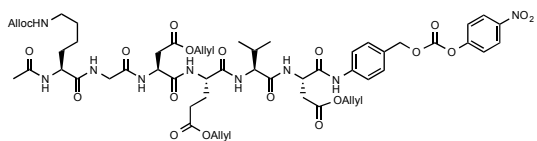
Table 5.1. Pharmacokinetic parameters in SD rats (1 mg/kg dox molar eq.)

	DEVD-S-DOX	EMC-DEVD-S-DOX
C_{\max} ($\mu\text{g/ml}$)	7.335 ± 1.175	14.49 ± 0.6180
$t_{1/2}$ (hr)	0.5002 ± 0.09237	19.13 ± 2.171
V_d (ml/kg)	464.2 ± 24.20	116.4 ± 10.09
CL (ml/kg/h)	655.2 ± 97.92	4.224 ± 0.1136
AUC_{last} (hr· $\mu\text{g/ml}$)	1.500 ± 0.2215	234.8 ± 7.064
AUC_{INF} (hr· $\mu\text{g/ml}$)	1.551 ± 0.2440	236.8 ± 6.370

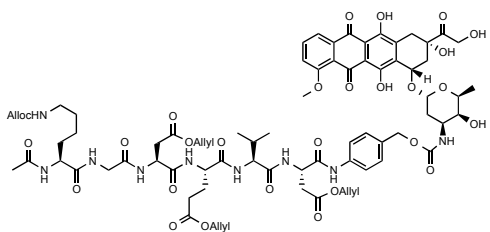
Data presented as mean \pm s.d.



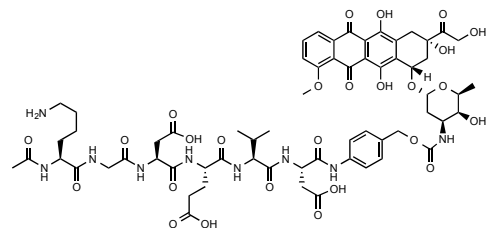
ii



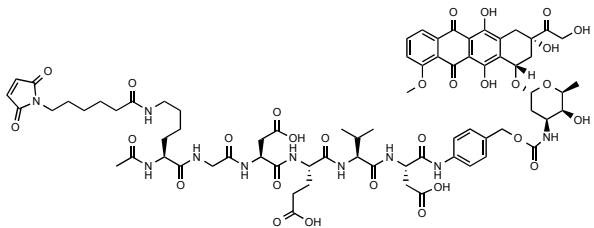
iii



iv



v



Scheme 5.1. Chemical synthesis of EMC-DEVD-S-DOX^a

^aReagents and conditions: (i) 4-aminobenzyl alcohol, EEDQ, DMF, rt. (ii) 4-NPC, 2,6-lutidine, DCM, DMF, rt. (iii) Doxorubicin HCl, DIEA, DMF, rt. (iv) Pd(PPh₃)₄, DMF, tributyltin hydride, acetic acid, rt. (v) EMCS, TEA, rt.

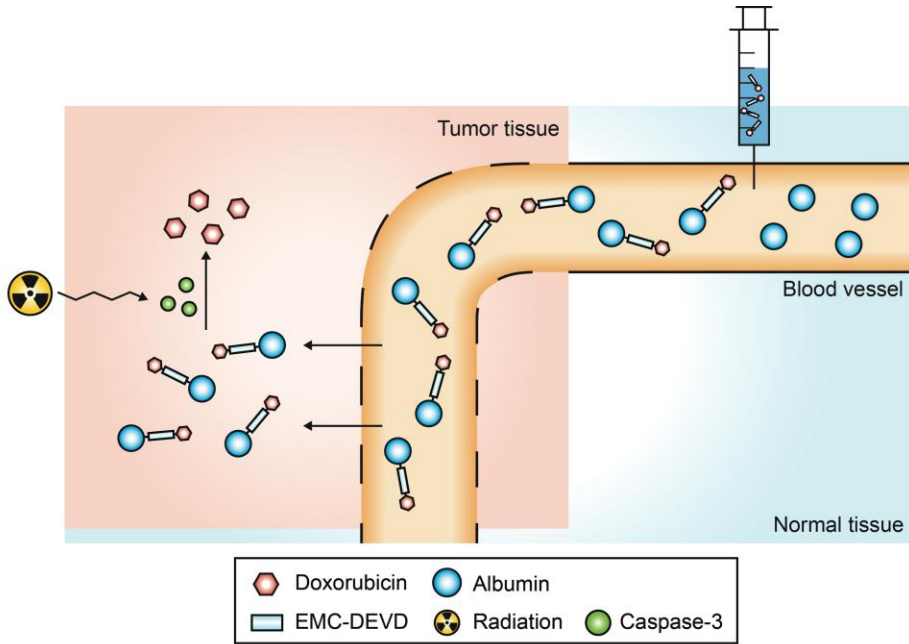
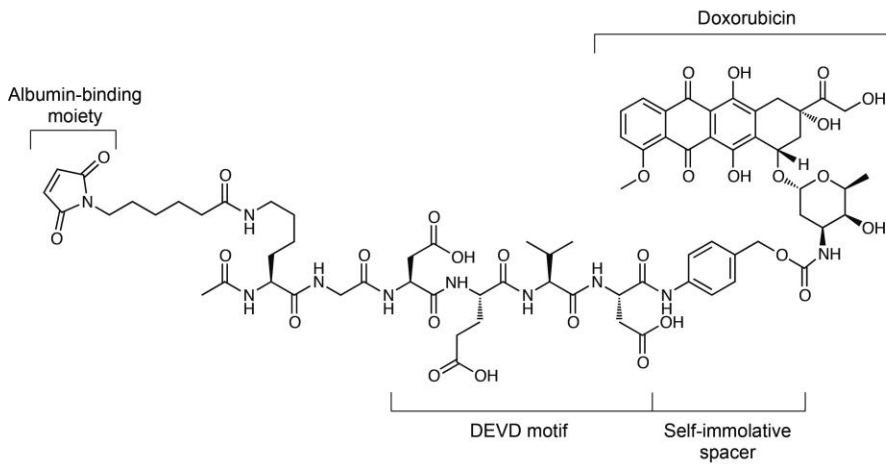
A**B**

Figure 5.1. (A) Schematic diagram of EMC-DEVD-S-DOX therapeutic strategy.
(B) Chemical structure of EMC-DEVD-S-DOX.

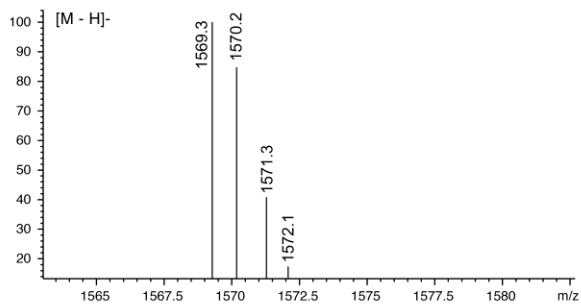
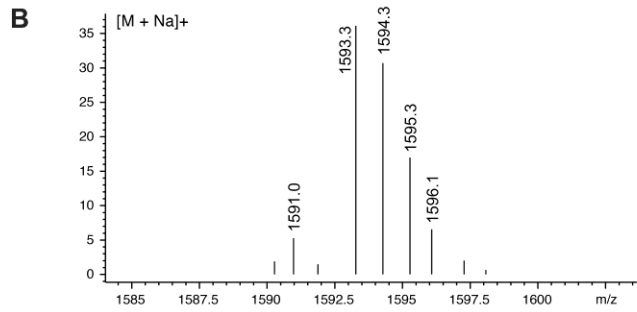
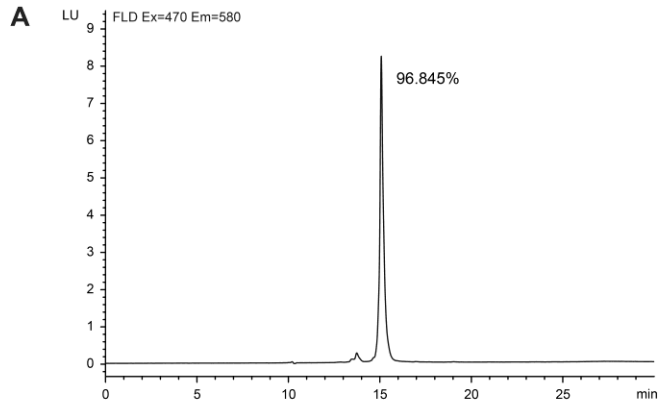


Figure 5.2. (A) Analytical HPLC chromatogram of the final product detected under fluorescence detector (470/580 nm). (B) Mass spectrum of the final product determined by LC/ESI-MS.

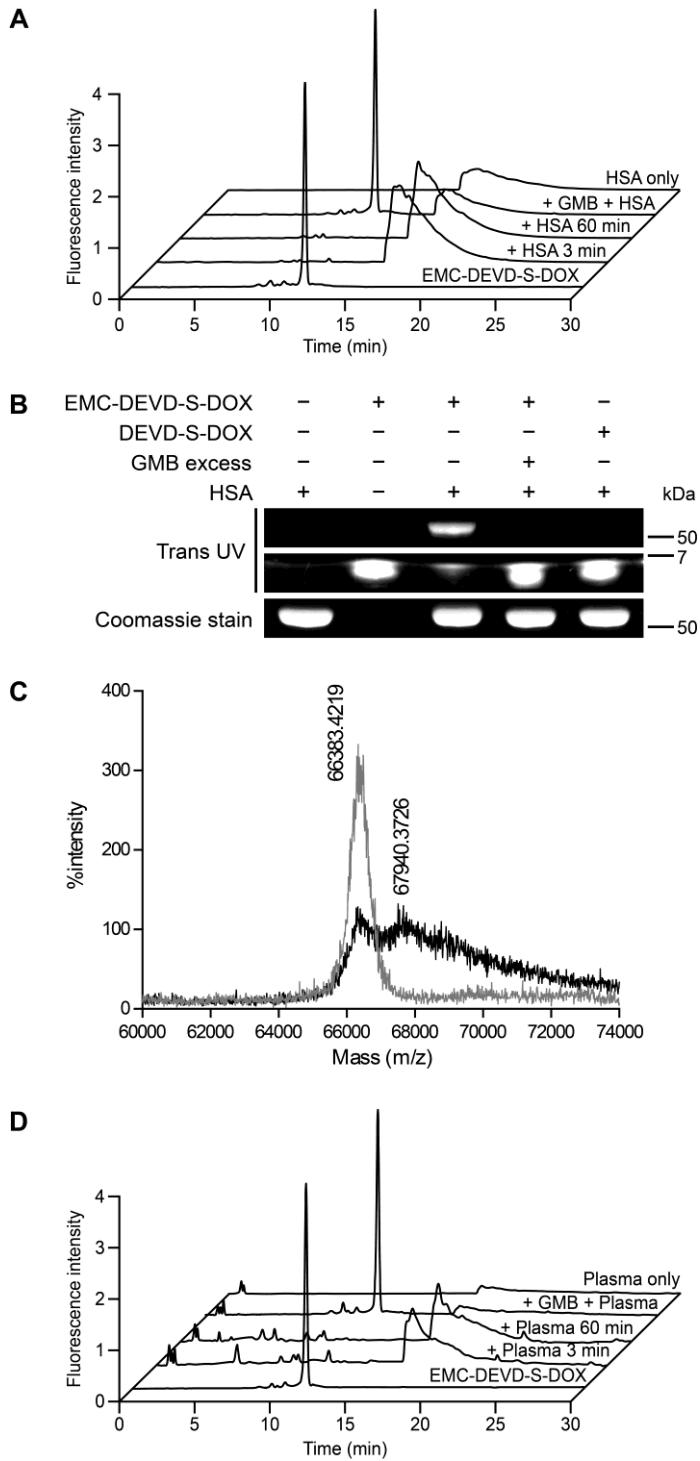


Figure 5.3. (A) HPLC chromatograms of EMC-DEVD-S-DOX and that incubated with commercially available HSA (3, 60 min), EMC-DEVD-S-DOX incubated with HSA blocked with excess GMB (60 min), and only HSA. (B) SDS-PAGE of EMC-DEVD-S-DOX or DEVD-S-DOX incubated with HSA or HSA blocked with excess GMB. (C) MALDI-TOF MS results of commercially available HSA (grey), and that incubated with EMC-DEVD-S-DOX in PBS (pH 7.4; black). (D) HPLC chromatograms of EMC-DEVD-S-DOX and that incubated in human plasma (3, 60 min), EMC-DEVD-S-DOX incubated with the plasma blocked with excess GMB (60 min), and only plasma.

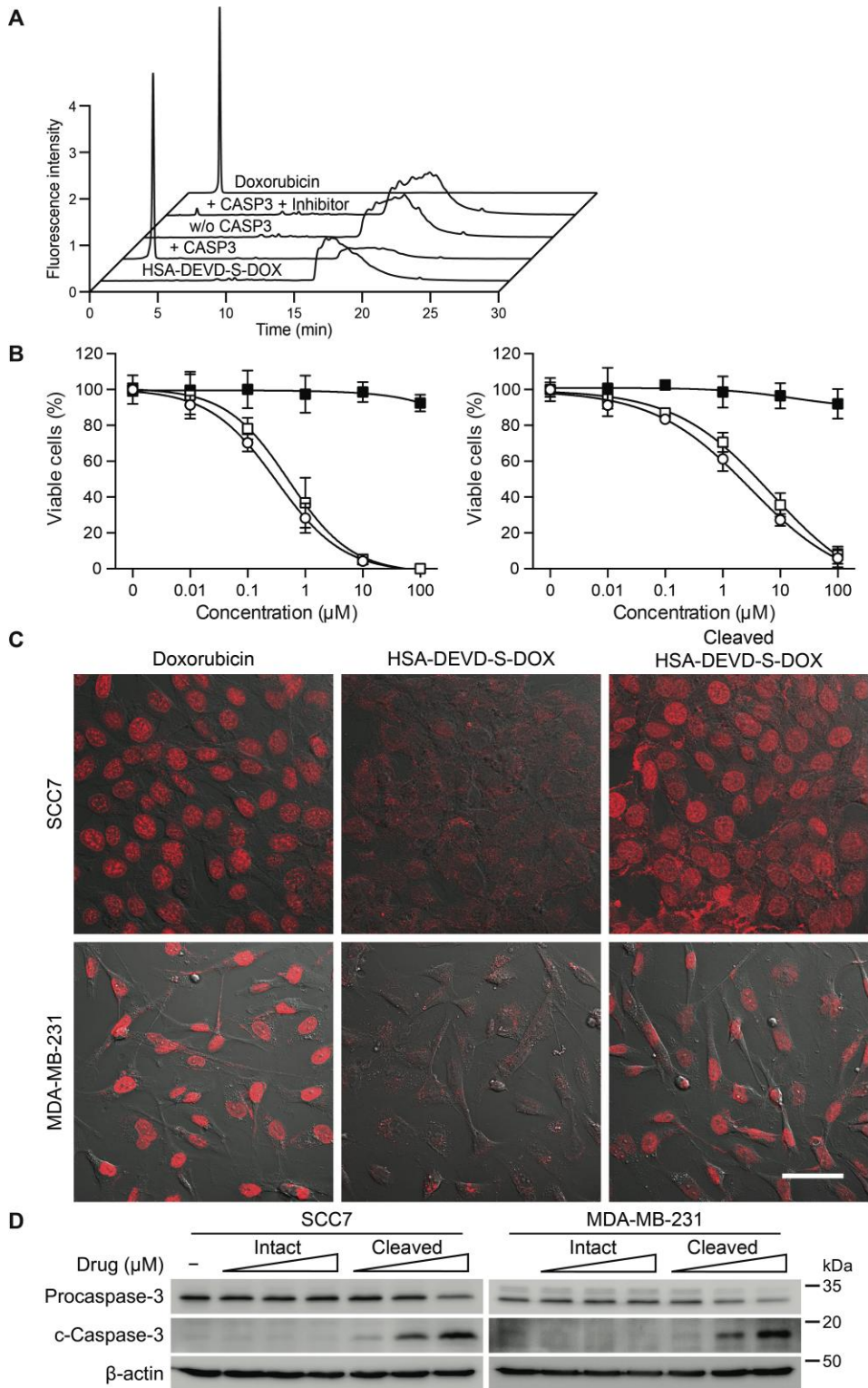


Figure 5.4. (A) HPLC chromatograms of HSA-DEVD-S-DOX and that incubated in the presence or absence of caspase-3, HSA-DEVD-S-DOX incubated with the caspase-3 pretreated with caspase inhibitor, and doxorubicin. (B) Concentration-dependent cytotoxicity of doxorubicin (○), HSA-DEVD-S-DOX (■), and HSA-DEVD-S-DOX incubated with recombinant human caspase-3 (□) on SCC7 (left) and MDA-MB-231 (right) cells determined by MTT assay. (C) Cellular uptake and intracellular distribution of doxorubicin (left), HSA-DEVD-S-DOX (center), and HSA-DEVD-S-DOX incubated with caspase-3 (right) in SCC7 (upper) and MDA-MB-231 (lower) cells observed under confocal microscopy. The substances were detected through intrinsic fluorescence of doxorubicin and represented as red color. Scale bar, 50 μm. (D) Western blots of SCC7 (upper) or MDA-MB-231 (lower) cells treated with HSA-DEVD-S-DOX or HSA-DEVD-S-DOX incubated with recombinant human caspase-3 (Cleaved HSA-DEVD-S-DOX) at a concentration of 1, 5, and 10 μM. The immunoblots were carried out using procaspase-3 (upper), cleaved caspase-3 (center), and β-actin (lower) antibodies.

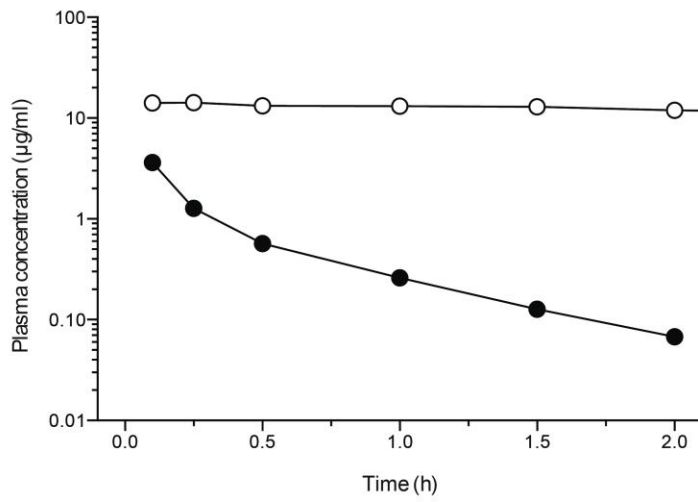
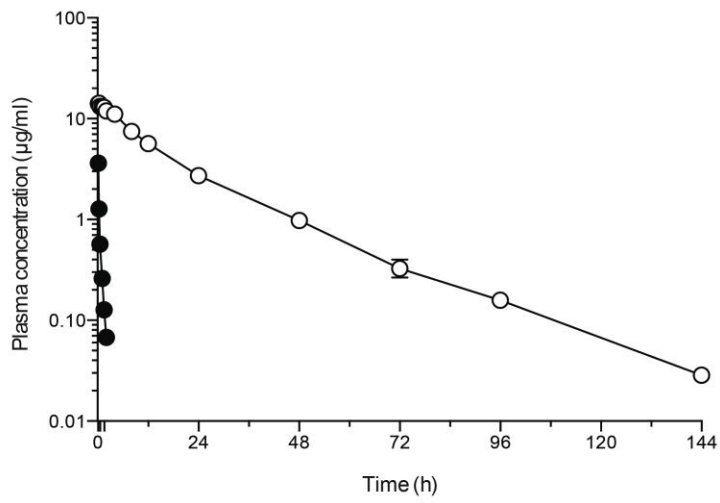
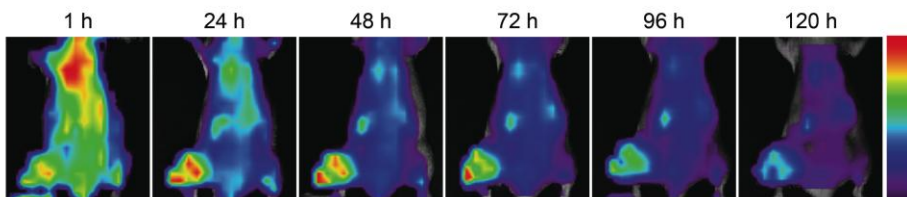
A**B**

Figure 5.5. (A) Logarithmic plasma concentration for time profiles of EMC-DEVD-S-DOX (○) and DEVD-S-DOX (●) administered to SD rats (n = 3) via intravenous route at a dose of 1 mg/kg molar equivalent to doxorubicin. The plasma concentration was calculated based on the mass concentration of doxorubicin content. Lower graph depicts enlarged plasma concentration profile showing until 2 h. (B) Ex vivo imaging of whole body distribution of EMC-DEVD-Cy5.5 in U87 MG tumor-bearing mice.

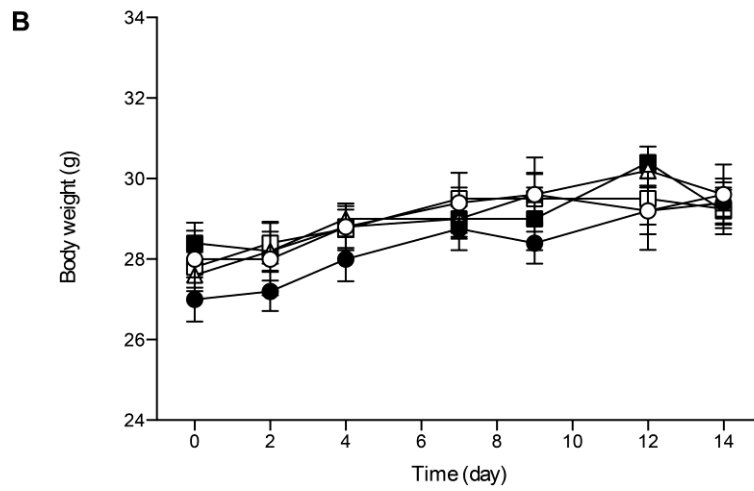
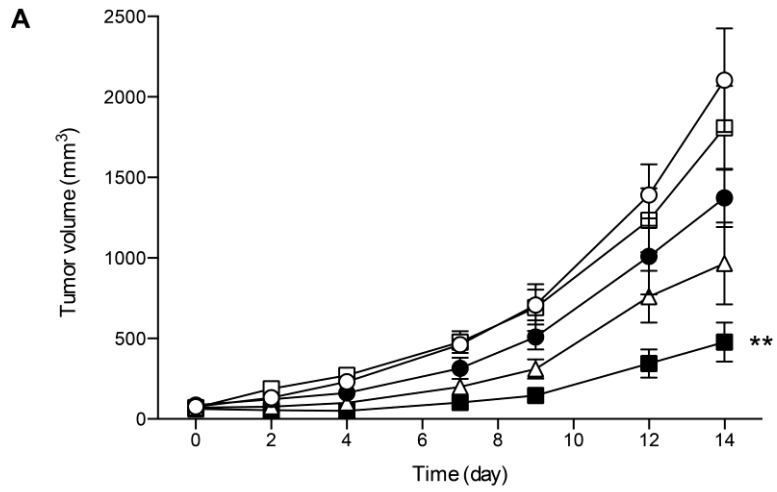


Figure 5.6. Animal study result of SCC7-tumor bearing C3H/HeN mice that received normal saline (○), radiation (●), DEVD-S-DOX accompanied by radiation (Δ), EMC-DEVD-S-DOX (□), or EMC-DEVD-S-DOX accompanied by radiation (■). EMC-DEVD-S-DOX or DEVD-S-DOX was intravenously administered daily for 7 days at 1 mg/kg molar equivalent to doxorubicin from day 0 (n = 5). Radiation was given at a dose of 4 Gy single time at day 0. Tumor growth profile (A) and body weight profile (B) are shown. Data are presented as mean ± s.e.m.

5.4. Discussion

The present study demonstrates about a prodrug comprising an *in situ* albumin-binding moiety (i.e. maleimide group), caspase-specific cleavable peptide, and doxorubicin as an active ingredient. The principle of the proposed prodrug system is as follows: (i) the prodrug instantly binds to an endogenous albumin, which acts as carrier molecule, in the blood stream after intravenous administration, (ii) the albumin-bound prodrug is delivered to the tumor that is exposed to a therapeutic radiation, (iii) caspase-3 that are upregulated in the irradiated tumor cells cleave the DEVD peptide spacer between albumin and doxorubicin, resulting in the release of free doxorubicin, (iv) the released free doxorubicin triggers apoptosis of the neighboring tumor cells, which again upregulate caspase-3, thereby repeatedly forcing the step (iii) and (iv). Hence, the activation of prodrug could be amplified in the site where apoptosis was first initiated by an exposure to radiation therapy.

The fundamental concept of the prodrug was recently proposed by our coworkers. The prodrug (DEVD-S-DOX) was prepared by conjugating a DEVD peptide to a doxorubicin via self-immolative spacer (*p*-aminobenzylcarbamate; PABC) and proved to be effective when combined with radiotherapy, so called as radiation-induced apoptosis-targeted chemotherapy (RIATC)⁴. However, hydrophilic peptides have very short plasma half-life with rapid renal excretion, which was also observed in the DEVD-S-DOX that had plasma half-life of 30 minutes in rats. Regarding that doxorubicin has a terminal half-life of 16.5 hours in SD rats¹², the significantly reduced plasma half-life is very disadvantageous in terms of therapeutic effect. Also, the previously prepared prodrug lacks tumor targeting capability that could selectively increase the local concentration of the agent within tumor

In order to overcome the aforementioned limitations, maleimide group, which acts as albumin-binding moiety, was introduced to the prodrug. Albumin has been recognized to be an excellent carrier for tumor targeting, and it was reported that maleimide group selectively reacts with the Cys34 of endogenous

albumin. EMC-DEVD-S-DOX, which was produced by simple modification of DEVD-S-DOX, was indeed capable in binding with the commercially available HSA as well as the albumins in plasma. The reaction was rapid, implying that the albumin binding of the EMC-DEVD-S-DOX would be immediate after entering the blood stream. The major concern was that the bound albumin might sterically hinder the caspase-3 recognizing the DEVD motif of EMC-DEVD-S-DOX. However, the results showed that the EMC-DEVD-S-DOX was well cleaved in the presence of caspase-3 regardless of HSA binding. As a result of the caspase-3-mediated cleavage, doxorubicin was liberated.

Our observations showed that albumin-bound form of EMC-DEVD-S-DOX (termed as HSA-DEVD-S-DOX) had almost no cytotoxic effect (or anticancer effect) *in vitro* as well as *in vivo*. The main reason of the inactivity is thought to be two-fold. One is the site of conjugation where the extra molecules are bound to the doxorubicin. The 3'-NH₂ group of the daunosamine sugar moiety plays critical role in stabilizing the DNA-doxorubicin complex when the doxorubicin is intercalated in the DNA. Therefore, this functional group is very important for the biological activity of doxorubicin¹³. As it could be seen in the chemical structure of EMC-DEVD-S-DOX, the DEVD peptide is conjugated to the 3'-NH₂ of doxorubicin via PABC spacer. Since the 3'-NH₂ is blocked by an amide bond, the conjugated doxorubicin loose its intrinsic anticancer effect. This was indeed proved in the previous study that showed loss of cytotoxic activity when KGDEVD-PABC was conjugated to 3'-NH₂ of doxorubicin. This was also supported by other study in our research group that screened the cytotoxic activity of doxorubicin with different molecule conjugated to the 3'-NH₂ (data not published). Another reason is the decreased cell penetration due to the bound albumin. There are no argument that doxorubicin should go into the cell to exert its anticancer effect. Since doxorubicin is a relatively hydrophobic and small molecule, it penetrates into the cell very easily as shown in the cellular uptake study. This is also supported by the fact that doxorubicin has a very large volume of distribution in pharmacokinetic study¹². In contrast, HSA-DEVD-S-DOX showed very low penetration into the cell. Since albumin is a

very hydrophilic macromolecule, it is obvious that the albumin interfered the penetration through the cell membrane. Consequently, EMC-DEVD-S-DOX had no observable cytotoxic effect. However, caspase-3 successfully cleaved the prodrug and allowed the recovery of the intrinsic biological activity of the doxorubicin, thereby proving its excellent property as a prodrug.

As a result of EMC-DEVD-S-DOX binding to the endogenous albumins, the plasma half-life of the agent increased 38-fold in comparison to DEVD-S-DOX (19 h versus 30 min), which is a non-albumin binding form of the prodrug. Especially for the chronic diseases, longer half-life of drugs is preferred for the ease of maintaining the plasma concentration in the therapeutic window and better patient compliance due to the less frequent dosing, leading to improved therapeutic outcomes. Apart from these typical benefits of the prolonged drug circulation time, there is an important advantage that is specific for the currently proposed prodrug system. Caspase-3, which is the principal molecular target, is expressed only temporarily unlike traditional molecular targets. However, it is difficult to estimate its time of maximum expression after stimulation (e.g. radiotherapy) and the duration of expression for every patient. Therefore, the prolonged circulation time of the prodrug is necessary to increase the possibility of encountering caspase-3 that would result in larger portion of the administered agent to be activated. The albumin-binding of EMC-DEVD-S-DOX also contributed in the selective accumulation of the prodrug in tumor. The elevated local concentration of the prodrug in the site of interest could further increase the chance of encountering the upregulated caspase-3.

5.5. Conclusion

EMC-DEVD-S-DOX is a novel anticancer drug that involves conventional approach of delivering drugs to tumor and our novel strategy of targeting the radiation-induced apoptosis. The prodrug system allows the comprised chemotherapeutic agent to act in highly selective manner in the tumor with very long plasma half-life, thereby greatly improving the therapeutic index.

Considering that the severe toxicities of the chemotherapeutic agents are one of the major limitations in the clinical oncology, this prodrug system is expected to contribute in overcoming those problems.

References

- 1 DiPaola, R. S., Rinehart, J., Nemunaitis, J., Ebbinghaus, S., Rubin, E., Capanna, T., Ciardella, M., Doyle-Lindrud, S., Goodwin, S., Fontaine, M., Adams, N., Williams, A., Schwartz, M., Winchell, G., Wickersham, K., Deutsch, P. & Yao, S. L. Characterization of a novel prostate-specific antigen-activated peptide-doxorubicin conjugate in patients with prostate cancer. *J Clin Oncol* **20**, 1874-1879 (2002).
- 2 Sapra, P., Stein, R., Pickett, J., Qu, Z., Govindan, S. V., Cardillo, T. M., Hansen, H. J., Horak, I. D., Griffiths, G. L. & Goldenberg, D. M. Anti-CD74 antibody-doxorubicin conjugate, IMMU-110, in a human multiple myeloma xenograft and in monkeys. *Clin Cancer Res* **11**, 5257-5264 (2005).
- 3 Gerlinger, M., Rowan, A. J., Horswell, S., Larkin, J., Endesfelder, D., Gronroos, E., Martinez, P., Matthews, N., Stewart, A., Tarpey, P., Varela, I., Phillimore, B., Begum, S., McDonald, N. Q., Butler, A., Jones, D., Raine, K., Latimer, C., Santos, C. R., Nohadani, M., Eklund, A. C., Spencer-Dene, B., Clark, G., Pickering, L., Stamp, G., Gore, M., Szallasi, Z., Downward, J., Futreal, P. A. & Swanton, C. Intratumor heterogeneity and branched evolution revealed by multiregion sequencing. *N Engl J Med* **366**, 883-892 (2012).
- 4 Lee, B. S., Cho, Y. W., Kim, G. C., Lee do, H., Kim, C. J., Kil, H. S., Chi, D. Y., Byun, Y., Yuk, S. H., Kim, K., Kim, I. S., Kwon, I. C. & Kim, S. Y. Induced phenotype targeted therapy: radiation-induced apoptosis-targeted chemotherapy. *J Natl Cancer Inst* **107** (2015).
- 5 Bucci, B., Misiti, S., Cannizzaro, A., Marchese, R., Raza, G. H., Miceli, R., Stigliano, A., Amendola, D., Monti, O., Biancolella, M., Amati, F., Novelli, G., Vecchione, A., Brunetti, E. & De Paula, U. Fractionated ionizing radiation exposure induces apoptosis through caspase-3 activation and reactive oxygen species generation. *Anticancer Res* **26**, 4549-4557 (2006).
- 6 Huang, Q., Li, F., Liu, X., Li, W., Shi, W., Liu, F. F., O'Sullivan, B., He, Z., Peng, Y., Tan, A. C., Zhou, L., Shen, J., Han, G., Wang, X. J., Thorburn, J., Thorburn, A., Jimeno, A., Raben, D., Bedford, J. S. & Li, C. Y. Caspase 3-mediated stimulation of tumor cell repopulation during cancer radiotherapy. *Nat Med* **17**, 860-866 (2011).

- 7 Delaney, G., Jacob, S., Featherstone, C. & Barton, M. The role of radiotherapy in cancer treatment: estimating optimal utilization from a review of evidence-based clinical guidelines. *Cancer* **104**, 1129-1137 (2005).
- 8 Kratz, F. Albumin as a drug carrier: design of prodrugs, drug conjugates and nanoparticles. *J Control Release* **132**, 171-183 (2008).
- 9 Dennis, M. S., Zhang, M., Meng, Y. G., Kadkhodayan, M., Kirchofer, D., Combs, D. & Damico, L. A. Albumin binding as a general strategy for improving the pharmacokinetics of proteins. *J Biol Chem* **277**, 35035-35043 (2002).
- 10 Kratz, F. & Beyer, U. Serum proteins as drug carriers of anticancer agents: a review. *Drug Deliv* **5**, 281-299 (1998).
- 11 Kratz, F., Muller-Driver, R., Hofmann, I., Dreves, J. & Unger, C. A novel macromolecular prodrug concept exploiting endogenous serum albumin as a drug carrier for cancer chemotherapy. *J Med Chem* **43**, 1253-1256 (2000).
- 12 Assumpção, J. U., Campos, M. L., Ferraz Nogueira Filho, M. A., Pestana, K. C., Baldan, H. M., Formariz Pilon, T. P., de Oliveira, A. G. & Peccinini, R. G. Biocompatible microemulsion modifies the pharmacokinetic profile and cardiotoxicity of doxorubicin. *J Pharm Sci* **102**, 289-296 (2013).
- 13 Jain, M., Barthwal, S. K., Barthwal, R., & Govil, G. Restrained molecular dynamics studies on complex of adriamycin with DNA hexamer sequence d-CGATCG. *Arch Biochem Biophys* **439**, 12-24 (2005).

Chapter 6

Integrin $\alpha\beta3$ targeted caspase-3-dependently activated doxorubicin prodrug

There have been numerous studies to deliver chemotherapeutic agents selectively to the tumor in attempt to increase their therapeutic index. One of the most popular approaches is to introduce an active targeting ligand that could recognize certain tumor-specific surface antigens. However, such approach has encountered a fundamental challenge due to the finding of intratumor heterogeneity, which conveyed the presence of distinct subclones of tumor cells in a single tumor mass. Paradoxically, specificity provided to the chemotherapeutic agents by conventional drug delivery approaches limit their therapeutic activity to only few subclones of tumor cells, potentially allowing tumor regrowth from the unaffected populations. In this study, a drug delivery strategy that could overcome such limitation of the conventional active targeting approach is proposed. As a model drug, RGDEV-D-DOX was prepared, which comprises integrin $\alpha\beta3$ recognizing sequence (RGD), caspase-3 cleavable sequence (DEV-D), and doxorubicin. The distinct feature of the proposed system is the presence of DEV-D sequence between the traditional targeting moiety (i.e., RGD) and the cytotoxic agent (i.e., doxorubicin). The RGD moiety selectively delivers the cytotoxic agent to the tumor and induces tumor cell apoptosis, leading to upregulation of caspase-3. The caspase-3 further activates other prodrug molecules, triggering the release of more hydrophobic form of the active compound that penetrates faster into the cell regardless of integrin $\alpha\beta3$ expression. Therefore, it could affect broader range of tumor cells in the tumor tissue, resulting in improved therapeutic outcome.

6.1. Introduction

Although newly developed drugs for clinical oncology are mostly focused in the targeted therapies, cytotoxic chemotherapeutic agents are still widely used in first-line therapy for their potent anticancer effect and availability in broad range of tumors. Their use, however, are often limited by the dose-dependent toxicities, which are sometimes even lethal¹. Therefore, many efforts have been made to deliver chemotherapeutic agents selectively to the tumor and minimize the distribution to the normal tissue. One of the most popular approaches is to introduce a molecular targeting moiety to the drugs, such as monoclonal antibodies or peptides that could selectively bind to tumor specific ligands, thereby alter the systemic pharmacokinetic properties and allow selective delivery of the agents to the tumor²⁻⁵. However, such an approach is fundamentally challenged by the intratumoral heterogeneity, which refers to the existence of genetically heterogeneous tumor cell population in a single tumor mass⁶. This finding implied that targeting a specific ligand would possibility affect only small portion of the tumor cells. Hence, there is a high possibility of tumor relapse from the unaffected subclones that do not express the target ligands. Moreover, the tumor growth is also aided by the tumor-associated stromal cells⁷, which are definitely not affected by the therapy. Therefore, effective cancer treatment demands delivery of chemotherapeutic agents to every tumor cells and the associated stromal cells, which differ in their genomic profiles. But targeting those cells that differ in their ligand expression pattern through the conventional approach is practically impossible.

In attempt to overcome the aforementioned limitations, it was hypothesized that the drug should approach to the site of interest in a selective manner, and then become non-selective, thereby allow the drug to affect every cell regardless of their genomic profile. To achieve such purpose, a peptide was prepared by which RGD and DEVD motif is combined, which is recognized by integrin $\alpha\beta3$ and caspase-3, respectively. In this peptide, RGD motif plays central role as an initial homing moiety to the tumor, since integrin $\alpha\beta3$ is

abundantly expressed on tumor endothelium as well as several types of tumor cells including late-stage glioblastoma, melanoma, ovarian, breast and prostate cancer^{8,9}. Moreover, RGD sequence could facilitate the cellular uptake of the RGD-bearing substance when bound to the integrins⁹. Many studies have, therefore, used RGD-containing peptides to deliver chemotherapeutic agents or particulate carrier systems to tumor¹⁰⁻¹².

The distinct property of the currently proposed system from the other studies that used RGD for tumor targeting comes from the insertion of the DEVD motif between the RGD moiety and the chemotherapeutic agent. The DEVD motif is the principal compartment in converting the drug from selective to non-selective drug. Caspase-3, which is activated as an executioner caspase during an apoptotic event, recognizes and enzymatically cleaves the DEVD sequence¹³. Therefore, when a sufficient number of cells that express integrin $\alpha\beta3$ are dead by the RGD-mediated delivery of chemotherapeutic agents, they could be liberated from the targeting moiety by the upregulated caspase-3 in the tumor. Generally, most of the chemotherapeutic agents lack selectivity. Therefore, the liberated drugs could diffuse into the nearby cells regardless of their integrin $\alpha\beta3$ expression and again induce cell death. After such event is initiated, the local concentration of caspase-3 is increased in the tumor by the apoptotic cells. Then the chemotherapeutic agents that are conjugated to the peptide could be continuously released in the tumor by the upregulated caspase-3 even after the cells that express integrin $\alpha\beta3$ are eliminated and kill the remaining integrin $\alpha\beta3$ -nonexpressing tumor cells, which would again increase caspase-3 (**Fig 6.1A**). Due to the cycling process, the concentration of the target molecule (i.e. caspase-3) would be sustained or even increased in the tumor as the therapy goes on, whereas the conventional targeted approach would eventually deplete the target molecule and become ineffective (**Fig. 6.1B**).

To prove the hypothesis, a model drug was synthesized. A peptide that has RGD and DEVD motif at the same time was prepared by addition of Arg-Gly sequence at the N-terminus of the DEVD, so that an Asp participating in RGD and DEVD motif. This pentapeptide is the shortest possible sequence that could

have both RGD and DEVD sequence. To the prepared peptide, doxorubicin was conjugated to produce a model prodrug for proof-of-concept in the current novel drug delivery strategy (**Fig. 6.1C**). This prodrug could be selectively delivered to the integrin $\alpha\beta3$ overexpressing cells including tumor endothelial cells and some types of tumor cells, and induce their apoptosis. Then by the upregulated caspase-3 in the tumor tissue, the further delivered prodrug could be cleaved and recover the non-selective and rapid penetrating characteristic of the doxorubicin, thus inducing further apoptosis of the tumor cell and the tumor-associated cells that does not express integrin $\alpha\beta3$.

6.2. Materials and Methods

6.2.1. Cell lines

Human umbilical vein endothelial cells (HUVEC) and human dermal microvascular endothelial cells (HDMEC) were purchased from PromoCell (Heidelberg, Germany). U87 MG and HT-29 cells were obtained from the American Type Culture Collection (ATCC; Manassas, VA). HUVECs and HDMECs were cultured in Endothelial Cell Growth Medium MV2 (ECGM; PromoCell). U87 MG and HT-29 cells were grown in high-glucose Dulbecco's modified eagle medium (Gibco, Carlsbad, CA) supplemented with 10% fetal bovine serum (Gibco). The cells were maintained in a humidified 5% CO₂ atmosphere at 37°C.

6.2.2. Synthesis

AcRGDEVDC-NH₂ and AcRDEVDC-NH₂ peptide was purchased from Pepton (Daejeon, South Korea). Daunorubicin hydrochloride was obtained from US Pharmacia (Rockville, MD). 1,4-Dioxane, anhydrous methanol, trimethyl orthoformate, propylene oxide, 48% hydrobromic acid and 1 M potassium butoxide in tetrahydrofuran were purchased from Sigma-Aldrich (St. Louis, MO). Bromine was obtained from Junsei Chemical (Tokyo, Japan). 4-Maleimidobutyric acid was from Santa Cruz Biotechnology (Dallas, TX). Cy5.5

maleimide was from Lumiprobe (Hallandale Beach, FL). All the other solvents were from Burdick & Jackson (Seoul, South Korea).

14-Doxorubicinyl maleimidobutyrate ester was synthesized according to Meyer-Losic et al. for conjugation with the prepared peptides¹⁴. Daunorubicin hydrochloride (100 mg, 177.3 μmol) was dissolved in a mixture of anhydrous methanol (3 ml) and anhydrous 1,4-dioxane (2.5 ml). Trimethyl orthoformate (89.2 μl , 815.6 μmol , 4.6 eq) was added followed by addition of bromine (15.7 μl , 306.8 μmol , 1.73 eq) at 11°C and reacted for 2 h under nitrogen. Propylene oxide (31.9 μl , 455.7 μmol , 2.57 eq) was added at 4°C and reacted for 75 min. Then mixture of acetone (8.6 ml) and 0.25 M hydrobromic acid (3 ml), and reacted for 48 h at room temperature. When the reaction was completed, the solution was diluted with distilled water (5 ml) and extracted with chloroform (10 ml \times 2). Saturated brine (5 ml) was added to the aqueous layer and the product was extracted into n-butanol until the aqueous layer was colorless. The collected n-butanol layer was concentrated at 35°C *in vacuo* and precipitated in 10 volume of n-hexane to obtain 14-halodaunorubicin as red solid. *m/z* (ESI-MS): 562.0 [M + H]⁺ for 14-chlorodaunorubicin, 605.9 [M + H]⁺ for 14-bromodaunorubicin.

Suspension of 4-maleimidobutyric acid was prepared and 0.1 M sodium bicarbonate was slowly added during stirring. The resulting solution was stirred for 20 min and concentrated at 30°C *in vacuo*. The concentrated solution was lyophilized to obtain sodium 4-maleimidobutyrate. The sodium 4-maleimidobutyrate (263 mg, 1.28 mmol) and 14-halodaunorubicin (138 mg, 237.2 μmol) were dissolved in acetone and refluxed under nitrogen for 4 h. The solution was cooled and filtered. The remaining solid was washed with acetone and the filtrate was evaporated under vacuum. The red residue was dissolved in water with 0.1% trifluoroacetic acid (TFA) and subjected to semi-preparative reverse-phase HPLC (Shimadzu, Kyoto, Japan) using ODS-A 5 μm semi-preparative column (150 mm \times 20 mm; YMC, Dinslaken, Germany) for further purification to obtain highly purified 14-doxorubicinyl maleimidobutyrate ester. A gradient system (Water and acetonitrile with 0.05% TFA as an additive) was

used with a flow rate of 8 mL/min. Each step of the reaction was monitored using normal phase TLC (CH₂Cl₂ : MeOH, 8 : 2). *m/z* (ESI-MS): 709.0 [M + H]⁺.

The 14-doxorubicinyl maleimidobutyrate ester and AcRGDEVDC-NH₂ was dissolved in anhydrous DMF and reacted overnight at 4°C. The solution was precipitated in diisopropyl ether and the precipitate was collected by filtration. The precipitate was washed three times with diisopropyl ether and dried *in vacuo*. The red solid was redissolved in water and subjected to a semi-preparative reverse-phase HPLC as mentioned above for further purification. Collected fractions were concentrated in reduced pressure and lyophilized to obtain final product RGDEVDC-DOX as red powder. The purity was confirmed by analytical HPLC with UV detection at 214 nm and was determined to be ≥ 95%. *m/z* (ESI-MS): 1542.0 [M + H]⁺.

AcRGDEVDC-NH₂ and AcRDEVDC-NH₂ peptides were fluorescently labeled using Cy5.5-maleimide with simple chemistry. The peptide (1 eq) and Cy5.5 maleimide (1.3 eq) was dissolved in DMF and reacted in dark at 4°C for 16 h. Then, 10 volume of dichloromethane was added to the solution and formed precipitate was recovered by filtration or centrifugation. The precipitate was dried *in vacuo* to obtain dark blue crude product. The solid was redissolved in small volume of DMF and subjected to a semi-preparative reverse-phase HPLC in purpose to remove any impurities, especially the unreacted Cy5.5 maleimide. The purity of the obtained AcRGDEVDC-Cy5.5 and AcRDEVDC-Cy5.5 was confirmed by analytical HPLC with UV detection at 214 nm and was determined to be ≥ 95%. In particular, no peak corresponding to Cy5.5-maleimide was detected, indicating the complete removal of unreacted Cy5.5-maleimide.

6.2.2. Integrin αvβ3 dependent cellular uptake imaging

HUVECs, HDMECs, and U87 MG cells were seeded on a cover-glass bottom dishes (SPL Life science, Pocheon, South Korea) at 3 × 10⁵ cells per dish and maintained for 48 h. When cells were at 80% confluence, AcRGDEVDC-Cy5.5

or AcRDEVDC-Cy5.5 were treated to the cells at final concentration of 1 μM and incubated for 5 min at 37°C. Then the cells were washed with cold PBS three times and fixed with 4% paraformaldehyde (Sigma-Aldrich, St. Louis, MO). The cell nucleus was stained with DAPI (Molecular Probes, Eugene, OR) and mounted with Slowfade gold anti-fade reagent (Molecular Probes). The cells were observed under a confocal laser-scanning microscope (LSM 710; Carl Zeiss, Oberkochen, Germany). Similar experiment using only AcRGDEVDC-Dy5.5 was carried out on HDMECs and U87 MG cells transfected with ITGAV siRNA (10 nM). The procedure was identical with above. The detailed description of siRNA transfection is shown below.

Another set of experiment was done using doxorubicin conjugated peptides. U87 MG cells were seeded on a cover-glass bottom dishes at 3×10^5 cells per dish and maintained for 48 h. When cells were at 80% confluence, RGDEVDDOX or RDEVDDOX were treated to the cells at final concentration of 10 μM and incubated for 30 min at 37°C. Then the cells were processed as described above and observed under a confocal laser-scanning microscope (LSM 710; Carl Zeiss, Oberkochen, Germany).

6.2.3. siRNA transfection.

Transient gene knockdown of HDMEC and U87 MG cells was carried out using Trilencer-27 siRNA duplexes against ITGAV (Cat. No. SR302468, ITGAV Trilencer-27 human siRNA; OriGene, Rockville, MD) or a scrambled control siRNA (OriGene). When the cells were at 80% confluency in 30 mm culture dish, the siRNA duplexes or the scrambled control siRNA were diluted at a concentration of 5 μM in siRNA dilution buffer (OriGene). Prepared siRNA solution (5 μl) was transferred to Opti-MEM (140 μl). Another set of solution containing transfection agent was prepared by addition of siTran1.0 (20 μl ; OriGene) to Opti-MEM (120 μl). The prepared solutions were combined and incubated 15 min at room temperature. The siRNA/siTrans complex solution was added to cells in complete medium (final volume 2.5 ml) to gain final concentration of 10 nM siRNA. The ratio between siRNA and siTran1.0 was

maintained in other concentrations of siRNA transfection. After 72 h incubation, the cells were applied for further experiments. The RNAi efficiency was confirmed through standard western blot using anti-integrin α v antibody (1:1000; Cell Signaling Technology, Danvers, MA).

6.2.4. Flow cytometry

U87 MG cells were cultured in 60 mm culture dishes. The cells were transfected with ITGAV or scrambled siRNA to produce integrin α v knock down or mock cells, respectively. The detailed siRNA transfection procedure is demonstrated above. When the transfection was completed, RGDEVDC-Cy5.5 was treated at a final concentration of 1 μ M for 5 min and washed twice with cold PBS. The cells were then detached with Trypsin/EDTA and collected by centrifuge at $400 \times g$ for 5 min. The cells were then fixed in 2% paraformaldehyde for 10 min at room temperature. After fixation, the cells were washed twice with and resuspended in 100 μ l of PBS containing 0.5% BSA. Then, Alexa 488-conjugated integrin α v β 3 antibody was added (1:100; R&D Systems, Minneapolis, MN) and incubated for 1 h at 4°C. The antibody-labeled cells were washed twice, resuspended in PBS containing 0.5% BSA, and subjected to flow cytometry (BD FACSCalibur, BD Biosciences, San Jose, CA) according to standard procedure.

6.2.5. HPLC determination of caspase-mediated activation

This experiment was carried out in purpose to determine the cleavage of RGDEVDC-DOX in presence of caspase-3. The RGDEVDC-DOX (100 μ M) was incubated with recombinant human caspase-3 (500 ng/mL; R&D Systems, Minneapolis, MN) in the caspase assay buffer (50 mM HEPES, pH 7.4, 100 mM NaCl, 0.1% CHAPS, 10 mM DTT, 1 mM EDTA, 10% glycerol; Enzo Life Sciences, Farmingdale, NY) at room temperature. Small portion of the solution was withdrawn at 15, 30, 60 min time point and quenched by addition of equal volume of DMSO to prevent the further reaction of the withdrawn samples. The samples were subjected to an analytical HPLC (Agilent 1300 series, Agilent

Technologies, Santa Clara, CA) using ODS-A 5 μm analytical column (150 mm \times 3 mm; YMC, Dinslaken, Germany). A gradient system (Water and ACN with 0.1% TFA as an additive, ACN 20-30%/5-25 min) was applied at a flow rate of 0.8 mL/min. The peaks were monitored under fluorescence detector at 470/580 nm. The ratio of the remaining RGDEVD-DOX and the released compound was determined in the basis of peak area. Additionally, the RGDEVD-DOX without caspase-3, and with caspase-3 (500 ng/ml) pretreated with caspase-3 inhibitor (Ac-DEVD-CHO, 10 μM ; Enzo Life Sciences), were incubated for 60 min at room temperature in the caspase assay buffer, and subjected to analytical HPLC using the identical experimental condition described above.

6.2.6. MTT cytotoxicity assay

The cytotoxicity of the prepared doxorubicin conjugates against cancer cells was examined on U87 MG and HT-29 cells. The cells were seeded in 96-well cell culture cluster plate (Corning, Tewksbury, MA) at 5×10^4 cells per well and incubated for 24 h in high-glucose Dulbecco's modified eagle medium with 10% FBS (Gibco). The medium was replaced with 100 μl of fresh medium containing the test compounds at final concentration of 0.1, 1, 10, and 100 μM and incubated for 1 h. The medium was then replaced with fresh medium and further incubated for 72 h at 37°C. Then 10 μl of MTT reagent (Trevigen, Gaithersburg, MD) was added to each well and incubated for 2 h at 37°C. When blue precipitate was clearly visualized inside the cells, 100 μl of detergent agent (Trevigen, Gaithersburg, MD) was added and further incubated for 4 h at room temperature. The absorbance was measured using microplate reader (Synergy HT, BioTek Instruments, Winooski, VT) at 570 nm. $n = 8$.

6.2.7. Western blots

U87 MG cells were treated with 0.1, 1, and 10 μM of the substance and incubated for 48 h. The cells were washed with cold PBS and lysed with RIPA buffer (Pierce, Rockford, IL) containing protease inhibitor cocktail (Pierce). The preparation of the samples and western blot were performed according to

the standard protocol. For immunoblotting, anti-Caspase-3 antibody (1:1000) and anti-cleaved Caspase-3 antibody (1:1000) from Cell Signaling Technology (Danvers, MA) were used as primary antibodies. HRP-conjugated anti-rabbit IgG (1:2000; R&D Systems) was used as secondary antibody. The blotted membranes were developed under ImageQuant LAS 4000 imaging system (GE Healthcare Life Sciences, Uppsala, Sweden).

6.2.8. Caspase-3 cellular activity assay

To determine the caspase-3 activity in the cells, the Calbiochem caspase-3 cellular activity assay kit (EMD Millipore, Darmstadt, Germany) was used following to the manufacturer's instruction. Briefly, U87 MG cells were treated with 0.1, 1, and 10 μM of RGDEVD-DOX with or without pretreatment of recombinant human caspase-3, and incubated for 48 h. The cells were washed once with cold PBS and lysed with CHAPS cell lysis buffer (50 mM HEPES, 5 mM DTT, 0.1 mM EDTA, 0.1% CHAPS, pH 7.4) without any addition of protease inhibitors, which may potentially inhibit the activity of caspase-3. The lysates were centrifuged in 14,000 rpm at 4°C for 15 min, and the supernatant was collected. The protein concentration was determined by BCA protein assay (Pierce) and all samples were diluted to equal concentration. The diluted cell lysate (10 μl), caspase substrate (10 μl , final concentration 200 μM ; Ac-DEVD-pNA), and assay buffer (80 μl ; 100 mM NaCl, 50 mM HEPES, 10 mM DTT, 1 mM EDTA, 10% glycerol 0.1% CHAPS, pH 7.4) were combined in half-area 96-well microplate in triplicate. Purified caspase-3 at final concentration 30 IU was used as control. The absorbance at 405 nm was measured at 10 min interval in microplate reader (Synergy HT, BioTek Instruments, Winooski, VT) for 60 min, and the slope ($\Delta\text{Abs}/\text{min}$) was calculated and averaged. The slope of the samples were divided by the slope of the purified caspase-3 and multiplied by 30 to calculate the specific activity (IU) of the samples. The values were further normalized by the amount of protein.

6.2.9. Cellular caspase-3 stain

U87 MG cells were seeded in 8-well cover glass chamber (Nalge Nunc, Rochester NY) at seeding density of 1×10^5 cells per well and grown until 80% confluence. RGDEVD-DOX or that preincubated with 500 ng/ml of recombinant human caspase-3 was treated to the cells at a final concentration of 1 μ M and incubated for 48 h. The activated caspase-3 within the cells was stained using Image-iT™ LIVE Green Caspase-3 Detection Kit (Molecular Probes, Eugene, OR) according to the manufacturer's instruction. The kit is based on a fluorescent inhibitor of caspases (FLICA) methodology, essentially an affinity label. Briefly, FAM-DEVD-FMK reagent was added to the cells and incubated for 60 min. Then, the cells were further stained with Hoechst 33342 (included in the kit). The cells were washed twice with the provided wash buffer and fixed with 4% paraformaldehyde. The fixed cells were then observed under a confocal laser-scanning microscope (LSM 710; Carl Zeiss, Oberkochen, Germany).

6.2.10. Animal study

U87 MG cells were suspended at 1×10^8 cell/ml in HBSS, and inoculated subcutaneously (100 μ l) into the thigh of 6 week-old male C3H/HeN mice. When the tumor volume reached 50-100 mm³, the mice were randomized and received saline (control), doxorubicin HCl (3 mg/kg), RDEVD-DOX (3 mg/kg doxorubicin equivalent), and RGDEVD-DOX (1, 3, 5 mg/kg doxorubicin equivalent) intravenously through tail vein for seven days daily. The mice were maintained for additional seven days after the last drug administration and sacrificed. The tumor length and width were measured by caliper and the volume was calculated using the modified ellipsoid formula ($L \times W^2/2$). Implanted tumors were isolated and weighed when sacrificed. All experimental procedures were approved by the Institutional Animal Care and Use Committee of the Seoul National University.

6.2.11. Statistical analysis

Data are presented as means \pm s.e.m. To test the differences between groups, the Mann-Whitney *U* test, which is a non-parametric statistics, was used. One-tailed test was performed. The GraphPad Prism version 6.0 (GraphPad Software, San Diego, CA) software was used for the statistical calculations. *P* values less than 0.05 were considered significant when compared to control and indicated with asterisks on the graphs.

6.3. Results

6.3.1. Synthesis of RGDEVD-DOX

Scheme 6.1 depicts the synthesis of RGDEVD-DOX. In order to retain the activity of doxorubicin when conjugated with the peptide, a location other than 3'-NH₂ was preferred as the conjugation site. In particular, the peptide was conjugated to the 14-OH of doxorubicin. For this, 14-doxorubicinyl maleimidobutyrate ester was first prepared according to Meyer-Losic et al., by using daunorubicin as a starting material¹⁴. This doxorubicin derivative allows conjugation of peptides that has sulfhydryl group in very mild condition via its maleimide group. Since RGDEVD peptide does not contain any sulfhydryl group, Cys was added to the C-terminus. The reaction was carried out in DMF by simply mixing the 14-doxorubicinyl maleimidobutyrate ester and AcRGDEVDC-NH₂. The final product was purified by semi-preparative HPLC. The purity was confirmed to be more than 95% using analytical HPLC (**Fig. 6.2A**). The mass was determined using ESI-MS (**Fig. 6.2B**).

6.3.2. Integrin $\alpha\beta3$ dependent cellular uptake of RGDEVD peptide

The facilitated cellular uptake of the RGDEVD peptide mediated by the RGD motif was determined in three different cell lines, U87 MG, HDMECs, and HUVECs, which overexpress integrin $\alpha\beta3$. RDEVDC peptide, which has defective RGD motif, was used as a control. The peptides that were labeled

with a fluorescent dye were used in the experimental studies. The labeled peptides – RGDEVD and RDEVD – were treated to the each cell line at 1 μ M for 5 minutes, which is a relatively short incubation time to avoid non-selective diffusion into the cells. When the cells were observed under confocal microscopy, RGDEVD peptide showed significantly higher accumulation than RDEVD peptide (**Fig. 6.3A**). Considering that the both peptides has almost identical structure except in the presence of one Gly residue, this result suggested that RGD motif within the RGDEVD peptide was involved in the facilitated cellular uptake in the integrin $\alpha\beta 3$ overexpressing cell lines.

This result was further supported with experiments on integrin αv siRNA transfected U87 MG and HDMECs (**Fig. 6.3B**) When RGDEVD peptide was treated to the cells, significant difference in the amount of that taken up between mock and siRNA transfected cells was found. The cells observed under confocal microscopy showed that integrin αv knocked down cells had drastically decreased uptake of the peptide than that in the mock cells. This was shown in both U87 MG cells and HDMECs (**Fig 6.3C**).

For U87 MG cells, their difference of the RGDEVD peptide uptake between siRNA transfected and mock cells were also determined by flow cytometry (**Fig. 6.3D**). After the treatment of RGDEVD peptide on the cells, both cells were also immunostained with fluorescent-labeled integrin $\alpha\beta 3$ antibody to confirm the integrin downregulation by siRNA transfection. The histogram plot showed a left shift of the integrin $\alpha\beta 3$ staining in the transfected cells, indicating a successful knock down of integrin αv in the U87 MG cells. Similar pattern of histogram was shown with the detector corresponding to the signal from RGDEVD peptide. The siRNA transfected U87 MG cells, which showed left shift of integrin $\alpha\beta 3$, also showed left shift of RGDEVD peptide uptake. This result manifested the correlation between the expression of integrin $\alpha\beta 3$ and uptake of RGDEVD peptide in the cells.

Same result was also shown in RGDEVD-DOX. When U87 MG cell was treated with RGDEVD-DOX or RDEVD-DOX, a facilitate drug uptake was

shown in RGDEVD-DOX, which has the RGD motif that interacts with integrin $\alpha\text{v}\beta\text{3}$ (**Fig. 6.3E**).

6.3.2. Caspase-3-mediated cleavage of RGDEVD-DOX

Cleavage of RGDEVD-DOX by caspase-3 was determined by HPLC analysis after incubation of RGDEVD-DOX (100 μM) with recombinant human caspase-3 (500 ng/ml) (**Fig. 6.4A**). When RGDEVD-DOX was subjected to HPLC analysis, the retention time of the peak showed 22.1 min. However, the incubation of the RGDEVD-DOX with the caspase-3 prior to the HPLC analysis shifted the retention time of the peak to 20.2 minute. The peak located at 22.1 min gradually decreased and that located at 20.2 minute gradually increased by time, showing more than 80% of the RGDEVD-DOX was cleaved within 30 minutes in the presence of the caspase-3. The peak of RGDEVD-DOX was undetectable when measure at 60 min time point, indicating the amount of uncleaved RGDEVD-DOX was decreased below the level of detection limit within 60 minutes. The mass spectrometry showed m/z value of 829.1 in the newly appeared peak, and the determined molecular weight was identical to the molecular weight of the anticipated cleaved product from RGDEVD-DOX. Also, m/z 732.2 was found, which corresponds to the mass of the peptide moiety after cleavage.

6.3.3. *In vitro* efficacy of RGDEVD-DOX

Therapeutic efficacy difference between RGDEVD-DOX and the active compound – RGDEVD-DOX pre-incubated with caspase-3 – was determined. The major difference between the two compounds was their influx rate into the cell regardless of the integrin $\alpha\text{v}\beta\text{3}$ expression. Initially, the U87 MG and HT-29 cells were incubated with doxorubicin, RGDEVD-DOX, or the active compound for 0.5, 1, 2, or 4 hours and observed under confocal microscopy. The acquired images were subjected to fluorescence intensity analysis to compare the cellular uptake as well as the influx rate into the cells (**Fig. 6.4B**). Not surprisingly, doxorubicin showed the most rapid accumulation in the cell

nuclei, whereas RGDEVD-DOX was significantly slower. However, the activation of RGDEVD-DOX by caspase-3 recovered its influx rate to that similar to doxorubicin. In the present observation, the cell influx rate of the active compound was slightly slower than doxorubicin, but the difference was insignificant. The representative images of compound accumulated into the two cell lines are shown in **Fig. 6.4C**.

The influx rate difference among the compounds was directly correlated with the cytotoxicity of the compounds. When U87 MG cells were exposed to doxorubicin, RGDEVD-DOX, and the active compound for two hours and further incubated for 72 hours, IC_{50} values were shown 0.104, 3.16, and 0.135 μM , respectively (**Fig. 6.5A**). The IC_{50} value of RGDEVD-DOX was significantly higher than doxorubicin, which was an agreement with the observation in cellular uptake. However, when the prodrug was cleaved by caspase-3, IC_{50} value was recovered to the level similar to that of doxorubicin.

Additionally, alteration of IC_{50} values according to the varying drug exposure time was determined (**Fig. 6.5B**). The doxorubicin, RGDEVD-DOX, or active compound was exposed to the U87 MG cells for 1, 2, or 4 hours with various concentration and the IC_{50} values were calculated. As it was reflecting the result shown in the cellular uptake study, longer exposure time resulted in decreased IC_{50} value. However, in the case of RGDEVD-DOX, it needed more than 3 hours of exposure to the cells to obtain similar IC_{50} value to an hour exposure of doxorubicin or active compound.

6.3.4. Caspase-3 upregulation induced by RGDEVD-DOX

For the concept of RGDEVD-DOX to be valid, the RGDEVD-DOX as well as the cleaved product of the prodrug should upregulate the active caspase-3 in the cells. To determine the upregulation of the active caspase-3 induced by the agents, three independent *in vitro* experiments were carried out: western blot, caspase activity assay, and cellular caspase staining. All these experiments were performed with U87 MG cells that were exposed for 48 hours to RGDEVD-DOX or to that pre-incubated with recombinant human caspase-3.

Western blot showed dose-dependently decreased procaspase-3 and increased cleaved (or active) caspase-3 for both compound treatments (**Fig. 6.6A**). Procaspase-3 is a zymogen of caspase-3, which is activated when cleaved into 17 and 19 kDa subunits. Hence, this result clearly shows activation of caspase-3 by both RGDEVD-DOX and cleaved RGDEVD-DOX. However, the amount the activate caspase-3 was shown more when treated with the cleaved RGDEVD-DOX.

Caspase-3 activation was further confirmed by cellular activity assay (**Fig. 6.6B**). This assay measures quantitative activity of the cellular caspase-3 rather than the amount of the protein itself, which is more important since the current prodrug strategy attempts to utilize the proteolytic feature of the caspase-3. The principle of the assay is based on the caspase-3-mediated cleavage of fluorometric substrate Ac-DEVD-AMC (7-amino-4-methylcoumarin), which in turn generates highly fluorescent AMC. Since the assay substrate comprises DEVD motif, which is also the peptide sequence adopted in current prodrug, the assay result could not only show the total activity of caspase-3 within cells, but also could indirectly reflect the potential of these apoptotic cells to further cleave the prodrug.

In a healthy U87 MG, which was not exposed to any cytotoxic agents, showed negligible caspase-3 activity in their cell lysate, whereas the cells treated with the RGDEVD-DOX or the cleaved RGDEVD-DOX had dose-dependent upregulation of caspase-3 activity. When RGDEVD-DOX and cleaved RGDEVD-DOX were treated to the cells at a concentration of 10 μ M, more than 99- and 128-fold increased caspase-3 activity was observed respectively when compared to the normal state cells. Also, similar to the western blot result, treatment of cleaved RGDEVD-DOX showed about 1.3-fold increased caspase-3 activity than when intact RGDEVD-DOX was treated.

Following study determined the cellular distribution of caspase-3 when the U87 MG cells were stimulated with the prodrug and the active compound (**Fig. 6.6C**). The caspase-3 staining method adopted in this study employs DEVD-FMK (fluoromethyl ketone), which is a fluorescent inhibitor of caspase-3.

DEVD peptide moiety of the compound is recognized by caspase-3 in specific manner followed by FMK irreversibly binding with a Cys residue within the protein. The FMK also acts as a fluorescent reporter for visualization. Thus this staining method could show the location within cell where the recognition of DEVD motif by caspase-3 actually occurs. As mentioned earlier, since the DEVD sequence is also an essential component of the currently suggested prodrug system, this method of caspase-3 staining could suggest where the caspase-3 mediated cleavage of the prodrug takes place in the cells. The cells treated with RGDEVD-DOX and the active compound showed high level of caspase-3 expression (green fluorescence) with highly accumulated doxorubicin moiety (red fluorescence) in the cell nuclei (nuclei were not properly stained with DAPI due to the competitive binding with the DNA-bound doxorubicin), whereas the untreated cells had almost no detectable staining of active caspase-3 within the cells (nuclei well stained with DAPI). The presence of the DEVD recognizing caspase-3 was observed throughout the cells regardless of any cell compartment.

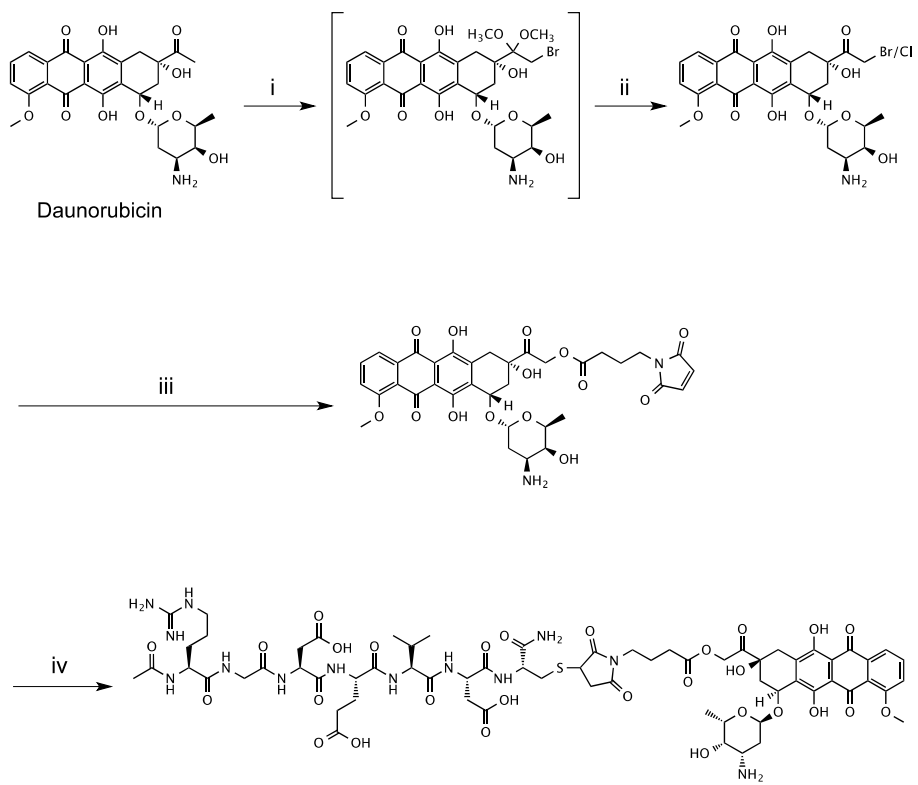
6.3.5. Tumor growth suppression of RGDEVD-DOX

Tumor growth suppression efficacy of RGDEVD-DOX was assessed in U87 MG tumor-bearing preclinical model (**Fig. 6.7**). The therapeutic efficacy of saline (control), doxorubicin, RDEVD-DOX, and RGDEVD-DOX were compared. When doxorubicin, RDEVD-DOX, and RGDEVD-DOX were administered to mice in identical dose (7×3 mg/kg molar equivalent to doxorubicin) the tumor growth rates of doxorubicin and RGDEVD-DOX received mice were similar, showing no noticeable increase in the tumor volumes during the course of study (8% decrease and 9% increase in final tumor volume compared to the initial volume, respectively), whereas the RDEVD-DOX received mice showed significantly increased tumor volume (4-fold increase) although smaller than the saline received control (5-fold increase). The average weight of the isolated tumors from doxorubicin, RDEVD-DOX, and RGDEVD-DOX treated groups at the last day of the study were reduced by

47.2, 83.2, and 85.0% compared to the control, respectively. Despite the similar therapeutic effect of doxorubicin and RGDEVD-DOX when administered in same dose, significant body weight loss was observed only in the doxorubicin received animals showing more than 30% decrease in their body weight. Moreover, three out of five examined mice were dead during the study in the doxorubicin treated group, but not in the other tested groups, indicating severe toxic effect of doxorubicin.

The systemic toxicity shown by the treatment of doxorubicin was even more severe than when RGDEVD-DOX was administered in higher dose (7×5 mg/kg molar equivalent to doxorubicin) despite the superior therapeutic efficacy of RGDEVD-DOX: 8% versus 70% reduction from the initial tumor volume in doxorubicin (7×3 mg/kg) and RGDEVD-DOX (7×5 mg/kg) received animal, respectively. As mentioned above, doxorubicin received animals showed more than 30% decreased average body weight in the last day of examination with 60% of the mice being dead. However, RGDEVD-DOX received animal showed maximum of 17% reduced body weight at day 12 and 14% reduced body weight at the end of examination. Also, in contrast to doxorubicin treated group, no mice were dead.

The therapeutic supremacy of RGDEVD-DOX over RDEVD-DOX in the same dose was already well described above. However, current study also showed RGDEVD-DOX had superior therapeutic effect even in a lower dose. While RDEVD-DOX (7×3 mg/kg) treated mice showed more than three-fold increase in their tumor volume during the course of the study, the mice received RGDEVD-DOX in 3 times lower dose (7×1 mg/kg) showed only 1.6-fold increase in that. The average weight of the isolated tumor from the RGDEVD-DOX treated animals were less than half of that from the RDEVD-DOX treated animals. Regarding that the physicochemical properties of these two compounds are nearly identical, the higher anticancer effect of RGDEVD-DOX clearly indicated the *in vivo* tumor targeting effect of RGD motif within the peptide.



Scheme 6.1. Chemical synthesis of RGDEVDC-DOX^a

^aReagents and conditions: (i) Trimethyl orthoformate, MeOH, 1,4-dioxane, Br₂, rt, and then propylene oxide, 2°C. (ii) 0.25 M HBr, acetone. (iii) sodium 4-maleimidobutyrate, acetone, refluxed. (iv) AcRGDEVDC-NH₂, DMF, rt.

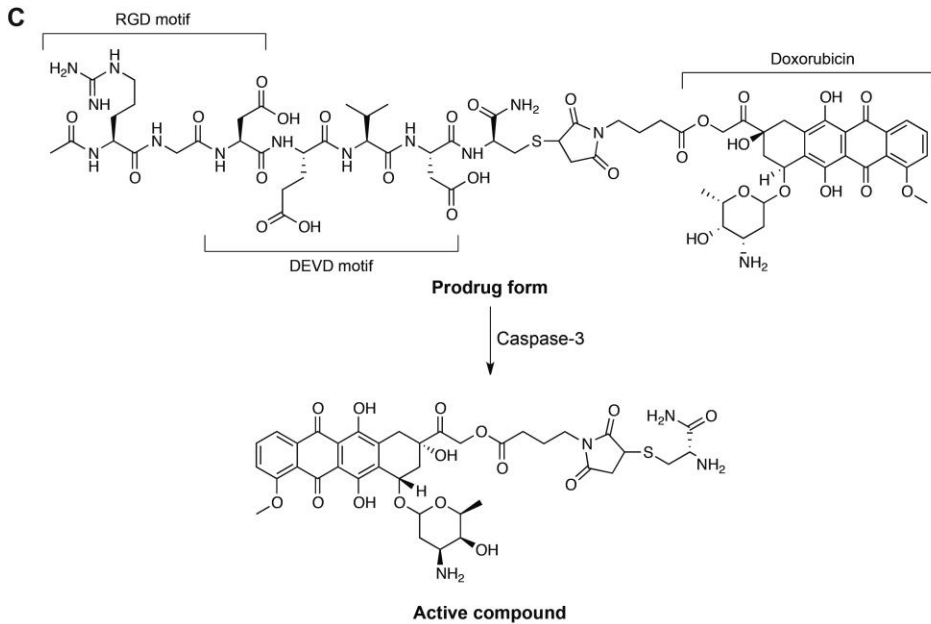
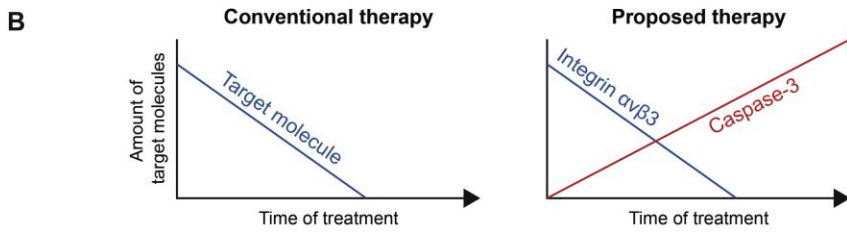
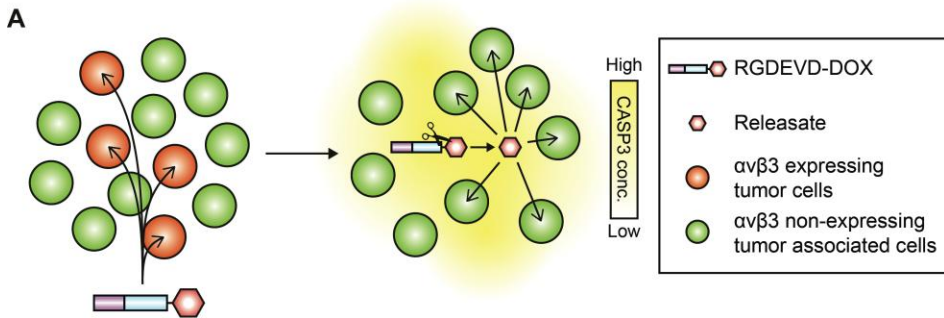


Figure 6.1. (A) Schematic diagram of the suggested prodrug strategy. (B) The major difference of the conventional targeted delivery system and the currently proposed targeted delivery system. (C) Chemical structure and compartment of the RGDEVD-DOX prodrug and its active compound.

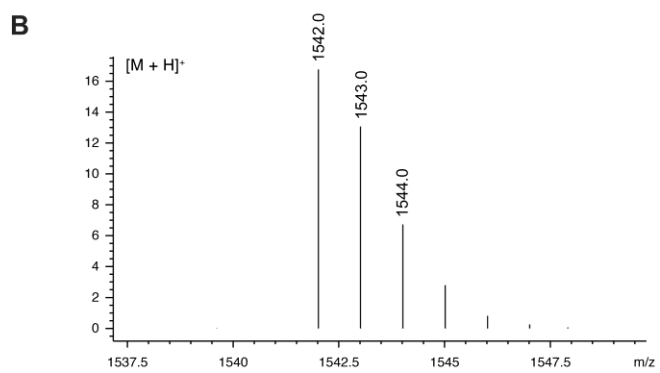
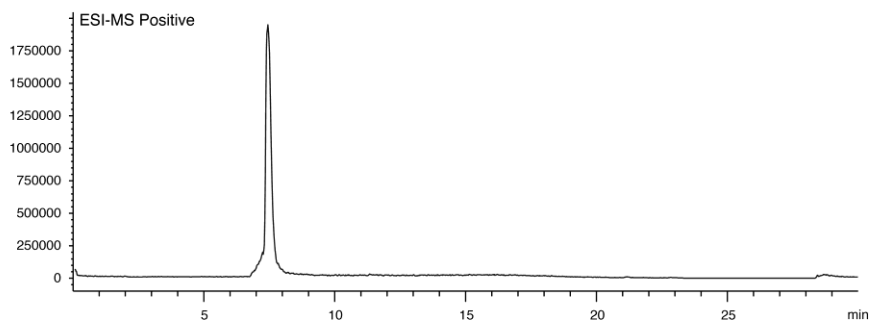
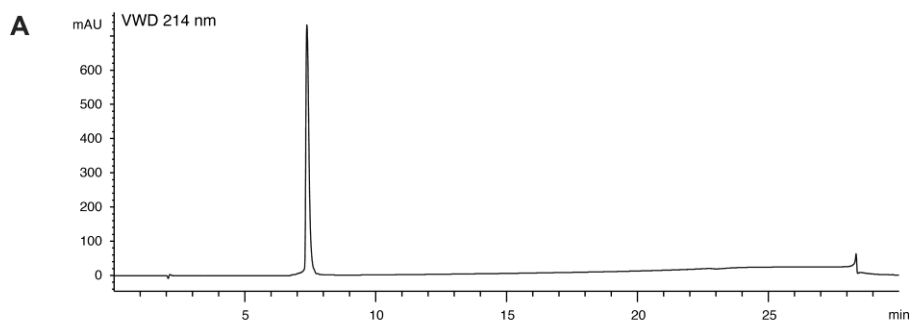


Figure 5.2. (A) Analytical HPLC chromatogram of the final product detected under UV detector (214 nm) and ESI-MS. (B) Mass spectrum of the final product determined by LC/ESI-MS.

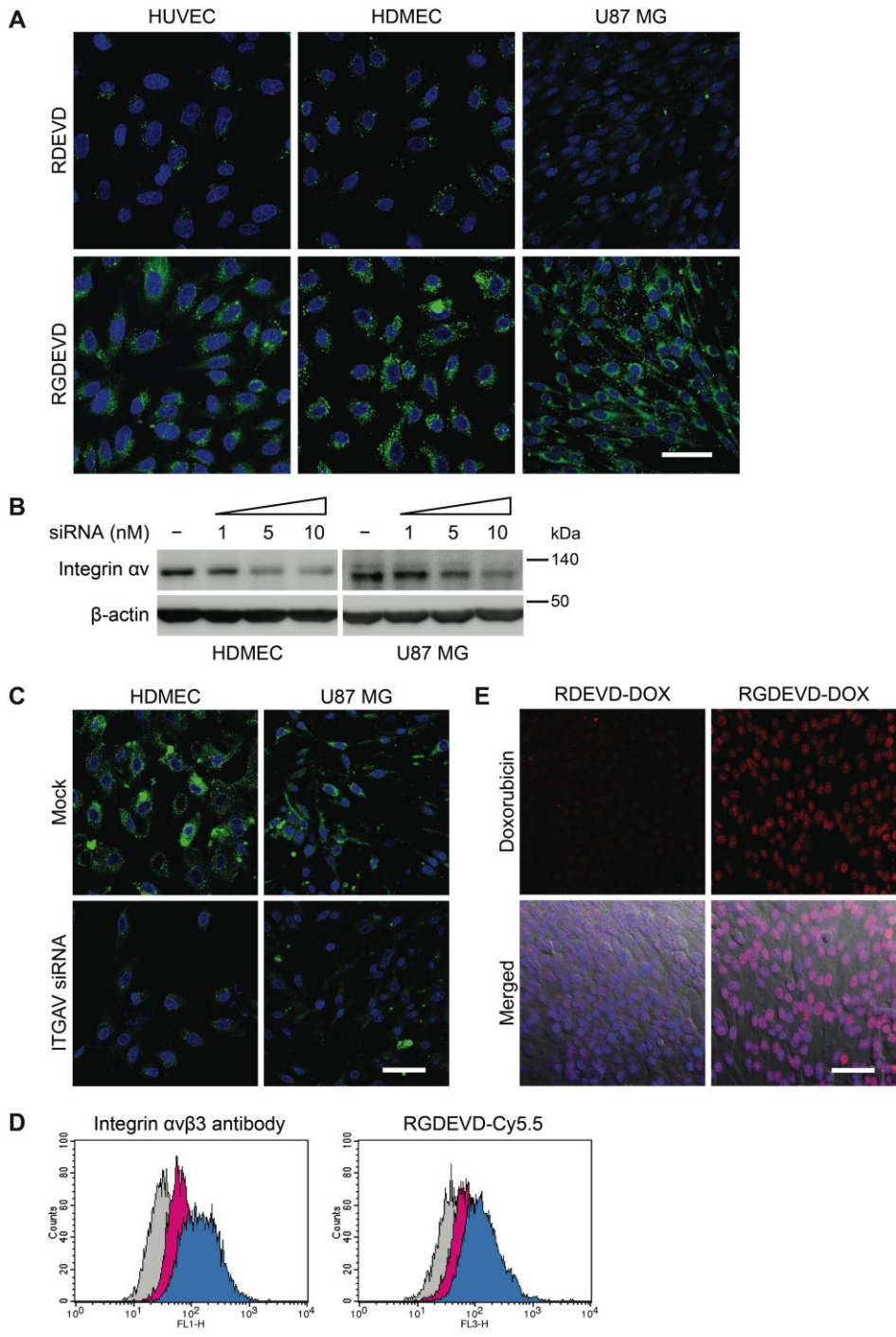


Figure 6.3. (A) Confocal microscopy images of HUVECs (left), HDMEC (center), and U87 MG cells (right) exposed to RDEVVD (upper panel) or RGDEVVD peptide (lower panel) labeled with Cy5.5. Green fluorescence represents the peptides. Cell nuclei are stained with DAPI (blue). Scale bar, 50 μ m. (B) Western blots of integrin α v after ITGAV siRNA transfection of HDMECs and U87 MG cells. (C) Confocal microscopy images of Cy5.5-labeled RGDEVVD peptide given to HDMECs (left) and U87 MG cells (right) that were mock-transfected (upper) or ITGAV siRNA transfected (lower). Green fluorescence represents the peptides. Cell nuclei are stained with DAPI (blue). Scale bar, 50 μ m. (D) Histograms of flow cytometry analysis. Mock-transfected (blue) and ITGAV siRNA transfected (pink) U87 MG cells were analyzed after RGDEVVD peptide treatment and integrin α v β 3 immunostaining. The cells were detected against Alexa488-labeled integrin α v β 3 antibody (left) and Cy5.5-labeled RGDEVVD peptide (right). Non-stained non-treated U87 MG cells were also analyzed (grey). (E) Confocal microscopy images of U87 MG cells exposed to RDEVVD-DOX (left) or RGDEVVD-DOX (right). The red fluorescence represents the doxorubicin moiety. The cells are also stained with DAPI (blue). All the acquired channels (red, blue, and DIC) were merged and shown in the lower panel. Scale bar, 50 μ m.

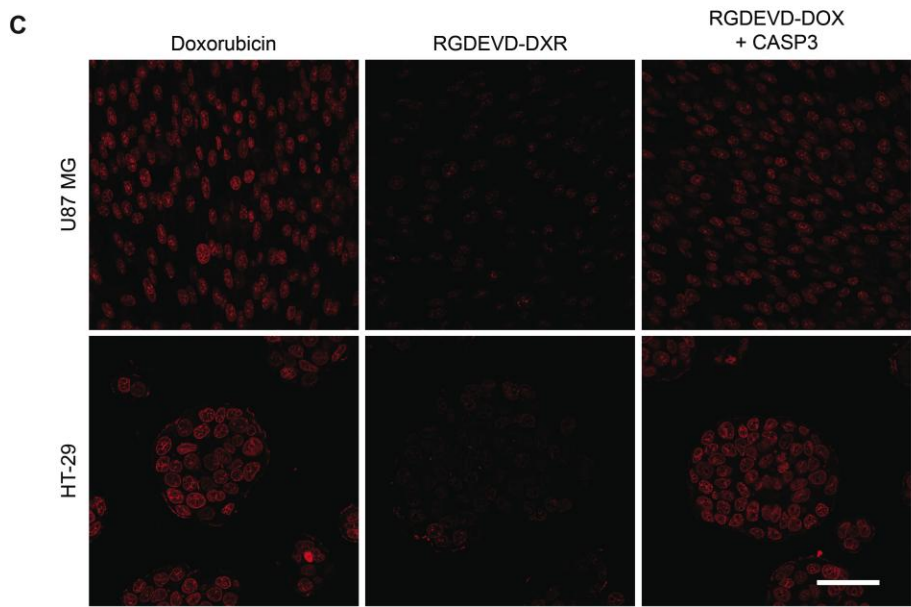
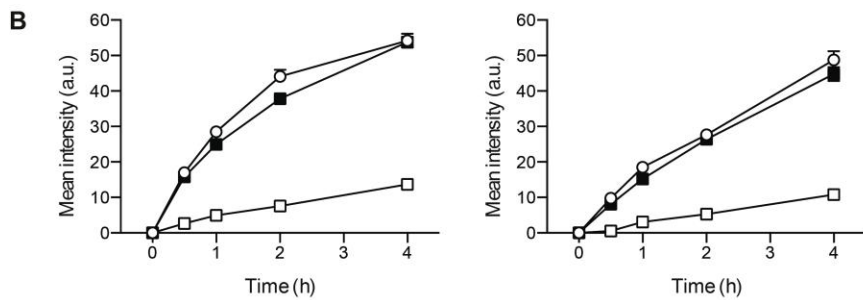
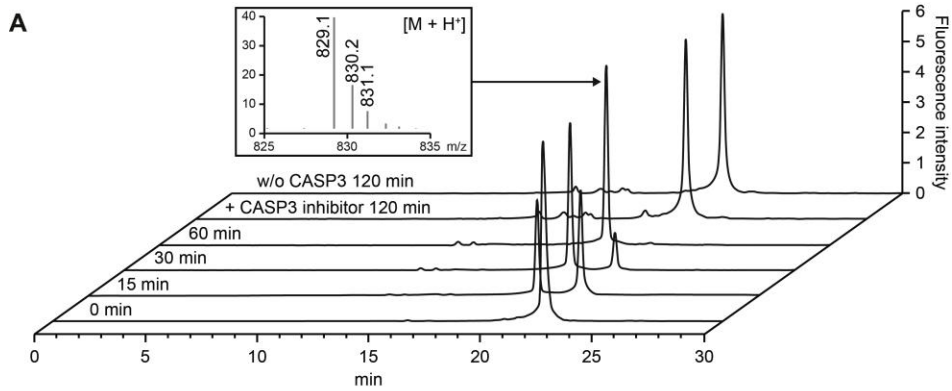


Figure 6.4. (A) HPLC chromatograms of RGDEVD-DOX incubated in the presence of recombinant human caspase-3 for 0, 15, 30, and 60 min. Chromatograms of RGDEVD-DOX incubated for 120 min with the caspase-3 pretreated with caspase inhibitor, and RGDEVD-DOX incubated for 120 min without addition of caspase-3 were also shown. (B) Mean intensity of doxorubicin fluorescence in the cell nuclei quantified depending on the drug exposure time. Doxorubicin (○), RGDEVD-DOX (□), or cleaved RGDEVD-DOX (■) was treated on U87 MG (left) and HT-29 (right) cells. Data are presented as mean ± s.e.m. (C) Representative images of doxorubicin (left), RGDEVD-DOX (center), and cleaved RGDEVD-DOX (right) treated on U87 MG (upper) and HT-29 (lower) cells for 1 h. Scale bar, 50 μm.

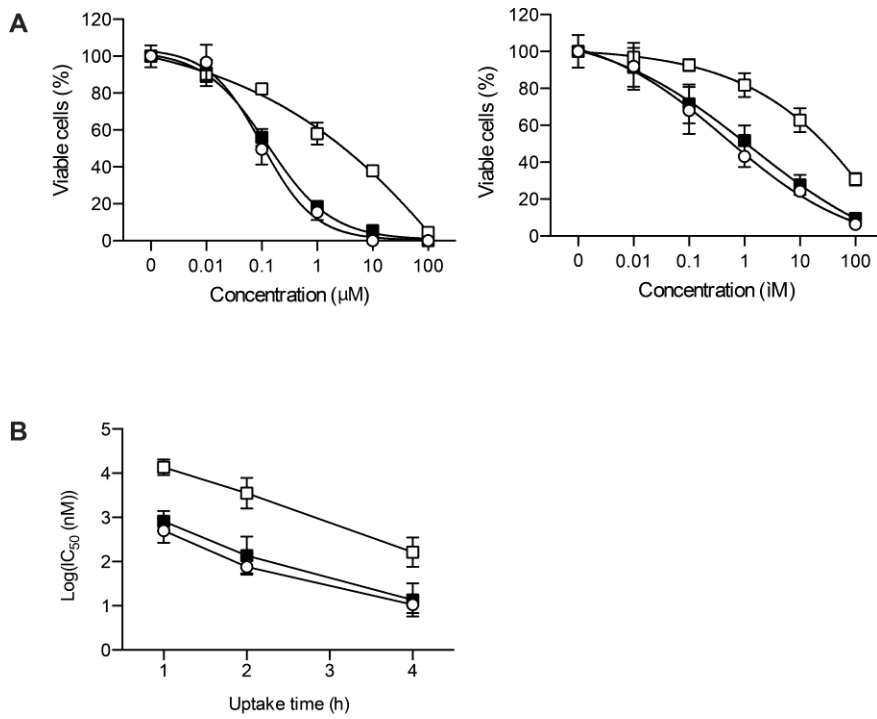


Figure 6.5. (A) Concentration-dependent cytotoxicity of doxorubicin (○), RGDEVD-DOX (□), and RGDEVD-DOX incubated with recombinant human caspase-3 (cleaved RGDEVD-DOX; ■) on U87 MG (left) and HT-29 (right) cells when exposed 2 h determined by MTT assay. (B) Exposure time-dependent IC50 values of the drugs on U87 MG cells. Data are presented as mean ± s.e.m.

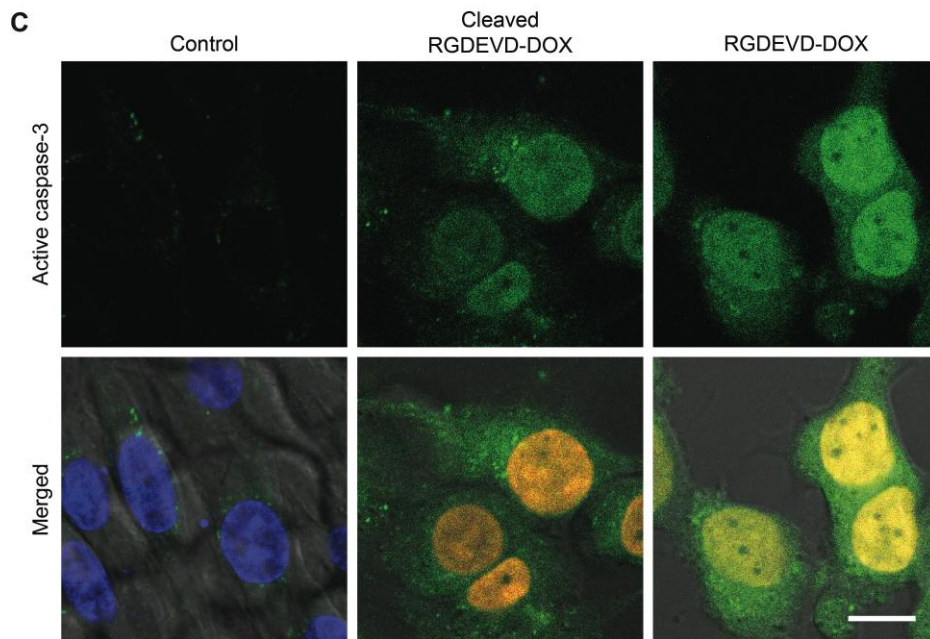
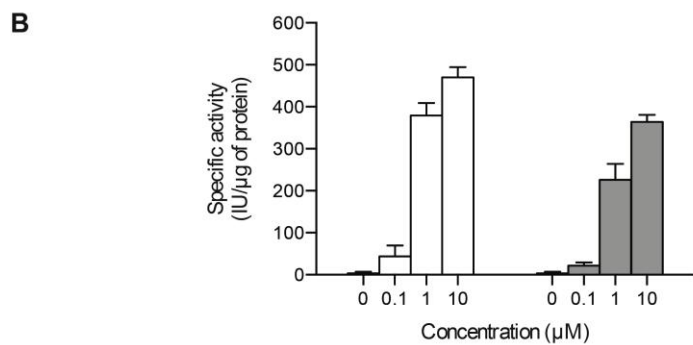
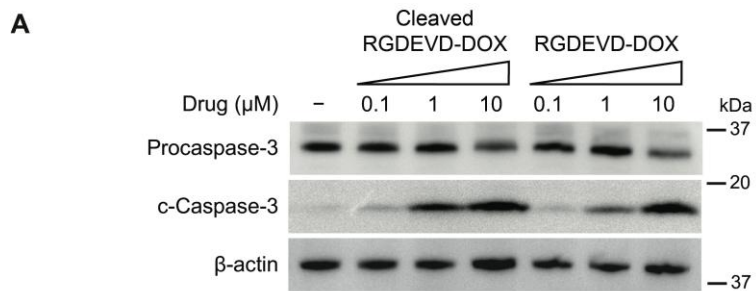


Figure 6.6. (A) Western blots of U87 MG cells treated with RGDEVD -DOX or RGDEVD-DOX incubated with recombinant human caspase-3 (cleaved RGDEVD-DOX) at a concentration of 0.1, 1, and 10 μ M. The immunoblots were carried out using procaspase-3 (upper), cleaved caspase-3 (center), and beta-actin (lower) antibodies. (B) Cellular caspase activities of U87 MG cells treated with cleaved RGDEVD-DOX (white) or RGDEVD-DOX (grey) at a concentration of 0, 0.1, 1, and 10 μ M. Data are presented as mean \pm s.e.m. (C) Cellular caspase-3 staining of U87 MG cells after 48 h exposure to cleaved RGDEVD-DOX (center) and RGDEVD-DOX (right). Control cells that have not been treated with any drugs were also shown (left). Green fluorescence represents the active caspase-3. Nuclei of control cells were stained with DAPI (blue). Nuclei of drug treated cells were accumulated with the drug (red) and were not stained with DAPI. Scale bar, 10 μ m.

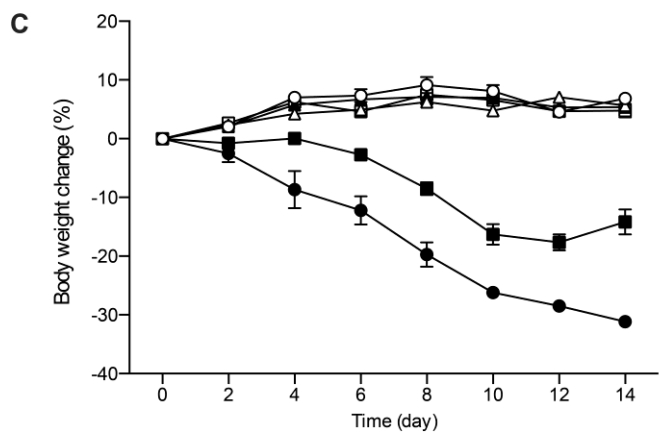
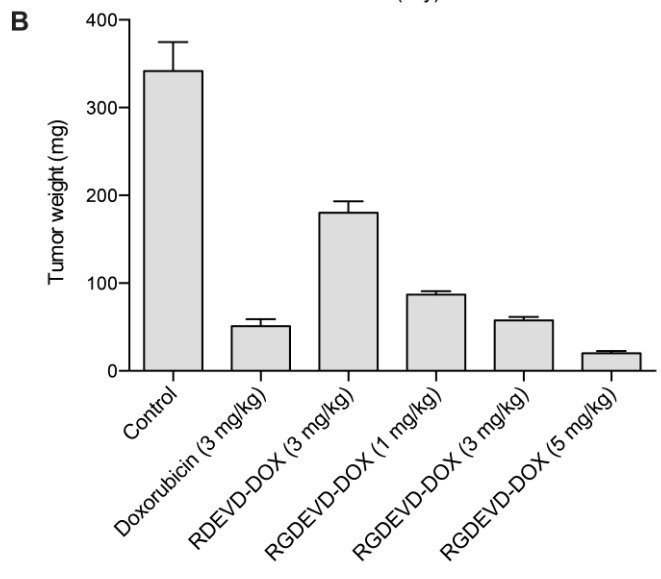
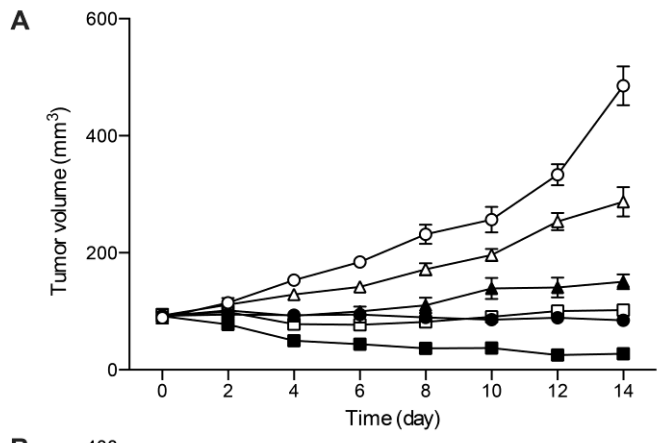


Figure 6.7. Animal study result of U87 MG-tumor bearing BALB/cSlc-nu mice that received normal saline (\circ), doxorubicin (7×3 mg/kg, \bullet), RDEV-D-DOX (7×3 mg/kg, Δ), and RGDEV-D-DOX in three different doses (7×1 mg/kg, \blacktriangle ; 7×3 mg/kg, \square ; 7×5 mg/kg, \blacksquare). The animals received the agents intravenously daily for 7 days. The doses are expressed at molar equivalent of doxorubicin. Tumor growth profiles (A), isolated tumor weights (C), and body weight profiles (B) are shown. Data are presented as mean \pm s.e.m.

6.4. Discussion

The present study demonstrates about the prodrug comprising an integrin $\alpha\beta3$ binding moiety, caspase-specific cleavable peptide, and a doxorubicin as an active cytotoxic compound. The principle of action of the current prodrug system are as followings: (i) the prodrug selectively targets integrin $\alpha\beta3$ overexpressing cells including certain tumor cells as well as endothelial cells constituting the angiogenic tumor blood vessels, and triggers apoptosis in those cells, (ii) due to the apoptosis induced in the integrin $\alpha\beta3$ overexpressing cell, local concentration of active caspase-3 increases within the tumor tissue, (iii) increased level of active caspase-3 cleave the prodrug and separate the peptide and doxorubicin compartment, (iv) since the peptide moiety is the one that provides the overall selectivity of the prodrug, the released doxorubicin compartment is non-selective with facilitated penetration into the cells due to its hydrophobicity, thus inducing cell death in the nearby cells regardless of their expression in integrin $\alpha\beta3$, and again upregulate caspase-3, which repeatedly force step (iii) and (iv) to occur. To put it shortly, during the initial phase of therapy, integrin $\alpha\beta3$ overexpressing cells are affected, and in the later phase, other tumor-associated cells are affected, potentially leading to complete remission of the tumor growth. A schematic illustration depicting this mode of action is shown in **Fig 6.1A**.

The importance of selectivity in development of anticancer agent has been always emphasized. However, this common sense is challenged by the finding of intratumor heterogeneity, which revealed the existence of different subclones of tumor cells in a single tumor mass. Moreover, many stromal cells constituting the tumor microenvironment also largely contribute to the growth of tumor. The selective targeting generally focuses on single molecule, which is likely to be expressed in the limited population of tumor cells according to the intratumor heterogeneity. Thus, such approach would be effective initially, but would soon be impotent by the regrowth of the unaffected tumor cells and the tumor-associated stromal cells.

In contrast, currently proposed strategy considers the selective delivery of chemotherapeutic agents to the tumor tissue, which in turn becomes non-selective within the tumor tissue. Therefore, it could possibly affect broad populations of tumor cells that differ in their biomarker expression pattern and also the tumor-associated stromal cells. This resembles intratumor injection of cytotoxic agents, which is generally not applicable for clinical use. Another significant difference between the current drug delivery strategy and the conventional one is that the target molecule increases as the therapy sustains, which is opposite in the conventional targeted therapies (see **Fig 6.2**).

As a model drug, RGDEVD-DOX was synthesized, which contains RGD and DEVD motif for targeting integrin $\alpha\beta3$ and caspase-3, respectively. These two amino acid sequences share one Asp and form fully functional single pentapeptide. This peptide was conjugated to the 14-OH position of doxorubicin to produce RGDEVD-DOX prodrug. This prodrug proved satisfactory integrin $\alpha\beta3$ targeting capability in various *in vitro* studies. It was also shown that RGDEVD-DOX was more potent than RDEVD-DOX in the U87 MG tumor-bearing preclinical model, indicating the benefit of the RGD motif *in vivo*.

The synthesized prodrug was rapidly cleaved in the presence of caspase-3, releasing a doxorubicin derivative. The cleavage of the prodrug significantly facilitated the penetration into the cell and nucleus of the active ingredient, similar to that of intact doxorubicin. It was considered that attachment of the very hydrophilic and negatively charged RGDEVD peptide on the doxorubicin had significantly delayed the cell and nucleus membrane penetration. Since cell surfaces are negatively charged due to the abundant phosphatidylserine, phosphatidylinositol¹⁵ and sialoglycoproteins¹⁶ on the membrane, negatively charged substances are difficult to penetrate through the cell membrane. Thus, detachment of this peptide from the doxorubicin compartment recovered the lipophilicity as well as the intrinsic rapid cell penetration capability. Hydrophilic molecules prefer their residence in the blood or plasma, whereas hydrophobic molecules prefer distribution in the tissue or cells. Therefore, the

conversion of the prodrug from hydrophilic form to hydrophobic form within the tumor tissue would consequently 'anchor' the conjugated doxorubicin in that location.

Not surprisingly, cell deaths induced by RGDEVD-DOX or the active form occurred through caspase-3-mediated pathway, hence showed upregulated caspase-3. The active caspase-3 was distributed evenly throughout the cells. In addition, caspases also leak out of the apoptotic cells¹⁷. Therefore, another molecules of RGDEVD-DOX reached to the tumor tissue could be further cleaved and activated by the easily accessible upregulated caspase-3.

6.5. Conclusion

RGDEVD-DOX has proven its efficacy for the proof-of-concept in the currently proposed drug delivery strategy as a model drug. This prodrug could selectively deliver the cytotoxic agent to the tumor tissue by the employed RGD motif, which could recognize tumor and tumor endothelial cells that overexpress integrin $\alpha v \beta 3$, during the initial phase of the therapy. Then the upregulated caspase-3 caused by the initially delivered cytotoxic agents could activate another molecule of the prodrug and facilitate their distribution into the nearby cells in non-selective manner.

As long as the DEVD moiety or other caspase-3-cleavable sequence is conserved in the prodrug, targeting moiety other than RGD and also other cytotoxic agents could be possibly adopted to achieve the same purposed delivery strategy. Therefore, current delivery strategy could be largely expanded and lead to development of various new prodrugs.

References

- 1 Allen, T. M. Ligand-targeted therapeutics in anticancer therapy. *Nat Rev Cancer* **2**, 750-763 (2002).
- 2 DiPaola, R. S., Rinehart, J., Nemunaitis, J., Ebbinghaus, S., Rubin, E., Capanna, T., Ciardella, M., Doyle-Lindrud, S., Goodwin, S., Fontaine, M., Adams, N., Williams, A., Schwartz, M., Winchell, G., Wickersham, K., Deutsch, P. & Yao, S. L.

- Characterization of a novel prostate-specific antigen-activated peptide-doxorubicin conjugate in patients with prostate cancer. *J Clin Oncol* **20**, 1874-1879 (2002).
- 3 Sapa, P., Stein, R., Pickett, J., Qu, Z., Govindan, S. V., Cardillo, T. M., Hansen, H. J., Horak, I. D., Griffiths, G. L. & Goldenberg, D. M. Anti-CD74 antibody-doxorubicin conjugate, IMMU-110, in a human multiple myeloma xenograft and in monkeys. *Clin Cancer Res* **11**, 5257-5264 (2005).
 - 4 Breij, E. C., de Goeij, B. E., Verploegen, S., Schuurhuis, D. H., Amirkhosravi, A., Francis, J. L., Breinholt Miller, V., Houtkamp, M., Bleeker, W. K., Satijn, D. & Parren, P. W. An antibody-drug conjugate that targets tissue factor exhibits potent therapeutic activity against a broad range of solid tumors. *Cancer Res* (2013).
 - 5 Deckert, J., Park, P. U., Chicklas, S., Yi, Y., Li, M., Lai, K. C., Mayo, M. F., Carrigan, C. N., Erickson, H. K., Pinkas, J., Lutz, R. J., Chittenden, T. & Lambert, J. M. A novel anti-CD37 antibody-drug conjugate with multiple anti-tumor mechanisms for the treatment of B-cell malignancies. *Blood* **122**, 3500-3510 (2013).
 - 6 Gerlinger, M., Rowan, A. J., Horswell, S., Larkin, J., Endesfelder, D., Gronroos, E., Martinez, P., Matthews, N., Stewart, A., Tarpey, P., Varela, I., Phillimore, B., Begum, S., McDonald, N. Q., Butler, A., Jones, D., Raine, K., Latimer, C., Santos, C. R., Nohadani, M., Eklund, A. C., Spencer-Dene, B., Clark, G., Pickering, L., Stamp, G., Gore, M., Szallasi, Z., Downward, J., Futreal, P. A. & Swanton, C. Intratumor heterogeneity and branched evolution revealed by multiregion sequencing. *N Engl J Med* **366**, 883-892 (2012).
 - 7 Wiseman, B. S. & Werb, Z. Stromal effects on mammary gland development and breast cancer. *Science* **296**, 1046-1049 (2002).
 - 8 Zitzmann, S., Ehemann, V. & Schwab, M. Arginine-glycine-aspartic acid (RGD)-peptide binds to both tumor and tumor-endothelial cells in vivo. *Cancer Res* **62**, 5139-5143 (2002).
 - 9 Chen, K. & Chen, X. Integrin targeted delivery of chemotherapeutics. *Theranostics* **1**, 189-200 (2011).
 - 10 Zhan, C., Gu, B., Xie, C., Li, J., Liu, Y. & Lu, W. Cyclic RGD conjugated poly(ethylene glycol)-co-poly(lactic acid) micelle enhances paclitaxel anti-glioblastoma effect. *J Control Release* **143**, 136-142 (2010).
 - 11 Xu, Q., Liu, Y., Su, S., Li, W., Chen, C. & Wu, Y. Anti-tumor activity of paclitaxel through dual-targeting carrier of cyclic RGD and transferrin conjugated hyperbranched copolymer nanoparticles. *Biomaterials* **33**, 1627-1639 (2012).
 - 12 Miura, Y., Takenaka, T., Toh, K., Wu, S., Nishihara, H., Kano, M. R., Ino, Y., Nomoto, T., Matsumoto, Y., Koyama, H., Cabral, H., Nishiyama, N. & Kataoka, K. Cyclic RGD-linked polymeric micelles for targeted delivery of platinum anticancer

- drugs to glioblastoma through the blood-brain tumor barrier. *ACS nano* **7**, 8583-8592 (2013).
- 13 Lien, S., Pastor, R., Sutherlin, D. & Lowman, H. B. A substrate-phage approach for investigating caspase specificity. *Protein J* **23**, 413-425 (2004).
 - 14 Meyer-Losic, F., Quinonero, J., Dubois, V., Alluis, B., Dechambre, M., Michel, M., Cailler, F., Fernandez, A. M., Trouet, A. & Kearsley, J. Improved therapeutic efficacy of doxorubicin through conjugation with a novel peptide drug delivery technology (Vectocell). *J Med Chem* **49**, 6908-6916 (2006).
 - 15 Goldenberg, N. M. & Steinberg, B. E. Surface charge: a key determinant of protein localization and function. *Cancer Res* **70**, 1277-1280 (2010).
 - 16 Wang, B. & Brand-Miller, J. The role and potential of sialic acid in human nutrition. *Eur J Clin Nutr* **57**, 1351-1369 (2003).
 - 17 Hentze, H., Schwoebel, F., Lund, S., Keel, M., Ertel, W., Wendel, A., Jaattela, M. & Leist, M. In vivo and in vitro evidence for extracellular caspase activity released from apoptotic cells. *Biochem Biophys Res Commun* **283**, 1111-1117 (2001).

Concluding remarks

Although heparin has been only approved and used clinically for its anticoagulant activity, it has been regarded as an interesting molecule for its capability to interact with broad range of endogenous molecules and regulatory effects in diverse pathophysiological states. This study was particularly focused in its potential role in tumor progression and angiogenesis. Regarding that angiogenesis inhibitors have recently encountered a problematic issue, in which showing adaptive resistance by upregulation of alternative pro-angiogenic factors, heparin could be an excellent lead compound for developing a novel angiogenesis inhibitor, since diverse pro-angiogenic factors are heparin-binding proteins. However, due to the potent anticoagulant activity of heparin, it cannot be directly applied clinically for use in indication other than venous thromboembolism.

In purpose to utilize heparin for treatment of cancer as an angiogenesis inhibitor, LMWH was chemically modified by introducing sodium taurocholates on the polysaccharide chain. Appropriate modification of LMWH allowed potentiation of anti-angiogenic activity while eliminating its anti-coagulant activity. It was found that such modifications resulted in blocking the ATIII-interacting pentasaccharide unit of heparin by a bulky molecule, in this case, the sterane core, and increasing the net anionic electrical charge by adding more sulfate groups that could enhance binding to VEGF. In addition, LHT7 retained the intrinsic capacity of heparin to bind with other pro-angiogenic molecules including FGF2 and PDGF-B, despite the chemical modification. In the aspect of increasing therapeutic efficacy and overcoming the acquired resistance, targeting VEGF, FGF2 and PDGF-B at the same time is critical for angiogenesis inhibition. Thus, LHT7 would potentially overcome the resistance and effectively inhibit angiogenesis as well as tumorigenesis. It was also confirmed that heparin is an excellent lead compound to develop multi-targeted agent due to its inherent capability to interact with broad range of pro-angiogenic factors.

Apart from development of heparin-based multitargeted angiogenesis inhibitor, two doxorubicin prodrugs were also developed according to a novel drug delivery strategy. Traditionally, one of the most popular approaches to deliver cytotoxic agents to the tumor tissue is by introducing tumor specific surface antigen recognition ligand to the drug. However, such approach has been severely challenged by the discovery of intratumor heterogeneity, which makes aware of presence of distinct subclones of cell populations within single mass of tumor. Ironically, due to the highly selective or specific nature of the employed ligand, the cytotoxic agents are conveyed to only limited subpopulations of tumor, ultimately resulting in regrowth of tumor by the unaffected tumor cells. Two different doxorubicin prodrugs, EMC-DEVD-S-DOX and RGDEVD-DOX, were synthesized that shares DEVD peptide sequence, an essential functional molecule for the currently suggested drug delivery strategy.

Firstly, the EMC-DEVD-S-DOX is delivered to the tumor tissue through the conventional passive targeting with long circulation time by the *in situ* albumin-binding capability. It is then specifically activated and recovers the cytotoxic activity by releasing free doxorubicin from the inactive form of the prodrug upon presence of caspase-3 induced by radiation exposure. Unlike the traditional target of tumor targeting, which the target molecules are invariably expressed on their cell surface unless there are significant changes in their environment, upregulation of caspase-3 is relatively a transitory event that occurs only during cell apoptosis. Therefore, long circulation and tumor accumulation capability provided by albumin binding significantly increases the possibility of prodrug to contact with the upregulated caspase-3 in the tumor tissue. Hence, the capabilities for albumin binding and radiation-stimulated prodrug activation are inseparable to achieve the purposed drug delivery strategy ideally. The major advantage of this strategy is that the site of drug action could be controlled more actively by determining the location of radiation exposure. Since there was a huge advance in stereotactic radiotherapy, the site where the prodrug is activated could be controlled very precisely, thus

leaving minimum sequelae to the patients. Already about half of the entire cancer patients commonly receive radiotherapy. Therefore, EMC-DEVD-S-DOX, which shows a perfect synergy with radiation, would be very attractive and ideal form of drug to treat the cancer patients.

By comparison with the EMC-DEVD-S-DOX, the RGDEVD-DOX comprises conventional active targeting moiety rather than the passive one. Although this drug delivery system employs the identical active targeting moiety with the conventional targeted delivery system, the insertion of DEVD sequence between the active ingredient and the targeting moiety totally differentiates the characteristics of the delivery mechanism. While the conventional active targeting strategy could affect only the limited subpopulation of the tumor, RGDEVD-DOX could affect broader range of tumor subpopulations that differ in their genomic profile within the site where integrin $\alpha\beta3$ overexpressing cells are located. The RGD moiety of the prodrug selectively delivers the cytotoxic agent to the tumor during the initial phase of administration and induces apoptosis in certain subclone of tumor cells as well as tumor endothelial cells that overexpress integrin $\alpha\beta3$, leading to upregulation of caspase-3. Then the caspase-3 further activates the other molecules of the prodrug, triggering to release more hydrophobic form of the active compound with facilitated penetration into the cell, regardless of their integrin $\alpha\beta3$ expression.

Since the upregulation of the caspase-3, which is a key event in the proposed drug delivery strategy, is common during the apoptosis of mammalian cells, the genomic diversity of tumor cells would hardly influence the efficacy of the currently developed prodrugs. Considering that conventional molecular targeted approach in any aspect of tumor therapy is seriously challenged by tumor heterogeneity, these two doxorubicin prodrugs could be outstanding alternatives. Also, current delivery strategy could be largely expanded and lead to development of various new prodrugs.

국문초록

현대의학에서 종양학의 비약적인 발전에도 불구하고 암은 여전히 난치병으로 간주된다. 이에 따라 많은 임상의를 및 연구자들이 암을 효과적으로 치료하기 위한 연구를 활발히 전개하고 있다. 하지만 현재까지 개발된 항암제들은 암의 유전적 다양성과 복잡성으로 인해 기대에 못 미치는 치료효과를 보이고 있으며 심각한 부작용과 같은 여러 문제점들 또한 갖고 있다. 따라서 보다 혁신적인 항암제가 요구되는 상황에서 기존 항암제와는 차별되는 신개념의 항암제를 연구 개발하였다.

본 학위논문에서는 크게 분류하여 두 종류의 항암제를 제시하였다. 첫 번째는 신개념의 혈관신생억제제로 헤파린을 기반으로 개발하였다. 혈관신생작용은 암의 성장에 있어서 필수적인 요소 중 하나이다. 종양이 어느 정도 이상의 크기로 성장하려면 이미 존재하고 있던 주변 혈관으로부터의 확산작용만으로는 조직 내의 모든 세포로 영양소나 산소를 공급받을 수가 없게 된다. 따라서 암 조직은 자가 생존을 위해 조직 내외로 새로운 혈관을 발생시키는데 이를 혈관신생작용이라고 한다. 일반적으로 저산소 상태에 처해진 암세포들은 이를 극복하고 생존하기 위해 여러 혈관신생성장인자들은 발현하여 혈관신생작용을 일으키게 되는데 이들 중 하나 이상의 신호전달과정을 차단하는 약물을 혈관신생억제제라고 한다. 본 연구에서 개발된 헤파린 기반의 혈관신생억제제(LHT7)는 VEGF와 FGF2, PDGF-B 등의 활성을 차단함으로써 종양 내 혈관신생작용 과정의 여러 단계에 동시에 억제작용이 있음을 확인하였다. 현재 임상적으로 사용되거나 개발되고 있는 혈관신생억제제 중 혈관신생인자를 다중으로 표적하는 약물은 찾아볼 수 없어 매우 획기적이다. 특히 여러 혈관신생인자에 대한 수용체의 티로신키나아제를 비특이적으로 억제하는 소분자

티로신키나아제 억제제에 비해 더 상위체계의 인자를 다중으로 표적하기 때문에 더 효과적인 혈관신생억제작용을 기대할 수 있다.

다른 하나는 세포사멸에 의해 활성화되는 독소루비신의 프로드럭이다. 일반적으로 세포독성 항암제의 가장 큰 문제점은 용량의존적으로 나타나는 심각한 독성 및 부작용이다. 이를 개선하기 위한 방편으로 세포독성 항암제를 선택적으로 암 조직에 전달하고 정상조직에서의 분포를 줄이기 위한 여러 시도들이 있어왔다. 본 연구에서는 널리 사용되고 있는 세포독성 화학요법제인 독소루비신을 기존 약물전달시스템과는 근본적으로 다른 이론적 배경으로 암조직에 보다 선택적으로 전달할 수 있도록 하였다. 이러한 약물전달시스템의 개발을 가능하게 할 방법으로 유도표현형질표적요법을 제안하였다. 유도표현형질표적요법이란 표적물질의 전달에 있어서 기존 방식의 암세포의 유전형질에 의존하는 것이 아닌 인위적으로 특정 표현형질을 유도시켜 그것을 표적하는 약물전달 방법이다. 본 연구에서는 특히 세포사멸을 유도시켜 이것을 표적하는 방법을 제안하였다. 종양 내 이질성에 의해 하나의 암을 유전형질에 기반을 두어 특정 지을 수 없으므로 유전형질에 의존하는 것보다 세포사멸을 외부자극으로 유도한 뒤 이것에 의존하여 세포독성 항암제를 전달하는 것이 보다 신뢰도가 높다. 특히 기존 약물전달시스템에 응용되는 수동적 수송과 능동적 수송 기술들 또한 접목하여 암조직에 매우 선택적으로 독소루비신이 수송될 수 있도록 하였다.

주요어 : 헤파린; 항암제; 혈관신생억제제; 다중표적형 치료제; VEGF; FGF; PDGF; 독소루비신; 프로드럭; 카스파제; DEVD; 알부민; RGD; 인테그린

학 번 : 2010-31129